

**VIBRATIONAL-ROTATIONAL  
EXCITATIONS IN  
NONLINEAR MOLECULAR  
SYSTEMS**

# **VIBRATIONAL-ROTATIONAL EXCITATIONS IN NONLINEAR MOLECULAR SYSTEMS**

**A. A. Ovchinnikov  
N. S. Erikhman**

and

**K. A. Pronin**

*Joint Institute of Chemical Physics  
Russian Academy of Sciences  
Moscow, Russia*

**Springer Science+Business Media, LLC**

Library of Congress Cataloging-in-Publication Data

---

Ovchinnikov, A. A. (Aleksandr Anatol'evich)

Vibrational-rotational excitations in nonlinear molecular systems/Alexander A.

Ovchinnikov, Nikolai S. Erikhman, and Kirill A. Pronin

p. cm.

Includes bibliographical references and index.

ISBN 978-1-4613-5494-9 ISBN 978-1-4615-1317-9 (eBook)

DOI 10.1007/978-1-4615-1317-9

1. Molecular dynamics. 2. Molecular rotation. I. Erikhman, Nikolai S. II. Pronin, Kirill A. III. Title.

QD461 .O915 2001

539'.6—dc21

2001038993

---

ISBN 978-1-4613-5494-9

© 2001 Springer Science+Business Media New York

Originally published by Kluwer Academic/Plenum Publishers, New York in 2001

Softcover reprint of the hardcover 1st edition 2001

<http://www.wkap.nl/>

10 9 8 7 6 5 4 3 2 1

A C.I.P. record for this book is available from the Library of Congress

All rights reserved

No part of this book may be reproduced, stored in a retrieval system, or transmitted in any form or by any means, electronic, mechanical, photocopying, microfilming, recording, or otherwise, without written permission from the Publisher

# Preface

"If there would be no God – then what a staff-captain am I?" – said one of the characters in a novel by Dostoevskii. In a similar way we can exclaim: "If there would be no nonlinearity – than what physics would that be?".

Really, the most interesting and exciting effects are described by nonlinear equations, and vanish in the linear approximation. For example, the general theory of relativity by A.Einstein comes to mind first — one of the most beautiful physical theories, which is in fact essentially nonlinear. Next, the phase transitions crystal – liquid and liquid – gas are due to the anharmonicity of inter-particle interactions, to dissociation and infinite motion. Similarly, transitions into the superconducting state or the superfluid would be impossible with purely harmonic interaction potentials. Another brilliant achievement in nonlinear physics was the construction of a laser and the subsequent development of nonlinear optics. The latter describes the interaction of the matter with light of super-high intensity, when multi-quanta intra-molecular transitions become essential. Last, we should note here the very beautiful mathematical theory – the theory of catastrophes. Its subject is the study of invariant general properties of multi-dimensional surfaces in the vicinity of bifurcation points with respect to continuous transformations. Assigning one or another physical meaning to multi-dimensional surfaces – for example, interpreting these either as potential surfaces of the interaction  $U(R, r)$ , or as a thermodynamic potential  $\Phi(P, T, \eta)$ , etc. – we can study the behavior of the systems in the vicinity of critical (bifurcation) points with the help of the theory of catastrophes.

Most monographs on intra - molecular vibrations and vibrational - rotational spectra of molecules are based on the theory of normal modes, while the nonlinearity is taken into account within perturbation theory. However, in high-intensity laser field the highly-excited intra-molecular vibrational-rotational modes are involved. The nonlinearity of motion plays then a decisive role and it should be taken into account properly in zero order approximation already. In the present book we will address the nonlinearity effects in polyatomic molecules exactly from that point of view. In the world of molecules we step away from the island of linearity into the intriguing ocean of nonlinearity. We hope, this journey will be interesting.

Recent progress in experimental laser technique provided extraordinary opportunities in the study of high vibrational / rotational overtones in the

spectra of polyatomic molecules. As it has been shown (A.A.Ovchinnikov, 1969), high excitations in nonlinear molecular systems give rise to local modes, which influence greatly the spectral properties and intramolecular kinetics. The theory of these effects is of great importance for the interpretation of experiments in IR spectroscopy, in the promising field of laser chemistry and molecular engineering (analysis, synthesis, and construction of complex organic molecules), in nonlinear optics, in the study of chemical transitions, etc. Besides, it forms an important inter-disciplinary part of fundamental theory at the border of chemical physics, physical chemistry, spectroscopy, quantum mechanics, and solid state physics.

This book is aimed at providing a comprehensive theoretical description of highly - excited long - living vibrational / rotational excitations in anharmonic molecules. It comprises the classical and quantum theory of local modes, their effect upon the infrared (IR) spectra of molecules and upon the kinetics of intramolecular relaxation, and presents a semi-empirical theory that relates the geometrical parameters of the molecule to the IR spectra. Besides, we added the material on breathers – local excitations of deformable lattices with inner vibrational structure, which attract much attention recently. At present the comprehensive analysis of the entire field is still lacking.

The following problems are considered in detail:

- a) Classification of oscillation spectra of strongly excited molecules and molecular crystals. The principal idea is to explain the vibronic excitation formation, its long - living nature, and relaxation of vibration energy with the account of vibration nonlinearity for CH and OH bonds, with special emphasis on the nonperturbative nature of these effects;
- b) Clusterization of vibrational and rotational energy levels;
- c) Dynamical breakdown of symmetry of vibrational and rotational motion in polyatomic molecules;
- d) Interpretation of IR spectra of organic molecules on the basis of local - mode theory;
- e) Calculation of relaxation time for highly - excited vibrations in polyatomic molecules;
- f) Existence of breathers, their stability and decay.

As to the form of the presentation of the material, our idea was to provide:

- a) a systematic and comprehensive presentation (unified theoretical approach to the problems; inclusion of all the important topics in the field from the basics to up-to-date research);
- b) a detailed form of presentation (only basic knowledge of quantum mechanics required as the background; all the important derivations performed in detail, without recourse to original literature);
- c) suitability to a wide auditorium, ranging from graduate students, specializing in spectroscopy, molecular physics, optics, etc. up to academic

researchers.

The book is structured as follows: The Introduction provides the basics of the conventional normal - mode theory of vibrations and a brief survey of the principal ideas of the local - mode theory. In Chapter 2 and Chapter 3 the classical theory of localization of vibrational excitations is presented on the basis of the model of two coupled nonlinear oscillators and is generalized consequently to an arbitrary number of weakly interacting nonlinear oscillators. Criteria for local - mode formation and decay are formulated and studied. The theory of breathers and its relation to the theory of local modes is described in Chapter 4. The quantum theory of local modes and vibrational - rotational spectra of polyatomic molecules is considered in Chapters 5 and 6. On the basis of the model of two coupled Morse oscillators the conditions for the emergence of localized vibrational / rotational modes in polyatomic molecules are specified with the account of nonlinear interactions, both potential and kinematic ones. The effect of clusterization of stretching - vibrational levels in the spectrum is addressed. Construction of model Hamiltonians for the vibrational / rotational motion of molecules, along with the method of contact transformations is discussed. Clusterization of rotational levels in the spectrum within the semiclassical approach is studied in Chapter 7, with the account of the symmetry of the molecule and its rigidity. The account of interaction of vibrations and rotations, and its effect upon the spectrum and level clusterization is considered in Chapter 8. The influence of Fermi resonances upon the spectrum and the structure of phase space is discussed. Intramolecular relaxation of vibrational energy in the presence of local modes is studied in Chapter 9 and Chapter 10, both for isolated molecules and for molecular crystals. Correlation between the molecular structure and IR spectra of polyatomic molecules is investigated within a semi-empirical approach in Chapter 10 as well.

The permissions to reproduce the copyrighted material are gratefully acknowledged:

- table 5.3 is reprinted from Chemical Physics Letters, volume 66, number 3, H. S. Moller, O. S. Mortensen "Vibrational motion in the local- and normal-mode pictures", page 540, ©1979 with permission from Elsevier Science;

- figures 4.1, 4.2, 4.3, 4.4 are reprinted from Physics Reports, volume 295, number 5, S. Flach, C. R. Willis, "Discrete breathers", page 184, ©1998, with permission from Elsevier Science;

- table 8.2 and figures 8.2, 8.3 are reprinted with permission from K. K. Lehmann "The Interaction of Rotation and Local Mode Tunneling in the Overtone Spectra of Symmetric Hydrides", Journal of Chemical Physics, volume 95, page 2361, ©1991 American Institute of Physics;

- figures 7.13, 7.19 are reprinted with permission from W. G. Harter, C. W. Patterson "Orbital Level Splitting in Octahedral Symmetry and SF<sub>6</sub> Rotational Spectra. I. Qualitative Features of High J Levels", Journal of Chem-

- ical Physics, volume 66, page 4872, ©1977 American Institute of Physics;
- tables 8.3, 8.4, figures 8.7, 8.8, 8.10, 8.11, 8.12, 8.13, 8.14 and Conclusions are reprinted with permission from D. A. Sadovskii, B. I. Zhilinskii, J. P. Champion, G. Pierre "Manifestation of Bifurcations and Diabolic Points in Molecular Energy Spectra", Journal of Chemical Physics, volume 92, page 1523, ©1990 American Institute of Physics;
  - tables 7.1, 7.2 and figures 7.2, 7.3, 7.6, 7.8, 7.10, 7.11 are reprinted with permission from W. G. Harter, C. W. Patterson "Rotational Energy Surfaces and High - J Eigenvalue Structure of Polyatomic Molecules", Journal of Chemical Physics, volume 80, page 4241, ©1984 American Institute of Physics;
  - table 3.1 and figures 2.17, 2.18, 2.19, 3.7, 3.9 are reprinted with permission from C. Jaffe, P. Brumer "Local and Normal Modes: A Classical Perspective", Journal of Chemical Physics, volume 73, page 5646, ©1980 American Institute of Physics;
  - figure 1.4 is reprinted with permission from E. L. Sibert, W. P. Reinhardt, J. T. Hynes "Classical Dynamics of Energy Transfer Between Bonds in ABA Triatomics", Journal of Chemical Physics, volume 77, page 3583, ©1982 American Institute of Physics;
  - tables 8.5, 8.6 and figures 8.15, 8.16, 8.17 are reprinted with permission from J. Svitak, Z. Li, J. Rose, M. E. Kellman "Spectral Patterns and Dynamical Bifurcation Analysis of Highly Excited Vibrational Spectra", Journal of Chemical Physics, volume 102, page 4340, ©1995 American Institute of Physics;
  - table 10.2 is reprinted with permission from D. J. Swanton, B. R. Henry, "A Theoretical Basis for the Correlation Between Bond Length and Local Mode Frequency", Journal of Chemical Physics, volume 86, page 4801, ©1987 American Institute of Physics;
  - figure 1.5 is reprinted with permission from A. C. Albrecht, "Thermal Lensing Spectroscopy in the Condensed Phase", in: "Advances in Laser Chemistry", ed. by A.H.Zewail, ©1978, Springer, Berlin, page 235;
  - a passage is reprinted from Progress Analytical Spectroscopy, volume 12, B. R. Henry, M. G. Sowa, "Intracavity Dye Laser Photoacoustic Spectroscopy and Application to High Energy Vibrational Overtone Spectra" "Conclusions", page 349, ©1989 with permission from Elsevier Science;
  - table 5.2 is reprinted from Spectrochim. Acta, volume 37A, I. A. Watson, B. R. Henry, I. G. Ross, "Local Mode Behaviour: The Morse Oscillator Model", page 857, ©1981 with permission from Elsevier Science;
  - figure 10.2 is reprinted with permission from A. Stuchebrukhov, S. Ionov, V. Letokhov, "IR - Spectra of Highly vibrationally Excited Large Polyatomic Molecules and Intramolecular Relaxation", Journal of Physical Chemistry, volume 93, page 5357, ©1989 American Chemical Society;
  - figure 10.6 is reprinted from Chemical Physics Letters, volume 134, A. Stuchebrukhov, I. E. Khromov, "IR Absorption Spectroscopy of Highly

Vibrationally Excited Polyatomic Molecules", page 251, ©1987 with permission from Elsevier Science;

- figure 10.7 is reprinted with permission from K. M. Gough, B. R. Henry, "Overtone Spectral Investigation of Substituent - Induced Bond - Length Changes in Gas - Phase Fluorinated Benzenes and their Correlations with AB Initio STO - 3G and 4 - 21G Correlations", Journal of American Chemical Society, volume 106, page 2781, ©1984 American Chemical Society.

The authors would like to thank Prof. M.Ya.Ovchinnikova and Prof. S. Flach for numerous stimulating discussions.

# Contents

<b>1</b>	<b>Introduction</b>	<b>1</b>
<b>2</b>	<b>Classical theory of nonlinear vibrational systems; local modes</b>	<b>17</b>
2.1	Survey of classical mechanics; introduction to local modes . . . . .	17
2.2	Method of averaging . . . . .	27
2.3	Two weakly coupled Morse oscillators: dynamics and local - mode formation . . . . .	30
2.4	Analysis of phase trajectories with the help of Poincare sections, numerical results . . . . .	46
<b>3</b>	<b>Coupled nonlinear oscillators: formation and decay of local modes</b>	<b>55</b>
3.1	Two weakly coupled nonlinear oscillators: decay of normal modes . . . . .	56
3.2	Multi-oscillator systems: local modes' and normal modes' representations . . . . .	60
3.3	Morse oscillators: calculation of resonance linewidths and criteria for the appearance of local modes . . . . .	68
3.4	Coupled nonlinear oscillators: localized vibrational excitations and their asymptotic stability . . . . .	77
3.5	Canonical transformation to local - mode representation . . . . .	89
<b>4</b>	<b>Discrete breathers</b>	<b>97</b>
4.1	Breathers in Hamiltonian lattices . . . . .	97
4.2	Discrete breathers in one-dimensional chains . . . . .	100
4.3	Arguments for the existence of discrete breathers: some mathematics . . . . .	105
4.4	Discrete breathers: numerical experiments . . . . .	107
4.5	Discrete breathers in lattices with a homogeneous potential .	112
4.6	An exactly solvable Hamiltonian lattice . . . . .	115

<b>5 Quantum theory of vibrational - rotational spectra in <math>XY_2</math> - type molecules</b>	119
5.1 Quantum theory of two Morse oscillators: stretching – vibration spectra in $XY_2$ molecules . . . . .	121
5.2 Stretching – vibration spectra: nonresonant modes' effect upon clusterization of levels . . . . .	130
5.3 Spectrum of stretching vibrations in $XY_2$ molecules: numerical studies . . . . .	136
<b>6 Quantum Hamiltonians of vibrational – rotational excitations in polyatomic molecules; method of contact transformations</b>	143
6.1 Quantum Hamiltonian of polyatomic molecules . . . . .	144
6.2 Molecular Hamiltonian in the inner basis representation 'coordinates - angles' . . . . .	153
6.3 Contact transformation . . . . .	160
6.4 Vibrational-rotational Hamiltonian for $XY_2$ molecule in the inner basis representation 'coordinates - angles' . . . . .	168
<b>7 Semiclassical rotational spectra of rigid and semi-rigid molecules; clusterization of levels and internal symmetry</b>	177
7.1 Spectrum of polyatomic molecules: clusterization of rotational levels . . . . .	178
7.2 Rotational spectrum of rigid and semi-rigid molecules: semiclassical approach . . . . .	191
7.3 Symmetry - based analysis of rotational clusters . . . . .	204
7.4 Tunnelling matrix . . . . .	216
7.5 Violation of permutation symmetry and the super-hyperfine structure . . . . .	229
<b>8 Interaction of vibrations and rotations; polyads and their spectra</b>	243
8.1 Interaction of local vibration modes and rotation in hydrides . . . . .	244
8.2 Rotational - vibrational spectrum in the vicinity of bifurcation points . . . . .	258
8.3 Spectral properties of systems with Fermi resonances . . . . .	274
<b>9 Intramolecular relaxation of vibrations in the presence of local modes</b>	283
9.1 Localized long - living vibrational states in molecular crystals . . . . .	286
9.2 Population inversion of localized long - living vibrational states in a cold lattice . . . . .	294
9.3 Interaction of isolated levels with the continuous spectrum . . . . .	298

<b>10 IR spectra and intramolecular relaxation</b>	313
10.1 Redistribution of intramolecular energy: influence of multi-mode resonance . . . . .	313
10.2 Relation between the absorption linewidths, intramolecular vibrations evolution, and unimolecular decay rates . . . . .	324
10.3 Effect of anharmonicity on IR spectra of polyatomic molecules	330
10.4 Correlation between structure and IR spectra in polyatomic molecules . . . . .	336
<b>11 Conclusion</b>	341
<b>Bibliography</b>	343
<b>Index</b>	353

# Chapter 1

## Introduction

The past decade has been marked by substantial progress in the studies of nonlinear effects in dynamic systems. Previously, major efforts have been dedicated to the elaboration of rigorous and effective computational methods for the treatment of weak nonlinearities. These methods originated from celestial mechanics and were associated with the names of Lagrange, Poincare, Kolmogorov, and others. However, recently physicists and mathematicians addressed new effects, where nonlinearity plays an essential role – such as solitons, long-living local vibrations, multiquanta transitions in an electromagnetic field, etc.

An interesting manifestation of nonlinear dynamic effects in vibrations of long molecular chains is the existence of solitons [1]. Soliton evolution differs drastically from phonon propagation mainly by the effect of preservation of the excitation shape, and by spatial concentration of the excitation in a bounded area in space. The mathematical theory of solitons and its numerous applications in quantum field theory, wave propagation, hydrodynamics, and plasma physics have been covered thoroughly in many monographs and review papers, e.g. [2, 3, 4], to cite only few. In the present book we address a different field of vibrational effects and their application to polyatomic molecules, polymers and simple molecular crystals. The vibrational – rotational spectra of polyatomic molecules have been considered in the fundamental monograph [5]. However, the nonlinear effects have been treated there as small perturbations, which lead to small quantitative changes. In the present monograph we address the nonlinearity in zero approximation already, so that it produces entirely new qualitative effects. Despite considerable progress in the understanding of essentially nonlinear anharmonic effects in the evolution of vibrational excitations [6], many topics need additional clarification and better theoretical understanding. However, a more or less systematic presentation of experimental results and of the underlying theoretical background seems already possible.

We start with the introductory notes on vibrational excitations in mole-

cules. Besides of presenting the basics of the traditional theory, one of the important ideas is to stress the difference between the weakly anharmonic case, treatable by perturbation theory, and the strongly nonlinear regime with new qualitative effects.

The traditional approach to the theory of small vibrations of polyatomic molecules is based upon the theory of normal modes. The latter is applicable to the so called rigid molecules (like  $H_2O$ ) and, with some modifications, to semi-rigid ones (like  $SF_6$ ).

According to the normal-mode theory the potential energy of inter-nuclear interaction in the vicinity of a local minimum is approximated by a positively - defined quadratic form. Thus the vibrational Hamiltonian is:

$$H = \sum_i \frac{p_i^2}{2m_i} + \frac{1}{2} \sum_{i,j} k_{i,j} q_i q_j. \quad (1.1)$$

Here  $q_i$  - are generalized coordinates that characterize small deviations of the molecule configuration from equilibrium,  $p_i$  are corresponding generalized momenta, and  $m_i$  - effective masses. The masses  $m_i$  are of the order of magnitude of atomic ones.

Within the classical approach, the problem with Hamiltonian (1.1) can be solved exactly. The solution can be expressed in a simple way in the normal - mode coordinates  $Q_\alpha$ . Really, introducing new variables:

$$P'_i = \frac{p_i}{\sqrt{m_i}}; \quad Q'_i = \sqrt{m_i} q_i, \quad (1.2)$$

one obtains the following expression for the Hamiltonian (1.1):

$$H = \sum_i P'^2_i + \sum_{i,j} K_{i,j} Q'_i Q'_j. \quad (1.3)$$

Transforming further the momentum  $P_\alpha = \hat{O}P'_i$  and position  $Q_\alpha = \hat{O}Q'_i$  with the help of a corresponding orthogonal matrix  $\hat{O}$ , one finds expression (1.3) to be:

$$H = \frac{1}{2} \sum_\alpha [P_\alpha^2 + \omega_\alpha^2 Q_\alpha^2]. \quad (1.4)$$

Hamiltonian (1.4) corresponds to a system of noninteracting harmonic oscillators. Each oscillator is called a normal mode, and each corresponding oscillation is termed normal oscillation. The solution of classical Hamiltonian equations with Eq. (1.4) is:

$$Q_\alpha = \sum_{\alpha=1}^N Q_{0\alpha} \sin(\omega_\alpha t + \varphi_\alpha),$$

$$P_\alpha = \sum_{\alpha=1}^N \omega_\alpha Q_{0\alpha} \cos(\omega_\alpha t + \varphi_\alpha), \quad (1.5)$$

where  $\varphi_\alpha$  is the initial phase of the normal mode  $\alpha$ .

Eq. (1.5) together with the explicit expression of the transformation from normal modes to the initial ones  $(p_i, q_i) = \Lambda(P_\alpha, Q_\alpha)$  provide the complete solution to the classical problem of small oscillations of polyatomic molecules.

Next we pass over to the quantum approach. Then the spectrum of the Hamiltonian (1.4) is a sum of spectra of  $N$  harmonic oscillators:

$$E_{n_1, \dots, n_\alpha, \dots, n_N} = \hbar \sum_{\beta=1}^N \omega_\beta \left( n_\beta + \frac{1}{2} \right), \quad (1.6)$$

where  $n_\alpha$  are quantum excitation numbers.

The wave function, corresponding to energy (1.6), is:

$$\Psi(Q_\alpha) = \prod_{\beta=1}^N H_{n_\beta}(Q_\beta). \quad (1.7)$$

Here  $H_{n_\beta}(Q_\beta)$  are the well known eigenfunctions of a harmonic oscillator with frequency  $\omega_\beta$ :

$$H_n(Q) = \frac{1}{\sqrt{2^n n! \sqrt{\pi} Q_0}} \exp \left[ -\frac{1}{2} \left( \frac{Q}{Q_0} \right)^2 \right] H_n \left( \frac{Q}{Q_0} \right),$$

and  $H_n$  are the Hermitian polynomials, with  $Q_0 = \sqrt{\hbar/m\omega}$  – the amplitude of zero vibrations.

Thus in the quantum case the problem of small oscillations is solved exactly as well.

The next step in the study of molecular vibrations is the incorporation of nonlinearity in the exact equations of motion. This anharmonicity comes from cubic, quartic, and higher-order terms in the potential energy of the molecule  $U(q_1, \dots, q_N)$ <sup>1</sup>. Typically this nonlinearity is assumed to be small and is accounted for by perturbation treatment. Here two different cases are possible.

(1) In the first case the shifts  $\delta\omega_\alpha$  of the frequencies due to the nonlinearity of oscillations are much smaller than the difference of normal mode frequencies:

$$|\delta\omega_\alpha| \ll \min_\beta |\omega_\alpha - \omega_\beta|. \quad (1.8)$$

---

<sup>1</sup>Besides, there are nonlinear terms, coming from interaction of vibrations with rotation of the molecule. These can be accounted for in a way, similar to the nonlinearities of the potential energy.

Then the perturbation theory is valid, and the classical trajectories are determined by Eq. (1.5) with slightly modified parameters  $Q_{0\alpha}, \omega_\alpha$  and  $\varphi_\alpha$ . The spectrum (1.6) in quantum treatment acquires small modifications:

$$\Delta E_{n_1, \dots, n_N} = \sum_{\alpha, \beta} x_{\alpha, \beta} \left( n_\alpha + \frac{1}{2} \right) \left( n_\beta + \frac{1}{2} \right), \quad (1.9)$$

where  $x_{\alpha, \beta}$  are parameters of anharmonicity,  $|x_{\alpha, \beta}| \ll |\omega_\alpha - \omega_\beta|$ . This correction term is calculated within perturbation theory with energy  $E$  (1.6) and wavefunction  $\Psi$  (1.7) as zero-order approximation. Corrections to  $\Psi$  can be found with perturbation theory as well.

(2) In the second case the inequality (1.8) does not hold, and in the limit of strong nonlinearity the opposite condition is satisfied:

$$|\delta\omega_\alpha| \gg \min_\beta |\omega_\alpha - \omega_\beta|. \quad (1.10)$$

Under condition (1.10) the conventional perturbation technique is unapplicable. In this case the classical trajectories differ radically from the curves (1.5), – the beat effect occurs, – and so do the quantum eigenfunctions, as compared to harmonic functions (1.7). In the limiting case (1.10) the latter are nearly orthogonal.

The inequality (1.10) specifies the physical phenomena, where the anharmonicity must be taken into account from the start in zero order approximation. Such a situation is realized in stretching vibrations of molecules with equivalent valence bonds, as  $H_2O$ ,  $CH_4$ ,  $C_6H_6$  and in many other substances. All these molecules possess highly anharmonic  $CH$  and  $OH$  bonds (anharmonic constants  $x_{\alpha, \beta}$  of order of  $100 \text{ cm}^{-1}$ ). The latter secures the validity of inequality (1.10) for highly excited vibrational overtones.

Let us illustrate the two cases (1.8) and (1.10), stated above, with the help of a simple analytic consideration of the model of two coupled harmonic oscillators. The Hamiltonian of the system is:

$$H = \frac{1}{2} (p_1^2 + \omega_1^2 q_1^2) + \frac{1}{2} (p_2^2 + \omega_2^2 q_2^2) + 2\beta^2 q_1 q_2, \quad \omega_1 > \omega_2, \quad (1.11)$$

where  $\beta^2$  is the interaction strength of the two modes.

The orthogonal transition matrix from normal coordinates  $Q_s$ ,  $Q_a$  to  $q_1$ ,  $q_2$  is:

$$\begin{pmatrix} q_1 \\ q_2 \end{pmatrix} = \begin{pmatrix} \frac{\sqrt{\Omega_1^2 - \omega_2^2}}{\sqrt{2\Omega_1^2 - \omega_1^2 - \omega_2^2}} & -\frac{\sqrt{\omega_2^2 - \Omega_2^2}}{\sqrt{\omega_1^2 + \omega_2^2 - 2\Omega_2^2}} \\ \frac{\sqrt{\Omega_1^2 - \omega_1^2}}{\sqrt{2\Omega_1^2 - \omega_1^2 - \omega_2^2}} & \frac{\sqrt{\omega_1^2 - \Omega_1^2}}{\sqrt{\omega_1^2 + \omega_2^2 - 2\Omega_2^2}} \end{pmatrix} \begin{pmatrix} Q_s \\ Q_a \end{pmatrix}. \quad (1.12)$$

The eigenfrequencies  $\Omega_1$  and  $\Omega_2$  are determined by secular equations:

$$\Omega_{1,2}^2 = \frac{1}{2} \left[ (\omega_1^2 + \omega_2^2) \pm \sqrt{(\omega_1^2 - \omega_2^2)^2 + 4\beta^4} \right]. \quad (1.13)$$

In the case of different frequencies  $\omega_1, \omega_2$  and sufficiently weak coupling constant  $\beta$ , the inequality (1.8) reduces to the following condition:

$$\frac{\beta^2}{\omega_1^2 - \omega_2^2} \ll 1. \quad (1.14)$$

With the account of (1.14) the transformation (1.12) and Eq. (1.13) gives:

$$\begin{aligned} \Omega_1^2 &= \omega_1^2 + \frac{\beta^4}{\omega_1^2 - \omega_2^2}, & \Omega_2^2 &= \omega_2^2 - \frac{\beta^4}{\omega_1^2 - \omega_2^2}, \\ q_1 &= Q_s - \frac{\beta^2}{\omega_1^2 - \omega_2^2} Q_a, & q_2 &= \frac{\beta^2}{\omega_1^2 - \omega_2^2} Q_s + Q_a, \\ Q_s &= A_s \sin(\Omega_1 t + \varphi_s), & P_s &= \Omega_1 A_s \cos(\Omega_1 t + \varphi_s), \\ Q_a &= A_a \sin(\Omega_2 t + \varphi_a), & P_a &= \Omega_2 A_a \cos(\Omega_2 t + \varphi_a). \end{aligned} \quad (1.15)$$

It can be seen from Eq. (1.15) that the account of interaction  $2\beta^2 q_1 q_2$  introduces only small changes in the evolution. By small modifications of evolution in the harmonic approximation we mean the identity of the functional dependence of position on time  $q_1, q_2 \longleftrightarrow Q_s, Q_a$  with minor changes of the frequency  $\omega_1 \approx \Omega_1$ ,  $\omega_2 \approx \Omega_2$ , of the amplitude  $A_s, A_a$ , and of the initial phase,  $\varphi_s, \varphi_a$ . In the general case in addition to the abovementioned harmonic term a bounded contribution ( $0 < t < \infty$ ) is added, which goes to zero with vanishing interaction. In other words, under (1.14) or (1.8) the interacting system closely resembles nearly the same pair of the initial noninteracting oscillators.

The qualitative similarity of the trajectories in configuration space can be clearly seen from the comparison of Lissajou curves of interacting and non-interacting oscillators.

It is well known that the Lissajou curves for incommensurate frequencies  $\omega_1, \omega_2$  or  $\Omega_1, \Omega_2$  fill densely some rectangle in position space. The sides of this rectangle are parallel to the axes of normal coordinates, the center coincides with the origin, while the lengths of the sides are twice the oscillation amplitudes  $A_s, A_a$  along reciprocal axes. According to (1.15), the coordinate transformation  $(q_1, q_2) \longleftrightarrow (Q_s, Q_a)$  is nearly unit. Thus  $A_s \approx A_1$ ,  $A_a \approx A_2$ , and the angle of the rotation of the axis is small:  $|\alpha| \sim \frac{\beta^2}{\omega_1^2 - \omega_2^2} \ll 1$ . It means that for similar initial conditions the Lissajou curves in both cases fill in two similar rectangles, rotated slightly one with respect to the other (Fig. 1.1). In the case of commensurate frequencies  $(\omega_1, \omega_2)$  and/or  $(\Omega_1, \Omega_2)$

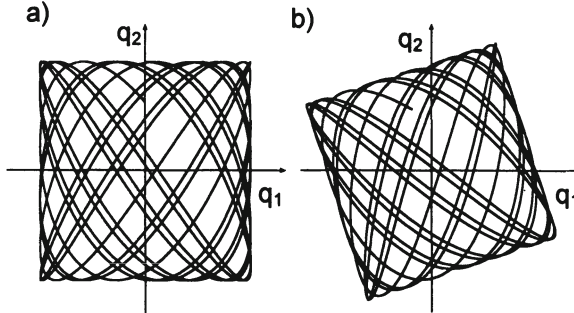


Figure 1.1: Lissajou curves of two harmonic oscillators a) without interaction (rectangle, parallel to the axes), and b) with weak interaction (rectangle, rotated slightly with respect to the origin).

the Lissajou curves change qualitatively, as the type of resonance changes. Three different cases are possible:

1) The frequencies  $(\omega_1, \omega_2)$  of noninteracting oscillators are incommensurate, while the perturbed frequencies  $(\Omega_1, \Omega_2)$  are commensurate. The Lissajou curve changes shape from the one filling densely some region of phase space to a closed algebraic curve.

2) The unperturbed frequencies are commensurate, while the frequencies of interacting oscillators are incommensurate – case opposite to 1).

3) Commensurate are both perturbed and unperturbed frequencies. Then the interaction changes the order of the resonance, and it does it in a pronounced way, as the reciprocal changes of the frequencies are small. For example,  $\omega_1 = \omega_2$  might change into  $21\Omega_1 = 23\Omega_2$ . In such a case the Lissajou curve changes its algebraic order significantly.

Obviously, in all these three cases the topology of the trajectories in configuration space is changed. Nevertheless, in the metrical sense these two trajectories are close to each other with the separating distance  $\sim \beta^2 (\omega_1^2 - \omega_2^2)^{-1}$  vanishing with the interaction strength.

The incommensurability of the frequencies  $(\omega_1, \omega_2)$  takes place with probability equal to unit, in contrast to the commensurate case with measure zero. Thus the close similarity of the harmonic oscillations is nearly always accompanied with the incommensurate nature of the evolution of the trajectory that fills up some region of phase space. In the cases 1)–3) the topology of Lissajou curves changes drastically, but in the metrical sense they remain close.

The qualitative similarity and small quantitative differences in the evolution of non-interacting and interacting pairs of oscillators can be seen most transparently by comparison of corresponding phase trajectories. If the fre-

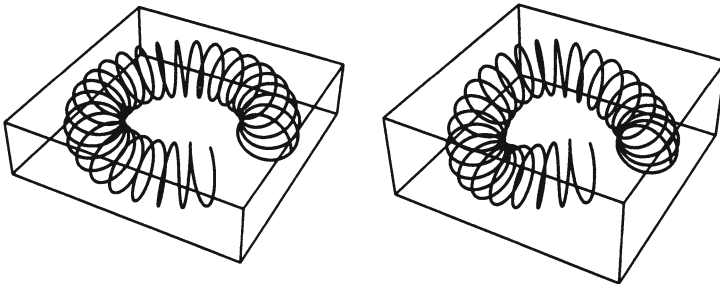


Figure 1.2: Phase curves of two harmonic oscillators with zero (a) and weak (b) interaction.

quencies  $\omega_1, \omega_2$  are incommensurate, the phase curves wind up uniformly and densely on a two - dimensional torus, embedded in a four - dimensional phase space [7]. Under condition (1.14) the interaction deforms this torus with the phase trajectory, wound up on it (Fig. 1.2) slightly. In fact, a more stringent statement is valid: an *arbitrary*, but weak enough interaction leads to only small deformations of the torus and the trajectory, if the frequencies  $\omega_1, \omega_2$  are incommensurate. The volume of the phase space, where this statement is violated, goes to zero with vanishing interaction strength  $\beta^2$ . The general idea of the proof of this important theorem on stability has been put forward by A.N.Kolmogorov in 1954 [8] for a weak nonlinearity with interaction Hamiltonian of arbitrary functional form  $\beta^2 V(q_1, q_2)$ . The rigorous proof of this theorem has been presented in the review paper by V.I.Arnold [9, 10]. The theory of stability of Hamilton systems is termed KAM, which is an abbreviation of the names of mathematicians Kolmogorov, Arnold, and Mozer, who made a decisive contribution to its formation. According to the principle of correspondence, this theorem remains valid for calculations of *quantum* vibrational spectra of polyatomic molecules. That provides an ideological justification to traditional calculations of nonlinear corrections to the energies of vibrational spectra of molecules [5, 11].

The considered system of two oscillators under conditions (1.14) corresponds to a couple of weakly interacting Local Modes (LM). Really, according to (1.15), the excitation of a normal oscillation  $Q_s$  influences presumably the coordinate  $q_1$  oscillation only, and, correspondingly,  $Q_a$  - vibrations influence presumably coordinate  $q_2$ . The energy of  $Q_s$  - vibrations is nearly completely localized on  $q_1$  - oscillators, while  $Q_a$  - vibrations – on  $q_2$  - oscillators. In other words, for a large difference between frequencies  $\omega_1$  and  $\omega_2$  (Eq.(1.14) satisfied) the pair of oscillators (1.11) constitutes weakly coupled local modes  $Q_s$  and  $Q_a$ . These LM change slightly under the influence

of inter-mode interaction ( $q_1 \sim Q_s$  and  $q_2 \sim Q_a$ ) <sup>2</sup>. In the language of quantum mechanics it means, that the eigenfunctions depend weakly on perturbations.

An opposite situation occurs in the so-called resonant case, when the frequencies are degenerate,  $\omega_1 \sim \omega_2$ , so that Eq. (1.14) is violated,  $|\omega_1^2 - \omega_2^2| \gtrsim \beta^2$ . In such a case even a small perturbation, as compared to the energy of the system, causes dramatic changes of the phase curves in the classical approach and of the eigenfunctions in the quantum consideration. As noted earlier, this is exactly the case for vibrations of polyatomic molecules with equivalent valence bonds, like  $CH_4$ ,  $C_2H_6$ ,  $H_2O$ , and so on. Due to the inapplicability of Kolmogorov theorem on stability, each problem in the resonant case should be considered separately. We will investigate here the system with Hamiltonian (1.11).

In the resonant case the formulae (1.12), (1.13) for the frequencies  $\Omega_1, \Omega_2$  and the orthogonal transformations  $(q_1, q_2) \longleftrightarrow (Q_s, Q_a)$  change to:

$$\Omega_1^2 = \omega^2 + \beta^2 + \frac{1}{2} \frac{\Delta^4}{\beta^2}, \quad \Omega_2^2 = \omega^2 - \beta^2 - \frac{1}{2} \frac{\Delta^4}{\beta^2},$$

$$\begin{pmatrix} q_1 \\ q_2 \end{pmatrix} = \frac{1}{\sqrt{2}} \begin{pmatrix} 1 + \frac{\Delta^2}{2\beta^2} & -1 + \frac{\Delta^2}{2\beta^2} \\ 1 - \frac{\Delta^2}{2\beta^2} & 1 + \frac{\Delta^2}{2\beta^2} \end{pmatrix} \begin{pmatrix} Q_s \\ Q_a \end{pmatrix}, \quad (1.16)$$

where  $2\omega^2 = \omega_1^2 + \omega_2^2$ , and  $2\Delta^2 = \omega_1^2 - \omega_2^2$ , ( $\omega_1^2 > \omega_2^2$ ).

Equation (1.16) is valid, provided the resonance condition is fulfilled:

$$\frac{\Delta^2}{\beta^2} = \frac{\omega_1^2 - \omega_2^2}{2\beta^2} \ll 1. \quad (1.17)$$

It can be seen easily from Eq. (1.16), that vibration  $Q_s$  causes nearly identical vibrations of coordinates  $q_1$  and  $q_2$ , while  $Q_a$  gives rise to vibrations of  $q_1$  and  $q_2$  in opposite phases. In contrast to the previously considered case of weakly coupled harmonic oscillators with incommensurate eigenfrequencies, here the vibrations  $Q_s$  and  $Q_a$  are the symmetrized and antisymmetrized delocalized normal modes. Consequently, in the present case the small changes of the original frequencies  $\frac{\beta^2}{\omega^2} \ll 1$  lead to drastic changes of original local modes  $q_1$  and  $q_2$  into delocalized normal modes  $Q_s$  and  $Q_a$ . Clearly, such a transition can not be obtained by perturbation theory.

The qualitative changes, mentioned above, can be made transparent with the help of the picture of phase curves. In the cases of interacting and non-interacting modes  $q_1$  and  $q_2$ , the curves differ drastically. The trajectories

---

<sup>2</sup>In the case of nonlinear interaction the survival or destruction of a local mode depends on its excitation energy. For example, if the excitation energy is greater than the energy of dissociation, the valence bond simply breaks apart.

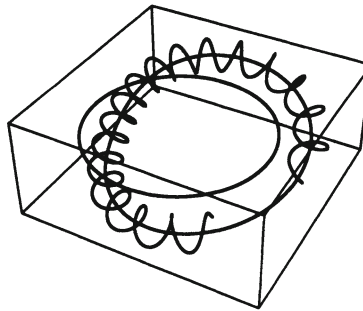


Figure 1.3: The phase curve of interacting oscillators in the vicinity of a stable resonance orbit, and the axis line of the unperturbed resonance torus.

of the interacting oscillators wind up on a torus, which has the closed orbit of the resonance torus of noninteracting oscillators as its axis line (Fig. 1.3).

It is important to note, that in a system of two weakly coupled harmonic oscillators with nearly identical eigenfrequencies  $\omega_1 \sim \omega_2$  only delocalized vibrations exist. Really, mean-square values over time  $\overline{q_1^2}$  and  $\overline{q_2^2}$  are equal one to another due to Eq. (1.16) and to practical incommensurability of the frequencies  $\Omega_1$  and  $\Omega_2$ <sup>3</sup>:

$$\overline{q_1^2} \approx \frac{1}{2} \overline{(Q_s + Q_a)^2} = \frac{1}{2} \left( \overline{Q_s^2} + \overline{Q_a^2} \right),$$

$$\overline{q_2^2} \approx \frac{1}{2} \overline{(Q_s - Q_a)^2} = \frac{1}{2} \left( \overline{Q_s^2} + \overline{Q_a^2} \right).$$

It means, that the vibrational energy is spread uniformly between the modes  $q_1$  and  $q_2$ , i.e. any vibration in the system is delocalized.

In summary, with the example of two weakly coupled harmonic oscillators we find that two drastically different vibrational regimes exist: In the case of significantly different eigenfrequencies  $|\omega_1^2 - \omega_2^2| \gg \beta^2$  these vibrations constitute local modes, which are weakly dependent on the interaction strength. Valence vibrations in molecule  $HDO$  can serve an example. On the other side, for nearly identical frequencies  $|\omega_1^2 - \omega_2^2| \ll \beta^2$  the vibrational modes  $Q_s(t)$  and  $Q_a(t)$  are delocalized. In this case the delocalized or Normal Modes (NM) differ most from the original LMs  $q_1$  and  $q_2$ . An example of it is provided by valence vibrations with small amplitude in molecule  $H_2O$  (vibrational levels with  $v_1 + v_2 = 0, 1, 2$ ).

In 1969 A.A.Ovchinnikov has shown that local vibrations are possible in the case of degenerate frequencies as well, provided the anharmonicity is

---

<sup>3</sup>The frequencies  $\Omega_1$  and  $\Omega_2$  can be in very high-order resonance only,  $m_1\Omega_1 + m_2\Omega_2 = 0$ ,  $|m_i| \gg 1$ .

strong enough and excitation level is high enough [12]. The physical origin of energy localization on one oscillator we will make clear with the use of the example of two weakly coupled anharmonic oscillators:

$$\begin{aligned} H = & \frac{1}{2}p_1^2 + \frac{1}{2}\omega^2q_1^2 + aq_1^3 + \dots \\ & + \frac{1}{2}p_2^2 + \frac{1}{2}\omega^2q_2^2 + aq_2^3 + \dots + 2\beta^2q_1q_2. \end{aligned} \quad (1.18)$$

Assume that initially ( $t = 0$ ) the first oscillator is excited while the second is not. If the amplitude of its vibration is small, the corresponding nonlinear terms in Eq. (1.18) can be neglected, and the system reduces to two harmonic oscillators with equal eigenfrequencies,  $\omega_1 = \omega_2 = \omega$ . As shown above, in this case the vibrations are delocalized and the energy is distributed uniformly between the two oscillators. On the contrary, if the amplitude of vibrational excitation is sufficiently large, the nonlinear terms in  $q_1$  in Eq. (1.18) become important. The latter change the frequencies of the first oscillator  $|\omega_1^2(A_1) - \omega_2^2| = |\omega_1^2(A_1) - \omega^2| \gg \beta^2$ . As a result we actually obtain a system of two oscillators with different frequencies and weak coupling. Then the vibrational modes will be local ones, according to previous considerations, as the energy transfer from the first oscillator to the second is impossible due to absence of resonance. This statement is rigorous as it is based on Kolmogorov theorem on stability. Given the oscillator frequencies  $\omega_1(A_1) \neq \omega_2 = \omega$  are different, the interaction  $\beta^2q_1q_2$  does not change the phase trajectories qualitatively, but introduces small quantitative corrections only. High excitation of the first oscillator and low excitation of the second one will therefore be preserved infinitely. Thus in systems with Hamiltonian (1.18) at high excitation of one of the oscillators a local vibration takes place.

Only some part of all the localized vibrations obtain the property of infinite stability in time. According to Kolmogorov's theorem, these local modes occupy a fraction of the phase space of nonzero measure. Nevertheless, all LMs are long-living with decay time  $\tau \gg \beta^{-1}$ , where  $\beta^{-1}$  is the classical beat period. The destruction of local modes in a system with Hamiltonian (1.18) occurs due to interaction of LMs via high-order resonances. The high-order nature of the destruction mechanism is the reason for the long life of the excitation.

In the quantum approach the energy of a LM is always localized on one of the oscillators. However, it goes over from one oscillator to another with the time period  $\tau = \hbar\varepsilon^{-1}$ , where  $\varepsilon$  is the energy splitting of symmetric and antisymmetric states with same excitation number  $v_1 = v_2 = v$ . Due to the non-equidistant nature of energy levels of an anharmonic oscillator, the splitting  $\varepsilon$  is typically smaller for higher excitation number:

$$E_n - E_{n-1} \neq E_1 - E_0. \quad (1.19)$$

Consequently one vibrational quantum can not pass from one oscillator to the other – due to the absence of resonance in such transfer,– but instead all the  $n$  quanta should go over at once. This last process is possible in high orders in small anharmonicity constants  $\sim (x_e/\omega)^n$  and in small inter-mode interaction  $\sim (\beta/x_e)^n$ . The very low probability of it leads to a pretty low transfer rate and long lifetime of the vibrational excitation on one oscillator.

An analogous situation takes place in a system of arbitrary number of weakly interacting identical anharmonic oscillators (Ovchinnikov 1969, 1972 [12, 13]). That provides a theoretical proof of the existence of long-living LMs in molecules with equivalent valent bonds ( $H_2O, CH_4, C_6H_6$ , etc.) and in simple molecular crystals ( $H_2, N_2, NO, CO$ , etc.). An estimate of the decay time of one intramolecular vibration into intermolecular vibrations (phonons) in  $N_2$  - crystal has been obtained in [12] :  $\tau \sim 1s$ . Later this estimate has been confirmed experimentally [14].

The advance of laser technology made possible the observation of high vibrational overtones. Numerous experiments have been performed on a wide range of molecules, having multiple  $CH$  bonds (Henry, [15]). The existence of long-living local modes in highly-excited  $CH$  valent-bond vibrational overtones has been proved unambiguously.

In summary, a weakly excited vibration of one valent bond in a molecule, containing multiple equivalent bonds, is a superposition of delocalized normal modes. A highly excited valent vibration, on the contrary, forms a long-living local mode. In the corresponding region of phase space the system forms a set of weakly interacting LMs. Each valent bond is a local mode. In a quantum treatment of LMs, the eigenfunctions of overtone  $v$  form a superposition of the type:

$$|\Psi_{LM}\rangle = C_1 |v, 0, 0, \dots\rangle + C_2 |0, v, 0, 0, \dots\rangle + C_3 |0, 0, v, 0, \dots\rangle + \dots \quad (1.20)$$

The linear manifold built on these functions can be considered as a band of vibrational excitons of  $v$ -levels.

The change of the evolution of vibrational excitations in passing from normal modes to local modes can be seen clearly with the help of Lissajou curves. These are shown on Fig.1.4 for a system of two weakly coupled anharmonic oscillators. In the normal-mode region Fig.1.4 (b) the Lissajou curves are symmetric with respect to the interchange  $q_1 \longleftrightarrow q_2$ . In the case of local modes Fig.1.4 (a) there are two curves, which change one into the other for  $q_1 \longleftrightarrow q_2$ .

We note that NM and LM can coexist in one and the same high order vibrational overtone (Fig.1.4). If the excitation energy is spread uniformly over valent bonds, the case of normal modes is realized ( $\omega_1(E_1) = \omega_2(E_2)$ )

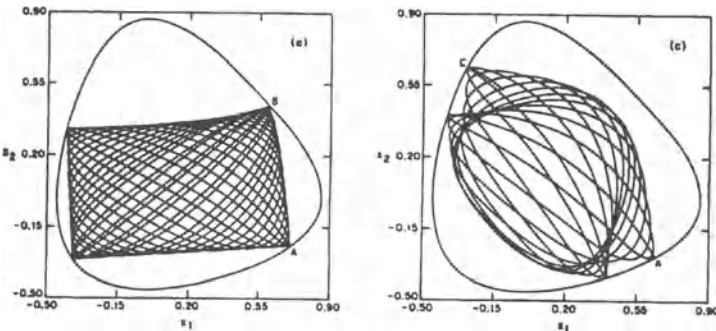


Figure 1.4: Trajectories, illustrating the vibrational motion of coupled non-linear oscillators: a) local mode and b) symmetrical normal mode. The energy of oscillators equals one third of the dissociation energy in all cases,  $E = D/3$ . From [16].

for  $E_1 = E_2$ ). On the contrary, if the excitation energy is distributed in a considerably non-uniform way, local-mode vibrations take place ( $\omega_1(E_1) \neq \omega_2(E_2)$  for  $E_1 > E_2$ ).

Progress in laser technique made possible lately the experimental investigations of high-order vibrational overtones ( $\nu \sim 10$ ) with high definition ( $\Delta\nu \sim 10^{-3} \text{cm}^{-1}$ ). In turn, the progress in the experimental studies urged the necessity to develop methods of calculation of vibrational-rotational spectra with high precision. Modern supercomputers and computational methods provide the necessary tools for it (see, e.g. [17]). On the other hand, to relate the qualitative and quantitative characteristics of the spectrum to the parameters of the inter-nuclear potential, one needs a simple, intuitively transparent physical picture of nuclear motion. The skill and ability to reconstruct the potential surface from the vibronic spectrum of the molecule and vice versa, obviously plays an important role in laser chemistry in synthesis of molecules with predetermined characteristics. The problem, mentioned above, can in principle be solved with quasiclassical methods of quantum mechanics.

Quasiclassical methods are applicable to a wide range of problems of interest to laser chemistry, including molecular dynamics and interpretation of vibrational-rotational spectra [18, 19, 20, 21]. Many processes of this kind involve excited molecules with high vibrational and rotational quantum numbers, for example LMs exist in high vibrational overtones.

In the quantum approach a localized long-living state is formed, when the transfer integrals to other analogous states (e.g. to another  $CH$  bond in  $CH_4$  molecule) are anomalously small. In the classical approach it corresponds

to several phase trajectories (one for each equivalent valent bond), that are transformed one into another by symmetry group transformations of the molecule, but, however, which are situated in distant regions of phase space. This correspondence of quantum and classical pictures provides a tool and a qualitative interpretation for the study of the area of localization of wavefunctions, makes possible the selection of local modes from normal ones, and enables the calculation of the LM energy spectrum with the help of Bohr-Sommerfeld quantization. Calculations of positions and widths of rotational levels with large momenta  $J$ , performed for molecules of type  $XY_2$  and  $XY_6$ , provide good agreement with exact results [18].

The existence of LMs and their decisive role in the formation of the vibrational spectrum in the region of energy, corresponding to classical stochasticization, have been discovered in  $H_3^+$  and  $O_3$  [22, 23, 24]. Localization in stochasticization region has been termed quantum localization [20]. The corresponding wavefunctions are localized either forever or for very long periods of time in the neighborhood of stable or nearly stable periodic orbits. The methods of calculation and observation in photodissociation spectra of these periodic orbits, and the computation of corresponding wavefunctions can be found in [25, 26, 27]. In the cited papers it has been shown besides, that local states (quasilevels) above the dissociation threshold in polyatomic molecules are possible.

It is easy to find the general feature of LM vibrational spectra, on the basis of the quasiclassical approach: the clusterization of levels that grows with the increase of the excitation energy. It is due to the reduction of the tunnel integral along the complex path that connects classical orbits. The distance between the latter grows with the increase of LM vibrational energy.

The concept of a LM permits one to describe in a natural way the structure of the vibrational spectrum of polyatomic molecules for high-order overtones [6]. It results in a smaller number of adjustable parameters, which is the consequence of the emergence of algebraic dependences between the anharmonicity constants  $x_{\alpha\beta}$  in Eq. (1.9). The particular form of these dependences is governed by the point group symmetry that transforms the equivalent bonds one into another.

Theoretical and experimental investigations of overtones in  $CH$  and  $OH$  vibrations within the concept of LMs are provided in [28, 29, 30, 31]. In Ref. [28] within the model of weakly coupled anharmonic oscillators Henry et.al. studied theoretically and experimentally the position and intensity of absorption lines in the IR spectrum of propane  $CH_3 - CH_2 - CH_3$ . Good agreement between theoretical and experimental results has been obtained. In [29, 30] the spectra of IR overtones of naphthalene and water  $H_2O$  have been calculated and interpreted. In Ref. [31] the interrelation between the models of local- and normal- modes in molecules  $XH_4$  and  $XH_3$  has been studied theoretically, and correspondence between the reciprocal parameters

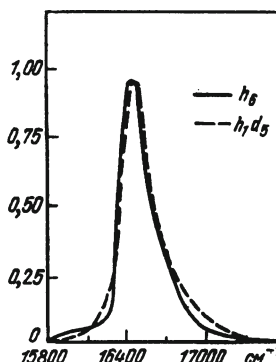


Figure 1.5: The absorption spectra of benzene  $C_6H_6$  and deuterated benzene  $C_6HD_5$  for the overtone  $\nu = 6$ , from [32].

has been obtained. The method, developed in [31], can be generalized to treat molecules with numerous equivalent bonds.

It turns out, that the position and shape of clusters of vibrational overtones for  $CH$  vibrations in IR spectrum of benzene  $C_6H_6$  does not depend on the degree of deuteration (Fig.1.5). The same is true for other molecules with several  $CH$  bonds [32]. These facts support the concept of LM as well.

The quasiclassical treatment of nuclear motion provides the possibility to relate the structure of the phase space to the structure of the rotational-vibrational spectrum. A forecast of dramatic reconstruction of the spectrum when the classical constants of motion pass through particular values and thus provoke radical changes of phase curves, is made possible [19]. An example of it is provided by the change in the nature of rotation of a rigid molecule (asymmetric top), when the precession axis of the momentum  $J$  changes orientation with respect to intramolecular coordinate basis. It happens, when the molecule momentum nearly coincides with the intramolecular unstable rotation axis, say  $y$  ( $I_x < I_y < I_z$ ). Then the rotation axis can be changed from one stable orientation (say,  $x$ ) to another ( $z$ ). Clearly, the rotational spectrum becomes more dense, as close to the separatrix lines the frequencies are small, and the level density correspondingly is high.

The number and variety of such effects is greatly enhanced with the introduction of semi-rigid molecules [18]. In this case the equipotential surface  $E(J) = const$  is no longer an ellipsoid, but some algebraic surface of a higher order. This surface can have many hills and hollows whose number can change depending on energy and total momentum of the molecule. At the moment when the number of hills or hollows changes, the shape of trajectories, depicted by the end of the vector  $J$  ( $|J| = const$ ) on the sur-

face  $E = \text{const}$  changes discontinuously. Correspondingly, the rotational spectrum changes discontinuously as well. Discontinuous transitions are a consequence of quasiclassical approach and are valid for high rotational momenta  $J \gg 1$  [18].

It is well known, that the rotational spectrum of a top at large values of momentum  $J$  form clusters of two levels each. Really, on the energy ellipsoid there are always pairs of trajectories that go over one into the other with the interchange  $\mathbf{J} \longleftrightarrow -\mathbf{J}$ . For  $J \gg 1$  in the vicinity of poles the trajectories are separated far apart, and the tunnelling integral between them is pretty small, which leads to anomalously small splitting of energy levels. The trajectories close to the equator, on the contrary, are overlapping considerably, and their levels do not form a cluster.

The presented scheme of analysis of the quasiclassical rotation spectrum implies, that the molecule is in a nondegenerate vibrational state, or that the tunnelling integral into another degenerate state is anomalously small:  $\Delta E_{\text{rot}}/\hbar \gg \Omega_{\text{vib}} \exp(-\text{Im } \Delta S/\hbar)$ .

An interesting analysis of the characteristics of vibrational spectra at high excitation level in the presence of Fermi-resonances has been performed by Kellman et.al. [33, 34, 35]. They undertook the study of the structure of phase space in the spirit of the theory of catastrophes to explain the qualitative peculiarities of vibrational spectra. Molecules  $H_2CO$ , benzophenone and acetylene have been considered.

Another interesting effect, analogous to clusterization of LM vibrational overtones, is the clusterization of vibrational -rotational levels. In fact, this clusterization is even stronger, than in the previous case due to additional suppression of tunnelling of vibrational excitations between similar LMs. The origin of this suppression lies in the necessity to reorient the momentum vector  $\mathbf{J}$  with respect to intramolecular coordinate basis during the transition. The probability of such a somersault (flip-flop) of the rotor decreases exponentially with the increase of rotation speed. Consequently the clusterization of vibrational - rotational levels increases with the increase of momentum  $J$ . This effect has been studied systematically in [36, 37, 38] for molecules with symmetry  $C_{2v}, C_{3v}$  and  $T_d : XY_2, XY_3, XY_4$ . If equivalent valent bonds are lacking, no tunnelling occurs. In such case the problem of vibrational - rotational states is reduced to clusterization of purely rotational levels of the effective Hamiltonian  $H_v(\mathbf{J})$ , which depends parametrically on the vibrational quantum numbers  $v$ .

We conclude, that the nonlinearity (anharmonicity) of nuclear motion produces clusterization of vibrational - rotational levels for high excitation numbers:  $v \gg 1, J \gg 1$ . The diversity of clusters grows with the increase of the number of equivalent LMs: similar valence bonds, valence angles, and other repeated geometrical structures. The higher is the point symmetry of the molecule, the more varied are the clusters.

Clustered levels in the vibrational - rotational spectrum of a molecule

reveal the existence of long-living vibrational excitations in it. The localization of vibrational modes influences the intramolecular relaxation greatly. For example, a single-quantum excitation of a *CH* bond in benzene  $C_6H_6$  gets delocalized over *CH* bonds in  $\tau \sim 10^{-12}s$ , while the tenth overtone  $\nu = 10$  – over the period of time, at least an order of magnitude longer.

A correct interpretation of the IR spectra with the help of semi-empirical formulae for structural and spectral characteristics makes possible the determination of geometrical parameters of the molecule – bond lengths, angles' magnitudes, etc. [15, 39].

The content and the principal idea of the book can finally be summarized as follows: the study of the peculiar features of vibrational - rotational spectra of polyatomic molecules due to the anharmonicity of the adiabatic nuclear motion, and the effect of this nonlinearity upon the intramolecular vibrational relaxation.

## Chapter 2

# Classical theory of nonlinear vibrational systems; local modes

In this Chapter we review briefly the basics of nonlinear Hamilton systems with a finite number of degrees of freedom. The representation in the variables 'action-angle' is introduced for harmonic and Morse oscillators. The perturbation theory, based on the method of canonical transformation is provided for Hamiltonians in the variables action-angle. The method of canonical transformation is closely related to the method of averaging, which has a clear physical meaning. The problems in the perturbation approaches due to small denominators are described. The theorem of Kolmogorov - Arnold - Moser (KAM) on the stability of trajectories for integrable Hamilton systems under the action of small perturbations is formulated. The KAM theorem is applied to the study of vibrations in the system of nonlinear weakly interacting oscillators.

For a proper understanding of the presented material the knowledge of mathematical methods of classical mechanics is implied in the amount of a university course in analytical mechanics. An advanced background is provided, for example, by Ref. [7, 40, 41]. The reader with less adherence to generalized mathematical constructions can use, for example, a more physics-oriented book [42, 43].

### 2.1 Survey of classical mechanics; introduction to local modes

The analysis of motion of weakly interacting mechanical systems can be conveniently performed in the space "action – angle", especially when one is interested in the long time limit. To illustrate the general scheme we

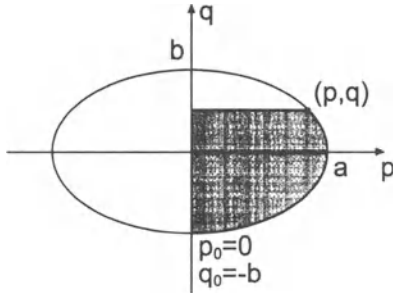


Figure 2.1: Phase trajectories of a harmonic oscillator.

will introduce the variables "action – angle" for the harmonic and Morse oscillators. Oscillator models of that kind are used widely in the study of molecular vibrations.

The Hamiltonian of a harmonic oscillator is:

$$H = \frac{p^2}{2m} + \frac{m\omega^2}{2}q^2, \quad (2.1)$$

where  $p$  and  $q$  are the momentum and position of the oscillator,  $m$  and  $\omega$  are the mass and oscillation frequency ( $m\omega^2 = k$  – the oscillator rigidity). The phase trajectories are determined by the equation  $H(p, q) = E$ , where  $E$  is the energy of the system. For the Hamiltonian Eq. (2.1) they form ellipses with the half-width parameters  $a = \sqrt{2mE}$ ,  $b = \sqrt{2E/m\omega^2}$ :

$$\frac{p^2}{a^2} + \frac{q^2}{b^2} = 1. \quad (2.2)$$

Action variable  $I(p, q)$  is determined by an integral along the phase trajectory Eq. (2.2):

$$I = \frac{1}{2\pi} \oint_{\gamma} pdq = \frac{\Pi}{2\pi} = \frac{E}{\omega}, \quad (2.3)$$

where  $\Pi$  is the area bounded by the phase trajectory (for an ellipsis  $\Pi = \pi ab$ ).

The angle variable  $\Phi$  is chosen in such a way, that the transformation  $(p, q) \rightarrow (I, \Phi)$  is canonical. For that purpose a generating function is introduced:

$$S(I, q) = \int_{p_0=0, q_0=-b}^q pdq, \quad (2.4)$$

where the integral is calculated along the phase trajectory Eq. (2.2) (this corresponds to the shaded area in Figure 2.1). With the help of the function

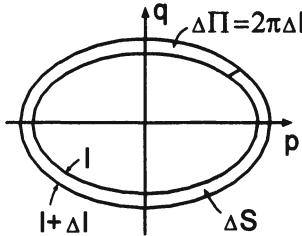


Figure 2.2: Geometrical definition of the angle variable  $\Phi$  as the proportion of the marked area to the area of the stripe between two close phase curves in the units  $2\pi$ .

$S(I, q)$  the canonical transformation  $(p, q) \rightarrow (I, \Phi)$  is determined by the following relations:

$$p = \frac{\partial S}{\partial q}, \quad \Phi = \frac{\partial S}{\partial I}. \quad (2.5)$$

Defining the momentum  $p$  with the help of Eqs. (2.1) and (2.3) via the variables  $(I, q)$ , and substituting  $p(I, q)$  in Eq. (2.4) and after that in Eq. (2.5), we obtain the expression of the angular variable:

$$\Phi = \frac{\partial}{\partial I} \int_{-b}^q \sqrt{2m \left( I\omega - \frac{m\omega^2}{2} \bar{q}^2 \right)} d\bar{q} = \arcsin \left( \sqrt{\frac{m\omega}{2I}} q \right) + \frac{\pi}{2}. \quad (2.6)$$

We note that  $S(q)$  and  $\Phi(q)$  are multi-valued functions of  $q$ . In the course of continuous evolution of  $q$  along the phase trajectory in the positive direction, the branches of the multi-valued function  $\Phi(q)$  should be chosen in such a way, that the change  $\Delta\Phi$  equals  $2\pi$  on return to the initial point. Obviously Eq. (2.5) makes it possible to satisfy this condition under the suitable choice of the branches of the function  $\arcsin x$ . Such a situation is maintained in the general case of one-dimensional finite motion as well.

From Eqs. (2.3) and (2.6) the following formulas of canonical transformation  $(p, q) \rightarrow (I, \Phi)$  are obtained:

$$\begin{aligned} I(p, q) &= \frac{p^2}{2m\omega} + \frac{m\omega^2}{2}q^2, \quad \Phi = \frac{\pi}{2} + \arcsin \left( \sqrt{\frac{m\omega}{2I}} q \right), \\ p &= \sqrt{2m\omega I} \sin \Phi, \quad q = -\sqrt{\frac{2I}{m\omega}} \cos \Phi, \quad H = \omega I. \end{aligned} \quad (2.7)$$

The variables  $(I, \Phi)$  can be easily interpreted in the following way: From Eqs. (2.3), (2.4) and (2.5) it can be easily seen that  $I\omega$  is the area bounded by the phase trajectory, while  $\Phi$  is the ratio of the marked stripe area in Figure

2.2 to the area of the entire stripe between two close phase trajectories, multiplied by  $2\pi$ , i.e.

$$I = \frac{\Pi}{2\pi}, \quad \Phi = 2\pi \frac{\Delta S}{\Delta \Pi} = \frac{\partial S}{\partial I}, \quad (2.8)$$

where  $\Delta \Pi$  is the area of the entire stripe, and  $\Delta S$  is the area of the marked stripe.

From the definition of the variables "action-angle" in the form of Eq. (2.8) the quantities  $(I, \Phi)$  are determined uniquely ( $\Phi$  – up to a constant) for any one-dimensional finite motion. With the account of Eq. (2.5) the transformation  $(p, q) \rightarrow (I, \Phi)$  becomes canonical. The latter means that  $(I, \Phi)$  satisfy Hamiltonian equations:

$$\begin{aligned} \dot{I} &= -\frac{\partial H}{\partial \Phi}, \quad \dot{\Phi} = \frac{\partial H}{\partial I}, \\ \dot{I} &= 0, \quad \dot{\Phi} = \omega \quad (\text{for oscillator Eq. (2.1)}). \end{aligned} \quad (2.9)$$

A detailed description of the variables "action - angle" can be found in textbooks on analytical mechanics, such as [7].

In the case of  $n$  non-interacting Hamilton systems with a single degree of freedom each, upon introduction of the variables  $(I_j, \Phi_j)$  according to Eqs. (2.3), (2.4), (2.8), we arrive at Eq. (2.9) for each degree of freedom. Moreover, in analytical mechanics the following theorem is proved: with  $n$  known independent integrals in involution<sup>1</sup>, in the case of finite motion the following variables  $(I_1, \dots, I_n, \Phi_1, \dots, \Phi_n)$  can be introduced in such a way, that the Hamiltonian of the system will depend upon the actions  $(I_1, \dots, I_n)$ , while the angular variables  $(\Phi_1, \dots, \Phi_n)$  will characterize the positions of the points, representing the state of the system on the  $n$ -dimensional torus  $T^n$ , the latter being determined by  $(I_1, \dots, I_n)$  (see, for example, Ref. [7]). Consequently, in this case the Hamilton equations and their solutions take the form:

$$\begin{aligned} \dot{I}_k &= -\frac{\partial H}{\partial \Phi_k} = 0, \quad \dot{\Phi}_k = \omega_k(I_1, \dots, I_n) = \frac{\partial H}{\partial I_k}, \\ I_k &= \text{const}, \quad \Phi_k = \omega_k t + \Phi_k(0). \end{aligned} \quad (2.10)$$

From Eq. (2.10) it follows that the phase trajectory  $\Phi(t)$  covers densely the  $n$ -dimensional torus in a spiral, if the frequencies  $\omega_k$  are out of resonance. The exact definition of resonance is the following: the frequencies  $\omega_k$  are termed to be in resonance of order  $K$ , if the following equation holds:

$$\sum_{k=1}^n m_k \omega_k = 0, \quad \sum_{k=1}^n |m_k| = K, \quad (2.11)$$

---

<sup>1</sup>They say, that functions  $F_1(p, q)$  and  $F_2(p, q)$  are in involution, if their Poisson brackets are equal to zero, i.e.  $\{F_1, F_2\} = \sum_k \left( \frac{\partial F_1}{\partial p_k} \frac{\partial F_2}{\partial q_k} - \frac{\partial F_1}{\partial q_k} \frac{\partial F_2}{\partial p_k} \right) = 0$ .



Figure 2.3: Phase trajectories on a two-dimensional torus in four-dimensional phase space.

where  $m_k$  are integers. If Eq. (2.11) does not hold for any  $K$ , the frequencies are termed incommensurate. In the particular case  $n = 2$  the trajectory covers the two-dimensional torus, embedded in the three-dimensional manifold of constant energy  $H(I) = E$ , Fig. 2.3. For the resonance  $\omega_1 = \omega_2$  the trajectory performs one rotation (revolution) along the meridian and one in latitude, returning to the starting point. The torus is split then into the one-parametric manifold of closed trajectories. Such a situation is realized in the motion of a particle in Coulomb potential. Thus, in the absence of resonance the phase trajectories cover densely the torus throughout. Such tori are called non-resonant. The motion, characterized by Eqs. (2.10) is termed conditionally-periodic. Hamiltonian systems, for which the solution reduces to Eq. (2.10), are called completely integrable. The evolution of such systems can be studied comprehensively in the entire time interval  $0 < t < \infty$ . In reality the mechanical systems, and the vibrations of polyatomic molecules in particular are not completely integrable, and their motion can not be described by Eq. (2.10). However, in the studies of molecular vibrations some small parameter  $\epsilon$  (weak anharmonicity, weak interaction between different modes, etc.) often appears. It allows the following representation of the Hamiltonian:

$$H = H_0 + H_{int}, \quad H_{int} = \epsilon V,$$

where  $H_0$  is the Hamiltonian of a completely integrable system with the equations of motion (2.10).

A question arises how do the phase trajectories of the Hamiltonian change under a small perturbation  $\epsilon V$ . The principal answer to this question has been found by A. N. Kolmogorov [8]: If the perturbation is weak enough, the majority of non-resonant tori of a nondegenerate system<sup>2</sup>, which are wound around by phase trajectories (Fig. 2.3), do not disappear. They

---

<sup>2</sup>A completely integrable system  $H_0(I_1, \dots, I_n)$  is termed nondegenerate, if its frequencies  $\omega_j$  as functions of  $I_1, \dots, I_n$  are independent, i.e.  $\det \left| \frac{\partial \omega_j}{\partial I_k} \right| \neq 0$ , and by small modifications of  $I_1, \dots, I_n$  these frequencies can always be made nonresonant.

are only deformed a little, remaining wound densely around by perturbed trajectories. The volume of phase space, occupied by destroyed tori tends to zero with  $\varepsilon \rightarrow 0$ . In other words, the majority of phase trajectories of the perturbed system remain being the winding of tori, the latter evolving from unperturbed tori under slight deformations. Phase trajectories, for which this assertion is not true, occupy a small volume, which tends to zero along with  $\varepsilon$ . Thus the conditionally-periodic character of motion of completely integrable systems is preserved under small perturbation. The rigorous description of this problem can be found in monographs [40, 41].

On the basis of this theorem, an interesting physical result on localization of all phase trajectories of two weakly interacting nonlinear oscillators can be obtained. Really, let us consider a Hamiltonian of the type:

$$H = H_1(I_1) + H_2(I_2) + \varepsilon V(I_1, I_2, \Phi_1, \Phi_2),$$

and let the variables  $(I_1, I_2)$  belong to the region of phase space, where the condition of nondegeneracy of  $H_1$  and of  $H_2$  holds.

The phase trajectories of the unperturbed system belong to the three-dimensional manifold  $H_1 + H_2 = E$ , which in turn is composed of two-dimensional tori  $T(E, I_1)$ , as shown in Fig. 2.3. According to the stated theorem, the non-resonant tori (which form the majority of all) get deformed slightly under the perturbation, along with the phase trajectories, wound on them. Any resonant torus in three-dimensional space can be squeezed between two non-resonant non-breaking-up tori, which separate a small volume between them, vanishing with  $\varepsilon$ . Thus, any phase trajectory of the perturbed system either belongs to a slightly deformed nonresonant torus, or is squeezed in a small volume between two tori of that kind, with that volume vanishing with  $\varepsilon$ . In particular, if the following inequality  $H_1(I_1) = E_1 \gg E_2 = H_2(I_2)$  holds on a nonperturbed trajectory, the same will be true on the perturbed one as well.

Defining a Local Mode (LM) as such a motion, in which the energy is localized presumably within one degree of freedom (mode), we arrive at the conclusion that in the system of two weakly interacting nonlinear oscillators the local vibrations are possible, when  $E_1 \gg E_2$  along the whole trajectory. For that the condition  $|\omega_1(E_1) - \omega_2(E_2)| \gg \varepsilon\omega(\bar{E})$  is required. The consideration above, however, does not apply to the case  $n > 2$ , as the  $n$ -dimensional tori do not separate the  $(2n - 1)$ -dimensional manifold of the energy surface into two non-connected parts, and thus the tori are not enclosed one into another, as it was in the case  $n = 2$ , Fig. 2.3. As a consequence, the trajectories from the destroyed tori can not be squeezed in a small volume between two deformed tori, and thus the trajectory leaves the vicinity of the initial unperturbed torus. Such motion is called Arnold diffusion.

Another important condition for the existence of LM at  $n = 2$  is the requirement of nondegeneracy  $\frac{\partial^2 H_0}{\partial I_a^2} \neq 0$ . As an example of a degenerate sys-

tem we consider two weakly bound harmonic oscillators with a Hamiltonian of the type:

$$\begin{aligned} H &= \frac{1}{2} \sum_{k=1}^2 (p_k^2 + \omega^2 q_k^2) + \beta \omega q_1 q_2 \\ &= \omega (I_1 + I_2) + 2\beta \sqrt{I_1 I_2} \cos \Phi_1 \cos \Phi_2. \end{aligned} \quad (2.12)$$

The system Eq. (2.12) is degenerate for  $\beta = 0$ , as in this case  $H = \omega(I_1 + I_2)$ , and the frequencies  $\omega_k = \omega$  do not depend upon the action variables  $I_k$ . All the unperturbed tori happen to be resonant  $\omega_1 = \omega_2 = \omega$ , and the requirements of the theorem are not satisfied. This leads to the fact, that the proof of LM existence for  $n = 2$ , mentioned above, is not valid. Really, as it is well known, in the system of two weakly bound harmonic oscillators Eq. (2.12) the beat effect occurs, that is the energy goes over from one oscillator to the other practically completely if  $\beta \ll \omega$ . Next we provide a rather instructive calculation, which proves the existence of beat effect.

The equations of motion for the Hamiltonian Eq. (2.12) have the form:

$$\begin{aligned} \dot{p}_1 &= -\omega^2 q_1 - \beta \omega q_2, & \dot{q}_1 &= p_1, \\ \dot{p}_2 &= -\omega^2 q_2 - \beta \omega q_1, & \dot{q}_2 &= p_2. \end{aligned} \quad (2.13)$$

Adding and subtracting the upper and lower equations, we obtain two independent sets of equations for the quantities  $P_{S,A} = p_1 \pm p_2$  and  $Q_{S,A} = q_1 \pm q_2$ :

$$\begin{aligned} \dot{P}_S &= -(\omega^2 + \beta\omega) Q_S, & \dot{P}_A &= -(\omega^2 - \beta\omega) Q_A, \\ \dot{Q}_S &= P_S, & \dot{Q}_A &= P_A. \end{aligned} \quad (2.14)$$

Eqs. (2.14) have the solution:

$$\begin{aligned} P_S &= -q_0 \omega_S \sin \omega_S t, & P_A &= -q_0 \omega_A \sin \omega_A t, \\ Q_S &= q_0 \cos \omega_S t, & Q_A &= q_0 \cos \omega_A t, \end{aligned} \quad (2.15)$$

where  $\omega_{S,A} = \sqrt{\omega^2 \pm \beta\omega}$ . The solution (2.15) corresponds to the following initial conditions:  $q_1(0) = q_0$ ,  $q_2(0) = p_1(0) = p_2(0) = 0$ . Expressing the energies  $E_1, E_2$  of the oscillators through the variables  $P_{S,A}, Q_{S,A}$ , and neglecting the terms of the order  $\beta/\omega$ , we obtain with the help of Eq. (2.15) the following formulas for  $E_1(t), E_2(t)$ :

$$\begin{aligned} E_1(t) &= \frac{\omega^2 q_0^2}{4} [1 + \cos(\Delta\omega t)] = E_0 \cos^2 \frac{\Delta\omega t}{2}, \\ E_2(t) &= \frac{\omega^2 q_0^2}{4} [1 - \cos(\Delta\omega t)] = E_0 \sin^2 \frac{\Delta\omega t}{2}, \end{aligned} \quad (2.16)$$

where  $\Delta\omega = (\omega_S - \omega_A) = \beta(1 + O(\beta))$ .

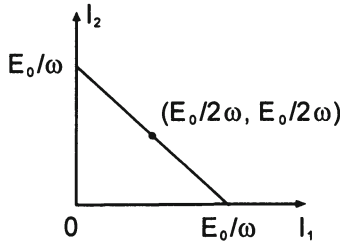


Figure 2.4: Beat phase trajectory in the plane  $(I_1, I_2)$ .

Thus, with the accuracy of  $\beta/\omega$  the energy is transferred totally from one oscillator to the other with the frequency  $\Delta\omega \sim \beta$ . It follows from Eqs. (2.3), (2.16) that the projection of the phase trajectory onto the plane of the action variables  $(I_1, I_2)$  is nothing but a segment of a straight line  $I_1 + I_2 = E_0/\omega$ ,  $(I_1, I_2) > 0$ , Fig. 2.4. The point  $(I_1(t), I_2(t))$  oscillates harmonically with respect to the center of the segment  $(\frac{E_0}{2\omega}, \frac{E_0}{2\omega})$ . The considered example of two weakly interacting oscillators demonstrates the qualitative changes in the character of motion (oscillation), provoked by interaction.

In the case of harmonic oscillators already weak interactions among them provoke the beat effect, when the energy is transferred totally from one oscillator to the other. The peculiarity of the beat effect is the profound change in the value of the integrals of the unperturbed system in its evolution along the phase trajectory, Fig. 2.4. In the general case of nonlinear interaction of two harmonic oscillators the phase trajectory covers densely all the energy surface. This is Arnold diffusion [44, 45].

Quite a different situation occurs if at least one oscillator is anharmonic. The nonlinearity of oscillations suppresses the effect of weak perturbations, so that the latter change only slightly the phase trajectories of the perturbed system, leaving them in the vicinity of the unperturbed ones. As a consequence, the value of any "constant of motion" of the unperturbed system varies only slightly along the perturbed phase trajectory. It is this property, that enables us to define the local mode as an oscillation with nearly all the energy localized on one of the oscillators. The excitation of two local modes corresponds to such an oscillation, when the reciprocal change of the energy for each oscillator, as well as the energy difference for these oscillators remain small along the entire phase trajectory. Clearly, this definition of LM is valid in the general case  $n > 2$  as well<sup>3</sup>. More to it, it is valid for the quantum consideration as well.

<sup>3</sup>The topological definition of local and normal modes is provided below, Eq. (2.55). From the point of view of physics, it is equivalent to the present one.

Thus, it has been shown that the nonlinearity of oscillations makes impossible any considerable energy transfer between a pair of identical oscillators after the introduction of a weak interaction between them. This fact leads to the existence of LMs with  $n = 2$ . It turns out that a similar situation is realized in the general case of an arbitrary number of similar oscillators,  $n > 2$ , [13]. We stress here that the Kolmogorov theorem is not applicable to this case, and a separate investigation is needed. Really, under strong excitation of a single oscillator the frequencies of all the other not excited ones remain equal, and consequently the resonance condition is fulfilled, Eq. (2.11). But the theorem guarantees the stability of nonresonant tori only. For the first time the absence of energy mixing between different degrees of freedom during a long time has been discovered in a numerical simulation of a system of bound nonlinear oscillators by Fermi, Pasta, and Ulam, [46]. Subsequent numerical calculations confirmed these results Eqs. [47, 48, 49].

In the present Chapter we prove the existence of LM in a system of similar weakly interacting nonlinear oscillators. (For non-resonant oscillators this fact follows from the Kolmogorov's theorem.) We will make it with the help of the method of averaging, widely used in analytical mechanics, in the studies of celestial motion, in particular.

To complete the present Section we calculate the variables "action-angle" for a Morse oscillator. The Morse potential provides good results for the description of stretching vibrations in molecules and is widely used in the calculations of vibrational frequencies and corresponding correction terms.

The Hamiltonian of Morse oscillator has the form:

$$H = \frac{p^2}{2m} + D [1 - \exp(-\alpha q)]^2, \quad (2.17)$$

where  $D$  is the dissociation energy, while the parameter  $\alpha$  is related to the frequency of small oscillations  $\omega_0$  according to the formula:

$$\omega_0^2 = \frac{2D\alpha^2}{m}. \quad (2.18)$$

The potential and the phase trajectories of the Hamiltonian Eq. (2.17) are depicted in Figs. 2.5 and 2.6.

Expressing the momentum  $p$  through the energy  $E$  and position  $q$  and substituting  $p(E, q)$  in Eq. (2.3), we obtain the action:

$$\begin{aligned} I &= \frac{1}{\pi} \int_{q_-}^{q_+} \sqrt{2m \left\{ E - D [1 - \exp(-\alpha q)]^2 \right\}} dq \\ &= \frac{\sqrt{2mD}}{\alpha} \left( 1 - \sqrt{1 - \frac{E}{D}} \right), \end{aligned} \quad (2.19)$$

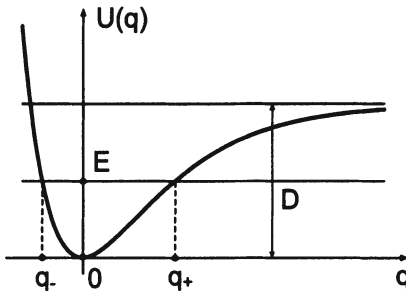


Figure 2.5: The potential curve of a Morse oscillator.

where  $q_+, q_-$  are the turning points (see Figs. 2.5 and 2.6). Inverting Eq. (2.19), we obtain the Hamiltonian in the variables "action-angle" along with the expression of the frequency  $\omega(I)$ :

$$H = \omega_0 I \left( 1 - \frac{I}{2I^b} \right), \quad \omega(I) = \omega_0 \left( 1 - \frac{I}{I^b} \right), \quad (2.20)$$

where  $I^b$  is the maximal possible value of  $I$ , when the energy equals the dissociation value,  $E = D$ :

$$I^b = \frac{\sqrt{2mD}}{\alpha}. \quad (2.21)$$

With the help of Eqs. (2.4), (2.5) we obtain the angular variable:

$$\Phi(E, q) = \frac{\partial S(I, q)}{\partial I} = \frac{\partial}{\partial I} \int_{q_-}^q p(E(I), \tilde{q}) d\tilde{q}$$

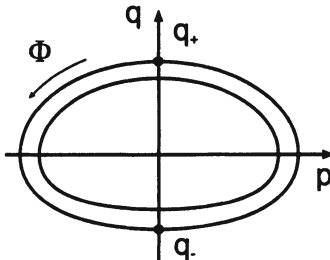


Figure 2.6: Phase trajectories of a Morse oscillator: an illustration.

$$= \arcsin \left[ \frac{\left(1 - \frac{I}{I^b}\right)^2 e^{\alpha q} - 1}{\sqrt{\left(2 - \frac{I}{I^b}\right) \frac{I}{I^b}}} \right] + \frac{\pi}{2}, \quad (2.22)$$

where  $\left[1 + \sqrt{\left(2 - \frac{I}{I^b}\right) \frac{I}{I^b}}\right]^{-1} = \exp(\alpha q_-)$ . It can be seen easily from Eq. (2.22), that  $\Phi(I, q_-) = 0$  at the left turning point. At the right turning point  $q = q_+$  the angular variable  $\Phi(I, q_-) = \pi$ . For the subsequent motion along the phase trajectory in the positive direction from  $q_+$  to  $q_-$  one should choose the branch of the function  $\arcsin x$  in such a way, that  $\Phi$  changes from  $\pi$  to  $2\pi$ , while  $q$  goes from  $q_+$  to  $q_-$ .

With the help of Eqs. (2.22), (2.20), and (2.17) we express new variables  $(p, q)$  through the old ones  $(I, \Phi)$ :

$$\begin{aligned} q &= \alpha^{-1} \ln \left( \frac{1 - \sqrt{1 - \lambda^2} \cos \Phi}{\lambda^2} \right), \\ p &= \frac{m\omega_0 \lambda}{\alpha} \frac{\sqrt{1 - \lambda^2} \sin \Phi}{1 - \sqrt{1 - \lambda^2} \cos \Phi}, \end{aligned} \quad (2.23)$$

where  $\lambda = (1 - \frac{I}{I^b})$ . The momentum  $p$  and position  $q$ , according to Eq. (2.23) are  $2\pi$ -periodic functions of the angular variable  $\Phi$ , as it should be for trajectories, winding around tori. Taking into account Eq. (2.20) we obtain the solution to Hamilton equations in the variables  $(I, \Phi)$ :

$$I = \text{const}, \quad \Phi = \omega_0 \left( 1 - \frac{I}{I^b} \right) t + \Phi_0. \quad (2.24)$$

In the subsequent Sections we will use Eqs. (2.20), (2.23), (2.24) for the qualitative analysis of phase trajectories for weakly interacting Morse oscillators.

## 2.2 Method of averaging

The method of averaging is one of the approaches to Hamiltonian systems, close to completely integrable ones, Eq. (2.10). In such a case the Hamiltonian of the system in the variables "action-angle" can be presented in the form:

$$H(I, \Phi) = H_0(I) + \varepsilon W(I, \Phi), \quad (2.25)$$

where  $(I, \Phi) = (I_1, \dots, I_s, \Phi_1, \dots, \Phi_s)$ , and  $\varepsilon$  is a small parameter.

As  $W(I, \Phi)$  is a periodic function of angular variables, it can be expanded in Fourier series:

$$W(I, \Phi) = \sum_{\substack{n=-\infty, \\ \left| \sum_1^s n_\nu \omega_\nu \right| \geq \varepsilon \bar{\omega}}}^{+\infty} W_{n_1, \dots, n_s}(I) \exp \left\{ i \sum_{\nu=1}^s n_\nu \Phi_\nu \right\}$$

$$+ \sum_{\substack{n=-\infty, \\ |\sum n_r \omega_r| \leq \varepsilon \bar{\omega}}}^{+\infty} W_{n_1, \dots, n_s}(I) \exp \left\{ i \sum_{r=1}^s n_r \Phi_r \right\}. \quad (2.26)$$

Here the first term corresponds to nonresonant contributions, the second — to resonant ones.

The method of averaging is based on the idea that the motion of the system (2.25) constitutes a displacement along the smooth trajectory with superimposed small oscillations. The latter give rise to small oscillations  $\sim \varepsilon$  in the right hand side of Hamiltonian equations, which can be averaged out over oscillation period  $T \sim \omega^{-1}$ . Substituting the unperturbed solution  $I = \text{const}$ ,  $\Phi_\nu = \omega_\nu t$  of the Hamiltonian equations into Eq. (2.25) and averaging over time period  $(\varepsilon \omega)^{-1} \gg T \gg \omega_\nu^{-1}$ , we obtain the averaged Hamiltonian:

$$\bar{H} = H_0(I) + \varepsilon V(I, \Phi), \quad (2.27)$$

where  $V(I, \Phi)$  is determined by the second term in Eq. (2.26):

$$V = \sum_{\substack{|\sum n_r \omega_r| \lesssim \varepsilon \bar{\omega}}} W_{n_1, \dots, n_s}(I) \exp \left( i \sum_r n_r \Phi_r \right). \quad (2.28)$$

The perturbation  $\varepsilon V$  produces the "secular" changes in the unperturbed phase trajectories during periods of time  $t \lesssim (\varepsilon \omega)^{-1}$ . If resonances are absent ( $\sum n_r \omega_r \neq 0$ ), there are no "secular" terms and  $V = 0$ . That provides a non-rigorous physical proof of Kolmogorov's theorem on stability of nonresonant tori.

Comparing Eqs. (2.26) and (2.27), we arrive at the following rule of averaging: to obtain the averaged Hamiltonian it is sufficient to keep in the Fourier expansion of the initial Hamiltonian in angular variables only the resonant terms ( $\left| \sum_r n_r \omega_r \right| \lesssim \varepsilon \bar{\omega}_\nu$ ). This method on averaging suffers two drawbacks: first, it is unclear how to transform the Hamiltonian to obtain the solution valid for time  $T_n \sim \varepsilon^{-n} \omega^{-1}$ ; second, this method provides a rigorous mathematical justification up to time  $T \sim \varepsilon^{-1}$ . Both these drawbacks can be bypassed in the method on canonical transformations which is described below. We will leave out the corresponding rigorous justifications, which can be found in monographs [40, 41] and in papers [9, 10, 50].

The basic idea of the method of canonical transformations is to find such a transformation  $(I, \Phi) \rightarrow (p, q)$ , which reduces the Hamiltonian (2.25) in variables  $(p, q)$  to the following form:

$$H(I, \Phi) = H(p, q) = H_0(p) + \varepsilon V(p, q) + O(\varepsilon^2). \quad (2.29)$$

This is achieved with the help of a canonical transformation:

$$I_\nu = \frac{\partial F(p, \Phi)}{\partial \Phi_\nu} = p_\nu + \varepsilon \frac{\partial S(p, \Phi)}{\partial \Phi_\nu},$$

$$q_\nu = \frac{\partial F(p, \Phi)}{\partial p_\nu} = \Phi_\nu + \varepsilon \frac{\partial S(p, \Phi)}{\partial p_\nu}. \quad (2.30)$$

The inverse transformation takes the form:

$$\begin{aligned} p_\nu &= I_\nu - \varepsilon \frac{\partial S(I, \Phi)}{\partial \Phi_\nu} + O(\varepsilon^2), \\ \Phi_\nu &= q_\nu - \varepsilon \frac{\partial S(I, \Phi)}{\partial I_\nu} + O(\varepsilon^2). \end{aligned} \quad (2.31)$$

Substituting Eqs. (2.30), (2.31) in Eq. (2.25), we obtain:

$$\begin{aligned} H(I, \Phi) &= H(p, q) \\ &= H_0 \left( p + \varepsilon \frac{\partial S(p, \Phi)}{\partial \Phi_\nu} \right) + \varepsilon W \left( p_\nu + \varepsilon \frac{\partial S(I, \Phi)}{\partial \Phi_\nu}, \Phi_\nu \right) \\ &= H_0(p) + \varepsilon \sum_{\mu} \omega_{\mu}(p) \frac{\partial S(p, \Phi)}{\partial \Phi_{\mu}} + \varepsilon W(p_\nu, \Phi_\nu) + O(\varepsilon^2). \end{aligned} \quad (2.32)$$

Next we choose  $S(p, \Phi)$  in such a way, that the terms of order  $\sim \varepsilon$  contain only the "secular" part:

$$\begin{aligned} \sum_{\mu} \omega_{\mu}(p) \frac{\partial S(p, \Phi)}{\partial \Phi_{\mu}} + W(p, \Phi) &= V(p, \Phi) \\ &= \sum_{|\sum n_r \omega_r| \lesssim \varepsilon \omega} W_{n_1, \dots, n_s}(I) \exp \left( i \sum_{r=1}^s n_r \Phi_r \right). \end{aligned} \quad (2.33)$$

In the right hand side of Eq. (2.33) the secular perturbation (2.28) appears. We look for the expression of  $S(p, \Phi)$  in the form of Fourier series in nonresonant harmonics:

$$S(p, \Phi) = \sum_{|\sum n_{\mu} \omega_{\mu}| > \varepsilon \omega} S_{n_1, \dots, n_s}(p) \exp \left( i \sum_{\mu=1}^s n_{\mu} \Phi_{\mu} \right). \quad (2.34)$$

Substituting Eqs. (2.26), (2.34) into Eq. (2.33) and comparing the coefficients for similar harmonics, we find  $S(p)$ :

$$S_{n_1, \dots, n_s}(p) = \frac{i W_{n_1, \dots, n_s}(p)}{\sum_{\nu=1}^s n_{\nu} \omega_{\nu}}. \quad (2.35)$$

Substituting Eq. (2.35) in Eq. (2.34) and Eq. (2.32) in Eq. (2.33), we obtain Eq. (2.29). It can be easily seen from Eq. (2.29) that the Hamiltonian of the system in variables  $(p, q)$  is equal to the averaged Hamiltonian Eq. (2.27) with the accuracy of  $\sim \varepsilon^2$ , if the substitution  $(I, \Phi) \rightarrow (p, q)$  is made in it:

$$H(p, q) = \overline{H}(I, \Phi)|_{\substack{I=p, \\ \Phi=q}} = H_0(p) + \varepsilon V(p, q). \quad (2.36)$$

Thus, from the mathematical point of view the method of averaging leads to the transition to the variables  $(p, q)$ , in which the Hamiltonian of the system coincides with the averaged Hamiltonian (2.36). Solving the Hamilton equations for  $p(t)$  and  $q(t)$ , and substituting the obtained solutions in Eq. (2.31), we find the required  $I(t)$  and  $\Phi(t)$ . From Eqs. (2.30) and (2.31) it follows that

$$\begin{aligned} |I_\nu(t) - p_\nu(t)| &\leq O(\varepsilon), \\ |\Phi_\nu(t) - q_\nu(t)| &\leq O(\varepsilon). \end{aligned} \quad (2.37)$$

Consequently, solving the problem with the averaged Hamiltonian  $\bar{H}(I, \Phi)$  for  $I_\nu(t)$  and  $\Phi_\nu(t)$ , we obtain the phase trajectory in the time interval  $T \lesssim \varepsilon^{-1}$  at least with the accuracy  $\sim \varepsilon$ . This is sufficient for a qualitative analysis of the phase curves, as in the absence of secular perturbations the variations of the unperturbed trajectory are small,  $\sim \varepsilon$ , which signifies the stability of the initial conditionally-periodic motion. While in the case of "secular" modifications of the phase trajectory (which can be considerable indeed) we obtain these changes with the accuracy of  $\sim \varepsilon$ .

Obviously, it is possible to make a canonical transformation  $(p, q) \rightarrow (P, Q)$  to get rid of the nonresonant terms of the order of  $\varepsilon^2$  in the Hamiltonian Eq. (2.29). As a result we obtain the Hamiltonian  $H_2(P, Q)$ , which provides the correct description of phase trajectories up to time  $\sim \varepsilon^{-2}\omega^{-1}$ . This whole process can be continued on to study consequently the Hamiltonians  $H_2, H_3, \dots$ , which determine correctly the character of phase trajectories up to time  $\sim \omega^{-1}\varepsilon^{-2}, \omega^{-1}\varepsilon^{-3}, \dots$  correspondingly. With the use of exactly that approach the asymptotic stability of local modes in the system of nonlinear weakly interacting similar oscillators up to time  $\omega^{-1} \exp(-\varepsilon^{-1/2})$  has been proved by Ovchinnikov in [13] (see below) and independently by Nehoroshev.

### 2.3 Two weakly coupled Morse oscillators: dynamics and local - mode formation

In the present Section we will consider the example of two weakly interacting Morse oscillators in order to demonstrate with the help of the method of averaging the general feature – the stability of the conditionally-periodic motion up to time  $(\omega\varepsilon)^{-1}$ . Besides, we will find out the conditions for the emergence of local modes (LM), and we will illustrate the topological differences in the position of tori referring to local and normal modes in phase space.

The Hamiltonian of the system of two Morse oscillators has the form:

$$H = \frac{1}{2} (p_1^2 + p_2^2) + D \sum_{i=1}^2 \left[ 1 - \exp \left( -\sqrt{\frac{1}{2D}} q_i \right) \right]^2 - \varepsilon p_1 p_2, \quad (2.38)$$

where  $D$  is the dissociation energy (for the  $OH$  bond it is of order of  $D \sim 10$ ),  $-\epsilon$  is the energy of kinematic interaction (which for stretching vibrations in  $H_2O$ ,  $CH_4$ , etc., molecules is negative and takes values of the order of  $10^{-2}$ ). In Eq. (2.38) the following units have been used:  $\hbar = 1$ ,  $m = 1$ ,  $\omega_0 = 1$ , where  $\omega_0 = \sqrt{\frac{u''(0)}{m}}$  is the vibration frequency in the harmonic approximation. The transition back to conventional units can be performed with the help of the following substitution:  $q \rightarrow q \left( \frac{\hbar}{m\omega_0} \right)^{-1/2}$ ,  $p \rightarrow \frac{p}{\sqrt{m\omega_0\hbar}}$ ,  $E \rightarrow \frac{E}{\hbar\omega_0}$ ,  $D \rightarrow \frac{D}{\hbar\omega_0}$ ,  $I \rightarrow \frac{I}{\hbar}$ . Inserting Eqs. (2.20)–(2.23) in Eq. (2.38), we obtain the following expression of the Hamiltonian in variables "action-angle":

$$H = I_1 \left( 1 - \frac{I_1}{2I^b} \right) + I_2 \left( 1 - \frac{I_2}{2I^b} \right) - \frac{2\epsilon D \sin \Phi_1 \sin \Phi_2 \left( 1 - \frac{I_1}{I^b} \right) \left( 1 - \frac{I_2}{I^b} \right) \sqrt{\left( 2 - \frac{I_1}{I^b} \right) \left( 2 - \frac{I_2}{I^b} \right) \frac{I_1 I_2}{(I^b)^2}}}{\left[ 1 - \sqrt{\left( 2 - \frac{I_1}{I^b} \right) \frac{I_1}{I^b}} \cos \Phi_1 \right] \left[ 1 - \sqrt{\left( 2 - \frac{I_2}{I^b} \right) \frac{I_2}{I^b}} \cos \Phi_2 \right]}.$$
(2.39)

Here the maximal value of the action  $I^b$  is defined by:

$$I^b = 2D.$$
(2.40)

Limiting our consideration to excitations that are not too high, i.e. when the following condition holds:

$$\frac{I_j}{I^b} = \frac{I_j}{2D} \ll 1,$$
(2.41)

we retain in Eq. (2.39) only the leading terms in that parameter. As a result we obtain:

$$H = I_1 \left( 1 - \frac{I_1}{4D} \right) + I_2 \left( 1 - \frac{I_2}{4D} \right) - 2\epsilon \sqrt{I_1 I_2} \sin \Phi_1 \sin \Phi_2.$$
(2.42)

Performing averaging over angular variables according to the rules, stated in the previous Section 2.2 (see Eq. (2.28)), we finally obtain the following Hamiltonian:

$$H = \sum_{j=1}^2 I_j \left( 1 - \frac{I_j}{4D} \right) - \epsilon \sqrt{I_1 I_2} \cos(\Phi_1 - \Phi_2).$$
(2.43)

In the derivation of Eq. (2.43) the formula (2.40) has been used.

In accordance with the results of Section 2.2 the Hamiltonian Eq. (2.43) provides a correct description of the phase trajectories of the initial Hamiltonian Eq. (2.39) for time up to  $\lesssim \epsilon^{-1}$ . In the analysis of motion of the averaged system and in the determination of conditions for local modes

existence the Hamiltonian Eq. (2.43) can be considered to be exact. The interaction term has a complicated form in variables  $(p, q)$ , while in new variables  $(I, \Phi)$  "action-angle" it takes up a simple shape  $\varepsilon\sqrt{I_1 I_2} \cos(\Phi_1 - \Phi_2)$ . Such an approach clarifies the physical reasons for local modes' existence, without distracting attention to the complicated mathematical issues dealing with the deviations introduced by the substitution of the initial Hamiltonian (2.39) by the averaged one, Eq. (2.43).

So, we have the Hamilton function (2.43). The question is: when and under what conditions the local vibrations emerge with oscillators' energies and oscillator energy differences changing slightly? As opposed to that case, the vibrations with the oscillator energy difference  $(E_1 - E_2)$  changing sign we term a normal mode (NM).

These definitions can be reformulated rigorously on the basis of notions of resonant and nonresonant tori. Within such an approach LM are in correspondence to nonresonant tori, while different normal modes correspond to the resonances of the general form  $n_1 : n_2$  (see next Section). In the case of NMs with resonance 1:1 the sign of the difference  $(E_1 - E_2)$  is always changed.

Let us consider the resonance  $\omega_1 = \omega_2$ . First we go over to new variables with the help of the following canonical transformation <sup>4</sup>:

$$\begin{cases} I = I_1 + I_2, & 2\Psi = \Phi_1 + \Phi_2, \\ J = I_1 - I_2, & 2\Theta = \Phi_1 - \Phi_2. \end{cases} \quad (2.44)$$

In the new variables the Hamiltonian (2.43) takes shape:

$$H = I - \frac{J^2}{8D} - \frac{\varepsilon}{2}\sqrt{I^2 - J^2} \cos 2\Theta. \quad (2.45)$$

It follows from Eq. (2.45) that  $I$  is constant ( $\Psi$  is a cyclic variable). Thus the problem is reduced to that for a system with one degree of freedom, when the phase trajectories  $(J, \Theta)$  are characterized by two parameters, energy  $E$  and total action  $I$ . Clearly, the role of the Hamiltonian for that one-dimensional system is played by the function:

$$\tilde{H}(J, \Theta) = -\frac{J^2}{8D} - \frac{\varepsilon}{2}\sqrt{I^2 - J^2} \cos 2\Theta, \quad (2.46)$$

which depends on  $I$  as a parameter. For the subsequent analysis it is convenient to introduce two functions, which depend upon energy  $E$  and action  $I$  as parameters:

$$h(E, I) = E - I + \frac{I^2}{8D}. \quad (2.47)$$

---

<sup>4</sup>The canonical nature of this transformation follows from the invariant character of the differential form:  $\omega^{(2)} = \sum dp \Lambda dq = dI_1 \Lambda d\Phi_1 + dI_2 \Lambda d\Phi_2 = d\frac{I+J}{2} \Lambda d(\Psi + \Theta) + d\frac{I-J}{2} \Lambda d(\Psi - \Theta) = dI \Lambda d\Psi + dJ \Lambda d\Theta$

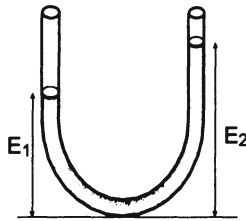


Figure 2.7: Oscillation of the level of a liquid in a U-shape tube.

and

$$\lambda(E, I) = h(E, I) + \frac{I^2}{8D}. \quad (2.48)$$

The phase trajectories are determined by the equations:

$$h(E, I) = \tilde{H}(J, \Theta) = -\frac{J^2}{8D} - \frac{\epsilon}{2} \sqrt{I^2 - J^2} \cos 2\Theta. \quad (2.49)$$

To find out if some particular vibration with some values of  $E, I$  is either a local or a normal mode, we have to investigate the phase curve  $(J(\Theta), \Theta)$  and to determine whether the action  $J$  changes sign or not. If  $J$  retains its sign, the vibration is an LM, while if the  $J$  sign is changed we deal with an NM.

It follows from Eq. (2.49), that if the point with coordinates  $(J, \Theta)$  belongs to the phase trajectory, the symmetrical point  $(-J, -\Theta)$  lies on the phase curve with the same values of  $E$  and  $I$  as well.

The transformation  $(J, \Theta) \rightarrow (-J, -\Theta)$  exchanges the oscillators (see Eq. (2.44)). Consequently, when the points  $(J, \Theta)$  and  $(-J, -\Theta)$  belong to the same phase curve, exchange of vibrational excitations between oscillators takes place. The energy difference  $(E_1 - E_2)$  flows continuously from the first oscillator to the second, and after that vice versa, and so on. This effect can be illustrated by the flow of a liquid in a U - shape tube, if viscosity can be neglected (see Fig. 2.7). The role of energy is played by the height of the fluid level. The oscillations in such a system reveal the beat effect, and the oscillator energy in this case changes from zero to the maximal sum value. In the general case the oscillator energy may not fall down to zero. The depicted oscillation process we call the normal vibration (NM).

In the opposite case, when the points  $(J, \Theta)$  and  $(-J, -\Theta)$  belong to various phase curves (the values of energy  $E$ , and of the action  $I$  remain equal for such a transformation) the local vibration takes place, and the excessive energy does not flow completely from one oscillator to the other. We say then, that there is a local mode (LM) in the system.

Next we pass over to the qualitative analysis of phase curves, determined

by Eq. (2.49). We imply that the total action satisfies the condition:

$$0 \leq I \leq I^b = 2D,$$

that is we limit the value of the action by the maximal value possible for an individual oscillator  $I_j$ . Besides, we imply the interaction  $\varepsilon$  to be weak enough, so that all the subsequent inequalities hold. Actually it is sufficient for  $\varepsilon$  to satisfy  $\varepsilon < 0.1$ . From Eqs. (2.46) and (2.49) it follows that the function  $H(J, \Theta)$  satisfies the following condition:

$$\tilde{H}_{\min}(I) \leq \tilde{H}(J, \Theta; I) \leq \tilde{H}_{\max}(I), \quad (2.50)$$

$$\tilde{H}_{\max}(I) = \frac{\varepsilon I}{2}, \quad \tilde{H}_{\min}(I) = \begin{cases} -\frac{1}{2}\varepsilon I, & \text{if } I \leq 2\varepsilon D \\ -\frac{1}{8}(I^2 + 4\varepsilon^2 D^2) D^{-1} & \text{if } I \geq 2\varepsilon D \end{cases}$$

According to Eq. (2.49) the function  $h(E, I)$  matches the similar condition. In other words, only those values of energy  $E$  and action  $I$  are possible, when the function  $h(E, I)$  belongs to the interval, characterized by the inequalities (2.50). It follows from Eqs. (2.47) and (2.49), that  $h'_I < 0$ . Consequently, the minimal  $I_{\min}(E)$  and maximal  $I_{\max}(E)$  possible values of the action with energy  $E$  fixed are determined by the solution of the following equations:

$$\begin{aligned} h_{\max} &= h(I_{\min}) = \tilde{H}_{\max}(I_{\min}), \\ E - I_{\min} + \frac{I_{\min}^2}{8D} &= \frac{\varepsilon I_{\min}}{2}; \\ h_{\min} &= h(I_{\max}) = \tilde{H}_{\min}(I_{\max}), \\ E - I_{\max} + \frac{I_{\max}^2}{8D} &= \begin{cases} -\frac{1}{2}\varepsilon I_{\max}, & \text{if } I_{\max} \leq 2\varepsilon D \\ -\frac{1}{8}(I_{\max}^2 + 4\varepsilon^2 D^2) D^{-1}, & \text{if } I_{\max} > 2\varepsilon D \end{cases}. \end{aligned} \quad (2.51)$$

Solving Eqs. (2.51) for  $I_{\min}$  and  $I_{\max}$ , we obtain the following expressions:

$$\begin{aligned} I_{\min} &= 4D \left(1 + \frac{\varepsilon}{2}\right) \left[1 - \sqrt{1 - \frac{E}{2D \left(1 + \frac{\varepsilon}{2}\right)^2}}\right] \\ &= \frac{E}{1 + \frac{\varepsilon}{2}} \left(1 + O\left(\frac{E}{D}\right)\right), \\ I_{\max} &= 4D \left(1 - \frac{\varepsilon}{2}\right) \left[1 - \sqrt{1 - \frac{E}{2D \left(1 - \frac{\varepsilon}{2}\right)^2}}\right] \\ &= \frac{E}{1 - \frac{\varepsilon}{2}} \left(1 + O\left(\frac{E}{D}\right)\right), \text{ if } I_{\max} \leq 2\varepsilon D, \text{ or} \\ I_{\max} &= 2D \left[1 - \sqrt{1 - \frac{E}{D} - \frac{\varepsilon^2}{2}}\right] \\ &= \frac{2E + \varepsilon^2 D}{2} \left(1 + O\left(\frac{E}{D}\right)\right), \text{ if } I_{\max} > 2\varepsilon D. \end{aligned} \quad (2.52)$$

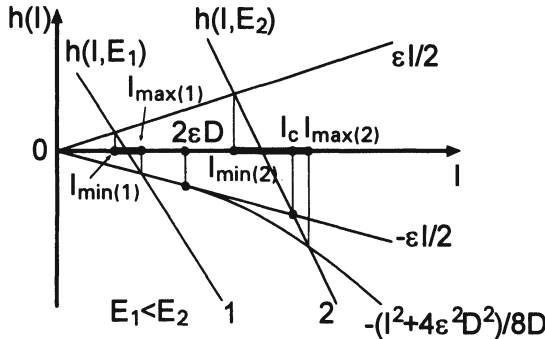


Figure 2.8: The graphical definition of  $I_{\min}(E)$  and  $I_{\max}(E)$ , and of the regions of NM and LM in the  $h - I$  plane.

As  $\epsilon \ll 1$ , from Eq. (2.52) we derive the conclusion, that the width of accessible values for the action  $\Delta I$  is  $\sim \epsilon E$ . The graphical determination of  $I_{\min}(E)$  and  $I_{\max}(E)$  is depicted in Fig. 2.8.

The allowed values of  $h$  and  $I$  for energies  $E_1$  (corresponding to NM) and  $E_2$  (corresponding to NM + LM) respectively correspond to the parts of the curves 1 and 2 between the straight line  $\epsilon I/2$  and the curve, combined from a straight line  $-\epsilon I/2$  and the curve  $-(I^2 + 4\epsilon^2 D^2)/8D$ . Projections of these segments upon axis  $I$  determine the allowed values of the action  $I_{\min}(E) < I < I_{\max}(E)$  with energy  $E$  fixed. All the points of the plane  $(h, I)$  between the curves mentioned above correspond to some allowed values of  $I$  and  $E$ , while all the other points do not represent any physical state of the oscillators. It will be shown later, that the area in Fig. 2.8 to the right of the point  $I = 2\epsilon D$  and bound by the straight line  $-\epsilon I/2$  and the curve  $-(I^2 + 4\epsilon^2 D^2)/8D$ , corresponds to local vibrations.

Next we pass over to the study of the phase trajectories (2.49), and to the analysis of the dependence of vibration features upon the energy  $E$  and action  $I$ . Let us consider three intervals of energy (NM),  $(LM_1)$ ,  $(LM_2)$ , determined by the following conditions:

$$(NM) \quad I_{\max}(E) \leq 2\epsilon D; \quad (2.53)$$

$$(LM_1) \quad 2\epsilon D \leq I_{\max}(E) \quad \text{and} \quad I_0(E) \leq 4\epsilon D; \quad (2.54)$$

$$(LM_2) \quad 4\epsilon D \leq I_0(E). \quad (2.55)$$

where  $I_0(E) = 2D \left(1 - \sqrt{1 - ED^{-1}}\right)$  is the solution of the equation  $\lambda(I_0) = 0$ .

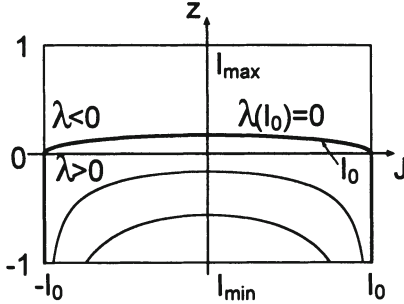


Figure 2.9: The set of phase trajectories  $z(J, I)$  for  $\lambda \geq 0$  and  $I_{\max}(E) < 2\varepsilon D$ .

First, let us consider the region ( $N$ ). With the account of Eq. (2.48) the equation (2.49) can be presented in the form:

$$z = \sqrt{\frac{\lambda}{2\varepsilon^2 D}} \left[ \sqrt{\frac{I^2 - J^2}{8D\lambda}} - \sqrt{\frac{8D\lambda}{I^2 - J^2}} \right] = \cos 2\Theta, \text{ if } \lambda(I) \geq 0, \quad (2.56)$$

$$z = \sqrt{\frac{|\lambda|}{2\varepsilon^2 D}} \left[ \sqrt{\frac{I^2 - J^2}{8D|\lambda|}} + \sqrt{\frac{8D|\lambda|}{I^2 - J^2}} \right] = \cos 2\Theta, \text{ if } \lambda(I) < 0. \quad (2.57)$$

The function  $z(J)$  for  $\lambda > 0$  grows monotonously from  $-\infty$  to  $z(0)$ , when  $J$  changes from  $I$  to 0.

The set of curves  $z(J)$  for  $0 \leq \lambda(I) \leq \lambda(I_{\min})$  is depicted in Fig. 2.9. The value of  $\cos 2\Theta$  at  $J = 0$  is determined by the formula:

$$z(J, I)|_{J=0} = z_0(I) = \left( \frac{I}{4\varepsilon D} - \frac{2\lambda(I)}{\varepsilon I} \right). \quad (2.58)$$

The function  $z_0(I)$  grows monotonously from  $-1$  to  $\frac{1}{4}I_0(\varepsilon D)^{-1}$ , while the action  $I$  changes from  $I_{\min}$  to  $I_0$ . The latter follows from  $\lambda'(I) < 0$  according to Eq. (2.48). Due to the inequality  $I \leq I_{\max} \leq 2\varepsilon D$  (region NM) the quantity  $z_0(I_0)$  satisfies  $z_0(I_0) = \frac{1}{4}I_0(\varepsilon D)^{-1} \leq \frac{1}{2}$ , and consequently the point  $(J = 0, \cos 2\Theta = \frac{1}{4}I_0(\varepsilon D)^{-1})$  belongs to the phase trajectory. Such a consideration leads to the shape of the phase trajectories Eq. (2.56), depicted in Fig. 2.9. Evidently, these trajectories correspond to normal (delocalized) vibrations, when the difference of actions  $J = I_1 - I_2$  for oscillators changes continuously between the minimal  $J_{\min} = -\bar{J}(I)$  and maximal  $J_{\max} = \bar{J}(I)$  values (see Fig. 2.9).

Next let us construct the phase trajectories Eq. (2.57) for  $\lambda(I) < 0$ . The action  $I$  belongs to the interval  $(I_0, I_{\max})$ . The quantity  $z_0(I)$  is determined

again by Eq. (2.58), and consequently it is a monotonous function of the action  $I$ . For the maximal value of the action  $I_{\max}$  the variable  $z_0(I_{\max})$  is characterized by:

$$z_0(I_{\max}) = \frac{I_{\max}}{4\varepsilon D} - \frac{2\lambda(I_{\max})}{\varepsilon I_{\max}} = 1, \quad (2.59)$$

that is  $\cos 2\Theta_0 = 1$ ,  $\Theta_0 = 0$ . In the derivation of Eq. (2.59) the formulas Eqs. (2.48), (2.51), and (2.53) have been taken into account. Equation (2.59) shows, that when the action  $I$  reaches its maximal value  $I_{\max}$ , the phase trajectory degenerates into a point, as it should in accordance with Eqs. (2.49) and (2.51). Next we take into account the following equalities:

$$\begin{aligned} \left( \frac{I^2}{8D|\lambda|} \right)' &= \left( \frac{I^2}{8D\left(I - E - \frac{r^2}{4D}\right)} \right)' \\ &= \frac{I - 2E}{8DI^3} \left( I^{-1} - EI^{-2} - \frac{1}{4D} \right)^{-2} < 0, \end{aligned} \quad (2.60)$$

$$\frac{I_{\max}^2}{8D|\lambda(I_{\max})|} = \frac{1}{\left(\frac{4\varepsilon D}{I_{\max}} - 1\right)} < 1, \text{ if } I_{\max} < 2\varepsilon D. \quad (2.61)$$

The inequality Eq. (2.60) is valid for low enough  $\varepsilon$  ( $\varepsilon < 0.1$ ) according to Eq. (2.52). Equation (2.61) is valid due to Eq. (2.52) and due to the condition  $I_{\max} < 2\varepsilon D$ . From Eqs. (2.60) and (2.61) it follows that the quantity  $\frac{1}{8}I^2(D|\lambda|)^{-1}$  decreases monotonously from  $+\infty$  to  $\beta < 1$ , when the action  $I$  changes from  $I_0$  ( $\lambda(I_0) = 0$ ) to  $I_{\max}$ . As a result the function  $z(J, I)$  determined by Eq. (2.57) has two minima in  $J$  for  $\frac{1}{8}(I^2 - J^2)(D|\lambda|)^{-1} = 1$  if  $\frac{1}{8}I^2(D|\lambda|)^{-1} > 1$ , and has no minima in the opposite case.

The set of curves  $z(J, I)$  for  $\lambda(I) < 0$  has the shape, depicted in Fig. 2.10. The action  $J$  along the phase trajectory changes from  $J_{\min} = -J_{\max}$  to  $J_{\max}(I)$  as in the case  $\lambda(I) > 0$ . So we arrive again at the conclusion that a normal delocalized vibration is realized. With the accuracy up to  $\sim \varepsilon$  the energy flows completely from one oscillator to the other. Thus for  $I_{\max}(E) < 2\varepsilon D$  there are normal delocalized vibrations exclusively. Determining  $E_{\max}$  through  $I_{\max}$  with the help of Eq. (2.51), we find the energy region with purely normal vibrations:

$$E_{\max} = E(I_{\max}) = I_{\max} - \frac{I_{\max}^2}{8D} - \frac{\varepsilon I_{\max}}{2} = 2\varepsilon D - \frac{3}{2}\varepsilon^2 D,$$

so that the following inequalities hold:

$$0 \leq E \leq 2\varepsilon D - \frac{3}{2}\varepsilon^2 D.$$

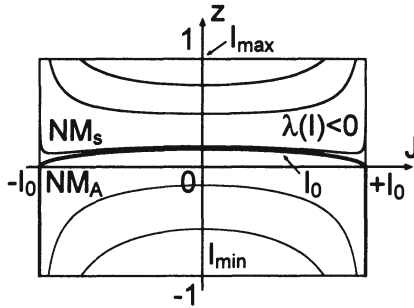


Figure 2.10: The set of curves  $z(J, I)$ , which correspond to phase trajectories with the action in the range  $I < I_{\max} \leq 2\varepsilon D$  and both  $\lambda(I) \leq 0$  and  $\lambda(I) > 0$ .

Phase trajectories in the plane  $(J, \Theta)$  for the entire range of the action variable  $I_{\min} \leq I \leq I_{\max} \leq 2\varepsilon D$  are depicted in Fig. 2.11.

Next let us consider the phase trajectories in the region  $(LM_1)$ , when the maximal value of action  $I_{\max}(E)$  and  $I_0(E)$  satisfy the condition (2.54). Then  $I_{\max}(E)$  is determined by the second formula in Eq. (2.52). The consideration of the function  $z(J, I)$  (2.56), provided above, remains valid in this case as well, with one exception: now  $z(0, I_0) = \frac{I_0}{4\varepsilon D} \leq 1$  (equal sign is realized for  $I_0(E) = 4\varepsilon D$ ). Consequently the phase curves in the case  $\lambda(I) > 0$  have the same shape, as in Fig. 2.9, and as in the region  $(NM_A)$  of Fig. 2.11. The only difference is that now the point  $z(0, I_0)$  can reach unit ( $\Theta = 0$ ), if  $I_0(E) = 4\varepsilon D$ . Thus, for  $\lambda(I) > 0$  we obtain again a normal vibration (NM).

A difference in the behavior of phase curves appears in the region of action  $I$ , where  $\lambda(I) < 0$ . In this case at some critical value of action  $I_{cr}$  a local mode arises, when  $J$  does not equal zero on the phase trajectory.

The critical value  $I_{cr}$  is determined by the condition:

$$\begin{aligned} h(I_{cr}) &= E - I_{cr} + \frac{I_{cr}^2}{8D} = -\varepsilon \frac{I_{cr}}{2}, \text{ or} \\ \lambda(I_{cr}) &= \frac{(I_{cr}^2 - 4\varepsilon D I_{cr})}{8D}. \end{aligned} \quad (2.62)$$

According to Eqs. (2.52) and (2.54) such  $I_{cr}$  can always be found in the region  $(L_1)$ , so that the inequality holds:

$$I_0(E) \leq I_{cr}(E) \leq 4\varepsilon D. \quad (2.63)$$

The equalities in (2.63) are reached simultaneously for  $E = 4\varepsilon D(1 - \varepsilon)$ .

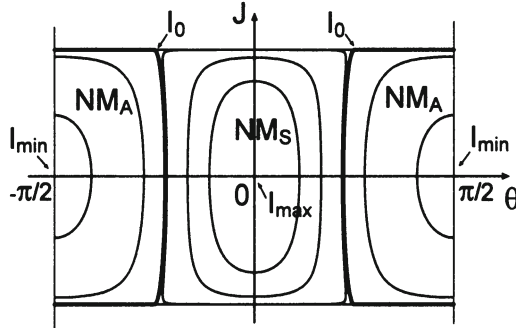


Figure 2.11: The set of phase trajectories of the system for  $E < 2\epsilon D - 1.5\epsilon^2 D$ . Solid curves (separatrix lines) separate the regions with  $\lambda(I) > 0$ , ( $NM_A$ ), and  $\lambda(I) < 0$ , ( $NM_S$ ) from each other.

From Eqs. (2.59) and (2.62) we obtain:

$$z_0(I_{cr}) = \cos 2\Theta|_{\substack{J=0 \\ I=I_{cr}}} = 1. \quad (2.64)$$

As it follows from Eqs. (2.48) and (2.58) the value of  $z'_0(I)$  is positive, and consequently for  $I > I_{cr}$  the equation  $z_0(I) = \cos 2\Theta$  has no solutions. Consequently the point  $J = (0, \Theta)$  does not belong to the phase trajectory. Thus, the vibration is local and in the present case  $\lambda(I) < 0$  the set of curves  $z(J, I)$  has the shape, depicted in Fig. 2.12. The set of curves  $z(J, I)$  for  $2\epsilon D \leq I_{max}$  and  $I_0(E) \leq 4\epsilon D$  (Fig. 2.12) on the phase plane  $(J, \Theta)$  is presented in Fig. 2.13.

From the definition of the functions  $I_0(E)$  (2.55) and  $I_{cr}(E)$  (2.62) it follows, that with the increase of energy  $E$  from some moment the following equality holds true:

$$I_0(E) = I_{cr}(E). \quad (2.65)$$

From the point of view of geometry, the latter corresponds to the situation, when the intersection point of the separatrix line  $I = I_0$  with the  $\Theta$  axis reaches the origin and touches there the separatrix, corresponding to  $I = I_{cr}$ .

Comparing Eqs. (2.65) and (2.62), we find that the discussed fact occurs when  $I_0 = 4\epsilon D$ . Then the quantity  $z_0(I_0)$ , defined by Eq. (2.58), becomes equal to unit, and the limiting curve of the set  $z(J, I)$  in Fig. 2.9,  $\lambda(I) \geq 0$ , touches the straight line  $z = 1$ . With the further increase of  $I_{max}(E)$  the quantity  $I_0(E)$  grows as well, and the following inequalities hold:

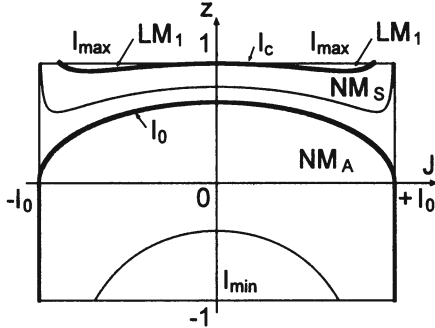


Figure 2.12: The set of phase trajectories  $z(J, I)$  of the system for  $2\epsilon D \leq I_{\max}(E)$  and  $I_0(E) \leq 4\epsilon D$ . The solid curve (separatrix line)  $I = I_c$  separates the regions of local ( $LM_1$ ) and normal symmetric ( $NM_S$ ) modes, while  $I = I_0$  separates normal symmetric modes ( $NM_S$ ) from antisymmetric ( $NM_A$ ) ones. The points  $I = I_{\max}$  and  $I = I_{\min}$  correspond to periodic orbits of local and normal vibrations respectively. The point  $(0, 1)$  corresponds to an unstable periodic orbit of a normal symmetric vibration.

$$\begin{aligned} 4\epsilon D &\leq I_{cr} \leq I_0 < I_{\max}(E), \text{ and} \\ z_0(I_0) &= \frac{I_0}{4\epsilon D} > 1. \end{aligned} \quad (2.66)$$

The curves with  $I_{cr} \leq I < I_0 (\lambda(I) < 0)$  in the region  $z \leq 1$  separate into two unconnected pieces, corresponding to phase trajectories of local modes with a monotonously changing angular variable  $\Theta$ . With the subsequent increase of the action  $I$  from  $I_0$  to  $I_{\max}(E)$  we pass over into the region of local vibrations, depicted in Fig. 2.13 (region ( $LM_1$ )), when the angle  $\Theta$  oscillates around zero value.

This picture is illustrated with phase portraits in the variables  $(z, J)$  and  $(\Theta, J)$  in Figs 2.14 and 2.15.

Let us determine the value of the action  $\tilde{I}_{\max}(\tilde{E})$  and the energy  $\tilde{E}$  when a new local mode with a monotonous change of the angle  $\Theta$  gets split off. According to Eq. (2.65) the LM gets split-up at  $I_0 = 4\epsilon D$ . Substituting this value into the equation  $\lambda(I_0) = 0$  and taking into account the definition Eq. (2.48), we obtain:

$$\lambda(\tilde{E}, I_0) = \lambda(\tilde{E}, 4\epsilon D) = \tilde{E} - 4\epsilon D + \frac{(4\epsilon D)^2}{4D} = 0,$$

and

$$\tilde{E} = 4\epsilon D(1 - \epsilon). \quad (2.67)$$

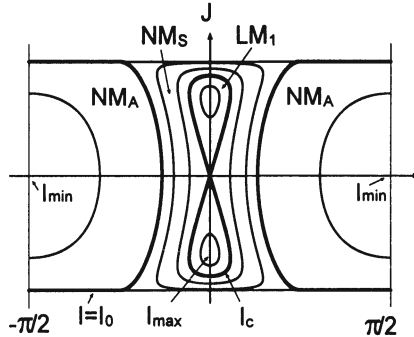


Figure 2.13: The set of phase trajectories in the plane  $(J, \Theta)$  of the system for  $2\varepsilon D < I_{\max}(E)$  and  $I_0(E) < 4\varepsilon D$ . All the notations are the same, as in Fig. 2.12 . The unstable periodic orbit of the normal symmetric vibration here corresponds to the origin.

Substituting Eq. (2.67) into Eq. (2.52), we find:

$$\tilde{I}_{\max} = 4\varepsilon D + \frac{15}{2}\varepsilon^2 D + O(\varepsilon^3 D). \quad (2.68)$$

Thus, in the case  $E > 4\varepsilon D(1 - \varepsilon)$  the phase trajectories of the system separate into three different classes: normal antisymmetric vibrations (region  $(NM_A)$  in Fig. 2.15); local vibrations with unbounded variation of the angle  $\Theta$  (region  $(LM_2)$  in Fig. 2.15); and local vibrations with bounded area for the changes of the angle (region  $(LM_1)$ ) in Fig. 2.15).

Each class of phase trajectories is in one to one correspondence with intervals for the values of the total action:

$$(NM) \quad I_{\min}(E) \leq I < I_{cr}(E), \quad (2.69)$$

$$(LM_2) \quad I_{cr}(E) \leq I \leq I_0(E), \quad (2.70)$$

$$(LM_1) \quad I_0(E) \leq I \leq I_{\max}(E), \quad (2.71)$$

where  $I_{\min}(E)$  and  $I_{\max}(E)$  are determined by the formula (2.52) while  $I_{cr}$  and  $I_0$  can be obtained from the equations:

$$h(I_{cr}) = -\frac{\varepsilon I_{cr}}{2}, \quad (2.72)$$

$$\lambda(I_0) = 0. \quad (2.73)$$

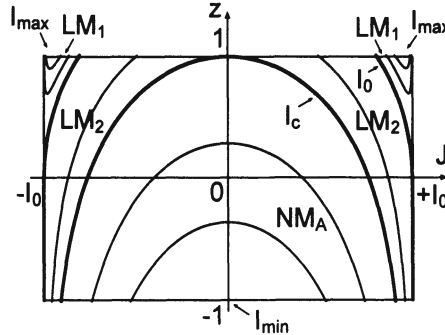


Figure 2.14: The set of phase trajectories  $z(J, I)$  of the system for  $I_0(E) > 4\epsilon D$ . The solid curve (separatrix line)  $I = I_0$  separates the regions of local ( $LM_1$ ) and local ( $LM_2$ ) modes, while  $I = I_c$  separates local modes ( $LM_2$ ) from normal antisymmetric ( $NMA$ ) ones. Normal symmetric modes ( $NMS$ ) in the present case are absent. The points  $I = I_{\max}$  and  $I = I_{\min}$  have the same meaning, as in Fig. 2.12.

The functions  $h(I)$  and  $\lambda(I)$  are determined by formulas Eq. (2.47) and (2.48). The condition for the split-off of the LM with unbounded interval for  $\Theta$  :

$$E \geq 4\epsilon D(1 - \epsilon), \quad (2.74)$$

along with the monotonous nature of the functions  $h(I), \lambda(I)$  at  $I < 2D$  secure the non-self-contradictory nature of the inequalities (2.69)–(2.71). We note here, that the volume of the region ( $LM_1$ ) is of the order of  $\epsilon^2$  in accordance with Eqs. (2.52) and (2.72),  $(I_0 - I_{\max}) \sim \epsilon^2 E$ . On the contrary, the volume of the region ( $LM_2$ ) is of the order of  $\sim E$  if  $E \lesssim D$  and does not depend on  $\epsilon$  when  $\epsilon \ll 1$ . For example in the case of stretching vibrations of the molecule of water  $\epsilon \sim 10^{-2}$  and  $D \sim 10$ , and the volume of the region ( $LM_1$ ) is  $\sim 10^{-4} \div 10^{-3}$ , whereas for the region ( $L$ ) it is  $\sim 1 \div 10$ . If one performs the quantization procedure according to Bohr-Sommerfeld, when a region of phase space with volume  $\sim 1$  ( $\hbar = 1$ ) corresponds to each quantum state, the region ( $LM_1$ ) does not correspond to any state at all. At the same time, local vibrations from region ( $LM_2$ ), starting with energy  $E \geq 2$  have a rather large number of quantum levels (see below).

The phase trajectories from ( $LM_1$ ) describe vibrations with all the phases of oscillators correlated,  $|\Theta| = |\Phi_1 - \Phi_2| \leq \Theta_{\max}$ . It means that the vibrations of oscillators interact strongly in some sense. Consequently the substitution of one oscillator by another one with a different frequency should change the character of vibrations in regions ( $LM_1$ ) considerably. On the

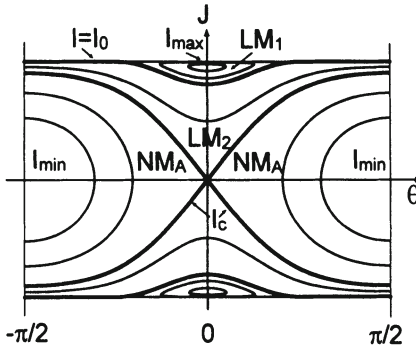


Figure 2.15: The set of phase trajectories in the plane  $(J, \Theta)$  of the system for  $I_0(E) > 4\epsilon D$ . All the notations are the same, as in Fig. 2.14. The set of orbits of normal symmetric vibrations has reduced here to a single point in the origin, which corresponds to an unstable periodic orbit (analogous to point  $(0,1)$  in Fig. 2.14).

contrary, vibrations in region  $(LM_2)$  are characterized by a monotonous increase in the phases  $|\Theta| = |\Phi_1 - \Phi_2|$ , like it would be for completely independent (non interacting) oscillators. Then the substitution of one weakly excited oscillator for another one with a different frequency should lead to a small change of the phase trajectory of the system. Really, the experimental results show, that upon substitution of hydrogen atoms for deuterium in molecules of the type  $H_2O$ ,  $C_6H_6$ , etc., the spectra, corresponding to stretching vibrations of valence bonds  $CH$  and  $OH$  change insignificantly (see, for example, the review [51]). A conclusion can be drawn, that in fact the LMs of the type  $(LM_2)$  in polyatomic molecules exist, while the vibrations of type  $(LM_1)$  do not exist, as it is

impossible to construct a stationary wavefunction, which could produce sufficient localization in momentum  $J$  and in position  $\Theta$ , as it is required for region  $(LM_1)$ .

To sum up the results let us study, how the regions  $(LM_2)$ ,  $(LM_1)$ , and  $(NM)$  transform upon the decrease of energy from  $\tilde{E} = 4\epsilon D(1 - \epsilon)$  to zero, and what happens to the inequalities (2.69)–(2.71). It can be easily shown, that when the energy decreases and moves from the region  $E > 4\epsilon D(1 - \epsilon)$  into  $E < 4\epsilon D(1 - \epsilon)$ , the inequalities (2.69)–(2.71) and the corresponding phase portraits of the system transform in the following way:

$$\begin{aligned}
 E(I_{\max} = 2\epsilon D) &< E < 4\epsilon D(1 - \epsilon); \\
 (NM_A) \quad I_{\min}(E) &\leq I \leq I_0(E); \\
 (NM_S) \quad I_0(E) &\leq I \leq I_{cr}(E); \\
 (LM_1) \quad I_{cr}(E) &\leq I \leq I_{\max}(E).
 \end{aligned} \tag{2.75}$$

The phase portrait corresponding to Eq. (2.75) is depicted in Fig. 2.13:

$$\begin{aligned} 0 \leq E \leq E(I_{\max} = 2\epsilon D); \\ (\text{NM}_A) \quad I_{\min}(E) \leq I \leq I_0(E); \\ (\text{NM}_S) \quad I_0(E) \leq I \leq I_{\max}(E) = 2\epsilon D. \end{aligned} \quad (2.76)$$

The phase portrait of Eq. (2.76) corresponds to Fig. 2.11. The inequalities (2.75) and (2.76) can be proved easily with the help of the definitions of  $I_{cr}$  and  $I_0$ , and with the use of Eqs. (2.72), (2.73).

Comparing the phase portraits in Fig. 2.15, 2.13, and 2.11 it can be seen easily, that with the decrease of energy  $E$  the curve with  $I = I_0$  approaches the curve with  $I = I_{cr}$ . The phase trajectories of local modes ( $\text{LM}_2$ ) are then ousted, and they vanish completely when the curve with  $I = I_{cr}$  coincides with  $I = I_0$  at energy  $E = 4\epsilon D(1 - \epsilon)$ . With the subsequent decrease of energy  $E$  the separatrix lines with  $I = I_{cr}$ ,  $I = I_0$  separate again, and between them there appears a region of phase trajectories, corresponding to symmetrical normal vibrations (region ( $\text{NM}_S$ ) in Fig. 2.13). The regions ( $\text{LM}_1$ ) and ( $\text{NM}_A$ ) of local and antisymmetric normal vibrations survive (in Fig. 2.13 the region of normal modes is marked as ( $\text{NM}_A$ )). And last for energy  $E < E(I_{\max} = 2\epsilon D)$  the curve with  $I = I_{cr}$  degenerates into a point ( $J = 0, \Theta = 0$ ) with  $I_{\max}(E) = I_{cr}$ . Simultaneously the regions of local vibrations ( $\text{LM}_1$ ) vanish completely, only regions ( $\text{NM}_A$ ) and ( $\text{NM}_S$ ) are left, which correspond to antisymmetric and symmetric normal vibrations (Fig. 2.11).

The described changes of phase portraits of the system with the changes in its energy lead to the conclusion on the instability of symmetric normal vibrations with respect to energy fluctuations. Really, due to the inequality  $\epsilon \ll 1$  the threshold for the disappearance of the region ( $\text{NM}_S$ ) of symmetric vibrations  $E = 4\epsilon D(1 - \epsilon)$  is a small quantity itself. Thus, even a small increase in energy destroys the symmetric normal mode.

As the volume of region ( $\text{NM}_S$ ) is of the order of  $4\epsilon D \ll 1$ , there are no quantum states, corresponding to a symmetric normal mode in the case of strong anharmonicity (not too large  $D$ ).

All the described rules on the emergence and disappearance of local and normal modes can be presented in graphic form (Fig. 2.16). The curves for  $h(I, E)$  are presented with energy  $E$  taking different values (lines  $h_1, h_2, h_3$  and  $h_I, h_{II}$ ). The curves  $\tilde{h}_{\max}(I)$  and  $\tilde{h}_{\min}(I)$  limit the maximal and minimal possible values of the function  $h(I, E)$ , i.e. of the Hamilton function  $\tilde{H}(J, \Theta; I)$  for given  $E$ . For a fixed energy  $E$  the physical states correspond to the points of the curve  $h(I, E)$  between the lines  $\tilde{h}_{\max}(I)$  and  $\tilde{h}_{\min}(I)$ , which are marked densely in Fig. 2.16. The values  $I$  and  $h$  for these points provide the possible intervals of the action  $I$  and of the Hamilton function  $\tilde{H}(J, \Theta; I)$  with energy  $E$  fixed. We note that the parabolic curve  $h = -\frac{1}{8}(I^2 + 4\epsilon^2 D^2)D^{-1}$  touches the straight line  $h = -\frac{1}{2}\epsilon I$

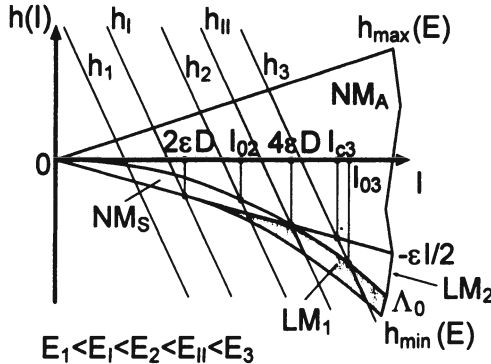


Figure 2.16: The graphical definition of  $I_{\min}(E)$  and  $I_{\max}(E)$ , and of the regions of NM and LM in the  $h$ - $I$  plane.  $NM_A$  is the region of antisymmetric normal vibrations;  $NM_S$  – symmetric normal vibrations;  $LM_1$  – region of local modes with bounded changes of angle  $\Theta$ ;  $LM_2$  – unbounded changes of  $\Theta$ .  $\Lambda_0$  is the curve  $\lambda(I_0) = 0$ .

at point  $(2\varepsilon D, -\varepsilon^2 D)$ , as shown in the picture, when the action takes the value  $I = 2\varepsilon D$ . The parabola  $h = -\frac{1}{8}I^2D^{-1}$  crosses the line  $h = -\frac{1}{2}\varepsilon I$  at  $I = 4\varepsilon D$ .

The diagram 2.16 illustrates the birth of LM and vanishing of the symmetrical NM with the increase of energy  $E$ . Really, if the curve  $h(I, E)$  (line  $h_I$ ) lies to the left of line  $h_I$ , it crosses regions  $(NM_A)$  and  $(NM_S)$  only, which correspond to the antisymmetric and symmetric NMs — there are no LMs. With the further increase in energy the curve  $h(I, E)$  moves to the right and at last finds itself between lines  $h_I$  and  $h_{II}$  (line  $h_2$ ). It crosses then three regions  $(NM_A)$ ,  $(NM_S)$ ,  $(LM_1)$ , that is normal modes of both types are possible in the system, and a local mode of type  $(LM_1)$  appears. With the subsequent increase in energy, when the curve  $h(I, E)$  crosses the line  $h_{II}$  and goes to the right of it, a local modes of type  $(LM_2)$  appears, while the normal mode  $(NM_S)$  vanishes. Vibrations of types  $(NM_A)$  and  $(LM_1)$  survive. The figure shows transparently the change of the sign in the inequality  $I_{cr} > I_0$  at the moment when the curve  $h(I, E)$  crosses the line  $h_{II}$ .

The discussion of the phase diagram Fig. 2.16 confirms the analysis of vibrations, which has been presented earlier on the basis of the comparison of phase parameters of the system, depicted in Fig. 2.11, 2.13, and 2.15.

## 2.4 Analysis of phase trajectories with the help of Poincare sections, numerical results

A qualitative analysis of phase trajectories for a system with two degrees of freedom can be conveniently performed with the help of Poincare section. The latter is defined as a crossing of an invariant torus with the trajectory wound up on it with the hyperplane  $q_1 = 0$ . As the torus in the four-dimensional phase space can be determined as the intersection of two hypersurfaces  $F_1(p_1, q_1, p_2, q_2) = 0$  and  $F_2(p_1, q_1, p_2, q_2) = 0$ , their intersection with the hyperplane  $q_1 = 0$  is a line in a four-dimensional space. The projection of this line upon the plane  $(p_2, q_2)$  provides an explicit representation of the vibrations of one of the oscillators (in this case, of the second one). In particular, the difference between the vibrations of a weakly bound oscillator and a free one becomes evident.

Let us construct the Poincare section for a system, characterized by Hamiltonian (2.43). The expressions for the momentum and position of the oscillator  $(p, q)$  can be obtained from Eq. (2.23) with the account of Eq. (2.41), which has been used in the transition from Eq. (2.38) to Eq. (2.43). As a result we obtain:

$$\begin{aligned} p_i &= \sqrt{2I_i} \sin \Phi_i, \\ q_i &= -\sqrt{2I_i} \cos \Phi_i, \quad i = 1, 2. \end{aligned} \quad (2.77)$$

In the derivation of Eq. (2.77) from Eq. (2.23) one should bear in mind the adopted set of units:  $m = \omega_0 = \hbar = 1$  and  $\alpha = (2D)^{-1/2}$ . From the condition  $q_1 = 0$  it follows  $\Phi_1 = \pm\pi/2$ <sup>5</sup>. Choosing  $\Phi_1 = \pi/2$  (that corresponds to the points of intersection with  $p_1 > 0$ ) and expressing the variables  $(J_j, \Phi_j)$  through  $(I, J, \Theta, \Psi)$  with the help of the formula (2.44), we obtain the following equations, which describe parametrically the projection of Poincare section upon the plane  $(p_2, q_2)$ :

$$\begin{aligned} p_2 &= \sqrt{I - J(\Theta)} \cos 2\Theta, \\ q_2 &= -\sqrt{I - J(\Theta)} \sin 2\Theta. \end{aligned} \quad (2.78)$$

The function  $J(\Theta)$  in Eq. (2.78) is determined by the Eq. (2.49). This equation determines the phase trajectory, wound up on a corresponding torus, for each value of energy  $E$  and total action  $I$ . (The projections of such trajectories on the plane  $(J, \Theta)$  for various values of  $(E, I)$  are shown

---

<sup>5</sup>The equation  $q_1 = 0$  has one more solution  $I_1 = 0$ . However this solution is special, as the phase trajectories pass through the point  $I_1 = 0$  only once for  $I = I_0(E)$  (see Section 2.3), whereas the value  $\Phi_1 = \frac{\pi}{2} + 2\pi n$  ( $n$ -integer) is reached periodically with  $T \sim \omega^{-1}$  on each trajectory.

in Figures 2.11, 2.13, and 2.15.) Thus we find that each invariant torus  $(E, I)$  has a Poincare section in correspondence, the projection of which upon the plane  $(p_2, q_2)$  is characterized by equation (2.78)<sup>6</sup>. Due to the weak interaction of oscillators each one will perform many oscillations before the energy of any one of them can change considerably (if there will be any change at all). For that reason the shape of the projection of Poincare section provides the information whether any energy transfer from one oscillator to the other takes place in the entire infinite time interval. If on the curve Eq. (2.78) there are points  $(p_2, q_2)$  where the energy of the second oscillator is much smaller (greater) than in other points of the curve, then the transition of energy takes place, and the vibrations are of normal type (NM). If there are no such points, then there is no energy transfer, and the vibration is a local mode (LM).

Let us calculate the Poincare section for a system of Morse oscillators (2.38) for the following values of the parameters:

$$D = 1, \varepsilon = 0.014, \quad (2.79)$$

and for two values of energy:

$$E_1 = 0.01, E_2 = 0.1. \quad (2.80)$$

Hamiltonian (2.38) has been used for model calculations of local and normal modes of stretching vibrations in the molecule  $XY_2$  ([52]). The applicability of this Hamiltonian for the calculation of stretching vibrations in the molecule without the account of the effect of the angle between the bonds and of the molecular rotation has been proved in [53]. Due to the smallness of  $\varepsilon$  and  $E/D$  the Hamiltonian (2.38) can be reduced to the form (2.45), as it has been shown above. In the calculation of  $J(\Theta)$ , which enters Eq. (2.78), we use the relations (2.56) and (2.57). The latter can be conveniently expressed in the following way:

$$\sqrt{I^2 - J^2} = 2\varepsilon D \left[ \cos(2\Theta) \pm \sqrt{\cos^2(2\Theta) - 4\gamma} \right], \quad (2.81)$$

where  $\gamma(I) = -\frac{\lambda(I)}{2\varepsilon^2 D} \leq \frac{1}{4}$ . The two signs in Eq. (2.81) signify the possibility that different pieces of phase curves might be described by various branches  $J_{\pm}^2(\Theta)$  of the multi-valued analytical function  $J^2(\Theta)$ <sup>7</sup>. One can show that local modes with no limits for the change of phase  $\Theta$  are described by the branch  $J_+^2(\Theta)$ , whereas the local modes with bounded changes of the angle  $\Theta$  are characterized by both branches  $J_{\pm}^2(\Theta)$  (Fig. 2.12, 2.15). As far as the symmetric normal vibrations (NMs) are concerned, in the case  $I_{\max}(E) \geq 2\varepsilon D$  all their phase trajectories consist of two branches  $J_{\pm}^2(\Theta)$  (Fig. 2.13),

<sup>6</sup>Another branch of the section corresponds to  $\Phi_1 = -\pi/2$  ( $p_1 < 0$ ).

<sup>7</sup>Analytical branches differing by sign  $\pm\sqrt{J^2(\Theta)}$  always exist, as it follows from the invariance of the Hamiltonian (2.45) with respect to the transformation  $J \rightarrow -J$ .

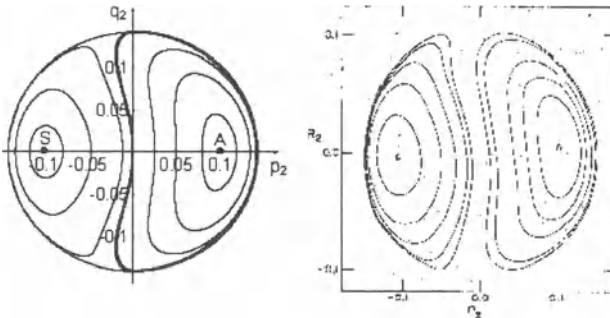


Figure 2.17: Poincare section: (a) analytical solution for Hamiltonian (2.43); (b) numerical calculation for Hamiltonian (2.38) from Ref. [52]. Parameters chosen:  $\epsilon = 0.014$ ,  $D = 1$ ,  $E = 0.01$ ,  $p_1 > 0$ .

$I_{NMA} =$	$p$	0.141	0.007	-0.002	-0.004	-0.001	0.003	0.010
0.010015	$q$	0.000	$\pm 0.129$	$\pm 0.115$	$\pm 0.100$	$\pm 0.082$	$\pm 0.058$	0.000
$I_{NMS} =$	$p$	-0.141	-0.042	-0.037	-0.032	-0.026	-0.019	-0.010
0.010035	$q$	0.000	$\pm 0.122$	$\pm 0.109$	$\pm 0.095$	$\pm 0.078$	$\pm 0.055$	0.000

Table 2.1: The coordinates  $(p_2, q_2)$  of the Poincare section. The energy is  $E = 0.01$ , and  $I_0 = 0.01$ , where  $I_0$  is the value of the action on the separatrix line,  $I_{NMA} < I_0 = 0.0100251 < I_{NMS}$ .

while in the case  $I_{\max}(E) \leq 2\epsilon D$  some part of phase trajectories has two branches, and some part — one branch  $J_-^2(\Theta)$  (Fig. 2.11).

The results of the calculation for Poincare sections according to formulas (2.78) and (2.81) with parameters (2.79) – (2.80) for several characteristic invariant tori are provided in Tables 2.1 and 2.2. The corresponding figures  $p_2(q_2)$  are presented in Figs. 2.17 and 2.18, along with the curves of the section which has been calculated numerically on the basis of the Hamiltonian (2.38) in [52]. The qualitative agreement of the curves obtained with the help of the method of averaging, and of the curves obtained numerically from the Hamiltonian (2.38) is transparent.

The quantitative discrepancy between the two curves is of the order of 20 %, as it can be seen from Figs. 2.17 and 2.18. Such a discrepancy agrees with the reciprocal error, introduced by the neglection of terms  $\sim \sqrt{\frac{I}{I_0}} \sim 0.1$  in the transition from Eq. (2.38) to Eq. (2.43). The curves in Figs. 2.17 and 2.18 are symmetrical with respect to  $p_2$ . This owes to the use of the expressions (2.7) for the momentum  $p_2$  and position  $q_2$  of the harmonic oscillator through the variables "action-angle"  $(I_2, \Phi_2)$ . The

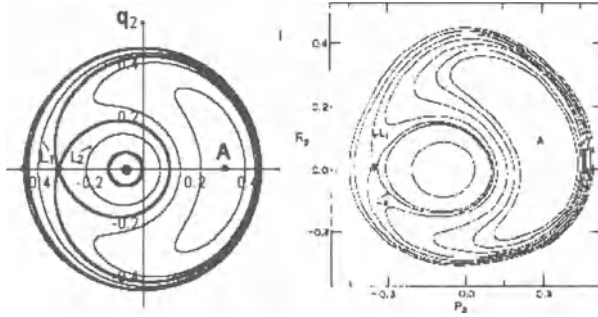


Figure 2.18: Poincare section: (a) analytical solution for Hamiltonian (2.43); (b) numerical calculation for Hamiltonian (2.38) from Ref. [52]. Parameters chosen:  $\varepsilon = 0.014$ ,  $D = 1$ , energy  $E = 0.1$ ,  $p_1 > 0$ .

$I_{NM_A} =$	$p$	0.342	0.322	0.308	0.298	0.292	0.289	0.290
0.100604	$q$	0.000	$\pm 0.087$	$\pm 0.106$	$\pm 0.110$	$\pm 0.101$	$\pm 0.078$	0.000
$I_{LM_2} =$	$p$	-0.159	-0.130	-0.101	-0.070	-0.039	-0.007	0.025
0.102531	$q$	0.000	$\pm 0.065$	$\pm 0.084$	$\pm 0.090$	$\pm 0.086$	$\pm 0.069$	$\pm 1.938$

Table 2.2: The coordinates  $(p_2, q_2)$  of the projection of Poincare section upon the plane  $(p_1 = q_1 = 0)$ . The energy is  $E_1 = 0.1$ , and  $I_{NM_A} = 0.999I_{cr}$ ,  $I_{LM_2} = 0.999I_0$ , where  $I_{cr} = 0.100705$ ,  $I_0 = 0.102633$ , are the values of the action on the separatrix lines which separate the normal modes  $NM_A$  from local  $LM_2$  ones, and  $LM_2$  from  $LM_1$  correspondingly.

latter is possible due to the smallness of the action ( $\frac{I}{\hbar} \ll 1$ ). The rigorous formulas for Morse oscillator and for the dependence of  $(p_2, q_2)$  upon  $(I_2, \Phi_2)$  with the subsequent use of the Hamiltonian (2.38) breaks that symmetry, as apparent from Figs. 2.17 and 2.18 (curves b). It can be seen that for low excitations  $(E_2/D) = 0.01$  local modes are absent (Fig. 2.17). This fact agrees with the condition  $E \sim I_{\max} \leq 2\varepsilon D$  (Eq. (2.76)). The energy of the oscillator along the section curve changes from nearly the value of the total energy  $E \sim 0.01$  to the value, significantly inferior to 0.01. The oscillator energy difference  $(E_1 - E_2)$  at least changes sign along the section curve. For example, the energy of the second oscillator in Fig. 2.17 in extreme right, upper and lower points of the curve  $I = I_0$  is  $\sim 0.01$ , while in the extreme left point of the curve it is much smaller than  $10^{-2}$ <sup>8</sup>. The same is true for the rest of the curves of Poincare sections in Figs. 2.18. It means, that

<sup>8</sup>The energy is calculated according to Eq. (2.38) with  $p_1 = q_1 = 0$ , while the values of  $p_2, q_2$  we take from Table 2.1. We remind, that  $p_2$  and  $q_2$  in Figs. 2.17 and 2.18 are measured in the units  $\alpha = D = m = 1$ .

the considered vibration is delocalized. The curves close to the separatrix line, which separates the  $NM_A$  modes, characterize the beat process, when the energy flows from one oscillator to the other completely. The curves  $I = I_{\min}$  and  $I = I_{\max}$  correspond to periodic orbits with oscillations in phase – point (S) and in opposite phase – point (A). It can be seen from Figs. 2.17, 2.18 that the energy of the second oscillator at these points is equal to  $E_2 \sim 0.005$  or  $0.05$  correspondingly, that is to one half the energy of the system. Thus, the points A with  $I = I_{\min}$  and S with  $I = I_{\max}$  correspond to oscillations with the total energy distributed equally among the two oscillators at any time. On the other curves corresponding to normal modes some part of the energy flows constantly from one oscillator to the other. More to it, on the curves close to separatrix lines the amount of the energy in the exchange is close to the total energy;  $\max |E_1 - E_2| \rightarrow E$  when the phase curve approaches the separatrix. In other words, in the vicinity of the separatrix lines the normal vibrations are represented by beats, while close to the periodic orbits A and S these are the states with nearly equal vibrational energies on each of the two oscillators at any time. The general feature of vibrations of NM type is the equivalence of vibrational states of oscillators with the accuracy up to a time shift. It is possible to determine analytically whether the NM vibration will occur with the given initial values of the moment and position of nonlinear oscillators, governed by Eq. (2.43), with the help of the following method. With the use of the formula Eq. (2.19) one has to calculate the total action  $I = I_1 + I_2$  and to verify the inequality  $I < I_{cr}(E)$  with Eq. (2.62). If the latter is satisfied, then the normal vibration takes place (NM), if the inequality is violated, then the vibration is local (LM).

Let us analyze next the curves of the section, depicted in Fig. 2.18, bearing in mind the properties of LMs and NMs. The energy is  $E = 0.1 > 4\varepsilon D(1 - \varepsilon) = 0.0591$ , and consequently the condition (2.74) for the splitting off of the local mode with unbounded changes of the angle  $\Theta$  (region  $LM_2$ ) is satisfied. The corresponding phase curves are shown in Fig. 2.15. The region  $NM_A$  between the curves  $L_1, L_2$  in Fig. 2.18 corresponds to the region of normal antisymmetric vibrations  $NM_A$  in Fig. 2.15. The typical curve of the section in this area has a sickle-like form. The points, situated further away from the origin, correspond to the states with higher energy on the second oscillator, while the points, closer to the origin, corresponds to lower energy on it. As the total action  $I$  tends to the minimal possible value  $I_{\min}$ , these curves reduce to a point (point A in the figure), which corresponds to the vibration of oscillators in opposite phase ( $2\Theta = \Phi_1 - \Phi_2 = \pi$ ). In this case, as noted before, the energy of the oscillators remain equal during all the time with the accuracy up to the interaction energy  $\sim \varepsilon E$ . The region of local vibrations with the unbounded change of phase  $\Theta$ <sup>9</sup> is bounded by

---

<sup>9</sup>In Figs. 2.17 and 2.18 the angle  $\Theta$  coincides with half the polar angle with the inverted

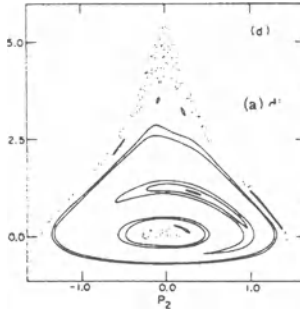


Figure 2.19: Poincare section for Hamiltonian (2.38) from Ref. [52] with energy  $E = 0.99D$  and other parameters same as in Fig. 2.17, 2.18. Remnants of destroyed toruses are seen clearly in the upper part of the plot.

the curves  $I = I_0$ ,  $I = I_{cr}$ , and its denoted by  $LM_2$  in Fig. 2.15. The points between the curves  $I_0$  and  $I_{cr}$  correspond to the states with higher energy on the first oscillator or on the second one. The regions of local vibrations with limited changes of the phase, which have been marked in Fig. 2.15 as  $LM_1$ , correspond to the region bounded by the curve  $I_0$  close to the origin or by the big circle with the center in the origin, Fig. 2.18.

A rough estimate of the areas in Fig. 2.18 belonging to the regions  $NM_A$ ,  $LM_2$  and  $LM_1$  give:  $S_{NM_A} : S_{LM_2} : S_{LM_1} = 0.61 : 0.33 : 0.06$ . Thus upon excitation to energy  $E = 0.1$  the system finds itself in the states  $NM_A$ ,  $LM_2$  and  $LM_1$  with the probabilities 0.61, 0.33 and 0.06 correspondingly. We stress, that the curves of Poincare section are not the phase trajectories for the second oscillator. In fact they may represent the set of points in phase space  $(p_2, q_2)$ , where the second oscillator finds itself, when the first oscillator is in  $q_1 = 0$  with  $p_1 > 0$ . If we observe the vibrations with time and fix the points  $(p_2, q_2)$  each time when  $q_1 = 0$ ,  $p_1 > 0$ , we will obtain the sequence of points  $p_2^{(n)}, q_2^{(n)}$ , which fill densely the section curves, depicted in Figs. 2.17 and 2.18. The distance  $d_{n,n+1}$  between the consecutive points  $(p_2^{(n)}, q_2^{(n)})$  and  $(p_2^{(n+1)}, q_2^{(n+1)})$  will be of order  $\varepsilon$  for normal modes ( $NM_A$ ), and  $\frac{\omega_1 - \omega_2}{\omega_0}$  for local modes with the unbounded change of phase  $\Theta$  ( $LM_2$ ). For the mode  $LM_1$  the distance between consecutive points is of the order of  $\sim I/D$ . These estimates are obtained on the basis of the calculation of the period  $T$  for phase trajectories (Hamiltonian (2.46)) and of the relation  $d_{n,n+1} \sim T^{-1}$ .

The presented estimate of the distance  $d_{n,n+1}$  for the  $LM_1$  leads to the in-

teresting conclusion that the emergence of  $\text{LM}_1$  provides the physical reason for stochastization of vibrations in some region of phase space (region  $\text{LM}_1$  in Fig. 2.18). Really the area of the region  $\text{LM}_1$  is of the order of  $\varepsilon^2$ , and consequently the curvature of the Poincare section is  $\sim \varepsilon^{-1}$ , which means that the curves are curved strongly provided  $\varepsilon$  is small enough. Next, as the distance  $d_{n,n+1}$  satisfies the inequality  $d_{n,n+1} \sim I/D \gg \varepsilon$ , the broken line through some number of consecutive points  $(p_2^{(n)}, q_2^{(n)})$  can not approximate any curve by the Poincare section. Thus, if we observe the position of the second oscillator in phase space during the period of time  $\varepsilon^{-1} \gg t \gg 2\pi/\omega_0$  at intervals  $2\pi/\omega_0$ , its motion will look like a chaotic random walk<sup>10</sup>. The section curves, corresponding to normal modes  $\text{NM}_A$  and the curves of local modes  $\text{LM}_2$ , lying close to the former, are, on the contrary, approximated by the broken lines through consecutive points  $(p_2^{(n)}, q_2^{(n)})$  in a nice way, as the distance is small then, while the curvature is of the order of 1. Consequently, an analogous measurement of the position  $(p_2, q_2)$  at time intervals  $2\pi/\omega_0$  during the period  $t \ll \varepsilon^{-1}$  provides a smooth curve  $p_2(q_2)$ . It should be noted, that the high resonances due to the interaction of oscillators lead to stochastization of vibrations (destruction of unperturbed tori) in the vicinity of closed trajectories. This is a general rule, in fact [44, 45]. Whereas for a system with two degrees of freedom  $n = 2$ , the phase trajectories remain in the close vicinity of the unperturbed trajectory, in systems with  $n > 2$ , on the contrary, they go far away from each other, so that the energy spreads over large regions of the iso-energetic surface in phase space. This can be seen clearly in Fig. 2.19, reproduced from [52], where the Poincare section for a system with Hamiltonian (2.38) for  $E/D = 0.99$  is shown. Some part of the trajectories demonstrate a highly irregular behavior (stochastic), so that the Poincare section constitutes a set of points that do not belong to any smooth curve. The reason for that lies in the fact that for  $E = 0.99D$  resonances of the type  $\omega_1 : \omega_2 \sim 10 : 1$  should be taken into account, as their influence in the first order in  $\varepsilon$  is in fact of the same magnitude, as that of the resonance  $1 : 1$ . In other words, terms of the order of  $I/2D$  in the expression of momentum through the action variables cannot be neglected.

Motion with bounded changes of the angle  $\Theta$  (modes  $\text{NM}_A$  and  $\text{LM}_1$  in Figs. 2.17 and 2.18) in mechanics is termed phase vibration. The trajectory of the latter in phase space winds around the closed trajectory. To put it rigorously, the trajectory of a phase vibration winds around a torus, the axis of which is constituted by a closed trajectory.

The position of invariant tori and the projection of their sections, described in the present Section, are equivalent to usual tori of a 3-dimensional

---

<sup>10</sup>In the case of a single oscillator such an experiment would produce a steady point  $(p_2, q_2)$ . In the case of a perturbation, which varies slightly during the period  $2\pi/\omega_0$ , a smooth curve  $p_2(q_2)$  would be produced, which signifies a small displacement of the oscillator in phase space during the period of oscillation.

Eucledean space, enclosed one into another<sup>11</sup>. Thus these tori can be imagined as usual two-dimensional tori in a usual three-dimensional space. tori with elliptic-like section correspond to local modes, while those with sickle-like section correspond to normal modes with resonant frequencies.

---

<sup>11</sup>This fact is a consequence of the topological equivalence of a salient hypersurface with an excluded point to a hyperplane.

## Chapter 3

# Coupled nonlinear oscillators: formation and decay of local modes

In this Chapter we study the conditions for the appearance and decay of Local Modes (LMs) and Normal Modes (NMs) in systems of equivalent weakly interacting nonlinear oscillators. A topological definition of LMs and NMs is provided, based on the study of the structure of phase space in the vicinity of the considered trajectory. According to such a definition an NM is a set of resonant trajectories  $n_i\omega_i = n_j\omega_j$  with its close vicinity. The sizes of such resonant regions, or in other words, the widths of the resonances are found. The definitions and the applied methods are based on the theory of canonical transformations and on the method of averaging developed in Chapter 2. With the help of the method of averaging the problems, considered in this Chapter, are reduced to a nonlinear Hamilton system with two degrees of freedom. These are studied with the help of Poincare surfaces of section (Poincare map). These are intersections of two-dimensional tori (with the studied trajectories on them) with the three-dimensional manifold, which fixes one of the coordinates of the system (for example,  $q_1 = 0$  and  $p_1 > 0$ ). In the 4-dimensional phase space the Poincare map is a one-dimensional manifold, the projection of which on the plane ( $p_2, q_2, p_1 = q_1 = 0$ ) is of interest to us. The plots of Poincare surfaces of section reveal clearly the changes of tori during the transition from local trajectories to the resonant trajectories of normal modes.

The background, required for the proper understanding of the material in this Chapter is provided in most books on classical mechanics, including those, cited in the introduction to the previous Chapter, for example, [7, 40, 41]. The construction of phase trajectories and the determination of stable points and saddle points for the averaged Hamiltonian require the basic knowledge of mathematical analysis and analytical geometry within the

undergraduate course. The required material is reviewed in brief, for example, in the handbook [54]. For the proper understanding of Sections 3.4 and 3.5 the knowledge of the theory of unitary transformations in quantum mechanics is required, along with the relation of the latter to the canonical transformations in classical mechanics. This can be found, for example, in Refs. [57] and [58]. We note also, that the basics of operator transformations, used in Sections 3.4 and 3.5, are provided also in the textbooks on the theory of operators in Hilbert space, or in any comprehensive handbook on the theory of matrices.

### 3.1 Two weakly coupled nonlinear oscillators: decay of normal modes

Let us consider the disappearance of normal modes in the system of two Morse oscillators when the interaction between them tends to zero,  $\varepsilon \rightarrow 0$ . In that case the straight lines  $\pm \frac{\varepsilon I}{2}$  (see Fig. 2.16) approach each other and coincide with the  $x$  axis for  $\varepsilon = 0$ . Then the regions  $(NM_A)$  and  $(NM_S)$  in Fig. 2.16 vanish and the area of local modes  $(LM_2)$  survives only. The latter is bounded by the axis  $(I)$  and by the curve  $\Lambda_0$  ( $h = -I^2/8D$ ), which approaches the curve  $\tilde{H}_{\min}(I)$ . With the decrease of  $\varepsilon$  the greater part of the curves  $h(I, E)$  from the physically accessible region goes over into the region of local modes  $(LM_2)$ , until they find themselves there entirely at  $\varepsilon = 0$  (see Fig. 2.16). The transformation of phase portraits of the system in the variables  $(J, \Theta)$  and  $(p_2, q_2)$  for  $\varepsilon \rightarrow 0$ , when the normal mode vanishes, is shown in Figs. 3.1 - 3.6.

The phase curves for the case when only normal modes exist are shown in Fig. 3.1. This condition holds for  $I_{\max}(E) < 2\varepsilon D$ , and consequently

$$I_{\min}(E) < I_0(E) < I_m(E) < I_{cr}(E) = I_{\max}(E) < 2\varepsilon D. \quad (3.1)$$

Here the quantities  $I_0$  and  $I_{cr}$  are determined by the equations (2.72) and (2.73), while  $I_m(E)$  corresponds to the value of action, which separates the salient and concave phase trajectories of symmetric normal modes  $NM_S$  (Fig. 3.1(a)). The emergence of the local mode LM with a bounded variation of angle  $\Theta$  is depicted in Fig. 3.2.

This happens at

$$I_m(E) = I_{cr}(E) = I_{\max}(E) = 2\varepsilon D. \quad (3.2)$$

In that case the symmetric normal mode  $NM_S$  has no salient phase curves at all, which can be seen clearly from the figure. With the subsequent decrease of  $\varepsilon$ , when the inequality holds

$$2\varepsilon D < I_{\max}(E), \quad I_0(E) \leq 4\varepsilon D,$$

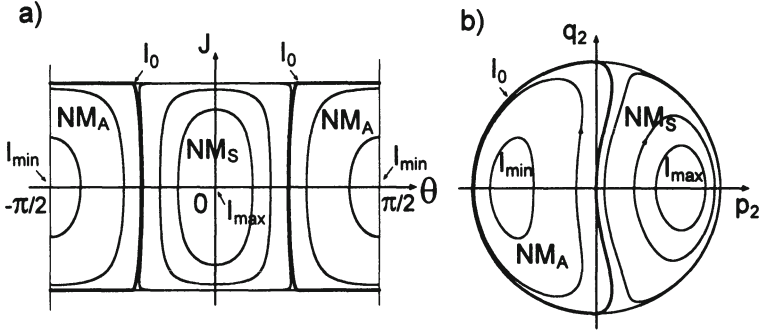


Figure 3.1: (a) Phase curves of the system (2.43) in the variables action – angle ( $J - \Theta$ ). (b) Poincaré section for the same system in local variables ( $q_1 = 0, p_1 > 0$ ). Parameters chosen:  $\varepsilon = 0.014, D = 1, E = 0.01D$ , so that  $I_{\max}(E) < 2\varepsilon D$ . Only normal symmetrical and antisymmetrical vibrations exist in this case.

and consequently when the following relation is true

$$I_{\min}(E) < I_0(E) < I_{cr}(E) < I_{\max}(E), \quad (3.3)$$

both symmetric and antisymmetric normal vibrations along with local modes having bounded changes of phase  $\Theta$  are possible (Fig. 3.3).

The appearance of the local mode  $LM_2$  with an unbounded change of phase  $\Theta$  is shown in Fig. 3.4.

This occurs with the realization of the following relations:

$$I_0(E) = I_{cr}(E) = 4\varepsilon D < I_{\max}(E). \quad (3.4)$$

Lowering the interaction strength  $\varepsilon$  further, we arrive at the situation, when there are two local vibrations  $LM_1$  and  $LM_2$ , and one normal vibration  $NM_A$ . The symmetric normal mode is absent (Fig. 3.5).

Then the following inequalities hold:

$$4\varepsilon D < I_{cr}(E, \varepsilon) < I_0(E) < I_{\max}(E, \varepsilon). \quad (3.5)$$

And, last, for  $\varepsilon = 0$  the normal mode  $NM_A$  and the local mode  $LM_1$  both disappear and only the  $LM_2$  mode with an unbounded variation of angle  $\Theta$  for  $J \neq 0$  and  $\Theta = const$  at  $J = 0$  is left (Fig. 3.6).

Then the following equalities are true:

$$I_{cr}(E) = I_{\min}(E), \quad I_0(E) = I_{\max}(E). \quad (3.6)$$

The phase portraits of the system, depicted in Figures 3.1 - 3.6 reveal clearly the fact, that all the vibrations can be classified into two types:

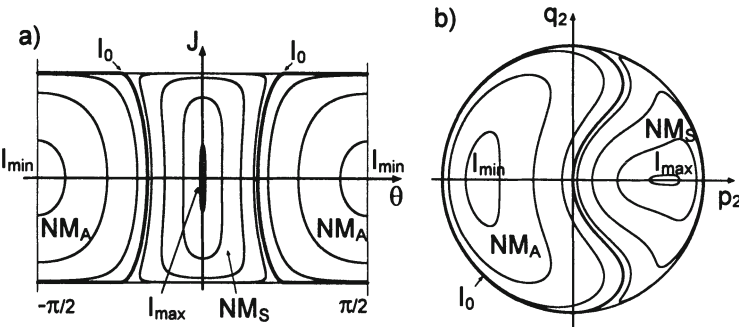


Figure 3.2: (a) Phase curves of the system (2.43) in the variables action – angle ( $J - \Theta$ ). (b) Poincare section for the same system in local variables ( $q_1 = 0, p_1 > 0$ ). Energy is chosen to satisfy  $I_{\max}(E) = 2\varepsilon D$ , when the first local mode appears in the continuum of normal symmetrical and antisymmetrical vibrations.

first type is the vibration with  $J$  changing from  $-J_{\max}$  to  $J_{\max}$ ; the second type is the one, when  $J$  keeps its sign, ( $J \neq 0$ ). In the first case the energy difference flows completely from one oscillator to the other, and the vibration is delocalized. These vibrations we classify as normal modes, as they prevail for large enough  $\varepsilon$ , when the picture of normal vibrations is obviously valid.

In the vibrations of the second type, on the contrary,  $J \neq 0$ , and the energy difference is localized on one oscillator without being transferred to the other one. Such vibrations are dominant for  $\varepsilon$  small enough, and for  $\varepsilon = 0$  they survive solely. Obviously, it should be exactly that way, as the vibrations of noninteracting oscillators are always of local type. Consequently, the second type of vibrations we denote as a local mode.

The consideration of phase curves in Figures 3.1 - 3.6 suggests the idea of a topological determination of a local mode as such a motion, when the corresponding tori can be obtained by continuous deformation of the unperturbed ones. Obviously the tori in Fig. 3.5(b), which are enclosed one in another and contain the point  $p_2 = q_2 = 0$ , can be obtained from the tori in Figure 3.6(b) by continuous deformation. At the same time the tori of normal modes, embracing the point  $(p_2(I_{\min}), q_2(I_{\min}))$ , have no topologically equivalent ones among the unperturbed tori (see Figs. 3.5 and 3.6). On the other hand, the tori of normal modes  $NM_A$  (Fig. 3.5(b)) can obviously be obtained by continuous deformation from the tori of  $NM_A$ , depicted in Fig. 3.1(b). The latter can be attributed to purely harmonic modes, as they correspond to the limiting case  $E/\varepsilon D \rightarrow 0$ , when vibrations are harmonic (see Fig. 2.17).

Such representations can be backed up by the following more rigorous

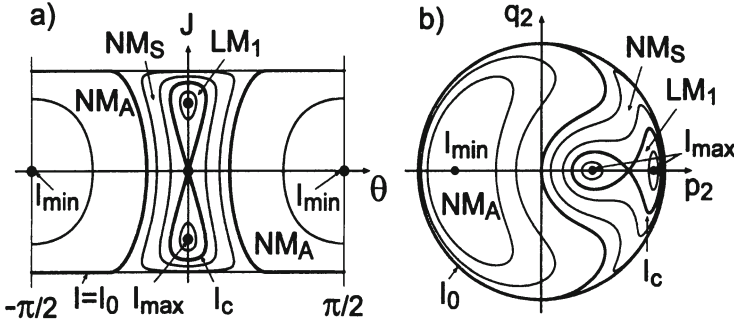


Figure 3.3: (a) Phase curves of the system (2.43) in the variables action – angle ( $J - \Theta$ ). (b) Poincare section for the same system in local variables ( $q_1 = 0$ ,  $p_1 > 0$ ). Parameters chosen:  $E = 0.04D$ ,  $\varepsilon = 0.015$ , so that  $2\varepsilon D < I_{\max}(E)$  and  $I_0(E) < 4\varepsilon D$ . Normal symmetrical and antisymmetrical vibrations exist along with the local mode  $LM_1$ .

considerations.

The tori of local modes are nonresonant ( $\omega_1 \neq \omega_2$ )<sup>1</sup>, and according to KAM theory they can be obtained from unperturbed tori by slight deformation ( $\varepsilon$  is small). Consequently the family of nonresonant unperturbed tori, enclosed one into another, are deformed slightly under the perturbation, and transform into a topological family of LM tori (see Fig. 3.5(b) and 3.6(b)). The tori of normal modes  $NM_A$  are enclosed one into another and are situated all in the space between the tori of local modes (Fig. 3.5). The axis line of this family of tori is a closed trajectory, which is formed from the resonance torus due to the decay under the action of the perturbation,  $\omega_1 = \omega_2$  (point  $I_{\min}$  in Fig. 3.5). This trajectory encircles in a spiral the family of enclosed LM tori – one rotation along the meridian and one rotation in latitude. It is clear, that the NM tori having this trajectory as an axis line and the LM tori, which are embraced by it are topologically non-equivalent, that is they cannot be transformed continuously one into another (Fig. 3.5).

Thus a genealogical relation between the form of the torus and the type of unperturbed vibration can be traced: 1) tori with the elliptical form of Poincare surfaces of section come from nonresonant tori of local vibrations when  $E/\varepsilon D \rightarrow \infty$ ; 2) tori with sickle-like sections originate from pure harmonic modes with  $E/\varepsilon D \rightarrow 0$ .

As a result, the following definition of LMs and NMs in the system of weakly interacting nonresonant oscillators can be provided.

<sup>1</sup> At present we neglect the higher resonances, as in the considered system they are revealed at considerably longer times, much greater than  $\varepsilon^{-1}$ .

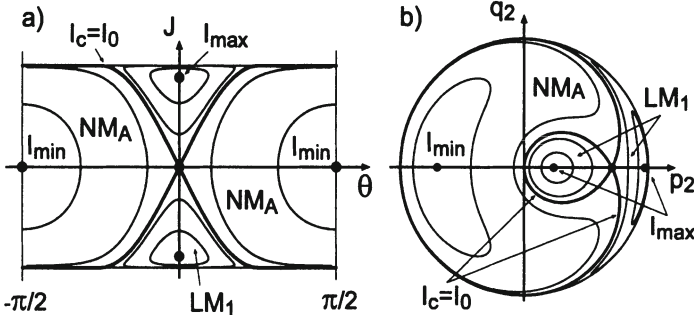


Figure 3.4: (a) Phase curves of the system (2.43) in the variables action – angle ( $J - \Theta$ ). (b) Poincare section for the same system in local variables ( $q_1 = 0, p_1 > 0$ ). Energy  $E$  chosen to satisfy  $I_0(E) = 4\varepsilon D$ , and  $\varepsilon = 0.015$ . The normal symmetrical mode disappears and the local mode  $LM_2$  with an unbounded change of angle  $\Theta$  appears.

Local modes are formed with the help of a slight deformation of non-resonant tori by a perturbation. If interaction is not weak, a sequence of small deformations is needed to obtain a local vibration from the initial non-resonant torus. tori corresponding to normal modes emerge in the place of resonant tori that decay under the action of the perturbation.

From this point of view any nonresonant torus generates a local vibration. Any resonant torus gives birth to normal vibrations, which in the present situation are in fact phase vibrations (any resonance is the source of phase vibrations [7]). Such an interpretation of local and normal modes has been presented in Ref. [52]. Within such an approach the width of the resonance is defined in a natural way as function of the phase volume, occupied by the tori of normal modes, which emerge in place of the resonant tori that have decayed (see below). The knowledge of the resonance width is necessary for the calculation of the lifetime of vibrational modes in the study of vibrational relaxation.

### 3.2 Multi-oscillator systems: local modes' and normal modes' representations

In this Section, following Ref. [52], we will simplify the problem of the determination of the type of vibrations (LM or NM) in a system of  $N$  weakly bound nonlinear oscillators by reducing it to the problem of two oscillators, that has been considered above in Sections 2.3 - 3.1.

Let us consider a system of Morse oscillators with the Hamiltonian:

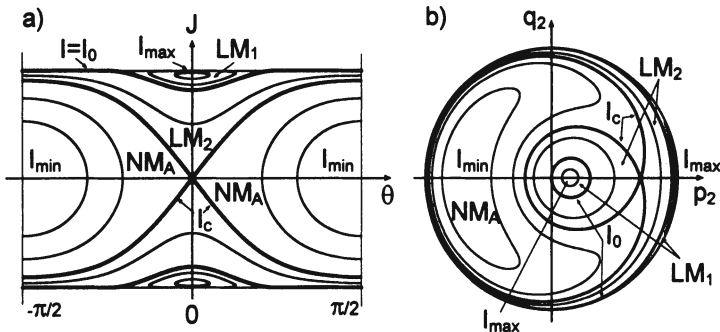


Figure 3.5: (a) Phase curves of the system (2.43) in the variables action – angle ( $J - \Theta$ ). (b) Poincaré section for the same system in local variables ( $q_1 = 0, p_1 > 0$ ). Parameters chosen:  $E = 0.1D, \varepsilon = 0.015$ , so that  $I_0(E) > 4\varepsilon D$ . The normal antisymmetrical vibrations exist along with local modes with bounded  $LM_1$  and unbounded  $LM_2$  changes of angle  $\Theta$ .

$$H = \left\{ \frac{1}{2} \sum_1^N G_{ii} p_i^2 + \sum_1^N D_i [1 - \exp(-\alpha_i q_i)]^2 \right\} + \sum_{i>j}^N G_{ij} p_i p_j + \sum_{i>j}^N K_{ij} q_i q_j = H_0 + \sum_{i>j} H_{ij}^{(k)} + \sum_{i>j} H_{ij}^{(p)}. \quad (3.7)$$

This Hamiltonian can be used for the description of valence-bond stretching vibrations in polyatomic molecules, when the anharmonicity of the vibration exceeds greatly the interaction between the bonds:

$$\frac{|G_{ij}|^2}{G_{ii}G_{jj}} \ll 1, \quad \frac{K_{ij}^2}{(D_i\alpha_i^2)(D_j\alpha_j^2)} = \frac{K_{ij}^2}{K_{ii}K_{jj}} \ll 1.$$

It has been used as a model Hamiltonian in many papers (for example, in Ref. [55] and [52]) for the calculation of stretching vibrations in the molecule of water  $H_2O$ . The correctness of such an approach has been proved in Ref. [53]. As it has been shown in Ref. [52], the delocalized vibration (a normal mode), viewed up to time

$$t \ll \left| \frac{G_{ii}}{G_{ij}} \omega^{-1} \right|, \left| \frac{K_{ii}}{K_{ij}} \omega^{-1} \right|,$$

is nothing but a vibration with resonant frequencies  $\omega_i = \omega_j$ . This fact enables the reduction of the problem of local vibrations to that of the existence (or lack) of resonance  $\omega_i = \omega_j$  between any two stretching vibrations.

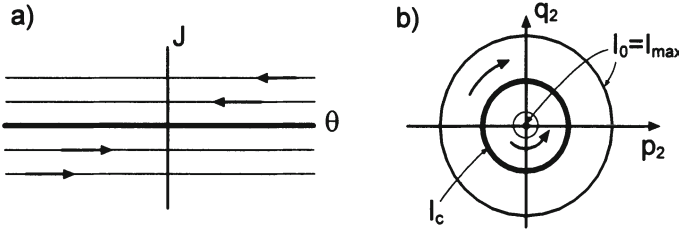


Figure 3.6: (a) Phase curves of the system (2.43) in the variables action – angle ( $J - \Theta$ ). (b) Poincare section for the same system in local variables ( $q_1 = 0, p_1 > 0$ ). Interaction strength between the oscillators  $\varepsilon$  is chosen to be zero. Only local modes  $LM_2$  with unbounded changes of angle  $\Theta$  are left for  $J \neq 0$ . In the case  $J = 0$  a set of periodic trajectories with  $\Theta = const$  exist.

It turns out, that in the vicinity of the resonant trajectory the vibration is of a delocalized nature. Really, for  $\omega_i \sim \omega_j$  the vibrations reveal a beat-like effect, and the excess of the energy is transferred periodically from one oscillator to another. With the help of the method of averaging the volume of the vicinity of resonant trajectory  $\omega_1 = \omega_2$  where vibrations have beat-like character can be found. Substituting Eq. (2.23) into Eq. (3.7) we obtain the following expressions for  $H_0$ ,  $H_{ij}^{(p)}$  and  $H_{ij}^{(k)}$ :

$$\begin{aligned} H_0 &= \frac{1}{2} \sum_1^N \omega_{i0} \left( 2 - \frac{I_i}{I_i^b} \right) I_i, \\ H_{ij}^{(k)} &= G_{ij} \frac{\omega_{i0} \omega_{j0} \lambda_i \lambda_j}{G_{ii} G_{jj} \alpha_i \alpha_j} \frac{\sqrt{1 - \lambda_i^2} \sqrt{1 - \lambda_j^2} \sin \Phi_i \sin \Phi_j}{\left( 1 - \sqrt{1 - \lambda_i^2} \cos \Phi_i \right) \left( 1 - \sqrt{1 - \lambda_j^2} \cos \Phi_j \right)}, \\ H_{ij}^{(p)} &= \frac{K_{ij}}{\alpha_i \alpha_j} \ln \left[ \frac{1 - \sqrt{1 - \lambda_i^2} \cos \Phi_i}{\lambda_i^2} \right] \ln \left[ \frac{1 - \sqrt{1 - \lambda_j^2} \cos \Phi_j}{\lambda_j^2} \right]. \end{aligned} \quad (3.8)$$

Here  $\lambda_i = \left( 1 - \frac{I_i}{I_i^b} \right)$ , and, as compared to Eq. (2.23), the substitution  $m_i \rightarrow G_{ii}^{-1}$  has been made. The functional dependence of the frequency on the action  $\omega_j (I_j)$  is determined by Eq. (2.20); the maximal value of the action  $I_i^b$  — by Eq. (2.21). Expanding  $H_{ij}^{(k)}$  and  $H_{ij}^{(p)}$  in Fourier series in the angular variables  $\Phi_i$  and  $\Phi_j$ , re-grouping and summing up partially the terms of the resultant series, we obtain the following expressions for the interaction:

$$\begin{aligned}
H_{ij}^{(k)} &= \frac{2G_{ij}\omega_{i0}\omega_{j0}\lambda_i\lambda_j}{G_{ii}G_{jj}\alpha_i\alpha_j} \\
&\times \sum_{n_i, n_j} \left\{ \frac{1 - a_i^{n_i} a_j^{n_j} \cos(n_i\Phi_i - n_j\Phi_j)}{1 - 2a_i^{n_i} a_j^{n_j} \cos(n_i\Phi_i - n_j\Phi_j) + (a_i^{n_i} a_j^{n_j})^2} \right. \\
&\quad \left. - \frac{1 - a_i^{n_i} a_j^{n_j} \cos(n_i\Phi_i + n_j\Phi_j)}{1 - 2a_i^{n_i} a_j^{n_j} \cos(n_i\Phi_i + n_j\Phi_j) + (a_i^{n_i} a_j^{n_j})^2} \right\}, \\
H_{ij}^{(p)} &= \frac{K_{ij}}{\alpha_i\alpha_j} \left\{ \ln\left(\frac{2\lambda_i^2}{1 + \lambda_i^2}\right) \ln\left(\frac{2\lambda_j^2}{1 + \lambda_j^2}\right) \right. \\
&\quad - \ln\left(\frac{2\lambda_i^2}{1 + \lambda_i^2}\right) \ln(1 - 2a_j \cos\Phi_j + a_j^2) \\
&\quad - \ln\left(\frac{2\lambda_j^2}{1 + \lambda_j^2}\right) \ln(1 - 2a_i \cos\Phi_i + a_i^2) \\
&\quad + \sum_{n_i, n_j} \frac{2}{n_i n_j} \sum_{l=1}^{\infty} \frac{(a_i^{n_i} a_j^{n_j})^l}{l^2} \{ \cos[l(n_i\Phi_i - n_j\Phi_j)] \\
&\quad \left. + \cos[l(n_i\Phi_i + n_j\Phi_j)] \} \}, \tag{3.9}
\end{aligned}$$

where  $(n_i, n_j)$  is a pair of positive relative primes. Summation goes over these pairs, which arise due to the substitution of indices in double Fourier series in harmonics  $\exp[i(m_1\Phi_1 + m_2\Phi_2)]$  according to the rule  $\sum_{m_1=1}^{\infty} \sum_{m_2=1}^{\infty} \rightarrow \sum_{n_i, n_j} \sum_{l=1}^{\infty}$ . As each pair  $m_1, m_2$  can be presented in the form  $m_1 = n_1 l, m_2 = n_2 l$  with some  $(n_1, n_2)$ , it is clear that the cited substitution can be performed always. The quantities  $a_j$ , entering Eq. (3.9) are determined by the expression:

$$a_j = (1 - \lambda_j)^{1/2} (1 + \lambda_j)^{-1/2}, \quad \lambda_j = \left(1 - \frac{I_j}{I_j^b}\right). \tag{3.10}$$

From Eq. (3.10) it follows, that  $a_j < 1$ , and, more to it,  $a_j \ll 1$  if the excitation level of the  $j$ -th oscillator is low  $I_j \ll I_j^b$ . The pairs  $(n_i, n_j)$ , satisfying the condition

$$n_i\omega_i(I_i) = n_j\omega_j(I_j), \tag{3.11}$$

correspond to the resonance interaction of  $i$ -th and  $j$ -th oscillators. Thus the terms  $\cos(n_i\Phi_i - n_j\Phi_j)$  with these  $(n_i, n_j)$  in the interaction Hamiltonian (3.9) vary slowly in time, and their interaction should be taken into account in the first place. The effect of this resonance interaction upon the phase

trajectories of the vibrations we will analyze in the first order in the interaction  $|H_{ij}|$  with the help of the method of averaging (see Sections 2.2, 2.3).

It should be noted, that the result of the averaging process will depend upon the choice of the region of phase space. In the terms of canonical transformations it means, that a different canonical transformation is needed for each region of phase space in order to take into account the resonance in the given area. In another region the resonance will be a different one with a different pair  $(n_i, n_j)$ , and consequently the canonical transformation should be different. Thus, both the method of averaging, and the method of canonical transformations, used to find the "secular perturbation", are primarily of a local character, than of the global one. Thus the particular Hamiltonian, obtained in the averaging procedure, reproduces accurately the vibrations in some limited region of phase space only.

Averaging Eq. (3.9) and substituting the resultant expressions of  $\overline{H}_{ij}^{(k)}$  and  $\overline{H}_{ij}^{(p)}$  into Eq. (3.8), we obtain the following Hamiltonian:

$$\begin{aligned} \overline{H} = & \frac{1}{2} \sum_{i=1}^N \omega_{i0} \left( 2 - \frac{I_i}{I_i^b} \right) I_i \\ & + \sum_{i=1}^N \sum_{j>i \geq 1}^N \left\{ \frac{K_{ij}}{\alpha_i \alpha_j} \ln \left( \frac{2\lambda_i^2}{1+\lambda_i} \right) \ln \left( \frac{2\lambda_j^2}{1+\lambda_j} \right) \right. \\ & + \sum_{n_i, n_j} \left\{ \frac{2K_{ij}}{\alpha_i \alpha_j n_i n_j} \sum_{l=1}^{\infty} \frac{(a_i^{n_i} a_j^{n_j})^l}{l^2} \cos [l(n_i \Phi_i - n_j \Phi_j)] \right. \\ & \left. \left. + \frac{2G_{ij}\omega_{i0}\omega_{j0}\lambda_i\lambda_j}{G_{ii}G_{jj}\alpha_i\alpha_j} \left[ \frac{1 - a_i^{n_i} a_j^{n_j} \cos(n_i \Phi_i - n_j \Phi_j)}{1 - 2a_i^{n_i} a_j^{n_j} \cos(n_i \Phi_i - n_j \Phi_j) + (a_i^{n_i} a_j^{n_j})^2} - 1 \right] \right\} \right\}. \end{aligned} \quad (3.12)$$

To obtain Eq. (3.12) from (3.9) it is sufficient to expand  $H_{ij}^{(k)}$  and  $H_{ij}^{(p)}$  in the harmonics  $\cos(n_i \Phi_i \pm n_j \Phi_j)$ , and to retain in the Fourier series the terms with  $\cos(n_i \Phi_i - n_j \Phi_j)$ ,  $n_i > 0, n_j > 0$  only<sup>2</sup>. The subsequent simplification of Eq. (3.12) is based on the assumption that each oscillator is in resonance with only one of the rest  $N - 1$  oscillators. In other words, each frequency  $\omega_i$  enters only one equation of the type (3.11). This is in fact a more typical situation, than the one, when the frequency  $\omega_i$  enters two equations of the type (3.11), as each additional equation limits the accessible region of phase

<sup>2</sup>This averaging procedure can be substituted for a canonical transformation with the generating function of the type  $F(\Phi, \bar{I}) = \Phi \bar{I} + \sum_{m\omega \neq 0} \frac{h_m(\bar{I})}{m\omega} \sin(m\Phi)$ , where  $\Phi \bar{I} = \sum \Phi_i \bar{I}_i$ ,  $m\omega = \sum m_i \omega_i$ , and  $h_m(\bar{I})$  is the Fourier coefficient of the Hamiltonian  $H(I, \Phi)$ .

space (nonresonant states fill up the phase space entirely, with the accuracy up to an area with measure zero).

In the analysis of stretching vibrations in polyatomic molecules with different bonds the situation with one sole resonance is typical for only one bond excited, as it usually is in spectroscopy. Clearly, there is a hierarchy of resonances, corresponding to that vibration. As the high-order resonances  $(n_i + n_j) \gg 1$  in the Hamiltonian (3.12) are suppressed by a small factor  $\left(a_i^{n_i} a_j^{n_j}\right) \ll 1$ , only the low-order resonance with small  $n_i + n_j$  is significant. In the molecules with two identical valent bonds, like  $H_2O$ ,  $CH_2Cl_2$ , etc. at low excitation only the resonance  $\omega_1 = \omega_2$  should be taken into account.

Thus the Hamiltonian (3.12) can be split effectively into a sum of pair Hamiltonians, which represent the resonance interaction of pairs of oscillators. Different pairs do not interact with each other. The pair Hamiltonian of  $i$ -th and  $j$ -th oscillators, which corresponds to the resonance (3.11), takes the form:

$$\begin{aligned} \overline{H}_{ij} = & \frac{1}{2} \left[ \omega_{0i} \left( 2 - \frac{I_i}{I_i^b} \right) I_i + \omega_{0j} \left( 2 - \frac{I_j}{I_j^b} \right) I_j \right] \\ & + \left\{ \frac{K_{ij}}{\alpha_i \alpha_j} \left[ \ln \left( \frac{2\lambda_i^2}{1 + \lambda_i} \right) \ln \left( \frac{2\lambda_j^2}{1 + \lambda_j} \right) \right. \right. \\ & \left. \left. + \frac{2}{n_i n_j} \sum_{l=1}^{\infty} \frac{\left(a_i^{n_i} a_j^{n_j}\right)^l}{l^2} \cos [l(n_i \Phi_i - n_j \Phi_j)] \right] \right. \\ & \left. + \frac{2G_{ij}\omega_{i0}\omega_{j0}\lambda_i\lambda_j}{G_{ii}G_{jj}\alpha_i\alpha_j} \frac{1 - a_i^{n_i} a_j^{n_j} \cos(n_i \Phi_i - n_j \Phi_j)}{1 - 2a_i^{n_i} a_j^{n_j} \cos(n_i \Phi_i - n_j \Phi_j) + \left(a_i^{n_i} a_j^{n_j}\right)^2} \right\}. \end{aligned} \quad (3.13)$$

In the derivation of Eq. (3.13) from Eq. (3.12) the last term in (3.12) has been omitted, as it is always small in the parameter  $\sim \left| \frac{G_{ij}}{G_{ii}} \right| \ll 1$  and does not depend upon the angular variable  $(n_i \Phi_i - n_j \Phi_j)$ . In fact it provides only a small renormalization of the unperturbed frequencies  $(\omega_{i0}, \omega_{j0})$ . Whereas the term with  $\ln \frac{2\lambda_i^2}{1 + \lambda_i}$  can not be neglected, as it becomes important at high excitations  $I_i \sim I_i^b$ , when  $\lambda_i \sim 0$ .

We stress that the possibility of splitting the Hamiltonian into a sum of noninteracting pair Hamiltonians arises due to the suppression of high-order resonances by the quickly decreasing quantity  $\left(a_i^{n_i} a_j^{n_j}\right)$  with the increase of resonance order  $n_i + n_j$ . Consequently, each oscillator participates in one resonance only, which has the lowest possible order at the current excitation level. The resonances with the frequencies of four participating oscillators

contribute to the second order in the interaction and should be taken into account for moments of time of the order of  $\sim G_{ij}^{-2}, K_{ij}^{-2}$ , etc.

The form of the Hamiltonian (3.13) shows, that the problem is reduced to that of two nonlinear oscillators, which has been considered in Sections 2.3 - 3.1. Consequently the qualitative behavior of phase curves, discussed earlier, applies in general to the phase curves of the Hamiltonian (3.13) (the appearance of the local mode, the disappearance of the symmetric normal mode, etc.).

Let us study the behavior of phase curves in the vicinity of the closed resonance orbit. Let us introduce the variables:

$$\begin{aligned} J_1 &= \frac{I_i}{n_i} + \frac{I_j}{n_j}, \quad J_2 = \frac{I_i}{n_i}, \\ \Theta_1 &= n_j \Phi_j, \quad \Theta_2 = n_i \Phi_i - n_j \Phi_j. \end{aligned} \quad (3.14)$$

This substitution is of canonical type (see the footnote to Eq. (2.44)). Substituting Eq. (3.14) into Eq. (3.13), we obtain  $\bar{H}_{ij}$  in the variables  $(J_1, J_2, \Theta_1, \Theta_2)$ :

$$\begin{aligned} \bar{H}_{ij} &= \frac{\omega_{i0}}{2} \left( 2 - n_i \frac{J_2}{I_i^b} \right) n_i J_2 + \frac{\omega_{j0}}{2} \left( 2 - n_j \frac{J_1 - J_2}{I_j^b} \right) n_j (J_1 - J_2) \\ &+ \frac{K_{ij}}{\alpha_i \alpha_j} \left[ \ln \left( \frac{2\lambda_i^2}{1 + \lambda_i} \right) \ln \left( \frac{2\lambda_j^2}{1 + \lambda_j} \right) + \frac{2}{n_i n_j} \sum_{l=1}^{\infty} \frac{(a_i^{n_i} a_j^{n_j})^l}{l^2} \cos [l\Theta_2] \right] \\ &+ \frac{2G_{ij}\omega_{i0}\omega_{j0}\lambda_i\lambda_j}{G_{ii}G_{jj}\alpha_i\alpha_j} \frac{1 - a_i^{n_i} a_j^{n_j} \cos \Theta_2}{1 - 2a_i^{n_i} a_j^{n_j} \cos \Theta_2 + (a_i^{n_i} a_j^{n_j})^2}. \end{aligned}$$

We note that here the quantities  $a_i, a_j$  are functions of the variables  $J_1, J_2$ . Due to the fact, that the variable  $\Theta_1$  does not enter the expression of  $\bar{H}_{ij}$ , the action  $J_1$  is a constant of motion, and consequently the problem of the calculation of the phase trajectory is reduced to a one-dimensional one. As the variables  $(J_1, \Theta_1)$  and  $(J_2, \Theta_2)$  have separated, and  $J_1$  is a constant of motion, there is a resonance orbit for each  $J_1$ , along which  $J_2 = \text{const}$ ,  $\Theta_2 = \text{const}$ . Thus the resonance orbit is determined by the equations:

$$\frac{\partial \bar{H}_{ij}}{\partial J_2} (J_{2r}, \Theta_{2r}) = 0, \quad \frac{\partial \bar{H}_{ij}}{\partial \Theta_2} (J_{2r}, \Theta_{2r}) = 0.$$

It can be shown easily, that due to the weak interaction of oscillators the first equation reduces to the condition of resonance for the unperturbed frequencies (3.11). The second equation gives  $\Theta_2 = 0, \pi$ . Thus for each  $J_1$

there are two stationary points  $(J_{2r}, 0)$  and  $(J_{2r}, \pi)$ , which correspond to the stable and unstable resonance orbits.

Expressing  $J_1$  and  $J_2$  in the form:

$$J_1 = \frac{I_{ir}}{n_i} + \frac{I_{jr}}{n_j}, \quad J_2 = \frac{I_{ir}}{n_i} + \delta_2,$$

and substituting these equations into the Hamiltonian  $\bar{H}_{ij}(J_1, J_2)$  with the constant term neglected, we obtain the expression of the resonance Hamiltonian in the vicinity of the resonance orbit:

$$\begin{aligned} H_{ij}^{(r)}(\delta_2, \Theta_2) = & -\frac{1}{2} \left( n_i^2 \frac{\omega_{i0}}{I_i^b} + n_j^2 \frac{\omega_{j0}}{I_j^b} \right) \delta_2^2 \\ & + \frac{2K_{ij}}{\alpha_i \alpha_j n_i n_j} \sum_{l=1}^{\infty} \frac{\left( a_i^{n_i}(\delta_2) a_j^{n_j}(\delta_2) \right)^l}{l^2} \cos[l\Theta_2] \\ & + \frac{2G_{ij}\omega_{i0}\omega_{j0}\lambda_i(\delta_2)\lambda_j(\delta_2) \left[ 1 - a_i^{n_i}(\delta_2) a_j^{n_j}(\delta_2) \cos \Theta_2 \right]}{G_{ii}G_{jj}\alpha_i\alpha_j \left\{ 1 - 2a_i^{n_i}(\delta_2) a_j^{n_j}(\delta_2) \cos \Theta_2 + \left[ a_i^{n_i}(\delta_2) a_j^{n_j}(\delta_2) \right]^2 \right\}}. \end{aligned} \quad (3.15)$$

We note that in the interaction terms the functional dependence of  $a_{i,j}(\delta_2)$  on  $\delta_2$  should be kept, in spite of the smallness of  $K_{ij}$  and  $G_{ij}$ . The substitution  $a_\beta(\delta_2) \rightarrow a_\beta(0)$  would produce an erroneous result in the determination of the threshold for the emergence of the local mode <sup>3</sup>.

From Eq. (3.15) it follows, that the point  $(J_{2r}, \Theta_2 = 0)$  corresponds to a stable resonance orbit, if  $K_{ij} > 0$  and  $G_{ij} > 0$ , and to an unstable one if  $K_{ij} < 0$  and  $G_{ij} < 0$ . For the orbit  $(J_{2r}, \Theta_2 = \pi)$  the correspondence rule is inverted: stability for  $K_{ij} < 0, G_{ij} < 0$  and instability for  $K_{ij} > 0, G_{ij} > 0$ . In the case when the signs of  $K_{ij}$  and  $G_{ij}$  are different, a special study of the character of stationary points  $(J_{2r}, 0)$  and  $(J_{2r}, \pi)$  is needed.

In the next paragraph we will calculate the resonance linewidth and the threshold value of the action  $J_{1cr}$  for the emergence of the local mode with the use of the expression (3.15) for the resonance Hamiltonian.

---

<sup>3</sup>In Ref. [52] the dependence of  $a_i(J_2) = a_i(J_{2r} + \delta_2)$  on the variable  $J_2$  has been ignored, and  $a_i(J_{2r})$  has been substituted into Eq. (3.15). This led to the increase of the threshold value of the splitting-off of the local mode  $J_{1cr}$  in the resonance  $\omega_i = \omega_j$  by two times (see Eqs. (3.23), (3.26) below).

### 3.3 Morse oscillators: calculation of resonance linewidths and criteria for the appearance of local modes

As we noted earlier (see Section 3.1), the interaction destroys the unperturbed resonant tori, so that the tori of phase oscillations are formed in their place [7]. In the resonant case  $\omega_1 = \dots = \omega_N$  these phase vibrations correspond to normal modes of different symmetry, which refer to the vibrations delocalized over all the  $N$  oscillators. Such a situation is realized in molecules with equivalent valent bonds at low excitation level, when the frequencies are approximately equal due to the smallness of the nonlinearity factor  $\frac{I}{J^2}$  (see Eq. (2.20)). The same type of vibrations will be realized in the case of similar excitation levels for all the  $N$  oscillators, as in this case the frequencies are equal due to the equality  $I_1 = \dots = I_N$  as well.

A question arises, how large is the area of phase space occupied by the tori of normal vibrations? The second question is the following: what is the total excitation level  $I_{cr \ min} = \sum_1^N I_\nu$ , when local modes emerge?

Let us find out the physical meaning of the quantity  $I_{cr \ min}$ . In the case of low excitation level with an arbitrary energy distribution between similar oscillators the vibration frequencies are approximately equal,  $\omega_1 = \dots = \omega_N$ , due to the smallness of the factor  $\frac{I}{J^2}$ , and a normal delocalized vibration takes place. At the same time, if the total action exceeds the critical value,  $I > I_{cr \ min}$ , then if the excitation energy concentrates on one of the oscillators, its frequency (say)  $\omega_1 (I_1)$  falls out of resonance with the others, and a local vibration is realized. Geometrically the meaning of the critical action  $I_{cr \ min}$  for two oscillators is depicted clearly in Figs. 3.3, 3.4, and 3.5. In fact, passing through the value  $I = I_{cr \ min}$  we go over from Fig. 3.3 through 3.4 to 3.5.

To characterize quantitatively the size of the area of phase (normal) vibrations in the case of two oscillators we introduce the quantity  $\Delta$  — the width of the resonance. In the presence of resonance Eq. (3.11) the Hamiltonian (3.7) is reduced to that situation exactly. The quantity  $\Delta$  measures half the maximal diameter of the region of phase vibrations in the direction of the axis  $J_2$  (Fig. 3.7).

When more than two frequencies take part in the resonance, several variable actions  $J_1, J_2, J_3, \dots, J_N$  exist, and such a simple characteristic as  $\Delta$  can not be introduced. In such a multidimensional case, however, some averaged parameter exists, exceeding the value of which we pass into the area of local vibrations. In the multidimensional case more delicate and precise characteristics are needed for the characterization of the emergence of local vibrations, as the emergence of the local mode depends upon the direction in the space of multiple action variables  $J_1, J_2, J_3, \dots$ . Localization of vibrations in a system of an arbitrary number of similar oscillators for

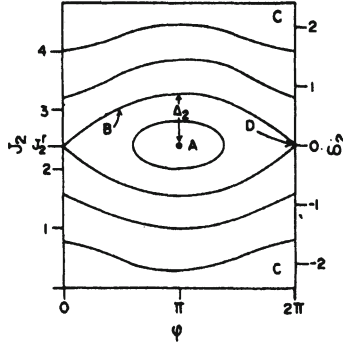


Figure 3.7: The qualitative structure of toruses, determined by the resonant Hamiltonian (3.15),  $J_2 = J_{2r} + \delta_2$ ,  $\varphi = \Theta_2$ ,  $\Delta_2 = \Delta$ , Eq. (3.14).

arbitrary time is considered below in Sections 3.4 and 3.5.

Let us calculate the resonance width  $\Delta$ . As it becomes clear from Fig. 3.7, the width  $\Delta$  is equal to the maximal value of  $\delta_2$  on the separatrix  $B$ . This maximal value is reached for  $\Theta = \pi$ . Really, the equation defining the separatrix is

$$H_{ij}^{(r)}(0,0) = H_{ij}^{(r)}(\delta_2, \Theta_2).$$

With the account of Eq. (3.15) it takes the form:

$$\begin{aligned} \frac{4\tilde{\eta}}{n_j n_i} \sum_{l=1}^{\infty} \frac{\left(a_{ir}^{n_i} a_{jr}^{n_j}\right)^l}{l^2} + \frac{4\tilde{\varepsilon} \lambda_{ir} \lambda_{jr}}{1 - a_{ir}^{n_i} a_{jr}^{n_j}} &= -\Lambda^{-1} \delta_2^2 \\ + \frac{4\tilde{\eta}}{n_j n_i} \sum_{l=1}^{\infty} \frac{\left(a_i^{n_i} a_j^{n_j}\right)^l}{l^2} \cos[l\Theta_2] + \frac{4\tilde{\varepsilon} \lambda_i \lambda_j \left(1 - a_i^{n_i} a_j^{n_j} \cos \Theta_2\right)}{1 - 2a_i^{n_i} a_j^{n_j} \cos \Theta_2 + \left[a_i^{n_i} a_j^{n_j}\right]^2}, \end{aligned}$$

where  $a_{ir}, a_{jr}, \lambda_{ir}, \lambda_{jr}$  are the values in the resonance points ( $J_{1r}, J_{2r}$ ) without the account of interaction. The quantities  $\tilde{\varepsilon}, \tilde{\eta}, \Lambda$  are determined by the formulas:

$$\begin{aligned} \tilde{\varepsilon} &= \frac{G_{ij} \omega_{i0} \omega_{j0}}{2G_{ii} G_{jj} \alpha_i \alpha_j}, \quad \tilde{\eta} = \frac{K_{ij}}{2\alpha_i \alpha_j}, \\ \Lambda &= \left( \frac{n_i^2 \omega_{i0}}{2I_i^b} + \frac{n_j^2 \omega_{j0}}{2I_j^b} \right)^{-1} \end{aligned} \quad (3.16)$$

It is convenient to transform this equation for the separatrix line to the following shape:

$$\delta_2^2 = -\Lambda \left\{ \frac{4\tilde{\eta}}{n_i n_j} \sum_{l=1}^{\infty} \frac{\left(a_{ir}^{n_i} a_{jr}^{n_j}\right)^l - \left(a_i^{n_i} a_j^{n_j}\right)^l \cos[l\Theta_2]}{l^2} \right. \\ \left. + 4\tilde{\epsilon} \left[ \frac{\lambda_{ir} \lambda_{jr}}{1 - a_{ir}^{n_i} a_{jr}^{n_j}} - \frac{\lambda_i \lambda_j (1 - a_i^{n_i} a_j^{n_j} \cos \Theta_2)}{1 - 2a_i^{n_i} a_j^{n_j} \cos \Theta_2 + \left(a_i^{n_i} a_j^{n_j}\right)^2} \right] \right\}. \quad (3.17)$$

The equation (3.17) defines implicitly the functional dependence  $\delta_2(\Theta_2)$ , as  $\delta_2$  enters the right hand side of the equation in the arguments of the functions  $a_i(I_{ir} + n_i \delta_2)$  and  $\lambda_i(I_{ir} + n_i \delta_2)$ , and similar for  $a_j, \lambda_j$ . From Eq. (3.17) it follows, that the derivative  $(\delta_2^2)'|_{\Theta_2=0,\pi} = 0$  equals zero, and as  $\delta_2^2(\Theta_2 = 0) = 0$ , the function  $\delta_2^2$  at  $\Theta_2 = 0$  has a minimum, and at  $\Theta_2 = \pi$  — a maximum. This can be proved easily with the help of the inequality  $0 < \left(a_i^{n_i} a_j^{n_j}\right) < 1$ . Consequently,  $\delta_2(\pi) = \Delta$ , as it is shown in Fig. 3.7.

Substituting the equation  $\Theta_2 = \pi$  into (3.17), we obtain the formula for the determination of the width  $\Delta$ <sup>4</sup>:

$$\Delta^2 = -\Lambda \left\{ \frac{4\tilde{\eta}}{n_i n_j} \sum_{l=0}^{\infty} \frac{\left(a_{ir}^{n_i} a_{jr}^{n_j}\right)^{2l+1} + \left(a_i^{n_i} a_j^{n_j}\right)^{2l+1}}{(2l+1)^2} \right. \\ \left. + \frac{4\tilde{\epsilon}}{n_i n_j} \sum_{l=0}^{\infty} \frac{\left(a_{ir}^{n_i} a_{jr}^{n_j}\right)^{2l+2} - \left(a_i^{n_i} a_j^{n_j}\right)^{2l+2}}{(2l+2)^2} \right. \\ \left. + 4\tilde{\epsilon} \left[ \frac{\lambda_{ir} \lambda_{jr}}{1 - a_{ir}^{n_i} a_{jr}^{n_j}} - \frac{\lambda_i \lambda_j}{1 + a_i^{n_i} a_j^{n_j}} \right] \right\}. \quad (3.18)$$

From the definition of  $a_i$  and  $\lambda_i$  (3.10) it follows that for  $I_{ir} \gg n_i \Delta$  the quantities  $a_\nu, \lambda_\nu$  in the right-hand-side of Eq. (3.18) can be substituted for  $a_{ir}, a_{jr}, \lambda_{ir}, \lambda_{jr}$ . As a result, we obtain the following expression for the resonance width  $\Delta$ :

$$\Delta = \Delta_0 = \left\{ -\Lambda \left[ \frac{8\tilde{\eta}}{n_i n_j} \sum_{l=0}^{\infty} \frac{\left(a_{ir}^{n_i} a_{jr}^{n_j}\right)^{2l+1}}{(2l+1)^2} \right. \right.$$

---

<sup>4</sup>In the case when the resonance orbit passes through the point  $J_2 = J_{2r}$ ,  $\Theta_2 = \pi$  the expression in curly brackets is always negative. When the latter takes positive values, the resonance orbit passes through the point  $(J_{2r}, \Theta_2 = 0)$ .

$$\left. +8\tilde{\epsilon}\lambda_{ir}\lambda_{jr}\frac{a_{ir}^{n_i}a_{jr}^{n_j}}{1-\left(a_{ir}^{n_i}a_{jr}^{n_j}\right)^2}\right\}^{\frac{1}{2}}. \quad (3.19)$$

With the low excitation level  $I_r \ll I^b$  the following estimates hold:  $\lambda_i, \lambda_j \sim 1$ , and  $a_i, a_j \ll 1$ , so that the formula (3.19) takes the form:

$$\Delta = \Delta_0 = \left\{ 4\Lambda \left[ -\frac{2\tilde{\eta}}{n_i n_j} - 2\tilde{\epsilon}\lambda_{ir}\lambda_{jr} \right] a_{ir}^{n_i}a_{jr}^{n_j} \right\}^{\frac{1}{2}}. \quad (3.20)$$

Eqs. (3.19) and (3.20) have been obtained by Juffe and Brumer in Ref. [52]. These formulas are valid until the following inequalities hold:

$$I_{ir} \gg n_i \Delta, \quad I_{jr} \gg n_j \Delta. \quad (3.21)$$

At the threshold the inequalities (3.21) are not satisfied, and to determine the width  $\Delta$  one should solve the equation (3.18) (see below).

Let us calculate the width  $\Delta$  with the use of Eq. (3.20) at resonance  $\omega_i = \omega_j$  for a system with Hamiltonian (2.43). According to Eq. (2.43) and (3.16) we have:  $n_i = n_j = 1$ ,  $\omega_i = \omega_j = 1$ ,  $I_i^b = I_j^b = 2D$ ,  $\alpha_i = \alpha_j = (2D)^{-1/2}$ ,  $\tilde{\eta} = 0$ ,  $\tilde{\epsilon} = -\epsilon D$ ,  $\Lambda = 2D$ .

Substituting these values into Eq. (3.20), we obtain <sup>5</sup>:

$$\Delta_0 = \sqrt{4\epsilon D I_{ir}}. \quad (3.22)$$

From Fig. 3.7 it is clear, that the minimal possible value of the action  $I_{ir\min}$ , when the local mode splits off, is determined by the condition  $\Delta = I_{ir\min}$ , that is:

$$I_{ir\min} = 4\epsilon D, \quad I_{cr\min} = 2I_{ir\min} = 8\epsilon D. \quad (3.23)$$

At the same time, according to Eq. (3.4) the local mode appears at  $I_{cr\min} = 4\epsilon D$ . This discrepancy aroused due to the neglection of the functional dependence of  $a(I_r + n\Delta)$  in the right-hand-side of equation (3.18) when the conditions (3.21) are violated. When LM appears, these conditions are violated always, as it will be seen below.

To determine the threshold for the split-off of the local mode correctly, let us solve the equation (3.18) with the account of the dependence of  $a_{i,j}(\Delta)$  and  $\lambda_{i,j}(\Delta)$  in the r.h.s. of Eq. (3.18). We assume:

$$n_i \geq n_j. \quad (3.24)$$

The resonant values of the action  $I_{ir}$  and  $I_{jr}$  satisfy the equation:

---

<sup>5</sup>Such  $\tilde{\epsilon}$  and  $\tilde{\eta}$  correspond to the following choice of  $G_{ij}$  and  $K_{ij}$  in Eq. (3.7):  $G_{ij} = -\epsilon \sqrt{G_{ii}G_{jj}}$ ,  $K_{ij} = -\eta \sqrt{K_{ii}K_{jj}}$ , with  $D_i = D_j = D$  due to the similarity of the bonds.

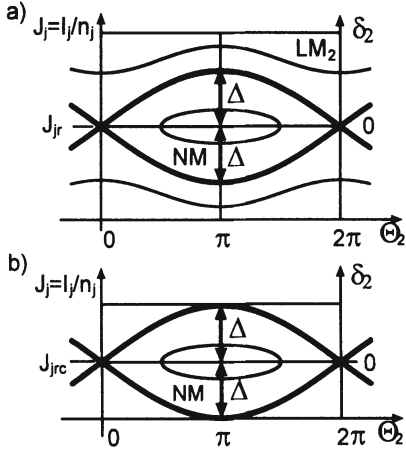


Figure 3.8: Phase portrait of two coupled oscillators in the variables  $(J_j, \Theta_2)$  in the vicinity of the resonance  $n_i : n_j$ . a) Local modes  $LM_2$  and normal modes  $NM$  coexist. The respective regions border along the solid separatrix line. b) The split-off of the local mode – when the separatrix line touches the axis  $\Theta_2$ .

$$\begin{aligned} n_i \lambda_{ir} &= n_j \lambda_{jr}, \\ I_{ir} &= \left(1 - \frac{n_j}{n_i}\right) I^b + \frac{n_j}{n_i} I_{jr}. \end{aligned} \quad (3.25)$$

The local mode gets split-off when the separatrix line touches the axis  $\Theta_2$ , Fig. 3.8:

$$\delta_2(\pi) = \Delta = \frac{I_{jrc}}{n_j} \ll I^b. \quad (3.26)$$

Then the action  $I_{irc}$  is determined from the equation (10.35):

$$I_{irc} = \left(1 - \frac{n_j}{n_i}\right) I^b + \frac{n_j^2}{n_i} \Delta. \quad (3.27)$$

In the touch - point the values of action are the following:

$$\begin{aligned} I_j &= I_{jrc} - n_j \Delta = 0, \\ I_i &= I_{irc} + n_i \Delta = \left(1 - \frac{n_j}{n_i}\right) I^b + \left(\frac{n_j^2}{n_i} + n_i\right) \Delta. \end{aligned} \quad (3.28)$$

Equation (3.28) is obtained from Eqs. (3.26) and (3.27). It has been taken into account that the change of the action is  $\delta I_j = -n_j \Delta$ ,  $\delta I_i = n_i \Delta$ , as  $I_i n_i^{-1} + I_j n_j^{-1}$  is a constant of motion.

With the use of Eqs. (3.26) - (3.28) the expressions of  $\lambda_i, \lambda_j, a_i, a_j$ , determined by Eq. (3.10) and entering Eq. (3.18), are given by:

$$\begin{aligned}
a_{ir} &= \left[ \frac{\left(1 - \frac{n_j}{n_i}\right) + \frac{n_j^2}{n_i} \frac{\Delta}{I^b}}{\left(1 + \frac{n_j}{n_i}\right) - \frac{n_j^2}{n_i} \frac{\Delta}{I^b}} \right]^{\frac{1}{2}}, \quad \lambda_{ir} = \frac{n_j}{n_i} - \frac{n_j^2}{n_i} \left( \frac{\Delta}{I^b} \right), \quad I_i = I_{irc}, \\
a_{jr} &= \left[ \frac{n_j \Delta}{2I^b} \right]^{\frac{1}{2}}, \quad \lambda_{jr} = 1 - n_j \left( \frac{\Delta}{I^b} \right), \quad I_j = I_{jrc}, \\
a_i &= \frac{\left(1 - \frac{n_j}{n_i}\right) + \left(\frac{n_j^2}{n_i} + n_i\right) \frac{\Delta}{I^b}}{\left(1 + \frac{n_j}{n_i}\right) - \left(\frac{n_j^2}{n_i} + n_i\right) \frac{\Delta}{I^b}}, \\
\lambda_i &= \frac{n_j}{n_i} - \frac{n_i^2 + n_j^2}{n_i} \left( \frac{\Delta}{I^b} \right), \quad I_i = I_{irc} + n_i \Delta, \\
a_j &= 0, \quad \lambda_j = 1, \quad I_j = I_{jrc} - n_j \Delta = 0.
\end{aligned} \tag{3.29}$$

Substituting Eq. (3.29) into (3.18) and keeping in the r.h.s. only the principal terms in the small parameter  $\frac{\Delta}{I^b}$ , we obtain the equation for the determination of the threshold value of the resonance width  $\Delta = I_{jrc} n_j^{-1}$  for LM split-off <sup>6</sup>.

$$\begin{aligned}
\Delta^2 &= \left( -\frac{4\tilde{\eta}\Lambda}{n_i n_j} \right) \left[ \frac{\Delta n_j}{2I^b} \right]^{\frac{n_j}{2}} \left[ \frac{\left(1 - \frac{n_j}{n_i}\right) + \frac{\Delta}{I^b} \frac{n_j^2}{n_i}}{\left(1 + \frac{n_j}{n_i}\right) - \frac{\Delta}{I^b} \frac{n_j^2}{n_i}} \right]^{\frac{n_i}{2}} \\
&\quad + (-4\tilde{\varepsilon}\Lambda) \\
&\quad \times \left\{ \frac{\Delta \left( n_i^2 - n_j^2 \right)}{I^b n_i} + \left[ \frac{\Delta n_j}{2I^b} \right]^{\frac{n_j}{2}} \left[ \frac{\left(1 - \frac{n_j}{n_i}\right) + \frac{\Delta}{I^b} \frac{n_j^2}{n_i}}{\left(1 + \frac{n_j}{n_i}\right) - \frac{\Delta}{I^b} \frac{n_j^2}{n_i}} \right]^{\frac{n_i}{2}} \right\}.
\end{aligned} \tag{3.30}$$

Three different cases are possible. The first one is given by the condition  $n_i = n_j = 1$ . Then equation (3.30) takes the form:

$$\Delta^2 = -4\Lambda (\tilde{\varepsilon} + \tilde{\eta}) \left( \frac{\Delta}{2I^b} \right).$$

---

<sup>6</sup>We note, that equivalent  $i$ -th and  $j$ -th modes are considered, when  $\omega_i = \omega_j = 1$ ,  $I_i^b = I_j^b = I^b$ ,  $D_i = D_j = D$ ,  $I^b = 2D$ .

From the last equation we find:

$$\Delta = I_{jrc} = 2(\varepsilon + \eta)D, \quad I_{cr,min} = 2I_{jrc} = 4(\varepsilon + \eta)D. \quad (3.31)$$

The parameters, entering Eq. (3.31) have chosen to be:

$$\begin{aligned} G_{ii} &= G_{jj} = m^{-1}, \quad G_{ij} = m^{-1}\varepsilon, \quad 2\alpha^2 = \frac{m\omega^2}{D}, \quad \alpha_i = \alpha_j = \alpha, \quad (3.32) \\ k_{ii} &= k_{jj} = m\omega^2, \quad k_{ij} = -\eta m\omega^2; \quad \tilde{\varepsilon} = -\varepsilon D, \quad \tilde{\eta} = -\eta D, \quad \Lambda = \frac{I^b}{\omega}. \end{aligned}$$

Taking into account the condition  $\omega = 1$ , we arrive at Eq.(3.31). Assuming  $\eta = 0$  we find that the local mode splits off at  $I_{cr,min} = 4\varepsilon D \ll I^b$ <sup>7</sup> in accordance with the results of Eq. (3.4) above.

The second case corresponds to the resonance with  $n_i > n_j > 2$ . From Eq. (3.30) we obtain the following expression of  $\Delta$ :

$$\Delta = \frac{4\varepsilon D \left( n_i^2 - n_j^2 \right)}{n_i \left( n_i^2 + n_j^2 \right)}. \quad (3.33)$$

We note here, that the strength of the potential interaction  $\eta$  escapes from the last expression. It will re-appear only in the next order terms in the small parameter  $\Delta(I^b)^{-1} \sim \varepsilon$ . If the i-th oscillator is close to the dissociation threshold,  $I_i \sim I^b$ , while the j-th is excited slightly,  $I_j \sim 0$ , the inequality holds:  $n_i \gg n_j$ . Then

$$\Delta = \frac{4\varepsilon D}{n_i}, \quad I_{cr,min} = \left( 1 - \frac{n_j}{n_i} \right) I^b + \left[ \left( \frac{n_j}{n_i} \right) + \left( \frac{n_j}{n_i} \right)^2 \right] 4\varepsilon D \sim I^b.$$

It can be seen, that at resonances of high order  $n_i \gg n_j > 2$  the width of the resonances (or the size of the region of normal vibrations) is inversely proportional to the order of the resonance,  $\Delta_{n_i \gg n_j} \sim 2\Delta_{1:1} (n_i + n_j)^{-1}$ .

And, last, in the third case  $n_i > n_j = 1$  for  $\Delta$  and  $I_{jrc}$  we find<sup>8</sup>:

$$\begin{aligned} \Delta &= 4 \left[ \frac{\varepsilon + \frac{\eta}{n_i}}{n_i^2 + 1} \right]^{\frac{2}{3}} \left( \frac{n_i - 1}{n_i + 1} \right)^{\frac{n_i}{3}} D, \\ I_{cr,min} &= \left( 1 - \frac{1}{n_i} \right) I^b + \left( 1 + \frac{1}{n_i} \right) \Delta \sim I^b, \quad \text{if } n_i \gg 1. \quad (3.34) \end{aligned}$$

<sup>7</sup>At high excitation level the NM and LM always coexist at  $n_i = n_j = 1$ .

<sup>8</sup>The case  $n_i > n_j = 2$  is reduced to the  $n_i > n_j > 2$  with renormalized  $\tilde{\varepsilon}_{ren}$ :

$$\tilde{\varepsilon}_{ren} = \tilde{\varepsilon} \left[ 1 + \frac{n_i}{n_i^2 - 4} \left( \frac{1 - 2n_i^{-1}}{1 + 2n_i^{-1}} \right)^{n_i/2} \left( 1 + \frac{\tilde{\eta}}{2n_i} \right) \right]$$

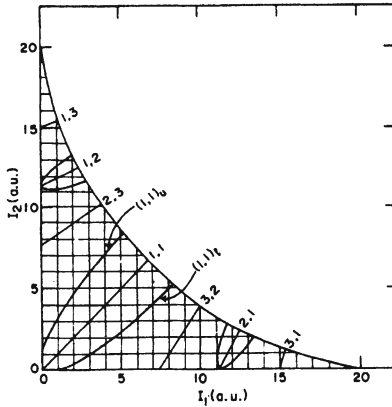


Figure 3.9: Location of various resonances in action space  $(I_1, I_2)$  for stretching vibrations in model  $H_2O$  molecule.

Comparing Eqs. (3.31), (3.32), and (3.33), (3.34), we arrive at the conclusion, that in the case of the resonance  $n_i > n_j = 1$  the dependence of the width of the resonance in the vicinity of the threshold is  $\Delta \sim |\varepsilon + \eta m_i^{-1}|^{2/3}$ , while in the other cases  $\Delta \sim |\varepsilon|, |\eta|$ . Far from the threshold the width of the resonance  $\Delta(I_r)$  should be estimated with the help of Eq. (3.19).

Figure 3.9 from [52] shows the resonance regions in the plane  $(I_1, I_2)$  for stretching vibrations in molecule  $H_2O$ . The calculation has been performed with the model Hamiltonian (3.7) using the values  $N = 2$ ,  $G_{11} = G_{22} = 1$ ,  $D = 10$ ,  $\omega = 1$ ,  $K_{12} = 0$ ,  $G_{12} = -0.014$ . The shape of resonance regions along with the resonance lines in the plane  $I_1, I_2$  are demonstrated in Fig. 3.10. The curve  $E(I_1, I_2) = D$ , which separates the region of phase space with unperturbed energy  $E \leq D$  is also provided.

In Ref. [56] Henry and Huang have shown with the help of IR spectroscopy methods that starting with  $v_{\min} = 2$  the stretching vibrations of  $CH$  bonds in the molecule  $CH_2Y_2$  ( $Y \neq F$ ) have a local character. With the use of the model Hamiltonian (3.7) and of the corresponding resonant Hamiltonian (3.13) in Ref. [52] Jaffe and Brumer calculated the minimal values of the number  $v_{\min}$  for stretching vibrations of  $CH$  bonds for such molecules when the vibrations become local. Their results are provided in Table 3.1.

These results for the molecule  $CH_2F_2$  are not correct as in this case the Fermi resonance should be taken into account. For other molecules the minimal value is  $I_{cr \min} \sim 2.1 \div 2.6$ ; in the experiments the local character of  $CH$ -bonds vibrations is manifested starting from  $v = 2$ . This discrepancy is eliminated if one takes into account the fact that the correct value  $I_{cr \min}$  is

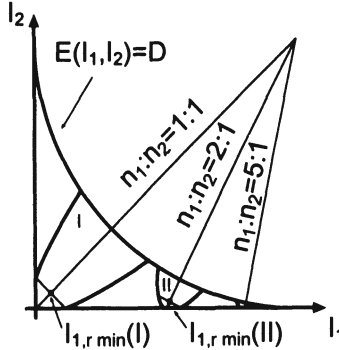


Figure 3.10: The resonance regions as functions of resonance type  $n_1 : n_2$ . The resonance lines are specified by the equation:  $n_1 I_1 - n_2 I_2 = (n_1 - n_2) I^b$ .

	$CH_2F_2$	$CH_2Cl_2$	$CH_2Br_2$	$CH_2I_2$
$I^b$	25.5	25.5	25.7	26.10
$\eta$	-0.008	-0.005	-0.002	-0.001
$\epsilon$	-0.014	-0.016	-0.022	-0.024
$I_{cr \min}$	2.2	2.1	2.5	2.6

Table 3.1: The minimal values of  $I_{cr \min}$  for which local modes appear. The quantities  $I^b$  are measured in units  $\hbar$ .

two times lower than the one found in Ref. [52]. Then the threshold for the emergence of LM will be  $I_{cr \min} = 1.05 \div 1.3$ , that is at  $v = 2$  the vibrations will be local with high probability in accordance with experimental data. Such a conclusion is reached with the account of the condition following from the quantization rules of Bohr - Sommerfeld, according to which each area of phase space  $(I_1, I_2)$  with volume  $\hbar^2$  corresponds to one quantum state. As for  $v = 2$  the volume of the resonance region is much smaller than that of localization, the local quantum states participating in the transitions with radiation absorption (emission) are observed in IR - experiment.

An analogous calculation for the molecules of water with  $I^b = 20$ ,  $\epsilon = 0.014$ ,  $\eta = 0$  produces  $I_{cr \min} = 0.6$ <sup>9</sup>, according to Eq. (3.31) ( $I$  is measured in units  $\hbar$ ). Consequently, one arrives to the conclusion, that for  $v \geq 2$  the stretching vibrations in the molecule are definitely of local nature. This can be revealed, for example, in the shape of IR spectrum, which correspond to the  $OH$  vibration overtones upon substitution of the molecule  $H_2O$  by  $HDO$ . Then the position of overtones corresponding to  $OH$  bond vibrations

<sup>9</sup>In Ref. [52] the following value is provided:  $I_{cr \min} = 1.2$ . The origin of the discrepancy is the same: the neglection of the dependence  $a_j(\Delta)$  in the r.h.s. of Eq. (3.18).

should not change with their intensity decreasing solely.

### 3.4 Coupled nonlinear oscillators: localized vibrational excitations and their asymptotic stability

In the present Section we will consider a system of similar weakly bound nonlinear oscillators. As it will be clear from the subsequent treatment, the method used will be valid for nonlinear systems of great generality. However, for the sake of transparency of consideration we will address the following particular Hamiltonian:

$$H(p, q) = \sum_{i=1}^N \frac{p_i^2 + q_i^2}{2} + \varepsilon \left( \lambda \sum_{i=1}^N q_i^4 + \beta \sum_{i \neq j} V_{ij} q_i q_j \right). \quad (3.35)$$

Here  $H(p, q)$  is a complete classical Hamiltonian of the system with mass and frequency of noninteracting oscillators equal to unit. The first term in the brackets in the right hand side characterizes the anharmonicity of the oscillators, while the second provides the linear bonding (interaction) between the oscillators. The small parameter  $\varepsilon$  will be used to construct the perturbation expansion.

Such a Hamiltonian has a direct application, for example, to simple molecular crystals like,  $N_2, O_2, NO, H_2$ , etc., Ref. [12].

In the absence of interaction ( $\beta = 0$ ), any local vibration in the system Eq. (3.35) (a small number of oscillators excited) satisfies the condition of resonance, Eq. (2.11). Such a vibration is in correspondence to a resonance torus in the phase space, which is constituted of tori of lower dimension. This situation is similar to the fact that a two-dimensional torus is composed of the one-parametric set of circles. The tori, mentioned above, have the dimension, equal to the number of excited oscillators. The phase trajectories of local vibrations are in fact wound on these tori. As it has been mentioned in Section 2.1, in this case the KAM theorem on stability of nonresonant tori does not work. Hence the problem of stability and local mode lifetime in the system of similar weakly interacting nonlinear oscillators requires a special consideration.

The solution to the problem, formulated above, has been obtained in 1972 by Ovchinnikov [13] and independently by Nehoroshev [59], who provided a mathematically rigorous consideration of it. It has been shown, that in the system of nonlinear oscillators (3.35) for  $\beta \ll \varepsilon \ll 1$  there exist local vibrations with exponentially long lifetimes  $\tau \sim \exp(\frac{M}{\varepsilon})$ , where the constant  $M$  does not depend on  $\beta$  and  $\varepsilon$ . The question on the nature of vibrations for  $t > \tau$  is still open.

From the method of analysis of the system (3.35) (see below) it follows, that the volume of phase space corresponding to local vibrations is nonzero. It means, that in systems with multiple degrees of freedom with probability nonzero there exist the states, in which the mixing of energy over various degrees of freedom does not take place over prolonged periods of time, which exceed considerably the characteristic relaxation time. Effects of this kind have been observed, for example, in the relaxation of vibrational excitations in  $N_2$  molecular crystal at low temperature (see the review [51]).

The absence of energy mixing has been observed in numerical experiments as well. For a system of bound nonlinear oscillators it has been observed for the first time in Ref. [46]. The subsequent numerical simulations Ref. [47, 48, 49] for systems of nonlinear oscillators confirmed these results.

The physical reason for the LM existence in the system (3.35) is the following: under strong excitation of one oscillator its frequency falls out of resonance with the rest part of the system<sup>10</sup>, and the energy transfer to the non-excited oscillators is impossible. Thus, having emerged once, the strong excitation remains on one oscillator.

First, to understand better the background of the mathematical approach used, we consider the case of two oscillators ( $N = 2$ ). Let us go over to the new variables  $a, \bar{a}$  according to the following formulas:

$$\begin{cases} a_i = \frac{1}{\sqrt{2}} (q_i - ip_i) e^{-it}, \\ \bar{a}_i = \frac{1}{\sqrt{2}} (q_i + ip_i) e^{it}, \end{cases} \quad \begin{cases} q_j = \frac{1}{\sqrt{2}} (a_j e^{it} + \bar{a}_j e^{-it}), \\ ip_j = \frac{1}{\sqrt{2}} (\bar{a}_j e^{-it} - a_j e^{it}). \end{cases} \quad (3.36)$$

The transition from the variables  $(q, ip)$  to  $(a, \bar{a})$  is canonical. The corresponding Hamilton equations take shape:

$$\begin{cases} i \frac{dq}{dt} = \{H, q\} = -\frac{\partial H}{\partial(ip)}, \\ i \frac{d(ip)}{dt} = \{H, ip\} = \frac{\partial H}{\partial q}, \end{cases} \quad \begin{cases} i \frac{da}{dt} = \{H', a\} = -\frac{\partial H'}{\partial(\bar{a})}, \\ i \frac{d(\bar{a})}{dt} = \{H', \bar{a}\} = \frac{\partial H'}{\partial a}. \end{cases} \quad (3.37)$$

The Poisson brackets are determined by the equations:

$$\begin{cases} \{f, g\} = \sum_k \left\{ \frac{\partial f}{\partial a_k} \frac{\partial g}{\partial \bar{a}_k} - \frac{\partial f}{\partial \bar{a}_k} \frac{\partial g}{\partial a_k} \right\} = \sum_k \left\{ \frac{\partial f}{\partial q_k} \frac{\partial g}{\partial(ip)_k} - \frac{\partial f}{\partial(ip)_k} \frac{\partial g}{\partial q_k} \right\}, \\ \{a_k, \bar{a}_l\} = \{q_k, ip_l\} = \delta_{k,l}, \quad \{a_i, a_j\} = \{\bar{a}_i, \bar{a}_j\} = 0. \end{cases} \quad (3.38)$$

The canonical nature of the transformation Eq. (3.36) follows from the definition (3.38) immediately. The generating function for this transformation has the form:

---

<sup>10</sup>Under weak excitation the nonlinearity can be neglected, so that for the rest of the oscillators we find the interval for the normal frequencies  $1 - \varepsilon\beta \leq \omega_\nu \leq 1 + \varepsilon\beta$ .

$$S(a, q) = -\sqrt{2}aqe^{it} + \frac{q^2}{2} + \frac{a^2}{2}e^{2it}.$$

With the help of the generating function the Hamiltonian  $H'(a, \bar{a})$  is defined by the formula:

$$\begin{aligned} H' &= H - i\frac{\partial S}{\partial t} = H(a, \bar{a}) - \sum_{j=1}^2 a_j \bar{a}_j \\ &= \varepsilon \left[ \lambda \sum_{j=1}^2 \left( \frac{a_j e^{it} + \bar{a}_j e^{-it}}{\sqrt{2}} \right)^4 \right. \\ &\quad \left. + \beta \frac{(a_1 e^{it} + \bar{a}_1 e^{-it})(a_2 e^{it} + \bar{a}_2 e^{-it})}{2} \right]. \end{aligned} \quad (3.39)$$

Thus the transformation (3.36) eliminates from the Hamiltonian (3.35) the noninteracting harmonic terms, leaving only the anharmonic part and the interaction terms. If the quantities  $p, q, a, \bar{a}$  are to be viewed as operators with commutation relations (3.38), the transformation  $(p, q) \rightarrow (a, \bar{a})$  corresponds to the transition to the interaction representation. The zero order Hamiltonian in this case is the oscillator Hamiltonian  $\sum \bar{a}a$ .

The analogy between the representation of physical quantities in the variables  $(a_j, \bar{a}_j)$  within the interaction representation in quantum mechanics and between the canonical and unitary transformations will be used below in the derivation of formulas for the generating functions.

Averaging the Hamiltonian (3.39) as it has been done above in Section 2.2, we obtain the Hamiltonian  $h(a, \bar{a})$ :

$$h(a, \bar{a}) = \varepsilon \left\{ \frac{3}{2} \lambda \left[ (a_1 \bar{a}_1)^2 + (a_2 \bar{a}_2)^2 \right] + \frac{\beta}{2} (a_1 \bar{a}_2 + \bar{a}_1 a_2) \right\}. \quad (3.40)$$

During the averaging process, as it can be seen from Eq. (3.40), in the expression of the Hamiltonian only the zero harmonic in time is left, while all the terms of the form  $\exp(itm)f(a, \bar{a})$  are neglected.

The rigorous mathematical derivation of the function  $h(A, \bar{A})$  is performed with the help of the canonical transformation of the following type:

$$\begin{aligned} A_j &= a_j + \varepsilon \frac{\partial \Lambda_0(a, \bar{A})}{\partial \bar{A}_j}, \\ \bar{A}_j &= \bar{a}_j - \varepsilon \frac{\partial \Lambda_0(a, \bar{A})}{\partial a_j}. \end{aligned} \quad (3.41)$$

The generating function for this transformation is determined by the formula:

$$\begin{aligned} S(a, \bar{A}) = & \sum_{j=1}^2 a_j \bar{A}_j \\ & + \varepsilon \sum_{j=1}^2 \frac{3\lambda}{8i} \left( a_j^4 e^{4it} - \bar{A}_j^4 e^{-4it} + 8a_j^3 \bar{A}_j e^{2it} - 8a_j \bar{A}_j^3 e^{-2it} \right) \\ & + \frac{\varepsilon\beta}{4i} (a_1 a_2 e^{2it} - \bar{A}_1 \bar{A}_2 e^{-2it}). \end{aligned} \quad (3.42)$$

It can be verified easily with the help of Eq. (3.39) that the new Hamiltonian  $H''$  in the new variables  $A, \bar{A}$  takes the shape:

$$h'(A, \bar{A}, t) = H''(A, \bar{A}, t) = h(A, \bar{A}) + \varepsilon^2 W(A, \bar{A}, t). \quad (3.43)$$

It follows from Eq. (3.43) that each local mode of the Hamiltonian  $h(A, \bar{A})$  is an LM of the exact Hamiltonian  $h'(A, \bar{A}, t)$  as well, at least during the period of time  $\tau \geq \varepsilon^{-2}$ . Really, if there exists a phase trajectory  $(a(t), \bar{a}(t))$ , the vicinity of which constitutes a minor part of the energy layer  $\Delta h$ <sup>11</sup>, then obviously the neighborhood of the exact trajectory  $(A(t), \bar{A}(t))$ , according to Eqs. (3.41) and (3.43) will form a minor part of the energy layer  $\Delta H$  as well, at least for time  $t \leq \tau \sim \varepsilon^{-2}$ . It is this property that makes possible the study of LM with the help of the averaged Hamiltonian  $h(a, \bar{a})$  in the variables  $(a, \bar{a})$ .

Let us find the LMs (3.40) and the conditions of their existence. The system (3.40) has, beside  $h(\bar{a}, a)$  one more constant of motion:

$$a_1 \bar{a}_1 + a_2 \bar{a}_2 = \frac{p_1^2 + q_1^2 + p_2^2 + q_2^2}{2} = I_1 + I_2 = I = R^2. \quad (3.44)$$

This is the total unperturbed action ( $\omega = 1$ ). In the considered approximation this quantity has been constant in the case of Morse oscillator as well (see formulas (3.13) and (3.14)). The fact that it is a constant of motion, is verified by the calculation of Poisson brackets:

$$\{I, h\} = \left\{ a_1 \bar{a}_1 + a_2 \bar{a}_2, \left[ \frac{3\lambda}{\beta} \left( (a_1 \bar{a}_1)^2 + (a_2 \bar{a}_2)^2 \right) + a_1 \bar{a}_2 + a_2 \bar{a}_1 \right] \right\} = 0.$$

Thus the phase trajectories of the system (3.40) belong to the cross-section of two surfaces:

---

<sup>11</sup>In the opposite case of ergodic motion the neighborhood of nearly any phase trajectory covers completely the whole energy layer  $\Delta h$ .

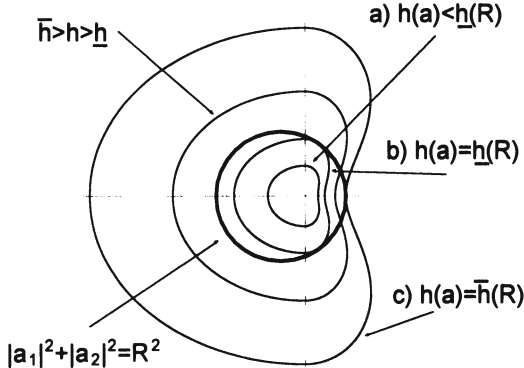


Figure 3.11: The geometrical illustration of conditions for the appearance and disappearance of solutions to the set of equations (3.45): (a)  $h < \underline{h}(R)$  – the surfaces  $R^2(a) = R^2$  and  $h(a) = h$  do not intersect – no solutions; (b) and (c)  $h = \underline{h}(R)$  or  $h = \bar{h}(R)$  – the surfaces touch each other – a solution appears. In the case, intermediate between (b) and (c)  $\underline{h}(R) < h < \bar{h}(R)$  the solution exists, and it survives small variations of  $h$  and of other constants of motion.

$$\begin{aligned} \varepsilon \frac{3}{2} \lambda \left( |a_1|^4 + |a_2|^4 \right) + \varepsilon \frac{1}{2} \beta (a_1 \bar{a}_2 + \bar{a}_1 a_2) &= h, \\ |a_1|^2 + |a_2|^2 &= R^2. \end{aligned} \quad (3.45)$$

From Eq. (3.45) it can be seen, that for  $R \sim 1$  and  $h \sim \varepsilon^2$  this set of equations has no solutions. It has no solutions for  $R \sim h$  either. The set (3.45) has a solution only for  $h \sim \varepsilon R^2$ . Thus for fixed values of  $R^2$  there are no solutions if  $h \ll R^2$  or  $h \sim R$ . So, for any  $R$  some value of the Hamiltonian function  $h(a, \bar{a}) = \underline{h}(R)$  exists, for which there appears a solution of the set of equations (3.45), and some value  $h(a, \bar{a}) = \bar{h}(R)$ , for which the solution disappears.

This situation is depicted schematically in Fig. 3.11.

It is clear from the figure, that with the increase of  $h$  for  $h = \underline{h}(R)$  there appears a solution of the set (3.45). With the subsequent increase of  $h$  from  $\underline{h}(R)$  to  $\bar{h}(R)$  the system always has a solution, which disappears when the inequality  $h > \bar{h}(R)$  is satisfied.

We note, that the cross-section of the surfaces, depicted in Fig. 3.11, refers to the hypersurfaces in the four-dimensional phase space. The cross-section is typically a two-dimensional surface. These two-dimensional surfaces degenerate into a line when the cross-section disappears. The line constitutes a closed phase trajectory, or the Poincaré cycle.

This assertion can be easily derived in analytical form, if one notes, that the solution of the system (3.45) forms at least a one-parametric set of points (a line), as the functions  $h(a, \bar{a})$  and  $R^2(a, \bar{a})$  are invariant with respect to the transformation  $(a \rightarrow ae^{i\varphi}, \bar{a} \rightarrow \bar{a}e^{-i\varphi})$ .

Let us perform the transformation  $t \rightarrow \frac{2t}{3\varepsilon\lambda}$ ,  $h \rightarrow \frac{3\varepsilon\lambda}{2}h$  with  $\gamma = \frac{\beta}{3\lambda}$ . Then the equations (3.45) take shape:

$$\begin{aligned} (a_1\bar{a}_1)^2 + (a_2\bar{a}_2)^2 + \gamma(a_1\bar{a}_2 + a_2\bar{a}_1) &= h, \\ a_1\bar{a}_1 + a_2\bar{a}_2 &= R^2. \end{aligned} \quad (3.46)$$

The equations (3.46) determine a two-dimensional surface to which the phase trajectories of the system belong. Let us demonstrate, that for each  $R^2$  on the three-dimensional manifold  $R^2(a) = R^2$  there exists an invariant manifold of nonzero measure, which consists of phase trajectories with one of the inequalities  $|a_1| \gg |a_2|$  or  $|a_2| \gg |a_1|$  satisfied. It means that the mentioned trajectories correspond to local vibrations. The latter means that in the phase space of the system (3.46) there exists a region of finite volume, which consists of LM phase curves.

Let us consider the case  $\gamma = 0$  first. Evidently, in the absence of inter-oscillator interaction local vibrations exist. Then the surfaces to which the phase trajectories belong are determined by the following equations, as it follows from Eq. (3.46):

$$a_1 = \sqrt{R^2 - \xi^2} e^{i\Psi}, \quad a_2 = \xi e^{i(\Psi+\Phi)}, \quad (3.47)$$

with the amplitude  $\xi$  satisfying

$$(R^2 - \xi^2)^2 + \xi^4 = h. \quad (3.48)$$

The family (3.47) is a one-parametric set of two-dimensional tori, which are numbered by the parameter  $h$ , and occupy entirely the whole hypersphere  $|a_1|^2 + |a_2|^2 = R^2$ . From Eq. (3.48) the inequality follows:

$$\underline{h} = \frac{R^4}{2} \leq R^4 = \bar{h}. \quad (3.49)$$

The geometrical interpretation of this inequality is shown in Fig. 3.12. For  $h = \bar{h} = R^4$  the tori (3.47) degenerate into a phase curve of the local vibration:

$$a_1 = Re^{i\Psi}, a_2 = 0, \quad \text{or} \quad a_1 = 0, a_2 = Re^{i\Phi}. \quad (3.50)$$

Thus the family of tori (3.47) for  $h \rightarrow \bar{h}$  has the trajectory of local vibration as the limiting manifold, whereas for  $h > \bar{h}$  ( $R^2$ ) the equation (3.46) has no solutions at all. This is seen clearly from Fig. 3.12: for  $h > \bar{h}$

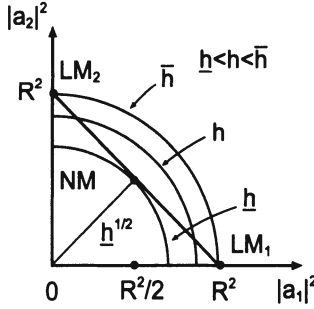


Figure 3.12: Graphical illustration to the solution of the system (3.46) with  $\gamma = 0$ .

the sphere  $|a_1|^2 + |a_2|^2 = h$  does not cross the straight line  $|a_1|^2 + |a_2|^2 = R^2$ . As the trajectory (3.50) corresponds to a local vibration, all the trajectories on tori (3.47) with  $h = \bar{h} - \delta$  correspond to local vibrations with small enough  $\delta$  as well. It means, that on the hypersphere  $R^2(a) = R^2$  there exists a region of finite volume ( $S \neq 0$ ), which is composed entirely of phase trajectories of local vibrations. Choosing a spherical layer with thickness  $\Delta R$ , we obtain a region of phase space with finite volume ( $V \neq 0$ ), which consists entirely of LM trajectories  $|a_1(t)| \gg |a_2(t)|$  (for all  $t$ ).

For the subsequent consideration it is convenient to determine the constructed region of phase space, corresponding to LM, with the help of the formula:

$$\mathcal{LM} = \bigcup_{R_0 < R < R_0 + \Delta R} ST(\bar{h}(R) - \delta), \quad (3.51)$$

where  $\mathcal{LM}$  is the region of phase space,  $ST(\bar{h}(R) - \delta)$  is the part of the hypersphere inside the torus (3.47), which in turn is the cross-section of the hypersurfaces  $h(a) = \bar{h}(R) - \delta$  and  $R^2(a) = R^2$ . The sum sign in Eq. (3.51) is used in the meaning of the manifold theory. The quantity  $\delta$  is small enough for  $|a_1| \gg |a_2|$  to be correct on all the tori; the layer thickness  $\Delta R$  is also low enough.

The introduction of a weak interaction ( $\gamma \ll 1$ ) between the oscillators leads to the following results: 1) the function  $\bar{h}(R)$  changes slightly; 2) the hypersurface  $h(a) = h$  and the tori of the section  $T(\bar{h}(R) - \delta)$  deform slightly; 3) the part of the hypersphere  $ST(\bar{h}(R) - \delta)$  inside the torus deforms slightly.

These changes have been taken into account in Eq. (3.51) and they lead to small deformations of the local mode region only. Thus, the consideration above proves that in the system characterized by the Hamiltonian (3.40) local vibrations exist, while in the system with Hamiltonian (3.43) such

vibrations decay during the time, not shorter than  $\tau \sim \varepsilon^{-2}$ . Consequently, in the general case  $N > 2$  for the proof of the LM existence it is sufficient to demonstrate the local character of the phase trajectory vibrations on the hypersphere  $R^2(a) = R^2$  close to the cross-section with the hypersurface  $h(a) = \bar{h}(R)$ , and then to construct these united surfaces in analogy with Eq. (3.51). In the consideration of the general case ( $N > 2$ ) below we will use this approach.

We note one more important consequence from the existence of the lower  $\underline{h}(R)$  and upper  $\bar{h}(R)$  bounds for the function  $h(a)$  on the hypersphere  $\sum |a_j|^2 = R^2$ . The existence of the conditional maximum and minimum of the function  $h(a, \bar{a})$  means that the equation for the conditional extremum with the Lagrange factor  $\omega$ :

$$\begin{cases} \frac{\partial h}{\partial \bar{a}_j} - \omega \frac{\partial R^2(a)}{\partial \bar{a}_j} = 0, \\ \frac{\partial h}{\partial a_j} - \omega \frac{\partial R^2(a)}{\partial a_j} = 0, \end{cases}, \quad \begin{cases} \frac{\partial h}{\partial \bar{a}_j} = \omega a_j, \\ \frac{\partial h}{\partial a_j} = \omega \bar{a}_j, \\ R^2(a) = R^2, \end{cases} \quad (3.52)$$

has two solutions at least. Comparing the Hamilton equations (3.37) and (3.52) we find that in the system there are Poincare cycles  $(a_j e^{i\omega t}, \bar{a}_j e^{-i\omega t})$ , where  $\omega$  and  $a_j$  are determined from Eq. (3.52). Obviously, this assertion is valid for any  $N$ . The LMs, correspondingly, lie in the vicinity of the cycle, which corresponds to the maximum of the Hamilton function  $\bar{h}(R)$ .

Let us demonstrate the validity of the obtained results on the LM existence by direct calculation of the Poincare cycles and of the phase trajectories in the vicinity of these cycles, when the values of the Hamilton function (3.46) differ slightly from their limiting values  $h = \bar{h} - \delta, h = \underline{h} + \delta$ . To find the boundary values  $\bar{h}$  and  $\underline{h}$ , and to construct the projections of phase trajectories on the two-dimensional plane (in analogy to Poincare sections, Sections 2.3 and 2.4) it is convenient to consider the solution of the system (3.46) under the condition:

$$a_1 = \bar{a}_1 = A, \quad a_2 = B e^{i\Phi}, \quad \bar{a}_2 = B e^{-i\Phi}. \quad (3.53)$$

This condition does not limit the generality of the treatment, as the solutions of Eq. (3.46) are obtained from Eq. (3.53) by a phase shift.

Substituting Eq. (3.53) into Eq. (3.46), we obtain the following equation for the lines in the section of tori (3.46) by the hyperplane (3.53)<sup>12</sup>:

$$h(A, \Phi) = A^4 + (R^2 - A^2)^2 + 2\gamma A \sqrt{R^2 - A^2} \cos \Phi = h. \quad (3.54)$$

Standard calculations lead to the following values of the parameters for the critical points of the function  $h(A, \Phi)$ :

---

<sup>12</sup>These lines in the section are nothing but the projections of phase curves, wound around the two-dimensional toruses (3.46).

a)  $\gamma < R^2$  :

$$\begin{aligned} \text{minimum } & \left( A^2 = \frac{R^2}{2}, \Phi = \pi \right), \quad h = \frac{R^4}{2} - \gamma R^2, \quad \omega = R^2 - \gamma; \\ \text{saddlepoint } & \left( A^2 = \frac{R^2}{2}, \Phi = 0 \right), \quad h_{sp} = \frac{R^4}{2} + \gamma R^2, \quad \omega = R^2 + \gamma; \\ \text{maximum } & \left( A_{1,2}^2 = \frac{R^2}{2} \left( 1 \pm \sqrt{1 - \frac{\gamma^2}{R^4}} \right), \Phi = 0 \right), \\ \bar{h} = h(A_{1,2}, 0) & = R^4 + \frac{\gamma^2}{2}, \quad \omega = 2R^2; \\ b) \gamma > R^2 : & \\ \text{minimum } & \left( A^2 = \frac{R^2}{2}, \Phi = \pi \right), \quad h = \frac{R^4}{2} - \gamma R^2, \quad \omega = R^2 - \gamma; \\ \text{maximum } & \left( A^2 = \frac{R^2}{2}, \Phi = 0 \right), \quad \bar{h} = \frac{R^4}{2} + \gamma R^2, \quad \omega = R^2 + \gamma. \end{aligned} \tag{3.55}$$

The frequencies  $\omega$  in Eq. (3.55) has been obtained with the help of equations (3.52). These critical points are in correspondence to the phase trajectories of Poincare cycles of the following form:

a)  $\gamma < R^2$  :

LM	$\begin{cases} a_1 = A_1 e^{i2R^2 t}, & a_2 = A_2 e^{i2R^2 t} \\ a_1 = A_2 e^{i2R^2 t}, & a_2 = A_1 e^{i2R^2 t} \end{cases}$	(3.56)
NMA	$\begin{cases} a_1 = \frac{1}{\sqrt{2}} Re^{i(R^2-\gamma)t}, & a_2 = \frac{1}{\sqrt{2}} Re^{i(R^2-\gamma)t+i\pi} \end{cases}$	
NMS	$\begin{cases} a_1 = \frac{1}{\sqrt{2}} Re^{i(R^2+\gamma)t}, & a_2 = \frac{1}{\sqrt{2}} Re^{i(R^2+\gamma)t} \end{cases}$	

b)  $\gamma \geq R^2$  : normal modes only.

Taking into account the definition (3.55) of the amplitudes  $A_1$  and  $A_2$ , we find that for LMs in every point of the phase trajectory either  $a_1 > a_2$  or  $a_1 < a_2$ , as it should be for a local vibration. On the contrary, for NMS and NMA the amplitudes  $a_1$  and  $a_2$  are equal, which means that these trajectories correspond to totally delocalized vibrations. Clearly, in the vicinity of LM cycle all the phase trajectories relate to local vibrations. As one can always choose  $R^2 > \gamma$ , regions of phase space with nonzero measure always exist, where the vibrations have local nature. As it follows from Eq. (3.55), for  $R^2 < \gamma$  local vibrations are absent.

The appearance / disappearance of LMs is depicted in Fig. 3.13. Here the lines of equal values of the function  $h(A, \Phi)$  are plotted for the two cases: a)  $\gamma < R^2$  and b)  $\gamma > R^2$ . These constant-value lines are the sections of two-dimensional tori, around which the phase trajectories wind up. These tori are obtained by rotation of constant-value lines around the axis  $A = 0$ . For such a rotation the axis perpendicular to the page is  $\text{Im } A$ , and consequently the quantity  $A\bar{A} = (\text{Re } A)^2 + (\text{Im } A)^2$  preserves its value. Thus the local or non-local nature of the phase trajectory (or of the corresponding torus) can

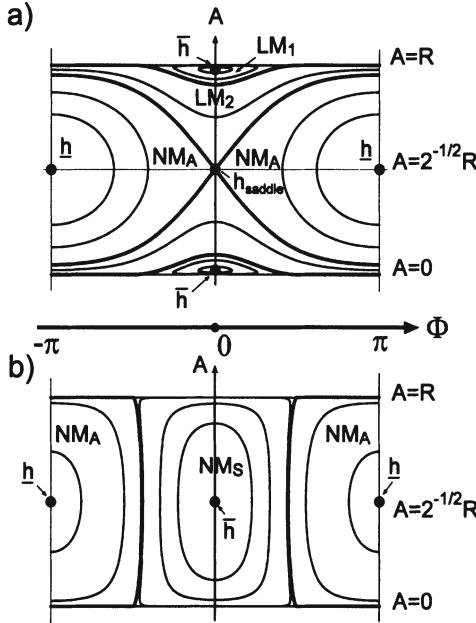


Figure 3.13: Level lines for the function  $h(A, \Phi)$ : (a)  $\gamma < R^2$ ; (b)  $\gamma > R^2$ .

be determined from the validity of the inequality  $A^2 - \frac{R^2}{2} \neq 0$ . For LM the latter is correct for all the points of the constant-value line, while for NM it is violated in two points. This last condition means, that the phase trajectory, wound on the corresponding torus almost periodically, visits all the time the points, for which  $|A|^2 = \frac{R^2}{2}$ . It can be noticed, that for  $\gamma > R^2$  all the lines of the section cross the point  $A^2 = \frac{R^2}{2}$  (no LMs), while for  $\gamma < R^2$  there are constant-value lines on which one of the two conditions is satisfied:  $|A|^2 > \frac{R^2}{2}$  or  $|A|^2 < \frac{R^2}{2}$  (LMs exist). The curves a) and b) of Fig. 3.13 are qualitatively similar to the phase portraits of Morse oscillators, depicted in Figs. 2.15 and 2.11 in Section 2.3. In both cases local vibrations disappear with the decrease of the excitation level: at  $R^2 < \gamma^2$  for oscillators with  $U = \epsilon q^4$ , and at  $I < 2\epsilon D$  for Morse oscillators. This is a general rule in fact, as with the diminishing excitation level the oscillator frequencies become closer in value, and thus the complete energy transfer from one oscillator to another becomes possible.

The proof of the existence of LMs with  $N = 2$  can be easily extended to the case  $N > 2$ , if it is possible to find a canonical transformation which transforms the Hamiltonian to the following shape:

$$h' = h(A, \bar{A}) + \varepsilon^2 P_{\bar{n}}(A, \bar{A}), \quad (3.57)$$

where

$$h = \frac{\varepsilon\lambda}{2} \sum_j |A_j^4| + \frac{\varepsilon\beta}{2} \sum_{i < j} V_{i,j} (A_i \bar{A}_j + \bar{A}_i A_j). \quad (3.58)$$

Here  $P_{\bar{n}}(A, \bar{A})$  is a polynomial of order  $\bar{n}$  in the variables  $(A_j, \bar{A}_j)$ , which does not depend on time explicitly, and does not change its form under the transformation  $(A_j, \bar{A}_j) \rightarrow (A_j e^{i\alpha}, \bar{A}_j e^{-i\alpha})$ . The latter means, that there exists a constant of motion:

$$R^2 = \sum_j^N (A_j, \bar{A}_j). \quad (3.59)$$

From Eqs. (3.59) and (3.57) it follows, that the function  $h'(A, \bar{A})$  reaches its maximum  $\bar{h}'$  and minimum  $h'$  values of the hypersphere  $R^2(A) = R^2$ . These limiting values are in correspondence to Poincare cycles, the positions and frequencies of which satisfy equations (3.52) for the conditional extremum.

The point from the vicinity of Poincare cycle in the maximum of the function  $h' = \bar{h}'$  corresponds to local modes. This fact becomes transparent from the following consideration. For  $\beta = 0$  the maximum value  $h' = \bar{h}'$  is reached, obviously, on the local mode (see Fig. 3.12),  $A_1 = R e^{i\Phi_1}, A_j = 0, j \neq 1$ . The close vicinity of this mode on the hypersphere represents the area

$$\left\{ A_1 = \sqrt{R^2 - \sum_2^N \delta_j^2 e^{i\Phi_1}}, \quad A_j = \delta_j e^{i\Phi_j} \right\},$$

$$(\bar{h}' - \delta) \leq h'(A) \leq \bar{h}', \quad \beta = 0. \quad (3.60)$$

For  $\delta \rightarrow 0$  this region reduces to a cycle of the local mode. The points of the manifold (3.60) belong to the unification of the crossed hypersphere  $R^2(A) = R^2$  with the family of hypersurfaces  $\bar{h}' > h' > \bar{h}' - \delta$ . For small enough  $\delta$  each point of the set (3.60) lies at a distance smaller than  $\delta$  from some limiting point of Poincare cycle. According to the theorem on continuous dependence of an implicit function on its parameter the position and form of the limiting cycle  $A_1 = R e^{i\Phi_1}$ , Eq. (3.51), as well as the  $(2n - 1)$ -dimensional parts of the hypersphere (3.60) depend continuously on the interaction constant  $\beta$  (with  $h(\beta)$  an analytic function), so that the introduction of interaction leads to their small deformation. Consequently, the points belonging to the manifold Eq. (3.60) remain in the vicinity of

the limiting cycle. Thus, according to Eq. (3.51), the unification of the parts of the hypersphere  $R^2(A) = R^2$ , obtained from the regions (3.60) by deformation due to the action of the interaction  $\beta \sum_{i,j} V_{i,j} q_i q_j$ , determine the region of phase space, which consists of LM phase trajectories.

Thus, we have shown, that in the system defined by Hamiltonian (3.57) there are local vibrations, phase trajectories of which fill in the region of phase space of finite volume  $v > 0$ . In the next Section we will provide a regular method for the construction of canonical transformations, which transform the Hamiltonian to the form of Eq. (3.57) plus the terms of the order of  $\exp(-\frac{1}{\epsilon})$ , which contribute at times  $t \gtrsim \exp(\frac{2}{\epsilon})$ . So we can state, that in the system of nonlinear oscillators with Hamiltonian (3.35) local vibrations exist, and their lifetime is  $\tau \gtrsim \exp(\frac{2}{\epsilon})$ , if the interaction constant  $\beta$  is low enough.

To conclude this Section let us construct the Poincare cycle, which corresponds two the LM in the system with Hamiltonian Eq. (3.58). The equations (3.52) for the cycle and the condition  $R^2(A) = R^2$  take shape:

$$\begin{aligned} \omega A_j &= \epsilon \lambda |A_j|^2 A_j + \frac{\epsilon \beta}{2} \sum_{k \neq j} V_{j,k} A_k, \\ A_1^2 + \sum_2^N A_k^2 &= R^2. \end{aligned} \quad (3.61)$$

The solution is sought for in the following form:

$$\begin{aligned} A_j &= R \delta_{1,j} + \beta x_j, \\ \omega &= \omega_0 + \beta z. \end{aligned} \quad (3.62)$$

Substituting Eq. (3.62) into (3.61) and picking up the coefficients preceding similar powers of  $\beta$ , we obtain the following solutions for  $A_j$  and  $\omega$ :

$$\begin{aligned} A_j &= \left( R - \frac{\beta^2}{8\lambda^2 R^3} \sum_{k=1}^N |V_{k,1}|^2 \right) \delta_{1,j} + \frac{\beta V_{1,j}}{2\lambda R} (1 - \delta_{1,j}), \\ \omega &= \epsilon \lambda R^2 [1 + O(\beta^2)]. \end{aligned} \quad (3.63)$$

From Eq. (3.63) we find, that the amplitudes of weakly excited oscillators ( $j \geq 2$ ) are lower in amplitude than those of highly excited ones ( $j = 1$ ) by the factor  $\sim \frac{A_j}{A_1} \sim \frac{\beta}{\lambda R^2}$ . This ratio decreases with the increase of the excitation level  $R^2$  and of the anharmonicity  $\lambda$ . The disappearance of the local mode can be determined in a natural way by the condition  $\frac{\beta}{\lambda R^2} \sim 1$ ,

which agrees with the accuracy up to a numerical factor  $\sim 1$  with the condition of LM disappearance in equation (3.56). Such an agreement could have been expected, as the energy transfer to one of the non-excited oscillators is fastest. The spreading of energy over all the oscillators is a much slower process.

### 3.5 Canonical transformation to local - mode representation

In the preceding Section it has been shown, that in the system with Hamiltonian Eq. (3.57) local vibrations exist. Let us construct the canonical transformation from Hamiltonian (3.35) to (3.57).

Going over from variables  $(p, q)$  to  $(a_j, \bar{a}_j)$  according to equation (3.36), we arrive at the canonical equations (3.37) of the form:

$$\begin{aligned} i \frac{da}{dt} &= \{U, a\} = -\frac{\partial U}{\partial \bar{a}}, \\ i \frac{d\bar{a}}{dt} &= \{U, \bar{a}\} = \frac{\partial U}{\partial a}. \end{aligned} \quad (3.64)$$

Here  $U(a, \bar{a})$  is the potential energy of the system (3.35), where the coordinates  $q_j$  are expressed through  $\bar{a}_j, a_j$  with the help of Eq. (3.36). Clearly, the function  $U(a, \bar{a}, t)$  will depend explicitly on time. The goal is to find the canonical transformation of the Hamilton function  $U(a, \bar{a}, t)$  into the Hamiltonian  $h'(\eta, \bar{\eta})$ , which does not depend on time explicitly. We will seek for the canonical transformation in the following form [13]:

$$\eta_j = a_j - i \{a_j, \Lambda\} + \frac{i^2}{2!} \{\{a_j, \Lambda\}, \Lambda\} + \dots \quad (3.65)$$

where  $\Lambda(a, \bar{a}, t)$  is some function, determined below. The canonical nature of the transformation (3.65) can be demonstrated in the most transparent way on the basis of the analogy with the unitary transformation in quantum mechanics. Really, the unitary transformation  $a_j \rightarrow \eta_j$  can be presented in the following form [57]:

$$\begin{aligned} \eta_j &= \exp[i\Lambda(a, \bar{a})] a_j \exp[-i\Lambda(a, \bar{a})] = \\ &= \bar{a}_j - i [a_j, \Lambda] + \frac{i^2}{2!} [[a_j, \Lambda], \Lambda] + \dots \end{aligned}$$

where  $\Lambda = \Lambda(a, \bar{a})$  is a Hermitian operator, expressed through  $(a_j, \bar{a}_j)$ , and  $[a, \Lambda]$  is the commutator of the operators  $a$  and  $\Lambda$ . Taking into account the fact, that in the classical limit the commutators are transformed into the

Poisson brackets [58], we immediately obtain Eq. (3.65). Here are some more details:

In the calculation of the commutator  $[A(a, \bar{a}), B(a, \bar{a})]$  the operators  $\bar{a}$  are moved to the left, while the operators  $a$  — to the right (normal representation). Then terms with one commutator  $[a, \bar{a}]$ , two commutators  $[a, \bar{a}][a, \bar{a}]$ , etc. emerge. Additional terms with the commutator  $[a, \bar{a}]$  provide contributions, lower in order with respect to the excitation number  $N$  (the number of boson 'particles'), and thus they can be neglected for  $N \gg 1$ . The classical limit corresponds to  $N \rightarrow \infty$ , so that the leading term in  $N$  is obtained for the provided unitary transformation, when only the terms, linear in  $[a, \bar{a}]$  are left in the calculation of the commutators. Such an approximation for the commutator  $[A(a, \bar{a}), B(a, \bar{a})] = C(a, \bar{a})$  leads to the fact, that the functional dependence of  $C(a, \bar{a})$  on the operator arguments  $(a, \bar{a})$  coincides (up to permutations) with  $C(a, \bar{a})$  from the Poisson brackets  $\{A(a, \bar{a}), B(a, \bar{a})\} = C(a, \bar{a})$  if  $\{a, \bar{a}\} = 1$ . Thus,  $\{\eta(a, \bar{a}), \bar{\eta}(a, \bar{a})\} = 1$ , which proves the canonical nature of the transformation  $(a, \bar{a}) \rightarrow (\eta, \bar{\eta})$ , and leads to the invariance of Poisson brackets with respect to the transformation:

$$\{F(a), \Phi(a)\}_{a, \bar{a}} = \{F(a(\eta)), \Phi(a(\eta))\}_{\eta, \bar{\eta}}.$$

The inverse transformation has the form:

$$a_j = \eta_j + i \{\eta_j, \Lambda\} + \frac{i^2}{2!} \{\{\eta_j, \Lambda\}, \Lambda\} + \dots \quad (3.66)$$

Then the following equality

$$\Lambda(a, \bar{a}) = \Lambda(\eta, \bar{\eta}) \quad (3.67)$$

holds due to the operational equation

$$\Lambda(a, \bar{a}) = e^{i\Lambda(a, \bar{a})} \Lambda(a, \bar{a}) e^{-i\Lambda(a, \bar{a})} = \Lambda(\eta, \bar{\eta}),$$

and due to the equivalence of the unitary and canonical transformations in the classical limit  $N \rightarrow \infty$  ( $N$  is the number of the excitation).

The Hamilton equations in the new variables can be written down in the form:

$$\begin{aligned} i \frac{d\eta_j}{dt} &= \{R, \eta_j\} = -\frac{\partial R}{\partial \bar{\eta}_j}, \\ i \frac{d\bar{\eta}_j}{dt} &= \{R, \bar{\eta}_j\} = \frac{\partial R}{\partial \eta_j}, \end{aligned} \quad (3.68)$$

which correspond to the form of Eqs. (3.64), as it should for canonical transformations.

The new Hamiltonian function is:

$$R(\eta, \bar{\eta}; t) = \varepsilon \left\{ U(\eta, \bar{\eta}; t) + i \{U, \Lambda\} + \frac{i^2}{2!} \{ \{U, \Lambda\}, \Lambda \} + \dots \right\} + iD, \quad (3.69)$$

where  $D(\eta, \bar{\eta}; t)$  is determined by the formula:

$$\begin{aligned} D(\eta, \bar{\eta}; t) &= \frac{\partial(i\Lambda(\eta, \bar{\eta}; t))}{\partial t} + \frac{1}{2!} \left\{ \frac{\partial(i\Lambda)}{\partial t}, i\Lambda \right\} \\ &\quad + \frac{1}{3!} \left\{ \left\{ \frac{\partial(i\Lambda)}{\partial t}, i\Lambda \right\}, i\Lambda \right\} + \dots \end{aligned} \quad (3.70)$$

For  $\frac{\partial\Lambda}{\partial t} = 0$  the canonical transformation (3.69) simply rewrites the old Hamiltonian  $U(a, \bar{a}; t)$  in the view variables  $U(a(\eta))$ . This becomes transparent from Eq. (3.69) with the account of Eqs. (3.66) and (3.67), and from the analogy between the canonical transformation (3.65) and the unitary transformation  $\hat{\eta} = e^{i\Lambda} \hat{a} e^{-i\Lambda}$ . In the general case  $\frac{\partial\Lambda}{\partial t} \neq 0$  a term  $iD \sim \frac{\partial\Lambda}{\partial t}$  is added to the function  $U(a)$ . In the end of the present Section we will prove rigorously the form (3.70) for the function  $D(\eta, \bar{\eta}; t)$  and (3.69) for the Hamiltonian  $R(\eta, \bar{\eta})$ .

To obtain the Hamiltonian of local modes  $h'(\eta, \bar{\eta})$  let us take the function  $\Lambda(\eta, \bar{\eta}; t)$  in a form such that  $R(\eta, \bar{\eta}; t)$  does not depend on time explicitly. We will look for  $\Lambda(\eta, \bar{\eta}; t)$  in the form of the series:

$$\Lambda = \varepsilon\Lambda_0 + \varepsilon^2\Lambda_1 + \dots + \varepsilon^p\Lambda_{p-1} + \dots \quad (3.71)$$

Let us introduce the following functions:

$$\left\{ \begin{array}{l} S_0 = \frac{\partial\Lambda}{\partial t}, \\ \dots \\ S_n = \underbrace{\left\{ \dots \left\{ \left\{ \frac{\partial\Lambda}{\partial t}, \Lambda \right\}, \Lambda \right\}, \dots, \Lambda \right\}}_{n \text{ times}}, \end{array} \right. \quad (3.72)$$

$$\left\{ \begin{array}{l} U_0 = \varepsilon U(\eta, \bar{\eta}; t), \\ \dots \\ U_n = \underbrace{\{ \dots \{ \{U_0, \Lambda\}, \Lambda \}, \dots, \Lambda \}}_{n \text{ times}}, \end{array} \right. \quad (3.73)$$

From Eqs. (3.72) and (3.73) it follows, that:

$$\left\{ \begin{array}{l} U_{n+1} = \{U_n, \Lambda\}, \\ S_{n+1} = \{S_n, \Lambda\}. \end{array} \right. \quad (3.74)$$

With the help of the variables  $U_n$  and  $S_n$  the Hamilton function  $R(\eta, \bar{\eta}; t)$ , defined by Eqs. (3.69) can be written down in the form:

$$R(\eta, \bar{\eta}; t) = \sum_{n=0}^{\infty} \left( U_n - \frac{S_n}{n+1} \right) \frac{i^n}{n!}. \quad (3.75)$$

Let us represent the functions  $U_n$  and  $S_n$  by series in  $\varepsilon$ :

$$\left\{ \begin{array}{l} S_n = \sum_{k=1}^{\infty} S_{n,k} \varepsilon^{n+k}, \\ U_n = \sum_{k=1}^{\infty} U_{n,k} \varepsilon^{n+k}, \quad U_{0,1} = U(\eta, \bar{\eta}; t), \quad U_{0,2} = U_{0,3} = \dots = 0. \end{array} \right. \quad (3.76)$$

Substituting Eqs. (3.71) and (3.76) into (3.75), and equating to zero the coefficients preceding time-dependent harmonics  $\exp(i\nu t)$  in all the orders in  $\varepsilon^{p+1}$ , we obtain the following set of recurrent equations for the determination of the Hamiltonian  $R(\eta, \bar{\eta})$  and of the function  $\Lambda_p(\eta, \bar{\eta}; t)$ :

$$\begin{aligned} p &= 1, \quad \varepsilon^1, \\ \frac{\partial \Lambda_0}{\partial t} &= S_{01} = U_{01} - \bar{U}_{01} = U(\eta, \bar{\eta}; t) - \overline{U(\eta, \bar{\eta}; t)}, \\ R(\eta, \bar{\eta}; t) &= \varepsilon (U_{01} - S_{01}) + O(\varepsilon^2) = \varepsilon \overline{U(\eta, \bar{\eta}; t)} + O(\varepsilon^2); \\ p &= 2, \quad \varepsilon^2, \\ \frac{\partial \Lambda_1}{\partial t} &= S_{02} = \frac{i}{1!} (U_{11} - \bar{U}_{11}) - \frac{i}{2!} (S_{11} - \bar{S}_{11}), \\ R(\eta, \bar{\eta}; t) &= \varepsilon (U_{01} - S_{01}) + \frac{i\varepsilon^2}{1!} \left( U_{11} - \frac{1}{2} S_{11} \right) - \varepsilon^2 S_{02} + O(\varepsilon^3) \\ &= \varepsilon \overline{U(\eta, \bar{\eta}; t)} + \frac{i\varepsilon^2}{2!} \overline{\left\{ U + \bar{U}, \int_t (U - \bar{U}) \right\}} + O(\varepsilon^3), \\ &\dots, \\ p &+ 1, \quad \varepsilon^{p+1}, \\ \frac{\partial \Lambda_p}{\partial t} &= S_{0,p+1} = \sum_{k=1}^p \frac{i^k}{k!} (U_{k,p+1-k} - \bar{U}_{k,p+1-k}) \\ &- \sum_{k=1}^p \frac{i^k}{(k+1)!} (S_{k,p+1-k} - \bar{S}_{k,p+1-k}), \\ R^{(p+1)}(\eta, \bar{\eta}; t) &= R^{(p)}(\eta, \bar{\eta}; t) \\ &+ \varepsilon^{p+1} \sum_{k=1}^p \frac{i^k}{k!} \overline{U}_{k,p+1-k} - \varepsilon^{p+1} \sum_{k=1}^p \frac{i^k}{(k+1)!} \overline{S}_{k,p+1-k}, \end{aligned} \quad (3.77)$$

where the bar in  $\overline{F(\eta, \bar{\eta}; t)}$  signifies the choice of zero time harmonic in the function  $F_0(\eta, \bar{\eta})$  (averaging over time), and  $\int_t$  is the integral in time:  $\int_t \{f(t)\} = \int dt \sum_{\nu \neq 0} f_\nu e^{i\nu t} = \sum_{\nu \neq 0} \frac{f_\nu}{i\nu} e^{i\nu t}$ . These recurrent equations make

possible the consecutive determination of the functions  $\Lambda_p(\eta, \bar{\eta}; t)$  in Eq. (3.71), and of the corresponding part of the Hamiltonian  $R(\eta, \bar{\eta})$ .

According to Eq. (3.77) the function  $R(\eta, \bar{\eta})$  is the zero-order harmonic of some real function  $K(\eta, \bar{\eta}; t)$ , which can be represented in the following form:

$$K(\eta, \bar{\eta}; t) = G(\eta e^{it}, \bar{\eta} e^{-it}),$$

where  $G(\eta, \bar{\eta})$  is some analytic function of  $2n$  variables  $(\eta_1, \dots, \eta_n, \bar{\eta}_1, \dots, \bar{\eta}_n)$ . The previous equation can be proved easily by mathematical induction with the help of recurrent equations (3.77) using the relations:

$$\begin{aligned} \{G_1(\eta e^{it}, \bar{\eta} e^{-it}), G_2(\eta e^{it}, \bar{\eta} e^{-it})\}_{\eta, \bar{\eta}} &= G_3(\eta e^{it}, \bar{\eta} e^{-it}), \\ \int_t [G(\eta e^{it}, \bar{\eta} e^{-it}) - \overline{G(\eta e^{it}, \bar{\eta} e^{-it})}] &= \tilde{G}(\eta e^{it}, \bar{\eta} e^{-it}), \\ U(\eta, \bar{\eta}; t) &= U(\eta e^{it} + \bar{\eta} e^{-it}). \end{aligned}$$

From Eq. (3.77) it follows, that the zero-order harmonic  $R(\eta, \bar{\eta}) = \tilde{K}(\eta, \bar{\eta}; t)$  in its expansion in variables  $\eta, \bar{\eta}$  contains the terms of the following form solely:  $\eta_1^{k_1} \dots \eta_N^{k_N} \bar{\eta}_1^{\bar{k}_1} \dots \bar{\eta}_N^{\bar{k}_N}$ , where

$$\sum_{j=1}^N k_j = \sum_{j=1}^N \bar{k}_j.$$

With the help of these relations one can prove easily, that

$$\left\{ R(\eta, \bar{\eta}), \sum_{j=1}^N |\eta_j^2| \right\} = 0,$$

and, consequently the quantity <sup>13</sup>

$$\sum_{j=1}^N |\eta_j^2| = R^2$$

is a constant of motion. The existence of such a constant has been used in the proof of the existence of local modes in the system with Hamiltonian  $R(\eta, \bar{\eta})$  (see Section 3.4).

According to the Eqs. (3.71) – (3.73), (3.76), for the determination of the quantities  $U_{k,p+1-k}$  and  $S_{k,p+1-k}$  with  $k \geq 1$  it is sufficient to find the functions  $\Lambda_m(\eta, \bar{\eta}; t)$  ( $m \leq p-1$ ). Thus the Eq. (3.77) enables us to

---

<sup>13</sup>Be sure not to mix the constant  $R$  with the transformed Hamiltonian  $R(\eta, \bar{\eta})$ .

find consecutively the functions  $\Lambda_p(\eta, \bar{\eta}; t)$  and the corresponding canonical transformation  $(a, \bar{a}) \rightarrow (\eta, \bar{\eta})$  along with the new Hamiltonian  $R(\eta, \bar{\eta}; t)$ .

If it were possible to pass to the limit  $p \rightarrow \infty$ , we would obtain the Hamiltonian  $R(\eta, \bar{\eta})$  without explicit time dependence, that is the Hamiltonian of local modes  $h'(\eta, \bar{\eta})$ , considered in the preceding Section.

Unfortunately the series (3.71) for the function  $\Lambda(\eta, \bar{\eta}; t)$  and Eq. (3.75) for the Hamiltonian do not converge, so that one has to truncate it for some  $p = \bar{n}$ . This procedure leads to the following representation of the Hamiltonian:

$$R(\eta, \bar{\eta}; t) = h(\eta, \bar{\eta}) + g_{\bar{n}} W(\eta, \bar{\eta}; t), \quad (3.78)$$

where  $|W(\eta, \bar{\eta}; t)| < 1$ . The constant  $g_{\bar{n}}$  satisfies the inequality:

$$|g_{\bar{n}}| < \varepsilon^{\bar{n}} M^{\bar{n}} \bar{n}! \Big|_{\bar{n}=(\varepsilon M)^{-1} \gg 1} \approx \exp \left( -\frac{1}{\varepsilon M} \right) \ll 1. \quad (3.79)$$

The latter follows from the fact that  $g_{\bar{n}} W(\eta, \bar{\eta}; t)$  contains terms proportional to  $S_{\bar{n}}$  and  $U_{\bar{n}}$ . According to Eqs. (3.72) and (3.73) these quantities are proportional to the product of the following derivatives:

$$\left( \frac{\partial U}{\partial \eta} \right)^{\bar{n}}, \left( \frac{\partial^{\bar{n}-m} U}{\partial \eta^{\bar{n}-m}} \frac{\partial^m U}{\partial \eta^m} \right), \frac{\partial^{\bar{n}} U}{\partial \eta^{\bar{n}}}, \text{ etc.}$$

Due to the analyticity of the function  $U(\eta)$  in each of its arguments, such terms are inferior to the quantities  $M^{\bar{n}} (\bar{n}!)$ , where  $M$  is some constant, dependent on the form of  $U(\eta, \bar{\eta})$ . This leads immediately to Eq. (3.79). In the present case the potential energy  $U(q)$  is a polynomial of order four<sup>14</sup> in the coordinates  $q_j$ . Then the transform (3.77) leads to Eq. (3.78), where the function  $h(\eta, \bar{\eta})$  is a polynomial of order  $\bar{n}$ .

The canonical transformation, determined by the function:

$$\Lambda_{\bar{n}} = \sum_{p=1}^{\bar{n}} \varepsilon^{p+1} \Lambda_p(\eta, \bar{\eta}; t)$$

generates the Hamiltonian (3.78) similar to Eqs. (3.43) and (3.57). It has been shown in the previous Section, that the latter corresponds to a system of nonlinear oscillators with local vibrations, which decay with the lifetime not less than  $\tau \gtrsim g_{\bar{n}}^{-2} \sim \exp \frac{2}{\varepsilon M}$ .

The obtained result is the following: in a system of nonlinear oscillators with Hamiltonian (3.35) for low enough values of  $\varepsilon$  it is always possible to choose small but nonzero values of the interaction strength  $\beta$ , so that local vibrations will be realized. The lifetime of these is  $\tau \gtrsim \exp \left( \frac{2}{\varepsilon M} \right)$  with  $M$

---

<sup>14</sup>Such a choice of  $U(q)$  is not a substantial limitation. The same conclusions remain valid for any analytical function  $U(q)$  in some bounded region  $|q_j| < Q$ .

independent of  $\varepsilon$ <sup>15</sup>. This estimate of the lifetime is close to the one obtained in [59].

To conclude we provide the derivation of Eq. (3.70) for the function  $D(\eta, \bar{\eta}; t)$ . Utilizing the analogy with the unitary transformation we will consider the quantities  $\eta, a$  to be Heisenberg operators, introduced according to the relations:

$$\eta = e^{i\Lambda(a,t)} a e^{-i\Lambda(a,t)}, \quad (3.80)$$

where  $a(t)$  satisfies the equation<sup>16</sup>:

$$i \frac{da}{dt} = [U(a, t), a].$$

Differentiating Eq. (3.80) over time explicitly, we obtain:

$$\begin{aligned} \frac{\partial \eta}{\partial t} &= \left( \frac{\partial}{\partial t} e^{i\Lambda(a,t)} \right) a e^{-i\Lambda(a,t)} + e^{i\Lambda(a,t)} a \left( \frac{\partial}{\partial t} e^{-i\Lambda(a,t)} \right) \\ &= [D(\eta, t), \eta]. \end{aligned} \quad (3.81)$$

where the operator  $D(a, t)$  is determined by the formula:

$$\begin{aligned} \frac{\partial}{\partial t} e^{i\Lambda(a, \bar{a}, t)} &= e^{i\Lambda(a, \bar{a}, t)} D(a, \bar{a}, t), \\ \frac{\partial}{\partial t} e^{-i\Lambda(a, \bar{a}, t)} &= D(a, \bar{a}, t) e^{-i\Lambda(a, \bar{a}, t)}. \end{aligned} \quad (3.82)$$

In the derivation Eq. (3.81) the equation (3.67) has been used.

The expression of  $D(a, \bar{a}, t)$  will be obtained later. From Eqs. (3.80) and (3.81) it follows that the derivative of the Heisenberg operator  $\eta(a, \bar{a}, t)$  satisfies:

$$\begin{aligned} i \frac{d\eta(a, \bar{a}, t)}{dt} &= i \frac{\partial \eta}{\partial t} + [U(a, \bar{a}, t), \eta] \\ &= \left[ e^{-i\Lambda(\eta, \bar{\eta}, t)} U(\eta, \bar{\eta}, t) e^{i\Lambda(\eta, \bar{\eta}, t)} + i D(\eta, \bar{\eta}, t), \eta \right] \\ &= [R(\eta, \bar{\eta}, t), \eta]. \end{aligned} \quad (3.83)$$

<sup>15</sup>The constant  $M$  depends only on the form of the function  $U(q)$  and of its derivatives.

<sup>16</sup>Typically the Heisenberg operators are introduced with the help of the equation  $i \frac{da}{dt} = [a, u(a)]$ . The difference comes from the form of Eqs. (3.64) and its quantum analogues, where  $\{u, a\}$  is substituted by  $[u, a]$ . Evidently, the physical meaning of the operators under consideration is not of any importance. What matters is the requirement, that the considered operator relations transform into valid equations upon the substitution of operator functions by usual numeric functions, and of the commutator  $[A, B]$  by the Poisson brackets  $\{A, B\}$ .

It is clear that the Hamilton equations (3.68) are the analogues of Eq. (3.83), when the commutator [ ] is substituted by the Poisson brackets { }. Then  $R(\eta, \bar{\eta}, t)$  will be determined by Eq. (3.69). The expression of the operator function  $D(\eta, \bar{\eta}, t)$  is to be found.

To find  $D(\eta, \bar{\eta}, t)$ , determined by Eq. (3.82), let us write down the derivative  $\frac{\partial \Lambda^{\bar{n}}(\eta, \bar{\eta}, t)}{\partial t}$  with all the powers of  $\Lambda^m$  moved with the help of commutator rules to the left. Then we obtain:

$$\begin{aligned} \frac{\partial}{\partial t} \Lambda^{n+1}(t) &= \left( \sum_{k=0}^n C_{n-k}^0 \right) \Lambda^n \Lambda' \\ &+ \left( \sum_{k=0}^{n-1} C_{n-k}^1 \right) \Lambda^{n-1} [\Lambda', \Lambda] + \left( \sum_{k=0}^{n-2} C_{n-k}^2 \right) \Lambda^{n-2} [[\Lambda', \Lambda], \Lambda] + \dots \\ &+ \left( \sum_{k=0}^0 C_n^m \right) \underbrace{[\dots [\Lambda', \Lambda], \dots \Lambda]}_{n \text{ times}}, \end{aligned} \quad (3.84)$$

where  $C_n^m = \frac{n!}{m!(n-m)!}$ . Utilizing the formula [60]:

$$\left( \sum_{k=\nu}^{n-1} C_k^\nu \right) = \frac{n(n-1)\dots(n-\nu)}{(\nu+1)!}$$

we obtain with the help of Eq. (3.84) the following relations:

$$\begin{aligned} \frac{\partial}{\partial t} e^{i\Lambda} &= \sum_{n=0}^{\infty} \frac{1}{(n+1)!} \frac{\partial}{\partial t} (i\Lambda)^{n+1} \\ &= e^{i\Lambda} \sum_{\nu=0}^{\infty} \frac{i^{\nu+1}}{(\nu+1)!} \underbrace{[\dots [\Lambda', \Lambda], \dots]}_{\nu \text{ times}} = e^{i\Lambda(\eta)} D(\eta). \end{aligned}$$

Thus for  $D(\eta)$  we find:

$$D(\eta, t) = \sum_{\nu=0}^{\infty} \frac{i^{\nu+1}}{(\nu+1)!} \underbrace{[\dots [[\Lambda', \Lambda], \Lambda], \dots]}_{\nu \text{ times}}. \quad (3.85)$$

Substituting [ , ] for { , } we derive the equation (3.70) for  $D(\eta, \bar{\eta}, t)$ , the latter entering the definition of the transformed Hamiltonian  $R(\eta, \bar{\eta}, t)$ .

In conclusion we note, that the energy localization effects in elastic homogeneous chains with quartic interaction has been observed in numerical experiments [49, 61, 62, 63].

## Chapter 4

# Discrete breathers

This Chapter is devoted to the theory of breathers. Breathers are localized vibrational excitations of Hamiltonian lattices. Breather-like objects form a natural generalization of the notion of a local mode — from a finite Hamiltonian system to an infinite lattice. This is why many notions are easily and transparently taken over from the world of finite-dimensional Hamiltonian systems to that of infinite-dimensional ones. Such examples are the notions of a constant of motion and of the integrability of the system. The latter denotes the fact, that the trajectories of the system belong to a differentiable manifold, which is in fact an intersection of an infinite number of surfaces with fixed values of constants of motion. In short, in the present Chapter we use the notions and assertions introduced in Chapter 2 plus the notions from the theory of phonons (plane waves). The phonons under some conditions are capable of destroying the breather, taking its energy away. The corresponding conditions are found and investigated. A review of the theory of breathers, comparison of the theoretical and experimental results, and references can be found in [64].

### 4.1 Breathers in Hamiltonian lattices

In this Section we will consider the physics of discrete breathers, i.e. of localized dynamical excitations in d-dimensional Hamiltonian lattices. The sites of the lattice are particles of mass  $m$ , which interact with a finite number of neighbors (typically the nearest ones) via anharmonic potentials. Such systems constitute a natural generalization of finite-dimensional Hamiltonian systems. Consequently, many notions and methods used in the study of finite-dimensional Hamiltonians can be successfully applied in the studies of Hamiltonian lattices. The corresponding material has been reviewed briefly in the first three Sections of Chapter 2 and in the Introduction. The knowledge of the presented material will be sufficient for the understanding of the consideration below.

In the studies of Hamiltonian lattices, however, new aspects of the problem arise due to the infinite number of degrees of freedom. For example, no analogy to the Kolmogorov-Arnold-Mozer (KAM) theorem exist. Thus, there is no general recipes for the analysis of changes of the trajectories for integrable systems under the action of small perturbation, so that special methods should be worked out in each separate case. This fact makes the study of the structure of phase space and of the type of trajectories much more complicated, even locally. The basic reason of these complications lies in the profound qualitative difference in the topology of manifolds with infinite number of dimensions and of the finite-dimensional differentiable manifolds. For example, the assertion that from each bounded infinite sequence a converging sub-sequence can be chosen no longer holds true. In finite-dimensional topological continuous manifolds that was always possible.

Due to the absence of KAM-like theorems, the analysis of motion of Hamiltonian lattices requires the use of exactly solvable models (if possible) on one hand, and numerical experiments on the other. Then the obtained information is generalized on the basis of heuristic physical principles. The rigorous mathematical construction of the theory of discrete breathers is still far ahead. Such an theory should formulate the conditions for the existence of breathers, the conditions of their stability, provide methods for the analysis of the stability of trajectories with respect to small perturbation of the potential and of the initial conditions. Below we provide a brief review of the theory of discrete breathers "within physical level of rigorousness". More details and the corresponding references can be found in the review [64].

Breathers correspond to local vibrations of an elastic lattice. As the lattice constant tends to zero, this solution on physical grounds should change into vibrations of an elastic medium. In other words, one should expect, that in a nonlinear elastic media breather-type solutions should exist. Really, the well-known nonlinear sine-Gordon (sG) equation

$$\psi_{tt} = \psi_{xx} - F(\psi), \quad F(\psi) = M^2 \sin \psi, \quad \psi \equiv \psi(x, t) \quad (4.1)$$

has a breather-type solution of the form:

$$\psi_b(x, t) = 4 \tan^{-1} \left[ \frac{m \sin(\omega t)}{\omega \cosh(mx)} \right], \quad \omega = \sqrt{M^2 - m^2}. \quad (4.2)$$

This solution oscillates periodically in time with frequency  $\omega$  and decays exponentially in space as  $\exp(-m|x|)$  with the increasing distance from the center of the breather  $x = 0$ . The solutions (4.2) form a one-parameter set of localized functions. In the general case the center of the breather can move in space.

The generalization of the solution (4.2) leads to the following heuristic physical definition of a breather: a breather is a local excitation of an elastic medium, which possesses some inner structure, changes periodically in time ("breathes"), and possibly propagates in space. In the particular case of zero oscillation frequency  $\omega = 0$  the breather is termed soliton.

We note from the beginning, that far from all the nonlinear equations for the vibrations of elastic media have breather-like solutions. For example, the wave equation with the nonlinearity of the type  $F(\psi) = -\psi + \psi^3$  instead of (4.1) has no breathers [65]. The decay rate of breather-like states with low energy in such a system has been calculated in Ref. [66].

The existence of breathers in the solutions of Eq. (4.1) is more of an exception, than of a rule. Really, the frequency spectrum  $\Omega(q)$  of a linearized equation (4.1) has the form:

$$\Omega(q) = \sqrt{q^2 + F'(0)}, \quad -\infty < q < +\infty, \quad (4.3)$$

where  $q$  is the wavevector. The frequency spectrum  $\Omega(q)$  extends from  $\sqrt{F'(0)}$  up to  $+\infty$ . Thus, any high enough harmonic  $(k, \omega)$  of a breather-like solution will be in resonance with the eigen-vibrations of the linear system, and will consequently generate phonons (plane waves) of frequency  $\Omega(q) = k\omega$ . The latter will take away the energy from the breather, leading to its decay. For the decay to be absent, the breather solutions should satisfy an infinite number of conditions. In other words, the nonlinear equation should possess a infinite number of symmetries. The sG equation is in fact totally integrable, which means that it has an enumerable (infinite) number of constants of motion, and, consequently, an enumerable number of symmetries. It is due to this fact, that the elastic media, described by sG equations, produces breathers. Small perturbations  $\sin \psi \rightarrow \sin \psi + \lambda V(\psi)$  typically destroy the integrability and lead to the decay of breathers.

The situation with Hamiltonian lattices is totally different <sup>1</sup>. Here the phonon spectrum is bounded by Debai frequency  $0 \leq \Omega(q) \leq \Omega_D$ . If the frequencies of the breather exceed the Debai frequency  $\omega > \Omega_D$  then no harmonics are in resonance with the phonons. Consequently, breathers are expected to exist in such a system. More to it, if there is a branch of optical phonons, the existence of breathers with frequency  $\omega < \Omega_0$ , satisfying  $2\omega > \Omega_D - \Omega_0$  is possible – as there are no resonances,  $k\omega \neq \Omega(q)$  for any  $k$ .

To illustrate the exceptional nature of breathers we note, that all the efforts to find breather-like solutions for Einstein-Maxwell equations, which describe the electrical vacuum, or for the equations describing a one - dimensional optical media with Kerr nonlinearity capable of self-induced transparency, met no success [67, 68]. Apparently, breather-like solutions of nonlinear equations of the sG type and of similar ones are of little use for the the-

---

<sup>1</sup>For simplicity we will consider primarily one-dimensional lattices.

oretical interpretation of experiments in various fields of nonlinear physics. Really, it is hard to believe, that isolated, nongeneric and structurally unstable (with respect to small perturbations of the potential) objects are useful for the description of phenomena in nature. More suitable and realistic are discrete breathers, which described local vibrations in Hamiltonian lattices.

## 4.2 Discrete breathers in one-dimensional chains

In this Section we will formulate, following Ref. [64], the concept of an approach, which allows one to predict the existence or nonexistence of breathers in lattice systems without actually solving the corresponding equations.

The idea of one approach to the proof of breather existence is the following. First, breathers are constructed for some trivial integrable system, which in some mathematical sense is close to the system of interest. Then the procedure of analytical continuation of breather solutions is performed in some small parameter, which characterizes the deviation of the original system from the trivial one.

The second approach is based on the analytical continuation of wavepackets of the linear system in the vicinity of the band edge in the small parameter of the nonlinear interaction, and on the subsequent study of the stability of such a continuation with respect to the variations of the potential and of the wavepacket form.

It has been shown with the help of these methods (see Ref. [64]), that stable breather solutions arise from continuations of only periodic orbits of integrable systems. The physical background for such a situation is the following. The non-periodic solutions for integrable systems can be expanded into Fourier series in time, which contain at least two fundamental incommensurate frequencies  $\omega_1$  and  $\omega_2$ . The superposition of these harmonics  $n_1\omega_1 + n_2\omega_2$  can be in resonance with any frequency of the phonon spectrum with the suitable choice of integer numbers  $n_1$  and  $n_2$ :

$$n_1\omega_1 + n_2\omega_2 \approx \Omega(q). \quad (4.4)$$

Consequently, any multi-frequency breather-like solution in an infinite translationally invariant elastic lattice will be a decaying one.

Thus, we arrive at the conclusion, that in Hamiltonian lattices with weak nonlinearity or with weak interaction between lattice sites the breathers are nothing but periodic orbits of an integrable system, slightly modified by interaction. The integrable system above is constructed from the real system under consideration with weak nonlinearity neglected, or with weak inter-site interaction neglected.

Next we formulate briefly the quantitative conditions for the existence of breathers. The fact, that stable breathers correspond necessarily to periodic

orbits will be revealed again. The conditionally-periodic local excitations decay inevitably. Of interest are the methods, which enable one to calculate the decay time of such breather-like structures. More details on that subject can be found in Refs. [69, 70, 71, 72].

We will demonstrate the method of the determination of existence/non-existence of breathers with the help of the system with the Hamiltonian:

$$H = \sum_{l=-\infty}^{+\infty} \left[ \frac{1}{2} \dot{u}_l^2 + V(u_l) + \Phi(u_l - u_{l-1}) \right]. \quad (4.5)$$

Here  $u_l$  is the displacement of the  $l$ -th particle with mass 1 from the equilibrium position at the  $l$ -th site. The potentials  $V(z)$  and  $\Phi(z)$  are determined by the formulas:

$$V(z) = \sum_{s=2}^{\infty} \frac{1}{s} V_s z^s, \quad \Phi(z) = \sum_{s=2}^{\infty} \frac{1}{s} \Phi_s z^s. \quad (4.6)$$

Widely used is the particular case, when  $V_2 = 1$ ,  $V_3 = -1$ ,  $V_4 = 0.25$ , and  $\Phi_2 = 0.1$ , while all the other coefficients in Eq. (4.6) are identically zero. Let us introduce the quantity – the energy density:

$$e_l = \left[ \frac{1}{2} \dot{u}_l^2 + V(u_l) \right] + \frac{1}{4} \Phi_2 \left[ (u_l - u_{l-1})^2 + (u_l - u_{l+1})^2 \right]. \quad (4.7)$$

The sum over the sites  $l$  provides the exact value of the total energy  $E$  if the coefficients satisfy  $\Phi_s = 0$  for  $s > 2$ . It is convenient to introduce the excitation energy according to the formula <sup>2</sup>:

$$e_{(2m+1)}(l_0) = \sum_{l_0-m}^{l_0+m} e_l. \quad (4.8)$$

With the help of a suitable choice of integer numbers  $l_0$  and  $m$  one can specify the excitation energy. More to it, having determined the time dependencies  $l_0(t)$  and  $m(t)$ , one can control the evolution of the breather energy distribution in space. This evolution characterizes the stability/instability of the breather, and in the latter case specifies its decay time. The numerical calculations are performed typically for the value  $l_0 = 0$ . Then if the center of mass of the breather stays still, there are only the quantities  $m(t)$  and the energy within some fixed localization interval  $(-m, +m)$  to be studied.

The Hamilton equations of the system (4.5) take the form:

$$\ddot{u}_l + V_2 u_l + \Phi_2 [2u_l - u_{l-1} - u_{l+1}] + f\{u_l\} = 0, \quad (4.9)$$

---

<sup>2</sup>In the case  $l_0 \equiv 0$  we will write this quantity in the simplified form as  $e_{2m+1}$ .

$$f\{u_l\} = \sum_{s=3}^{\infty} V_s u_l^{s-1} + \sum_{s=3}^{\infty} \Phi_s \left[ (u_l - u_{l-1})^{s-1} + (u_{l+1} - u_l)^{s-1} \right].$$

Equation (4.9) contains the linear terms, responsible for the phonon branch of vibrations, and the nonlinear part  $f\{u_l\}$ , which forms the breathers.

Assuming that the breathers are formed solely from the conditionally-periodic solutions for integrable systems<sup>3</sup>, we look for breather-like solutions in the form:

$$u_l(t) = \sum_{k_1, \dots, k_n = -\infty}^{\infty} A_{l;k_1, \dots, k_n} \exp[i(k_1 \omega_1 + k_2 \omega_2 + \dots + k_n \omega_n)]. \quad (4.10)$$

Then a breather exists under the following condition:

$$A_{l;k_1, \dots, k_n} \rightarrow 0, \quad \text{when } l \rightarrow \pm\infty. \quad (4.11)$$

From Eq. (4.11) it follows in general, that the nonlinear part  $f\{u_l\}$  in Eq. (4.9) goes to zero faster, than the linear terms. Then the necessary and sufficient conditions for the existence of breathers are reduced to the demand, that the solutions of the linear part of Eq. (4.9) should provide decaying exponents for  $l \rightarrow \pm\infty$ . Obviously, the frequencies  $\omega_\nu$  and their harmonics  $k_\nu \omega_\nu$  must not fall into the region of the phonon spectrum, as then the linear part of Eq. (4.9) has a solution in the form of an exponent, oscillating in space. Substituting Eq. (4.10) into Eq. (4.9) and neglecting the nonlinear terms, we present the linear part in the following form:

$$\begin{aligned} A_{l+1;k} &= [\kappa_k(\omega) + 2] A_{l;k} - A_{l-1;k}, \\ \kappa_k(\omega) &= \left[ V_2 - \left( \sum_{\nu=1}^n k_\nu \omega_\nu \right)^2 \right] \Phi_2^{-1}. \end{aligned} \quad (4.12)$$

Equation (4.12) is a linear two-dimensional map, and  $A_{l;k} = 0$  is a fixed point of this map, as it is for the original nonlinear map with the retained nonlinear terms. This linear map is defined by the transformation with the following two-dimensional matrix  $G$ :

$$\begin{pmatrix} A_{l+1;k} - A_{l;k} \\ A_{l+1;k} \end{pmatrix} = \begin{pmatrix} 1 & \kappa_k(\omega) \\ 1 & \kappa_k(\omega) + 1 \end{pmatrix} \begin{pmatrix} A_{l;k} - A_{l-1;k} \\ A_{l;k} \end{pmatrix}. \quad (4.13)$$

The eigenvalues of matrix  $G$  are:

---

<sup>3</sup>This hypothesis is backed up by the results of numerical experiments.

$$\lambda_{1,2} = \left[ 1 + \frac{1}{2} \kappa_k(\omega) \right] \pm \sqrt{\left[ 1 + \frac{1}{2} \kappa_k(\omega) \right]^2 - 1}, \quad \lambda_1 \lambda_2 = 1. \quad (4.14)$$

Equations (4.14) suggest, that the following three cases are possible:

a)  $\kappa_k(\omega) > 0$ , so that  $0 < \lambda_2 < 1$  and (4.15)

$\lambda_2 \rightarrow 1$ , when  $\kappa_k(\omega) \rightarrow 0$ ,  $\lambda_2 \rightarrow 0$ , when  $\kappa_k(\omega) \rightarrow \infty$ .

b)  $\kappa_k(\omega) < -4$ , so that  $-1 < \lambda_1 < 0$  and (4.16)

$\lambda_1 \rightarrow 0$ , when  $\kappa_k(\omega) \rightarrow -\infty$ ,  $\lambda_1 \rightarrow -1$ , when  $\kappa_k(\omega) \rightarrow -4$ .

c)  $-4 \leq \kappa_k(\omega) \leq 0$ , so that  $|\lambda_1| = |\lambda_2| = 1$ . (4.17)

From Eqs. (4.15), (4.16) it follows, that in the cases a) and b) the existence of breathers is possible, as the linear solutions contain exponents, which decay in space. In case c), on the contrary, breathers can not exist, as the amplitudes  $A_{l;k}$  do not decay for  $|\lambda_1| = |\lambda_2| = 1$ . As the transformation (4.13) is invariant with respect to the substitution  $l+1 \leftrightarrow l-1$  with the transformation matrix  $G$  left intact, all the consideration above, concerning the decay of  $A_{l;k}$  in space for  $l \rightarrow \infty$  remains valid in the limit  $l \rightarrow -\infty$  as well.

Next we note, that for  $l \rightarrow \pm\infty$  the nonlinear terms are small compared to the linear ones. The latter, taken into account, will preserve the exponential decay, introducing only slight modifications into the space dependence of  $A_{l;k}$ . On the other hand, changing either the energy or the frequency  $\omega_\nu$  one can make the solution, which decayed for  $l \rightarrow -\infty$ , transform into the exponentially decaying one for  $l \rightarrow +\infty$  when  $l$  changes from  $-\infty$  to  $+\infty$ . This situation is in complete analogy to the choice of energy eigenvalue in the Schroedinger equation: first a function, decaying for  $x \rightarrow -\infty$  is selected, then the energy  $E$  is chosen in such a way, that this function with  $x$  growing transforms into a decaying solution for  $x \rightarrow +\infty$ . To make sure breathers exist one has to verify the realization of the discussed conditions for all Fourier components  $A_{l;k_1,\dots,k_n}$  simultaneously. Below we will demonstrate, that it can be fulfilled typically for single-frequency solutions ( $n = 1$ ) only, or, in other words, for periodic orbits. In the case of quasi-periodic solutions with  $n \geq 2$  some amplitude  $A_{l;k_1,\dots,k_n}^{(\omega_1, \dots, \omega_n)}$  typically will not decay in space. The reason has been stated above — it is always possible to construct some linear combination of fundamental (basic) frequencies  $(\omega_1, \dots, \omega_n)$ , which will be at resonance with the frequencies of the phonon

spectrum (see Eq. (4.4)). Multi-frequency breathers can be realized as exceptional cases only, when the system possesses some additional symmetries and, consequently, the corresponding constants of motion [73].

Let us consider in more detail the conditions of existence of a single-frequency (or periodic) breather,  $n = 1$ . Then we find:

$$\kappa_{k_1}(\omega_1) = \frac{V_2 - (k_1\omega_1)^2}{\Phi_2}, \quad (4.18)$$

where  $V_2$  and  $\Phi_2$  are the parameters of the quadratic terms in the potential (4.6). According to Eq. (4.12), these terms determine the position of the band in the phonon spectrum  $\Omega(q)$ :

$$V_2 \leq \Omega^2(q) \leq V_2 + 4\Phi_2. \quad (4.19)$$

The condition (4.19) for  $\Omega^2(q)$  coincides with Eq. (4.17) for the harmonics  $k_1\omega_1$ . Thus the condition for nonexistence of a breather (4.17) can be formulated briefly in the following form: if any harmonics  $k_1\omega_1$  gets into the phonon band:

$$(k_1\omega_1)^2 = \Omega^2(q), \quad (4.20)$$

the breather is destroyed. The substitution of Eq. (4.20) into Eq. (4.19) provides an equation, which determines the band of  $\omega_1$  - frequencies with no breathers:

$$V_2 < (k_1\omega_1)^2 \leq V_2 + 4\Phi_2, \quad (4.21)$$

where  $k_1$  is an integer. If some value of  $k_1$  satisfies Eq. (4.21), then breathers are absent, as the  $k_1$  - harmonic  $A_{l,k_1}(\omega_1)$  decays, and the other harmonics decay through it as well. Thus all the energy of localized vibrations is transferred to the phonons.

From Eq. (4.21) it follows, that breathers with frequencies

$$\omega_1 > V_2 + 4\Phi_2 \quad (4.22)$$

should be anticipated, as Eq. (4.21) can not be satisfied then. Another conclusion is that a stable multi-frequency breather can not exist, as one can always find some set of integers  $k_1, \dots, k_n$  ( $n \geq 2$ ) that will satisfy the equation:

$$V_2 \leq (k_1\omega_1 + k_2\omega_2 + \dots + k_n\omega_n)^2 \leq V_2 + 4\Phi_2. \quad (4.23)$$

If  $V_2 \neq 0$ , then the phonon spectrum is of an optical type,  $\Omega_{\min}^2 = V_2$ . Then breathers with frequencies  $\omega$  below  $\Omega_{\min}$  can exist. The condition for it is the following:

$$0 < \Omega_{\min} - \omega < [\omega - (\Omega_{\max} - \Omega_{\min})], \quad (4.24)$$

where  $\Omega_{\max}^2 = V_2 + 4\Phi_2$  is the maximal phonon frequency. Equation (4.24) secures the fact that the frequency of the breather  $\omega$  lies below  $\Omega_{\min}$ , ( $\omega < \Omega_{\min}$ ), while its second harmonic  $2\omega$  exceeds  $\Omega_{\max}$ , ( $2\omega > \Omega_{\max}$ ).

The condition (4.24) can be generalized easily to the case, when the harmonics up to  $k\omega$  fit the band gap, ( $k\omega < \Omega_{\min}$ ), while the harmonic  $(k+1)\omega$  lies above the phonon band, ( $(k+1)\omega > \Omega_{\max}$ ):

$$0 < \Omega_{\min} - k\omega < [\omega - (\Omega_{\max} - \Omega_{\min})], \quad (4.25)$$

with some  $k$  from the set  $1, 2, 3, \dots$ .

To summarize, we formulate in brief the conditions under which the existence of breathers is possible. Only single-frequency breathers can be stable. Breathers can exist, if the frequency of the breather  $\omega$  exceeds the maximal phonon frequency  $\Omega_{\max}$ . Low-frequency breathers  $\omega < \Omega_{\min}$  are possible for an optical phonon spectrum  $\Omega_{\min} > \delta > 0$ . In the last case the frequency  $\omega$  should satisfy equation (4.25) with some integer value of  $k$ .

We would like to note also, that, according to Eqs. (4.14)-(4.17) and (4.12), the spatial localization of the harmonics  $A_{l;k}$  diminishes as the frequency  $(k, \omega)$  approaches the edge of the phonon band. The localization radius of a high-frequency breather  $\omega > \Omega_{\max}$  is determined by the first harmonic  $A_{l;1}$ . The localization of a low-frequency breather  $\omega < \Omega_{\min}$  is governed by the harmonic  $A_{l;k}$ , whose number  $k$  satisfies Eq. (4.25), or by  $A_{l;k+1}$ .

Results of numerical experiments and additional references on the subject can be found in the review [64].

### 4.3 Arguments for the existence of discrete breathers: some mathematics

The principal idea of a powerful method of the study of existence of discrete breathers is based on the continuation of periodic solutions of exactly solvable models in the interaction  $\varepsilon$  between the sites of a Hamiltonian lattice. The possibility of such a continuation with the localization feature preserved can be proven with the help of a theorem, analogous to the one on an implicit function in an infinite-dimensional space.

Let us present the equation of motion in the form:

$$F(u, t) = \{F_1(u, t), F_2(u, t) \dots\} \equiv 0, \quad (4.26)$$

where

$$F_l(u, t) = \ddot{u}_l + \frac{\partial H}{\partial u_l}. \quad (4.27)$$

Here  $H(u)$  is the Hamiltonian of the system:

$$H(u) = \sum_{l=-\infty}^{\infty} \left( \frac{\dot{u}_l^2}{2} + V(u_l) \right) + \varepsilon \sum_{l=-\infty}^{\infty} \Phi(u_l - u_{l+1}). \quad (4.28)$$

To employ the theorem on implicit functions, first one chooses the space of periodic functions with fixed frequency and with time-reversal symmetry. For example, the one with

$$u(t) = u\left(t + \frac{2\pi}{\omega_b}\right), \quad u(t) = u(-t). \quad (4.29)$$

In the space (4.29) the solutions of Eq. (4.26) with  $\varepsilon = 0$  are presented by isolated points. This fact enables one to prove the existence of solutions  $u(t, \varepsilon)$  of the equation (4.26) at small enough  $\varepsilon$ . These solutions have the same period  $\omega_b$  and the same symmetry for  $t \rightarrow -t$  as the functions (4.29). For the applicability of the theorem on implicit functions it is sufficient to prove the reversibility of the Newton operator in the vicinity of the point  $\varepsilon = 0$ :

$$\frac{\partial F(u(\varepsilon); \varepsilon)}{\partial u} \frac{du(\varepsilon)}{d\varepsilon} + \frac{\partial F(u(\varepsilon); \varepsilon)}{\partial \varepsilon} = 0. \quad (4.30)$$

Equation (4.30) states that the corresponding differential form, defined on an infinite-dimensional manifold equals zero. Such an approach has been used in Ref. [74] in the study of the problem of existence of exponentially localized breathers in Hamiltonian lattices with time-reversal symmetry. This consideration is valid for lattices of arbitrary dimension, both finite and infinite, and for both single-site breathers and multiple-site ones. In the latter case the unperturbed solution is a vibrational excitation of several lattice sites, at a large enough distance. With the interaction switched on, these excitations decay exponentially with the increase of the distance from the initial localization sites. Thus, in general, breather solutions can have a much more complicated inner structure, than in the simplest one-site case.

However, we would like to note, that the consideration, provided above, is not the proof in a strict mathematical sense, but more likely a heuristic argument in favour of the existence of breathers. In fact it is very problematic to prove the differentiability of  $u(\varepsilon)$  with respect to  $\varepsilon$ . More to it, if one tries to make it with the help of Newtonian perturbation methods, the proof within the spirit of KAM theory can not be obtained due to small denominators (resonances). On the other hand, the KAM theory does not state the non-differentiability of  $u(\varepsilon)$ . Obviously, the question needs additional attention.

Another wide enough class of Hamiltonian lattices, where the existence of breathers can be proved and exact solutions demonstrated, are lattices with a homogeneous potential. Then the variables  $t$  and  $l$  can be separated, so that the construction of a solution becomes much more simple.

Really, for example in the case of the potential  $V(z) = V_{2m}z^{2m}(2m)^{-1}$  and  $\Phi(z) = \Phi_{2m}z^{2m}(2m)^{-1}$  after the substitution of it in Eq. (4.9) we obtain the equation:

$$\ddot{u}_l = -V_{2m}u_l^{2m-1} - \Phi_{2m}(u_l - u_{l-1})^{2m-1} - \Phi_{2m}(u_l - u_{l+1})^{2m-1}. \quad (4.31)$$

We seek for the solution in the following form:

$$u_l(t) = G(t)f_l(-1)^l, \quad f_l > 0. \quad (4.32)$$

Substituting Eq. (4.32) into Eq. (4.31), we find the following equations for the functions  $G(t)$  and  $f_l$ :

$$\begin{aligned} \ddot{G}(t) + \varkappa G^{2m-1} &= 0, \\ \varkappa f_l &= V_{2m}f_l^{2m-1} + \Phi_{2m}(f_l + f_{l-1})^{2m-1} + \Phi_{2m}(f_l + f_{l+1})^{2m-1}, \end{aligned} \quad (4.33)$$

where  $\varkappa > 0$  is the separation parameter. If for the values  $\varkappa > 0$  the solution  $f_l$  tends to zero with  $l \rightarrow \pm\infty$ , the breather exists. The existence of solutions to Eq. (4.33) with such properties has been proven in Ref. [70]. We note, that this proof is valid even in the case  $V_{2m} = 0$ , when the theorem on implicit functions, cited above is not applicable, so that the proof of the existence of a discrete breather, provided in Ref. [74], does not work.

The material, presented in this Section, provides new insight, which supplements the results of the paper [13] on the existence of classical local vibrations in simple molecular crystals. It turns out, that multi-frequency vibrations are stable only asymptotically, while the strictly periodical (single-frequency) ones might be stable ever.

## 4.4 Discrete breathers: numerical experiments

Progress in super-computer technology provided new opportunities for numerical modeling of vibration dynamics in Hamiltonian lattices. At present, the number of works, addressed at numerical studies of breather-like objects in nonlinear lattices is big enough. Numerical solutions of Hamilton equations for the lattice typically make use of Runge-Kutt methods or Verlet (leap-frog) algorithms [75]. The results are typically presented in the form of time- or space- dependencies of the amplitudes and of the energy in the course of actual integration of equations. These numerical experiments suggest, that there exist lattice solitons, the dynamics of which resemble that of the breathers. Most part of the numerical experiments addresses one-dimensional chains, which by no means signifies the non-existence of breathers in multi-dimensional lattices,  $d \geq 2$ . It has been demonstrated, that sometimes breathers move as some structures with inner vibrations.

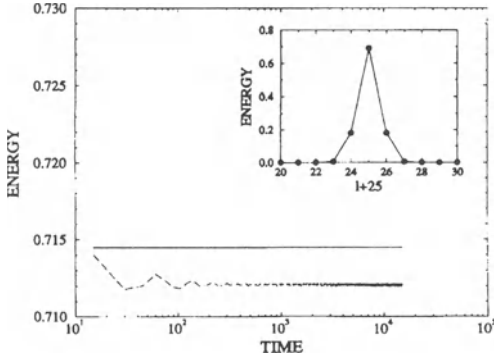


Figure 4.1: The time dependence of the energy  $e_{(5)}$  of five sites in a breather (dashed line). Total energy of the chain (solid line). Inset: energy distribution as function of the particle number for the same solution, measured for time  $1000 < t < 1150$ .

Next we review briefly some results of numerical calculations from Ref. [64].

Let us look for a breather-like solution of Eq. (4.9) with periodic boundary conditions in a chain of  $N = 3000$  sites. The parameters of the potentials  $V(z)$  and  $\Phi(z)$  in Eq. (4.9) are chosen in the form:

$$\begin{aligned} V_2 &= 1, \quad V_3 = -1, \quad V_4 = \frac{1}{4}; \quad \Phi_2 = 0.1, \\ V_s &= 0, \quad s > 4; \quad \Phi_s = 0, \quad s > 2. \end{aligned} \quad (4.34)$$

Typically the existence of breather-like objects is assumed proven, if the time of its observation exceeds largely the small characteristics time  $\tau$  of the transition of the excitation between two adjacent lattice sites. The latter transition is governed by the linear part of Eq. (4.9). For the parameters of the potential (4.34) chosen, the quantities  $t$  and  $\tau$  satisfy the inequality:

$$t \gg \frac{\sqrt{2(V_2 + \Phi_2)}}{2\Phi_2} = 7.416\dots \quad (4.35)$$

Figure 4.1 shows the time dependence of the total energy on five sites  $e_{(5)}$  (see Eq. (4.8)) for the following initial conditions:  $u_0(t=0) = 2.3456$ ,  $u_{l \neq 0}^{(0)} = 0$ ,  $\dot{u}_l(0) = 0$ . The plot demonstrates clearly that the local excitation exists. This breather-like object is observed during the time  $7.416 \ll t \ll 10^4$ . After a short transition time  $t \sim 100$  the energy on five sites reaches a constant value.

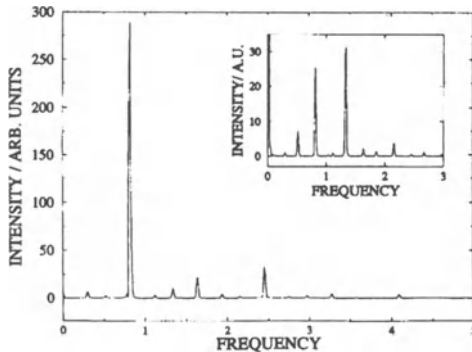


Figure 4.2: Spectral energy density with the same initial conditions, as in Fig. 4.1 for site  $l = 0$ . Inset: for  $l = \pm 1$ .

The distribution of energy over lattice sites within the object ( $l - 2, l + 2$ ) is shown in the inset of Figure 4.1. Obviously, only three sites are involved in the vibration. The solution is localized clearly within the observation time. The central atom oscillates with a big amplitude (energy), its nearest neighbors – with small equal amplitudes, while all the rest practically stand still. The qualitative physics of the effect signify, that principally only two degrees of freedom take part in the vibrations: namely, the displacement of the central atom and the symmetrical displacements of its two neighbors. Thus, the numerical experiment reveals the fact, that the system with an infinite number of degrees of freedom is reduced effectively to the problem with only two degrees of freedom.

This last assertion is backed up by the results of Fourier analysis of the time dependencies of displacement amplitudes for the central atom in the breather and of the nearest-neighbor atoms, see Fig. 4.2.

A careful analysis of Fig. 4.2 reveals the existence of two independent basic frequencies  $\omega_1 = 0.822$  and  $\omega_2 = 1.34$ . All the other peaks in the figure correspond to linear combinations of these,  $\omega_{mn} = m\omega_1 + n\omega_2$ , with integer values  $m$  and  $n$ . This fact provides another proof of the statement, that the motion of the system is equivalent to vibrations of two equivalent weakly bound nonlinear oscillators. The vibration represents a conditionally-periodic motion with two basic frequencies  $\omega_1, \omega_2$ . It can be noted from Fig. 4.2, that the central atom oscillates primarily with the frequency  $\omega_1$ , while the neighboring atoms vibrate in-phase with each other with frequency  $\omega_2$ . It is these frequencies that correspond to the maximal peaks in the dependencies  $A_0(\omega)$  and  $A_{\pm 1}(\omega)$  correspondingly.

The considered breather solution of Eq. (4.9) with the potential (4.34)

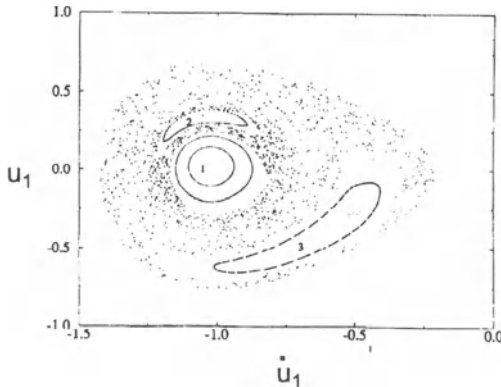


Figure 4.3: Poincare intersection between the trajectory and the subspace  $(\dot{u}_1, u_1, u_0 = 0, \dot{u}_0 > 0)$  for the symmetric reduced three-particle problem and energy  $E = 0.58$ .

reveals clearly the typical behavior of a nonlinear system with two degrees of freedom. This suggests the idea to use the results for the reduced problem with two degrees of freedom to study the types of initial excitations which produce breathers in infinite lattices. The corresponding investigation has been performed successfully in Ref. [76]. First, the frequency spectrum of different trajectories, both regular and chaotic is studied. Then, the trajectories of particles, which lie outside the bounded linear phonon spectrum are selected out, as possible candidates for breather-like objects in an infinite lattice. Other trajectories have frequencies in resonance with the phonon spectrum. Even if these trajectories correspond to breather-like solutions, these will decay in time. For these latter structures the point of interest is the calculation of their lifetime.

A nonlinear two-dimensional system typically is not fully integrable, but only locally integrable. In other words, within some regions of phase space the motion of the system is conditionally-periodic with two frequencies, and the trajectory gets wound on two-dimensional tori. The Poincare crossection of the trajectory of the reduced system ( $s = 2$ ) (which characterizes the vibration of the central atom and of its two neighbors) with the manifold  $\{u_1, \dot{u}_1, u_0 = 0, \dot{u}_0 > 0\}$  is depicted in Fig. 4.3 from Ref. [64].

Here the regions 1 and 2 correspond to a regular conditionally-periodic motion with a two-frequency spectrum, which does not overlap with the phonon spectrum. These trajectories are natural candidates for breather-like objects. The irregular dots correspond to chaotic trajectories. The frequency spectrum of such a motion is continuous. Thus, the spectrum of chaotic trajectories will overlap with the phonon spectrum, so that such

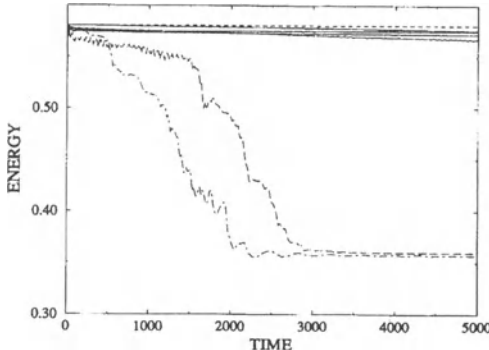


Figure 4.4: The time dependence of the energy  $e_{(5)}$  of five sites in a breather. Upper short dashed line – total energy of all simulations; solid lines – initial conditions of fixed points in islands 1,2 from Fig. 4.3 and larger torus in island 1 and torus in island 2; long dashed line – initial condition of torus in island 3; dashed-dotted line – initial condition of chaotic trajectory.

trajectories will decay in an infinite lattice. And, last, the third region in Fig. 4.3 corresponds to a regular motion, the frequencies of which, however, are in resonance with the phonon frequencies, so that in an infinite lattice such trajectories decay as well. Figure 4.4 shows the decay of the total energy  $e_{(5)}(t)$  on five lattice sites for some trajectories of the reduced system from Fig. 4.3. The comparison of Figs. 4.3 and 4.4 reveals the fact, that different objects decay at different rates. The slowest is the decay of initial excitations which correspond to periodic orbits of the reduced system. These trajectories correspond to the centers of regions 1 and 2 in Fig. 4.3. The center of region 3, on the contrary, corresponds to a periodical orbit with frequency  $\omega_3$ , which is in resonance with the phonon frequency and consequently decays fast.

To summarize, we conclude, that the numerical experiments confirm reliably enough the assumption, that breathers are formed from periodic orbits of low-dimensional subsystems of infinite Hamiltonian lattices. The necessary and, most probably, the sufficient condition for the existence of such a breather is the absence of resonance between the basic frequency of the periodic orbit and of its harmonics — with the phonon frequencies of the infinite lattice.

In the next Section we will consider an exactly solvable model with a homogeneous potential, which backs up all the assumptions, provided here on the basis of numerical experiments [77].

## 4.5 Discrete breathers in lattices with a homogeneous potential

A d-dimensional Hamiltonian lattice with a homogeneous interaction potential between the lattice sites has been studied recently by Ovchinnikov and Flach in [77]. A number of analytical solutions for breathers have been obtained. The stability of these solutions with respect to the variations of the interaction potential has been investigated. A regular method of construction of solutions for multi-site breathers in a d-dimensional lattice with a homogeneous potential of a special type is presented. An algorithm for the selection of a special class of homogeneous potentials, which can be solved exactly, is provided.

Let us first consider a one-dimensional Hamiltonian chain with the Hamiltonian of the type:

$$\begin{aligned} H &= W_k + W_p, \quad W_k = \frac{1}{2} \sum_l p_l^2, \quad W_p = \frac{1}{2} \sum_l (x_l - x_{l+1})^2 h(s_l), \\ s_l &= \frac{x_l}{x_{l+1}} + \frac{x_{l+1}}{x_l}. \end{aligned} \quad (4.36)$$

Here the index  $l$  refers to the lattice sites. The equations of motion with the account of  $\dot{x}_l = p_l$  take the form:

$$\ddot{x}_l + \frac{\partial W_p}{\partial x_l} = 0. \quad (4.37)$$

The solutions of this equation, which tend to zero at large distances,  $x_l \rightarrow 0, |l| \rightarrow \infty$ , are called breathers. It is such solutions that we are looking for. The homogeneity of the potential  $W_p(\lambda x) = \lambda^2 W_p(x)$  makes possible the separation of variables in Eq. (4.37). Really, making the substitution

$$x_l(t) = G(t) u_l \quad (4.38)$$

in Eq (4.37), we obtain the following equations for  $G(t)$  and  $u_l$ :

$$\ddot{G} + kG = 0, \quad ku_l = \frac{\partial W_p(u_l)}{\partial u_l}. \quad (4.39)$$

The condition  $|x_l(t)| < \infty$  requires the separation parameter  $k$  be positive:

$$k = \omega^2 > 0, \quad |G(t)| = |A \cos(\omega t + \Phi)| < M < \infty. \quad (4.40)$$

The explicit form of equation (4.39) for the component  $u_l$ , which describes the space dependence, is

$$\begin{aligned}
k &= \left(1 - \frac{u_{l+1}}{u_l}\right) h(s_l) + \left(1 - \frac{u_{l-1}}{u_l}\right) h(s_{l-1}) \\
&+ \frac{1}{2} \left(1 - \frac{u_{l+1}}{u_l}\right)^2 h'(s_l) \left(\frac{u_l}{u_{l+1}} - \frac{u_{l+1}}{u_l}\right) \\
&+ \frac{1}{2} \left(1 - \frac{u_{l-1}}{u_l}\right)^2 h'(s_{l-1}) \left(-\frac{u_{l-1}}{u_l} + \frac{u_l}{u_{l-1}}\right), \\
s_l &= \frac{x_l}{x_{l+1}} + \frac{x_{l+1}}{x_l} = \frac{u_l}{u_{l+1}} + \frac{u_{l+1}}{u_l}.
\end{aligned} \tag{4.41}$$

Let us seek the solution  $u_l$  of this equation in the form:

$$u_l = (-1)^l e^{-\beta|l|}, \quad \beta > 0. \tag{4.42}$$

The solution (4.42) is a localized excitation of the lattice ground state  $u_l \equiv 0$  – a breather. Substituting Eq. (4.42) into Eq. (4.41) we obtain the following set of equations for  $l > 0$ ,  $l < 0$ , and  $l = 0$ :

$$\begin{aligned}
k &= \left(1 + e^{-\beta}\right) h(-s) + \left(1 + e^{\beta}\right) h(-s) - \\
&\left(1 + e^{-\beta}\right)^2 h'(-s) \sinh \beta + \left(1 + e^{\beta}\right)^2 h'(-s) \sinh \beta, \quad l \neq 0, \\
k &= 2 \left(1 + e^{-\beta}\right) h(-s) - 2 \left(1 + e^{-\beta}\right)^2 h'(-s) \sinh \beta, \quad l = 0, \\
s &= -s_l = \text{const} = 2 \cosh \beta.
\end{aligned} \tag{4.43}$$

Subtracting the second equation (4.43) from the first one, we obtain the equation in  $s$ , and the expression of  $k$ :

$$h'(-s) = -\frac{2h(-s)}{s(s+2)}, \tag{4.44}$$

$$\begin{aligned}
k &= [2 + s(1 - \gamma)] \left[1 + \frac{\gamma}{s+2} \left(1 + \frac{s}{2}(1 - \gamma)\right)\right] h(-s), \\
\gamma &= \sqrt{1 - \left(\frac{2}{s}\right)^2}.
\end{aligned} \tag{4.45}$$

If the solution  $s_\nu$  of Eq. (4.44) satisfies

$$s_\nu > 2, \quad h(-s_\nu) > 0, \tag{4.46}$$

then the inequality  $k > 0$  holds true. Consequently, according to Eqs. (4.40), (4.42), and (4.43), the solution  $x_l^{(\nu)}(t) = G^{(\nu)}(t) u_l^{(\nu)}$  corresponds to a breather. This solution is structurally stable, as under small variations of

$\delta h(s)$  the roots of Eq. (4.44) change insignificantly, so that the conditions (4.46) are still fulfilled. If the condition  $h(s) > 0$  is realized for arbitrary  $s$ , then  $x_l \equiv 0$  is the ground state – the one with minimal energy. Then the obtained solution can be considered a localized excitation of the ground state ("vacuum" with  $E_{\min} = 0$ ). The solution always can be multiplied by an arbitrary constant factor to give another solution, – due to the homogeneous nature of the potential, – producing thus a one-parameter family of localized excitations. The number of such sets is equal to the number of solutions to Eq. (4.44), which satisfy the conditions (4.46).

Let us consider a particular example with the potential  $W(x_l)$ , where

$$h(s) = 1 + a \exp(-bs^2), \quad (4.47)$$

and the parameters  $a$  and  $b$  satisfy

$$a > \frac{e^{3/2}}{2 + 3\sqrt{3/2b}}, \quad b > \frac{3}{8}. \quad (4.48)$$

There exists at least one solution to Eq. (4.44), which satisfies the conditions (4.46). For example, for  $a = 0.7$  and  $b = 0.5$  we find the root  $s \approx 2.06781\dots$ , and, correspondingly,  $\beta \approx 0.25967\dots$  This solution is obviously structurally stable with the perturbations  $h(s)$  from Eq. (4.47).

The consideration, provided in the previous Sections suggest, that the obtained breather solution is formed from the periodic orbit of a phonon with the frequency from the upper edge of the band  $\Omega_D$ . It is exactly for the phonons from the upper edge of the band that the space-dependence of the amplitude has the form  $u_l \sim (-1)^l$ . In this case the higher harmonics of the breather frequency satisfy  $m\omega > \Omega_D$ , so that the breather does not decay.

We would like to note, that the search for this breather as a continuation of the phonon solution with  $h(s) \equiv 1$  to the region  $h(s) \neq 1$  is problematic. The reason lies in the fact, that the linearization of equations (4.39) in the vicinity of  $x_l \equiv 0$  is impossible, as the potential  $W_p(x_l)$  incorporates the factor  $h\left(\frac{x_l}{x_{l+1}} + \frac{x_{l+1}}{x_l}\right)$  with a singularity in  $x_l \equiv 0$ .

However, the linearization of Eq. (4.39) is possible in the vicinity of  $x_l \equiv c$ , when the potential energy  $W_p$  can be expressed in the form:

$$W_p = \frac{c^2}{2} \sum_l \left[ h(2)(\delta_l - \delta_{l+1})^2 + h'(2)(\delta_l - \delta_{l+1})^4 + O(\delta^5) \right], \quad \delta_l = \frac{x_l}{c} - 1. \quad (4.49)$$

In the case  $h(s) > 0$  all the states  $x_l = c$  have the minimal energy  $E = 0$ . Thus, the ground state in the system (4.36) is definitely degenerate for  $h(s) > 0$ . As it has been shown above, the excited states with  $x_l \equiv 0$  contain breathers. The same is true for the states with  $x_l = c \neq 0$  as well.

Really, the system with the potential energy (4.49) with the term  $O(\delta^5)$  neglected is the well-known chain of Fermi-Pasta-Ulam. It is well known, that Eq. (4.49) has discrete breather-type solutions for  $h'(2) > 0$  [78, 79, 80]. Though this solution can not be presented in closed analytical form, it has been proven to exist.

In short, the excitations of the ground state with  $x_l = c$  corresponding to discrete breathers for the model (4.36) exist and are localized,  $|x_l - c| \rightarrow 0$  for  $|l| \rightarrow \infty$ . In the particular case  $c = 0$  the solution is presented in closed analytic form (4.42).

## 4.6 An exactly solvable Hamiltonian lattice

Let us consider a d-dimensional hyper-cubic lattice with a scalar coordinate  $x_{\underline{l}}$ , associated with each lattice site. The index  $\underline{l} = (l_1, \dots, l_d)$  is a set of integer numbers ranging from  $-\infty$  to  $+\infty$ , which enumerates the lattice sites. It is convenient to introduce an operator  $L$ , which acts upon a scalar function  $f_{\underline{l}}$  according to the rule:

$$L f_{\underline{l}} = \sum_{\underline{l}' \rightarrow |\underline{l}' - \underline{l}|=1} f_{\underline{l}'} . \quad (4.50)$$

Here  $|\underline{l}|^2 = l_1^2 + l_2^2 + \dots + l_d^2$ . The operator  $L$  puts in correspondence to the quantity  $f_{\underline{l}}$  a sum of analogous quantities, corresponding to the nearest-neighbor (with respect to  $\underline{l}$ ) sites in the hyper-cube lattice. For example, in a square lattice the nearest neighbors to site  $(l_1, l_2)$  are the following four:  $(l_1 - 1, l_2)$ ,  $(l_1 + 1, l_2)$ ,  $(l_1, l_2 - 1)$ , and  $(l_1, l_2 + 1)$ . The generalization to the d-dimensional case is straightforward. Next let us define the quantity:

$$s_{\underline{l}} = \frac{Lx_{\underline{l}}}{x_{\underline{l}}} . \quad (4.51)$$

The Hamiltonian of the system we introduce as:

$$H = \frac{1}{2} \sum_{\underline{l}} p_{\underline{l}}^2 + W_p, \quad W_p = \sum_{\underline{l}} (Lx_{\underline{l}})^2 h(s_{\underline{l}}) . \quad (4.52)$$

Equation (4.52) allows the separation of variables  $x_{\underline{l}} = G(t) u_{\underline{l}}$ . For the quantities  $G(t)$  and  $u_{\underline{l}}$  we obtain the following equations:

$$\ddot{G} + kG = 0, \quad k > 0, \quad (4.53)$$

and

$$ku_{\underline{l}} = -\frac{1}{2} u_{\underline{l}} s_{\underline{l}}^3 h'(s_{\underline{l}}) + \frac{1}{2} L \left\{ u_{\underline{l}} s_{\underline{l}}^2 h'(s_{\underline{l}}) \right\} + L \left\{ u_{\underline{l}} s_{\underline{l}} h(s_{\underline{l}}) \right\} . \quad (4.54)$$

Here the operator  $L$  sums up contributions of the products  $u_{\underline{l}} s_{\underline{l}}^2 h'(s_{\underline{l}})$  and  $u_{\underline{l}} s_{\underline{l}} h(s_{\underline{l}})$  over the nearest neighbors of site  $\underline{l}$ . Let us assume the following:

$$\begin{aligned} s_{\underline{l}} &\equiv s_1, \quad |\underline{l}| \neq 0, \\ s_{\underline{l}} &\equiv s_0, \quad |\underline{l}| = 0. \end{aligned} \quad (4.55)$$

Then the quantities  $s_{\underline{l}}$ ,  $h(s_{\underline{l}})$ , and  $h'(s_{\underline{l}})$  can be taken out from the figure brackets the operator  $L$  acts upon, so that Eq. (4.54) takes the form:

$$\begin{aligned} k &= s_1^2 h(s_1), \quad |\underline{l}| > 1, \\ k &= s_1^2 h(s_1) + \frac{u_0}{u_1} \left\{ [s_0 h(s_0) - s_1 h(s_1)] + \frac{1}{2} [s_0^2 h'(s_0) - s_1^2 h'(s_1)] \right\}, \\ &\quad |\underline{l}| = 1, \\ k &= s_0 s_1 h(s_1) + \frac{1}{2} s_0 [s_1^2 h'(s_1) - s_0^2 h'(s_0)] \\ &= s_0^2 h(s_0) + s_0 \left\{ \left[ s_1 h(s_1) + \frac{1}{2} s_1^2 h'(s_1) \right] - \left[ s_0 h(s_0) + \frac{1}{2} s_0^2 h'(s_0) \right] \right\}, \\ &\quad |\underline{l}| = 0. \end{aligned} \quad (4.56)$$

Let us introduce the function:

$$g(s) = \frac{1}{2} s^2 h(s), \quad g'(s) = s h(s) + \frac{1}{2} s^2 h'(s). \quad (4.57)$$

Next we impose, that the quantities  $s_0$  and  $s_1$  satisfy the following equations:

$$g(s_0) = g(s_1), \quad g'(s_0) = g'(s_1). \quad (4.58)$$

With Eq. (4.58) fulfilled, the equation (4.56) is satisfied, and the separation parameter is given by:

$$k = 2g(s_0) = 2g(s_1). \quad (4.59)$$

Equations (4.58) enable one to construct the function  $h(s)$  in such a way, that the Hamiltonian (4.52) can be solved exactly in analytic form. In fact it is sufficient to choose the function  $g(s)$  in the form which satisfies Eq. (4.58). After that the function  $h(s)$  is reconstructed with the help of Eq. (4.57) and the homogeneous interaction potential  $W_p$ , (4.52) is obtained.

The solutions to Eq. (4.54) decay exponentially for  $|\underline{l}| \rightarrow \infty$  if  $|s_1| > 2d$ . For one-dimensional chains this fact can be verified easily. Really,

$$const = |s_1| = \left| \frac{u_{\underline{l}+1}}{u_{\underline{l}}} + \frac{u_{\underline{l}-1}}{u_{\underline{l}}} \right| = e^{-\beta} + e^{\beta}. \quad (4.60)$$

For  $|s_1| > 2$  this equation always has a real solution with  $\beta > 0$ . In the general case the proof is somewhat more complicated.

We note also, that this method can be generalized to build solutions, which characterize multi-site breathers in a homogeneous potential. In fact, it is sufficient to substitute in Eq. (4.54) the following values:

$$\begin{aligned} s_l &= s_\infty, \quad \text{for } l \neq l_m, \\ s_{l_m} &= s_m. \end{aligned} \tag{4.61}$$

The number of sites  $l_m$  is finite, and  $|l_m - l_{m'}| < \infty$  for any pair  $(m, m')$ . This gives a system of equations for the quantities  $(s_1, s_2, \dots, s_m)$  and  $k$ , as we obtained Eq. (4.56) for  $(s_0, s_1)$  and  $k$  before. Solving the obtained equations we find the quantities  $(s_1, s_2, \dots, s_m)$  and  $k$ , which determine the physical parameters of the multi-site breather and the conditions which should be satisfied by the function  $h(s)$  for the breather to exist.

## Chapter 5

# Quantum theory of vibrational - rotational spectra in $XY_2$ - type molecules

Recently a large amount of theoretical and experimental work has been devoted to the analysis of nonlinear effects in vibrational-rotational spectra of polyatomic molecules. The nonlinearity is revealed in a particularly pronounced way in stretching vibrations of valence bonds of the type  $C - H$ ,  $N - H$ ,  $O - H$ , formed by a hydrogen atom and some other heavy atom.

The strong nonlinearity of such vibrations leads to the necessity of the introduction of the concept of a local mode (LM). The LM is characterized by its frequency  $\omega$  and the anharmonicity parameter  $x_e$ . Besides, a parameter  $\beta$ , characterizing the interaction of local modes, is required. It turns out that the description of vibrational overtones in these terms is more transparent and informative, than in conventional normal mode theory. In fact, within normal mode approach the picture of overtones is too vague and complex, and needs too many adjustable parameters to achieve agreement with the experimental spectra (see, for example, [51, 6]).

One of the unusual and interesting consequences of vibration anharmonicity is the effect of clusterization (formation of a hyperfine structure of very closely positioned levels – doublets, triplets, etc., depending on the symmetry and complexity of the molecule) of highly-excited levels. Contrary to the theory of normal modes, this is not an accidental degeneration, but an inherent effect. The same reasons, that provoke clusterization, lead to the extreme stability of highly-excited nonlinear vibrations, whose lifetime can reach several seconds (see review [51]).

These effects were first considered by A.A.Ovchinnikov in Ref. [12]. A clear physical picture of long-living highly excited vibrational states has been

presented there as well. The long - living nature of the latter originates from the lack of resonance for the transitions between weakly- and highly- excited states, as it has been shown in Chapter 2 for classical oscillators.

In the paper [82] Ovchinnikov and Erikman within the model of two weakly bound Morse oscillators calculated the splitting of vibronic levels  $\epsilon_N(n)$ , which corresponds to the symmetric and antisymmetric excitation of valence bonds' vibrations. Here  $N$  is the overtone number – the total number of vibrational quanta on the oscillators, and  $n$  – the excitation number of one of the two bonds. In particular, the following value for the  $H_2O$  molecule has been found:  $\epsilon_{10}(0) \simeq 2 * 10^{-8} cm^{-1}$ . Further calculations with the use of more complicated model Hamiltonians confirmed the tendency to the clusterization of high overtones [6]. More to it, as it turned out, the interaction of vibrations with the rotation of the molecule can reduce significantly the splitting of energy of high overtones for some particular orientations and for high values of the molecule's rotational momenta  $J$  ([36, 38]).

Another reason for the interest to the studies of high overtone spectra is due to the possibility of obtaining information on the structure of the potential surface of stretching vibrations. The characteristics of these highly-excited vibrations depend weakly on the surrounding, and are determined primarily by the interaction potential  $U(r)$ . For example, the anharmonicity parameters  $x_e$  in  $C-H$  vibrations in the molecules  $C_2H_2$ ,  $C_6H_6$ ,  $C_2H_2I_2$  are roughly equal, and take the values of the order of  $60 cm^{-1}$  ([83, 32]). On the other hand, the frequency of normal oscillations (low excitations) depend strongly on the interaction between different degrees of freedom, and this makes it problematic to obtain information on the shape of the potential  $U(r)$ .

In short, this Chapter is devoted to the study of anharmonicity effects in the system of two weakly interacting highly anharmonic quantum oscillators. It will be shown, that the anharmonicity leads to strong clusterization of vibrational levels. More to it, for highly-excited levels this clusterization is anomalously large. The highly-excited overtones include a whole set of states, which correspond to excitations localized on a single valance bond. The energy splitting of levels for such excitations decreases exponentially with the increasing number of the vibrational overtone. Mathematical formulas for this splitting are derived. Comparison of analytical and numerical results is provided. The theoretically calculated and experimentally measured spectra of vibrational overtones (for example, for molecules  $H_2O$ ,  $H_2S$  and other of the type  $XY_2$ ) are compared. The comparison of the two interpretations of vibrational spectra within conventional normal mode theory and the theory of local modes is provided. It is demonstrated that for high anharmonicity the latter provides a natural interpretation and requires a smaller number of fitting parameters.

For the proper understanding of the material the basic knowledge of

quantum mechanics is required, for example within the course [81]. The basics of vibrational spectra of polyatomic can be found, for example, in the fundamental monograph [5].

## 5.1 Quantum theory of two Morse oscillators: stretching – vibration spectra in $XY_2$ molecules

Let us consider two weakly-bound Morse oscillators, characterized by the following Hamiltonian <sup>1</sup>:

$$\begin{aligned} H &= H_0 + W, \\ H_0 &= \left[ -\frac{\omega}{2} \frac{\partial^2}{\partial x^2} + U(x) - \frac{\omega}{2} \frac{\partial^2}{\partial y^2} + U(y) \right], \\ W &= -2\beta_k \frac{\partial^2}{\partial x \partial y} + 2\beta_d xy, \\ U(x) &= \frac{\omega^2}{4x_e} \left[ 1 - \exp \left( -\sqrt{\frac{2x_e}{\omega}} x \right) \right]^2. \end{aligned} \quad (5.1)$$

Here  $\omega$  and  $x_e$  are the frequency and the anharmonicity parameter in spectroscopic units  $cm^{-1}$ ;  $\beta_k$  and  $\beta_d$  are parameters of kinematic- and potential- interaction of stretching vibrations. The Morse potential has been introduced in such a way, that the energy spectrum takes the form:

$$E(n) = \omega \left( n + \frac{1}{2} \right) - x_e \left( n + \frac{1}{2} \right)^2. \quad (5.2)$$

Position in (5.1) is measured in units  $\sqrt{\frac{\hbar}{m\omega}}$ , the energy – in spectroscopic units  $[\frac{E}{\hbar c}] = [cm^{-1}]$ . The dissociation energy  $D$  is expressed through the frequency  $\omega$  and the anharmonicity parameter  $x_e$  with the help of the formula (see (5.1)):

$$D = \frac{\omega^2}{4x_e}.$$

For the stretching vibrations of  $C-H$  and  $O-H$  bonds the parameters, entering (5.1) are of the following order of magnitude:  $\omega \sim 3000 cm^{-1}$ ;  $x_e \sim 100 cm^{-1}$ ;  $\beta \sim 50 cm^{-1}$ . These estimates allow one to consider the interaction  $W$  as a perturbation both with respect to the initial Hamiltonian of noninteracting vibrations, and to the nonlinearity  $(\frac{\beta}{x_e} < 1)$ . The latter is especially important, as for high overtones  $(\frac{\beta}{N x_e} \ll 1)$  it requires the use of local mode representation for the zero order approximation.

---

<sup>1</sup>In this Section we follow Ref. [82].

The exact analytic calculation of the vibration spectrum of the Hamiltonian (5.1) is certainly impossible. However, under the condition

$$\frac{x_e}{\omega} \ll \frac{\beta}{x_e} \ll 1 \quad (5.3)$$

the asymptotically exact analytic expressions for the vibrational overtones are accessible. In fact, a less stringent condition  $\frac{\beta}{N x_e} \ll 1$ , ( $N$  – the overtone number), than (5.3), is sufficient.

We want to prove that with the increase of the overtone number  $N$  the clusterization of vibrational levels takes place. The vibronic levels group in pairs, with small energetic splitting  $\varepsilon_N(n) \ll \min\{\beta, x_e\}$ . Here  $N$  is the overtone number,  $n$  is the number of vibronic quanta on one bond, with  $(N - n)$  quanta on the other bond.

Due to small splitting, the local vibration in a molecule is extremely stable. The lifetime of a highly excited vibration of a single bond, excited for example with laser or due to molecular collisions, is very long:

$$\tau = \frac{\pi \hbar}{\varepsilon_N} \gg \max \left\{ \frac{\pi \hbar}{\beta}, \frac{\pi \hbar}{x_e} \right\} \sim 10^{-12} \div 10^{-10} \text{ s},$$

Thus if some physical process proceeds for a period of time  $\sim 10^{-12} \div 10^{-10} \text{ s}$ , as for example, the interaction of vibrations with rotations, a dynamical violation of symmetry will take place ( $C_{2v}$  symmetry for  $XY_2$  molecules, for example). This effect should be properly accounted for in the calculations of the vibrational-rotational spectrum, vibronic energy relaxation rate, and so on.

For the calculation of energy splitting  $\varepsilon_N(n)$  let us introduce symmetric and antisymmetric vibronic states:

$$\begin{aligned} |n, N - n\rangle_{(S)} &= \frac{1}{\sqrt{2}} (|n, N - n\rangle + |N - n, n\rangle), \\ |n, N - n\rangle_{(A)} &= \frac{1}{\sqrt{2}} (|n, N - n\rangle - |N - n, n\rangle), \end{aligned} \quad (5.4)$$

where  $|n, N - n\rangle$  – the eigenfunctions of the Hamiltonian  $H_0$  (5.1) – are represented by a product of Morse functions  $|n, N - n\rangle = \Psi_n^{(M)}(x) \Psi_{N-n}^{(M)}(y)$ . Later we will need the expressions of the matrix elements of the operators  $x$  and  $p$ , calculated with Morse functions. These have been found in [84] to be:

$$\begin{aligned} \langle N - n | x | n \rangle &= \frac{C(N - n, n)}{\sqrt{\frac{2x_e}{\omega} (N - 2n)}}, \\ C(n_1, n_2) &= (-1)^{n_1+n_2+1} \sqrt{\frac{\left[1 - (2n_1 + 1) \frac{x_e}{\omega}\right] \left[1 - (2n_2 + 1) \frac{x_e}{\omega}\right]}{\left[1 - (n_1 + n_2 + 1) \frac{x_e}{\omega}\right]^2}} \end{aligned}$$

$$\begin{aligned}
& \times \sqrt{\frac{\left(\frac{x_e}{\omega}\right)^{n_1-n_2} n_1!}{[1 - (n_2 + 1) \frac{x_e}{\omega}] [1 - (n_2 + 2) \frac{x_e}{\omega}] \dots [1 - n_1 \frac{x_e}{\omega}] n_2!}} \\
& \approx_{(n_1+n_2)\frac{x_e}{\omega} \ll 1} \sqrt{\frac{\left(\frac{x_e}{\omega}\right)^{n_1-n_2} n_1!}{n_2!}}, \quad n_1 > n_2, \\
& \langle N - n | p | n \rangle = i(N - 2n) \left[ 1 + (N + 1) \frac{x_e}{\omega} \right] \langle N - n | x | n \rangle. \quad (5.5)
\end{aligned}$$

In the first order in the interaction  $W$ , the splitting energy with the account of (5.1), (5.5) is provided by the expression:

$$\begin{aligned}
\varepsilon_N^{(1)}(n) &= 2 \langle N - n, n | W | n, N - n \rangle \\
&= 2 \frac{(N - 2n)^2 \beta_k + \beta_d}{\frac{x_e}{\omega} (N - 2n)^2} \left(\frac{x_e}{\omega}\right)^{N-2n} \frac{(N - n)!}{n!}. \quad (5.6)
\end{aligned}$$

In the preceding calculation a condition  $n x_e \ll \omega$  has been used. For the values  $\omega \sim 3000 \text{ cm}^{-1}$ ;  $x_e \sim 100 \text{ cm}^{-1}$ ;  $n \sim N \sim 10$  this condition is fulfilled. Substituting the parameters of the molecules  $H_2O$  and  $D_2O$ :

$$\begin{aligned}
H_2O : \\
\omega &\sim 3900 \text{ cm}^{-1}; \frac{\beta_k}{\omega} = -0.008; \frac{\beta_d}{\omega} = -0.01; \frac{x_e}{\omega} = 0.025, \\
D_2O : \\
\omega &\sim 3000 \text{ cm}^{-1}; \frac{\beta_k}{\omega} = -0.032; \frac{\beta_d}{\omega} = -0.006; \frac{x_e}{\omega} = 0.013 \quad (5.7)
\end{aligned}$$

in (5.6), we obtain the following expressions for  $\varepsilon_{10}(0)$ :

$$\begin{aligned}
H_2O, \quad \varepsilon_{10} &= \varepsilon_{10}(0) = 8.6 * 10^{-7} \text{ (cm}^{-1}), \\
D_2O, \quad \varepsilon_{10} &= \varepsilon_{10}(0) = 7.3 * 10^{-9} \text{ (cm}^{-1}). \quad (5.8)
\end{aligned}$$

Eq. (5.8) specifies the principal term in the energy splitting  $\varepsilon_{10}(0)$  in powers of the small parameter  $\frac{x_e}{\omega}$ . This contribution, however, happens to be anomalously small. Thus it is natural to look for the main term of the expansion of the energy in another small parameter  $\left(\frac{\beta}{2x_e}\right) = \gamma$  ( $\gamma \approx 0.25$  for  $H_2O$ , for example). The latter is equivalent to the calculation of the matrix elements of the interaction  $W = 2\beta_k p_x p_y + 2\beta_d xy$  with the wavefunctions of a harmonic oscillator. Such an approximation provides satisfactory results for a wide class of molecules, like dihalomethanes, for example. It is used extensively in the calculations of vibrational spectra with the help of fitting Hamiltonians, ([6]).

This contribution can be found by diagonalization of the matrix  $H$ , calculated with the states of the overtones (5.4). The harmonic approximation

for the matrix elements  $\langle N - m, m | W | n, N - n \rangle$  is sufficient. With the use of (5.1), (5.2), (5.5) the matrix  $H_{m,n}$  can be found to be:

$$H_{m,n} = \langle N - m, m | H | N - n, n \rangle = 2x_e n (N - n) \delta_{m,n} + \beta \left[ \sqrt{n(N-n+1)} \delta_{m,n-1} + \sqrt{(n+1)(N-n)} \delta_{m,n+1} \right], \quad (5.9)$$

where  $\beta = \beta_k + \beta_d$ . In the calculation of (5.9) a constant term  $(N+1)\omega\delta_{m,n}$  for the  $N^{\text{th}}$  overtone has been omitted, which obviously does not influence the overtone inter-level spacing. The secular equation, corresponding to the matrix (5.9), has the form:

$$\begin{aligned} & \beta \left[ \sqrt{n(N-n+1)} C_{n-1} + \sqrt{(n+1)(N-n)} C_{n+1} \right] \\ & + 2x_e n (N - n) C_n = EC_n, \end{aligned} \quad (5.10)$$

where  $C_n$  are the coefficients of the expansion of an eigenvector of the operator  $H$  (5.9) in the states  $|N - n, n\rangle$ .

Let us go over to the variables

$$C_n = \frac{\psi_n}{\sqrt{n!(N-n)!}}, \quad \gamma = \frac{\beta}{2x_e}, \quad \lambda = \frac{E}{2x_e}. \quad (5.11)$$

Substituting (5.11) into (5.10) we obtain:

$$\begin{aligned} & n(N-n)\psi_n + \gamma [n\psi_{n-1} + (N-n)\psi_{n+1}] = \lambda\psi_n, \quad \text{or} \\ & (H_0 + \gamma W)\psi = \lambda\psi. \end{aligned} \quad (5.12)$$

For the stretching vibrations of valence bonds  $C-H$ ,  $O-H$  the condition (5.3) holds, and, correspondingly,  $\gamma \ll 1$ . Thus the equation (5.12) can be solved with the use of perturbation theory.

It is convenient to solve equation (5.12) in the basis of symmetric and antisymmetric vectors:

$$\begin{aligned} \psi_n^\pm &= \frac{1}{2} (\psi_n \pm \psi_{N-n}), \quad 0 \leq n \leq \frac{N}{2}, \quad N - \text{even}, \\ \psi_n^\pm &= \frac{1}{2} (\psi_n \pm \psi_{N-n}), \quad 0 \leq n \leq \frac{N-1}{2}, \quad N - \text{odd}. \end{aligned} \quad (5.13)$$

Adding and subtracting equations (5.12) with indices  $n$  and  $N - n$ , we obtain the following set of equations for  $\psi_n^+$  and  $\psi_n^-$ :

$N - \text{even} :$

$$n(N-n)\psi_n^+ + \gamma [n\psi_{n-1}^+ + (N-n)\psi_{n+1}^+] = \lambda\psi_n^+, \quad 0 \leq n \leq \frac{N}{2} - 1,$$

$$\frac{N^2}{4}\psi_{\frac{N}{2}}^+ + \gamma N\psi_{\frac{N}{2}-1}^+ = \lambda\psi_{\frac{N}{2}}^+, \quad n = \frac{N}{2}, \quad (5.14)$$

$$n(N-n)\psi_n^- + \gamma [n\psi_{n-1}^- + (N-n)\psi_{n+1}^-] = \lambda\psi_n^-, \quad 0 \leq n \leq \frac{N}{2} - 1;$$

$N - \text{odd} :$

$$\begin{aligned} n(N-n)\psi_n^\pm + \gamma[n\psi_{n-1}^\pm + (N-n)\psi_{n+1}^\pm] &= \lambda\psi_n^\pm, \quad 0 \leq n \leq \frac{N-3}{2}, \\ \left[ \frac{N(N-1)}{2} - \left( \frac{N-1}{2} \right)^2 \right] \psi_{\frac{N-1}{2}}^\pm + \gamma \left[ \frac{N-1}{2} \psi_{\frac{N-3}{2}}^\pm \pm \frac{N+1}{2} \psi_{\frac{N-1}{2}}^\pm \right] \\ &= \lambda\psi_{\frac{N-1}{2}}^\pm, \quad n = \frac{N-1}{2}. \end{aligned} \quad (5.15)$$

To make calculations transparent we write out the nondiagonal terms of the matrices (5.14), (5.15):

1.  $N - \text{even} :$

$$\begin{aligned} \begin{pmatrix} Z_+ & Z_c & 0 \\ Z_r & 0 & 0 \\ 0 & 0 & Z_- \end{pmatrix}, \quad Z_c = \begin{pmatrix} 0 \\ \vdots \\ 0 \\ \frac{N}{2} + 1 \end{pmatrix}, \quad Z_r = (0 \dots 0 N), \\ Z_+ = Z_- = \begin{pmatrix} 0 & N & 0 & \cdot & & & \\ 1 & 0 & N-1 & \cdot & & 0 & \\ 0 & 2 & 0 & \cdot & & & \\ \cdot & \cdot & \cdot & \cdot & \cdot & \cdot & \\ & & & \cdot & 0 & \frac{N}{2} + 3 & 0 \\ 0 & & & \cdot & \frac{N}{2} - 2 & 0 & \frac{N}{2} + 2 \\ & & & & \cdot & 0 & \frac{N}{2} - 1 \\ & & & & & \cdot & 0 \end{pmatrix}, \end{aligned}$$

2.  $N - \text{odd} :$

$$\begin{aligned} \begin{pmatrix} Z_+ & 0 \\ 0 & Z_- \end{pmatrix}, \quad Z_+ = \begin{pmatrix} 0 & N & 0 & \cdot & & & \\ 1 & 0 & N-1 & \cdot & & 0 & \\ 0 & 2 & 0 & \cdot & & & \\ \cdot & \cdot & \cdot & \cdot & \cdot & \cdot & \\ & & & \cdot & 0 & \frac{N+4}{2} & 0 \\ 0 & & & \cdot & \frac{N-3}{2} & 0 & \frac{N+3}{2} \\ & & & & \cdot & 0 & \frac{N-1}{2} \\ & & & & & \cdot & \frac{N+1}{2} \end{pmatrix}, \\ Z_- = Z_+ - (N+1) \delta_{m, \frac{N-1}{2}} \delta_{n, \frac{N-1}{2}}. \end{aligned} \quad (5.16)$$

Eqs. (5.16) represent Jacobi matrices. Their symmetric and antisymmetric parts, denoted by  $Z_+$  and  $Z_-$  correspondingly, differ by the element  $Z_{\frac{N-1}{2}, \frac{N-1}{2}}$  for  $N - \text{odd}$ , and have an extra row and extra column with numbers  $\frac{N}{2}$  for  $N - \text{even}$ . This fact, together with the smallness of the parameter  $\gamma$  leads to an anomalously low splitting of the levels  $\lambda_0^+$  and  $\lambda_0^-$ . Really, the calculation of correction terms to the energy and to the wavefunctions of the symmetric and asymmetric states produce similar results for both symmetries, with differences appearing only in the order  $\gamma^{\frac{N-1}{2}} {}^2$ .

---

<sup>2</sup>In fact, the nonzero difference in energy  $\lambda_0^+ - \lambda_0^-$  appears in the order  $\gamma^N$  (see below,

Equations (5.14) and (5.15) constitute an eigenvalue problem for a non-Hermitian matrix. Let us solve this problem with the help of perturbation theory.

For convenience let us denote a one-column matrix, which the matrices (5.15), (5.16) act upon, by  $|\psi\rangle$ . The states of the unperturbed matrix  $H_0$  we denote by  $|\psi_n\rangle$ , where the index  $n$  refers to the energy level  $\lambda_n^{(0)} = n(N-n)$ . Thus the eigenvectors  $|\psi\rangle$ ,  $|\psi_n\rangle$  have the form:

$$|\psi\rangle \sim \begin{pmatrix} \psi_1 \\ \dots \\ \psi_n \\ \dots \\ \psi_{\frac{N}{2}} \end{pmatrix}, \quad |\psi_n\rangle = \begin{pmatrix} 0 \\ \dots \\ 1 \\ \dots \\ 0 \end{pmatrix},$$

where in  $|\psi_n\rangle$  unit number is positioned in the  $n$ -th row. For  $N$  – even the vector contains  $\frac{N}{2}$  rows, for  $N$  – odd, the number of rows is  $\frac{N-1}{2}$ .

The exact solution of the equations (5.13), (5.14) we denote by  $|\Psi_n\rangle$ , where the index  $n$  characterizes the unperturbed state  $\psi_n$ , the vector  $|\Psi_n\rangle$  has been obtained from.

In these notations the equations (5.13) and (5.14) read:

$$(H_0 + \gamma W) |\Psi_n\rangle = \lambda_n |\Psi_n\rangle. \quad (5.17)$$

Let us seek for the solution in the form:

$$\begin{aligned} |\Psi_n\rangle &= |\psi_n\rangle + |\varphi_n\rangle, \\ \langle \psi_n | \varphi_n \rangle &= 0. \end{aligned} \quad (5.18)$$

The vector  $|\varphi_n\rangle$  and the eigenvalue  $\lambda_n$  are expansions in  $\gamma$ :

$$\begin{aligned} |\varphi_n\rangle &= \gamma |\varphi_n^{(1)}\rangle + \gamma^2 |\varphi_n^{(2)}\rangle + \gamma^3 |\varphi_n^{(3)}\rangle + \dots \\ \lambda_n &= \lambda_n^{(0)} + \Delta\lambda_n = n(N-n) + \Delta\lambda_n. \end{aligned} \quad (5.19)$$

Substituting Eqs. (5.18) and (5.19) into Eq. (5.17) we obtain:

$$(\lambda_n^{(0)} - H_0) |\varphi_n\rangle = (\gamma W - \Delta\lambda_n) |\varphi_n\rangle + (\gamma W - \Delta\lambda_n) |\psi_n\rangle. \quad (5.20)$$

Multiplying Eq. (5.20) by  $\langle \psi_n |$ , taking into account Eq. (5.18), the Hermitian nature of  $H_0$ , and the conditions  $\langle \psi_n | W |\psi_n\rangle = 0$ ,  $\langle \psi_n | \psi_n\rangle = 1$ , we obtain:

$$\Delta\lambda_n = \gamma \langle \psi_n | W |\varphi_n\rangle. \quad (5.21)$$

Eq. (5.21) forms the basis of the calculation of the splitting of nondegenerate levels.

---

(5.23)).

Substituting Eq. (5.19) in (5.20), and collecting terms of the same power in  $\gamma$ , we obtain with the use of (5.21) the following system of recurrent equations for  $|\varphi_n^{(m)}\rangle$ :

$$\begin{aligned}
 (\lambda_n^{(0)} - H_0) |\varphi_n^{(1)}\rangle &= W |\psi_n\rangle, \\
 (\lambda_n^{(0)} - H_0) |\varphi_n^{(2)}\rangle &= W |\varphi_n^{(1)}\rangle - \langle \psi_n | W |\varphi_n^{(1)}\rangle |\psi_n\rangle, \\
 (\lambda_n^{(0)} - H_0) |\varphi_n^{(3)}\rangle &= W |\varphi_n^{(2)}\rangle - \langle \psi_n | W |\varphi_n^{(2)}\rangle |\psi_n\rangle \\
 &\quad - \langle \psi_n | W |\varphi_n^{(1)}\rangle |\varphi_n^{(1)}\rangle, \\
 (\lambda_n^{(0)} - H_0) |\varphi_n^{(4)}\rangle &= W |\varphi_n^{(3)}\rangle - \langle \psi_n | W |\varphi_n^{(3)}\rangle |\psi_n\rangle \\
 &\quad - \langle \psi_n | W |\varphi_n^{(2)}\rangle |\varphi_n^{(1)}\rangle - \langle \psi_n | W |\varphi_n^{(1)}\rangle |\varphi_n^{(2)}\rangle, \\
 &\dots, \\
 (\lambda_n^{(0)} - H_0) |\varphi_n^{(m+1)}\rangle &= W |\varphi_n^{(m)}\rangle - \langle \psi_n | W |\varphi_n^{(m)}\rangle |\psi_n\rangle \\
 &\quad - \langle \psi_n | W |\varphi_n^{(m-1)}\rangle |\varphi_n^{(1)}\rangle - \langle \psi_n | W |\varphi_n^{(m-2)}\rangle |\varphi_n^{(2)}\rangle - \dots \\
 &\quad - \langle \psi_n | W |\varphi_n^{(1)}\rangle |\varphi_n^{(m-1)}\rangle. \tag{5.22}
 \end{aligned}$$

It can be noted from Eq. (5.22) and from the structure of matrices (5.15) and (5.16) that the distinctions between the symmetric and antisymmetric states arise in the calculations for the first time in the term  $|\varphi_n^{(k)}\rangle$  with  $k = \frac{N}{2} - n$  for  $N$ –even, and with  $k = \frac{N-1}{2} - n + 1$  for  $N$ –odd. Really, in the state  $|\varphi_n^{(\frac{N}{2}-n)}\rangle$  an admixture of  $|\psi_{\frac{N}{2}}\rangle$  appears for  $N$ –even, while for antisymmetric vectors such states are absent. With  $N$ –odd, an admixture of the state  $|\psi_{\frac{N-1}{2}}^{(n)}\rangle$  will enter  $|\varphi_n^{(\frac{N-1}{2}-n+1)}\rangle$ . The former will give corrections of opposite signs for symmetric and antisymmetric levels:

$$\left\langle \psi_{\frac{N-1}{2}}^+ \middle| W \middle| \psi_{\frac{N-1}{2}}^+ \right\rangle = - \left\langle \psi_{\frac{N-1}{2}}^- \middle| W \middle| \psi_{\frac{N-1}{2}}^- \right\rangle.$$

From the consideration above it follows that the differences in the correction terms to the energies of symmetric and antisymmetric states appear for the first time, when we substitute the vector  $|\varphi_n\rangle$ , calculated up to  $|\varphi_n^{(N-2n)}\rangle$ , into Eq. (5.21). Really, if  $N$  is odd, the first difference in the admixture of the state  $|\psi_{\frac{N-1}{2}}\rangle$  appears after  $\frac{N-1}{2} - n + 1$  steps.

After that one needs  $\frac{N-1}{2} - n - 1$  steps to go up to the state  $|\varphi_n^{(N-n-1)}\rangle$ , in which the admixture of the state  $|\psi_{n+1}\rangle$  is different for symmetric and

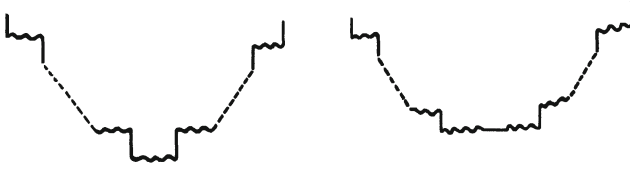


Figure 5.1: Diagrammatic representation of Eq. (5.23). The left picture is for  $N$  even, the right one – for  $N$  odd. The vertical solid line corresponds to the matrix element  $W_{n,n\pm 1}$ , a horizontal one – to  $W_{\frac{N-1}{2},\frac{N-1}{2}}$ , the wavy line corresponds to the factor  $(E_n - E_m)^{-1}$ .

antisymmetric states, and which provides a nonzero contribution to the matrix element (5.21). An analogous consideration shows, that in the case of  $N$  - even, the first distinctions between  $\lambda_n^+$  and  $\lambda_n^-$  appear upon substitution of  $|\varphi_n^{(N-2n-1)}\rangle$  into Eq. (5.21). A diagrammatic illustration of it is presented in Fig. 5.1.

The expression of energy level splitting  $\varepsilon_N(n)$  follows immediately from the consideration above:

$$\varepsilon_N(n) = \lambda_n^+ - \lambda_n^- = \begin{cases} \gamma^{N-2n} \langle \psi_n | W \left( \frac{1}{\lambda_n^{(0)} - \hat{H}^{(0)}} W \right)^{N-2n-1} | \psi_n \rangle, & N - \text{even}, \\ 2\gamma^{N-2n} \langle \psi_n | W \left( \frac{1}{\lambda_n^{(0)} - \hat{H}^{(0)}} W \right)^{N-2n-1} | \psi_n \rangle, & N - \text{odd}. \end{cases} \quad (5.23)$$

Substituting (5.15), (5.16) and  $\lambda_n^{(0)} = n(N-n)$  in (5.23), we obtain:

$$\begin{aligned} \varepsilon_N(n) &= \frac{\gamma^{N-2n} W_{n,n+1} W_{n+1,n+2} \dots W_{\frac{N}{2}-1, \frac{N}{2}} W_{\frac{N}{2}, \frac{N}{2}-1} \dots W_{n+1,n}}{(E_n - E_{n+1}) \dots (E_n - E_{\frac{N}{2}-1}) (E_n - E_{\frac{N}{2}}) (E_n - E_{\frac{N}{2}+1}) \dots (E_n - E_{n+1})} \\ &= -2\gamma^{N-2n} \frac{(N-n)!}{n! [(N-2n-1)!]^2}, \quad N - \text{even}, \\ \varepsilon_N(n) &= 2\gamma^{N-2n} \frac{W_{n,n+1} W_{n+1,n+2} \dots W_{\frac{N-3}{2}, \frac{N-1}{2}} W_{\frac{N-1}{2}, \frac{N-1}{2}} W_{\frac{N-1}{2}, \frac{N-3}{2}} \dots W_{n+1,n}}{(E_n - E_{n+1})^2 (E_n - E_{n+2})^2 \dots (E_n - E_{\frac{N-1}{2}})^2} \\ &= 2\gamma^{N-2n} \frac{(N-n)!}{n! [(N-2n-1)!]^2}, \quad N - \text{odd}. \end{aligned}$$

Thus for even and odd values of  $N$  the expressions of  $\varepsilon_N(n)$  coincide up to

	$\omega$ ( $cm^{-1}$ )	$\beta$ ( $cm^{-1}$ )	$x_e$ ( $cm^{-1}$ )	$\varepsilon_{10}, (5.6)$ ( $cm^{-1}$ ) <sup>3</sup>	$\varepsilon_{10}, (5.24)$ ( $cm^{-1}$ )	$\tau_{10}$ ( $c$ )
$H_2O$	3900	50	100	$1.7 * 10^{-6}$	$10^{-8}$	$2 * 10^{-5}$
$D_2O$	3000	50	50	$3.6 * 10^{-8}$	$5 * 10^{-6}$	$7 * 10^{-6}$
$H_2Se$	2500	8	42	$6 * 10^{-9}$	$3 * 10^{-13}$	$6 * 10^{-3}$
$H_2S$	2790	5	50	$7 * 10^{-9}$	$5 * 10^{-16}$	$6 * 10^{-3}$

Table 5.1: The energy splitting  $\varepsilon_{10}$  of symmetric and antisymmetric levels  $|10, s\rangle$  and  $|10, a\rangle$  in some molecules of  $XY_2$  type.

the accuracy of the sign. Combining these two formulas, we obtain:

$$\varepsilon_N(n) = \lambda_n^+ - \lambda_n^- = (-1)^{N+1} \frac{2(N-n)!}{n! [(N-2n-1)!]^2} \left( \frac{\beta}{2x_e} \right)^{N-2n} 2x_e. \quad (5.24)$$

Here we have gone back to the initial units of measurement:

$$\gamma = \frac{\beta}{2x_e}, \quad \varepsilon = E^+ - E^-.$$

Next we use the Eqs. (5.6),(5.24) to calculate the energy splitting  $\varepsilon_{10}(0) = \varepsilon_{10}$ , and the time of the excitation transfer from one bond to the other in molecules  $H_2O, D_2O, H_2Se, H_2S$ . The results of the calculation are presented in Table 5.1 with the parameters of molecules taken from Ref. [85].

The results of the calculations show, that in both limiting cases  $\frac{N x_e}{\omega} \ll \frac{\beta}{N x_e} \ll 1$ , and  $\frac{\beta}{N x_e} \ll \frac{N x_e}{\omega} \ll 1$ , the splitting is anomalously small,  $\varepsilon \ll \beta$ , and  $\varepsilon \ll x_e$ , and decreases fast with  $N$ . Correspondingly, the  $N$ - quanta excitation transfer time between the bonds grows fast (exponentially) with the increase of  $N$ , remaining, however, anomalously long compared to the characteristic time of single-quanta excitation transfer ( $\tau \sim \beta^{-1} \sim 10^{-12}$  s).

The exact calculation of the energy level splitting  $\varepsilon_N(n)$  requires the diagonalization of the Hamiltonian matrix (5.1), defined on Morse states of the overtone manifold. Such calculations for several overtones will be presented below. It will prove the pronounced clusterization of high overtones. More to it, these results will show, that Eqs. (5.6), (5.24) reproduce the exponential decay of the splitting  $\varepsilon_N$  with the increase of  $N$  in a correct way. In the next paragraph we will show, that the account of nonresonant modes does not change the obtained results. Thus the consideration above is applicable to real molecules of the type  $XY_2$ , which have an additional angular oscillation mode ( $\Omega \sim 1500 cm^{-1}$ ).

## 5.2 Stretching – vibration spectra: nonresonant modes' effect upon clusterization of levels

In the preceding Section we have considered the model of two weakly-interacting anharmonic quantum oscillators, and we have demonstrated the clusterization of highly-excited vibrational levels, corresponding to the states  $|n, N-n\rangle_+$  and  $|n, N-n\rangle_-$ . The magnitude of the splitting  $\varepsilon_N(n)$  is defined by Eqs. (5.6) and (5.24). As it can be seen, the splitting decreases exponentially with the increase of  $N$ :  $\varepsilon_N(n) \sim \max \left[ \left( \frac{Nx_e}{\epsilon\omega} \right)^N, \left( \frac{\beta e^2}{2Nx_e} \right)^N \right]$ , for  $Nx_e \ll \omega$ . Such a dependence leads to an extremely strong clusterization ( $\varepsilon_N \ll \beta$ ), which grows rapidly with the increase of  $N$ . A question arises: how do nonresonant vibration modes influence the effect of clusterization of levels? It turns out, that these modes renormalize the frequency  $\omega$  and interaction strength  $\beta$  of stretching vibrations only, reducing thus the problem to that of two nonlinear oscillators (5.1). Here are the corresponding calculations [6].

Following [6], we write down the Hamiltonian of the molecule in the following form:

$$\begin{aligned}
 H &= H_0 + W_a + W_b + W_{ab}, \\
 H_0 &= \frac{1}{2} [g_{aa}(p_a^2 + p_b^2) + k_{aa}(x_a^2 + x_b^2) + \Delta u(x_a) + \Delta u(x_b)] \\
 &\quad + \frac{1}{2} \sum_{\mu} (g_{\mu\mu} p_{\mu}^2 + k_{\mu\mu} x_{\mu}^2), \\
 W_{ab} &= g_{ab} p_a p_b + k_{ab} x_a x_b, \\
 W_{\nu} &= \sum_{\mu} (g_{\nu\mu} p_{\nu} p_{\mu} + k_{\nu\mu} x_{\nu} x_{\mu}), \quad \nu = a, b
 \end{aligned} \tag{5.25}$$

Here  $(a, b)$  correspond to two equivalent vibrational modes,  $\mu$  – to other nonresonant modes,  $\Delta u_{a,b}$  – to the nonlinear part of Morse potential.

Let us calculate the correction terms of the first order to the state  $|m, n, 0\rangle$ , and second order corrections to the energy  $E_{m,n}^{(0)}$ , where  $m$  and  $n$  are the excitation numbers of the oscillators  $a$  and  $b$ , while  $|0\rangle$  – is the vacuum state of nonresonant oscillators  $\prod_{\mu} |0_{\mu}\rangle$ . According to the formulas (5.21) and (5.22) of the standard perturbation theory, we obtain:

$$\begin{aligned}
 |\Psi_{m,n}\rangle &= |m, n, 0\rangle + \frac{1}{E_{m,n}^{(0)} - H_0} (W_a + W_b + \widetilde{W}_{ab}) |m, n, 0\rangle, \\
 \Delta E_{m,n}^{(2)} &= E_{m,n} - E_{m,n}^{(0)} \\
 &= \langle m, n, 0 | (W_a + W_b + \widetilde{W}_{ab}) (|\Psi_{m,n}\rangle - |m, n, 0\rangle).
 \end{aligned} \tag{5.26}$$

Here by  $\widetilde{W}_{ab}$  we denote the part of the operator  $W_{ab}$ , which extends beyond the overtone ( $m + n$ ). In Eq. (5.26) we have taken into account the fact that the diagonal matrix elements of the operator  $W_\nu$  equal zero. Utilizing the matrix elements of the operators  $p$  and  $x$ <sup>4</sup>:

$$\begin{aligned}\langle v+1| p_\mu |v\rangle &= i \sqrt{\frac{k_{\mu\mu}}{g_{\mu\mu}}} \sqrt{\frac{v+1}{2}}, \\ \langle v+1| x_\mu |v\rangle &= \sqrt{\frac{g_{\mu\mu}}{k_{\mu\mu}}} \sqrt{\frac{v+1}{2}},\end{aligned}\quad (5.27)$$

and using Eq. (5.26), we obtain the following expression for the correction term to the energy,  $\Delta E_{m,n}^{(2)}$  (a standard expression of the energy correction in the second order in interaction strength):

$$\begin{aligned}\Delta E_{m,n}^{(2)} &= \\ &= \langle m, n, 0 | \left( W_a + W_b + \widetilde{W}_{ab} \right) \frac{1}{E_{m,n}^{(0)} - H_0} \left( W_a + W_b + \widetilde{W}_{ab} \right) | m, n, 0 \rangle \\ &= \sum_\mu \left\{ \frac{| g_{a\mu} \langle m | p_a | m+1 \rangle \langle 0 | p_\mu | 1_\mu \rangle + k_{a\mu} \langle m | x_a | m+1 \rangle \langle 0 | x_\mu | 1_\mu \rangle |^2 }{-\omega - \Omega_\mu} \right. \\ &\quad \left. + \frac{| g_{a\mu} \langle m | p_a | m-1 \rangle \langle 0 | p_\mu | 1_\mu \rangle + k_{a\mu} \langle m | x_a | m-1 \rangle \langle 0 | x_\mu | 1_\mu \rangle |^2 }{\omega - \Omega_\mu} \right\} \\ &\quad + \sum_\mu \left\{ \frac{| g_{b\mu} \langle n | p_b | n+1 \rangle \langle 0 | p_\mu | 1_\mu \rangle + k_{b\mu} \langle n | x_b | n+1 \rangle \langle 0 | x_\mu | 1_\mu \rangle |^2 }{-\omega - \Omega_\mu} \right. \\ &\quad \left. + \frac{| g_{b\mu} \langle n | p_b | n-1 \rangle \langle 0 | p_\mu | 1_\mu \rangle + k_{b\mu} \langle n | x_b | n-1 \rangle \langle 0 | x_\mu | 1_\mu \rangle |^2 }{\omega - \Omega_\mu} \right\} \\ &\quad + \frac{| g_{ab} \langle m | p_a | m+1 \rangle \langle n | p_b | n+1 \rangle + k_{ab} \langle m | x_a | m+1 \rangle \langle n | x_b | n+1 \rangle |^2 }{-2\omega} \\ &\quad + \frac{| g_{ab} \langle m | p_a | m-1 \rangle \langle n | p_b | n-1 \rangle + k_{ab} \langle m | x_a | m-1 \rangle \langle n | x_b | n-1 \rangle |^2 }{2\omega} \\ &= -(m+n) \left\{ \frac{(\alpha - \beta)^2}{2\omega} + \sum_\mu \left[ \frac{(\alpha_\mu - \beta_\mu)^2}{\omega + \Omega_\mu} - \frac{(\alpha_\mu + \beta_\mu)^2}{\omega - \Omega_\mu} \right] \right\} \\ &\quad - \left\{ \frac{(\alpha - \beta)^2}{2\omega} + 2 \sum_\mu \frac{(\alpha_\mu - \beta_\mu)^2}{\omega + \Omega_\mu} \right\},\end{aligned}\quad (5.28)$$

---

<sup>4</sup>In Eqs. (5.25)-(5.27) and below we measure the momentum and position in the units  $\sqrt{\hbar m \omega}$  and  $\sqrt{\frac{\hbar}{m\omega}}$ , and the energy in spectroscopic units ( $\frac{E}{\hbar c}$ ),  $\text{cm}^{-1}$ . Consequently, the quantities  $\omega, \Omega_\mu, g, k$  below in this Section are measured in  $\text{cm}^{-1}$ .

where

$$\begin{aligned}\alpha &= \frac{g_{ab}}{2} \sqrt{\frac{k_{aa}}{g_{aa}}}, \quad \beta = \frac{k_{ab}}{2} \sqrt{\frac{g_{aa}}{k_{aa}}}, \\ \alpha_\mu &= \frac{g_{a\mu}}{2} \sqrt{\frac{k_{aa} k_{\mu\mu}}{g_{aa} g_{\mu\mu}}}, \quad \beta_\mu = \frac{k_{a\mu}}{2} \sqrt{\frac{g_{aa} g_{\mu\mu}}{k_{aa} k_{\mu\mu}}}, \\ \omega^2 &= g_{aa} k_{aa}, \quad \Omega_\mu^2 = g_{\mu\mu} k_{\mu\mu}.\end{aligned}\quad (5.29)$$

In the derivation of Eq. (5.28) we took into account the equivalence of the bonds  $a$  and  $b$ :  $g_{a\mu} = g_{b\mu}$ ,  $k_{a\mu} = k_{b\mu}$ ,  $g_{aa} = g_{bb}$ ,  $k_{aa} = k_{bb}$ . Besides, in the denominators  $E_{m,n,0}^{(0)} - E_{m\pm 1,n\pm 1,\mu}^{(0)}$  we neglected the anharmonic terms, which lead to higher-order corrections to  $\Delta E_{mn}^{(2)}$  in the parameter  $\frac{x_e}{\omega - \Omega_\mu} \ll 1$ .

It follows immediately from Eq. (5.28) that the renormalized frequency is:

$$\omega' = \omega - \left\{ \frac{(\alpha - \beta)^2}{2\omega} + \sum_\mu \left[ \frac{(\alpha_\mu - \beta_\mu)^2}{\omega + \Omega_\mu} - \frac{(\alpha_\mu + \beta_\mu)^2}{\omega - \Omega_\mu} \right] \right\}, \quad (5.30)$$

and that the energy of the  $n$ -th excitation of the stretching vibration is governed by the formula (5.2), with  $\omega$  is substituted by  $\omega'$ . We note also, that the anharmonic part in the spectral formula (5.2) is left unchanged with the same anharmonicity parameter  $x_e$ .

Next we pass over to the calculation of the renormalized interaction strength  $\beta$ . We note, that the investigation of the spectrum of an operator is equivalent to the study of the zeros of the corresponding Fredholm determinant of the operator  $H - \lambda I$ , or, in other words, in the case of finite-dimension basis, to the calculation of the determinant  $|H_{mn} - \lambda I_{mn}| = \Delta(\lambda)$ , and to solving the equation  $\Delta(\lambda) = 0$ . The important fact is that the matrix of the operator  $(H - \lambda I)_{mn}$  can be calculated in any basis set. In particular, the basis might not be orthogonal and normalized.

Let us look for the spectrum of the overtone manifold  $N = (m + n)$  of the Hamiltonian (5.25) in the basis  $|\Psi_{m,n}\rangle$ , which is determined by Eq. (5.26). To determine the matrix  $H_{mn;m'n'}$  of the Hamiltonian  $H$  in this nonorthogonal basis<sup>5</sup>, we use the equalities, following from (5.26):

$$\begin{aligned}(H_0 + W') |\Psi_{m,n}\rangle &= \\ &= (H_0 + W') \left[ |m, n, 0\rangle + \frac{1}{E_{m,n}^{(0)} - H_0} W' |m, n, 0\rangle \right] \\ &= \left( E_{m,n}^{(0)} + \Delta E_{m,n}^{(2)} \right) |\Psi_{m,n}\rangle\end{aligned}$$

<sup>5</sup>As in the overtone manifold the denominators are small  $\sim x_e$ , the knowledge of the states  $|\Psi_{mn}\rangle$ , and consequently, of the matrix  $H_{mn;m'n'}$  is sufficient for the determination of the spectrum of this manifold.

$$\begin{aligned}
& + \sum_{(m'n') \neq (mn)} \langle m', n', 0 | W' \frac{1}{E_{m,n}^{(0)} - H_0} W' | m, n, 0 \rangle |\Psi_{m',n'}\rangle \\
& - \left\{ \Delta E_{m,n}^{(2)} \frac{1}{E_{m,n}^{(0)} - H_0} W' | m, n, 0 \rangle \right. \\
& + \sum_{(m'n') \neq (mn)} \langle m', n', 0 | W' \frac{1}{E_{m,n}^{(0)} - H_0} W' | m, n, 0 \rangle \\
& \times \left. \left( \frac{1}{E_{m',n'}^{(0)} - \hat{H}_0} W' | m', n', 0 \rangle \right) \right\}. \tag{5.31}
\end{aligned}$$

where  $W' = W_a + W_b + \widetilde{W}_{ab}$  in accordance with (5.26).

In Eq. (5.26) only the resonant part of the operator  $W_{ab}$ , acting within overtone manifold states, is not taken into account. It will be considered later on.

The last term in curly brackets in Eq. (5.31) is of the order of  $(W')^3$ . Consequently, expanding it in an analogous way in the states of the overtone manifold  $|\Psi_{m',n'}\rangle$ , we will obtain corrections to the coefficients of the first two terms in the next order in the small parameter,  $\sim (W')^3$ . Thus, neglecting the term in curly brackets, we obtain the matrix of the operator  $H_0 + \gamma W'$  in the nonorthogonal basis with the accuracy up to  $\sim (W')^2$ :

$$\begin{aligned}
(H_0 + W') |\Psi_{m,n}\rangle &= \left( E_{m,n}^{(0)} + \Delta E_{m,n}^{(2)} \right) |\Psi_{m,n}\rangle \\
&+ \sum_{(m'n') \neq (mn)} \langle m', n', 0 | W' \frac{1}{E_{m,n}^{(0)} - H_0} W' | m, n, 0 \rangle |\Psi_{m',n'}\rangle, \text{ or} \\
(H_0 + W')_{mn}^{m'n'} &= \left( E_{m,n}^{(0)} + \Delta E_{m,n}^{(2)} \right) \delta_m^{m'} \delta_n^{n'} \\
&+ \langle m', n', 0 | W' \frac{1}{E_{m,n}^{(0)} - H_0} W' | m, n, 0 \rangle \left( 1 - \delta_m^{m'} \delta_n^{n'} \right). \tag{5.32}
\end{aligned}$$

Regarding Eq. (5.32) we would like to note the following. The neglected terms in Eq. (5.31) and the contributions from other manifolds give rise to terms of two different types in the Hamiltonian  $H_{mn}$ . The first modify slightly the nonzero matrix element, causing relative changes of the order  $\sim \frac{g}{\omega}$ . The second type of terms cause new transitions like  $(m, n) \rightarrow (m+2, n-2)$ . However, the intensity of the latter is  $\sim g \left( \frac{g}{\omega} \right)^3$ , i.e. low as compared to the intensity of a similar transition  $\sim g \left( \frac{\pi \epsilon}{\omega} \right)^3$ , caused by the anharmonicity of Morse functions. Really, for the stretching vibrations of the bonds like  $CH$ ,  $OH$ , etc., the following inequality holds:  $\frac{g}{\omega} \ll \frac{\pi \epsilon}{\omega}$ . Thus the renormalization of the frequency  $\omega$  and the interaction strength  $\beta$  keeps us within the model of two oscillators (5.1), and allows the usage of the formulas (5.6) and (5.24) to estimate the principal term of the level splitting  $\epsilon_N(n)$ .

The contribution of the resonance part  $W_{ab}^{(r)}$  of the operator  $W_{ab}$ , which causes transitions within the manifold  $(m, n) \rightarrow (m \pm 1, n \mp 1)$ , is not taken into account in (5.32). Adding the corresponding terms, we obtain the matrix of the total Hamiltonian  $H_{mn}^{m'n'}$  in the basis of the considered overtone manifold  $m + n = m' + n' = N$ . In the end we obtain the following final expression of  $H_{mn}^{m'n'}$ :

$$\begin{aligned} H_{mn}^{m'n'} &= (H_0 + W)_{mn}^{m'n'} \\ &= \left( H_0 + W_a + W_b + \tilde{W}_{ab} + W_{ab}^{(r)} \right)_{mn}^{m'n'} = \left( H_0 + W' + W_{ab}^{(r)} \right)_{mn}^{m'n'} \\ &= \left( E_{m,n}^{(0)} + \Delta E_{m,n}^{(2)} \right) \delta_m^{m'} \delta_n^{n'} + \langle m', n', 0 | W_{ab}^{(r)} | m, n, 0 \rangle \\ &\quad + \langle m', n', 0 | W' \frac{1}{E_{m,n}^{(0)} - H_0} W' | m, n, 0 \rangle \left( 1 - \delta_m^{m'} \delta_n^{n'} \right). \end{aligned} \quad (5.33)$$

In Eq. (5.33) the estimate  $\langle \Psi_{m',n'} | W^{(r)} | \Psi_{m,n} \rangle - \langle m', n', 0 | W^{(r)} | m, n, 0 \rangle \sim \frac{g^3}{\omega^2}$  has been used, which allows us to neglect this expression.

Next we have to find the matrix elements, entering Eq. (5.33). Utilizing the expressions (5.25) for the operators  $W_a, W_b, W_{ab}$  and the formula (5.27) for the matrix elements of momentum  $p$  and position  $x$ , after elementary but tedious calculations we obtain:

$$\begin{aligned} &\left\langle \begin{array}{c} m+1, n-1 \\ m-1, n+1 \end{array} \middle| W' \frac{1}{E_{m,n}^{(0)} - H_0} W' \middle| m, n \right\rangle \\ &= \left\langle \begin{array}{c} m+1, n-1 \\ m-1, n+1 \end{array} \middle| W_a \frac{1}{E_{m,n}^{(0)} - H_0} W_b \middle| m, n \right\rangle \\ &\quad + \left\langle \begin{array}{c} m+1, n-1 \\ m-1, n+1 \end{array} \middle| W_b \frac{1}{E_{m,n}^{(0)} - H_0} W_a \middle| m, n \right\rangle \\ &\quad + \left\langle \begin{array}{c} m+1, n-1 \\ m-1, n+1 \end{array} \middle| \tilde{W}_{ab} \frac{1}{E_{m,n}^{(0)} - H_0} \tilde{W}_{ab} \middle| m, n \right\rangle \\ &= 2 \sum_{\mu} \left[ \frac{(\alpha_{\mu} + \beta_{\mu})^2}{\omega - \Omega_{\mu}} - \frac{(\alpha_{\mu} - \beta_{\mu})^2}{\omega + \Omega_{\mu}} \right] \left\{ \begin{array}{c} \frac{\sqrt{n(n+1)}}{2} \\ \frac{\sqrt{m(n+1)}}{2} \end{array} \right\}, \quad (5.34) \\ &\left\langle \begin{array}{c} m+1, n-1 \\ m-1, n+1 \end{array} \middle| W_{ab}^{(r)} \middle| m, n \right\rangle = 2(\alpha + \beta) \left\{ \begin{array}{c} \frac{\sqrt{n(n+1)}}{2} \\ \frac{\sqrt{m(n+1)}}{2} \end{array} \right\}, \end{aligned}$$

where the coefficients  $\alpha, \beta, \alpha_{\mu}, \beta_{\mu}$  are determined in (5.29). In the figure brackets, Eq. (5.34), upper and lower lines correspond to two possible resonant transitions within the vibrational overtone. Like in the derivation of Eq. (5.28), here the anharmonic corrections in the denominators  $E_{m,n}^{(0)} - E_{m',n'}^{(0)}$  have been omitted. Due to this omission the matrix  $H_{mn}^{m'n'}$  is Hermitian.

Taking into account the equations (5.2), (5.28), (5.30), and (5.34) the matrix of the total Hamiltonian in the basis of the overtone manifold (5.33) can be presented in the form:

$$H_{mn}^{m'n'} = \left[ (m+n+1)\omega' - \left( m + \frac{1}{2} \right)^2 x_e - \left( n + \frac{1}{2} \right)^2 x_e \right] \delta_m^{m'} \delta_n^{n'} + 2g \left[ \frac{\sqrt{n(m+1)}}{2} \delta_{m+1}^{m'} \delta_{n-1}^{n'} + \frac{\sqrt{m(n+1)}}{2} \delta_{m-1}^{m'} \delta_{n+1}^{n'} \right], \quad (5.35)$$

$$g = \alpha + \beta + \sum_{\mu} \left[ \frac{(\alpha_{\mu} + \beta_{\mu})^2}{\omega - \Omega_{\mu}} - \frac{(\alpha_{\mu} - \beta_{\mu})^2}{\omega + \Omega_{\mu}} \right]. \quad (5.36)$$

To determine the spectrum of the matrix (5.35) we have to solve the equation:

$$\left| H_{mn}^{m'n'} - \lambda \delta_m^{m'} \delta_n^{n'} \right| = 0, \text{ with } m+n=N. \quad (5.37)$$

On the other hand, as it can be easily seen, the matrix, Eq. (5.35), corresponds to the Hamiltonian of two Morse oscillators with linear interaction:

$$H = \frac{1}{2} \left[ \frac{\omega'^2}{\omega^2} g_{ab} (p_a^2 + p_b^2) \right] + [u_{\mu}(x_a) + u_{\mu}(x_b)] + 2gp_a p_b, \quad (5.38)$$

The matrix elements of the operator  $p_a p_b$  are calculated in the harmonic approximation, which is applicable under the condition  $\frac{x_e}{\omega} \ll \frac{g}{x_e} \ll 1$ . Thus the problem of the calculation of the high overtone spectrum, interacting weakly with a set of nonresonant modes, is reduced to the problem of two nonlinear weakly bounded oscillators, which has been considered in the previous Section. Consequently the influence of nonresonant modes is manifested in a weak renormalization of the frequency  $\omega$  and of the interaction strength  $g_{ab}$  of the stretching vibrations of the bond ( $ab$ ), while the anharmonicity parameter  $x_e$  remains unchanged.

Thus, all the results obtained previously for the model of two nonlinear oscillators are correct in this case as well. In particular, the basic result of the increase in the clusterization of degenerate levels with the growing overtone number, is maintained.

We arrive at an important result signifying the clusterization of levels (doublets, in this particular case), corresponding to stretching vibrations of valence bonds of molecular fragments  $XY_2$ , no matter how complicated the molecule it enters is, with the only condition of absence of other resonant modes<sup>6</sup>. In particular, this is true for the molecule  $H_2O$ , as its deformation vibration (frequency  $\omega_2 = 1600 \text{ cm}^{-1}$ ) is nonresonant, and thus has little influence upon the stretching vibration of the valence bond.

---

<sup>6</sup>Fermi resonances are considered in Chapter 8, Section 8.3.

The same is true for the molecules  $CH_4$ ,  $C_6H_6$ , etc., as the deformation frequencies  $\sim 1080\text{ cm}^{-1}$  are much lower than the frequencies of valence bonds' stretching  $\sim 3000\text{ cm}^{-1}$ .

### 5.3 Spectrum of stretching vibrations in $XY_2$ molecules: numerical studies

In this Section we provide the results of numerical calculations of the vibrational spectrum of the molecule  $XY_2$ , based on the model of two oscillators which has been studied previously in Sections 5.1 and 5.2. As it will be made apparent later, these results back up the model approach of two weakly interacting nonlinear oscillators and the concept of local modes (LM) in whole, as compared to the conventional normal mode (NM) theory, which takes nonlinearity into account within perturbation theory.

The first advantage of the LM approach is in the simplicity of the representation of eigenstates through LM states. Typically the vibrational eigenstates are either symmetric or antisymmetric combinations of the local modes in accordance with Eq. (5.4). In more complicated molecules like  $CH_4$ ,  $C_6H_6$ , etc., the corresponding combinations are determined by irreducible representations of the group of transmutations of positions of equivalent nuclei, which are responsible for the vibrations of equivalent bonds. For the examples above these are atoms of hydrogen. On the other hand, the representation of a high-overtone vibrational eigenstate in the basis of normal modes provides an extremely wide spectral mixture (see Table 5.3 below). This proves the fact that the LM concept characterizes the essential physical nature, and is not for calculation convenience only. The analogy can be drawn with the wave function  $\psi_0(r)$  for an  $S$  state of an electron in hydrogen atom, which corresponds to electron probability density spread in the area  $a \sim 1$ , as opposed to the wavepacket  $k\Delta p \sim \frac{\hbar}{a}$ , which is delocalized over the whole space of plain waves  $\exp\left(\frac{i\mathbf{p}\mathbf{r}}{\hbar}\right)$ .

Another advantage of the concept of local modes is the considerably smaller number of variable parameters, needed to achieve agreement of the theoretical and experimental spectra. This is another manifestation of the adequacy of the LM concept to physics of nonlinear highly excited vibrations.

Here we provide the results of calculation of the first five overtones in molecule  $H_2O$  on the basis of Hamiltonian (5.35). The use of such an approximation is reasonable due to the inequality:

$$\left| \left( \frac{N x_e}{e \omega} \right)^{N-1} \right|_{N=5} \sim 10^{-6} \ll \left| \left( \frac{g e}{2 N x_e} \right)^{N-1} \right|_{N=5} \sim 10^{-4}, \quad (5.39)$$

The latter means that the main contribution to the splitting  $\epsilon_N(n)$  is governed by the formula of the type of (5.24), which may be obtained under

the condition, that the matrix of interaction operator  $2gp_a p_b$  is calculated in the harmonic approximation. Under this condition Eq. (5.35) follows from the Hamiltonian (5.38). With the account of renormalization of  $\omega$  and  $\beta$  the latter is equivalent to the Hamiltonian (5.1), which has been used in the derivation of Eq. (5.24) for the energy splitting  $\epsilon_N(n)$ .

Thus we calculate the overtone spectrum by diagonalizing the matrix (5.35). Let us find the form of this matrix in the basis of symmetrized states (5.4). The matrix is reducible, as its elements between states of different symmetry equals zero. The matrix elements for symmetric and antisymmetric manifolds equal one another, except for the transitions between the states  $|mn_{\pm}\rangle$  with  $m - n = 0, \pm 1$ . Calculations for the first five overtones  $m + n = 0, 1, \dots, 5$  provide the following expressions for the manifolds of different symmetry:

$$\begin{aligned}
 H^{(\pm)}(1) &= \omega' - 2x_e \pm g, \quad m + n = N = 1, \\
 \left\{ \begin{array}{l} H^{(+)}(2) = \begin{pmatrix} 2\omega' - 6x_e & 2g \\ 2g & 2\omega' - 4x_e \end{pmatrix}, \quad m + n = N = 2, \\ H^{(-)}(2) = \begin{pmatrix} 2\omega' - 6x_e & \\ & \end{pmatrix} \end{array} \right. \\
 H^{(\pm)}(3) &= \begin{pmatrix} 3\omega' - 12x_e & \sqrt{3}g \\ \sqrt{3}g & 3\omega' - 8x_e \pm 2g \end{pmatrix}, \quad m + n = N = 3, \\
 \left\{ \begin{array}{l} H^{(+)}(4) = \begin{pmatrix} 4\omega' - 20x_e & 2g & 0 \\ 2g & 4\omega' - 14x_e & 2\sqrt{3}g \\ 0 & 2\sqrt{3}g & 4\omega' - 12x_e \end{pmatrix}, \\ H^{(-)}(4) = \begin{pmatrix} 4\omega' - 20x_e & 2g \\ 2g & 4\omega' - 14x_e \end{pmatrix} \end{array} \right. \\
 m + n = N = 4, \\
 H^{(\pm)}(5) &= \begin{pmatrix} 5\omega' - 30x_e & \sqrt{5}g & 0 \\ \sqrt{5}g & 5\omega' - 22x_e & 2\sqrt{2}g \\ 0 & 2\sqrt{2}g & 5\omega' - 18x_e \pm 3g \end{pmatrix}, \\
 m + n = N = 5,
 \end{aligned} \tag{5.40}$$

In Eq. (5.40) we neglected the constant terms of the matrix (5.35), independent of  $m$  and  $n$ . It corresponds to the measurement of energy from the ground state  $E_{00} = 0$ . Comparing matrices (5.16), and (5.40) we find, that the differences between the symmetric and antisymmetric manifolds are in complete agreement with form of matrices (5.16) for arbitrary  $N$ .

With the help of Eq. (5.40) the energy levels of the first five overtones have been calculated. The required parameters

$$\omega' = 3860 \text{ (cm}^{-1}\text{)}, \quad x_e = 80 \text{ (cm}^{-1}\text{)}, \quad g = -27 \text{ (cm}^{-1}\text{)} \tag{5.41}$$

have been taken from Ref. [86], where the energy levels have been calculated on the basis of Hamiltonian (5.38). The matrix elements in Eq. (5.40),

LM	$E_{\text{exp}}$	$E_{\text{exact}}$	$E_{\text{appr}}$
01 <sup>+</sup>	3657.1	3673.5	3673
01 <sup>-</sup>	3755.9	3747	3727
02 <sup>+</sup>	7201.5	7223	7223
02 <sup>-</sup>	7249.8	7240	7240
11	7445	7416	7417
03 <sup>+</sup>	10599.7	10608.5	10612
03 <sup>-</sup>	10613.4	10611.3	10614
12 <sup>+</sup>	10868.9	10896	10894
12 <sup>-</sup>	11032.4	10994	11000
04 <sup>+</sup>	13828.3	13826.1	13834
04 <sup>-</sup>	13830.9	13825.5	13834
13 <sup>+</sup>	14221.1	14282	14286
13 <sup>-</sup>	14318.8	14324	14326
22	14536.9	14513	14520
05 <sup>+</sup>	16898.4	16880.6	16899
05 <sup>-</sup>	16898.4	16880.7	16899
14 <sup>+</sup>	17458.2	17517	17520
14 <sup>-</sup>	17496.5	17526	17527
23 <sup>+</sup>	17748.1	17803	17803
23 <sup>-</sup>		17934	17956

Table 5.2: The energies of symmetric and antisymmetric levels in the molecule  $H_2O$  with  $v_3 = 0$ . Results of an exact quantum mechanical calculation of  $E_{\text{exact}}$  with Morse functions from Ref. [86] are presented in the third column, energy  $E_{\text{appr}}$  calculated with the help of the approximate formula (3.40) - in the fourth column.

however, have been found with the use of the exact Morse functions with the accuracy up to the principal terms in the anharmonicity  $x_e$  and interaction  $g$ . The results of both calculations are presented in Table 5.2, together with experimental data from [6].

The results of experiments in Table 5.2 refer to the case, when the deformation mode is not excited  $\nu_2 = 0$ .

It can be seen easily, that the calculation of matrix elements in the harmonic approximation in Table 5.2 (matrix (5.40)) produces an error of 1% at maximum (compare columns 3 and 4 in the Table), which is of the order of  $(\frac{x}{\omega}) \sim 0.02$ . The agreement with experimental data (deviation less than 5%) becomes better for higher overtones. Within the overtone the agreement is better for the states with the higher localization energy, in passing from  $|23^{\pm}\rangle$  to  $|05^{\pm}\rangle$ . This is another confirmation of the fact that the high excitation of stretching vibrations are described well in the LM

concept within the model of weakly interacting nonlinear oscillators. For the molecule  $H_2O$  there are two oscillators, for  $C_6H_6$ —six, etc.

We note that the worse agreement of the theoretical and experimental values of the energy of low-lying levels and levels with a uniform distribution of energy over the bonds is in complete agreement with the definition of normal modes as a 1:1 resonance, which has been given in [52] (see also Section 3.2 in Chapter 3 and Figs. 3.9, 3.10). Really, in the case of a uniform energy distribution over valence bonds the vibrations are described better in the terms of normal modes (see Fig. 3.9, 3.10). Therefore the account of deformation vibrations (especially with Fermi resonances  $\nu_{1,3} = 2\nu_2$ ) becomes important, while in the model of two oscillators it is neglected. The same is true for low excitation of deformation vibration  $E = \nu_2, 2\nu_2$ , [87],[88].

The data in Table 5.2 reveal clearly the increasing clusterization of levels for higher overtones. This tendency, together with the nature of the dependence of clusterization on the overtone number agrees fully with Eq. (5.24) for the splitting  $\varepsilon_N(n)$ . The numerical discrepancies between the values of  $\varepsilon_N(n)$  from Table 5.2 and the results of calculations based on (5.24) come from the numerical errors, which for the overtone with number  $N = 5$  exceed the value of the splitting  $\sim 8 * 10^{-3}$  ( $cm^{-1}$ ) for  $|05^\pm\rangle$ <sup>7</sup>. For the overtones with  $N \leq 4$  the agreement is satisfactory. Now we demonstrate that the expression of  $\varepsilon_N(n)$ , obtained with the matrices (5.40) for  $N = 2, 3$  coincide fully with Eq. (5.24), as it should. The secular equations in both cases are quadratic. Their solutions are:

1.  $N = 2$ :

$$\begin{aligned} E_2^+(0) &= 2\omega' - 5x_e - \sqrt{x_e^2 + 4g^2} \\ &= 2\omega' - 6x_e - 2\frac{g^2}{x_e} + O(g^4), \\ E_2^-(0) &= 2\omega' - 5x_e, \\ \varepsilon_2 &= E_2^+(0) - E_2^-(0) = -2\frac{g^2}{x_e}; \end{aligned}$$

2.  $N = 3$ :

$$\begin{aligned} E_3^\pm(0) &= 3\omega' - 10x_e \pm g - \sqrt{(2x_e \pm g)^2 + 3g^2} \\ &= 3\omega' - 12x_e + 3\frac{g^2}{4x_e} \pm \frac{3g^3}{8x_e^2} + O(g^4), \\ \varepsilon_3 &= E_3^+(0) - E_3^-(0) = \frac{3g^3}{4x_e^2}, \\ E_2^\pm(1) &= 3\omega' - 10x_e \pm g + \sqrt{(2x_e \pm g)^2 + 3g^2} \end{aligned}$$

---

<sup>7</sup>The accuracy  $\sim 10^{-3}$  ( $cm^{-1}$ ) in the calculation of the energy was not needed, as the comparison with experimental data requires the accuracy of  $\sim 0.1$  ( $cm^{-1}$ ) only.

LM energy, ( $cm^{-1}$ )	basis expansion density	NM energy, ( $cm^{-1}$ )	basis expansion density
3676	$0.99 1,0\rangle_s$	3676	$0.85 1,0\rangle ; 0.10 2,0\rangle$
3730	$0.99 1,0\rangle_a$	3730	$0.90 0,1\rangle ; 0.09 1,1\rangle$
7223	$0.93 2,0\rangle_s ;$	7223	$0.44 2,0\rangle ; 0.15 3,0\rangle ; 0.14 0,2\rangle$
	$0.07 1,1\rangle$		$0.11 1,0\rangle ; 0.09 1,2\rangle$
7240	$0.98 0,2\rangle_a ;$	7240	$0.59 1,1\rangle ; 0.21 2,1\rangle ; 0.09 0,1\rangle ;$
7422	$0.93 1,1\rangle ;$	7422	$0.62 0,2\rangle ; 0.18 2,0\rangle ; 0.09 1,2\rangle$
	$0.07 2,0\rangle_s$		
10598	$0.98 3,0\rangle_s$	10618	$0.22 2,2\rangle ; 0.15 2,0\rangle ; 0.14 1,2\rangle ;$
			$0.10 3,0\rangle ; 0.10 4,0\rangle$
10600	$0.99 3,0\rangle_a$	10620	$0.25 1,1\rangle ; 0.23 3,1\rangle ; 0.18 2,1\rangle ;$
			$0.10 1,3\rangle ; 0.06 4,1\rangle$
10899	$0.98 2,1\rangle_s$	10903	$0.25 3,0\rangle ; 0.21 4,0\rangle ; 0.18 1,2\rangle ;$
			$0.08 2,0\rangle ; 0.08 0,2\rangle$
10996	$0.99 2,1\rangle_a$	10998	$0.59 0,3\rangle ; 0.15 1,3\rangle ; 0.10 2,1\rangle ;$
			$0.08 3,1\rangle$
13798	$0.99 4,0\rangle_s$	13998	$0.30 2,1\rangle ; 0.14 2,3\rangle ; 0.12 4,1\rangle ;$
			$0.08 0,3\rangle ; 0.08 3,3\rangle$
13798	$0.99 4,0\rangle_a$	13988	$0.26 1,2\rangle ; 0.18 3,2\rangle ; 0.12 3,0\rangle ;$
			$0.10 4,2\rangle ; 0.05 1,4\rangle$
14276	$0.85 3,1\rangle_s ;$	14333	$0.25 5,0\rangle ; 0.21 3,0\rangle ; 0.08 1,2\rangle ;$
	$0.14 2,2\rangle$		$0.08 1,4\rangle ; 0.07 4,0\rangle$

Table 5.3: Energy eigenvalues and the densities in the expansion of the eigenvectors within LM and NM pictures for a Morse potential. NM - basis vector  $|n_1, n_2\rangle$  corresponds to  $n_1$  quanta of a symmetric vibration and to  $n_2$  antisymmetric ones. In the LM basis the indices  $s$  and  $a$  denote symmetrized and antisymmetrized states respectively.

$$\begin{aligned}
&= 3\omega' - 8x_e \pm 2g + O(g^2), \\
\varepsilon_3(1) &= E_2^+(1) - E_2^-(1) = 4g.
\end{aligned} \tag{5.42}$$

In conclusion we provide the results of the calculation of the vibrational overtone spectrum, performed in [89], Table 5.3. These results have been obtained in the model of two Morse oscillators. The calculations have been performed in both LM and NM basis. In the third and forth columns of Table 5.3 the contributions of different basis functions to the eigenenergies of vibrational levels are provided. We note the impressive simplicity of the representation of eigenstates in LM basis, as compared to the very complicated mixture of eigenvectors in NM representation. This is another demonstration of the adequacy of LM concept in physics of stretching vibrations in

molecules with  $C - H$ ,  $O - H$ ,  $N - H$  and similar bonds, as compared to the normal-mode picture. It is due to this reason, that the calculation of vibrational overtones in the model of Morse oscillators, containing only two adjustable parameters  $\omega'$  and  $x_e$ <sup>8</sup>, provides good agreement with experimental data, especially for high overtones and states of the type  $|n, m^\pm\rangle$  with  $|n - m| \gg 1$ .

We also note, that the calculation with a quartic potential  $U_0x^4$  instead of Morse gives qualitatively similar results: a simple description in the LM picture, and a complicated representation in normal mode approach [89]. Besides, in the calculations with the quartic potential the three-oscillators-model has been employed – valence angle oscillations has been added. Complicated mixtures of basis functions in the LM picture evolves only in the presence of some accidental resonance like the Fermi resonance in the model of three oscillators<sup>9</sup>.

---

<sup>8</sup>The parameter  $2g = \frac{m}{M} \cos \Theta_0$ , where  $m$  and  $M$  are the masses of atoms of hydrogen and oxygen correspondingly, and  $\Theta_0$  is the angle between  $O - H$  bonds, is fixed

<sup>9</sup>Fermi resonances are considered in Chapter 8, Section 8.3.

## Chapter 6

# Quantum Hamiltonians of vibrational – rotational excitations in polyatomic molecules; method of contact transformations

This Chapter is devoted to the principles of construction of the total vibrational-rotational Hamiltonian of a polyatomic molecule. The basic idea of the method relies upon the transformation of the Laplace operator into its covariant form, as in tensor analysis. Thus, the kinetic energy operator is calculated from the classical expression  $2T = \sum g_{ik}q^i q^k$  through the components of the metric tensor  $g_{ik}$ . The transition to quantum description of particle motion in Euclidean space for  $g_{ik} \neq \delta_{ik}$  is equivalent to a transition into a non-orthogonal basis. For a mechanical system, whose configuration space has some curvature, this method is essentially the definition of quantization. It makes the determination of the quantum Hamiltonian for a mechanical system with bonds rather simple and transparent. An example can be provided by a molecule with valent bonds of fixed lengths and variable angles between them. In Sections 6.1 and 6.2 this technique will be used to write down the full vibrational-rotational Hamiltonian of the molecule. Sections 6.3 and 6.4 are devoted to the method of contact transformations, which enables one to represent the Hamiltonian of a molecule in the form of power series in the small parameter  $(m_{\text{electron}}/M_{\text{nucleus}})^{1/4}$ . The terms of this expansion can be separated into three classes: the first one – purely vibrational operators, the second – purely rotational operators, and the third – operators describing the interaction of vibrations and rotations,  $H = H_{\text{vib}} + H_{\text{rot}} + H_{\text{vib,rot}}$ .

From the mathematical point of view, a contact transformation is a se-

quence of unitary transformations, close to unit,  $\sim \left[ 1 + O \left( \left( \frac{m_{\text{electron}}}{M_{\text{nucleus}}} \right)^{1/4} \right) \right]$ .

In practice, the contact transformation for a molecular Hamiltonian is chosen in such a way, that the order of the interaction operator  $H_{\text{vib},\text{rot}}$  be minimal in the small parameter  $(m_{\text{electron}}/M_{\text{nucleus}})^{1/4}$ . A regular method of construction of the required sequence of unitary transformations is provided in Section 6.3. The resultant Hamiltonian for such a transformation describes well some vibrational-rotational multiplet. The treatment of several different multiplets requires different contact transformations. In Section 6.4 the methods of Sections 6.1 – 6.3 are used to construct the Hamiltonian for the molecule  $XY_2$  in inner coordinates, and to study it with the help of a suitable contact transformation.

For the proper understanding of this Chapter, the knowledge of the technique of unitary and canonical transformations within the material of the cited books [7, 90, 81, 54] is sufficient. The required information on tensor analysis for the covariant form of the equations in curved space can be found in the second part of the textbook [90]. A better understanding of the physical meaning of various terms in molecular Hamiltonians during contact transformations require basic knowledge of the theory of the interaction of vibrations with rotations in polyatomic molecules, which can be found, for example, in the monograph [96, 98].

## 6.1 Quantum Hamiltonian of polyatomic molecules

In the studies of vibrations of polyatomic molecules above we utilized model Hamiltonians which are more or less adequate for the analysis of strongly anharmonic stretching vibrations of  $C - H$  and  $O - H$  bonds. It has been shown, that the vibration nonlinearity leads to a highly pronounced clusterization of highly excited vibrational levels. As the inter-level spacings in the cluster are comparable or even much smaller than the rotational frequencies  $\omega_r \sim 10 \text{ cm}^{-1}$  the question of the influence of molecular rotation upon its vibrational spectrum arises.

We would like to stress, that presently we mean not the accidental coincidence of vibrational and rotational frequencies  $\Delta E_v \sim \Delta E_r$  as it happens in the case of weakly excited normal modes. We are talking about their inevitable coincidence for higher overtones, as the energy splitting of two similar stretching vibrations  $\epsilon_N(n)$  diminishes rapidly with increasing  $N$  for strongly nonlinear vibrations (see Eqs. (5.6) and (5.24)). In other words, will the tendency to clusterization of highly excited vibrational levels of polyatomic molecules remain valid, if the interaction of vibrations with the rotation of the molecule is taken into account. It is necessary to study the molecular Hamiltonian, which incorporates the terms corresponding to

vibrations, rotations, and their interaction, and to analyze the corresponding modifications of the vibrational spectrum.

The molecule constitutes a complicated system of interacting electrons and the nuclei with the following Hamiltonian:

$$H = \frac{\hbar^2}{2} \sum_i m^{-1} \Delta_i + \frac{\hbar^2}{2} \sum_j M_j^{-1} \Delta_j + \sum_{i < k} \frac{e^2}{|r_i - r_k|} + \sum_{j < k} \frac{e_j e_k}{|R_j - R_k|} + \sum_{i,j} \frac{e e_j}{|R_j - r_i|}, \quad (6.1)$$

where  $\Delta_i$  is the Laplace operator for the  $i$ -th particle,  $m, e$  are the mass and the charge of the electron,  $M_j, e_j$  are the mass and the charge of  $j$ -th nuclei,  $r_i, R_j$  - the position of  $i$ -th electron and  $j$ -th nucleus. The Hamiltonian (6.1) is extremely complicated, so that the corresponding problem cannot be solved directly.

However, Born and Oppenheimer (1927) suggested to utilize the small parameter  $\frac{m}{M_j} \sim 10^{-4}$  in the adiabatic approximation, representing the wavefunction of the system in the form of the product  $\Phi(r, R) = \Psi_e(r, R) \Psi(R)$ . Here the function  $\Psi_e(r, R)$  is the solution of the equation (6.1), where the kinetic energy of the nuclei  $\sum_j M_j^{-1} \Delta_j$  is omitted, while the energy eigenvalues  $U_n(R_j)$  depend on the nuclei positions  $R_j$  as parameters. The nuclear wavefunction  $\Psi(R)$  satisfies the Schrödinger equation in which the electron energy  $U_n(R)$  plays the role of the potential:

$$\left[ \frac{\hbar^2}{2} \sum_j M_j^{-1} \Delta_j + U(R_j) \right] \Psi(R_j) = E \Psi(R_j). \quad (6.2)$$

We omitted the index  $n$  in the electron energy  $U_n(R_j)$  assuming that the electronic subsystem of the molecule is in the ground state:  $U_0(R_j) = U(R_j)$ . In the present book throughout we consider the molecule in the ground electronic state with the assumption that the excited states of the electrons are situated high enough in energy, ( $\Delta E_e \sim 10^5 \text{ cm}^{-1}$ ), and do not influence the qualitative structure of the vibrational-rotational spectrum ( $\Delta E_v \sim 10^3 \text{ cm}^{-1}$ ) <sup>1</sup>.

Thus in the adiabatic approximation the motion of nuclei in polyatomic molecules is governed by Eq. (6.2). The potential energy of the nuclei  $U(R_j)$  is obtained as a result of the quantum-chemical calculation of the ground electronic state of the molecule. For a very wide class of molecules the function  $U(R_j)$  has an extremely profound minimum for some configuration of nuclei. In that case the nuclei execute motion presumably in a

<sup>1</sup>Excited electronic states contribute to the vibrational spectrum correction terms of the relative order  $\sim \frac{m}{M}$ .

multidimensional vicinity of that minimum ( $\mathbf{R}_j \sim \mathbf{R}_{j0}$ ) with superimposed small vibrations and rotations. Such molecules are termed semirigid; they will be the subject of the study in the present book. Molecules like  $H_2O$ ,  $C_6H_6$ ,  $CH_4$ ,  $SnF_6$  and others belong to that type. The molecule  $NH_3$ , on the contrary, is not a semirigid one, as it can go over easily enough from one conformation to another, which is obtained by the inversion of all the nuclei with respect to the center of mass. The inversion barrier for such a transition is of the order of  $\sim 2000\text{ cm}^{-1}$  — comparable to the vibrational frequencies. We will not study such molecules here.

In the analysis of rotational – vibrational interactions in a semirigid polyatomic molecule it is convenient to pass over to the set of coordinates  $Q_1, \dots, Q_{3n-6}, \alpha, \beta, \gamma, R_{cx}, R_{cy}, R_{cz}$ . Here the coordinates  $Q_j$  measure the deviation from the equilibrium configuration, the Euler angles  $(\alpha, \beta, \gamma)$  characterize the orientation of the equilibrium configuration  $\{\mathbf{R}_{j0}\}$  with respect to the laboratory coordinates' set, and  $\mathbf{R}_c$  is the position of the center of mass of molecule.

This coordinates set can be conveniently introduced in two stages. First we introduce the coordinates  $\mathbf{r}_1, \dots, \mathbf{r}_{N-2}, \alpha, \beta, \gamma, \mathbf{R}_c$  according to the formulas:

$$\begin{aligned} \mathbf{R}_j &= \mathbf{R}_c + S^{-1}(\alpha\beta\gamma)(\mathbf{a}_j + \mathbf{r}_j), \\ \sum_j^N \mathbf{a}_j m_j &= \sum_j^N \mathbf{r}_j m_j = 0, \\ \sum_j^N m_j (\mathbf{a}_j \times \mathbf{r}_j) &= 0, \end{aligned} \quad (6.3)$$

where  $\mathbf{a}_j$  is the vector from the molecule center of mass to the equilibrium position of the  $j$ -th nuclei,  $\mathbf{r}_j$  is the shift of the  $j$ -th nuclei from its equilibrium in the new frame,  $(\alpha, \beta, \gamma)$  – are the Euler angles, and  $S$  is the rotation matrix of the new frame with respect to the old one. The last two equations in (6.3) are called Eckart conditions.

Obviously, equations (6.3) determine a mutually unambiguous correspondence rule between the sets of old  $(\mathbf{R}_1, \dots, \mathbf{R}_N)$  and new  $(\mathbf{r}_1, \dots, \mathbf{r}_{N-2}, \alpha, \beta, \gamma, \mathbf{R}_c)$  coordinates. Really, given the  $(N-2)$  vectors  $(\mathbf{r}_1, \dots, \mathbf{r}_{N-2})$ , from the Eckart conditions we determine  $\mathbf{r}_{N-1}$ ,  $\mathbf{r}_N$ , and subsequently from the first equality we find  $\mathbf{R}_1, \dots, \mathbf{R}_N$ . And vice versa, with  $\mathbf{R}_1, \dots, \mathbf{R}_N$  given, we obtain  $\mathbf{R}_c = \frac{\sum m_j \mathbf{R}_j}{\sum m_j}$ , and upon substitution into the second Eckart condition  $\mathbf{r}_j = -\mathbf{a}_j + S(\alpha, \beta, \gamma)(\mathbf{R}_j - \mathbf{R}_c)$  we find  $(\alpha, \beta, \gamma)$  and subsequently from the first equation –  $\mathbf{r}_1, \dots, \mathbf{r}_{N-2}$ .

The transformation of variables (6.3) corresponds to the following geometrical object. First we consider a polyhedron corresponding to the equilibrium configuration of the molecule. The apexes of the polyhedron have the "weight" equal to the masses of the nuclei. The origin of the orthogonal coordinate set is put in the center of mass, and the axes are positioned

with respect to the polyhedron in such a way, that the Eckart conditions are fulfilled. Then the positions of the nuclei in the frame of the polyhedron ( $\mathbf{r}_j + \mathbf{a}_j$ ) are in the relationship with the nuclei positions  $\mathbf{R}_j$  in the laboratory frame, governed by Eq. (6.3). Such a frame is bound rigidly with the molecule: its origin moves with the center of mass, and axes rotate in such a way, that the Eckart conditions are fulfilled.

If the rigidity is infinitely high, then  $\mathbf{r}_j = 0$ . The vibration amplitude is zero, and the molecule represents a rigid top. Its wavefunction  $D(\alpha, \beta, \gamma)$  is defined on the configuration manifold of Euler angles  $(\alpha, \beta, \gamma)$  with the elementary volume  $d\alpha \sin \beta d\beta d\gamma$ .

It is obvious that the transition into such a frame provides a transparent physical picture of the nuclear motion of semirigid molecules, and makes it possible to reveal the general features of their vibrational-rotational spectra. Additionally we have the freedom to take into account the individual features of a particular molecule by the choice of coordinate transformation  $\{\mathbf{r}_j\} \rightarrow \{\mathbf{Q}_j\}$ , which will simplify the form of the potential  $U(R_j(Q))$  to a maximal extent. For example, in the case of normal modes the coordinates  $\{\mathbf{Q}_j\}$  are introduced in such a way, that the quadratic part of the vibration energy  $\sum_{j=1}^N m\dot{r}_j^2 + U(R_j(Q))$  acquires a diagonal form. In the case of highly anharmonic stretching vibrations the potential energy is reduced to the form  $U(Q) = (\sum_{j=1}^N U_j(Q_j) + \text{small correction terms})$ . After the coordinates  $Q$  with the account of individual characteristics of the molecule are chosen, the construction of the vibrational-rotational Hamiltonian reduces to rewriting the operator (6.2) in the new set of variables. As the transition to the new variables in the potential  $U(R_j)$ <sup>2</sup> is trivial, the main difficulty lies in the transformation of the kinetic energy operator  $\sum_j M_j^{-1} \Delta_j$ .

To transform the multidimensional Laplace operator to the non-Decart frame we will use the formulas of tensor analysis [90]. Other derivations of the Hamiltonian, based on the quantization of the classical Hamilton function or on the transformation of the derivatives to non-Decart coordinates can be found in Refs. [94] and [95] respectively.

As it is known from tensor analysis, the Laplace operator in non-Decart frame has the form:

$$\Delta = \frac{1}{\sqrt{g}} \cdot \frac{\partial}{\partial q^i} \cdot \sqrt{g} \cdot g^{ik} \cdot \frac{\partial}{\partial q^k}, \quad (6.4)$$

---

<sup>2</sup>We assume, that the quadratic terms in the operator of electron momentum  $\langle \Psi(r) | I_{ik}^{-1}(R) L_i L_k | \Psi_{el}(r) \rangle$  which arise during the transition to the rotating frame (body axes), are incorporated in  $U(R)$  ([96]). Obviously, the point symmetry of the function  $U(R)$  will not change. Terms, linear in the operator  $\langle \Psi_{el} | L_i | \Psi_{el} \rangle$  vanish according to Jahn – Teller rule [100], as the stable configuration of the molecule has a non-degenerate electronic ground state with the exception of linear molecules. In the case of linear molecules terms linear in the averaged operator of electronic momentum  $L$  should be included in the formulas below [96]. However, we will not consider linear molecules here.

where  $g = |g_{ik}|$  is the determinant of the metric tensor  $g_{ik}$ , which defines the elementary distance:

$$ds^2 = g_{ik} dq^i dq^k. \quad (6.5)$$

The metrics of the contravariant metric tensor  $g^{ik}$  is inverse to  $g_{ik}$ :

$$g^{ik} = (g_{ik})^{-1}. \quad (6.6)$$

Equation (6.4), as usual in tensor analysis, implies summation over indices which are repeated twice. In the Decart frame  $g_{ik} = \delta_{ik}$  and Eq. (6.4) transforms into the usual multidimensional Laplace operator  $\sum_i \frac{\partial^2}{\partial q_i^2}$ .

It can be easily seen, that the relation between the operators  $\Delta$  and  $\left(\frac{ds}{dt}\right)^2$  in Eqs. (6.4) and (6.5) up to derivatives of the function  $\sqrt{g(q)}$  is the same as the relation between the kinetic energy  $2T = g_{ik} \dot{q}^i \dot{q}^k$  in Lagrange formulation and the kinematic part of the Hamilton function  $2H(p, q) - 2U(q) = g^{ik} p_i p_k$  in Hamilton representation. Really, the momenta  $p_i$  are determined by equation (5.20):

$$p_i = \frac{\partial T}{\partial \dot{q}^i} = g_{ik} \cdot \dot{q}^k. \quad (6.7)$$

Then we find:

$$\dot{q}^i = g^{ik} p_k, \quad (6.8)$$

and upon substitution of Eq. (6.8) into the formula  $2T = g_{ik} \dot{q}^i \dot{q}^k$  we obtain  $2(H(p, q) - U(q)) = g^{ik} p_i p_k$ . Then a simple rule governing the form of the Laplace operator in non-Decart coordinates can be formulated: The kinetic energy should be represented in the form  $2T = \sum_j M_j \dot{R}_j^2 = \sum_{i,k} g_{ik}(q) \dot{q}^i \dot{q}^k$ ,

then the inverse matrix  $\|g_{ik}\|^{-1}$  should be found along with the determinant  $|g_{ik}|$ , and subsequently equation (6.4) should be used. Such an approach to the calculation of the operator  $\Delta$  in the non-Decart frame with the use of Eq. (6.3) is most convenient, as the expression of the kinetic energy through the particle velocity  $\dot{r}_j$  in the frame rotating with the molecule and of the derivatives of Euler angles  $\dot{\alpha}, \dot{\beta}, \dot{\gamma}$  are known (see, i.e. [42]), so that the expression of the tensor  $g_{ik}(q)$  can be written down immediately. For small amplitude vibrations the elements  $g_{ik}$  have a transparent physical meaning, as well as the elements of the inverse matrix  $g^{ik}$  (see, i.e., [96]).

We would like to stress once more, that the algorithm of calculation of Laplace operator in non-Decart coordinates, described above, is equivalent to the transition performed by direct substitution of partial derivatives  $\frac{\partial}{\partial x^i} = \frac{\partial q^j}{\partial x^i} \frac{\partial}{\partial q^j}$  into the expression of Laplace operator. Really the expression (6.4) is

invariant with respect to all continuous transformations of the coordinates, when the tensor  $g^{ik}$  is transformed according to the formula:

$$(g^{ik})' = \frac{\partial q^i}{\partial x^m} \cdot \frac{\partial q^k}{\partial x^n} \cdot g^{mn}. \quad (6.9)$$

One can transform the metric tensor to the new coordinates  $g_{ik} \rightarrow g'_{ik}$ , and calculate subsequently  $\|g'\|^{-1} = \|g'_{ik}\|^{-1}$  – the result will be the same. In fact the transition  $g_{ik} \rightarrow g'_{ik}$  corresponds to the calculation of the kinetic energy  $2T = g_{ik} \dot{X}^i \dot{X}^k$  in non-Decart coordinates  $2T = g_{ik} \dot{q}^i \dot{q}^k$ .

The operator (6.4) is Hermitian, as the elementary volume is transformed according to the formula:

$$dv = \sqrt{|g|} dx = \sqrt{|g'|} dq. \quad (6.10)$$

With the account of Eq. (6.10) the probability  $dP$  to find the system in the elementary volume  $dx$  of the Euclidean space, expressed in non-Decart coordinates  $q$  has the form <sup>3</sup>:

$$dP = |\Psi(x)|^2 dx = \left( \prod_{i=1}^{3N} M_i^{\frac{1}{2}} \right)^{-1} \cdot |\Psi(x(q))|^2 \cdot \sqrt{g'(q)} dq. \quad (6.11)$$

Next we pass over to the direct derivation of the vibrational-rotational Hamiltonian by performing the transition to non-Decart coordinates (6.3) in the operator (6.2). The kinetic energy in the laboratory frame has the form <sup>4</sup>:

$$T = \frac{1}{2} \sum_j M_j \cdot \dot{\mathbf{R}}_j^2. \quad (6.12)$$

In the non-Decart frame (6.3) the kinetic energy  $T$  takes the shape ([42, 96]):

$$\begin{aligned} T &= \frac{1}{2} \sum_{j=1}^N M_j \dot{\mathbf{R}}_c^2 + \frac{1}{2} \sum_{j=1}^N M_j \{[\boldsymbol{\omega} \times (\mathbf{a}_j + \mathbf{r}_j)] + \dot{\mathbf{r}}_j\}^2 = \\ &= \frac{1}{2} M \dot{\mathbf{R}}_c^2 + \frac{1}{2} \sum_{\gamma, \nu} I_{\gamma \nu} \omega_\gamma \omega_\nu + \boldsymbol{\omega} \sum_{j=1}^N M_j [\mathbf{r}_j \times \dot{\mathbf{r}}_j] \\ &\quad + \frac{1}{2} \sum_{j=1}^N M_j \dot{\mathbf{r}}_j^2, \quad M = \sum_j M_j. \end{aligned} \quad (6.13)$$

<sup>3</sup>Here  $M_1 = M_2 = M_3$ ,  $M_4 = M_5 = M_6$  and so on.

<sup>4</sup>From the last equation it becomes obvious, that  $g_{ik} = \sqrt{M_i} \delta_{ik}$ . At the same time,  $M_1 = M_2 = M_3$ ,  $M_4 = M_5 = M_6$ , etc. (cf. 6.11).

Here  $\dot{\mathbf{r}}_j$  is the velocity of the  $j$ -th particle with respect to the rotating frame,  $\dot{\mathbf{R}}_c$  is the velocity vector of the molecule center of mass with respect to the laboratory frame,  $\omega_\nu$  is the projection of the angular velocity of the rotating frame (body axes) upon the axes ( $\nu - \bar{x}, \bar{y}, \bar{z}$ ). The projections of the angular velocity upon the rotating axis are related to the time derivatives of Euler angles in the following way:

$$\begin{aligned}\dot{\omega}_{\bar{x}} &= \sin \gamma \cdot \dot{\beta} - \sin \beta \cdot \cos \gamma \cdot \dot{\alpha}, \\ \dot{\omega}_{\bar{y}} &= \cos \gamma \cdot \dot{\beta} + \sin \beta \cdot \sin \gamma \cdot \dot{\alpha}, \\ \dot{\omega}_{\bar{z}} &= \cos \beta \cdot \dot{\alpha} + \dot{\gamma}.\end{aligned}\quad (6.14)$$

The inverse transformation is:

$$\begin{aligned}\dot{\alpha} &= -\frac{\cos \gamma}{\sin \beta} \cdot \omega_{\bar{x}} + \frac{\sin \gamma}{\sin \beta} \cdot \omega_{\bar{y}}, \\ \dot{\beta} &= \sin \gamma \cdot \omega_{\bar{x}} + \cos \gamma \cdot \omega_{\bar{y}}, \\ \dot{\gamma} &= \cot \beta \cdot \cos \gamma \cdot \omega_{\bar{x}} - \cot \beta \cdot \sin \gamma \cdot \omega_{\bar{y}} + \omega_{\bar{z}}.\end{aligned}$$

And last,  $I_{\nu\lambda}$  is the inertia (momentum) tensor of the molecule, corresponding to the momentary position of nuclei, and calculated in the body system:

$$\begin{aligned}I_{\nu\lambda} &= \sum_{j=1}^N M_j \cdot \left\{ (\mathbf{a}_j + \mathbf{r}_j)^2 \delta_{\nu\lambda} - (\mathbf{a}_j + \mathbf{r}_j)_\nu (\mathbf{a}_j + \mathbf{r}_j)_\lambda \right\}, \\ I_{\nu\lambda}^{(0)} &= I_{\nu\lambda}^{(0)} = \sum_{j=1}^N M_j \left\{ \mathbf{a}_j^2 \delta_{\nu\lambda} - (\mathbf{a}_j)_\nu (\mathbf{a}_j)_\lambda \right\}, \quad \mathbf{r}_j = 0.\end{aligned}\quad (6.15)$$

The second formula in Eq. (6.15) corresponds to the case of a rigid molecule.

As the potential energy  $U(\mathbf{R}_j)$  does not depend upon the position of the center of mass  $\mathbf{R}_c$ , and as the vector  $\mathbf{R}_c$  enters only the first term in Eq. (6.13) and does not mix with the vector  $\mathbf{r}_j$ , the motion of the center of mass separates out completely. Below we assume  $\mathbf{R}_c = \dot{\mathbf{R}}_c = 0$  throughout.

Let us introduce inner coordinates  $(Q_1, \dots, Q_{3N-6})$  which characterize the momentary configuration (positions) of the nuclei. We impose the requirement, that for  $Q = 0$  the initial equilibrium configuration is reproduced, and the quadratic form  $\sum_{j=1}^N M_j \dot{\mathbf{r}}_j^2$  transforms into the sum of squares  $\sum_{k=1}^{3N-6} \dot{Q}_k^2$ .

This can be performed always with the help of the linear transformation:

$$\begin{aligned} r_{j\lambda} &= M_j^{-\frac{1}{2}} \sum_{k=1}^{3N-6} \Lambda_{j\lambda,k} Q_k, \\ \dot{r}_{j\lambda} &= M_j^{-\frac{1}{2}} \sum_{k=1}^{3N-6} \Lambda_{j\lambda,k} \dot{Q}_k, \end{aligned} \quad (6.16)$$

where the coefficients  $\Lambda_{j\lambda,k}$  depend upon the vectors  $\left\{ \sqrt{\frac{M_j}{M}} \mathbf{a}_j \right\}$  and upon the quantities  $\left\{ \sqrt{\frac{M_j}{M}} \right\}$ . The factors  $\Lambda_{j\lambda,k}$  can be found, for example, in the following way. From Eckart conditions (6.3) we obtain  $\mathbf{r}_N$  and  $\dot{\mathbf{r}}_{N-1}$ , which are linear functions of  $(\mathbf{r}_1, \dots, \mathbf{r}_{N-2})$ . After that we substitute  $\dot{\mathbf{r}}_1, \dots, \dot{\mathbf{r}}_{N-2}, \dot{\mathbf{r}}_{N-1}(\dot{\mathbf{r}}_1, \dots, \dot{\mathbf{r}}_{N-2}), \dot{\mathbf{r}}_N(\dot{\mathbf{r}}_1, \dots, \dot{\mathbf{r}}_{N-2})$  into the expression of the kinetic energy  $\sum M_j \dot{\mathbf{r}}_j^2$  and transform the obtained bilinear expression  $T_Q(\dot{\mathbf{r}}_1, \dots, \dot{\mathbf{r}}_{N-2})$  to the canonical form. Then with the help of the scale transformation  $Q_i \rightarrow \lambda_i Q_i$  we reduce the expression of the kinetic energy to  $2T_Q = \sum_{k=1}^{3N-6} \dot{Q}_k^2$ . The matrix of the resultant transformation provides the linear relation between  $(\mathbf{r}_1, \dots, \mathbf{r}_{N-2})$  and  $(Q_1, \dots, Q_{3N-6})$ , and produces equations (6.16) in an obvious way, determining the factors  $\Lambda_{j\lambda,k}$ .

Substituting Eq. (6.16) into (6.13) and taking into account the consideration provided during the derivation of coordinates  $Q_i$ , we obtain the following expressions for the kinetic energy of the molecule:

$$2T = \sum_{\lambda, \nu = \bar{x}, \bar{y}, \bar{z}} I'_{\nu\lambda} \omega_\nu \omega_\lambda + 2 \sum_{\nu = \bar{x}, \bar{y}, \bar{z}} \omega_\nu \sum_{k,l=1}^{3N-6} \iota_{kl}^\nu Q_k \dot{Q}_l + \sum_{k=1}^{3N-6} \dot{Q}_k^2, \quad (6.17)$$

where  $\iota_{kl}^\nu$  is determined by the formula:

$$\iota_{kl}^\nu = \sum_j (\Lambda_{j\lambda,k} \Lambda_{j\theta,l} - \Lambda_{j\theta,k} \Lambda_{j\lambda,l}), \nu \neq \theta \neq \lambda, \quad (6.18)$$

The permutation  $(\bar{x}, \bar{y}, \bar{z}) \rightarrow (\nu, \lambda, \theta)$  is even. Obviously,  $\iota_{kl}^\nu$  is antisymmetric in the indices  $(l, k)$ :

It is convenient to represent Eq. (6.17) in the following form:

$$\begin{aligned} 2T &= \sum_{\lambda, \nu = \bar{x}, \bar{y}, \bar{z}} I'_{\nu\lambda} \omega_\nu \omega_\lambda + \sum_{k=1}^{3N-6} \left( Q_k + \sum_{\nu, l} \omega_\nu \iota_{lk}^\nu Q_l \right)^2, \\ I'_{\nu\lambda} &= I_{\nu\lambda} - \sum_{k, l, m=1}^{3N-6} \iota_{k,m}^\nu \iota_{l,m}^\lambda Q_k Q_l. \end{aligned} \quad (6.19)$$

The momenta of the system are determined by the formulas:

$$\begin{aligned} P_k &= \frac{\partial T}{\partial Q_k} = Q_k + \sum_{\nu,l} \omega_\nu \iota_{lk}^\nu Q_l; \\ J_\nu &= \frac{\partial T}{\partial \omega_\nu} = \sum_{\lambda=\bar{x},\bar{y},\bar{z}} I'_{\nu\lambda} \omega_\lambda + \sum_{l,k} \iota_{lk}^\nu Q_l P_k \\ &= \sum_{\lambda=x,y,z} I'_{\nu\lambda} \omega_\lambda + \pi_\nu, \end{aligned} \quad (6.20)$$

where

$$\pi_\nu = \sum_{l,k} \iota_{lk}^\nu Q_l P_k \quad (6.21)$$

is called the vibrational momentum of the molecule. All the vectors in Eqs. (6.19) – (6.21) are calculated with respect to the axis of the body frame. From Eq. (6.20) we find the expression of  $\omega_\nu$ :

$$\omega_\nu = \sum_{\lambda=x,y,z} \mu_{\nu\lambda} (J_\lambda - \pi_\lambda), \quad (6.22)$$

where the matrix  $\mu_{\nu\lambda}$  is inverse to  $I'_{\nu\lambda}$ :

$$\mu_{\nu\lambda} = (I')_{\nu\lambda}^{-1}. \quad (6.23)$$

The matrix  $\mu_{\nu\lambda}$  is function of position  $Q_k$  solely.

Substituting Eqs. (6.22) and (6.20) into Eq. (6.19) we find the part of the Hamilton function ( $H - U$ ), which corresponds to the kinetic energy of the molecule:

$$2T = \sum_{k=1}^{3N-6} P_k^2 + \sum_{\nu\lambda} \mu_{\nu\lambda} (J_\nu - \pi_\nu) (J_\lambda - \pi_\lambda). \quad (6.24)$$

In Eq. (6.24) the momenta  $J_\nu$  should be expressed through the momenta conjugate (corresponding) to Euler angles  $(\alpha, \beta, \gamma)$  with the help of the formula:

$$J_\nu = J_\alpha \frac{\partial \dot{\alpha}}{\partial \omega_\nu} + J_\beta \frac{\partial \dot{\beta}}{\partial \omega_\nu} + J_\gamma \frac{\partial \dot{\gamma}}{\partial \omega_\nu}, \quad (6.25)$$

where the derivatives  $\frac{\partial \dot{\alpha}}{\partial \omega_\nu}$ ,  $\frac{\partial \dot{\beta}}{\partial \omega_\nu}$ , and  $\frac{\partial \dot{\gamma}}{\partial \omega_\nu}$  should be found with the help of Eqs. (6.14). The vibrational momentum in Eq. (6.24) should be expressed according to the definition (6.21). Thus the kinetic energy of the system has been written down through the momenta ( $P_k$ ,  $J_\alpha$ ,  $J_\beta$ ,  $J_\gamma$ ) and through the

coordinates ( $Q$ ,  $\alpha$ ,  $\beta$ ,  $\gamma$ ), that is the Hamilton function of the system has been found <sup>5</sup>:

$$H = \frac{1}{2} \sum_{k=1}^{3N-6} P_k^2 + \frac{1}{2} \sum_{\nu\lambda} \mu_{\nu\lambda} \left( J_\nu - \sum_{l,k} \iota_{lk}^\nu Q_l P_k \right) \left( J_\lambda - \sum_{l,k} \iota_{lk}^\lambda Q_l P_k \right) + U(Q_1 \cdots Q_{3N-6}). \quad (6.26)$$

Now what is left: to write out the elements of the tensor  $g^{ik}, g^{\nu k}, g^{\nu\lambda}$ , to calculate the corresponding factor  $|g| = |g^{ab}|^{-1}$ , and according to the algorithm provided above to determine the quantum Hamiltonian with the momenta  $P_a \rightarrow (-i\hbar \frac{\partial}{\partial a})$ . Such a construction corresponds to the transition from the laboratory frame to non-Decart frame which rotates with the molecule.

## 6.2 Molecular Hamiltonian in the inner basis representation 'coordinates - angles'

Let us find the explicit form of the quantum vibrational-rotational Hamiltonian, corresponding to the Hamilton function (6.26). With the help of the method, described in the preceding Section we will demonstrate that the Hamilton function (6.26) corresponds to the Hamiltonian of the following form:

$$H = \frac{1}{2} \mu^{\frac{1}{2}} \sum_{k=1}^{3N-6} P_k \mu^{-\frac{1}{2}} P_k + \frac{1}{2} \mu^{\frac{1}{2}} \sum_{\nu\lambda} (J_\nu - \pi_\nu) \mu^{-\frac{1}{2}} \mu_{\nu\lambda} (J_\lambda - \pi_\lambda) + U(Q), \quad (6.27)$$

where the operators  $P_k, J_\nu$ , and  $\pi_\nu$  are determined with the help of Eqs. (6.21), (6.25), and the following formulas <sup>6</sup>:

$$\begin{aligned} P_k &= -i\hbar \frac{\partial}{\partial Q_k}, \quad \pi_\nu = \sum_{l,k} \iota_{lk}^\nu Q_l P_k, \text{ and } \iota_{kl}^\nu = -\iota_{lk}^\nu; \\ J_{\bar{x}} &= -\cos \gamma (\cos^{-1} \beta) \left( -i\hbar \frac{\partial}{\partial \alpha} \right) + \sin \gamma \left( -i\hbar \frac{\partial}{\partial \beta} \right) \\ &\quad + \cot \beta \cos \gamma \left( -i\hbar \frac{\partial}{\partial \gamma} \right), \\ J_{\bar{y}} &= \sin \gamma (\cos^{-1} \beta) \left( -i\hbar \frac{\partial}{\partial \alpha} \right) + \cos \gamma \left( -i\hbar \frac{\partial}{\partial \beta} \right) \end{aligned}$$

<sup>5</sup>Strictly, in Eq. (6.26) one should substitute the expression of  $J_\nu$ , expressed through the variables  $J_\alpha, J_\beta, J_\gamma$ , conjugate to  $\alpha, \beta, \gamma$  with the help of Eq. (6.25).

<sup>6</sup>All the repeated indices below imply summation.

$$\begin{aligned}
& -\cot \beta \sin \gamma \left( -i\hbar \frac{\partial}{\partial \gamma} \right), \\
J_{\bar{x}} &= -i\hbar \frac{\partial}{\partial \gamma}, \text{ or} \\
J_{\nu} &= g_{\nu}^a J_a, \text{ where } a = \alpha, \beta, \gamma; \quad \nu = \bar{x}, \bar{y}, \bar{z}. \tag{6.28}
\end{aligned}$$

Taking into account the expression of the elementary volume in non-Decart coordinate set:

$$dv = \sin \beta d\alpha d\beta d\gamma \mu^{-\frac{1}{2}} (Q) dQ, \tag{6.29}$$

one can verify easily, that the momentum operators with respect to the mobile axes  $J_{\bar{x}}, J_{\bar{y}}, J_{\bar{z}}$  are Hermitian. We note here that in this frame the momenta are not Hermitian, but the operator  $H$  in fact is. To prove the validity of Eq. (6.27) let us consider the case of a rigid molecule first. The classical Hamilton function and the corresponding quantum Hamiltonian are:

$$\begin{aligned}
H &= \frac{1}{2} \sum_{\nu\lambda} J_{\nu} \mu_{\nu\lambda}^{(0)} J_{\lambda}, \\
H &= -\frac{\hbar^2}{2} \sum_{\nu\lambda} \mu_{\nu\lambda}^{(0)} g^{-\frac{1}{2}} \sum_{a,b} \frac{\partial}{\partial a} g_{\nu}^a g^{\frac{1}{2}} g_{\lambda}^b \frac{\partial}{\partial b}. \tag{6.30}
\end{aligned}$$

Here  $(a, b)$  enumerate the Euler angles  $(\alpha, \beta, \gamma)$ ,  $(\nu, \lambda)$  correspond to the axes of the mobile frame,  $(\bar{x}, \bar{y}, \bar{z})$  is the  $g_{\lambda}^a$  - matrix of the linear transformation of momenta (6.28), and  $g$  is the determinant of the following matrix:

$$\begin{aligned}
g^{-1} &= \left| \sum_{\nu\lambda} g_{\nu}^a \mu_{\nu\lambda}^{(0)} g_{\lambda}^b \right| = |g_{\nu}^a| \cdot |\mu_{\nu\lambda}^{(0)}| \cdot |g_{\lambda}^b| \\
&= |\mu_{\nu\lambda}^{(0)}| \cdot |g_{\lambda}^{a2}| = \frac{|\mu_{\nu\lambda}^{(0)}|}{\sin^2 \beta} = \frac{\mu(0)}{\sin^2 \beta}, \tag{6.31}
\end{aligned}$$

where  $\mu(0) = |\mu_{\lambda\nu}^{(0)}|$  is the determinant of the matrix  $\mu_{\lambda\nu}^{(0)}$ . It has been taken into account here, that the determinant of the linear transformation has the form  $|g_{\nu}^a| = -\sin^{-1} \beta$ , which can be verified easily with the help of the explicit expressions of  $g_{\nu}^a$  in Eq. (6.28). It can be proved also, that

$$\frac{1}{\sin \beta} \sum_a \frac{\partial}{\partial a} (g_{\nu}^a \sin \beta) = \sum_a g_{\nu}^a \frac{\partial}{\partial a}. \tag{6.32}$$

Really, for example with  $\nu = x$  one finds using Eq. (6.28):

$$\begin{aligned}
& \frac{1}{\sin \beta} \left\{ \frac{\partial}{\partial \alpha} (-\cos \gamma \cos^{-1} \beta) + \frac{\partial}{\partial \beta} \sin \gamma + \frac{\partial}{\partial \gamma} \cot \beta \cos \gamma \right\} \sin \beta \\
= & -\cos \gamma \cos^{-1} \beta \frac{\partial}{\partial \alpha} + \sin \gamma \frac{\partial}{\partial \beta} + \sin \gamma \cot \beta - \cot \beta \sin \gamma + \cot \beta \cos \gamma \frac{\partial}{\partial \gamma} \\
= & \sum_a g_x^a \frac{\partial}{\partial a}.
\end{aligned} \tag{6.33}$$

Substituting Eq. (6.31) into (6.30) and taking into account Eq. (6.32) we obtain the following Hamiltonian of a rigid molecule (top):

$$\begin{aligned}
H = & -\frac{\hbar^2}{2} \frac{\sqrt{\mu(0)}}{\sin \beta} \sum_{a,b} \frac{\partial}{\partial a} \frac{\sum_{\nu \lambda} g_{\nu}^a \mu_{\nu \lambda}^{(0)} g_{\lambda}^b}{\sqrt{\mu(0)}} \sin \beta \frac{\partial}{\partial b} \\
= & \frac{1}{2} \sum_{\nu \lambda} J_{\nu} \mu_{\nu \lambda}^{(0)} J_{\lambda} = \frac{1}{2} \sum_{\nu \lambda} (I^{(0)})_{\nu \lambda}^{-1} J_{\nu} J_{\lambda}.
\end{aligned} \tag{6.34}$$

The Hamiltonian (6.34) describes the motion of a top, the orientation of which is characterized by Euler angles  $(\alpha, \beta, \gamma)$ . If the principal axes have been chosen for the body frame, then  $(I^{(0)})_{\nu \lambda}^{-1} = \delta_{\nu, \lambda} I_{\nu}^{-1}$ , and the Hamiltonian  $H$  takes the form:

$$H = \frac{1}{2} \left( \frac{J_x^2}{I_x} + \frac{J_y^2}{I_y} + \frac{J_z^2}{I_z} \right), \tag{6.35}$$

where  $I_{\nu}$  are the inertia momenta with respect to the axis  $(\bar{x}, \bar{y}, \bar{z})$ .

Comparing Eqs. (6.30) and (6.34) we find that the Hamiltonian is obtained from the Hamilton function by the following manipulations: the latter is multiplied by the factor  $\sqrt{\mu(0)}$ , the substitution  $\mu_{\nu \lambda}^{(0)} \rightarrow \frac{\mu_{\nu \lambda}^{(0)}}{\sqrt{\mu^0}}$  is performed, and this factor is placed between the operators of momenta. The expression (6.27) demonstrates, that this recipe is valid in the general case as well, when  $\mu_{\nu \lambda}$  depends upon  $Q$ , and the vibration momenta  $\pi_{\nu}$  is function of the operators  $P_k, Q_k$ . This fact gives the idea, that the determinant  $g^{-1}$  does not depend upon the coordinates operators  $Q_k$ , which enter the expression (6.21) of the vibration momentum. Next we demonstrate the validity of this statement.

We have to find the derivatives  $\frac{\partial g}{\partial Q_k}$ , assuming that  $\mu_{\nu \lambda}(Q)$  does not depend on  $Q$  explicitly, that is we will differentiate upon only those  $Q_i$ , which enter the operator of vibrational momentum  $\pi_{\nu}$ . In the calculation we will use the formula for the derivative of the determinant of a symmetric matrix  $g_{uv}$ :

$$\frac{\partial}{\partial Q_i} |g_{uv}| = \frac{\partial}{\partial Q_i} g = -g \sum_{uv} \frac{\partial g^{uv}}{\partial Q_i} \cdot g_{uv}. \quad (6.36)$$

Here  $\|g^{uv}\|$  is the matrix inverse to  $\|g_{uv}\|$ , symmetric as well. The indices  $(u, v)$  take the values  $i = 1, \dots, 3N - 6$ ,  $a = \alpha, \beta, \gamma$ . The elements  $g^{uv}$  are the components of a covariant tensor, which relates the generalized momenta in the Hamilton function (6.26), while  $g_{uv}$  are the components of the contravariant tensor, relating the velocities  $\dot{Q}_i, \dot{\alpha}, \dot{\beta}, \dot{\gamma}$  in the kinetic energy in Eq. (6.19), where  $I'_{\nu\lambda}$  is considered independent of  $Q_i$ .

Let us introduce the matrix  $g_a^\nu$ , inverse to the matrices  $g_\lambda^b$  (6.28), which enables us to represent the momenta  $J_a$  through  $J_\nu$ :

$$J_a = g_a^\nu J_\nu, \quad g_a^\nu g_\lambda^a = \delta_\lambda^\nu, \quad g_a^\nu g_\nu^b = \delta_a^b. \quad (6.37)$$

Comparing Eqs. (6.25), (6.28), and (6.18) – (6.15) the relations between the angular velocities  $(\omega_x, \omega_y, \omega_z)$  and  $(\dot{\alpha}, \dot{\beta}, \dot{\gamma})$  can be presented in the following form:

$$\dot{a} = g_\lambda^a \cdot \omega_\lambda, \quad \omega_\lambda = g_\lambda^a \cdot \dot{a}. \quad (6.38)$$

Now everything is ready for the calculation of the derivative (6.36). From Eq. (6.26) the following expressions of the derivatives emerge:

$$\begin{aligned} \frac{\partial g^{ik}}{\partial Q^m} &= \sum_{v,\lambda} \mu_{\nu\lambda} \sum_l \left( \iota_{mi}^\nu \iota_{lk}^\lambda + \iota_{li}^\nu \iota_{mk}^\lambda \right) Q^l, \\ \frac{\partial g^{ab}}{\partial Q^m} &= 0, \\ \frac{\partial g^{ia}}{\partial Q^m} &= - \sum_{v,\lambda} \mu_{\nu\lambda} g_\lambda^a \iota_{mi}^\nu. \end{aligned} \quad (6.39)$$

The expression of the kinetic energy (6.19) provides the formulas for the components of the contravariant tensor  $g_{ik}$  and  $g_{ia}$ :

$$g_{ik} = \delta_{ik}, \quad g_{ia} = \sum_v g_a^\nu \sum_l \iota_{li}^\nu Q^l. \quad (6.40)$$

In the derivation of Eqs. (6.39) and (6.40) the formulas (6.28) and (6.38) which express the variables  $(J_{\bar{x}}, J_{\bar{y}}, J_{\bar{z}})$  through  $(J_\alpha, J_\beta, J_\gamma)$  and  $(\omega_{\bar{x}}, \omega_{\bar{y}}, \omega_{\bar{z}})$  through  $(\dot{\alpha}, \dot{\beta}, \dot{\gamma})$  respectively have been used.

Substituting Eqs. (6.39) and (6.40) into (6.36), and taking into account the relations (6.37) between  $g_a^\nu$  and  $g_\nu^a$ , we find the required derivatives:

$$\begin{aligned}
g^{-1} \frac{\partial g}{\partial Q^m} = & - \sum_{v,\lambda} \mu_{v\lambda} \sum_{l,i,k} \left( \iota_{mi}^\nu \iota_{lk}^\lambda + \iota_{li}^\nu \iota_{mk}^\lambda \right) Q^l \delta_{ik} \\
& + 2 \sum_{i,a,\nu,\lambda} (g_\lambda^a \mu_{v\lambda} \iota_{mi}^\nu) \sum_\theta g_a^\theta \sum_l \iota_{li}^\theta Q^l = -2 \sum_{v,\lambda} \mu_{v\lambda} \sum_{i,l} \iota_{mi}^\nu \iota_{li}^\lambda Q^l \\
& + 2 \sum_{v,\lambda} \mu_{v\lambda} \sum_{i,l} \iota_{mi}^\nu \iota_{li}^\theta Q^l \underbrace{\left( \sum_a g_a^\theta g_\lambda^a \right)}_{\delta_\lambda^\theta} = 0, \text{ that is} \\
& \frac{\partial g}{\partial Q^m} = 0, \text{ if } \mu_{v\lambda} = \text{const.} \tag{6.41}
\end{aligned}$$

From the fact that the derivatives  $\frac{\partial g}{\partial Q^m}$  equal zero it follows that the determinant of the metric tensor  $g = |g_{uv}|$  does not depend upon the values of the coordinates  $Q_i$  which enter the expression of the vibration momentum  $\pi_\nu$  (6.21). Then for the calculation of  $g^{-1}$  we can put  $\pi_\nu = 0$ , that is  $Q_i = 0$  in the expression of  $\pi_\nu$ . Then the calculation of  $g^{-1}$  can be performed in full analogy with the one for the rigid molecule (top) with the only difference, that now  $\mu_{\lambda\nu}(Q)$  depends upon  $Q$ . In other words, we can utilize Eq. (6.31) in the calculation of  $g^{-1}$ , which leads to the following result:

$$g^{-1} = \frac{\mu(Q)}{\sin^2 \beta}. \tag{6.42}$$

Together with the identity (6.32) the latter provides for the Hamilton function (6.26) the quantum Hamiltonian (6.27). To make the Hamiltonian Hermitian with respect to the usual scalar product

$$\langle \psi | \varphi \rangle = \int \psi \varphi dQ \sin \beta d\alpha d\beta d\gamma,$$

it is transformed according to  $H \rightarrow \mu^{-\frac{1}{4}} H \mu^{\frac{1}{4}}$ . As a result the Hamiltonian (6.27) takes the form which is typically used as a starting point in the calculations of the vibrational-rotational spectra of molecules:

$$\begin{aligned}
H = & \frac{1}{2} \mu^{\frac{1}{4}} \sum_{k=1}^{3N-6} P_k \mu^{-\frac{1}{2}} P_k \mu^{\frac{1}{4}} \\
& + \frac{1}{2} \mu^{\frac{1}{4}} \sum_{\nu,\lambda=\{\bar{x},\bar{y},\bar{z}\}} \left( J_\nu - \sum_{l,k=1}^{3N-6} \iota_{lk}^\nu Q_l P_k \right) \mu^{-\frac{1}{2}} \mu_{v\lambda}(Q) \\
& \times \left( J_\lambda - \sum_{l,k=1}^{3N-6} \iota_{lk}^\lambda Q_l P_k \right) \mu^{\frac{1}{4}} + U(Q). \tag{6.43}
\end{aligned}$$

The operators of angular momentum are defined by Eqs. (6.28). Obviously, they act only upon the angular variables of the wavefunction and commute with all the operator functions of  $Q_i$ . Such a form of  $H$  has been provided in the monograph [96]. Then the operators  $P_k = -i\hbar \frac{\partial}{\partial Q_k}$  become Hermitian as well.

The Hamiltonian (6.43) provides a good approximation for the description of vibrational-rotational spectra in the case, when the energy of electronic transitions from the given electronic term exceed greatly the energy of vibrational-rotational transitions, that is when the adiabatic approximation of Born-Oppenheimer is valid. For a wide class of molecules in the ground electronic state the adiabatic approximation holds. This fact is also backed up by the validity of IR spectra description on the basis of calculations with Hamiltonian (6.43). With the increasing accuracy of such calculations more subtle features of molecular IR spectra can be described.

However, the Hamiltonian (6.43) is still too complicated for calculations. To overcome the difficulties we will separate out the principal terms and estimate the magnitude of the rest. We remind here, that the coordinates  $Q_i$  characterize the deviations of nuclei positions from the equilibrium configuration, so that for a semi-rigid molecule they are small compared to the inter-nuclei distances  $a \sim 1 \text{ \AA}$ . Let us denote by  $d$  the amplitude of nuclei vibrations. Then the terms entering the Hamiltonian (6.43) are of the following order of magnitude:

$$\begin{aligned} E_e &\sim \frac{\hbar^2}{ma^2}, \quad \frac{E_e}{\hbar c} \sim 10^4 \div 10^5 \text{ sm}^{-1}, \\ E_v &\sim \frac{\hbar^2}{Md^2}, \quad E_v \sim U''(0) Q^2 \sim \frac{E_e}{a^2} d^2 \sim \frac{\hbar^2 d^2}{ma^4}, \text{ that is} \\ &\frac{\hbar^2}{Md^2} \sim \frac{\hbar^2 d^2}{ma^4} \text{ and } \left(\frac{d}{a}\right)^4 \sim \frac{m}{M} = k^4 \sim 10^{-4}, \text{ that is} \\ E_v &\sim E_e \frac{m}{M} \left(\frac{a}{d}\right)^2 \sim E_e k^2, \quad P_k^2 \sim E_e k^2, \text{ and} \\ U(Q) - U(0) &\sim U''(Q) Q^2 \sim E_v \sim E_e k^2 \sim 1000 \text{ cm}^{-1}. \end{aligned} \quad (6.44)$$

If we introduce dimensionless variables  $q_i = a^{-1} \left(\frac{m}{M}\right)^{-\frac{1}{4}} Q_i$ , where  $\overline{M}$  is some average nuclei mass and  $a$  is some average inter-nuclei distance, then in the unit set  $\hbar = 1, m = 1, a = 1$  the molecular Hamiltonian (6.43) can be presented in the form:

$$H = F(kp, kq, k^2 J_\nu), \quad (6.45)$$

where  $k = \left(\frac{m}{M}\right)^{\frac{1}{4}}$ . Eq. (6.45) follows from Eq. (6.43) with the account of Eq. (6.44) and with the use of the expressions for the inertia tensor  $I'_{\nu\lambda}$  and the inverse to it  $\mu_{\nu\lambda}$ :

$$\begin{aligned} I'_{\nu\lambda}(r) &= I_{\nu\lambda}^{(0)\prime} \left[ 1 + c_1 \frac{r}{a} + c_2 \left( \frac{r}{a} \right)^2 + \dots \right] \sim \overline{M} a^2, \\ \mu_{\nu\lambda} &= \mu_{\nu\lambda}^{(0)} \left[ 1 + \tilde{c}_1 \frac{r}{a} + \tilde{c}_2 \left( \frac{r}{a} \right)^2 + \dots \right] \sim \frac{1}{\overline{M} a^2}, \end{aligned} \quad (6.46)$$

where  $\frac{r_i}{a} = k\sqrt{\frac{\overline{M}}{M_i}}q \sim k$ . The Hamiltonian (6.43) can be separated into three parts: The first one does not contain the momentum operators  $J_\nu$  and constitutes a purely vibrational Hamiltonian  $H_{vib}(kp_i, kq_i)$ . The quadratic part of the vibration Hamiltonian determines the normal modes, the energy of which according to Eq. (6.45) is of the order of magnitude  $\sim k^2 v$ , where  $v$  is the overtone number (we note, that the energy in Eq. (6.45) is measured in the units  $E_{el} = \frac{\hbar}{ma^2}$ ). The second part of the Hamiltonian (6.43) is composed of terms, linear in the momentum operator  $J_\nu$ . This part is called Coriolis interaction. Its principal term is  $\sim k^4 J$ , Eq. (6.45). And, last, the third part of the Hamiltonian (6.43) consists of terms quadratic in  $J_\nu$ , which determine the rotation energy of the molecule and the corrections due to centrifugal energy. The rotation energy has the order of magnitude  $\sim k^4 J^2$ , as it can be seen from Eq. (6.45). Thus the Hamiltonian of the molecule (6.43) can be represented in the following form <sup>7</sup>:

$$\begin{aligned} H &= H_{vib} + H_{rot} + H_{cor}, \\ H_{vib} &= H_{20} + H_{30} + \dots + H_{m0} + \dots, \\ H_{rot} &= H_{02} + H_{12} + \dots + H_{m2} + \dots, \\ H_{cor} &= H_{21} + H_{31} + \dots + H_{m1} + \dots, \end{aligned} \quad (6.47)$$

where the indices in the symbol  $H_{m,n}$  signify that the operator  $H_{m,n}$  is composed of a sum of products of  $m$  vibration operators ( $p, q$ ) and  $n$  rotation operators  $J_\nu$ . According to Eq. (6.45) the operator  $H_{m,n}$  is of the following order of magnitude:

$$H_{mn} \sim \left( k^{m+2n} v^{\frac{m}{2}} J^n \right) \frac{\hbar^2}{ma^2} \sim k^{m+2n-2} v^{\frac{m}{2}} J^n \cdot E_{vib}. \quad (6.48)$$

With the help of Eq. (6.48) the magnitude of different terms in the Hamiltonian (6.47) can be estimated. Depending on the conditions of the physical experiment the principal terms can be separated out, while the small corrections can be accounted for by perturbation theory. For example, if we study the spectrum of high rotational states of the molecule in the ground electronic state at room temperature ( $T \sim 200 \text{ cm}^{-1}$ ), then,

---

<sup>7</sup>It can be shown, that the vibrational part of the Hamiltonian (which does not contain the operators  $J$ ) has no terms linear in  $P$ , that is the terms  $H_{10}$ , Eq. (6.43) and (6.47) are absent [97].

assuming  $J \sim k^{\varepsilon-2}$ , we find that the principal term will be the following:  $H_{02} \sim k^{2\varepsilon}$ , ( $\varepsilon \rightarrow 0$ ). The next term in  $k$  will be the operator  $H_{12} \sim k^{1+2\varepsilon}$ , and the following —  $H_{20} \sim k^2$ . In this case the operator  $H_{02} + H_{20}$  can be adopted as the zero Hamiltonian for the study of the rotation spectrum. For the rotational levels it provides the asymmetrical top spectrum with the molecule in the ground vibrational state, as  $T \ll \omega_v \sim 1000 \text{ cm}^{-1}$ . The principal correction terms to the rotation spectrum come from the perturbation  $H_{12}$  and have the order  $\sim k^{4\varepsilon}$ , with the corresponding contribution appearing only in the second order. In the study of vibrational spectra of molecules in the IR region  $\sim 1000 \text{ cm}^{-1}$  at room temperature the rotation quantum numbers  $J$  are of order  $\sim 1 \div 10$ , so that the principal terms in Eq. (6.47) are  $H_{20} \sim k^2$ ,  $H_{30} \sim k^3$ ,  $H_{40} \sim k^4$ , ..., while the interactions  $H_{12}$  and  $H_{21}$  are small perturbations. The operators  $H_{12}$  and  $H_{21}$  contribute only in the second order with contributions  $\sim k^6$  and  $\sim k^8$  respectively. Thus in this case we obtain merely the vibrational spectrum of an anharmonic oscillator.

Due to the progress of experimental technique which made possible the resolution of lines in the IR spectrum with the accuracy up to  $\sim 10^{-2} \div 10^{-4} \text{ cm}^{-1}$ , there emerged the possibility to study the subtle details of the potential surface of inter-nuclei interaction on the basis of spectroscopic information. However, for such an approach high accuracy calculations of the vibration-rotation spectra are required to derive the information on the potential surface  $U(q)$  from comparison with experimental spectra. Such a calculation requires the account of a large number of terms in Eq. (6.47) and heavy use of computers. Because of that the maximal possible automatization of spectrum calculations by perturbation theory approaches is needed. The method of contact transformations developed for the application to vibrational-rotational Hamiltonian (6.43) in the form of series (6.47) is used. The principal idea of the method will be described in the next Section. The detailed consideration and the list of corresponding formulas, as well as the references to original work can be found in [96, 98, 99].

### 6.3 Contact transformation

The basic idea of the method lies in the unitary transformation of the initial Hamiltonian (6.43):

$$H' = e^{iS} H e^{-iS} = \dots e^{iS_2} e^{iS_1} H e^{-iS_1} e^{-iS_2} \dots \quad (6.49)$$

This transformation is chosen in such a way, that the newly produced operator  $H'$ , called effective Hamiltonian, is more convenient for the calculation of the spectrum, which does not change upon unitary transformations. In the present case the Hamiltonian (6.43) in the form of Eq. (6.47) has

the shape of a sum of terms of various orders in  $k = \left(\frac{m}{M}\right)^{\frac{1}{4}}$ . Depending on the physical situation these terms can be grouped in such a way, that each group will bear a small parameter  $\lambda^n$  with some factor  $H_n$ , so that the whole initial Hamiltonian takes the form:

$$H = H_0 + \lambda H_1 + \lambda^2 H_2 + \dots \quad (6.50)$$

Let us consider the sequence of contact transformations  $\exp(i\lambda S_1)$ ,  $\exp(i\lambda^2 S_2)$ , etc., that produce the Hamiltonians:

$$\begin{aligned} H^{(1)} &= e^{i\lambda S_1} H e^{-i\lambda S_1} = H_0 + \lambda \{H_1 + i[S_1, H_0]\} \\ &+ \lambda^2 \left\{ H_2 + i[S_1, H_1] - \frac{1}{2} [S_1, [S_1, H_0]] \right\} + \dots, \end{aligned} \quad (6.51)$$

$$\begin{aligned} H^{(2)} &= e^{i\lambda^2 S_2} H^{(1)} e^{-i\lambda^2 S_2} = H_0 + \lambda \{H_1 + i[S_1, H_0]\} \\ &+ \lambda^2 \left\{ H_2 + i[S_1, H_1] - \frac{1}{2} [S_1, [S_1, H_0]] + i[S_2, H_0] \right\} \\ &+ \lambda^3 H_3 + \lambda^3 \left\{ i[S_1, H_2] - \frac{1}{2} [S_1, [S_1, H_1]] \right. \\ &\quad \left. - \frac{i}{6} [S_1, [S_1, [S_1, H_0]]] + i[S_2, H_1] \right\} + \dots, \end{aligned} \quad (6.52)$$

In the end the sequence of such transformations produces the required effective Hamiltonian. Obviously, the operators accompanying  $\lambda$  in  $H^{(1)}$  and  $\lambda^2$  in  $H_2^{(2)}$  do not change during the subsequent transformations. Thus we can write:

$$H' = H'_0 + \lambda H'_1 + \lambda^2 H'_2 + \dots, \quad (6.53)$$

where

$$\begin{aligned} H'_0 &= H_0, \\ H'_1 &= H_1 + i[S_1, H_0], \\ H'_2 &= H_2 + i[S_1, H_1] - \frac{1}{2} [S_1, [S_1, H_0]] + i[S_2, H_0], \\ &\dots, \end{aligned} \quad (6.54)$$

and so on. Let us assume, that the spectrum of the operator  $H_0$  is nondegenerate and the interlevel spacing is big enough. We will choose the Hermitian operators  $S_1, S_2, \dots$  in such a way, that  $H'_1 H'_2, \dots$  be diagonal in the basis of eigenfunctions of the operator  $H_0$ . As the operators  $H'_1, H'_2, \dots$ , etc. depend

on the momentum operators  $J_\nu$ , while  $H_0$  does not depend upon them, the diagonal shape of  $H'_n$  means that they are in fact block-diagonal: in place of the element  $H_{vv}$  there is some operator – function of momentum operator  $J_\lambda$ , and its functional dependence upon  $J_\lambda$  is determined by the number of the vibrational level  $v$ . Then the block-diagonal operator  $H'_1$  and  $S_1$  from Eq. (6.54) can be obtained from the following equations:

$$\begin{aligned} \langle v | H'_1 | v \rangle &= \langle v | H_1 | v \rangle, \\ 0 = \langle a | H'_1 | b \rangle|_{a \neq b} &= \langle a | H_1 | b \rangle - i(E_a - E_b) \langle a | S_1 | b \rangle. \end{aligned} \quad (6.55)$$

Correspondingly  $H'_2$  is determined by:

$$\begin{aligned} \langle v | H'_2 | v \rangle &= \langle v | H_2 | v \rangle + i \langle v | [S_1, H_1] | v \rangle - \\ &\quad \frac{1}{2} \langle v | [S_1, [S_1, H_0]] | v \rangle, \\ \langle a | H'_2 | b \rangle|_{a \neq b} &= \langle a | H_2 | b \rangle + i \langle a | [S_1, H_1] | b \rangle - \\ &\quad \frac{1}{2} \langle a | [S_1, [S_1, H_0]] | b \rangle + i \langle a | [S_2, H_0] | b \rangle = 0. \end{aligned} \quad (6.56)$$

The quantities  $\langle a | H | b \rangle$ ,  $\langle v | H | v \rangle$  in Eqs. (6.55) and (6.56) are operators, which depend upon the momenta  $J_\lambda$ . The equation (6.55) provides some freedom in the determination of the diagonal part of operator  $S'_1$ . The same is true for operators  $S_2, S_3$ , etc. This arbitrariness can be used to get rid of some terms in the operators  $H_v$ .

The equation for  $S_n$  has a solution always, if  $E_a - E_b \neq 0$  and  $\langle a | H_2 | b \rangle \ll E_a - E_b$ . If there is approximate degeneracy  $E_a \sim E_b$ , then the matrix element  $\langle a | S_n | b \rangle$  becomes large  $\sim \langle a | H_n | b \rangle (E_a - E_b)^{-2}$ . The corresponding transformation  $\exp(iS_n\lambda^n)$  differs considerably from unit, and the correction to the energy  $E^{(n+1)}$  will be much bigger than the quantity  $\lambda^{n+1}$ . It means, that the perturbation theory is not valid in this case. To overcome the problem, we put the matrix element  $\langle a | S_n | b \rangle$  equal to zero, while the corresponding operator  $H'_n$  acquires matrix elements between nearly degenerate states  $\langle a | H'_n | b \rangle \neq 0$ . Thus, if there are nearly degenerate levels in the spectrum of the operator  $H_0$ , then the block-diagonal terms of some  $H'_n$  will have nonzero matrix elements between these degenerate states.

Applying such a unitary transformation (6.49) to the Hamiltonian (6.43), we obtain the following form of the effective Hamiltonian  $H'$  in place of Eq. (6.47):

$$H' = \left( H'_{20} + \sum_{m=3}^{\infty} \hat{H}'_{m0} \right) + \sum_{n=2}^{\infty} H'_{0n} + \sum_{m=1, n=1}^{\infty} H'_{mn}. \quad (6.57)$$

The first sum in Eq. (6.57) describes the molecule vibrations, the second one – the rotations, the third sum characterizes the interaction of vibrations and rotations. The terms  $H'_{mn}$  in the sum (6.57) are of the same order of magnitude, as the operators  $H_{mn}$  in Eq. (6.47), as it can be easily seen from Eqs. (6.55) and (6.56):

$$H'_{mn} \sim k^{m+2n} E_e \sim k^{m+2n-2} E_{vib}. \quad (6.58)$$

We note, that in Eq. (6.57) there are operators  $H'_{0n}$  with  $n > 2$ , whereas in Eq. (6.47) operators  $H_{0n}$  with  $n > 2$  are lacking. On the contrary, for nondegenerate frequencies of the operator  $H_{20}$  the operators  $H'_{12}$  and  $H'_{21}$  are equal to zero according to Eq. (6.55). This is due to the fact, that in the harmonic approximation (see Eq. (6.43)) the averages  $\langle v | q | v \rangle$  and  $\langle v | p_\mu q_\nu | v \rangle$  for  $\mu \neq \nu$  equal zero. At the same time in Eq. (6.47) the terms  $H_{12}$  and  $H_{21}$  are present. The expressions of some operators  $H'_{mn}$  through the parameters of the initial Hamiltonian (6.43) and their application to particular types of molecules can be found in [96, 97, 98, 99]. Let us demonstrate the way how the term  $H_{12} \sim qJ^2$  in Eq. (6.47) after a contact transformation with  $\exp[iS_{12}]$ , where  $S_{12} \sim pJ^2$  gives birth to a term  $H'_{04} \sim J^4$  in Eq. (6.57). Really, according to Eq. (6.56) the second order in  $S_{12}$  gives:

$$\begin{aligned} \langle v | H'_2 | v \rangle &\sim \frac{1}{2} \langle v | [S_{12}, [S_{12}, H_0]] | v \rangle + i \langle v | [S_{12}, H_{12}] | v \rangle \\ &\sim \frac{1}{2} \left\langle v \left| \left[ pJ^2, \left[ pJ^2, \frac{p^2 + q^2}{2} \right] \right] \right| v \right\rangle + i \langle v | [pJ^2, qJ^2] | v \rangle \\ &\sim \frac{1}{2} J^4 \sim H'_{04}. \end{aligned} \quad (6.59)$$

The calculation of  $H'_{04}$  according to the formula (6.56) with the perturbation  $H_{12}$  leads to the following expression of  $H'_{04}$  [98]:

$$H'_{04} = \sum_{\nu, \lambda} T_{\nu \lambda} J_\nu^2 J_\lambda^2, \quad (6.60)$$

where the factors  $T_{\nu \lambda}$  are expressed through the parameters of the initial Hamiltonian. The freedom in the choice of the form of operator  $S_{12}$  is used to eliminate all the terms like  $J_\nu^2 J_\lambda J_\gamma$ ,  $J_\gamma J_\lambda J_\nu^2$ , etc. Of importance for the subsequent consideration is the fact that  $T_{\nu \lambda} \sim k^8$ , so that with  $J \sim k^{-2+\epsilon}$  these terms provide corrections to the rotational levels  $\Delta E_J \sim k^{4\epsilon} E_{el}$ , whereas  $E_J \sim k^{2\epsilon} E_{el}$  ( $\epsilon \rightarrow 0$ ). As it has been noted earlier, the operator (6.60) provides the main contribution to the energy of rotational levels of the Hamiltonian  $H'_{02} + H'_{04}$  at high values of the quantum number  $J$ .

The form of the effective Hamiltonian (6.57) and the estimates of its terms (6.58), along with the formulas of contact transformations (6.51) – (6.56) suggest the following conclusions. In the study of the spectrum of high vibrational levels with lifted degeneracy of frequencies the main contribution to the energy of vibrational-rotational levels is provided by the terms of the vibrational Hamiltonian  $H'_{n0}$ , with the superimposed structure

of the rotation Hamiltonian  $H'_{02} + H'_{04} + \dots$ <sup>8</sup>. The interaction between them is described by the terms  $H'_{22} \sim k^6 E_{el}$ ,  $(H'_{21})^2 \sim k^8 E_{el}$ ,  $(\langle H'_{21} \rangle = 0)$ , as  $\langle v | p_\mu q_\nu | v \rangle = 0$  for  $\mu \neq \nu$  due to the nondegeneracy of vibrational levels)<sup>9</sup>. These estimates lead to the conclusion, that in the study of nonlinearity effects in vibrations at high excitation level the vibration-rotation interaction can be neglected. In particular, the clusterization of vibrational levels due to the anharmonicity of vibrations is preserved. Due to this fact the model of valent forces provides a good approximation for stretching vibrations of valent bonds.

On the other hand, in the studies of nonlinearity effects in the rotation spectrum  $E_{rot} = BJ(J+1)$ , which will be considered in the next Section, the vibration-rotation interaction can be neglected also. Really, in this case  $J \sim k^{-2+\epsilon}$ ,  $H'_{02} \sim k^{2\epsilon}$ ,  $H'_{04} \sim k^{4\epsilon}$ , while the interaction satisfies  $H'_{22} \sim k^{2\epsilon+2}$ ,  $(H'_{21})^2 \sim k^{\epsilon+4} \ll k^{4\epsilon}$ , and can be neglected in fact. Thus, in the studies of high rotational levels one can limit oneself to the consideration of the effective Hamiltonian  $H'_{rot} = H'_{02} + H'_{04}$ . So, the conclusion can be drawn, that the clusterization of highly excited vibrational-rotational levels is influenced by the interaction between vibrations and rotations weakly.

The case of degeneracy of normal mode frequencies, however, provides an exception. In the Coriolis interaction  $H'_{21}$  the non-diagonal terms which connect the degenerate vibrational levels  $|v_i, v_k\rangle$  and  $|(v_i - 1), (v_k + 1)\rangle$  should be kept. These terms provide corrections to the spectrum  $\Delta E \sim k^4 J E_{el} \sim Jk^2 \omega_{vib}$  of the same order of magnitude, as rotation frequencies  $\sim k^4 J E_{el} \sim Jk^2 \omega_{vib}$ . Due to this reason in the vibrational-rotational spectrum the terms  $\mu_{v\lambda} J_v J_\lambda \sim J^2 k^2 \omega_{vib}$  and the Coriolis interaction  $H'_{21}$  should be taken into account simultaneously.

We are interested in the study of nonlinearity effects in molecule vibrations. Most transparently these effects are revealed in the vibrations of light nuclei, as the anharmonicity  $\frac{x_e}{\omega_{vib}} \sim k^2 \sim \sqrt{\frac{m}{M}}$  is proportional to  $M^{-\frac{1}{2}}$  (for hydrogen nuclei  $k_H^2 \sim 0.022$ , for  $C^{12} \sim \frac{x_e}{\omega_{vib}} \sim 0.006$ ). Consequently, the stretching vibrations of bonds like  $CH$ ,  $OH$ , etc. in big organic molecules of the type  $C_6H_6$ ,  $CH_4$ ,  $C_2H_6$ ,  $C_2H_5OH$ , etc. are essentially nonlinear, whereas other modes might be accounted for by the theory of normal vibrations with anharmonicity as a small perturbation. If the molecule is big enough, the inertia tensor depends primarily on the position of the heavier nuclei,  $C^{12}$ ,  $O^{16}$ , etc. Then the operators  $J_\nu$  and  $q^2$  will enter the molecule Hamiltonian (6.45) with the small parameter  $k^2 \sim 0.006$  or  $\sim \frac{M_H}{M_C} k_H^2 \sim 0.0023$ . The latter means, that the influence of the Coriolis and centrifugal interactions upon the spectrum of highly anharmonic vibrations

<sup>8</sup>Due to the symmetry  $H(\mathbf{J}) = H(-\mathbf{J})$  the following equation holds:  $H'_{03} = H'_{05} = \dots = 0$

<sup>9</sup>In the case of degenerate vibrational frequencies the operator  $H'_{21}$  provides correction terms of the order of  $k^4 E_{el}$  – first order in  $H_{21}$ .

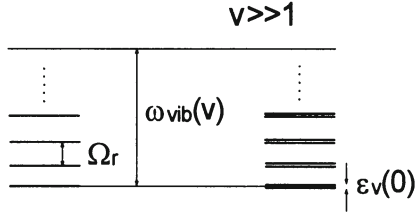


Figure 6.1: The vibrational-rotational spectrum of the  $v$  - overtone in the case of strong excitation of one  $CH$  bond.  $\epsilon_v(n)$  is the splitting of vibrations of different symmetry, see Eq. 5.6 and 5.24.

of  $CH$  and  $OH$  bonds will be an order of magnitude weaker, than the one coming from the nonlinearity of the inter-nuclei potential  $U(Q)$ .

To sum up, we can present the following scheme for the calculation of vibrational-rotational spectrum of highly excited strongly anharmonic stretching vibrations of  $XH$  bonds.

1. Rotation numbers are of order 1. Then:

$$H = H_0 + H_{int}, \quad (6.61)$$

$$H_0 = H_{vib} + H_r, \quad (6.62)$$

$$\begin{aligned} H_{vib} &= \sum_{k=1}^{3N-6} \mu^{\frac{1}{4}} P_k \mu^{-\frac{1}{2}} P_k \mu^{\frac{1}{4}} + \sum_{m=2}^{\infty} U_{m0}(Q), \\ \sum_{m=2}^{\infty} U_{m0}(Q) &= \sum_{a,b} U_{a,b}(\mathbf{R}_{a,b}(Q)) \\ &+ \sum_{(a,b),(a,c)}^{\infty} U_{ab,ac} \{ \Theta(\mathbf{R}_{a,b}(Q), \mathbf{R}_{a,c}(Q)) \} \\ &+ W(\mathbf{R}_1(Q), \dots, \mathbf{R}_N(Q)), \end{aligned} \quad (6.63)$$

where  $R_{a,b}$  is the length of valent bonds,  $\Theta_{ab,ac}$  is the angle between the bonds,  $W(\mathbf{R}_1, \dots, \mathbf{R}_N)$  is the small correction term which characterizes the difference between the potential  $U(Q)$  and the potential of valence forces. The operator  $H_{rot}$  is given by the equality:

$$H_{rot} = \sum_{v,\lambda} \mu_{v\lambda}^{(0)} J_v J_\lambda \sim k^2 E_{vib}. \quad (6.64)$$

The parameter  $k^2 \sim 0.0224$  refers to the most anharmonic vibrations of hydrogen nuclei. From Eqs. (6.62) – (6.64) it can be seen, that the zero-order vibration-rotation spectrum, for example, of a highly excited vibration of a single  $XH$  bond will reveal the structure, depicted in Fig. 6.1. In this case the vibrations and rotations get separated completely. From Eqs. (6.43) and (6.47) it becomes obvious that for  $H_{int}$  in Eq. (6.61) the following operator should be chosen:

$$\begin{aligned}
H_{int} &= H_{12} + H_{22} + H_{21} + T_{40}, \\
H_{12} &= \sum_{v,\lambda} \left( \sum_i \frac{\partial \mu_{v\lambda}^{(0)}}{\partial Q_i} Q_i \right) J_\nu J_\lambda \sim k^3 \omega_{vib} \sim k^5, \\
H_{22} &= \frac{1}{2} \sum_{v,\lambda} \left( \sum_{i,j} \frac{\partial^2 \mu_{v\lambda}^{(0)}}{\partial Q_i \partial Q_j} Q_i Q_j \right) J_\nu J_\lambda \sim k^4 \omega_{vib} \sim k^6, \\
H_{21} &= - \sum_{v,\lambda} \mu_{v\lambda}^{(0)} \pi_\nu J_\lambda \sim k^2 \omega_{vib} \sim k^4, \\
T_{40} &= \frac{1}{2} \sum_{v,\lambda} \mu_{v\lambda}^{(0)} \pi_\nu \pi_\lambda \sim k^2 \omega_{vib} \sim \omega_r \sim k^4. \tag{6.65}
\end{aligned}$$

Here  $\pi_\nu$  is the vibration momentum, (6.21). The operator  $T_{40}$  is much smaller, than the vibration Hamiltonian  $H_{vib}$ , and thus it can be viewed as a small perturbation. This perturbation leads to a small shift of the vibration level  $\sim k^2 \omega_{vib}$  with all its accompanying rotational sub-levels. It will not change the anomalously small splitting  $\varepsilon_v(0)$  of vibrational levels of the type  $|v, 0, 0, \dots\rangle$ , as the matrix elements between them take small values of the same order  $\sim k^4$  as the matrix elements of the anharmonic part of the potential energy  $U(q)$ .

The operator of centrifugal interaction  $H_{12}$  gives rise to correction terms in the energy of the order of  $\sim k^3 \omega_{vib}$ , as the matrix elements for anharmonic wavefunctions can be estimated as  $\langle v | Q | v \rangle \sim O(k)$ . Besides,  $H_{12}$  mixes the states of the type  $|v, 0\rangle D_s^J \tau$  and  $|v \pm 1, 0\rangle D_{s\pm 2}^J \tau$ , with the admixture of the order of  $\sim k^3$  — the separation of vibrations with rotations is slightly violated.

The operator of Coriolis interaction  $H_{21}$  in first order gives corrections to the energy due to the matrix elements of the type  $\langle v | p | 0 \rangle \langle 0 | Q | v \rangle \sim k^{2\nu-2} \sim \left(\frac{x_e}{\omega_{vib}}\right)^{\nu-1} \ll k^4$  only, if  $\nu \gg 1$ . Such corrections emerge, when there are several identical stretching vibrations. The eigenfunctions of different permutation symmetry for these bonds can have a nonzero vibration moment  $\pi_\nu$ , during the calculation of which the cited matrix elements emerge,  $\pi_\nu \sim k^{2\nu-2}$ . For the case of only two bonds the eigenfunctions will be provided by a symmetric and antisymmetric combinations of real func-

tions  $|v, 0\rangle$  and  $|0, v\rangle$ . Thus the vibration momentum  $\pi \sim i \frac{d}{dx_m} x_n$  in this case will equal zero as well with vanishing energy correction  $\Delta E \sim H_{21}$ <sup>10</sup>. The operator  $H_{21}$  mixes the states  $|v, 0\rangle D_{st}^J(\Omega)$  and  $|v - 2, 2\rangle D_{s,t\pm 1}^J(\Omega)$ .

Thus the vibration-rotation interaction produces the shift of energy levels  $\lesssim k^{2v} \omega_{vib} J^2 \sim \left( \frac{x_e}{\omega_{vib}} \right)^v \omega_{vib} J^2$ , which corresponds to highly excited vibrations of a single  $XH$  bond. The magnitude of the energy splitting for  $XH$  vibrations of various permutation symmetry ( $\varepsilon_N(n)$  for  $XH_2$  molecules) is preserved, that is the effect of level clusterization is not destroyed by the interaction.

Thus, (1) to separate out the vibrational-rotational spectrum of the molecule for highly excited  $XH$  vibrations ( $v \gg 1$ ) with the accuracy up to terms of order  $\sim k^2 \omega_{vib} \sim \omega_r \sim k^4$  it is sufficient to choose the Hamiltonian in the form Eq. (6.61) with  $H_{int} = 0$ . The latter follows from the fact, that

$$H_{int} = (T_{40} + H_{21} + H_{12} + H_{22}) \sim (k^{4v} + k^{2v+2} + k^5 + k^6) \ll k^4 \ll 1.$$

(2) If the rotational quantum number is big,  $J \sim k^{-2} \leq 50$ , the rotation frequencies can be estimated as  $\sim k^2 \omega_\nu J \sim k^2$ . It means, that  $H_{int} = (T_{40} + H_{21} + H_{12} + H_{22}) \sim (k^{4v} + k^{2v} + k + k^2) \sim k$ . Then the initial Hamiltonian should be chosen in the form:

$$H = H_{vib} + H_{rot} + H_{12} + H_{22}. \quad (6.66)$$

This Hamiltonian secures the accuracy of  $\sim k \sim 7\%$  for the calculation of rotation transitions on the highly excited  $XH$  vibration level ( $v \gg 1$ ). The pronounced clusterization of levels with different permutation symmetry is preserved. That is, each level gets split into a dense series of levels, with the distance between them diminishing fast with the increase in the excitation number  $v$  and, as it will be shown below, of the momentum  $J$ . And, last, (3) when the vibration excitation is low, while the rotation excitation is high the following estimates hold:

$$v \sim 1, \quad J \sim k^{-2}. \quad (6.67)$$

Then the Hamiltonian should be used in the form:

$$H = H_{02} + H_{12} + H_{22} + H_{20}. \quad (6.68)$$

With the help of the contact transformation the latter can be reduced to a sum of a rotational and vibrational Hamiltonians:

$$H' = H'_{02} + H'_{04} + H'_{20}, \quad (6.69)$$

where  $H'_{04}$  is provided in Eq. (6.60). This Hamiltonian will be used subsequently for the analysis of clusterization of purely rotational levels, which

---

<sup>10</sup>The second order correction term in  $H_{21}$  is of the order of  $k^4$ .

arises due to the nonlinearity of the rotation spectrum and has no relation to the anharmonicity of vibrations of light nuclei, as it was in the previous cases (1) and (2). The effect of clusterization of rotation levels originates from the low effectiveness of the tunneling re-orientation of the rotation axis in the body frame bound to the molecule. A detailed consideration of this effect will be provided in the subsequent Sections. This effect is manifested in case (2) as well, when the stretching vibration  $XH$  is highly excited as well. Then the low effectiveness of the two tunneling processes: of the vibrational excitation to another bond, and of the re-orientation of molecule rotation axis into another position with respect to the equilibrium configuration, makes the clusterization of vibration-rotation levels even more pronounced.

To conclude, we note, that the transition to valent-bond coordinates  $\{Q_i\} \rightarrow \{r_{ab}, \Theta_{ab;ac}\}$  in the vibration Hamiltonian (6.63) within the approximation of valence-bond-force potential with the neglection of the term  $\sum_k \mu^{\frac{1}{4}} [p_k \mu^{-\frac{1}{2}} (p_k \mu^{\frac{1}{4}})]^{11}$  leads to the Hamiltonian, which has been used previously:

$$H = \frac{1}{2} \sum_i P_i^2 + \sum_{i < k} \beta_{ik} P_i P_k + \sum_i U_i(X_i). \quad (6.70)$$

The potential  $U_i(X_i)$  has been used in Morse form. This Hamiltonian provides the accuracy of the vibration spectrum up to terms of order  $k^2$ , which for  $XH$  bond vibrations corresponds to  $\leq 2\%$ . This estimate justifies the usage of the Hamiltonian (6.70) for the calculation of the features of molecular vibration spectrum: of the dependence of vibration frequencies upon the excitation level; of level clusterization effects; of the number of levels in the cluster; of the dependence of cluster spectral width upon excitation level, etc.

#### 6.4 Vibrational-rotational Hamiltonian for $XY_2$ molecule in the inner basis representation 'coordinates - angles'

When the anharmonicity of the stretching vibration due to the nonlinearity of the potential  $U(R_{XY})$  plays the decisive role in the determination

---

<sup>11</sup>This term can be included in the potential energy, so that the Hamiltonian (6.70) preserves its form. For the vibrations of light nuclei  $H$  this term leads to small corrections  $\sim \frac{M\mu}{M_X} Q_i Q_j$ . Its principal term has the shape  $\frac{M\mu}{M_X} Q_i Q_j$ , and it can be accounted for by the addition of a similar interaction into Eq. (6.70). For small molecules with  $CH$  and  $OH$  bonds this potential interaction is much smaller, then the corresponding kinematic interaction  $\beta_{ij} p_i p_j$ . In any case, it does not change the order of the splitted levels  $|v, 0\rangle$  and  $|0, v\rangle$ , as it can be seen from the derivation of Eqs. (5.6) and (5.24). Calculations for molecules  $H_2O$  and  $C_6H_6$  with the account of the purely kinematic interaction  $\beta_{ij} p_i p_j$  reproduce the vibrational levels with the accuracy up to  $1 \text{ cm}^{-1}$ , [53].

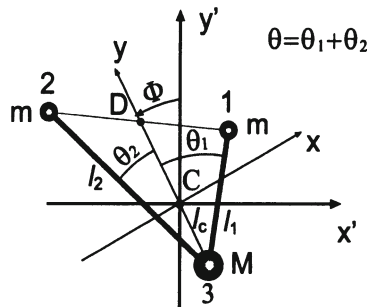


Figure 6.2: The scheme of valence coordinates in molecule  $XY_2$ :  $C$  is the center of mass and  $D$  – the middle of the segment  $[1, 2]$ . Axes  $(x, y)$  denote the body frame, related to the molecule, while  $(X', Y')$  form the laboratory frame if the motion takes place in the plane  $(X', Y')$ . The valence coordinates are the lengths  $l_1, l_2$ , and  $\Theta$  – the angle between the bonds  $(3, 2)$  and  $(3, 1)$ .

of the vibration-rotation spectrum, as compared to the nonlinearity due to Coriolis interaction and the functional dependence of inertia tensor upon vibration coordinates, it is convenient to express the Hamiltonian through the valence-bond (stretching) coordinates. In such a representation the molecule vibrations in zero approximation constitute a set of independent local modes (LMs), in which the anharmonicity of the valence-bond potential  $(U(R_{XY}), U(\Theta_{XY,XY'}))$  is accounted for completely. The next approximation should incorporate the weak interaction between LMs due to Coriolis and centrifugal interactions, as well as the slight deviations of the potential from the potential of valence forces. Such a scheme works well in the analysis of vibrations for  $CH$  and  $OH$  bonds due to the considerable anharmonicity of valence potential  $U(R)$ , modeled quite satisfactorily by Morse potential [56, 6]. Detailed derivation and examples of Hamiltonians in valence coordinates for various molecules can be found in [11]. Here we will derive such a Hamiltonian for the molecule  $XY_2$ . We assume that the mass of atom  $X$  is much bigger than that for atom  $Y$ :

$$\beta = \frac{M_Y}{M_X} = \frac{m}{M} \ll 1, \quad m = M_Y, \quad M = M_X. \quad (6.71)$$

We will derive the vibration-rotation Hamiltonian up to terms of order  $\sim \beta$  with the account of the smallness of  $\beta$  ( $\beta \lesssim 0.1$ ), neglecting terms  $\sim \beta^2, \beta^3$ , etc. For the study of  $CH$  vibration spectrum in big organic molecules, when  $M$  is the mass of the molecule backbone, such an approximation is quite natural. Let us introduce valence coordinates  $(l_1, l_2, \Theta)$ , and Euler angles

$(\alpha, \beta, \gamma = \Phi)$ <sup>12</sup> to determine the molecule position in the frame, where the center of mass is immobile (Fig. 6.2). The body axis we define in the following way: the  $y$  axis goes through the center of mass and through the heavy atom 3; the axis  $x$  is perpendicular to it and lies in the molecule plane; the axis  $z$  is perpendicular to the latter plane. The Euler angles are defined in the usual way, so that  $(\alpha, \beta)$  are the azimuth and polar angles of the  $z$  axis in the laboratory frame;  $\gamma = \Phi$  is the angle of molecule rotation for given values of  $(l_1, l_2, \Theta)$  with respect to the mobile axis  $z$  ( $\alpha$  and  $\beta$  fixed). The axes  $(x', y')$  in Fig. 6.2 correspond to the position of mobile axes  $(x, y)$  before the last turn upon angle  $\Phi$ . The axes  $(x', y')$  are immobile completely only in the case, when all the atoms 1, 2, and 3 move in one and the same plane. The valence coordinates in the molecules  $XY_2$  are introduced in the following way: point  $C$  is the molecule center of mass; point  $D$  is the middle of the segment [1, 2];  $(x', y')$  are the intermediate mobile axes;  $(x, y)$  are the mobile body axes bound to the molecule;  $l_1, l_2$  are valent coordinates,  $\Theta$  is the angle between the bonds (3, 2) and (3, 1). The axes  $(x', y')$  rotate together with the molecule plane, the position of which is determined by the mobile axis  $z$ . Obviously, the kinetic energy of molecule plane rotation

$$T_z = \frac{M}{2} v_{3z}^2 + \frac{m}{2} (v_{1z}^2 + v_{2z}^2) \quad (6.72)$$

is determined completely by the angular velocity  $\omega$  of the mobile axes  $(x, y, z)$  rotation with respect to the laboratory frame  $(x'', y'', z'')$  (the latter are not shown in Fig. 6.2), and by the value of the inertia moment tensor  $I_{ik}$  ( $l_1, l_2, \Theta$ ). Defined through  $\omega_i, I_{ik}$  the energy  $T_z$  takes the shape:

$$T_z = \frac{1}{2} (I_{xx}\omega_x^2 + 2I_{xy}\omega_x\omega_y + I_{yy}\omega_y^2). \quad (6.73)$$

As  $I_{zx} = I_{zy} = 0$  the angular velocities  $\omega_x, \omega_y$  are expressed through the projections of the total momentum  $J_x, J_y$  only:

$$\begin{aligned} \omega_x &= (I^{-1})_{xx} J_x + (I^{-1})_{xy} J_y, \\ \omega_y &= (I^{-1})_{xy} J_x + (I^{-1})_{yy} J_y. \end{aligned} \quad (6.74)$$

Substituting Eq. (6.74) into (6.73) we obtain the usual expression of the kinetic energy through the momenta:

$$T_z = \frac{1}{2} \left( (I^{-1})_{xx} J_x^2 + 2(I^{-1})_{xy} J_x J_y + (I^{-1})_{yy} J_y^2 \right). \quad (6.75)$$

Taking into account the fact, that the momentum projections upon the body axes are expressed through the Euler angles and the corresponding conjugate momenta, we find, that Eq. (6.75) characterizes the part of the

---

<sup>12</sup>The Euler angle  $\beta$  should not be falsely identified with the parameter  $\frac{m}{M}$  in Eq. (6.71).

molecule Hamiltonian, which corresponds to the atomic motion perpendicular to the molecular plane. Thus, to obtain the total Hamiltonian of the molecule, the kinetic energy of motion inside the plane should be expressed through the momenta, and then the expression (6.75) should be added to it. In the subsequent consideration we assume  $v_z = 0$ , the motion is implied to take place within the plane, while the axes  $x', y'$  are, consequently, immobile. By  $T$  we denote below the kinetic energy of motion within the molecular plane.

The kinetic energy  $T$  with the accuracy up to terms  $\sim \beta = \frac{m}{M}$ , or, equivalently, the component of Lagrange function  $\mathcal{L}$ , which corresponds to that energy, is determined by the following expression:

$$\begin{aligned}\mathcal{L} &= \mathcal{L}_0 + \delta\mathcal{L}, \\ \mathcal{L}_0 &= \frac{m}{2} (l_1^2 + l_2^2) + \frac{m}{2} l_1^2 (\dot{\theta}_1 - \dot{\Phi}) + \frac{m}{2} l_2^2 (\dot{\theta}_2 + \dot{\Phi}) = \frac{m}{2} (\mathbf{v}_1^2 + \mathbf{v}_2^2), \\ \delta\mathcal{L} &= -\frac{M}{2} (l_c^2 + l_c^2 \dot{\Phi}) = -\frac{M}{2} \mathbf{v}_3^2 = -\beta \frac{m}{2} (\mathbf{v}_1 + \mathbf{v}_2)^2,\end{aligned}\quad (6.76)$$

where  $l_c$  is the distance from the center of mass to the heavy ( $M$ ) atom,  $\Theta_1$  and  $\Theta_2$  are the angles between the  $y$  axis and the bonds  $l_1, l_2$  correspondingly (see Fig. 6.2). The distance  $l_c$  is function of  $l_1, l_2$ , and  $\theta$ :

$$l_c = \beta \sqrt{l_1^2 + l_2^2 + 2l_1 l_2 \cos \theta} = \beta L_D, \quad (6.77)$$

where  $L_D$  is twice the length of the median of the triangle, which goes through the molecular center of mass. The formula (6.76) is obtained from the expression of the kinetic energy in the frame, where the total momentum of the molecule  $\mathbf{P}$  is zero upon neglection of the terms of order  $\beta^2$  and up. The angles  $\theta_1$  and  $\theta_2$  are provided by the expressions:

$$\sin \theta_1 = \frac{l_2 \sin \theta}{L_D}, \quad \sin \theta_2 = \frac{l_1 \sin \theta}{L_D}. \quad (6.78)$$

Equations (6.77) and (6.78) make it possible to express the velocities  $\dot{\theta}_1, \dot{\theta}_2, \dot{l}_c$  through  $l_1, l_2, \dot{\theta}$ , and thus to determine the Lagrange function of the molecule  $\mathcal{L}(l_1, l_2, \dot{\theta}, \dot{\Phi}; (l_1, l_2, \theta))$ .

The Hamilton function of the molecule (its kinetic part) is determined by the formula:

$$H = H_0 + \delta H, \quad H_0 = \mathcal{L}_0, \quad \delta H = -\delta\mathcal{L}, \quad (6.79)$$

where the momenta, conjugate to  $l_1, l_2, \theta$ , and  $\Phi$ , are derived with the help of  $\mathcal{L}_0$ :

$$\begin{aligned}
 P_1 &= \frac{\partial \mathcal{L}_o}{\partial l_1} = ml_1 + ml_1^2 (\dot{\theta}_1 - \dot{\Phi}) \theta_{11} + ml_2^2 (\dot{\theta}_2 + \dot{\Phi}) \theta_{21}, \\
 P_2 &= \frac{\partial \mathcal{L}_o}{\partial l_2} = ml_2 + ml_1^2 (\dot{\theta}_1 - \dot{\Phi}) \theta_{12} + ml_2^2 (\dot{\theta}_2 + \dot{\Phi}) \theta_{22}, \\
 P_3 &= \frac{\partial \mathcal{L}_o}{\partial l_3} = ml_1^2 (\dot{\theta}_1 - \dot{\Phi}) \theta_{13} + ml_2^2 (\dot{\theta}_2 + \dot{\Phi}) \theta_{23}, \\
 J_\phi &= \frac{\partial \mathcal{L}_o}{\partial \dot{\Phi}} = -ml_1^2 (\dot{\theta}_1 - \dot{\Phi}) + ml_2^2 (\dot{\theta}_2 + \dot{\Phi}). \tag{6.80}
 \end{aligned}$$

Here  $\theta_{11}, \theta_{12}, \theta_{13}$  are partial derivatives of the functions  $\theta_i(l_1, l_2, \theta)$  over  $l_1, l_2$  and  $\theta$  correspondingly.

From Eq. (6.80) we obtain the expressions of the velocities  $\dot{l}_1, \dot{l}_2, (\dot{\theta}_1 - \dot{\Phi})$  and  $(\dot{\theta}_2 + \dot{\Phi})$  through the momenta  $P_1, P_2, P_3$  and  $J_\phi$ :

$$\begin{aligned}
 ml_1 &= P_1 + \frac{\theta_{11} - \theta_{21}}{2} J_\Phi, \\
 ml_2 &= P_2 + \frac{\theta_{12} - \theta_{22}}{2} J_\Phi, \\
 \dot{\theta}_1 - \dot{\Phi} &= \frac{P_3 - \theta_{23} J_\Phi}{ml_1^2}, \\
 \dot{\theta}_2 + \dot{\Phi} &= \frac{P_3 + \theta_{13} J_\Phi}{ml_2^2}. \tag{6.81}
 \end{aligned}$$

In the derivation of equations (6.81) and (6.80) we took account of the following identities:

$$\theta_{13} + \theta_{23} = 1, \quad \theta_{11} + \theta_{21} = \theta_{12} + \theta_{22} = 0. \tag{6.82}$$

We note here, that it is most convenient to consider the velocities  $(\dot{\theta}_1 - \dot{\Phi})$  and  $(\dot{\theta}_2 + \dot{\Phi})$ , and not  $\dot{\theta}, \dot{\Phi}$ , as through the former the velocities of atoms  $\mathbf{v}_1, \mathbf{v}_2$  and  $\mathbf{v}_3$  are expressed in the most simple way:

$$\begin{aligned}
 v_{3x} &= -\beta (l_1 \sin \theta_1 - l_2 \sin \theta_2) \\
 &\quad -\beta [l_1 (\dot{\theta}_1 - \dot{\Phi}) \cos \theta_1 - l_2 (\dot{\theta}_2 + \dot{\Phi}) \cos \theta_2], \\
 v_{3y} &= -\beta (l_1 \cos \theta_1 + l_2 \cos \theta_2) \\
 &\quad +\beta [l_1 (\dot{\theta}_1 - \dot{\Phi}) \sin \theta_1 + l_2 (\dot{\theta}_2 + \dot{\Phi}) \sin \theta_2]. \tag{6.83}
 \end{aligned}$$

Substituting Eqs. (6.81) and (6.83) into Eq. (6.76) and subsequently into Eq. (6.79), and adding up the kinetic energy  $T_z$  (6.75) with the potential

energy  $U(l_1, l_2, \theta)$ , we obtain the Hamiltonian function of  $XY_2$  molecule  $XY_2$  in valence coordinates up to terms  $\sim \beta = \frac{m}{M}$ :

$$\begin{aligned} H(P, J) = & \left\{ (\mu + \mu_3) (P_1^2 + P_2^2) + 2\mu_3 P_1 P_2 \cos \theta \right. \\ & - 2\mu_3 \sin \theta \left( \frac{P_1}{l_2} + \frac{P_2}{l_1} \right) P_3 \\ & + \left. \left( (\mu + \mu_3) \left( \frac{1}{l_1^2} + \frac{1}{l_2^2} \right) - \frac{2\mu_3 \cos \theta}{l_1 l_2} \right) P_3^2 + U(l_1, l_2, \theta) \right\} \\ & + \left\{ 2(\mu + 2\mu_3) \left[ \frac{\sin \theta}{L_D^2} (P_2 l_1 - P_1 l_2) J_z + \frac{\cos \theta (l_1^2 - l_2^2)}{l_1 l_2 L_D^2} P_3 J_z \right] \right\} \\ & + \left\{ \frac{2(\mu + 2\mu_3)}{L_D^2} J_z^2 + \frac{1}{2} \left( (I^{-1})_{xx} J_x^2 + 2(I^{-1})_{xy} J_x J_y + (I^{-1})_{yy} J_y^2 \right) \right\}, \end{aligned} \quad (6.84)$$

where

$$\mu = \frac{1}{2m}, \quad \mu_3 = \frac{\beta}{2m} = \frac{1}{2M}, \quad J_z = J_\Phi, \quad (6.85)$$

and  $(I^{-1})_{ik}$  is the element of the inverse matrix of inertia momentum tensor, which is function of  $l_1, l_2$ , and  $\theta$ . The momenta  $J_k$  are expressed through Euler angles  $(\alpha, \beta, \gamma)$  and conjugate momenta  $(J_\alpha, J_\beta, J_\gamma)$  according to formulas (6.28). In the case of different masses of light atoms  $m_1 \neq m_2$ , the equation (6.84) remains valid, if in its kinetic part the following substitutions are made:

$$l_1 \rightarrow \left( \frac{m_1}{m_2} \right)^{\frac{1}{4}} l_1, \quad l_2 \rightarrow \left( \frac{m_2}{m_1} \right)^{\frac{1}{4}} l_2, \quad P_1 \rightarrow \left( \frac{m_2}{m_1} \right)^{\frac{1}{4}} P_1, \quad P_2 \rightarrow \left( \frac{m_1}{m_2} \right)^{\frac{1}{4}} P_2, \quad (6.86)$$

along with  $m = \sqrt{m_1 m_2}$ . This follows from the fact, that for such a value of  $m$  the substitution (6.86) transforms the Lagrangian (6.76) into the kinetic energy of the molecule, with masses of light atoms equal to  $m_1$  and  $m_2$ . For the study of the quantum Hamiltonian, corresponding to (6.84), the determinant  $|g^{ik}|$  should be found, and after that, according to the rules from Chapter 6, Section 6.2, the required differential operator acting upon the function  $\psi(l_1, l_2, \theta, \alpha, \beta, \gamma)$  can be written out immediately. This procedure is straightforward, but a bit lengthy, so that we do not provide it here. In the particular cases of importance to us the calculations and the resulting formulas are much simpler, and we will provide these below.

The Hamilton function (6.84) is a sum of three terms, which have a transparent physical meaning. The first term in figure brackets describes the inner motion of the molecule, and, in fact, is nothing but the vibrational Hamiltonian of the molecule. The second term corresponds to the Coriolis

interaction of rotation with vibrations. The third term contains the rotational part of the total Hamiltonian, along with the centrifugal interaction of vibration and rotation.

The advantage of stretching (valence) coordinates is in the simpler expression of the potential energy, especially in the case, when the latter is represented by a sum of potentials for valence bonds and sites. However, for that simplification one has to pay a higher price in the form of a more complex kinematic part of the Hamiltonian as compared to the expression of it in normal coordinates, when Eckart conditions hold. In valence coordinates the vibrational momentum (6.84) is nonzero already in the equilibrium configuration, so that the magnitude of Coriolis interaction  $\sim \frac{\Delta l}{l} E_{vib}$  is greater in order than the rotation energy  $\sim (\frac{\Delta l}{l})^2 E_{vib}$ . The latter makes it impossible to separate the rotational and vibrational motion of the molecule, which could have been done in normal coordinates. Another inconvenience of valence coordinates lies in the complexity of the expression for the determinant  $|g^{ik}(l_1, l_2, \theta)|$ . However, for strong anharmonicity of the valence forces potential  $U(l_1, l_2, \theta)$ , when it exceeds greatly the anharmonicity arising from the kinematic part of the Hamiltonian (6.84), the use of valence coordinates is quite reasonable (for example, for molecules  $H_2O$ ,  $C_6H_6$ , etc.). Then in the analysis of vibration-rotation spectrum the Hamiltonian (6.84) should be taken for the initial one, with  $l_1, l_2$ , and  $\theta$  equal to their equilibrium values. Then there is no need to calculate  $|g^{ik}| = const$ , and the Hamiltonian coincides with Eq. (6.84) where  $P_i$  and  $J_i$  are operators ( $J_i J_k \rightarrow \frac{1}{2} (J_i J_k + J_k J_i)$ ). We imply the bond lengths  $l_i$  and the angles  $\theta$ , entering the kinematic part of the Hamiltonian (6.84) to be constants, equal to their average values.

For the terms, entering Eq. (6.84) the following estimates hold:

$$\begin{aligned}
\mu P_{1,2}^2 &\sim \frac{\hbar^2}{m(\Delta l)^2} \sim E_{vib} \sim \hbar\omega_{vib}, \\
\frac{\mu P_3^2}{l^2} &\sim \frac{\hbar^2}{ml^2(\Delta\theta)^2} \sim \frac{\hbar^2}{m(\Delta l)^2} \sim E_{vib}, \\
\mu_3 P_1 P_2 &\sim \frac{m}{M} \frac{\hbar^2}{m(\Delta l)^2} \sim \beta E_{vib}, \\
\frac{\mu_3 P_{1,2} P_3}{l} &\sim \frac{m}{M m(\Delta l) l(\Delta\theta)} \sim \beta E_{vib}, \\
\frac{\mu P_{1,2} J_z}{l} &\sim \frac{\hbar^2}{m(\Delta l) l} \sim \frac{(\Delta l)}{l} E_{vib}, \\
\frac{\mu P_3 J_z}{l^2} &\sim \frac{\hbar^2}{m(\Delta\theta) l^2} \sim \frac{(\Delta l)}{l} E_{vib},
\end{aligned}$$

$$\frac{\mu J_z^2}{l^2} \sim \frac{\hbar^2}{ml^2} \sim \frac{(\Delta l)^2}{l^2} E_{vib}. \quad (6.87)$$

In the case, when  $U(l_1, l_2, \theta) = U(l_1) + U(l_2) + V(\theta)$  and all the terms in this sum are strongly anharmonic, the following scheme for the calculation of vibrational-rotational molecular spectrum can be put forward:

In zero order the Hamiltonian gets split into a sum of three Hamiltonians with each one describing vibrations of the bonds  $l_1, l_2$  and of the angle  $\theta$  correspondingly. The vibration wavefunction is a product of three wavefunctions  $\psi_1(l_1)\psi_2(l_2)\psi_3(\theta)$ , each one describing a corresponding local mode. The rotational part of the molecule wavefunctions is determined by the rotational part of the Hamiltonian (6.84) — the last term in figure brackets, averaged over vibrations.

The next approximation is in the account of the term  $2\mu_3 \cos \theta P_1 P_2 = \beta(2\mu \cos \theta P_1 P_2)$ , which in second order provides corrections to the energy  $\sim \frac{\beta^2}{x_c} E_{vib}$ . The remaining terms of the Hamiltonian give corrections of the order of  $\beta^2 E_{vib}$ , or  $(\frac{\Delta l}{l})^2 E_{vib}$ , according to the estimates (6.87). The latter are much smaller than the former, as the anharmonicity parameter satisfies  $x_c \ll 1$ . This scheme of calculations corresponds to the usage of Hamiltonian (5.1) in the analysis of vibration spectrum for highly excited valence bonds. That same Hamiltonian has been used in Chapter 2 in the classical analysis of two weakly interacting nonlinear oscillators. As noted before, the quantum calculation of high  $OH$  vibration overtones in molecule  $H_2O$ , performed in [53], provides the accuracy up to  $10 \text{ cm}^{-1}$ , which corresponds to the order of rotation frequencies  $\omega_r$ . The next approximation, which provides correction terms to the energy  $\sim \beta^2 \omega_{vib}$  and  $\sim (\frac{\Delta l}{l})^2 \bar{\omega}_{vib}$ , requires the account of the interaction  $(P_1 + P_2)P_3$  and of Coriolis terms  $P_i J_z$ , which is equivalent to the use of the total Hamiltonian (6.84). The Coriolis interaction makes it impossible to separate rotations from vibrations. The molecule wavefunction is formed by a sum of products of vibrational and rotational wavefunctions. The vibration wavefunctions depend upon rotation quantum numbers as parameters. The latter is manifested explicitly when the molecule is a symmetric top. Then  $I_{xx} = I_{yy}, I_{xy} = 0$ , and the Hamiltonian (6.84) contains operators of the momentum squared  $J^2$ , and the  $z$ -projections of momentum  $J_z$ , which commute with each other. Thus, the quantum problem is reduced to the consideration of a purely vibrational Hamiltonian, which depends upon  $J^2 = J(J+1)$  and  $k = J_z$  as parameters. The calculation technique for the vibration-rotation spectrum of formaldehyde, when the Coriolis interaction is not small as compared to the rotation energy, has been developed in Refs. [101, 102]. In these works, however, the vibration modes have been considered in the harmonic approximation. We stress, that Eq. (6.84) can be used as a vibration-rotation Hamiltonian only in the case of strong anharmonicity of the potential  $U(l_1, l_2, \theta)$  and, simultaneously, of small vibration amplitudes  $\frac{\Delta l}{l} \ll 1, \frac{\Delta \theta}{\theta} \ll 1$ . Then the nonlinearity arising

from the kinematic part of the Hamiltonian can be neglected, and the quantities  $l_1, l_2, \theta_1, \theta_2$  and  $\theta$  in the kinematic part can be substituted by their average values. In the opposite case the determinant  $|g^{ik}|$  should be found in accordance with Eqs. (6.4) and (6.43).

For a symmetric top with  $I_{xy} = 0$ ,  $I_x = I_y$ , when  $J_z$  is a constant of motion, the Hamiltonian (6.84) with the help of a contact transformation

$$H' = \exp [iJ_z (A_{11}l_1 + A_{12}l_2 + A_{13}\theta)] H \exp [-iJ_z (A_{11}l_1 + A_{12}l_2 + A_{13}\theta)], \quad (6.88)$$

where the coefficients  $A_{ik}$  are functions of the averaged angles  $\bar{\theta}_i$  and bond lengths  $\bar{l}_i$ , can be transformed into:

$$H' = \left\{ \sum_{i,k} G^{i,k} (l, \theta) P_i P_k + U(l_1, l_2, \theta) \right\} + \frac{1}{2} \left( \frac{J_x^2}{I_x} + \frac{J_y^2}{I_y} + \frac{J_z^2}{I_z} \right). \quad (6.89)$$

In Eq. (6.89) the inertia momenta  $I_j$  are functions of averaged  $\bar{\theta}_i, \bar{l}_i$ . Thus the transformed Hamiltonian splits into a sum of purely vibrational and purely rotational Hamiltonians. The coefficients  $A_{ik}$  (6.88) can be expressed through the coefficients of the kinetic part of Hamiltonian (6.84) in an obvious way.

If the molecule constitutes an asymmetric top, the rotational part of the Hamiltonian (6.89) retains the term of the type  $I_{xy}^{-1} J_x J_y$ , which remains small for  $\frac{I_{xy}}{I_{xx} - I_{yy}} \ll 1$ , but can change significantly in the opposite case.

The analysis provided demonstrates, that for relatively small changes of angles and bond lengths of the strongly anharmonic vibrating molecule the Hamiltonian in valence (stretching) coordinates can be transformed into a sum of a purely vibrational and a purely rotational Hamiltonian (6.89). The parameters of this Hamiltonian are functions of the averaged angles and bond lengths. The first term in brackets in Eq. (6.89) forms the model Hamiltonian, which has been used by R.Wallace [53] in the calculations of high vibrational overtones in molecule  $H_2O$ .

For high values of the momentum  $J$ , when the reciprocal changes of angles and bond lengths lead to significant Coriolis and centrifugal interactions, the Hamiltonian should be constructed in accordance with Eq. (6.4), viewing Eq. (6.84) as a starting expression of the classical Hamilton function.

## Chapter 7

# Semiclassical rotational spectra of rigid and semi-rigid molecules; clusterization of levels and internal symmetry

In this Chapter we consider the effect of clusterization of the rotational levels of rigid and semi-rigid molecules at high values of rotation momenta  $J \gg 1$ . The 'degree' of clusterization can be calculated with the use of the quasiclassical approach (method WKB) due to the inequality  $J \gg 1$ . For the rotation Hamiltonian the rotational part  $H_{rot}(J)$  of the total rotation-vibration molecular Hamiltonian can be chosen after a suitable contact transformation. The contact transformation minimizes the effect of the rotation — vibration interaction, and in the first approximation the latter can be neglected.

Both rigid and semi-rigid molecules have been considered. The semiclassical quantization of the rotational motion is introduced with the help of the notion of an RE surface. The classical rotation of the molecule is considered on this surface as well. The trajectories of this motion are nothing but the phase curves of the Hamiltonian system with one degree of freedom. Its phase space is topologically equivalent to a two-dimensional sphere. Quantizing these trajectories after Bohr-Sommerfeld, we obtain the quasiclassical rotation spectrum. The trajectories belonging to different parts of the RE surface and transforming one into another by symmetry transformations correspond to clusterized levels. The splitting of these levels is governed by sub-barrier tunneling which is being considered. The tunneling matrix is being built, and the splitting of levels with different symmetries inside the cluster is calculated. In the last Section we take into account the nuclear

spin and we calculate the corresponding superstructure in the rotational spectrum, produced by the permutation symmetry of equivalent spins.

For the proper understanding of this Chapter the knowledge of WKB method is required, along with the classification methods for the rotational levels of a polyatomic molecule according to point group symmetries and permutation group, closely related to the nuclear spins. These are reviewed, for example, in Ref. [81]. The theory of symmetry has been considered in the classical monograph [113]. Examples of symmetry analysis of the energy levels in polyatomic molecules can be found, for example, in Sections 12 and 13 of Ref. [81], and in Ref. [5]

## 7.1 Spectrum of polyatomic molecules: clusterization of rotational levels

As we have shown in the preceding Sections, the nonlinearity of molecule vibrations slows down considerably the vibration energy transfer from one part of the molecule to the other. This leads to the formation of intramolecular local vibrations – local modes(LM). In molecules with identical valent bonds ( $H_2O$ ,  $CH_4$ , etc.) the vibration spectrum becomes strongly clusterized due to the pronounced degeneracy of states, which correspond to high vibration overtones on equivalent bonds<sup>1</sup>. The strong degeneracy of vibration levels is the consequence of Hamiltonian nonlinearity and of weak interaction of equivalent degrees of freedom (for example,  $CH$ ,  $OH$  vibrations in  $CH_4$  and  $H_2O$ ), which can be transformed one into another with the help of some point group transformation. Consequently, the rotational states of an asymmetric free top, differing by the orientation of rotation axis with respect to the proprietary axes of the top, will be strongly degenerate<sup>2</sup>. Really, the free top is a nonlinear Hamilton system, i.e. its Hamilton equations are nonlinear. States with the opposite direction of rotation are transformed one into another with the help of the operation of time inversion  $t \rightarrow -t$ ,  $J \rightarrow -J$ , which signifies their equivalence. These states are bound weakly, as it is difficult to inverse the axis for a highly spinning top. The goal of the present Section is to prove the existence of rotation levels' clusterization effect for a wide class of effective rotational Hamiltonians  $H(J)$ . The analysis of vibration-rotation spectra in molecules  $SF_6$ ,  $SiF_4$ ,  $UF_6$  (see, for example, [103, 104, 105]), and in similar "heavy" spherical top molecules led to the amazing experimental discovery of spectral clusterization effect. Due to it the anticipated complex rotation spectrum represents a

---

<sup>1</sup>The terms "pronounced degeneracy", " strong degeneracy" define the situation, when there exist two or more levels, the splitting of which is anomalously small. In other words, these levels form a cluster, whose width is much smaller, than any interaction strength entering the initial vibration-rotation Hamiltonian.

<sup>2</sup>For a symmetric top the states  $|J, k\rangle$  and  $|J, -k\rangle$  are degenerate in the strict sense.

fine structure of highly degenerate rotation multiplets. The splitting within the multiplet for high values of  $J$  turns out to be so small, that the hyperfine interaction of the nuclear spin with rotation becomes important. The hyper-fine interaction produces the mixing of molecular states with different nuclei symmetry and leads to the appearance of IR lines, which have been forbidden in the absence of such mixing [106]. The relative simplicity of the clusterized spectrum leads to a relatively simple theory of dynamic "spontaneous" violation of symmetry, which describes the superfine structure inside the spectral clusters [107, 18]. Below the theory of rotation levels clusterization is described after W.G.Harter and C.W.Patterson [18]. It will be shown below, that the physical reason for clusterization of rotation levels at high  $J$  is the same as the reason why the highly excited vibration levels of equivalent LMs (for example,  $OH$  bonds in the molecule  $H_2O$ ) stick together. The profound reason for that coincidence lies in the strong nonlinearity of Hamilton equations.

In the analysis of the rotation structure of the given vibration level two different cases are possible: first, the vibration level is nondegenerate, and second, when the vibration level is degenerate and the degenerate levels are bound by the operator of vibration-rotation interaction of relatively low order. In the first case the vibration-rotation Hamiltonian  $H(\xi, \Omega)$  of the molecule with the help of the contact transformation (6.49) can be reduced to a purely rotational Hamiltonian  $H_v(J)$ , which has its specific functional form for each nondegenerate vibration level  $|v\rangle$ , numbered by the index  $v$ . For example, if  $H_v(J)$  is given by Eq. (6.60), the coefficients  $T_{\nu\lambda}(v)$  in that formula will depend upon the excitation number  $v$ . If the vibration level is degenerate, then with the help of the contact transformation (6.49) the molecule Hamiltonian can be reduced to the operator matrix  $H_{vv'}(J)$ , where the indices  $(v, v')$  enumerate all the degenerate levels of the given vibrational excitation  $E(v) = E(v') = E$ . In the present Section we will consider the case of a nondegenerate vibration level, which is always realized for the ground vibrational state at least. The degenerate case will be considered in the next Sections.

Thus, the rotational structure of the nondegenerate vibration level is described by the effective rotation Hamiltonian  $H_v(J)$ , which is obtained from the initial molecular Hamiltonian with the help of the contact transformation (6.49). As the initial Hamiltonian is invariant with respect to the inversion of time  $p \rightarrow -p$ ,  $J \rightarrow -J$ , and as the nondegenerate vibration state is also invariant with respect to that transformation ( $\varphi_v^* = \lambda\varphi_v$ ), the effective rotation Hamiltonian  $H_v(J)$  is an even function of  $J$ <sup>3</sup>:

---

<sup>3</sup>The symmetry of the operator function  $H(J)$  means that after all the possible reductions of the order of operators  $J_\mu$  with the help of the formula  $[J_\mu, J_\nu] = -ie_{\mu\nu\lambda}J_\lambda$  the resultant operator  $H(J)$  satisfies Eq. (7.1).

$$H_v(J) = H_v(-J). \quad (7.1)$$

The simplest operators that satisfy the condition (7.1) are the top Hamiltonian that describes the rotation of a rigid molecule:

$$H = AJ_x^2 + BJ_y^2 + CJ_z^2, \quad (7.2)$$

and the Hamiltonian of a semi-rigid molecule of octahedral symmetry, like  $SF_6$ :

$$H = BJ^2 + 10t_{044} \left[ J_x^4 + J_y^4 + J_z^4 - \frac{3}{5}J^4 \right]. \quad (7.3)$$

Here  $J_x, J_y, J_z$  are the projections of the momentum operator  $\mathbf{J}$  upon the axis bound tightly to the molecule (see Section 6.1),  $t_{044}$  is a constant, which depends upon the excitation level  $t_{044}(v)$  (for  $SF_6$ :  $B \sim 0.09 \text{ cm}^{-1}$ ,  $t_{044} \sim 2 \cdot 10^{-10} \text{ cm}^{-1}$ ). Below we calculate the rotation spectrum with the use of the explicit form of operators (7.2) and (7.3), and confirm its clustered nature for high values of the momentum  $J$ . The quasi-classical calculation ( $J \gg 1$ ) below will reveal the fact, that the clusterization of the spectrum is the consequence of high values of  $J$  and of the existence of point symmetry group ( $J'_\mu = O_{\mu\nu}J_\nu$ ), which preserves the operators (7.2) and (7.3). As any rotation Hamiltonian satisfies the condition (7.1), and, consequently, is invariant with respect to transformations  $\mathbf{J} \rightarrow -\mathbf{J}$ , for high values of  $J$  the spectrum of any rotation Hamiltonian  $H_v(J)$  will get split into clusters of highly degenerate rotation levels (two sub-levels at minimum).

From the point of view of classical physics the Hamiltonian (7.2) describes rotation, when the molecule is assumed to be absolutely rigid, that is the interaction of inner degrees of freedom (vibrational and electronic motions) with rotation is absent. In the next approximation the molecule in the course of rotation deforms slightly, so that the elastic forces are compensated by centrifugal forces. In this case the average distances between the nuclei increase by  $\Delta r \sim \frac{J^2}{r_0^3 \omega_v^2 M^2}$ . In turn, that changes that elastic and kinetic energy of the molecule by  $\Delta E \sim \frac{J^4}{r_0^6 \omega_v^2 M^3}$ , that is, it gives rise to terms of order  $J^4$  in the Hamiltonian. As a result, the effective rotational Hamiltonian of the semi-rigid molecule takes the shape of Eq. (7.3).

We note, that the deformation of the molecule during rotation decreases the symmetry of the rotational Hamiltonian. Thus, for example, the quadratic part of the Hamiltonian (7.3) is spherically symmetric, whereas its quartic part has octahedral symmetry only. The effect of reduction of rotation symmetry due to the interaction of molecule rotation with vibrational and electronic degrees of freedom is called the dynamical symmetry breaking. Despite the fact, that the non-rigidity of the molecule reduces the symmetry of rotation Hamiltonian, the latter always retains the point symmetry of

the molecule. Thus, Eq. (7.3) has the octahedral symmetry of the molecule  $SF_6$ .

For the picture of rotation of the semi-rigid molecule, described above, to be valid, the rotation should be much slower, then the vibrational motion. Then the molecule vibrations follow adiabatically the changes of rotation states of the molecule, that is, tune up to it. Consequently the molecule energy is determined completely by its rotational state, which in the classical approach is characterized by vector  $\mathbf{J}$  in the frame, bound to the molecule. This correspondence between the vector  $\mathbf{J}$  and the molecule energy  $E(\mathbf{J})$  enables the introduction of the classical Hamilton function, which within the quantum approach has the sense of an effective rotation Hamiltonian of the type (7.2) or (7.3). On the contrary, if the vibration level  $|v\rangle$  is degenerate, there is no unambiguous relation between the moment  $\mathbf{J}$  and energy  $E$ , as for the determination of energy the vibration state should be specified additionally. Within the classical approach it makes impossible the construction of the Hamilton function  $H(J)$ <sup>4</sup>, while in the quantum case it precludes from transforming the molecule Hamiltonian to the effective rotation form of the type (7.2) or (7.3). The operator expressions (7.2) and (7.3) are the principal terms in the expansion of the effective rotation Hamiltonian  $H_v(J)$  in powers of the momentum operator  $\mathbf{J}$ . As the clusterization of rotation levels is revealed most really at high values of the momentum  $J \gg 1$ , we will calculate the rotation spectrum within the quasi-classical approximation. Thus we choose the function  $H_v(J)$  for the Hamiltonian of the classical system. With the help of it we find the Hamilton-Jacobi equations, solve them, and find the action  $S(\bar{\alpha}, \bar{\beta}, \bar{\gamma})$ , where  $(\bar{\alpha}, \bar{\beta}, \bar{\gamma})$  are the Euler angles, which define the molecule orientation in the laboratory frame  $(x, y, z)$ <sup>5</sup>. After that the rotation spectrum is obtained from the condition of Bohr-Sommerfeld quantization<sup>6</sup>. The splitting inside the cluster can be found in full analogy with the calculation of the splitting which is produced by the tunneling of the particle through a potential barrier.

However, the straightforward calculation of the rotation spectrum with

<sup>4</sup>The index  $v$  in the function  $H_v(J)$  within the classical approach characterizes the adiabatic invariant, which preserves its value in the course of slow rotation and gives rise to the one-to-one correspondence between the momentum  $\mathbf{J}$  and the energy  $E$ :  $E = H_v(\mathbf{J})$ , see, for example, Ref. [7].

<sup>5</sup>The Euler angles  $(\bar{\alpha}, \bar{\beta}, \bar{\gamma})$  play the role of coordinates in the configuration manifold of molecule orientations. The momentum projections  $J_{\bar{\alpha}}, J_{\bar{\beta}}, J_{\bar{\gamma}}$  (or  $-i\frac{\partial}{\partial \bar{\alpha}}, -i\frac{\partial}{\partial \bar{\beta}}, -i\frac{\partial}{\partial \bar{\gamma}}$  in the quantum approach) play the role of conjugate momenta .

<sup>6</sup>The quantization rules are applied in this case to a multidimensional mechanical system (the dimensionality of phase space is 6). The technique of quantization and construction of a quasi-classical solution in the multidimensional case can be found in the papers by V.P.Maslov (see, for example, Appendix 2 in the Russian edition of the monograph by J. Heading [108], and the brief consideration in the paper by V.Arnold [7]). Luckily, the problem of quantization of a rotator  $H_v(J)$  can be reduced to the one-dimensional case, tractable by the quantization method of Bohr- Sommerfeld (see below).

the help of the method, described above, is complicated by the necessity to solve the complex nonlinear equation in partial derivatives  $H\left(\frac{\partial S}{\partial \bar{\alpha}_\nu}, \bar{\alpha}_\nu\right) = E$ , ( $\bar{\alpha}_\nu = \bar{\alpha}, \bar{\beta}, \bar{\gamma}$ ). This problem, however, can be bypassed with the help of a canonical transformation to new variables, in which the Hamilton-Jacobi equations can be solved by the method of separation of variables. After the separation of variables the multidimensional problem is reduced to a one-dimensional one, and the energy spectrum along with the tunnel splitting can be found easily with the help of the quasi-classic method.

The following logical justification of the rotation spectrum calculation for the effective Hamiltonian  $H_\nu(J)$  can be provided additionally. Due to the inequality  $J \gg 1$  the quasi-classical approximation can be used. We look for a canonical transformation  $(\bar{\alpha}_\nu, \bar{J}_\nu) \rightarrow (\alpha_\nu, J_\nu)$  such that in the new variables the solution of Hamilton-Jacobi equations take the form:

$$S(\alpha_\nu) = \sum_\nu S_\nu(\alpha_\nu | I_1, I_2, I_3), \quad (7.4)$$

where  $I_1, I_2, I_3$  are the action variables. Performing the quantization procedure of each term  $S_\nu(\alpha_\nu)$  in Eq. (7.4) according to Bohr-Sommerfeld, we obtain the energy spectrum of the system. To obtain the splitting inside the cluster with the accuracy up to exponential terms, we find the imaginary correction to the action  $S_\nu(\alpha_\nu | I)$  performing the analytic continuation in the coordinate  $\alpha_\nu$  from a classically accessible region into another one. Then the width of the cluster can be estimated as  $\sim \exp(-\frac{\text{Im} S_\nu}{\hbar})$ . The validity of the obtained spectrum is guaranteed by the fact, that each canonical transformation and, consequently, each new form of Hamilton function  $H'_\nu(\alpha, J)$  corresponds to some unitary transformation of the initial effective rotation Hamiltonian  $H'_\nu = U H_\nu U^{-1}$  [58]. Thus, with the help of the function  $H'_\nu(\alpha, J)$  we find the spectrum of the operator  $H'_\nu$ , which coincides with the spectrum of the initial Hamiltonian  $H_\nu(J)$  due to their unitary equivalence.

Let us go over to the classical problem of the top with Hamiltonian  $H_\nu(J)$ , where  $(J_{\bar{x}}, J_{\bar{y}}, J_{\bar{z}})$  are the projections of the top momentum upon the body axes  $(\bar{x}, \bar{y}, \bar{z})$ , which are bound to the molecule (the top). The point of the phase space of such a system (or, in other words, the state of the top) is characterized by three Euler angles  $(\bar{\alpha}, \bar{\beta}, \bar{\gamma})$ , which specify the orientation of the body axes  $(\bar{x}, \bar{y}, \bar{z})$  in the laboratory frame  $(x, y, z)$ , and by three canonical momenta  $J_{\bar{\alpha}}, J_{\bar{\beta}}, J_{\bar{\gamma}}$ . The physical meaning of the momenta  $J_{\bar{\alpha}}, J_{\bar{\beta}}, J_{\bar{\gamma}}$  is the following:  $J_{\bar{\alpha}}$  is the projection of top momentum upon the laboratory axis  $z$ ;  $J_{\bar{\beta}}$  is the projection of momentum upon the body axis  $\bar{y}$  for  $\gamma = 0$ <sup>7</sup>;  $J_{\bar{\gamma}}$  is the projection of momentum upon the axis  $\bar{z}$ . Thus the phase point of the top is the set of three coordinates and three canonically

---

<sup>7</sup>To be precise,  $J_{\bar{\beta}}$  is the momentum projection upon the line of nodes.

conjugated momenta  $(\bar{\alpha}, \bar{\beta}, \bar{\gamma}; J_{\bar{\alpha}}, J_{\bar{\beta}}, J_{\bar{\gamma}})$ . The momenta  $(J_{\bar{\alpha}}, J_{\bar{\beta}}, J_{\bar{\gamma}})$  are related to the momenta projections upon the laboratory axes  $(J_x, J_y, J_z)$  and the body axes  $(J_{\bar{x}}, J_{\bar{y}}, J_{\bar{z}})$  with the help of the following equations [96, 18]:

$$\begin{aligned} J_x &= -\cos \bar{\alpha} \cot \bar{\beta} J_{\bar{\alpha}} - \sin \bar{\alpha} J_{\bar{\beta}} + \frac{\cos \bar{\alpha}}{\sin \bar{\beta}} J_{\bar{\gamma}}, \\ J_y &= -\sin \bar{\alpha} \cot \bar{\beta} J_{\bar{\alpha}} + \cos \bar{\alpha} J_{\bar{\beta}} + \frac{\sin \bar{\alpha}}{\sin \bar{\beta}} J_{\bar{\gamma}}, \\ J_z &= J_{\bar{\alpha}}; \\ J_{\bar{x}} &= -\frac{\cos \bar{\gamma}}{\sin \bar{\beta}} J_{\bar{\alpha}} + \sin \bar{\gamma} J_{\bar{\beta}} + \cot \bar{\beta} \cos \bar{\gamma} J_{\bar{\gamma}}, \\ J_{\bar{y}} &= \frac{\sin \bar{\gamma}}{\sin \bar{\beta}} J_{\bar{\alpha}} + \cos \bar{\gamma} J_{\bar{\beta}} - \cot \bar{\beta} \sin \bar{\gamma} J_{\bar{\gamma}}, \\ J_{\bar{z}} &= J_{\bar{\gamma}}. \end{aligned} \quad (7.5)$$

Equations (7.5) agree completely with the provided definition of the momenta  $J_{\bar{\alpha}}, J_{\bar{\beta}}, J_{\bar{\gamma}}$  as projections of momentum upon the corresponding axis.

With the help of Eqs. (7.5) the following equations can be verified easily:

$$\{J_a, J_b\} = 0, \quad J^2 = J_x^2 + J_y^2 + J_z^2 = J_{\bar{x}}^2 + J_{\bar{y}}^2 + J_{\bar{z}}^2, \quad (7.6)$$

where  $\{f, g\}$  are the classic Poisson brackets of the functions  $f(\bar{\nu}, J_{\bar{\nu}})$  and  $g(\bar{\nu}, J_{\bar{\nu}})$  with respect to the variables  $(\bar{\alpha}, \bar{\beta}, \bar{\gamma}), (J_{\bar{\alpha}}, J_{\bar{\beta}}, J_{\bar{\gamma}})$ , where  $\bar{\nu}$  is from the set  $(\bar{\alpha}, \bar{\beta}, \bar{\gamma})$ . It follows from Eq. (7.6), that in any system with a Hamiltonian of the type  $H(J_{\bar{x}}, J_{\bar{y}}, J_{\bar{z}})$ , where  $(J_{\bar{x}}, J_{\bar{y}}, J_{\bar{z}})$  are defined by Eqs. (7.5), the projections of momentum upon the laboratory axes  $J_x, J_y, J_z$  preserve their values. That is, the vector of momentum  $\mathbf{J}$  is a constant of motion, and it preserves its value and orientation along any phase trajectory. As the effective rotation Hamiltonian  $H_v(\mathbf{J})$  is a scalar function, it can always be presented in the form of some function  $H_v(J_{\bar{x}}, J_{\bar{y}}, J_{\bar{z}})$ , in agreement with the previous expressions (7.2) and (7.3). Thus, the canonical variables  $(\bar{\nu}, J_{\bar{\nu}})$  enter the Hamilton function of the top in combinations  $J_{\bar{x}}, (\bar{\nu}, J_{\bar{\nu}})$  only. Consequently, the vector of momentum  $\mathbf{J}$  is constant, and the top energy does not depend upon the orientation of this vector in the laboratory frame, and upon the quantities  $\bar{\alpha}$  and  $\frac{J_x}{J} = \frac{J_{\bar{x}}}{J}$  in particular. The system energy  $E = H(\bar{\beta}, \bar{\gamma}, J_{\bar{\beta}}, J_{\bar{\gamma}})$  depends upon four variables at most. Now we will demonstrate, that it depends in fact upon the two canonical conjugated variables  $(\gamma, J_{\gamma})$  and upon the modulus of the momentum  $J$ . Besides, we will provide an explicit determination of the new variables  $(\gamma, J_{\gamma})$ . In addition we will describe explicitly the transition from the Hamilton function  $H(\bar{\beta}, \bar{\gamma}, J_{\bar{\beta}}, J_{\bar{\gamma}})$  to  $H(\gamma, J_{\gamma}, J)$ , reducing thus the multidimensional problem

to the one-dimensional Hamiltonian, function of parameter  $J$ . As the system energy and, consequently, the Hamiltonian do not depend upon other canonical variables, there is no need in the derivation of their explicit form, as long as we are interested in the spectrum of the quantum problem solely. We will provide only a brief description of the method of construction of other canonical variables. In fact that would be the canonical transformation  $(\bar{\nu}, J_{\bar{\nu}}) \rightarrow (\nu, J_{\nu})$ , mentioned above.

Now we make this qualitative consideration transparent with the help of the following derivation. Let us consider the state of a top with  $J_x = J_y = 0$ ,  $J_z = J_{\alpha} = J$ . From the first three equations we find:

$$J_{\alpha} = J, \quad J_{\beta} = 0, \quad \cos \bar{\beta} = \frac{J_{\gamma}}{J}. \quad (7.7)$$

Equations (7.7) are obvious in fact, as in this case the axis  $z$  coincides with the direction of vector  $\mathbf{J}$ , and, consequently, the momentum projection upon the top axis is  $J_{\bar{z}} = J_{\gamma} = J \cos \bar{\beta}$ , while its projection on the perpendicular axis  $z$  is zero, so that  $J_{\beta} = 0$  (the line of nodes is perpendicular to  $z$  and  $\bar{z}$ ). From Eqs. (7.5) and (7.7) the relations follow:

$$\begin{aligned} \frac{\partial J_{\bar{x}}}{\partial \bar{\beta}} &= \cos \bar{\gamma} \left\{ \frac{-J_{\gamma}}{\sin^2 \bar{\beta}} + \frac{J_{\alpha} \cos \bar{\beta}}{\sin^2 \bar{\beta}} \right\} \\ &= \frac{J \cos \bar{\gamma}}{\sin^2 \bar{\beta}} \left( \cos \bar{\beta} - \frac{J_{\gamma}}{J} \right) = 0, \\ \frac{\partial J_{\bar{y}}}{\partial \bar{\beta}} &= \frac{J \sin \bar{\gamma}}{\sin^2 \bar{\beta}} \left( \frac{J_{\gamma}}{J} - \cos \bar{\beta} \right) = 0, \quad \frac{\partial J_{\bar{z}}}{\partial \bar{\beta}} = \frac{\partial J_{\gamma}}{\partial \bar{\beta}} = 0. \end{aligned} \quad (7.8)$$

Eqs. (7.8) demonstrate, that for any Hamilton function of the type  $H_{\nu}(J_{\bar{x}}, J_{\bar{y}}, J_{\bar{z}})$  the equations (7.7) are true along the whole phase trajectory, if Eqs. (7.7) hold at least in one point of the trajectory. In fact, it is the Euler angle  $\bar{\gamma}$  and the momentum  $J_{\gamma}$  corresponding to the frame with  $J_z = J_{\alpha} = J$  that give rise to the new variables  $\gamma$  and  $J_{\gamma}$ , mentioned above. However, we will keep the notations  $\bar{\gamma}$  and  $J_{\gamma}$  bearing in mind the adopted choice of the coordinate system.

Thus the calculation of the phase trajectory can be reduced to the solution of a one-dimensional Hamilton problem. Really, due to the equations (7.7) and (7.8) the following equations of motion for  $\bar{\gamma}$  and  $J_{\gamma}$  hold:

$$\begin{aligned} j_{\bar{\gamma}} &= - \left\{ \frac{\partial H}{\partial J_{\bar{x}}} \frac{\partial J_{\bar{x}}}{\partial \bar{\gamma}} + \frac{\partial H}{\partial J_{\bar{y}}} \frac{\partial J_{\bar{y}}}{\partial \bar{\gamma}} + \frac{\partial H}{\partial J_{\bar{z}}} \frac{\partial J_{\bar{z}}}{\partial \bar{\gamma}} \right\} \\ &= - \frac{\partial}{\partial \bar{\gamma}} H(J_{\bar{x}}(\bar{\gamma}, \bar{\beta}; J_{\alpha}, J_{\beta}, J_{\gamma}), J_{\bar{y}}(\bar{\gamma}, \bar{\beta}; J_{\alpha}, J_{\beta}, J_{\gamma}), J_{\bar{z}} = J_{\gamma}) \\ &= - \frac{\partial}{\partial \bar{\gamma}} H(J_{\bar{x}}(\bar{\gamma}, \bar{\beta}; J, 0, J_{\gamma}), J_{\bar{y}}(\bar{\gamma}, \bar{\beta}; J, 0, J_{\gamma}), J_{\bar{z}} = J_{\gamma}), \end{aligned}$$

$$\begin{aligned}
\dot{\bar{\gamma}} &= \frac{\partial H}{\partial J_{\bar{x}}} \frac{\partial J_{\bar{x}}}{\partial J_{\bar{\gamma}}} + \frac{\partial H}{\partial J_{\bar{y}}} \frac{\partial J_{\bar{y}}}{\partial J_{\bar{\gamma}}} + \frac{\partial H}{\partial J_{\bar{\gamma}}} \\
&= \frac{\partial}{\partial J_{\bar{\gamma}}} H(J_{\bar{x}}(\bar{\gamma}, \bar{\beta}; J, 0, J_{\bar{\gamma}}), J_{\bar{y}}(\bar{\gamma}, \bar{\beta}; J, 0, J_{\bar{\gamma}}), J_{\bar{\gamma}}) \\
&= \frac{\partial}{\partial J_{\bar{\gamma}}} H(J_{\bar{x}}(\bar{\gamma}, \bar{\beta}(J, J_{\bar{\gamma}}); J, 0, J_{\bar{\gamma}}), J_{\bar{y}}(\bar{\gamma}, \bar{\beta}(J, J_{\bar{\gamma}}); J, 0, J_{\bar{\gamma}}), J_{\bar{\gamma}}) \\
&\quad - \left\{ \frac{\partial H}{\partial J_{\bar{x}}} \frac{\partial J_{\bar{x}}}{\partial \bar{\beta}} \frac{\partial \bar{\beta}}{\partial J_{\bar{\gamma}}} + \frac{\partial H}{\partial J_{\bar{y}}} \frac{\partial J_{\bar{y}}}{\partial \bar{\beta}} \frac{\partial \bar{\beta}}{\partial J_{\bar{\gamma}}} \right\}, \\
\frac{\partial J_{\bar{x}}}{\partial \bar{\beta}} &= \frac{\partial J_{\bar{y}}}{\partial \bar{\beta}} = 0, \\
\dot{\bar{\gamma}} &= \frac{\partial}{\partial J_{\bar{\gamma}}} H(J_{\bar{x}}(\bar{\gamma}, \bar{\beta}(J, J_{\bar{\gamma}})), J_{\bar{y}}(\bar{\gamma}, \bar{\beta}(J, J_{\bar{\gamma}})), J_{\bar{\gamma}}, J_{\bar{\beta}} = 0). \quad (7.9)
\end{aligned}$$

In the calculation of  $\dot{\bar{\gamma}}$  the Eq. (7.8) has been taken into account. The time dependence of  $\bar{\gamma}(t)$ ,  $J_{\bar{\gamma}}(t)$  is determined by the Hamilton equations (7.9). The Hamiltonian for the latter is obtained from the initial one by substitution of Eq. (7.7) into (7.5), and then in  $H(J_{\bar{x}}, J_{\bar{y}}, J_{\bar{z}})$ . The resultant expression of the Hamilton function is:

$$\begin{aligned}
H(\bar{\gamma}, J_{\bar{\gamma}}; J) &= H(J_{\bar{x}}(\bar{\gamma}, J_{\bar{\gamma}}; J), J_{\bar{y}}(\bar{\gamma}, J_{\bar{\gamma}}; J), J_{\bar{\gamma}}), \\
\cos \beta &= \frac{J_{\bar{\gamma}}}{J}, \quad J_{\bar{\alpha}} = J, \quad J_{\bar{\beta}} = 0. \quad (7.10)
\end{aligned}$$

For any given phase trajectory it is always possible to choose the orientation of the laboratory frame so that the axis  $z$  coincides with the direction of momentum vector  $\mathbf{J}$ . Then Eqs. (7.7) hold, and the equations of motion will be determined by the one-dimensional Hamiltonian (7.10). Important is the fact that the functional form of  $H(\bar{\gamma}, J_{\bar{\gamma}}; J)$  for all phase trajectories will be similar, which follows readily from Eq. (7.10). These Hamiltonians differ solely in the fact, that for different directions of vector  $\mathbf{J}$  the Euler angles  $(\bar{\alpha}, \bar{\beta}, \bar{\gamma})$  characterize the orientation of the top in different laboratory systems. More to it, these body systems are chosen in such a way, that the motions with equal values of  $E$  and  $J$ , but with different orientations of  $\mathbf{J}$  look quite similar — each one in its own body frame (the functions  $\bar{\alpha}(t), \bar{\beta}(t), \bar{\gamma}(t)$  are similar). Thus the determination of the spectrum of the quantum problem is reduced to the quasi-classical quantization of the Hamiltonian (7.10), which characterizes the energy of the classic top. According to Eq. (7.10) this energy depends upon three quantities:  $J$  and two canonical variables  $\bar{\gamma}, J_{\bar{\gamma}}$ . The latter means, that the determination of the energy spectrum of the rotation Hamiltonian  $H_v(J_{\bar{x}_i})$  in the quasi-classic approximation is reduced to the quantization of a Hamiltonian with one degree of freedom.

Each level, defined in such a way, is  $(2J + 1)$  times degenerate in accordance with the number of different possible values of the  $J_z$  projection,

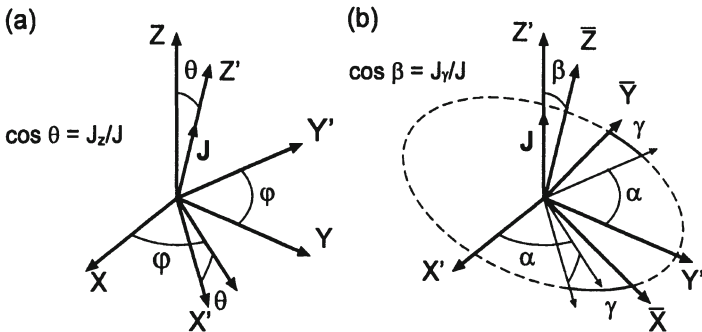


Figure 7.1: The plot, illustrating the new canonical variables introduced:  $(\varphi, \alpha, \gamma)$  and  $(J_\varphi = J_z, J, J_\gamma)$ .

taking integer values from  $-J$  to  $J$ . In the classic approach this corresponds to the independence of the Hamiltonian (or energy) (7.10) of the direction of vector  $\mathbf{J}$ . Phase trajectories with similar  $E$  and  $J$  form a two-parametric manifold: each direction of vector  $\mathbf{J}$  has one phase trajectory in correspondence. Defining the energy  $E$ , the momentum magnitude  $J$ , and its direction (for example, its polar angle and azimuth) we define the phase trajectory unambiguously. Thus the phase trajectories form a four-parametric set. It can be seen easily from Eqs. (7.5), (7.7), and (7.9), that each trajectory covers a two-dimensional torus in phase space. While the four-parametric set of two-dimensional tori fills all the phase space of the top throughout. Now it is possible to introduce new variables  $\{(\varphi, J_z), (\alpha, J), (\gamma, J_\gamma)\}$  with the help of a canonical transformation, so that the Hamiltonian acquires the form (7.10). The quantization problem is reduced to the solution of a one-dimensional equation of Hamilton-Jacobi.

The physical meaning of the new variables can be seen transparently from Fig. 7.1. The angle  $\varphi$  is the azimuth of  $\mathbf{J}$ ,  $J_z$  is the momentum projection upon axis  $z$ , the polar angle of  $\mathbf{J}$  is determined through  $J_z$  and  $J$  according to  $\cos \theta = \frac{J_z}{J}$ . Obviously,  $\varphi$ ,  $J_z$ , and  $J$  are constants of motion. Next, we introduce the intermediate frame  $(x', y', z')$  according to Fig. 7.1: the axis  $z'$  is directed along vector  $\mathbf{J}$ , axis  $y'$  belongs to the plane  $x'0y$ , axis  $x'$  is defined unambiguously as a perpendicular to the plane  $x'0y'$ . The orientation of molecular axes  $(\bar{x}, \bar{y}, \bar{z})$  with respect to  $(x', y', z')$  determines three Euler angles  $\alpha, \beta$  and  $\gamma$ . As  $\beta$  is the angle between the vector  $\mathbf{J}$  and the axis  $\bar{z}$ , the momentum projection  $J_\gamma$  upon axis  $\bar{z}$  is expressed through  $J$  and  $\beta$  by formula  $J_\gamma = J \cos \beta$ . Thus  $J_\gamma$  can be chosen instead of the angle  $\beta$  as the independent variable. Then we obtain the following set of canonically conjugated variables:  $(\varphi, J_z), (\alpha, J), (\gamma, J_\gamma)$ , where the polar

angle is determined by  $\cos \theta = \frac{J_z}{J}$ , the Euler angle is  $\cos \beta = \frac{J_\gamma}{J}$ , and the momentum projection is zero,  $J_\beta = 0$ . These formulas are the consequence of the special choice of the frame  $(x', y', z')$ , and of the orientation of the top in this basis set. We note, that the angle  $\alpha$  is the canonical conjugate to the momentum projection  $J_{z'} = J$ , so that  $\dot{\alpha} = \frac{\partial H}{\partial J_{z'}} = \frac{\partial H}{\partial J} = \frac{\partial H}{\partial J_\alpha}$ . Clearly, the inter-relation between the old and new variables is unambiguous,  $(\bar{\alpha}, \bar{\beta}, \bar{\gamma}; J_{\bar{\alpha}}, J_{\bar{\beta}}, J_{\bar{\gamma}}) \leftrightarrow (\varphi, \alpha, \gamma; J_z, J, J_\gamma)$ . From the definition of the new variables the equalities follow:

$$E = H(J_{\bar{x}_i}(\bar{\nu}, J_{\bar{\nu}})) = H(J_{\bar{x}_i}(J, J_\gamma, \gamma)) = H(\gamma, J_\gamma; J),$$

where  $H(\gamma, J_\gamma; J)$  coincides with the function (7.10) exactly. The variables  $\gamma, J_\gamma J_\alpha$  play the same role in the basis set  $(x', y', z')$ , as the variables  $(\bar{\gamma}, J_{\bar{\gamma}}, J_z = J, \bar{\alpha})$  in  $(x, y, z)$  for the phase trajectories (7.7). Thus the time dependence of the functions  $\gamma(t), J_\gamma(t), \alpha(t)$  is the same as the one in Eq. (7.10). Consequently the new equations of motion in the new variables are of Hamilton type, with the new Hamiltonian obtained from the initial (old) one with the help of the straightforward substitution of old variables by their expressions through the new ones:  $H'(P, Q) = H(p(P, Q), q(P, Q))$ . Thus the transformation  $(\bar{\alpha}, \bar{\beta}, \bar{\gamma}; J_{\bar{\alpha}}, J_{\bar{\beta}}, J_{\bar{\gamma}}) \rightarrow (\varphi, \alpha, \gamma; J_z, J, J_\gamma)$  we seek for is canonical. Quantizing the classical Hamiltonian in the new variables, we find the spectrum of the quantum Hamiltonian, which is unitary equivalent to the initial rotation Hamiltonian  $H_v(J_{\bar{x}_i})$ , and, consequently, obtains the same energy spectrum. So, the conclusion can be drawn, that the determination of top spectrum can be reduced to the one-dimensional problem with Hamiltonian of the type (7.10), where  $J$  enters as a parameter.

On the other hand, the Hamiltonian  $H(\gamma, J_\gamma, J)$  can be viewed as the Hamilton function upon the six-dimensional phase space  $(\varphi, \alpha, \gamma; J_z, J, J_\gamma)$ . As the function  $H(\gamma, J_\gamma, J)$  does not depend upon the variables  $(\alpha, \varphi, J_z)$ , the conjugate quantities  $(J, J_z, \varphi)$  are constants of motion. The latter means, that the momentum vector  $\mathbf{J}$  preserves its value, as  $\varphi$  is the azimuth of  $\mathbf{J}$ ,  $\theta = \arccos \frac{J_z}{J}$  is the polar angle of  $\mathbf{J}$ , and  $J$  is its modulus. The fact, that momentum  $\mathbf{J}$  is constant, is trivial, however, it is instructive to express it in the notations of canonical variables. Below we will consider the Hamilton function of the type (7.10) with the canonical variables (see Fig. 7.1) as arguments. The classical action  $S$ , which is the phase of the wavefunction, takes the shape:

$$S(\varphi, \alpha, \gamma) = J\alpha + J_z\varphi + S(\gamma; J, E),$$

where  $S(\gamma)$  is determined by the equation:

$$H\left(\frac{\partial S}{\partial \gamma}, \gamma; J\right) = E. \quad (7.11)$$

From the properties of the wavefunction (its single-valued and continuous nature) it follows, that  $J, J_z$  are the integers. Further, from the inequalities  $J \geq J_z \geq -J$  we find, that  $J_z = -J, -J+1, \dots, J$ . Then for the total action we obtain:

$$\begin{aligned} S_{\text{tot}}(\varphi, \alpha, \gamma) &= J\alpha + J_z\varphi + S(\gamma; J, E), \\ J_z &= -J, -J+1, \dots, J-1, J, \quad J = 1, 2, \dots \end{aligned} \quad (7.12)$$

The transition from Eq. (7.11) to (7.12) is nothing but the quasi-classical quantization of the total momentum  $J$  and of its projection  $J_z$ . Next we have to quantize the action  $S(\gamma; E, J)$ , and to determine the energy levels  $E$ . The quantization conditions depend essentially upon the shape of phase trajectories  $H(J_\gamma, \gamma; J) = E$ : whether the variation of angle  $\gamma$  along the whole trajectory is finite or infinite. This fact can be illustrated with the help of the analogy with the pendulum: the quantization conditions are entirely different for the cases, when the pendulum either rotates around its axis, or oscillates only. To determine the quantization conditions for all the types of classical trajectories, it is convenient to introduce the notion of the rotation energy surface RE. This surface is two-dimensional, and is essentially the phase space of the Hamilton system with one degree of freedom, defined by the Hamiltonian  $H(\gamma, J_\gamma; J)$ <sup>8</sup>. It is interesting to note, that the considered phase space is non-Euclidean, and in the topological sense is equivalent to a sphere. The RE surface is constructed in the following way: In the  $(J_{\bar{x}}, J_{\bar{y}}, J_{\bar{z}})$  basis set, bound to the molecule, vector  $E = H(\gamma, J_\gamma; J)$  is plotted in the direction of  $\mathbf{J}$ , where  $\tilde{\gamma} = \pi - \gamma$  and  $\beta = \arccos \frac{J_\gamma}{J}$  are the azimuth and polar angle of  $\mathbf{J}$  while  $J_\gamma = J_{\bar{z}} = J \cos \beta$ . By RE surface we denote the surface, which is drawn by the end point of the plotted radius-vector, when  $\mathbf{J}$  takes all the possible directions with its modulus unchanged. The phase trajectories of such a system belong to the cross-section of the RE surface with the sphere  $E = \text{const}$ . The motion along this trajectory is determined by Hamilton equations:

$$\dot{\gamma} = \frac{\partial H}{\partial J_{\bar{\gamma}}}, \quad \dot{J}_\gamma = -\frac{\partial H}{\partial \gamma}, \quad (7.13)$$

according to Eq. (7.9) and to the canonical nature of the transformation:

$$(\bar{\alpha}, \bar{\beta}, \bar{\gamma}; J_{\bar{\alpha}}, J_{\bar{\beta}}, J_{\bar{\gamma}}) \rightarrow (\varphi, \alpha, \gamma; J_z, J, J_\gamma).$$

The RE surfaces for a rigid molecule with the Hamiltonian of a symmetric and an asymmetric top (7.2) and for a semi-rigid molecule of the type

---

<sup>8</sup>The elementary area upon this surface is defined by:  $d\sigma_{RE} = dJ_\gamma d\gamma = J d \cos \beta d\gamma = J \sin \beta d\beta d\gamma$ .

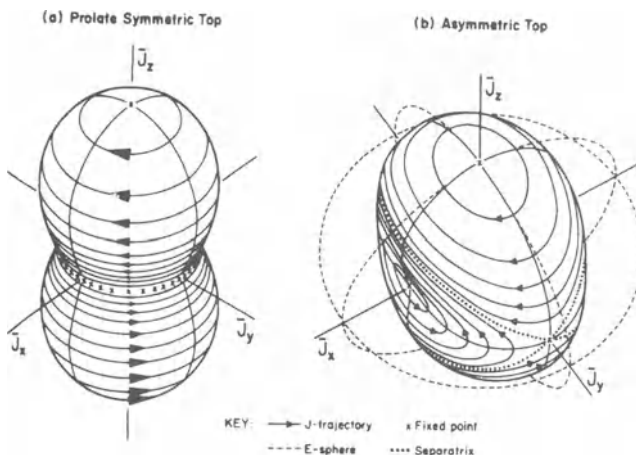


Figure 7.2: Molecular RE - surfaces: symmetric top (a) and asymmetric top (b).

$SF_6$  with Hamiltonian (7.3) are depicted in Figs.7.2 and 7.3<sup>9</sup>. The phase trajectories and the corresponding directions of motion are shown there as well.

The relation between the physical properties of the molecule, and the shape of its RE surface can be understood easily with the help of the example of molecule  $SF_6$ , see Fig. 7.4. This molecule has high rigidity with respect to the changes of  $SF$  bond, and rather low rigidly for the variations of angles between bonds. During rotation around the  $SF$  bond the inertia momentum does not change due to the rigidity of the  $SF$  bond, and the energy is  $E_0 = 0.5I_0^{-1}J^2$  (where  $I_0$  is the inertia momentum of a spherical top). Such rotation corresponds to the trajectories in the vicinity of the vertices of RE surface, which embrace the symmetry axes of fourth order (axes  $\bar{J}_x$ ,  $\bar{J}_y$ ,  $\bar{J}_z$ ). On the other hand, the molecule rotation around the symmetry axis of third order  $C_3$  changes the angles due to the low angular rigidity in such a way, that the distance of atom  $F$  from the rotation axis, and, correspondingly, the inertia momentum  $I > I_0$  increase both. The latter signifies the decrease of rotation energy  $E = 0.5I^{-1}J^2 < E_0$ <sup>10</sup>.

<sup>9</sup>The RE surfaces in the figures are the plots of the energy  $E(\tilde{\gamma}, \beta)$  in polar coordinates  $\tilde{\gamma} = \pi - \gamma$ ,  $\beta = \arccos \frac{J_x}{J_\gamma}$ . The variables  $\tilde{\gamma}$  and  $J_\gamma$  obey canonical equations:  $\frac{d}{dt}\tilde{\gamma} = -\frac{\partial E}{\partial J_\gamma}$ ,  $\frac{d}{dt}J_\gamma = \frac{\partial E}{\partial \tilde{\gamma}}$ . These equations determine the direction of motion along the phase curves in the pictures.

<sup>10</sup>The account of the increasing elastic energy  $U$  does not change the conclusion upon the decrease of the total energy  $E = T_{rot} + U$ , see below, end of Section 7.3.

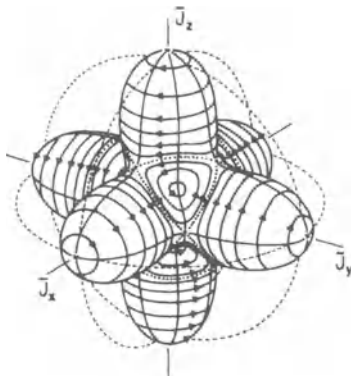


Figure 7.3: The RE - surface of a semirigid octahedral spherical top molecule.

The considered direction of momentum  $\mathbf{J}$  on the RE surface will have in correspondence the valleys, as shown in Fig.7.3.

Thus, we have shown, that the determination of the fine and superfine structure of rotation spectrum for a polyatomic molecule in nondegenerate electronic-vibrational states (in the ground state, for example) at high rotational excitation levels ( $J \gg 1$ ) is reduced to the quasi-classical quantization of a Hamilton system with one degree of freedom (7.13). For  $H(\gamma, J_\gamma; J)$  the effective rotation Hamiltonian  $H(J_{\bar{x}}, J_{\bar{y}}, J_{\bar{z}})$  is chosen, where the momenta  $(J_{\bar{x}}, J_{\bar{y}}, J_{\bar{z}})$  are expressed through  $(\gamma, J_\gamma; J)$  with the help of Eq. (7.5), and with the  $z$  axis of the laboratory frame directed along vector  $\mathbf{J}$ . Then the following equalities hold:  $J_\alpha = J$ ,  $J_\beta = 0$ ,  $\cos \beta = \frac{J_\gamma}{J}$ . With the help of  $H(\gamma, J_\gamma; J) = H(\pi - \tilde{\gamma}, J_\gamma; J)$  the molecule RE surface  $E(\tilde{\gamma}, \beta = \arccos \frac{J_\gamma}{J})$  can be constructed. The phase trajectories of the system are obtained as the cross-section of the RE surface with the sphere  $R = E$ . The structure of phase trajectories enables the qualitative analysis of vector  $\mathbf{J}$  motion with respect to the molecular axes, and, vice versa, of any molecular axis with respect to the direction of  $\mathbf{J}$ . These phase curves illustrate the quasi-classical quantization procedure (see next Section).

To calculate the rotation spectrum in the adiabatic approximation exactly, the diagonalization of the effective rotation Hamiltonian matrix  $H(J_{\bar{x}}, J_{\bar{y}}, J_{\bar{z}})$  for each value of  $\mathbf{J}^2 = J(J+1)$ ,  $J = 0, 1, 2, \dots$  should be performed. The results of an exact and a quasi-classical calculation will be compared in the next Section.

Finally we note, that according to Eqs. (7.2), (7.3), and (7.5) the Hamiltonian  $H(\gamma, J_\gamma; J)$  describes a nonlinear system, the energy levels of which

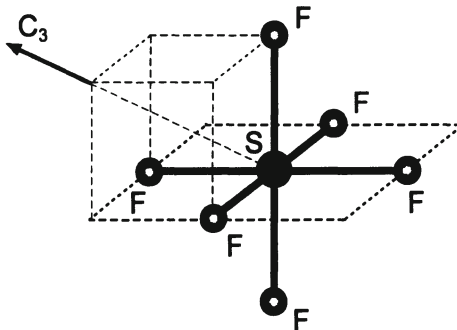


Figure 7.4: Structure of molecule \$SF\_6\$.

are positioned non-equidistantly. Consequently, the energy exchange between molecules in different rotation states is problematic. This property slows down the energy relaxation for highly excited rotation levels.

## 7.2 Rotational spectrum of rigid and semi-rigid molecules: semiclassical approach

In this Section we will provide the quasi-classical calculation of the rotation spectrum of an asymmetric top with Hamiltonian (7.2), and in a more schematic way the calculation of the spectrum with Hamiltonian (7.3), which describes the semi-rigid molecule of octahedral symmetry, like \$SF\_6\$. As it has been shown in the preceding Section, the quasi-classical approach is applicable to any effective Hamiltonian \$H(\mathbf{J})\$ for \$J \gg 1\$, if the molecule is in a nondegenerate electronic-vibrational state.

Let us consider the asymmetric top first. As we have shown in the preceding Section, the classical problem of an asymmetric top can be reduced to the Hamiltonian (7.10) with one degree of freedom. This Hamiltonian is obtained from Eq. (7.2) by substitution of Eq. (7.5) with the account of (7.7). The last relation arises due to the coincidence of the directions of vector \$\mathbf{J}\$ and of the axis \$z\$ in the laboratory frame. As a result, the Hamiltonian (7.10) with a single degree of freedom, corresponding to the studied asymmetric top takes the shape<sup>11</sup>:

$$H(\gamma, J_\gamma) = A(J^2 - J_\gamma^2) \cos^2 \gamma + B(J^2 - J_\gamma^2) \sin^2 \gamma + CJ_\gamma^2. \quad (7.14)$$

The momentum projections upon the molecular axes \$J\_{\bar{x}}, J\_{\bar{y}}\$, and \$J\_{\bar{z}}\$ are related to \$\gamma, J\_\gamma\$, and \$J\$ by the equations:

---

<sup>11</sup>Below we will denote the Euler angles by \$(\alpha, \beta, \gamma)\$ instead of \$(\bar{\alpha}, \bar{\beta}, \bar{\gamma})\$ for brevity.

$$J_{\bar{x}} = -J \sin \beta \cos \gamma, \quad J_{\bar{y}} = J \sin \beta \sin \gamma, \quad J_{\bar{z}} = J \cos \beta = J_\gamma. \quad (7.15)$$

Equations (7.15) follow from Eqs. (7.5) and (7.7). The angles  $\beta$  and  $\tilde{\gamma} = \pi - \gamma$  are the polar angle and the azimuth of vector  $\mathbf{J}$  in the molecular body frame. At the same time they are the polar angle and the azimuth of a point on RE surface. Simultaneously,  $\gamma = \pi - \tilde{\gamma}$  and  $J_\gamma = J \cos \beta$  are the canonical variables on the RE surface in the phase space of the system. The correspondence relation  $\{(\gamma, J_\gamma) \leftrightarrow \text{point of RE surface}\}$  has singularities in the vicinity of RE surface poles, where  $\beta = 0, \pi$  and  $J_\gamma = \pm J$  correspondingly.

From Eq. (7.14) and the equation

$$H(\gamma, J_\gamma) = H\left(\gamma, \frac{\partial S}{\partial \gamma}\right) = E \quad (7.16)$$

the momentum  $J_\gamma(E)$  can be found:

$$J_\gamma(E) = \pm \sqrt{\frac{J^2(A \cos^2 \gamma + B \sin^2 \gamma) - E}{(A \cos^2 \gamma + B \sin^2 \gamma) - C}}. \quad (7.17)$$

Then the expression of action follows:

$$S(\gamma, J, E) = \int J_\gamma(E) d\gamma + S_0. \quad (7.18)$$

Eqs. (7.18) and (7.12) provide the complete solution for the total action  $S_{tot}(\varphi, \alpha, \gamma)$  of a free asymmetric top. The energy spectrum of a top is determined by the quantized action (7.18), as the energy enters only this part of the total action  $S_{tot}$ .

In the quasi-classical approximation the action  $S(\gamma)$  characterizes the phase of the wavefunction  $\psi \sim \exp[iS(\gamma)]$ . Consequently, the condition that  $\psi(\gamma)$  be a single-valued function leads to the following condition for quantization:

a) For trajectories with unbounded variations of azimuth  $\gamma$ :

$$\Delta S = \int_{\gamma}^{\gamma+2\pi} J_\gamma(E) d\gamma = 2\pi k_C, \quad k_C = J, J-1, \dots, \quad -\infty \leq \gamma \leq +\infty; \quad (7.19)$$

b) For trajectories with bounded variations of  $\gamma$ <sup>12</sup>:

---

<sup>12</sup>The Planck's constant is assumed unit,  $\hbar = 1$ , in Eq. (7.19) and below.

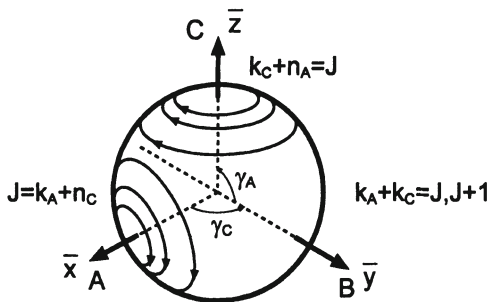


Figure 7.5: The shape of finite and infinite trajectories in azimuth angles  $\gamma_C$  and  $\gamma_A$ .

$$\Delta S = \oint J_\gamma(E) d\gamma = 2\pi \left( n_C + \frac{1}{2} \right), \quad n_C = 0, 1, 2, \dots, \quad \gamma_{\min} \leq \gamma \leq \gamma_{\max}. \quad (7.20)$$

The first condition in Eq. (7.19) is analogous to the quantization of the magnetic number  $m$  for particle motion in a centrally-symmetric field. The second quantization condition is the condition of Bohr-Sommerfeld for a particle in a one-dimensional potential well with two turning points.

If  $\gamma$  is the azimuth with respect to axis  $\bar{z}$ , then the first quantization condition corresponds to trajectories on the RE surface, which embrace axis  $\bar{z}$ . The second quantization condition corresponds to trajectories, embracing axis  $\bar{x}$  (see Fig. 7.5). The latter makes it possible to substitute the second quantization condition by the first one with axis  $\bar{x}$  substituted for  $J_\gamma$ . Then during the calculation of  $J_\gamma(E)$  according to Eq. (7.17) the parameters  $A$  and  $C$  should be exchanged one for another. In Eq. (7.19) the quantum number  $k_C$  corresponds to the precession of vector  $\mathbf{J}$  around the molecular axis  $\bar{z}$  with angular constant  $C$ . The quantum number  $n_C$  refers to the motion, finite in angle  $\gamma$ , when the vector  $\mathbf{J}$  precesses around the molecular axis  $x$  with the rotation constant  $A$  (Fig. 7.5).

With  $x$  axis taken for  $J_\gamma$  axis, the trajectories with  $k_C$  and  $n_C$  will have in correspondence the quantum numbers  $n_A$  and  $k_A$ . These numbers are determined by equations (7.19) and (7.20) as well, with  $A$  and  $C$  substituted one for another. Below we will prove the validity of the relations:

$$\begin{aligned} k_C + n_A &= J, \quad k_A + n_C = J, \\ k_C + k_A &= J \quad \text{or} \quad k_C + k_A = J + 1. \end{aligned} \quad (7.21)$$

Equations (7.21) demonstrate, that the choice of quantization axis is of

no importance: if Eqs. (7.19) and (7.20) are valid for axis  $z$ , they are valid for axis  $x$  as well. Substituting Eq. (7.17) into (7.19), and calculating the corresponding elliptic integrals, we arrive at the following equations for the energy spectrum:

1.  $\mathbf{J}$  precesses around axis  $z$ .

$$\begin{aligned}
 k_C &= \frac{J}{2\pi} \int_{\gamma}^{\gamma+2\pi} \sqrt{\frac{\varepsilon + \cos 2\gamma}{\varepsilon_0 + \cos 2\gamma}} d\gamma = \frac{J}{\pi} \int_{-1}^{+1} \sqrt{\frac{\varepsilon + x}{(\varepsilon_0 + x)(1 - x^2)}} dx \\
 &= \frac{2J}{\pi\sqrt{(\varepsilon + 1)(\varepsilon_0 - 1)}} \cdot \{(\varepsilon_0 + 1)\Pi - (\varepsilon_0 - \varepsilon)F\}, \\
 \Pi &= \Pi\left(\frac{\pi}{2}, \frac{-2}{(\varepsilon_0 - 1)}, \sqrt{\frac{2(\varepsilon_0 - \varepsilon)}{(\varepsilon + 1)(\varepsilon_0 - 1)}}\right), \\
 F &= F\left(\frac{\pi}{2}, \sqrt{\frac{2(\varepsilon_0 - \varepsilon)}{(\varepsilon + 1)(\varepsilon_0 - 1)}}\right), \\
 \varepsilon_0 &= \left(2\frac{C-A}{B-A} + 1\right) \geq \varepsilon = \left(2\frac{EJ^{-2}-B}{B-A} + 1\right) \geq 1, \\
 C &\geq B \geq A, \quad CJ^2 \geq E \geq BJ^2; \quad k_C = J, J-1, \dots
 \end{aligned} \tag{7.22}$$

and

$$\begin{aligned}
 n_A + \frac{1}{2} &= \frac{J}{2\pi} \int_{-\arccos(-\alpha)}^{\arccos(-\alpha)} \sqrt{\frac{\alpha + \cos \gamma}{\alpha_0 + \cos \gamma}} d\gamma \\
 &= \frac{J}{\pi} \int_{-\alpha}^{1} \sqrt{\frac{\alpha + x}{(\alpha_0 + x)(1 - x^2)}} dx, \\
 -1 &\leq \alpha = 1 - 2\frac{\varepsilon - 1}{\varepsilon_0 - 1} \leq \alpha_0 = 1 + \frac{4}{\varepsilon_0 - 1}, \\
 n_A &= 0, 1, 2.
 \end{aligned} \tag{7.23}$$

In Eqs. (7.22) and (7.23) the quantization formulas for one and the same trajectory with respect to the axes  $\bar{z}$  and  $\bar{x}$  are written out. The functions  $F(\varphi, k)$  and  $\Pi(\varphi, n, k)$  are elliptic integrals of I and III kind, respectively:

$$\begin{aligned}
 F(\varphi, k) &= \int_0^\varphi \frac{d\psi}{\sqrt{1 - k^2 \sin^2 \psi}}, \\
 \Pi(\varphi, n, k) &= \int_0^\varphi \frac{d\psi}{(1 - n \sin^2 \psi) \sqrt{1 - k^2 \sin^2 \psi}}.
 \end{aligned}$$

The precession of  $\mathbf{J}$  around axis  $x$  is calculated in an analogous way, and we will not consider it here in more detail. With the use of the formula

$$\int_b^a \sqrt{\frac{x-b}{(a-x)(x-c)(x-d)}} dx = \frac{2}{\sqrt{(a-c)(b-d)}} \times \left[ (d-a) \prod \left( \frac{\pi}{2}, \frac{b-a}{b-d}, \sqrt{\frac{(a-b)(c-d)}{(a-c)(b-d)}} \right) - (b-d) F \left( \frac{\pi}{2}, \sqrt{\frac{(a-b)(c-d)}{(a-c)(b-d)}} \right) \right], \quad d < c < b < a,$$

and with the use of equation (7.22), which relates the parameters  $(\varepsilon, \varepsilon_0)$  and  $(\alpha, \alpha_0)$ , it can be shown easily, that

$$\int_{-\alpha}^1 \sqrt{\frac{x+\alpha}{(x+\alpha_0)(1-x^2)}} dx = \int_{\varepsilon}^{\varepsilon_0} \sqrt{\frac{x-\varepsilon}{(\varepsilon_0-x)(x^2-1)}} dx. \quad (7.24)$$

From Eqs. (7.22) and (7.23) with the help of Eq. (7.24) the expression (7.21) can be obtained:

$$k_C + n_A + \frac{1}{2} = J + \frac{1}{2}.$$

The relation between  $k_C$  and  $k_A$  follows from the previous equation with the use of the following argument. The quantum numbers  $(k_C, n_A)$  (and, analogously,  $(k_A, n_C)$ ) are determined unambiguously with the help of Eq. (7.22) and (7.23) for each classical trajectory, which embraces axis  $\bar{z}$  ( $\bar{x}$ ). These are good quantum numbers, if the corresponding trajectories lie in the quasi-classical region of RE surface. At high values of  $\mathbf{J}$  the applicability of quasi-classical approach  $J_\gamma^2 \gg J_\gamma$  is violated only in the vicinity of the saddle point of RE surface, where  $\frac{\partial J_\gamma}{\partial E} \rightarrow \infty$ . In other words, the quasi-classical method breaks down only for trajectories, close to the separatrix line (the vicinity of dashed lines in Figs. 7.2 and 7.3). We note, that  $k_C$  and  $k_A$  can be interpreted as momentum projections upon axes  $C$  and  $A$  only in the limiting case of a symmetric top, when  $A = B$  or  $C = B$ . In the opposite case of an asymmetric top with a stationary axis of rotation and an arbitrary RE surface, these numbers are adiabatic invariants according to Eq. (7.19), and are good quantum numbers in the range of validity of the quasi-classical approach.

Each level with  $(k_C, n_A)$  and  $(k_A, n_C)$  is double-degenerate in accordance with the symmetric position of two phase curves (see Figs. 7.2, 7.3, and 7.5)

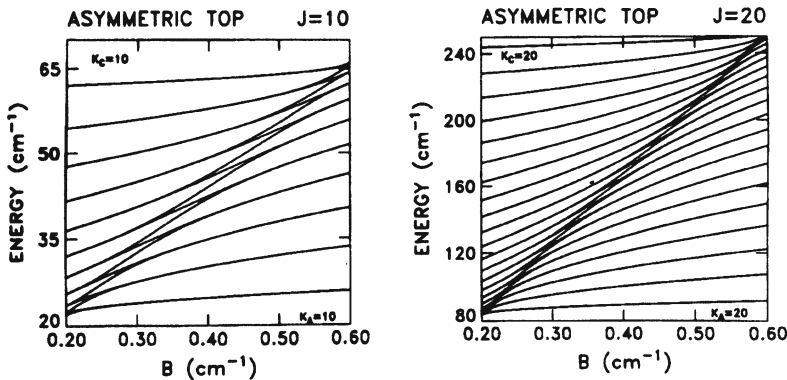


Figure 7.6: Level correlations of an asymmetric top molecule for  $J = 10$  (a) and  $J = 20$  (b). The constants  $A = 0.2 \text{ cm}^{-1}$  and  $C = 0.6 \text{ cm}^{-1}$  are fixed, while  $B$  varies in the range  $A < B < C$ . All the levels are clustered except those along the diagonals of the separatrix region on the RE - surface.

<sup>13</sup>. Let us examine, how the quantum level  $E(k_C, n_A)$  and the corresponding phase curve transforms into the level  $E(k_A, n_C)$  and its phase curve, when the rotation constant  $B$  tends to  $C$  (Fig. 7.6). As long as the classical trajectory goes far from the separatrix, the energy  $E_{k_C}(B)$  varies slowly with  $B$ . In the vicinity of the separatrix line, when  $E_{k_C}(B) \sim BJ^2$ , the level splits into two terms. For each one of these the quasi-classical nature of motion is violated, so that the action integrals (7.22) suffer abrupt changes on passing through the vicinity of the separatrix. Simultaneously, the phase curves from the ones, embracing axis  $\bar{z}$ , transform into the ones embracing axis  $\bar{x}$ . On leaving the vicinity of the separatrix line, when the difference  $|E - BJ^2|$  becomes big enough and the quasi-classical approach becomes valid, the action (7.22) becomes constant independent of  $B$ , but with respect to axis  $\bar{x}$  this time. Then the phase integral  $(n_A + \frac{1}{2})$  transforms into the integral along the curve, embracing axis  $A$ , and, according to quantization conditions, takes an integer value  $k_A$ , and, analogously, the integral  $k_C$  becomes  $(n_C + \frac{1}{2})$ .

The values of  $k_A$  will remain close to the preceding half-integer value  $(n_A + \frac{1}{2})$ , that is for one term  $k_A = n_A$ , whereas for the other  $k_A = n_A + 1$ . Analogously, in the reverse change of  $B$  from  $C$  to  $A$ , the term with quantum number  $n_C$  splits into two terms with  $k_C = n_C$  and  $k_C = n_C + 1$ .

Thus, each pair of symmetric phase curves in the quasi-classical region,

<sup>13</sup>In fact, these levels have anomalously low splitting due to sub-barrier tunneling (see below).

embracing axis  $C$ , has in correspondence two quantum levels with quantum numbers  $(k_C, k_A = n_A)$  and  $(k_C, k_A = n_A + 1)$ , whereas for curves embracing axis  $A$  the numbers are  $(k_A, k_C = n_C)$  and  $(k_A, k_C = n_C + 1)$ . Obviously, the pair  $(k_A, k_C)$  satisfies equation (7.21):  $k_A + k_C = J$  or  $k_A + k_C = J + 1$ .

The behavior of terms  $E_{k_C}(B) = E_{n_A}(B)$  and  $E_{k_A}(B) = E_{n_C}(B)$  can be seen clearly in Fig. 7.6 from Ref. [18]. For example, the level with  $(k_C = 7, n_A = 3)$  upon the change of  $B$  from  $A = 0.2$  to  $C = 0.6$  splits into two levels with  $(k_A = 3, n_C = 7)$  and  $(k_A = 4, n_C = 6)$ . The phase integrals (7.22) and (7.23), that is the numbers  $(k_C, n_A + \frac{1}{2})$  and  $(n_C + \frac{1}{2}, k_A)$ , suffer abrupt changes of the order of  $\frac{1}{2}$  in the vicinity of the separatrix line ( $E \sim BJ^2$ ), where level splitting occurs. Such behavior agrees completely with the preceding discussion of quantum numbers  $k_A$  and  $k_C$ .

Due to the symmetry of RE surface with respect to the transformation  $\mathbf{J} \rightarrow -\mathbf{J}$  the quasi-classical energy levels of the effective rotation Hamiltonian  $H(\mathbf{J})$  are at least two times degenerate. In the general case of an arbitrary RE surface the degeneracy of a level is equal to the number of equivalent stable stationary axes of rotation. For example, the system with RE surface in Fig. 7.3 has a six-time degenerate level, which corresponds to six symmetric phase curves, embracing the symmetry axes of fourth order, and another eight-times degenerate quantum level, which corresponds to eight symmetrical phase curves, embracing axes of third order. These degenerate levels reveal super-fine splitting due to sub-barrier tunneling. In the vicinity of the separatrix this splitting transforms into the usual one — of the order of rotation quantum  $BJ$ . In this area rotation terms of different symmetry transform one into another, — just as in the case of an asymmetric top the precession around axis  $\bar{z}$  goes over into precession with respect to axis  $\bar{x}$ :  $(k_C, n_A + \frac{1}{2}) \rightarrow (n_C + \frac{1}{2} = k_C \pm \frac{1}{2}, k_A = n_A + \frac{1}{2} \mp \frac{1}{2})$ . Obviously, the relation between the quantum numbers of terms for such a transition depends upon the symmetry of RE surface solely: the formula  $k_A = n_A + \frac{1}{2} \mp \frac{1}{2}$  does not depend upon the particular values of rotation constants for an asymmetric top.

The group of superfine split levels we will term a rotation cluster, and the level structure inside the cluster — the super-fine structure, as opposed to the fine structure, which characterizes the rotation levels for constant  $J$ . The splitting due to the interaction with nuclear spins in this context is termed hyperfine splitting.

To sum up, we have demonstrated the clusterization of rotation levels at high values of momentum  $J \gg 1$ , at least for molecules in the ground electronic-rotational state. The higher is the molecule symmetry, and, consequently, the symmetry of RE surface, the higher is the multiplicity of the cluster. For octahedral symmetry the cluster can consist of eight levels. Now let us prove this by a direct calculation. To find the spectrum of an asymmetric top in a quasi-classical approximation we utilize Eq. (7.22). The

$n_z$	$E_n(QM)^{(a)}$	$E_n(SC)^{(b)}$	$S(QM)^{(a)}$	$S(SC)^{(b)}$
$J = 10$				
10	63.181	63.176	$2.16 \cdot 10^{-7}$	$1.96 \cdot 10^{-7}$
9	57.851	57.842	$1.93 \cdot 10^{-5}$	$1.87 \cdot 10^{-5}$
8	53.147	53.133	$6.98 \cdot 10^{-4}$	$6.91 \cdot 10^{-4}$
7	49.113	49.084	$1.27 \cdot 10^{-2}$	$1.29 \cdot 10^{-2}$
6	25.833	45.781	$1.11 \cdot 10^{-1}$	$1.20 \cdot 10^{-1}$
$J = 20$				
20	246.392	240.347		$1.25 \cdot 10^{-14}$
19	235.360	235.354	$2.84 \cdot 10^{-12}$	$2.66 \cdot 10^{-12}$
18	224.977	224.970	$2.55 \cdot 10^{-12}$	$2.49 \cdot 10^{-10}$
17	215.214	215.205	$1.42 \cdot 10^{-8}$	$1.40 \cdot 10^{-8}$
16	206.013	206.071	$5.33 \cdot 10^{-7}$	$5.29 \cdot 10^{-7}$
15	197.603	197.586	$1.41 \cdot 10^{-5}$	$1.41 \cdot 10^{-5}$
14	189.801	189.777	$2.71 \cdot 10^{-4}$	$2.72 \cdot 10^{-4}$
13	182.721	182.884	$3.76 \cdot 10^{-3}$	$3.80 \cdot 10^{-3}$
12	176.448	176.382	$3.64 \cdot 10^{-2}$	$3.75 \cdot 10^{-2}$
11	171.132	171.029	$2.18 \cdot 10^{-1}$	$2.38 \cdot 10^{-1}$

Table 7.1: <sup>(a)</sup>  $QM$  — Quantum-mechanical diagonalization, Eq. (7.2). <sup>(b)</sup>  $SC$  — Semi-classical calculation. In both cases  $A = 0.2$ ,  $B = 0.4$ ,  $C = 0.6$ . The energy is measured in units  $cm^{-1}$ . The quantum number  $n_z$  is  $n_z = k_C = k_z$ . In our notations  $S$  is the overlap integral denoted by  $W$ , Eq. (7.25).

elliptic integrals, entering Eq. (7.22) have to be calculated, and the functional dependence  $k_C(E)$  plotted. Then the inverse function  $E(k_C)$  can be obtained in graphical form, its values in integer points reproducing the required spectrum. Alternatively, the quantum calculation by direct diagonalization of the Hamiltonian (7.2) enables the verification of the accuracy of the quasi-classical approximation, and the quantitative proof of the clusterization effect, which has been discussed within the concept of RE surface. The results of both approaches are provided in Table 7.1. The calculations have been performed for an asymmetric top  $A = 0.2$ ,  $B = 0.4$ ,  $C = 0.6 \text{ cm}^{-1}$  with  $J = 10, 20$ . It can be seen easily, that the quasi-classical calculation reproduces the result with the accuracy at least up to three orders. For  $J = 20$  the agreement is better, than for  $J = 10$ , as it should be on the basis of general principles. The two last columns reproduce the quantity  $S$ , which characterizes the overlap integral for the top wavefunction in the sub-barrier region of phase space<sup>14</sup>. The quantity  $S$  determines the super-fine splitting of rotation terms. Let us demonstrate that in more detail.

As it is well known, the escape probability for the particle to leave the well per unit time (or the decrease of the probability to stay in the well  $\frac{dP}{dt} = \Gamma$ ) due to sub-barrier tunneling, is determined by the equation  $\Gamma = T^{-1} \exp(-2\theta)$ , where  $\theta = \text{Im} \int_{C_t} J(\gamma) d\gamma$  is the sub-barrier action, and  $T$  is the period of motion in the well (see, for example, Ref. [81]). On the other hand, the probability to leave the well, according to Fermi golden rule, can be presented in the form:

$$\Gamma = \left| \frac{dP}{dt} \right| = \frac{2\pi}{\hbar} |W|^2 \frac{dn}{dE},$$

where  $W = \langle 1 | H | 2 \rangle$  is the matrix element between the states of the particle in different wells, which is produced by the part of the total Hamiltonian  $H$  introducing inter-well transitions. Obviously, this matrix element is determined by the overlap of states in different wells  $\langle 1 | 2 \rangle$ . The density of states at energy  $E$  is given by  $\frac{dn}{dE} \sim (\hbar\omega_E)^{-1} = T(2\pi\hbar)^{-1}$ . Equating the two expressions of  $\Gamma$  we find the matrix element  $W = |\langle 1 | H | 2 \rangle|$ :

$$\langle 1 | H | 2 \rangle = W = \frac{\hbar}{T} \exp \left[ -|\theta| \pm i \text{Re} \int_{C_t} J_\gamma d\gamma \right]. \quad (7.25)$$

Equation (7.25) expresses the nondiagonal matrix element between two degenerate quasi-classical levels through the tunnel integral along the path  $C_t$  from the state  $|1\rangle$  into  $|2\rangle$ . If there are several equivalent paths, then, obviously, the matrix element  $W$  is provided by the corresponding sum  $W = \sum_i W_i$ , as  $\langle 1 | H | 2 \rangle$  is proportional to the sum of all possible integral overlaps

---

<sup>14</sup>For tunneling between wells this is the region of  $q$ -space beneath the barrier  $U(q) > E$ . For above-barrier reflection this is the region of  $p$ -space between the two wave-packets at the points  $\mathbf{p}_0$  and  $-\mathbf{p}_0$  respectively.

of wavefunctions  $\langle q | 1 \rangle$  and  $\langle q | 2 \rangle$ . Here only the overlap integrals with the leading terms in the exponent  $\exp(|\theta|)$  are taken into account [81]. The path, along which the integral  $\theta$  is calculated, lies in the complex plane of phase space, as the classical transition between the starting and end points is impossible. The path is chosen in such a way, that the quasi-classical wavefunction  $\psi \sim \exp[iS(\gamma)]$  decreases along it. Correspondingly, the probability of the transition  $|1\rangle \rightarrow |2\rangle$  is low<sup>15</sup>.

For an asymmetric top the action  $S(\gamma)$  is given by Eq. (7.22), where the upper limit  $2\pi$  should be substituted by  $\gamma$ . Then the phase  $S(\gamma)$  of the wavefunction after the overturn of vector  $\mathbf{J}$  in a symmetric position is given by:

$$S(\gamma) = J \int_0^\gamma \sqrt{\frac{\varepsilon + \cos 2\gamma'}{\varepsilon_0 + \cos 2\gamma'}} d\gamma'.$$

The last equation reveals the fact, that the integral over the specified contour reverses the sign of the wavefunction phase  $\exp[iS(r)] \rightarrow \exp[-iS(r)]$ , that is it describes the transition of vector  $\mathbf{J}$  to the symmetrical phase curve on the RE-surface. The tunneling integral is provided by the imaginary part of this expression:

$$\begin{aligned} \theta &= \text{Im } S(\gamma) = 2J \int_{\frac{\pi}{2}}^{\frac{\pi}{2}+i\gamma} \sqrt{\frac{\varepsilon + \cos(\pi + 2i\beta)}{\varepsilon_0 + \cos(\pi + 2i\beta)}} d\beta \\ &= J \int_1^\varepsilon \sqrt{\frac{\varepsilon - z}{(\varepsilon_0 - z)(z^2 - 1)}} dz = J \frac{2(\varepsilon_0 - \varepsilon)}{\sqrt{(\varepsilon_0 - 1)(\varepsilon + 1)}} \cdot (\Pi - F), \\ \Pi &= \Pi \left( \frac{\pi}{2}, \frac{\varepsilon - 1}{\varepsilon_0 - 1}, \sqrt{\frac{(\varepsilon - 1)(\varepsilon_0 + 1)}{(\varepsilon_0 - 1)(\varepsilon + 1)}} \right), \\ F &= F \left( \frac{\pi}{2}, \sqrt{\frac{(\varepsilon - 1)(\varepsilon_0 + 1)}{(\varepsilon_0 - 1)(\varepsilon + 1)}} \right). \end{aligned} \quad (7.26)$$

The overlap integral (7.25) with the account of Eq. (7.26) is given in the last column of Table 7.1. In the third column the results of a quantum calculation with the help of Hamiltonian (7.2) are provided. Obviously, the agreement is very good, though the quasi-classical approach guarantees only the exponential accuracy.

In the calculation of splitting of terms one should take into account, that there are two paths for tunneling:  $\gamma_+ = \frac{\pi}{2} + i\beta$  and  $\gamma_- = -\frac{\pi}{2} + i\beta$ . In the end, for the matrix element  $\langle 1 | H | 2 \rangle$  of an asymmetric top we obtain:

---

<sup>15</sup>The probability  $\exp[iS(\gamma)]$  increases along the path, corresponding to the inverse transition  $|2\rangle \rightarrow |1\rangle$ .

$$\langle 1 | H | 2 \rangle = \frac{2}{T} e^{-|\theta|}, \quad (7.27)$$

Consequently, the splitting inside the cluster is  $\Delta E = \frac{4}{T} \exp(-|\theta|)$ .

For  $J = 20$  the "less split-up" cluster in Table 7.1 is the one with  $k_z = 20$ , for which the tunneling integral is  $T^{-1} \exp(-|\theta|) = 1.25 \cdot 10^{-14} \text{ cm}^{-1}$ , and the splitting is  $5 \cdot 10^{-14} \text{ cm}^{-1}$ , according to Eq. (7.27). Such a splitting corresponds to beat evolution with the period  $\tau \sim \hbar(\Delta E)^{-1} \sim 22 \text{ (min)}$ . It means, that in physical processes with the duration less than 22 minutes, as for example, the hyperfine interaction of the nuclear spin with rotation, the molecule reveals reduced symmetry, and can be considered as rotating around the fixed axis  $\bar{z}$ . During this time the vector  $\mathbf{J}$  will not overturn with respect to the molecule, whereas the nuclear wavefunctions of different symmetry can get mixed completely due to the hyper-fine interaction of nuclear spins with molecule rotation. As a consequence in the spectra of rotation bands there will appear the lines, which are typically prohibited by selection rules due to symmetry of nuclear spins.

The rotation Hamiltonian (7.3) of a semi-rigid molecule of octahedral symmetry can be considered in an analogous way. We will not provide the corresponding details here. Instead, we write out the quasi-classical Hamiltonian  $H(\gamma, J_\gamma)$  for the two cases: 1) when the axis of fourth order is chosen as axis  $\bar{z}$ ; 2) when for axis  $\bar{z}$  the axis of third order is chosen (see Fig.7.3).

1) An axis of fourth order is chosen for  $\bar{z}$ .

$$H(J_\gamma, \gamma) = BJ^2 + 10t_{044}J_\gamma^4 (\cos^4 \gamma + \sin^4 \gamma + 1) - 10t_{044} \left[ 2J^2 J_\gamma^2 (\cos^4 \gamma + \sin^4 \gamma) - J^4 \left( \cos^4 \gamma + \sin^4 \gamma - \frac{3}{5} \right) \right], \quad (7.28)$$

where  $(J_\gamma, \gamma)$  are related to  $J_{\bar{x}}, J_{\bar{y}}, J_{\bar{z}}$  by equations (7.15), which are substituted further in Eq. (7.3).

2) An axis of third order is chosen for  $\bar{z}$ :

$$H(J_\gamma, \gamma) = BJ^2 + 10t_{044} \left[ -\frac{7}{6}J_\gamma^4 + J^2 J_\gamma^2 + \frac{2\sqrt{2}}{3}J_\gamma (J^2 - J_\gamma^2)^{3/2} \times \sin 3\gamma - \frac{1}{10}J^4 \right]. \quad (7.29)$$

For the derivation of Eq. (7.29) new momenta  $J'_{\bar{x}}, J'_{\bar{y}}, J'_{\bar{z}}$  are introduced according to the formulas:

$$J'_{\bar{x}} = \frac{1}{\sqrt{2}} (J_{\bar{x}} - J_{\bar{y}}),$$

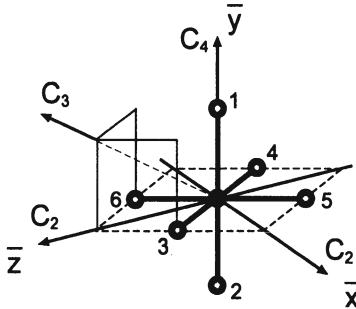


Figure 7.7: Body axes for a molecule of octahedral symmetry  $SF_6$ , used in the semi-classical analysis of clusters  $|m_3\rangle$

$$\begin{aligned} J'_{\bar{y}} &= \frac{1}{\sqrt{6}} (J_{\bar{x}} + J_{\bar{y}} - 2J_{\bar{z}}), \\ J'_{\bar{z}} &= \frac{1}{\sqrt{3}} (J_{\bar{x}} + J_{\bar{y}} + J_{\bar{z}}). \end{aligned} \quad (7.30)$$

These are expressed subsequently with the help of Eqs. (7.15) through  $(J_\gamma, \gamma)$  in the new basis set, and after the substitution of  $J_{\bar{x}_i}$  ( $J'_{\bar{x}_i}(J_\gamma, \gamma)$ ) into equation (7.3) reproduce Eq. (7.29).

The system with Hamiltonian (7.28) within the quasi-classical approach can be solved in analytic form, as the equation  $H(J_\gamma, \gamma) = E$  is bi-quadratic with respect to  $J_\gamma$ , and thus it can be solved exactly. The analogous equation for the Hamiltonian (7.29) should be solved numerically.

The results of the calculation of the rotation spectrum and overlap integrals (7.25) are provided in Table 7.2, reproduced from Ref. [18]. The calculation has been performed for molecule  $SF_6$  with  $B = 0.091083 \text{ cm}^{-1}$ ,  $t_{044} = 5.44 \text{ Hz}$ . The energy is measured from  $E_0 = BJ^2$ . Positive values of energy correspond to the precession of  $\mathbf{J}$  around the axis of fourth order, while negative energy is for axes of third order. More details of the calculation can be found in [109]. In Refs. [110, 111, 112] one can find details of the calculation of the super-fine structure by the method of tunnel matrix with the use of overlap integrals, provided in Table 7.2. Besides, the classification of clusters according to the symmetry of octahedral group depending on the local symmetry (see below), i.e. as function of quantum numbers  $k_C, k_A$ , is provided there as well.

In conclusion, we provide the expression of the rotation Hamiltonian for a semi-rigid molecule (7.28), when two axes of second order are chosen for axes  $\bar{z}$  and  $\bar{x}$ , while  $\bar{y}$  is the axis of fourth order, perpendicular to them (see Fig. 7.7):

$n_{\bar{z}}$	$E_n(QM)^{(a)}$	$E_n(SC)^{(b)}$	$S(QM)^{(a)}$	$S(SC)^{(b)}$
$J = 30$				
$n_4$				
30	$5.31 \cdot 10^{-4}$	$5.29 \cdot 10^{-4}$	$2.63 \cdot 10^{-11}$	$2.50 \cdot 10^{-11}$
29	$3.54 \cdot 10^{-4}$	$3.53 \cdot 10^{-4}$	$9.55 \cdot 10^{-10}$	$9.57 \cdot 10^{-10}$
28	$2.04 \cdot 10^{-4}$	$2.03 \cdot 10^{-4}$	$1.53 \cdot 10^{-8}$	$1.56 \cdot 10^{-8}$
27	$0.80 \cdot 10^{-4}$	$0.79 \cdot 10^{-4}$	$1.42 \cdot 10^{-7}$	$1.47 \cdot 10^{-7}$
26	$-0.20 \cdot 10^{-4}$	$-0.22 \cdot 10^{-4}$	$8.32 \cdot 10^{-7}$	$8.65 \cdot 10^{-7}$
25	$-0.97 \cdot 10^{-4}$	$-1.00 \cdot 10^{-4}$	$2.34 \cdot 10^{-6}$	$3.20 \cdot 10^{-6}$
$n_3$				
30	$-3.57 \cdot 10^{-4}$	$-3.54 \cdot 10^{-4}$	$1.75 \cdot 10^{-7}$	$1.69 \cdot 10^{-7}$
29	$-2.48 \cdot 10^{-4}$	$-2.44 \cdot 10^{-4}$	$-2.02 \cdot 10^{-6}$	$2.15 \cdot 10^{-6}$
28	$-1.68 \cdot 10^{-4}$	$-1.66 \cdot 10^{-4}$	$6.59 \cdot 10^{-6}$	$7.40 \cdot 10^{-6}$
$n_4$				
$J = 88$				
88	$4.206 \cdot 10^{-2}$	$4.205 \cdot 10^{-2}$	$1.73 \cdot 10^{-23}$	$1.62 \cdot 10^{-23}$
87	$3.728 \cdot 10^{-2}$	$3.727 \cdot 10^{-2}$	$2.17 \cdot 10^{-21}$	$2.13 \cdot 10^{-21}$
86	$3.275 \cdot 10^{-2}$	$3.273 \cdot 10^{-2}$	$1.31 \cdot 10^{-19}$	$1.30 \cdot 10^{-19}$
85	$2.845 \cdot 10^{-2}$	$2.844 \cdot 10^{-2}$	$5.12 \cdot 10^{-18}$	$5.11 \cdot 10^{-18}$
84	$2.440 \cdot 10^{-2}$	$2.438 \cdot 10^{-2}$	$1.44 \cdot 10^{-16}$	$1.44 \cdot 10^{-16}$
83	$2.056 \cdot 10^{-2}$	$2.055 \cdot 10^{-2}$	$3.12 \cdot 10^{-15}$	$3.13 \cdot 10^{-15}$
82	$1.695 \cdot 10^{-2}$	$1.604 \cdot 10^{-2}$	$5.41 \cdot 10^{-14}$	$5.44 \cdot 10^{-14}$
81	$1.356 \cdot 10^{-2}$	$1.355 \cdot 10^{-2}$	$7.71 \cdot 10^{-13}$	$7.77 \cdot 10^{-13}$
80	$1.038 \cdot 10^{-2}$	$1.037 \cdot 10^{-2}$	$9.19 \cdot 10^{-12}$	$9.28 \cdot 10^{-12}$
79	$0.741 \cdot 10^{-2}$	$0.739 \cdot 10^{-2}$	$9.30 \cdot 10^{-11}$	$9.40 \cdot 10^{-11}$
78	$0.473 \cdot 10^{-2}$	$0.452 \cdot 10^{-2}$	$8.04 \cdot 10^{-10}$	$8.15 \cdot 10^{-10}$
77	$0.205 \cdot 10^{-2}$	$0.204 \cdot 10^{-2}$	$5.99 \cdot 10^{-9}$	$6.09 \cdot 10^{-9}$
76	$-0.033 \cdot 10^{-2}$	$-0.034 \cdot 10^{-2}$	$3.86 \cdot 10^{-8}$	$3.93 \cdot 10^{-8}$
75	$-0.252 \cdot 10^{-2}$	$-0.254 \cdot 10^{-2}$	$2.15 \cdot 10^{-7}$	$2.20 \cdot 10^{-7}$
74	$-0.542 \cdot 10^{-2}$	$-0.454 \cdot 10^{-2}$	$1.04 \cdot 10^{-6}$	$1.06 \cdot 10^{-6}$
73	$-0.633 \cdot 10^{-2}$	$-0.636 \cdot 10^{-2}$	$4.23 \cdot 10^{-6}$	$4.24 \cdot 10^{-6}$
72	$-0.794 \cdot 10^{-2}$	$-0.798 \cdot 10^{-2}$	$1.44 \cdot 10^{-5}$	$1.56 \cdot 10^{-5}$
71	$-0.933 \cdot 10^{-2}$	$-0.939 \cdot 10^{-2}$	$4.46 \cdot 10^{-5}$	$4.54 \cdot 10^{-5}$
$n_3$				
88	$-2.86 \cdot 10^{-2}$	$-2.804 \cdot 10^{-2}$	$1.24 \cdot 10^{-11}$	$1.17 \cdot 10^{-11}$
87	$-2.493 \cdot 10^{-2}$	$-2.491 \cdot 10^{-2}$	$6.06 \cdot 10^{-10}$	$5.97 \cdot 10^{-10}$
86	$-2.204 \cdot 10^{-2}$	$-2.201 \cdot 10^{-2}$	$1.37 \cdot 10^{-8}$	$1.37 \cdot 10^{-8}$
85	$-1.938 \cdot 10^{-2}$	$-1.935 \cdot 10^{-2}$	$1.90 \cdot 10^{-7}$	$1.94 \cdot 10^{-7}$
84	$-1.697 \cdot 10^{-2}$	$-1.693 \cdot 10^{-2}$	$1.79 \cdot 10^{-6}$	$1.87 \cdot 10^{-6}$
83	$-1.482 \cdot 10^{-2}$	$-1.477 \cdot 10^{-2}$	$1.17 \cdot 10^{-5}$	$1.22 \cdot 10^{-5}$
82	$-1.297 \cdot 10^{-2}$	$-1.290 \cdot 10^{-2}$	$5.07 \cdot 10^{-5}$	$5.63 \cdot 10^{-5}$
81	$-1.146 \cdot 10^{-2}$	$-1.142 \cdot 10^{-2}$	$1.48 \cdot 10^{-5}$	$1.50 \cdot 10^{-5}$

Table 7.2: <sup>(a)</sup>  $QM$  — Quantum-mechanical diagonalization, Eq. (7.3). <sup>(b)</sup>  $SC$  — Semi-classical calculation.

$$\begin{aligned}
E = & H(J_\gamma, \gamma) = BJ^2 \\
& + 10t_{044} [J_\gamma^4 (\cos^4 \gamma + 2 \sin^4 \gamma - 6 \cos^2 \gamma) / 2 \\
& - J_\gamma^2 J^2 (\cos^4 \gamma + 2 \sin^4 \gamma - 3 \cos^2 \gamma) \\
& + J^4 (\cos^4 \gamma + 2 \sin^4 \gamma - 6/5) / 2] .
\end{aligned} \tag{7.31}$$

The expression (7.31) is convenient for the semi-classical analysis of the structure of rotation clusters, which correspond to the rotation of the molecule  $SF_6$  with respect to soft axes of third order. The equation  $E = H(P_\gamma, \gamma)$  in the form (7.31) is bi-quadratic with respect to  $J_\gamma$ , and thus it enables the determination of function  $J_\gamma(\gamma, E)$  and of the corresponding tunnel integral  $|\theta|$  with the tunnel action  $S \sim \exp(-|\theta|)$ .

We note, that for large  $J_\gamma$  the motion with respect to angle  $\gamma$  is always finite (the trajectory embraces axis  $C_3$ , but not axis  $\bar{z}$ ). This can be seen readily from Fig.7.3. Thus, the change of the direction of rotation axis  $C_3$  in terms of Hamiltonian (7.31) is a process, analogous to particle tunneling from one potential well into another. In the present case it is the molecular rotation axis, which tunnels in the body system. In the laboratory frame that looks like an abrupt spontaneous overturn of the molecule.

### 7.3 Symmetry - based analysis of rotational clusters

In this Section we will consider the symmetry properties of rotational levels in the cluster. We will also provide examples of diagonalization of the tunneling matrix and of the corresponding splitting of levels inside the cluster, following the works of W.G.Harter and C.W.Patterson [110, 111, 112].

The clusterization of rotation levels is revealed most transparently for large values of  $J$ , when the quasi-classical approximation is valid. Thus, below we will use the term rotation cluster for the set of classical trajectories on RE-surface (Fig.7.2 and 7.3), which for the transformations from the molecular symmetry group (symmetry of RE-surface) go one into another. This does not limit the generality of the symmetry analysis, but provides additional clarity of consideration. This is most convenient in the analysis of the emerging and vanishing stable rotation axes with the change of momentum  $J$  or of other parameters of the molecule (see Section 8.2 and below).

The main idea of symmetry analysis of rotational clusters, and the smallness of level splitting inside the cluster is illustrated most transparently by Fig.7.8 from [18]. It shows the RE-surfaces of Hamiltonian (7.3) with the trajectories, corresponding to the rotation around axes of third order ( $C_3$

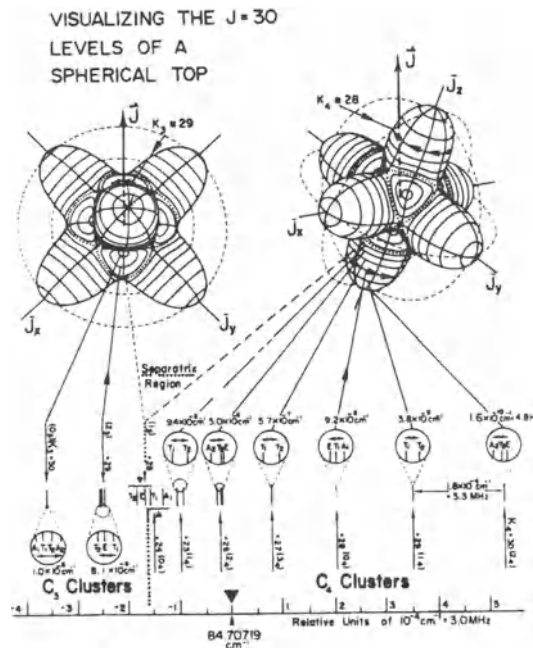


Figure 7.8: Rotational spectrum of an octahedral spherical top molecule for  $J = 30$  with the corresponding semiclassical trajectories.

clusters) and axes of fourth order ( $C_4$  cluster). The symmetry of split-up levels and the magnitude of splitting (cluster width) are provided there as well. We note the extremely small magnitude of the splitting  $\sim 10^{-6} \div 10^{-10} \text{ cm}^{-1}$ , which resembles the analogous small splitting of local modes for the stretching vibrations. This is no coincidence in fact, as in both cases we have equivalent weakly bound nonlinear Hamilton systems. These properties always provoke clusterization of levels, as it has been discussed above.

The molecule  $XY_6$  can be imagined as a system of nuclei, bound by elastic springs along  $XY$  bonds. The springs, related to angular vibrations have low rigidity. Then the  $C_3$  axis will be a "soft axis", while  $C_4$  axis — a "hard" one. The deformation of the molecule during rotation with respect to these axes are shown in Fig. 7.9 from Ref. [112].

The symmetry type of the rotation level (state) can be defined conveniently within the terms of RE-surface and classical trajectories, which are generated on this surface by vector  $j$  in the course of molecule rotation, see Fig. 7.8. The point group, which leaves the RE-surface intact, is called its symmetry group. The regular representation of this group is the sub-group

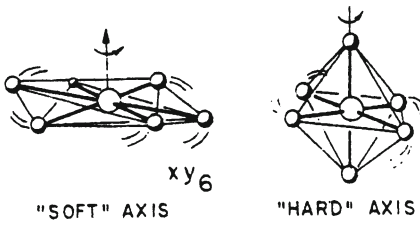


Figure 7.9: Rotation and deformation of molecule  $XY_6$  with respect to axes  $C_3$ , (a) and  $C_4$ , (b).

of orthogonal matrices from  $O(3)$ , which, upon transforming the momenta  $J_{\bar{x}}, J_{\bar{y}}, J_{\bar{z}}$ , leave the rotation Hamiltonian of the molecule  $H(J_{\bar{x}_i})$  invariant. For the asymmetric top this is the Hamiltonian (7.2) and the corresponding group is  $D_2 \otimes C_i = D_{2h}$ . For a semi-rigid molecule of octahedral symmetry this is the Hamiltonian (7.3), and the corresponding groups are  $O \otimes C_i = O_h$  for  $XY_6$  and  $T_d \otimes C_i$  for  $XY_4$ <sup>16</sup>. If the rotational wavefunctions of the molecule are represented as  $\Psi(\varphi, \theta, \gamma)$ , where  $(\varphi, \theta, \gamma)$  are Euler angles, then the representation of the point symmetry group acts upon these functions in the following manner<sup>17</sup>:

$$\begin{aligned} J_{\bar{x}'_i} &= \Lambda_{ij} J_{\bar{x}_j}, \quad J_{\bar{x}'_i} = \exp [iJ_\nu n_\nu(\Lambda)] J_{\bar{x}_i} \exp [-iJ_\nu n_\nu(\Lambda)], \\ \Psi'(\varphi, \theta, \gamma) &= \exp [iJ_\nu n_\nu(\Lambda)] \Psi(\varphi, \theta, \gamma), \\ \nu &= \bar{x}, \bar{y}, \bar{z}, \Lambda_{ij} \in O(3). \end{aligned} \quad (7.32)$$

Here  $n_\nu(\Lambda)$  is the component of the rotation vector, around which the body axes turn;  $\Lambda_{ij}$  is the orthogonal matrix of the group  $O(3)$ , corresponding to this rotation. The matrix elements of the rotation operator (7.32) calculated with the wavefunctions of the symmetric top  $|J, M, K\rangle$  are given by the known Wigner functions  $D_{M,K}^J(\varphi, \theta, \gamma)$ <sup>18</sup>.

The operator (7.32) realize the so called representation of the inner molecular symmetry group [96], as opposed to the representation of the external field symmetry group ( $O(3)$  for the free molecule,  $O(2)$  for the molecule in

<sup>16</sup>The symmetry group of RE-surface is the product of the molecular symmetry group and of inversion  $C_i$ . The invariance of the rotation Hamiltonian with respect to the transformation  $J_{\bar{x}} \rightarrow -J_{\bar{x}_i}$  follows from time reversibility.

<sup>17</sup>The new functions  $\Psi'$  in the old system are chosen in such a way that  $J_{\bar{x}'_i} \Psi' = \lambda \Psi'$  follows from  $J_{\bar{x}} \Psi = \lambda \Psi$ .

<sup>18</sup>The functions  $D_{M,K}^J(\varphi, \theta, \gamma)$  during orthogonal transformations of the internal axes of the molecule are transformed in the same way as the spherical functions  $(Y_J^K(\theta, \varphi))^*$  are transformed during the similar transformation of the laboratory frame.

a uniform external electric field, etc.). In the quasi-classical limit the representation (7.32) can be imagined as the property of classical trajectories on the RE-surface to get transformed one into another in the course of RE-surface transformations into itself. Within such an approach the top state, corresponding to  $C_3$  and  $C_4$  clusters are represented by the following linear combination of Dirac ket-vectors:

$$\begin{aligned} |\Psi_{C_4}\rangle &= \sum_{i=1}^6 |k_4, i\rangle \psi_i^{(4)}, \quad C_4 \text{ — cluster;} \\ |\Psi_{C_3}\rangle &= \sum_{i=1}^8 |k_3, i\rangle \psi_i^{(3)}, \quad C_3 \text{ — cluster.} \end{aligned} \quad (7.33)$$

Here  $|k_4, i\rangle$  is the ket-vector, corresponding to the classical trajectory on the  $i$ -th hill of RE-surface, which received after the quasi-classical quantization the quantum number  $k_4$ . Analogously, the vector  $|k_3, i\rangle$  corresponds to the trajectory in  $i$ -th hollow of RE-surface, which received during quantization along the  $C_3$  axis  $i$  the quantum number  $k_3$ , Fig. 7.8.

Obviously the action of the symmetry group representation of RE-surface in the space (7.33) is reduced to the linear transformation of coefficients  $\psi_i^{(3,4)}$  one through the other. The representation, acting in this space, is typically a reducible one. Expanding this representation into irreducible ones, we determine the number of levels of different symmetry, which compose one rotation cluster. Levels with different  $k_3, k_4$  correspond to different rotation clusters. For the molecule  $SF_6$  the distance between clusters is  $\sim 10^{-4} \text{ cm}^{-1}$  for  $J = 30$  and  $\sim 10^{-2} \text{ cm}^{-1}$  for  $J = 88$ , see Table 7.2. The splitting between levels inside the cluster are of the order of magnitude of the overlap integral  $S$ , and according to the cited Table is at least two orders of magnitude smaller, than the distance between the clusters. For clusters with  $k \sim J$  the splitting inside them are many orders of magnitude smaller, than the distance between them. From Table 7.2 it can be seen, that for  $J = n_4 = 30$ ,  $S$  is  $\sim 10^{-11} \text{ cm}^{-1}$  with  $\Delta E_{k_4} \sim 10^{-4} \text{ cm}^{-1}$ , while for  $J = n_4 = 88$ ,  $S$  is  $\sim 10^{-23} \text{ cm}^{-1}$  with  $\Delta E_{k_4} \sim 10^{-2} \text{ cm}^{-1}$ .

A regular method of expansion into irreducible representations of cluster sub-spaces in the form (7.33) is described in Ref. [112]. Here we will give a brief summary of it.

The symmetry analysis of the rotation cluster is based on the correlation of irreducible representations of two symmetry groups. One of them is the symmetry of RE-surface, while the other is the local symmetry of the considered classical trajectory. For example,  $D_2 = \{1, R_{2\bar{x}}, R_{2\bar{y}}, R_{2\bar{z}}\}$  is the rotational symmetry of RE-surface for an asymmetric top (Fig. 7.2), while  $\{R_{2\bar{z}}, 1\} = C_2(\bar{z})$  is the local symmetry of the trajectory with respect to axis  $\bar{z}$ . Analogously  $C_2(\bar{x}) = \{1, R_{2\bar{x}}\}$ , is the local symmetry of trajectories

with respect to axis  $\bar{x}$ . The group  $C_2(\bar{x}_i)$  is the sub-group  $D_2$  of the group  $D_2$ . Obviously, this is a general property: the local symmetry group of the trajectory always is a sub-group of the RE-surface symmetry group.

Below we demonstrate for the RE-surface of an asymmetric top (Fig. 7.2), how the irreducible components of the rotation cluster can be obtained.

Let us consider a  $C_2(\bar{z})$  cluster. The representation of the  $D_2$  group can be split into two sub-spaces: one corresponds to the symmetric representation of the  $C_2(\bar{z})$  group, while the other — to the antisymmetric one. The vectors of a symmetric representation we denote by  $|0_{2\bar{z}}\rangle$ , while those of the antisymmetric one — by  $|1_{2\bar{z}}\rangle$ . The first are formed by linear combinations of Wigner functions  $D_{MK}^J(\varphi, \theta, \gamma)$  with even  $K$ , while the second — with odd  $K$ . In the terms of quasi-classical quantization the first one correspond to even quantum numbers  $k_C$ , while the second — to odd  $k_C$ , see Eq. (7.22). In the course of rotation by  $180^\circ$  around axis  $\bar{z}$  the first ones are multiplied by +1, while the second — by  $-1$ <sup>19</sup>. Consequently, the space of rotational cluster states (7.33) can be of two sorts, depending on which one of the vectors  $|0_2\rangle$  or  $|1_2\rangle$  have initiated it. Let us consider each case separately. Below we write out the form of the space (7.33) and the action of operators  $R_{2\bar{x}}$ ,  $R_{2\bar{y}}$ ,  $R_{2\bar{z}}$  from the group  $D_2$ .

1. The initial vector is  $|0_2\rangle$ ,  $R_{2\bar{z}}|0_2\rangle = |0_2\rangle$ . The space basis of the rotation cluster is given by:  $|e^{A_1}\rangle = 2^{-\frac{1}{2}}(|0_2\rangle + R_{2\bar{y}}|0_2\rangle)$ ,  $|e^{B_2}\rangle = 2^{-\frac{1}{2}}(|0_2\rangle - R_{2\bar{y}}|0_2\rangle)$ . The action of operators from group  $D_2$  is:

$$\begin{aligned}
 & \text{1. Rotation cluster reper} \\
 |0_2\rangle &= R_{2\bar{z}}|0_2\rangle, \\
 |e^{A_1}\rangle &= 2^{-1/2}(|0_2\rangle + R_{2\bar{y}}|0_2\rangle), \\
 |e^{B_2}\rangle &= 2^{-1/2}(|0_2\rangle - R_{2\bar{y}}|0_2\rangle). \\
 R_{2\bar{z}}|e^{A_1}\rangle &= 2^{-1/2}(R_{2\bar{z}}|0_2\rangle + R_{2\bar{z}}R_{2\bar{y}}|0_2\rangle) \\
 &= 2^{-1/2}(|0_2\rangle + R_{2\bar{z}}R_{2\bar{y}}R_{2\bar{z}}^2|0_2\rangle) \\
 &= 2^{-1/2}(|0_2\rangle + R_{2\bar{y}}|0_2\rangle) = |e^{A_1}\rangle, \\
 R_{2\bar{x}}|e^{A_1}\rangle &= R_{2\bar{z}}R_{2\bar{y}}|e^{A_1}\rangle = R_{2\bar{z}}|e^{A_1}\rangle = |e^{A_1}\rangle, \text{ or} \\
 &|e^{A_1}\rangle - A_1 \text{ representation of group } D_2; \\
 R_{2\bar{z}}|e^{B_2}\rangle &= |e^{B_2}\rangle, R_{2\bar{y}}|e^{B_2}\rangle = -|e^{B_2}\rangle, R_{2\bar{x}}|e^{B_2}\rangle = -|e^{B_2}\rangle, \text{ so} \\
 &|e^{B_2}\rangle - B_2 \text{ representation of group } D_2. \tag{7.34}
 \end{aligned}$$

2. The initial vector is  $|1_2\rangle$ . The space basis of the rotation cluster is given by  $|1_2\rangle$  and  $R_{2\bar{y}}|1_2\rangle$ . The action of group operators is governed by:

---

<sup>19</sup>The action on quantum orbits is given by  $\int_{\gamma}^{\gamma+\pi} J_{\gamma}(\gamma) d\gamma = \pi k_C$ , see Eq. (7.22). This equation proves the statement in the text.

## 2. Rotation cluster reper

$$\begin{aligned}
 |1_2\rangle &= -R_{2\bar{z}}|1_2\rangle, \\
 |e^{A_2}\rangle &= 2^{-1/2}(|1_2\rangle + R_{2\bar{y}}|1_2\rangle), \quad |e^{B_1}\rangle = 2^{-1/2}(|1_2\rangle - R_{2\bar{y}}|1_2\rangle). \\
 R_{2\bar{z}}|e^{A_2}\rangle &= -|e^{A_2}\rangle, \quad R_{2\bar{y}}|e^{A_2}\rangle = |e^{A_2}\rangle, \quad R_{2\bar{x}}|e^{A_2}\rangle = -|e^{A_2}\rangle, \text{ so} \\
 &\quad |e^{A_2}\rangle - A_2 \text{ representation of group } D_2; \\
 R_{2\bar{z}}|e^{B_1}\rangle &= -|e^{B_1}\rangle, \quad R_{2\bar{y}}|e^{B_1}\rangle = -|e^{B_1}\rangle, \quad R_{2\bar{x}}|e^{B_1}\rangle = |e^{B_1}\rangle, \text{ so} \\
 &\quad |e^{B_1}\rangle - B_1 \text{ representation of group } D_2. \tag{7.35}
 \end{aligned}$$

Here  $R_{2\bar{x}}$ ,  $R_{2\bar{y}}$ ,  $R_{2\bar{z}}$  are the rotation operators with respect to the principal axes of the molecule.

In the derivation of Eqs. (7.33) – (7.34) only the rules of group multiplication for group  $D_2$ , and the action of operators of the local sub-group  $C_{2\bar{z}}$  upon the initial vectors  $|0_2\rangle$ ,  $|1_2\rangle$  have been used. The particular form of the matrices of rotation operators (7.32) was not required. In fact, this is the general rule in the expansion into irreducible components of the rotation clusters, worked out in Refs. [110, 111, 112].

Thus, we arrive at the conclusion, that the rotation cluster, induced by the state  $|0_{2\bar{x}}\rangle$ , consists of levels of symmetry  $(A_1, B_2)$ , while the one for the state  $|1_{\bar{x}}\rangle$  – from the levels of symmetry  $(A_2, B_1)$ . A similar analysis of clusters, induced by the states  $|0_{2\bar{x}}\rangle$  and  $|1_{2\bar{x}}\rangle$ , leads to the following results: is the representation of group

$$\begin{aligned}
 |f^{A_1}\rangle &= \frac{1}{\sqrt{2}}(|0_{2\bar{x}}\rangle + R_{2\bar{y}}|0_{2\bar{x}}\rangle), \quad -A_1 \text{ representation of group } D_2; \\
 |f^{B_1}\rangle &= \frac{1}{\sqrt{2}}(|0_{2\bar{x}}\rangle - R_{2\bar{y}}|0_{2\bar{x}}\rangle), \quad -B_1 \text{ representation of group } D_2; \\
 |f^{A_2}\rangle &= \frac{1}{\sqrt{2}}(|1_{2\bar{x}}\rangle + R_{2\bar{y}}|1_{2\bar{x}}\rangle), \quad -A_2 \text{ representation of group } D_2; \\
 |f^{B_2}\rangle &= \frac{1}{\sqrt{2}}(|1_{2\bar{x}}\rangle - R_{2\bar{y}}|1_{2\bar{x}}\rangle), \quad -B_2 \text{ representation of group } D_2. \tag{7.36}
 \end{aligned}$$

Here  $R_{2\bar{x}}|0_{2\bar{x}}\rangle = |0_{2\bar{x}}\rangle$ ,  $R_{2\bar{x}}|1_{2\bar{x}}\rangle = -|1_{2\bar{x}}\rangle$ .

From these equations it can be found, that the precession of vector  $\mathbf{J}$  around axis  $\bar{x}$  gives rise to rotation clusters of two types:  $(A_1, B_1)$  and  $(A_2, B_2)$ . The first is induced by the state  $|0_{2\bar{x}}\rangle$  and consists of rotation levels with  $A_1$  and  $B_1$  symmetry, while the second is induced by the state  $|1_{2\bar{x}}\rangle$  and incorporates rotation levels of  $A_2$  and  $B_2$  symmetry.

All these results are united in the correlation Tables 7.3. Here the columns are numbered by the irreducible representations of the local group

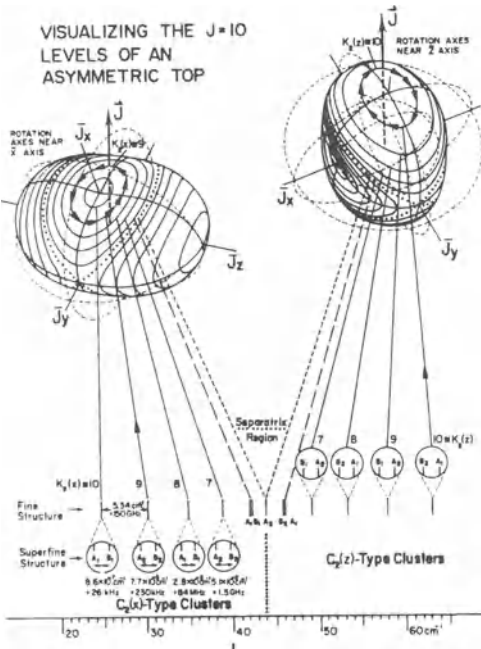


Figure 7.10: Rotational spectrum of a most-asymmetric top molecule for  $J = 10$  with the corresponding semiclassical trajectories. Rotational constants are for a hypothetical heavy asymmetric top with  $A = 0.2 \text{ cm}^{-1}$ ,  $B = 0.4 \text{ cm}^{-1}$ ,  $C = 0.6 \text{ cm}^{-1}$ . From Ref. [18].

$C_{2\bar{x}_i}$ , while the rows are numbered by the representations of the group  $D_2$ . The number in the column shows, how many irreducible representations, corresponding to the number of the row are there in the cluster for that column. For example, the cluster  $|1_{2\bar{z}}\rangle$  consists of one representation  $A_2$  and one  $B_1$ , while the cluster  $|0_{2\bar{y}}\rangle$  --- of one representation  $A_1$  and one  $A_2$ . The classical trajectories on the RE-surface, the corresponding clusters, and level splittings inside these clusters for a hypothetical asymmetric top with  $A = 0.2$ ,  $B = 0.4$ , and  $C = 0.6 \text{ cm}^{-1}$  are depicted in Fig. 7.10.

In the third part of Table 7.3 the correlation of groups  $C_{2\bar{y}}$  and  $D_2$  is given. For a rigid asymmetric top this correlation is of no special interest, as the axis  $\bar{y}$  is unstable, and there are no classical trajectories that embrace it. However, for a semi-rigid molecule of asymmetric top type an RE-surface with split-up separatrix lines can be imagined easily, with three sorts of classical trajectories, each embracing one of the three corresponding orthogonal axes. Such an RE-surface is depicted in Fig. 7.11 from Ref. [18]. It could be

$k_{\bar{z}}, C_{2\bar{z}}$			$k_{\bar{x}}, C_{2\bar{x}}$			$k_{\bar{y}}, C_{2\bar{y}}$		
	$0_2$	$1_2$		$0_2$	$1_2$		$0_2$	$1_2$
$A_1$	1	—	$A_1$	1	—	$A_1$	1	—
$A_2$	—	1	$A_2$	—	1	$A_2$	1	—
$B_1$	—	1	$B_1$	1	—	$B_1$	—	1
$B_2$	1	—	$B_2$	—	1	$B_2$	—	1

Table 7.3: Correlation tables of local groups  $C_{2\bar{x}_i}$  and of group  $D_2$ , the symmetry group of RE-surface of an asymmetric rotator: a)  $k_{\bar{z}}, C_{2\bar{z}}$ , b)  $k_{\bar{x}}, C_{2\bar{x}}$ , c)  $k_{\bar{y}}, C_{2\bar{y}}$ .

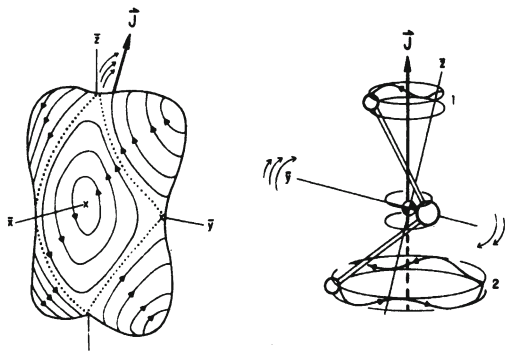


Figure 7.11: Rotational energy surface and associated rotational dynamics for a hypothetical semirigid asymmetric molecule: (a) RE surface and trajectories are sketched in body frame. (b) Rotational motion of an  $XY_2$  molecule associated with one corner trajectory is sketched in the laboratory frame.

generated by a molecule with an infinitely heavy atom  $X$  and soft bending mode, when momentum  $J$  is big enough, and the angle between  $XY$  bonds equals  $90^\circ$  approximately. In this case the stable rotation axes are turned with respect to the initial principal axes  $(\bar{x}, \bar{y}, \bar{z})$  by  $45^\circ$  around axis  $\bar{x}$ , see Fig. 7.11. It is clear, that all the three types of rotation clusters  $|k_{2\bar{x}}\rangle$ ,  $|k_{2\bar{y}}\rangle$ ,  $|k_{2\bar{z}}\rangle$  are possible, where  $(\bar{x}, \bar{y}, \bar{z})$  denote the new axes, rotated with respect to the previous basis set so that two of them are directed along the valence bonds  $XY$ .

Next we go over to the classification of rotation clusters for the RE-surface of octahedral symmetry, Fig. 7.8. Let us consider the  $C_4$  cluster. It has in correspondence six classical trajectories on the hills of the RE-surface, which transform one into the other under the action of group  $O$ , see Fig.

Classes of conjugated elements	$E$	$4C_3^{1(a)}$ $4C_3^2$	$3C_4^{2(b)}$	$3C_4^{1(b)}$ $3C_4^3$	$6R_2^{(c)}$
$A_1$	1	1	1	1	1
$A_2$	1	1	1	-1	-1
$E$	2	-1	2	0	0
$T_2$	3	0	-1	-1	1
$T_1, \bar{x}, \bar{y}, \bar{z}$	3	0	-1	1	-1

Table 7.4: The characters of the irreducible representation of the octahedral group  $O$ . <sup>(a)</sup> $C_3^1, C_3^2$  — rotations by 120 and 240 degrees with respect to the axes of third order (three fold axes) — diagonals of the cube, Fig. 7.12; <sup>(b)</sup> $(C_4^1, C_4^3) R_4^2$  — equivalent rotations by 90 and 270 degrees, and rotation by 180 degrees with respect to the axis of forth order (axes  $\bar{x}, \bar{y}, \bar{z}$  in Fig. 7.12); <sup>(c)</sup> $R_2$  — rotation by 180 degrees with respect to axes of second order, passing through the middles of cube edges, belonging to different faces and parallel to each other, Fig. 7.12.

### 7.8. Each trajectory has in correspondence a quasi-classical state

$$|m_4, 1\rangle, |m_4, 2\rangle, \dots, |m_4, 6\rangle, \quad (7.37)$$

where  $m_4$  is the quantum number resulting from quasi-classical quantization, and the second number refers to the hill, where the trajectory resides. Each vector  $|m_4, j\rangle$  from the set (7.37) realizes the representation

$$R_4(j)|m_4, j\rangle = e^{im_4\pi/2}|m_4, j\rangle, \quad (7.38)$$

of group  $O$ , sub-group  $C_4(j)$ . Here  $j$  is the number of  $C_4$  axis (hill). Our goal is to expand it into irreducible representations (IR) of group  $O$ , space (7.37). To achieve that we find the character of the representation (7.37), and, having expanded it into characters of irreducible representations, obtain the required result.

The characters of the irreducible representation of the octahedral group  $O$ .

Clearly, only those rotations  $R(G)$ , for which some of the vectors (7.37) are eigenfunctions, will contribute to the character  $\chi(G)$ . It follows from the fact, that all the operators  $R(G)$  of group  $O$  either leave the vector  $|m_4, j\rangle$  intact, or transform it into some other one  $|m_4, j'\rangle$  from the same set (see Tables 7.4 and Fig. 7.12, which specify the characters and elements of group  $O$ ). Really, after rotation the trajectory, which embraced axis  $C_4(j)$ , either remains in its place, that is on the  $j$ -th hill of RE-surface, or goes over to the other  $j'$ -th hill. Then with the account of Eq. (7.38) we obtain the following characters  $|0_4\rangle, |1_4\rangle, |3_4\rangle, |2_4\rangle$  for clusters:

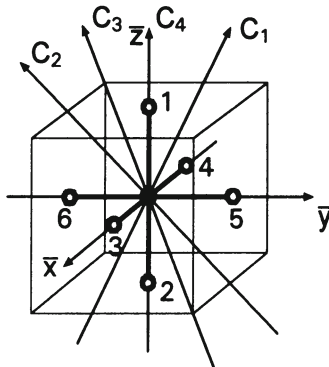


Figure 7.12: The symmetry axes of the octahedral group, molecule  $XY_6$ .  $C_1$  is the axis of first order. In a molecule of an octahedral symmetry there are 24 equivalent one-sided  $C_1$  axes.

1.  $(0_4)$  – cluster

$$\chi_{o_4}(E) = \sum_{j=1}^6 \langle 0_4, j | E | 0_4, j \rangle = \sum_{j=1}^6 1 = 6,$$

$$\chi_{o_4}\left(R_4^{(1,3)}\right) = \langle 0_4, j | R_4^{(1,3)} | 0_4, j \rangle + \langle 0_4, \bar{j} | R_4^{(1,3)} | 0_4, \bar{j} \rangle = 2,$$

$$\chi_{o_4}\left(R_4^{(2)}\right) = \langle 0_4, j | R_4^{(2)} | 0_4, j \rangle + \langle 0_4, \bar{j} | R_4^{(2)} | 0_4, \bar{j} \rangle = 2,$$

here  $|j, 0_4\rangle$  and  $|\bar{j}, 0_4\rangle$  are the states, the classical trajectories of which are situated on the hills, corresponding to two oppositely directed axes  $C_4$  (for example, at the positive and negative sides of axis  $\bar{z}$ , as shown in Fig. 7.8). For other elements of the group we have  $\chi(G) = 0$ . Thus,

$$(\chi_{o_4}(G), \chi_{A_1}(G)) = \frac{1}{24} [6 \cdot 1 + (2 \cdot 1) \cdot 3 + (2 \cdot 1) \cdot 6] = 1, 1A_1,$$

$$(\chi_{o_4}(G), \chi_{A_2}(G)) = \frac{1}{24} [6 \cdot 1 + (2 \cdot 1) \cdot 3 - (2 \cdot 1) \cdot 6] = 0, 0A_2,$$

$$(\chi_{o_4}(G), \chi_E(G)) = \frac{1}{24} [6 \cdot 2 + (2 \cdot 2) \cdot 3] = 1, 1E,$$

$$(\chi_{o_4}(G), \chi_{T_1}(G)) = \frac{1}{24} [6 \cdot 3 - (2 \cdot 1) \cdot 3 + (2 \cdot 1) \cdot 6] = 1, 1T_1,$$

$$(\chi_{o_4}(G), \chi_{T_2}(G)) = \frac{1}{24} [6 \cdot 3 - (2 \cdot 1) \cdot 3 - (2 \cdot 1) \cdot 6] = 0, 0T_2,$$

$$\text{that is } (0_4) = A_1 \oplus E \oplus T_1.$$

$$\begin{aligned}
 & (1_4) - \text{cluster} \\
 \chi_{1_4}(E) &= 6, \\
 \chi_{1_4}\left(R_4^{(1,3)}\right) &= e^{i\pi/2} + e^{-i\pi/2} = 0, \\
 \chi_{1_4}\left(R_4^{(2)}\right) &= e^{i\pi} + e^{-i\pi} = -2,
 \end{aligned}$$

and on other elements of the group  $\chi(G) = 0$ .

$$\begin{aligned}
 (\chi_{1_4}(G), \chi_{A_1}(G)) &= \frac{1}{24}(6 - 6) = 0, \\
 (\chi_{1_4}(G), \chi_{A_2}(G)) &= \frac{1}{24}(6 \cdot 1 - (2 \cdot 1) \cdot 3) = 0, \\
 (\chi_{1_4}(G), \chi_E(G)) &= \frac{1}{24}(6 \cdot 2 - (2 \cdot 2) \cdot 3) = 0, \\
 (\chi_{1_4}(G), \chi_{T_1}(G)) &= \frac{1}{24}(6 \cdot 3 + (2 \cdot 1) \cdot 3) = 1, \\
 (\chi_{1_4}(G), \chi_{T_2}(G)) &= \frac{1}{24}(6 \cdot 3 + (2 \cdot 1) \cdot 3) = 1, \\
 \text{that is } (1_4) &= T_1 \oplus T_2.
 \end{aligned}$$

$$\begin{aligned}
 & (2_4) - \text{cluster} \\
 \chi_{2_4}(E) &= 6, \\
 \chi_{2_4}\left(R_4^{(1,3)}\right) &= e^{i\pi} + e^{-i\pi} = -2, \\
 \chi_{2_4}\left(R_4^{(2)}\right) &= 1 + 1 = 2.
 \end{aligned}$$

On other elements of the group  $\chi(G) = 0$ .

$$\begin{aligned}
 (\chi_{2_4}(G), \chi_{A_1}(G)) &= \frac{1}{24}(6 \cdot 1 + (2 \cdot 1) \cdot 3 - (2 \cdot 1) \cdot 6) = 0, \\
 (\chi_{2_4}(G), \chi_{A_2}(G)) &= \frac{1}{24}(6 \cdot 1 + (2 \cdot 1) \cdot 3 + (2 \cdot 1) \cdot 6) = 1, \\
 (\chi_{2_4}(G), \chi_E(G)) &= \frac{1}{24}(6 \cdot 2 + (2 \cdot 2) \cdot 3) = 1, \\
 (\chi_{2_4}(G), \chi_{T_1}(G)) &= \frac{1}{24}(6 \cdot 3 - (2 \cdot 1) \cdot 3 - (2 \cdot 1) \cdot 6) = 0, \\
 (\chi_{2_4}(G), \chi_{T_2}(G)) &= \frac{1}{24}(6 \cdot 3 - (2 \cdot 1) \cdot 3 + (2 \cdot 1) \cdot 6) = 1, \\
 \text{that is } (2_4) &= A_2 \oplus E \oplus T_2.
 \end{aligned}$$

	$0_4^{(a)}$	$1_4$	$2_4$	$3_4$	$0_3^{(b)}$	$1_{3,2_3}$	$0_2^{(c)}$	$1_2$	$0_1^{(d)}$
$A_1$	1	—	—	—	1	—	1	—	1
$A_2$	—	—	1	—	1	—	—	1	1
$E$	1	—	1	—	—	1	1	1	2
$T_1$	1	1	—	1	1	1	1	2	3
$T_2$	—	1	1	1	1	1	2	1	3

Table 7.5: Correlation symmetry group  $O$  and groups  $C_4$ ,  $C_3$ ,  $C_2$ , and  $C_1$ .  
 (a)  $m_4$  – representation of group  $C_4(\bar{z})$ ; (b)  $m_3$  – representation of group  $C_3(\bar{z})$ ;  
 (c)  $0_2$  – representation of group  $C_2(\bar{z})$ ; (d)  $0_1$  – representation of group  $C_1(\bar{z})$ .

Thus, there are three sorts of  $C_4$  clusters:

$$(0_4) = A_1 \oplus E \oplus T_1, \quad (1_4) = T_1 \oplus T_2, \quad (2_4) = A_2 \oplus E \oplus T_2. \quad (7.39)$$

These levels, composing  $C_4$  clusters, have been depicted in circles on the right hand side of Fig. 7.8.

A similar calculation for  $C_3$  clusters leads to the following result:

$$\begin{aligned} & 2. \quad C_3 - \text{cluster} \\ (0_3) &= A_1 \oplus A_2 \oplus T_1 \oplus T_2, \\ (1_{3,2_3}) &= E \oplus T_1 \oplus T_2. \end{aligned} \quad (7.40)$$

These clusters are depicted on the left hand side of Fig. 7.8.

Equations (7.39) and (7.40) solve the problem of symmetry classification of rotation clusters, corresponding to stable rotation axes ( $C_4$  and  $C_3$ ) in semi-rigid molecules of octahedral symmetry, like  $XY_6$ .

If in a molecule of octahedral symmetry under some conditions (see below) a stable rotation axis of first order ( $C_1$  – axis) emerges, the corresponding rotation cluster consists of 24 rotation states <sup>20</sup>. These states form a regular representation of group  $O$ , so that the  $C_1$  – cluster can be expanded in the irreducible representations (IR) in the following way <sup>21</sup>:

$$(0_1) = A_1 \oplus A_2 \oplus 2E \oplus 3T_1 \oplus 3T_2. \quad (7.41)$$

The results we present with the help of correlation Tables 7.5.

In this Table we provided also the expansion in irreducible representations for  $C_2$  – clusters ( $0_2$  and  $1_2$ ). On the octahedral RE-surface (Fig. 7.3) of the Hamiltonian (7.3) they have in correspondence six unstable rotation

<sup>20</sup>In the general case there are 24 equivalent  $C_1$  - axis, see Fig. 7.12.

<sup>21</sup>Here the group theory has been used, according to which each irreducible representation is contained in the regular representation as many times, as its dimension [113].

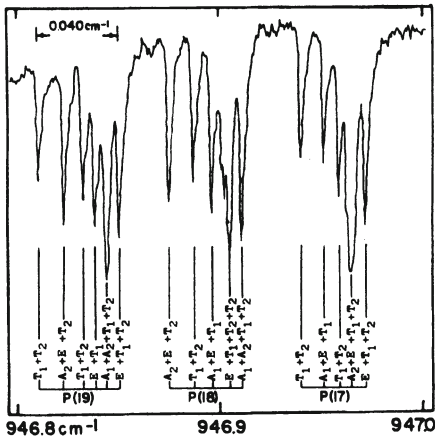


Figure 7.13: Tunable laser diode absorption spectra of  $SF_6$ .

axes of second order  $C_2$ , which go through the cross-section points of separatrix lines. Due to this instability there are no quantum rotation levels, corresponding to these axes, or, in other words, there are no trajectories on the surface around these axes. However, if the separatrix lines get split for high values of  $J$ , when next order terms in  $J$  into the rotation Hamiltonian (7.3) are taken into account, the  $C_2$  – axes may become stable, and then in the spectrum the levels of  $C_2$  – clusters will emerge. This effect resembles the phase transition of second order, and it will be considered in next Sections.

## 7.4 Tunnelling matrix

In the preceding Section the symmetry analysis of the rotation cluster has been provided. Now we will describe briefly the calculation of level splitting in the cluster, following Refs. [110, 111, 112]. The magnitude of this splitting is of the order of tunneling between the states of the rotation cluster (to be exact, of the overlap integral  $S$ ) (7.37) or (7.44), and is very small in fact – see Tables 7.1, 7.2, and Eqs. (7.26), (7.27). Fig. 7.13 from Ref. [110] shows the absorption spectrum of molecule  $SF_6$ . The lines of the spectrum are classified according to the rotation clusters they belong to. It can be seen easily, that the distance between clusters is  $\sim 10^{-2} \text{ cm}^{-1}$ , while the splitting of levels inside the cluster is at least  $\sim 10^{-3} \div 10^{-4} \text{ cm}^{-1}$ .

Let us consider the  $C_4$  – cluster. It has the set of states (7.37) in correspondence. The trajectories of these states are depicted on the right hand side of Fig. 7.8. Each state (trajectory) of this kind has four nearest equiv-

alent states (trajectories), and one more state (trajectory) on the opposite side of the rotation axis, Fig. 7.8. The matrix element of the rotation Hamiltonian  $\langle j | H(J) | j' \rangle$ , corresponding to the tunneling between nearest states we denote by  $S$ , while those for the states with opposite directions of the rotation axis ( $m_c$  and  $-m_c$ ) we denote by  $T$ . In these notations the Hamiltonian matrix in the representation of Eq. (7.37) has the form <sup>22</sup>:

$$\langle i | H_4 | j \rangle = \begin{pmatrix} H_m & T_m & S_m & S_m & S_m & S_m \\ T_m & H_m & S_m & S_m & S_m & S_m \\ S_m & S_m & H_m & T_m & S_m & S_m \\ S_m & S_m & T_m & H_m & S_m & S_m \\ S_m & S_m & S_m & S_m & H_m & T_m \\ S_m & S_m & S_m & S_m & T_m & H_m \end{pmatrix}. \quad (7.42)$$

Here the states with opposite directions of rotation axes are chosen in the following way:  $|m_4, 1\rangle$  and  $|m_4, 2\rangle$ ,  $|m_4, 3\rangle$  and  $|m_4, 4\rangle$ ,  $|m_4, 5\rangle$  and  $|m_4, 6\rangle$  (see Fig. 7.12). The elements  $S_m$  and  $T_m$  of the matrix depend upon the number of the cluster  $m$ , which is determined for large  $J$  after the quasi-classical quantization (7.19). The elements of the  $i$ -th row can be assumed real, which is no limitation in fact (see the footnote to Eq. (7.42)). For clusters  $1_4$  and  $3_4$ , according to the theorem of Wigner – Eckart, we have  $T_m = 0$ , as  $\langle 1_4 | H | 3_4 \rangle$  and  $[C_4^1(\bar{z}), H] = 0$ .

Analogous manipulations for the  $C_3$  – cluster lead to the matrix:

$$\langle i | H_3 | j \rangle = \begin{pmatrix} H_k & T_k & S_k & T_k & S_k & T_k & S_k & U_k \\ T_k & H_k & S_k & T_k & S_k & T_k & U_k & S_k \\ S_k & S_k & H_k & S_k & T_k & U_k & T_k & T_k \\ T_k & T_k & S_k & H_k & U_k & T_k & S_k & S_k \\ S_k & S_k & T_k & U_k & H_k & S_k & T_k & T_k \\ T_k & T_k & U_k & T_k & S_k & H_k & S_k & S_k \\ S_k & U_k & T_k & S_k & T_k & S_k & H_k & T_k \\ U_k & S_k & T_k & S_k & T_k & S_k & T_k & H_k \end{pmatrix}. \quad (7.43)$$

The footnote to Eq. (7.42) applies to the matrix elements of Eq. (7.43) as well.

A  $C_3$  – cluster has eight equivalent rotation axes of third order, and, correspondingly, the cluster has eight rotation states:

$$|k_3, 1\rangle, |k_3, 2\rangle, |k_3, 3\rangle, |k_3, 4\rangle, |k_3, 5\rangle, |k_3, 6\rangle, |k_3, 7\rangle, |k_3, 8\rangle. \quad (7.44)$$

---

<sup>22</sup>Strictly speaking, this matrix and the matrix (7.43) have the provided form only for  $0_{3,4}$  – clusters. However, the first row is correct for any cluster ( $1_3, 1_4, 2_4$ ). It enables the calculation of the spectrum of these matrices (see below). The fact, that the elements of the first row are real is proved in the next footnote.

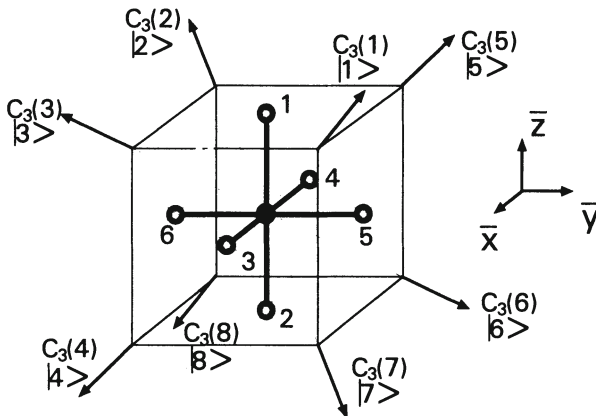


Figure 7.14: The labeling of  $C_3$  axes and of the rotational states in  $C_3$  cluster, molecule  $XY_6$ .

The numbers of equivalent axes and states (7.44) with respect to molecular axes are shown in Fig. 7.14, which correspond to the matrix (7.43). Tunneling along the axes with an edge in common is equal to  $S_k$ ; with a diagonal of a side in common –  $T_k$ ; with a diagonal of the cube in common –  $U_k$  (see Fig. 7.14). The quantities  $U_k$  are equal to zero for  $1_3$ ,  $2_3$  – clusters due to the  $C_3$  symmetry of the Hamiltonian. In this case the footnote to Eq. (7.42) holds true, stating that only the first row in the matrix Eq. (7.43) remains real and retains the form, provided above for an arbitrary cluster. The other rows remain the same only in a  $0_3$  – cluster.

For the first rows in the matrices (7.42) and (7.43) to be real, we will use only rotations by  $180^\circ$  for the construction of cluster basis sets from the initial rotational state<sup>23</sup>. For the octahedral group this is always possible, see Figs. 7.12 and 7.14. With  $(S, U, T)$  given, the matrices Eq. (7.42), (7.43) of the rotation Hamiltonian (7.3) can be determined with the help of the constructed basis functions. By the diagonalization of these matrices we find the energy of rotational states in the clusters, that is, their super-fine structure. It should be born in mind, however, that the basis sets of rotation clusters (7.37) and (7.44) are non-orthogonal in the general case<sup>24</sup>.

In the quasi-classical limit, when  $J \rightarrow \infty$ , and this non-orthogonality can be neglected, the matrix elements  $S$ ,  $T$ , and  $U$  can be calculated through the tunneling integrals according to Eq. (7.25). The corresponding results in Ta-

<sup>23</sup>The operators of rotation by  $180^\circ$  are Hermitian. Thus, due to  $[H(J), R_2] = 0$  the operator  $HR_2$  is Hermitian as well. Correspondingly, the quantity  $\langle j | H | j' \rangle = \langle j | HR_2 | j' \rangle$  is real. The equation  $\text{Im} \langle 1 | H | j \rangle = \text{Im} \langle 1 | HR_2 (1 \rightarrow j) | 1 \rangle = 0$  can always be met. However, it may turn out, that  $\text{Im} \langle j | H | j' \rangle \neq 0$ . The first row can always be made real.

<sup>24</sup>In the non-orthogonal basis the secular equation takes the form  $|\langle i | H | k \rangle - \lambda \langle i | k \rangle|$ .

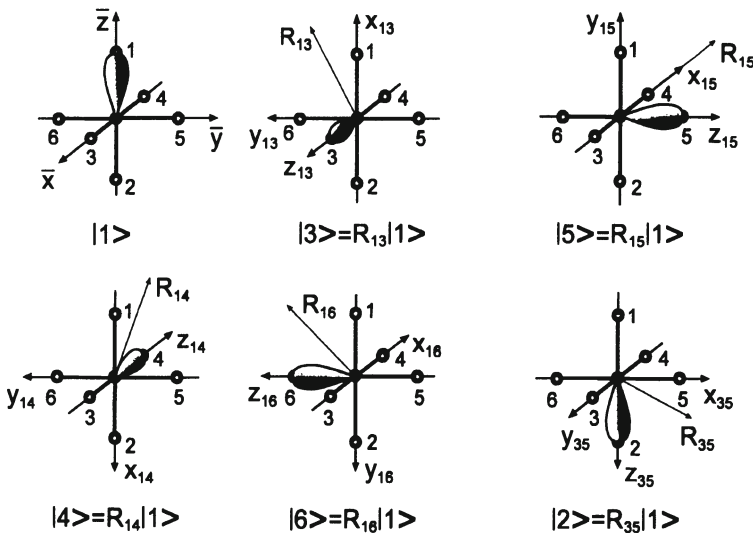


Figure 7.15: The basis vectors of  $C_4$  cluster and the corresponding orientations of equivalent axes.  $R_{kj}$  is the operator of rotation by 180 degrees with respect to the axis – bisector of the angle  $k0j$ .

bles 7.1 and 7.2 reveal good agreement of the approximate and exact results for  $J \geq 30$ . Next we demonstrate, how the matrices (7.42) and (7.43) can be diagonalized in the quasi-classical limit. To perform the diagonalization of these matrices it is sufficient to find the vectors of irreducible representations in the space of states of rotational clusters (7.37) and (7.44). These vectors will be consequently the eigenvectors of the matrices (7.42) and (7.43) due to the fact, that these matrices commute with the operations of group  $O$ . This is guaranteed by the fact, that the tunneling matrix elements between equivalent states in the matrices (7.42) and (7.43) are implied equal to one another. For example, if  $|a\rangle$  and  $|b\rangle$  are equivalent to the states  $|a'\rangle = R|a\rangle$  and  $|b'\rangle = R|b\rangle$  respectively, the matrix elements  $H_{a,b}$  and  $H_{a',b'}$  are assumed equal.

Let us construct the basis for the  $C_4$  – cluster, along with the corresponding vectors of the irreducible representations. Fig. 7.15 shows the vectors of this basis and the corresponding molecular axes for each vector – such axes, where the wavefunction depends upon the Euler angles (characterizing the orientations of these axes in the laboratory coordinate set) in the same way, as does the wavefunction of the initial state, denoted by ket – vector  $|1\rangle$ . This wavefunction characterizes the probability of orientations of the molecular axes ( $\bar{x}, \bar{y}, \bar{z}$ ) with respect to the laboratory coordinate set.

The intra-molecular rotations are defined with respect to these axes. Thus,  $C_4^2(\bar{z})$  denotes the rotation by  $180^\circ$  with respect to axis  $\bar{z}$ , and is characterized by the operator  $\exp(iJ_{\bar{z}}\pi)$ ;  $R_{15}$  denotes rotation by  $180^\circ$  around the axis of second order, which splits the angle between the valent bonds of atoms 1 and 6 into two equal parts. The latter rotation corresponds to the operator  $\exp[i2^{-\frac{1}{2}}\pi(J_{\bar{z}} - J_{\bar{y}})]$ . It is easy to find with the help of Fig. 7.15, that the basis vectors  $|j\rangle$  in the course of rotations  $C_4^1(\bar{z})$ ,  $C_4^1(\bar{y})$ , and  $C_4^1(\bar{x})$  are transformed in the following way:

$$\begin{aligned}
 & \left( \begin{array}{c} C_4^1(\bar{z})|1\rangle \\ C_4^1(\bar{z})|2\rangle \\ C_4^1(\bar{z})|3\rangle \\ C_4^1(\bar{z})|4\rangle \\ C_4^1(\bar{z})|5\rangle \\ C_4^1(\bar{z})|6\rangle \end{array} \right) = \left( \begin{array}{ccc} 1 & \pm i & -1 \\ 1 & \pm i & -1 \end{array} \right) \left( \begin{array}{c} |1\rangle \\ |2\rangle \\ |5\rangle \\ |6\rangle \\ |4\rangle \\ |3\rangle \end{array} \right), \\
 & \left( \begin{array}{c} C_4^1(\bar{x})|1\rangle \\ C_4^1(\bar{x})|2\rangle \\ C_4^1(\bar{x})|3\rangle \\ C_4^1(\bar{x})|4\rangle \\ C_4^1(\bar{x})|5\rangle \\ C_4^1(\bar{x})|6\rangle \end{array} \right) = \left( \begin{array}{ccc} 1 & -1 & 1 \\ 1 & \pm i & -1 \\ 1 & \pm i & -1 \\ 1 & \mp i & -1 \\ 1 & -1 & 1 \\ 1 & \mp i & -1 \end{array} \right) \left( \begin{array}{c} |6\rangle \\ |5\rangle \\ |3\rangle \\ |4\rangle \\ |1\rangle \\ |2\rangle \end{array} \right), \\
 & \left( \begin{array}{c} C_4^1(\bar{y})|1\rangle \\ C_4^1(\bar{y})|2\rangle \\ C_4^1(\bar{y})|3\rangle \\ C_4^1(\bar{y})|4\rangle \\ C_4^1(\bar{y})|5\rangle \\ C_4^1(\bar{y})|6\rangle \end{array} \right) = \left( \begin{array}{ccc} 1 & -1 & 1 \\ 1 & \mp i & -1 \\ 1 & \pm i & -1 \\ 1 & -1 & 1 \\ 1 & \pm i & -1 \\ 1 & \mp i & -1 \end{array} \right) \left( \begin{array}{c} |3\rangle \\ |4\rangle \\ |2\rangle \\ |1\rangle \\ |5\rangle \\ |6\rangle \end{array} \right); \\
 & \text{reper of cluster } \left( \begin{array}{c} |1\rangle \\ |2\rangle \\ |3\rangle \\ |4\rangle \\ |5\rangle \\ |6\rangle \end{array} \right) = \left( \begin{array}{c} |1\rangle \\ R_{3,5}|1\rangle \\ R_{1,3}|1\rangle \\ R_{1,4}|1\rangle \\ R_{1,5}|1\rangle \\ R_{1,6}|1\rangle \end{array} \right). \tag{7.45}
 \end{aligned}$$

We illustrate the idea of the derivation of transformations (7.45) with the help of the following example. Under the action of the rotation  $C_4^1(\bar{x})$  upon the state  $|1\rangle$  from cluster (14) the axis  $\bar{z}$  is transformed into  $z_{16}$  of the state  $|6\rangle$ , while the axes  $(\bar{x}, \bar{y})$  will be directed oppositely to  $(x_{16}, y_{16})$  of the state  $|6\rangle$ , i.e.  $C_4^1(\bar{x})|1\rangle = C_4^2(\bar{y})|6\rangle = -|6\rangle$ . The state from the clusters (04) and (24) will be transformed into  $|6\rangle$ . In short, the state emerging due

to rotation, is determined by the new position of the axis  $\bar{z}_{jj'}$ , while the corresponding coefficient is determined by the angle of rotation of the new position of  $\bar{z}_{jj'}$  until the new position of the axes  $\bar{x}, \bar{y}$  coincides with the new positions of the axes  $(x_{16}, y_{16})$  of the old state.

As an arbitrary rotation from group  $O$  is a product of some number of  $C_4^1(\bar{x}_i)$  rotations, the Eqs. (7.45) provide the opportunity to obtain all the matrices of the reducible representation of group  $O$ , realized by the states of the rotation cluster. Below we find the rotational states of the cluster  $(0_4)$  irreducible representations along with the corresponding energies in detail.

The states of the cluster  $(0_4)$  are grouped into the following eigenvectors of operator  $C_4^1(\bar{z})$ :

$$\begin{aligned}
& C_4^1(\bar{z}) \cdot \begin{pmatrix} |1\rangle \\ |2\rangle \\ (|3\rangle + |4\rangle + |5\rangle + |6\rangle) \end{pmatrix} \\
&= \begin{pmatrix} |1\rangle \\ |2\rangle \\ (|3\rangle + |4\rangle + |5\rangle + |6\rangle) = |A_1; 1\rangle \end{pmatrix}, \quad \lambda = 1; \\
& C_4^1(\bar{z}) \cdot \begin{pmatrix} (|3\rangle + |4\rangle - |5\rangle - |6\rangle) \\ (|3\rangle - |4\rangle + i|5\rangle - i|6\rangle) \\ (|3\rangle - |4\rangle - i|5\rangle + i|6\rangle) \end{pmatrix} \\
&= \begin{pmatrix} -(|3\rangle + |4\rangle - |5\rangle - |6\rangle) \\ -i(|3\rangle - |4\rangle + i|5\rangle - i|6\rangle) \\ i(|3\rangle - |4\rangle - i|5\rangle + i|6\rangle) \end{pmatrix} = \begin{pmatrix} -|E; -1\rangle \\ -i|T_1; -i\rangle \\ i|T_1; i\rangle \end{pmatrix}. \tag{7.46}
\end{aligned}$$

Eq. (7.46) is obtained from Eq. (7.45). Comparing the correlation Table 7.5 and the Table of characters 7.4, we find, that the vectors  $|T_1; -i\rangle$  and  $|T_1; i\rangle$  can enter only the irreducible representation  $(T_1)$ , while the vector  $|E; -1\rangle$  can enter only the representation  $(E)$ . The representation  $(E)$  comprises only vectors with  $\lambda = 1$  and  $\lambda = -1$ , as  $\chi_E(C_4^2) = 2$ ,  $\chi_E(C_4^1) = 0$ .

As it has been noted before, only the first rows in matrices (7.42) and (7.43) preserve their form, written out explicitly above. Thus, to find the energy spectrum of clusters, we look for the vectors of irreducible representations, which have a nonzero projection upon the state  $|1\rangle$ . We act with the operator  $C_4^1(\bar{y})$  upon the vectors  $|E; -1\rangle, |T_1; -i\rangle$ . The vectors obtained belong to the same irreducible representation, but have nonzero projections upon  $|1\rangle$  and, consequently, allow the determination of their energy. Thus we find:

$$\begin{aligned}
C_4^1(\bar{y})|E; -1\rangle &= C_4^1(|3\rangle + |4\rangle - |5\rangle - |6\rangle) = (|2\rangle + |1\rangle \\
&- |5\rangle - |6\rangle), \quad \text{so that} \quad |E\rangle = (|1\rangle + |2\rangle - |5\rangle - |6\rangle);
\end{aligned}$$

$$\begin{aligned}
H|E\rangle &= \begin{pmatrix} H_0 & T_0 & S_0 & S_0 & S_0 & S_0 \\ \cdot & \cdot & \cdot & \cdot & \cdot & \cdot \\ \cdot & \cdot & \cdot & \cdot & \cdot & \cdot \\ \cdot & \cdot & \cdot & \cdot & \cdot & \cdot \\ \cdot & \cdot & \cdot & \cdot & \cdot & \cdot \\ \cdot & \cdot & \cdot & \cdot & \cdot & \cdot \end{pmatrix} \cdot \begin{pmatrix} 1 \\ 1 \\ 0 \\ 0 \\ -1 \\ -1 \end{pmatrix} \\
&= \begin{pmatrix} H_0 + T_0 - 2S_0 \\ \cdot \\ \cdot \\ \cdot \\ \cdot \\ \cdot \end{pmatrix} = E^E |E\rangle,
\end{aligned}$$

so that  $E^E = H_0 + T_0 - 2S_0$ .

$$\begin{aligned}
C_4^1(\bar{y})|T_1; -i\rangle &= C_4^1(\bar{y})(|3\rangle + |4\rangle + i|5\rangle - i|6\rangle) = -(|1\rangle - |2\rangle \\
&\quad + i|5\rangle - i|6\rangle) \quad \text{so that} \quad |T_1\rangle = (|1\rangle - |2\rangle + i|5\rangle - i|6\rangle) \quad \text{and} \\
H|T_1\rangle &= \begin{pmatrix} H_0 & T_0 & S_0 & S_0 & S_0 & S_0 \\ \cdot & \cdot & \cdot & \cdot & \cdot & \cdot \end{pmatrix} \cdot \begin{pmatrix} 1 \\ -1 \\ \cdot \\ \cdot \end{pmatrix} \\
&= (H_0 - T_0)|T_1\rangle, \text{ so that } E^{T_1} = (H_0 - T_0). \tag{7.47}
\end{aligned}$$

The vector of representation ( $A_1$ ) should be orthogonal to vectors (7.47), and should belong to the eigenvalue  $\lambda = 1$  of operator  $C_4^1(\bar{z})$ . Thus, it should be represented by a linear combination of vectors  $|1\rangle$ ,  $|2\rangle$ , and  $|3\rangle + |4\rangle + |5\rangle + |6\rangle$ , this combination being unique. These conditions are satisfied by a vector with the energy:

$$\begin{aligned}
|A_1\rangle &= |1\rangle + |2\rangle + |3\rangle + |4\rangle + |5\rangle + |6\rangle, \\
H|A_1\rangle &= \begin{pmatrix} H_0 & T_0 & S_0 & S_0 & S_0 & S_0 \\ \cdot & \cdot & \cdot & \cdot & \cdot & \cdot \end{pmatrix} \cdot \begin{pmatrix} 1 \\ 1 \\ \cdot \\ \cdot \end{pmatrix} \\
&= \begin{pmatrix} H_0 + T_0 + 4S_0 \\ \cdot \\ \cdot \end{pmatrix}, \text{ so that} \\
E^{A_1} &= H_0 + T_0 + 4S_0. \tag{7.48}
\end{aligned}$$

Combining Eqs. (7.47) and (7.48) we arrive at the following vectors of irreducible representations and their energies for the cluster( $O_4$ ):

( $O_4$ ) -cluster

$$\begin{aligned}
|A_1\rangle &= |1\rangle + |2\rangle + |3\rangle + |4\rangle + |5\rangle + |6\rangle, \\
E^{A_1} &= H_0 + T_0 + 4S_0; \\
(E), \quad \left( \begin{array}{c} |E, 1\rangle \\ |E, 2\rangle \end{array} \right) &= \left( \begin{array}{c} |1\rangle + |2\rangle - |5\rangle - |6\rangle \\ |3\rangle + |4\rangle - |5\rangle - |6\rangle \end{array} \right), \\
E^E &= H_0 + T_0 - 2S_0; \\
(T_1), \quad \left( \begin{array}{c} |T_1, 1\rangle \\ |T_1, 2\rangle \\ |T_1, 3\rangle \end{array} \right) &= \left( \begin{array}{c} |1\rangle - |2\rangle \\ |3\rangle - |4\rangle \\ |5\rangle - |6\rangle \end{array} \right), \quad E^{T_1} = H_0 - T_0. \quad (7.49)
\end{aligned}$$

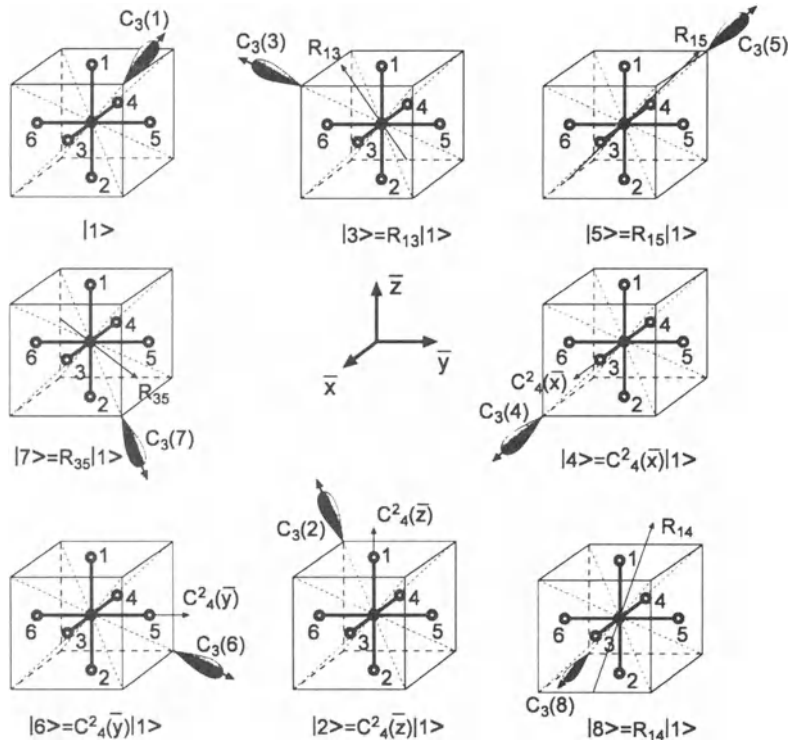
In Eq. (7.49) the vectors of representation  $(T_1)$  are obtained from the vector  $|T_1\rangle$  in Eq. (7.47) by the action of operators  $C_4^1(\bar{z})$  and  $C_4^1(\bar{x})$  upon it, with a subsequent construction of corresponding linear combinations. The fact, that the vectors of  $T_1$  – representation in Eq. (7.49) have been found correctly is backed up by their orthogonality to the vectors from representations  $(A_1)$ ,  $(E)$ , and their orthogonality to each other. Analogous calculations lead to the following results for  $(1_4, 3_4)$  and  $(2_4)$  clusters <sup>25</sup>:

$$\begin{aligned}
&\text{\bf $(1_4, 3_4)$-cluster} \\
(T_1), \quad \left( \begin{array}{c} |T_1, 1\rangle \\ |T_1, 2\rangle \\ |T_1, 3\rangle \end{array} \right) &= \left( \begin{array}{c} |3\rangle + |4\rangle + i(|5\rangle - |6\rangle) \\ (|1\rangle - i|2\rangle) - (|3\rangle + |4\rangle) \\ (|1\rangle + i|2\rangle) - (|5\rangle + |6\rangle) \end{array} \right), \\
E^{T_1} &= H_1 - 2S_1; \\
(T_2), \quad \left( \begin{array}{c} |T_2, 1\rangle \\ |T_2, 2\rangle \\ |T_2, 3\rangle \end{array} \right) &= \left( \begin{array}{c} |3\rangle - |4\rangle - i(|5\rangle - |6\rangle) \\ (|1\rangle - i|2\rangle) + (|3\rangle + |4\rangle) \\ (|1\rangle + i|2\rangle) + (|5\rangle + |6\rangle) \end{array} \right), \\
E^{T_2} &= H_1 + 2S_1. \quad (7.50)
\end{aligned}$$

$$\begin{aligned}
&\text{\bf $(2_4)$-cluster} \\
(A_2), \quad |A_2\rangle &= |1\rangle - |2\rangle - |3\rangle - |4\rangle - |5\rangle - |6\rangle, \\
E^{A_{21}} &= H_2 - T_2 - 4S_2; \\
(E), \quad \left( \begin{array}{c} |E, 1\rangle \\ |E, 2\rangle \end{array} \right) &= \left( \begin{array}{c} |1\rangle - |2\rangle - \frac{1}{2}(|3\rangle + |4\rangle + |5\rangle + |6\rangle) \\ |3\rangle + |4\rangle - |5\rangle - |6\rangle \end{array} \right), \\
E^E &= H_2 - T_2 + 2S_2; \\
(T_2), \quad \left( \begin{array}{c} |T_2, 1\rangle \\ |T_2, 2\rangle \\ |T_2, 3\rangle \end{array} \right) &= \left( \begin{array}{c} |1\rangle + |2\rangle \\ (|3\rangle - |4\rangle) + i(|5\rangle - |6\rangle) \\ (|3\rangle - |4\rangle) - i(|5\rangle - |6\rangle) \end{array} \right), \\
E^{T_2} &= H_2 + T_2. \quad (7.51)
\end{aligned}$$

---

<sup>25</sup>As noted earlier, the parameter  $T_1$  in the matrix (7.42) for the  $(1_4)$  – cluster equals zero.

Figure 7.16: Basis states of clusters  $0_3$  and  $1_3$  in the body frame  $(\bar{x}, \bar{y}, \bar{z})$ 

Equations (7.49) – (7.51) solve the problem of classification of rotation levels for clusters  $(0_4)$ ,  $(1_3, 3_4)$ ,  $(2_4)$  according to the symmetry of group  $O$  (irreducible representations), and of energy level determination as function of the quantized quasi-classical energy of cluster  $H_m$  and of tunneling matrix elements  $S_m$ ,  $T_m$ . The latter are expressed through the tunneling integrals with the help of equations (7.25).

Next let us perform a similar analysis of rotation clusters  $(0_3)$  and  $(1_3, 2_3)$ . Now there are 8 basis states, obtained from the initial rotation state  $|1\rangle$  with the help of rotations by  $180^\circ$ , as shown in Fig. 7.16. In accordance with the definition of basis states in Fig. 7.16, we find the rule of transformation of these states one into another under the action of rotations  $C_4^1(\bar{x})$ ,  $C_4^1(\bar{y})$ , and  $C_4^1(\bar{z})$ .

0 <sub>3</sub> – cluster				(1 <sub>3</sub> , 2 <sub>3</sub> ) – clusters		
j⟩ \ G	C <sub>4</sub> <sup>1</sup> (z̄)	C <sub>4</sub> <sup>1</sup> (ȳ)	C <sub>4</sub> <sup>1</sup> (x̄)	C <sub>4</sub> <sup>1</sup> (z̄)	C <sub>4</sub> <sup>1</sup> (ȳ)	C <sub>4</sub> <sup>1</sup> (x̄)
1⟩	5⟩	7⟩	3⟩	$e^{\mp i2\pi/3} 5\rangle$	$e^{\mp i2\pi/3} 7\rangle$	$e^{\mp i2\pi/3} 3\rangle$
2⟩	3⟩	3⟩	8⟩	$e^{\pm i2\pi/3} 3\rangle$	3⟩	$e^{\mp i2\pi/3} 8\rangle$
3⟩	1⟩	4⟩	4⟩	$e^{\mp i2\pi/3} 1\rangle$	4⟩	$e^{\pm i2\pi/3} 4\rangle$
4⟩	7⟩	8⟩	7⟩	7⟩	8⟩	$e^{\pm i2\pi/3} 7\rangle$
5⟩	2⟩	1⟩	2⟩	$e^{\pm i2\pi/3} 2\rangle$	$e^{\mp i2\pi/3} 1\rangle$	2⟩
6⟩	8⟩	5⟩	5⟩	$e^{\pm i2\pi/3} 8\rangle$	$e^{\pm i2\pi/3} 5\rangle$	5⟩
7⟩	6⟩	6⟩	1⟩	6⟩	$e^{\pm i2\pi/3} 6\rangle$	$e^{\mp i2\pi/3} 1\rangle$
8⟩	4⟩	2⟩	6⟩	$e^{\mp i2\pi/3} 4\rangle$	2⟩	$e^{\pm i2\pi/3} 6\rangle$

(7.52)

With the help of the transformation formulas we obtain the vectors of irreducible representations and the corresponding energies. As an illustration we provide the detailed calculation for a (1<sub>3</sub>) cluster.

The rotation operator C<sub>4</sub><sup>1</sup>(z̄) has the following eigenvectors:

$$\begin{aligned}
 |\uparrow, +1\rangle &= [C_4^4(z̄) + C_4^1(z̄) + C_4^2(z̄) + C_4^3(z̄)]|1\rangle \\
 &= [|1\rangle + e^{-i2\pi/3}|5\rangle + |2\rangle + e^{i2\pi/3}|3\rangle], \\
 |\downarrow, +1\rangle &= [C_4^4(z̄) + C_4^1(z̄) + C_4^2(z̄) + C_4^3(z̄)]|8\rangle \\
 &= [|8\rangle + e^{-i2\pi/3}|4\rangle + e^{-i2\pi/3}|7\rangle + e^{-i2\pi/3}|6\rangle], \quad \lambda_+ = 1; \\
 |\uparrow, -1\rangle &= [C_4^4(z̄) - C_4^1(z̄) + C_4^2(z̄) - C_4^3(z̄)]|1\rangle \\
 &= [|1\rangle - e^{-i2\pi/3}|5\rangle + |2\rangle - e^{i2\pi/3}|3\rangle], \\
 |\downarrow, -1\rangle &= [C_4^4(z̄) - C_4^1(z̄) + C_4^2(z̄) - C_4^3(z̄)]|8\rangle \\
 &= [|8\rangle - e^{-i2\pi/3}(|4\rangle - |7\rangle + |6\rangle)], \quad \lambda_- = -1; \\
 |\uparrow, \pm i\rangle &= [|1\rangle \pm ie^{-i2\pi/3}|5\rangle - |2\rangle \mp ie^{i2\pi/3}|3\rangle], \\
 |\downarrow, \mp i\rangle &= [|8\rangle \pm ie^{-i2\pi/3}|4\rangle - e^{-i2\pi/3}|7\rangle \mp ie^{-i2\pi/3}|6\rangle], \\
 \lambda_i &= \mp i.
 \end{aligned} \tag{7.53}$$

As the cluster (1<sub>3</sub>) according to Table 7.5 consists of the representations E ⊕ T<sub>1</sub> ⊕ T<sub>2</sub>, with the help of the characters of representation (Table 7.4) we find, that the vectors (7.53) enter these irreducible representations in the following way:

$$(E) : \{[\alpha_1|\uparrow, +1\rangle + \alpha_2|\downarrow, +1\rangle], [\beta_1|\uparrow, -1\rangle + \beta_2|\downarrow, -1\rangle]\};$$

$$\begin{aligned} (T_1) & : [\alpha_2^* |\uparrow, +1\rangle - \alpha_1^* |\downarrow, +1\rangle], \dots; \\ (T_2) & : [\beta_2^* |\uparrow, -1\rangle - \beta_1^* |\downarrow, -1\rangle], \dots \end{aligned} \quad (7.54)$$

Obviously, the vectors  $|\uparrow, \pm i\rangle$  and  $|\downarrow, \pm i\rangle$  in Eq. (7.53) enter the representations  $T_1$  and  $T_2$  only. Thus, acting, for example, with the operator  $C_4^1(\bar{y})$  upon vector  $|\uparrow, -i\rangle$  we obtain a vector, which will be necessarily orthogonal to the vectors  $\alpha_1 |\uparrow, +1\rangle + \alpha_2 |\downarrow, +1\rangle$  and  $\beta_1 |\uparrow, -1\rangle + \beta_2 |\downarrow, -1\rangle$  from the  $E$ -representation. Consequently,  $C_4^1(\bar{y}) |\uparrow, -i\rangle$  will have nonzero projections only upon vector  $\alpha_2^* |\uparrow, +1\rangle - \alpha_1^* |\downarrow, +1\rangle$  from sub-space  $\lambda_{\bar{z}} = 1$ , and upon vector  $\beta_2^* |\uparrow, -1\rangle - \beta_1^* |\downarrow, -1\rangle$  from sub-space  $\lambda_{\bar{z}} = -1$ . Thus, the correct linear combinations of vectors with  $\lambda_{\bar{z}} = 1$  and with  $\lambda_{\bar{z}} = -1$  can be found according to the formulas:

$$\begin{aligned} \frac{\langle \uparrow, +1 | C_4^1(\bar{y}) | \uparrow, -i \rangle}{\langle \downarrow, +1 | C_4^1(\bar{y}) | \uparrow, -i \rangle} &= -\frac{\alpha_2^*}{\alpha_1^*} = \exp\left(i\frac{\pi}{3}\right), \\ \frac{\langle \uparrow, -1 | C_4^1(\bar{y}) | \uparrow, -i \rangle}{\langle \downarrow, -1 | C_4^1(\bar{y}) | \uparrow, -i \rangle} &= -\frac{\beta_2^*}{\beta_1^*} = -\exp\left(i\frac{\pi}{3}\right). \end{aligned} \quad (7.55)$$

In the derivation of Eq. (7.55) the definition of vector  $|\uparrow, -i\rangle$  in Eq. (7.53) has been taken into account along with the equality:

$$C_4^1(\bar{y}) |\uparrow, -i\rangle = i \exp\left(i\frac{2\pi}{3}\right) |1\rangle - i \exp\left(i\frac{2\pi}{3}\right) |3\rangle + \exp\left(-i\frac{2\pi}{3}\right) |7\rangle,$$

which follows from the transformation (7.52).

From Eqs. (7.54) and (7.55) it can be found, that the rotational levels of symmetry  $(T_1)$ ,  $(T_2)$  and  $(E)$  have in correspondence the following vectors of states and energies:

$(1_3)$ -cluster

$$(T_1) : |T_1, 1\rangle = [ |1\rangle + |2\rangle + e^{i2\pi/3} |3\rangle - |4\rangle + e^{-i2\pi/3} |5\rangle - |6\rangle - |7\rangle + e^{-i\pi/3} |8\rangle ],$$

$$H |T_1, 1\rangle = \begin{pmatrix} H_1 & T_1 & S_1 & T_1 & S_1 & T_1 & S_1 & U_1 = 0 \\ \cdot & \cdot \\ \cdot & \cdot \end{pmatrix}$$

$$\times \begin{pmatrix} 1 \\ 1 \\ e^{i2\pi/3} \\ \vdots \\ \vdots \end{pmatrix} = \begin{pmatrix} H_1 - T_1 - 2S_1 \\ \vdots \end{pmatrix} \quad \text{so} \quad E^{T_1} = H_1 - T_1 - 2S_1;$$

$$(T_2) : |T_2, 1\rangle = [ |1\rangle + |2\rangle - e^{-2i\pi/3} |3\rangle - |4\rangle ]$$

$$\begin{aligned}
& -e^{-i2\pi/3} |5\rangle - |6\rangle + |7\rangle - e^{-i\pi/3} |8\rangle \Big], \\
H|T_2, 1\rangle &= (H_1 - T_1 + 2S_1)|T_2, 1\rangle, \quad E^{T_2} = H_1 - T_1 + 2S_1; \\
(E) : \quad |E, 1\rangle &= \left[ |1\rangle + |2\rangle + e^{2i\pi/3} |3\rangle + |4\rangle \right. \\
& \left. + e^{-i2\pi/3} |5\rangle + |6\rangle + |7\rangle - e^{-i\pi/3} |8\rangle \right], \\
H|E, 1\rangle &= \\
& \left[ H_1 + T_1 + S_1 e^{2i\pi/3} + T_1 + S_1 e^{-2i\pi/3} + T_1 + S_1 \right] |E, 1\rangle, \\
E^E &= H_1 + 3T_1. \tag{7.56}
\end{aligned}$$

The cluster  $(2_3)$  realizes the equivalent representation of group  $O$ , so that its eigenvectors are obtained from Eq. (7.56) by substitution  $i \rightarrow -i$ , with the energies remaining the same. A similar calculation for the  $0_3$ -cluster leads to the following result:

$$\begin{aligned}
& (0_3)\text{-cluster} \\
(A_1) : \quad |A_1\rangle &= |1\rangle + |2+\rangle |+3\rangle + |4\rangle + |5\rangle + |6\rangle + |7\rangle + |8\rangle, \\
H|A_1\rangle &= \begin{pmatrix} H_0 & T_0 & S_0 & T_0 & S_0 & T_0 & S_0 & U_0 \\ \cdot & \cdot \end{pmatrix} \cdot \begin{pmatrix} 1 \\ \cdot \end{pmatrix} = \\
&= \begin{pmatrix} H_0 + 3T_0 + 3S_0 + U_0 \\ \cdot \end{pmatrix} = (H_0 + 3T_0 + 3S_0 + U_0)|A_1\rangle, \\
E^{A_1} &= H_0 + 3T_0 + 3S_0 + U_0; \\
(A_2) : \quad |A_2\rangle &= |1\rangle + |2\rangle - |3\rangle + |4\rangle - |5\rangle + |6\rangle - |7\rangle - |8\rangle, \\
H|A_2\rangle &= (H_0 + 3T_0 - 3S_0 - U_0)|A_2\rangle, \quad E^{A_2} = H_0 + 3T_0 - 3S_0 - U_0; \\
(T_1) : \quad |T_1, 1\rangle &= |1\rangle + |2\rangle + |3\rangle - |4\rangle + |5\rangle - |6\rangle - |7\rangle - |8\rangle, \\
H|T_1, 1\rangle &= (H_0 + T_0 + S_0 - T_0 + S_0 - T_0 - S_0 - U_0)|T_1, 1\rangle \quad \text{so} \\
E^{T_1} &= H_0 - T_0 + S_0 - U_0; \\
(T_2) : \quad |T_2, 1\rangle &= |1\rangle + |2\rangle - |3\rangle - |4\rangle - |5\rangle - |6\rangle + |7\rangle + |8\rangle, \\
H|T_2, 1\rangle &= (H_0 + T_0 - S_0 - T_0 - S_0 - T_0 + S_0 + U_0)|T_2, 1\rangle \quad \text{so} \\
E^{T_2} &= H_0 - T_0 - S_0 + U_0. \tag{7.57}
\end{aligned}$$

The results, obtained for the superfine structure of rotation clusters are summarized in Table 7.6.

We note, that as the tunneling parameter  $S_k$  corresponds to the transitions between nearest equivalent axes, and thus depends upon the "distance" between the axes in an exponential manner, the inequality  $S_k \gg (T_k, U_k)$  holds, and the level splitting inside the cluster is determined primarily by parameter  $S_k$ . With this property in mind, we find with the help of Table 7.6 the energy width of the rotation clusters:

$c \setminus s$	$A_1(1)$	$A_2(1)$	$E(2)$	$T_1(3)$	$T_2(3)$
$0_4$	$T_0 + 4S_0$	—	$T_0 - 2S_0$	$-T_0$	—
$1_4, 3_4$	—	—	—	$-2S_1$	$2S_1$
$2_4$	—	$-T_2 - 4S_2$	$-T_2 + 2S_2$	—	$T_2$
$0_3$	$3(T_0 + S_0)$ $+U_0$	$3(T_0 - S_0)$ $-U_0$	—	$-T_0 + S_0$ $-U_0$	$-T_0 - S_0$ $+U_0$
$1_3, 2_3$	—	—	$3T_1$	$-T_1 - 2S_1$	$-T_1 + 2S_1$

Table 7.6: Superfine energy structure of rotation clusters relative to their centers. Here  $A_\nu, E, T_\nu$  are the types of irreducible representations of the group  $O$ , their arguments ( $n$ ) characterize the dimensionality of the representation.  $\dot{H}_k$  is the energy of the non-splitted rotational level from cluster ( $k_{3,4}$ );  $S_k, T_k, U_k$  are the Hamiltonian matrix elements with respect to non-splitted levels, arising from tunneling between equivalent rotation axes;  $E^g$  is the energy of  $g$  - level (level of symmetry  $g$ )

$$\begin{aligned} \Delta E(0_4) &= 6S_0, \quad \Delta E(1_4) = 4S_1, \quad \Delta E(2_4) = 6S_2, \\ \Delta E(0_3) &= 6S_0, \quad \Delta E(1_3) = 4S_1. \end{aligned} \quad (7.58)$$

Thus, the complete analysis of the symmetry of cluster rotation levels has been performed, and the super-fine structure of these levels, produced by tunneling of rotational states between equivalent rotation axes, has been found. This tunneling turns out to be extremely small for high values of the molecular momentum  $J$ , and can take values of the order of  $10^{-2} \div 10^{-24} \Omega_{rot}$ , where  $\Omega_{rot}$  is the rotation frequency (see Tables 7.1, 7.2). The low value of tunneling originates from the small overlap of top wavefunctions, corresponding to different rotation axes, if  $J$  goes to infinity. This fact can be illustrated by the transition from one top wavefunction to the other with the account of the fact, that the Wigner functions  $D_{MK}^J$  which govern this transition, tend to zero exponentially for  $J \rightarrow \infty$ , when  $M \sim K \sim J$ . We would like to note further, that the provided analysis of the symmetry and of the super-fine structure of rotation clusters can be taken over without any changes to the study of the highly-excited vibration overtones in molecules of octahedral symmetry, like  $XY_6$ . The only modification is of a purely verbal type: the basis states of the cluster (7.37) are understood now as vibrational states with some valence bond (stretching vibration) highly excited,  $k = 1, 2, \dots, 6$ . The tunneling matrix elements  $S_k, T_k$  are the matrix elements of the interaction of stretching modes, calculated with the anharmonic functions of Morse type, or some generalized matrix elements of high order in inter-mode interaction, like the equations (5.6) and (5.24) used in Section 5.1 in the model calculation of stretching vibrations in  $XY_2$  molecules. Clusters of local modes in vibrational overtones of molecule  $XY_6$  have

been studied up to levels with  $20\nu_3$  in Ref. [114].

The anomalously small splitting of levels inside the rotation cluster leads to extremely slow changes of the direction of the rotation axis (the overturn of the molecule is an extremely rare event). Thus, according to Table 7.2 the splitting in the clusters ( $k_4$ ) with  $J = 88 = k_4$  is of the order of  $\sim 2 \cdot 10^{-23}$ , which corresponds to one overturn in 50 000 years. Consequently, in all the physical processes the intra-molecular precession axis for momentum vector  $\mathbf{J}$  will in practice remain unchanged. As these axes are of third or fourth order, the precession of vector  $\mathbf{J}$  resembles the precession in a symmetric top. In other words, the semi-rigid molecule  $XY_6$  at high values of  $J$  looks like a symmetric top, and its rotation spectrum resembles that of a symmetric top.

In the opposite case, when the splitting inside the cluster is comparable to the distance between the clusters, as it typically happens for not too large  $J$ , the molecule resembles some averaged spherical top – its rotation axes are changed fast enough, and the continuous overturns resemble the spinning of a spherical top.

The effect of "freezing" of the rotation axis in a semi-rigid molecule is augmented considerably, if excitation of local mode vibrations along the rotation axis is possible. Then the change of the rotation axis must take place simultaneously with the transfer of a vibration quantum from one mode to the other. The latter slows down the overturn of the molecule even more, so that the behavior of the molecule becomes closer to that of a symmetrical top. This fact will be considered in more detail in the next Sections.

## 7.5 Violation of permutation symmetry and the super-hyperfine structure

In this Section we will consider the origins and the consequences of mixing of spin wavefunctions for rigid and semi-rigid molecules  $XY_2$ . As we have shown above, the splitting of the rotation cluster due to tunneling between equivalent rotation axes turns out to be extremely small ( $\sim 10^{-2} \div 10^{-20} \hbar\Omega_{rot}$ ) for large values of  $J$ . As a result, the energy levels inside the cluster might be influenced to a great extent by the interaction of rotation with nuclear spins and of the nuclear spins with each other. Thus, the states of different symmetry within the rotation cluster, and, consequently, various spin wavefunctions get mixed<sup>26</sup>. In the IR spectra of the rotation cluster superfine structure there may emerge new lines, which were prohibited by

---

<sup>26</sup>The correct wavefunction is constructed as a bilinear combination of coordinate and spin wavefunctions, which belong to one type of symmetry for integer values of the spin and to the adjoint types of symmetries for semi-integer spin (the transposed schemes of Jung for groups of equivalent nuclei in the latter case). The coordinate component

the symmetry of the coordinate wavefunction. Really, due to the mixing of functions of different symmetry the inactive levels acquire appreciable active components (the interaction of rotation with the nuclear spins is comparable to tunneling), so that prohibited lines appear in the spectra.

The first experimental proof of spin wavefunction's mixing in a molecule  $SF_6$  has been obtained in Ref. [116]. Many more examples of such mixing, termed super-hyperfine structure, is provided in Refs. [115, 117]. The mathematical origin of such mixing lies in the fact, that the operator of the interaction of rotations with nuclear spins is not symmetric in the permutations of position coordinates and spin coordinates separately, but symmetrical only in the permutation of both at the same time. Thus, in general, nonzero are the matrix elements for the transitions between functions of different point symmetry<sup>27</sup> or different spin symmetry, so that different wavefunctions get mixed. On the contrary, if the interaction with the nuclear spin is ignored, the molecule Hamiltonian becomes symmetric separately with respect to position and to spin coordinates of the nuclei, and thus the functions of different point and corresponding spin-symmetry do not mix. In other words, in the latter case the molecules of different spin symmetry behave like various modifications of the substance, as, for example, ortho- and para- water. From the point of view of spectroscopy, the neglection of mixing is equivalent to such a resolution of the spectrometer, when all the lines of the rotation cluster are perceived as a single mature line with no intra-cluster structure. In the high-definition spectra, when the intra-cluster lines can be resolved (resolution not lower, than  $10^{-4} \text{ cm}^{-1}$ ) the clusterized level structure becomes an important object of investigation. In this case the nature and the amount of mixing for wavefunctions of different symmetry should be accounted for.

From the point of view of a physical experiment the situation is characterized best by the following citations from Ref. [18]:

"As previously, transitions between rotational levels of different (overall) species are very strictly forbidden, since the coupling of the nuclear spin with the rest of the molecule is so extremely weak... . These selection rules hold even for collisions, and therefore any particular gas consists of as many almost nonconvertible modifications as there are rotational species of its molecules."

And in the case of mixing of species:

"Let us emphasize that, as a consequence of these mixings, superfine and

---

(  $r_1 \ r_2 \ r_3$  ) and the spin component  $\begin{pmatrix} \sigma_1 \\ \sigma_2 \\ \sigma_3 \end{pmatrix}$  for the value of nuclear spin  $S = 3/2$

can serve as examples. Thus the mixing of coordinate functions is accompanied by mixing of spin functions as well [81, 113].

<sup>27</sup>Point groups are sub-groups of the permutation group, so that the violation of the permutation symmetry leads to the violation of point group symmetry as well.

hyperfine structures cannot be treated separately.”

Two necessary conditions of mixing can be formulated: First, states with like parity with respect to inversion of nuclear coordinates should be present in the cluster<sup>28</sup>; Second, the tunneling matrix elements should be small, or be at least of the same order, as the matrix elements of rotation – nuclear-spin interaction. The most interesting and delicate is the first condition of similar parity of levels in the cluster, as it is sensitive to dynamic violation of symmetry due to molecule rotation. Below we investigate the effect of parity upon the mixing of wavefunctions for molecules  $XY_2$ . The effect of parity upon the mixing of functions in the molecule  $SF_6$  has been considered in Refs. [116, 115, 117, 118].

Before we start the investigation of rotation clusters and of their relation to spin wavefunctions, let us remind the basics of the group approach. The molecule wavefunctions with rotation momentum  $J$  are represented by a direct sum  $L_+^j \oplus L_-^j$ , where

$$L_+^j = \sum_{m,k} C_+^{m,k} \begin{pmatrix} D_{m,k}^J(\varphi, \theta, \chi) \\ D_{m,k}^J(\varphi, \theta, \chi) \end{pmatrix}, \quad L_-^j = \sum_{m,k} C_-^{m,k} \begin{pmatrix} D_{m,k}^J(\varphi, \theta, \chi) \\ -D_{m,k}^J(\varphi, \theta, \chi) \end{pmatrix}.$$

These functions with the help of operators  $\exp(iJ_{x_i}N_{x_j})$  implement the representation of the group of rotations  $O(3)$ , characterized by integer number  $J$ . The operators  $\exp(-iJ_{\bar{x}_j}N_{\bar{x}_j})$  realize the representation of the inner rotation group  $\overline{O}(3)$  of the same symmetry type  $J$ . The transformations of this group provide such overturns of the molecule (the top), which keep the momentum vector  $\mathbf{J}$  constant.

The matrices of the representation group  $O(3)$  act upon the first index  $m$  of functions  $D_{m,k}^J$ , while the matrices of representation of the inner group  $\overline{O}(3)$  – upon the second index  $k$ . The operators of representations of these groups commute with each other, as  $[J_{x_i}, J_{\bar{x}_j}] = 0$ .

The inversion operation  $I$ , acting in the representation  $L_+^j \oplus L_-^j$  according to the rule  $IL_+^j = L_+^j$ ,  $IL_-^j = -L_-^j$  should be added. All the three types of operations  $\exp(-iJ_{\bar{x}_j}N_{\bar{x}_j})$ ,  $\exp(iJ_{x_i}N_{x_j})$  and  $I$  determine the combined symmetry of the space of states  $L_+^j \oplus L_-^j$ .

---

<sup>28</sup>The action of inversion operator upon the rotational wavefunctions as functions of Euler angles, can be presented in the form  $I \begin{pmatrix} D(\Omega) \\ P D(\Omega) \end{pmatrix} = \begin{pmatrix} 0 & 1 \\ 1 & 0 \end{pmatrix} \begin{pmatrix} D(\Omega) \\ P D(\Omega) \end{pmatrix} = P \begin{pmatrix} D(\Omega) \\ P D(\Omega) \end{pmatrix}$ , where  $P = \pm 1$  is the parity of the state. In this representation the operators, commuting with inversion, have the form:  $A = \begin{pmatrix} a & 0 \\ 0 & a \end{pmatrix}$ . More details are provided in Ref. [112]. The described inversion operation corresponds to the inversion of coordinates of all the nuclei; the axes bound to the molecule change their direction to the opposite one, and the body system changes from the right one into the left one, and vice versa. Important is the fact, that under such a transformation the Euler angles of the left and right body system in the laboratory frame remain the same.

We denote this symmetry by the symbol  $O(3)^*\bar{O}(3)$  [119, 120]. The first letter specifies the type of external symmetry of the rotation function. In the present case this is the symmetry of the complete orthogonal group in the three-dimensional Euclidean space  $O(3)$ , which is characterized by the momentum  $J$  and parity  $P$ , that is  $J^P$ . The spaces  $L_{\pm}$  are parts of the regular representation of this group, so that each one of them has the dimension  $(2J+1)^2$ . If the molecule is in a uniform field, this is the symmetry group  $O(2) = C_{\infty}(z) \otimes \{1, I\}$ , while for a molecule in a crystal lattice this will be the symmetry of one of the crystalline groups, etc.

The second part of the symbol  $O(3)^*\bar{O}(3)$  denotes the type of inner symmetry, that is the group, the representations of which are realized with the help of operators  $\exp(-iJ_{\bar{x}_j}N_{\bar{x}_j})$  and  $I$  in the space  $L_+^j \oplus L_-^j$ . In the present case this is the symmetry of a spherical top, that is a representation of a complete orthogonal group. For a molecule  $XY_2$  the inner symmetry group will be  $\bar{C}_{2v} = C_2 \otimes C_i$ , while for an octahedral molecule  $XY_6$  we obtain the group  $\bar{O}_h = O \otimes C_i$ . We took into account the fact, that the symmetry of rotation cluster are determined by the symmetry of the RE surface of the rotation Hamiltonian. The group of the RE surface is represented by the direct product of the point symmetry group of the molecule, and of the group  $C_i = (1, I)$ . Thus, free molecules  $XY_2$  and  $XY_6$  have in correspondence the combined symmetries of the type  $O(3)^*\bar{C}_{2v}$  and  $O(3)^*\bar{O}_h$  correspondingly.

Let us consider the molecule  $XY_2$ . The symmetry of its states with respect to group  $O(3)$  is characterized by momentum and  $J^P$ , where  $P$  is parity. These states are described by Wigner functions  $D_{m,k}^J(\Omega)$ , and at the same time represent the symmetry of type  $J^P$  with respect to the inner symmetry group  $\bar{O}(3)$ . On the other hand the inner symmetry group of molecule  $XY_2$  is the group  $C_{2v}$ , so that we have to compose linear combinations of functions  $D_{m,k}^J(\Omega)$  to obtain functions of symmetry  $C_{2v}$ . Thus we arrive again at the necessity of construction of correlation between the representations of the two groups, in the present case of  $\bar{O}(3)$  and  $C_{2v}$ .

From the correlation table of representations we can determine which representations of the group  $C_{2v}$  are contained in each vector of representation  $J^P$ , and vice versa, from which type of states  $D_{m,k}^J(\Omega)$  the states of definite symmetry types of group  $C_{2v}$  are being composed. The symmetry types and the characters of groups  $C_{2v}$  and  $D_2$  are provided in Table 7.7<sup>29</sup>.

To obtain the correlation of representations, one has to find the action of operators of group  $C_{2v}$ , upon the basis states of the representation  $J^P$ , group  $\bar{O}(3)$ . The basis states are chosen in the form:

$$|J^P, k\sigma\rangle = |J^P, k\rangle + \sigma |J^P, -k\rangle, \quad \sigma = \pm 1, \quad P = \pm 1. \quad (7.59)$$

<sup>29</sup>The operation  $R_{2\bar{x}_k}$  is a rotation by  $180^\circ$  around axis  $\bar{x}_k$ .

The operator  $I$  is an inversion, so that  $IR_x$  is the inversion in the plane of the molecule  $XY_2$ .

$D_2$	1	$R_{2\bar{x}}$	$R_{2\bar{y}}$	$R_{2\bar{z}}$
$C_{2v}$	1	$IR_{2\bar{x}}$	$R_{2\bar{y}}$	$IR_{2\bar{z}}$
$A_1$	1	1	1	1
$A_2$	1	-1	1	-1
$B_1$	1	1	-1	-1
$B_2$	1	-1	-1	1

Table 7.7: Characters of groups  $D_2$  and  $C_{2v}$ .

Here the index  $m = J_z$  has not been written out explicitly, as it is not changed under the action of operations of inner symmetry  $\overline{C}_{2v}$ . During rotations from  $\overline{O}(3)$ , the functions  $|J^P, k\rangle$  are transformed as the conjugate spherical functions  $Y_k^{*j}(\mathbf{n})$ . Thus, we obtain the following transformations:

$$\begin{aligned} IR_{2\bar{x}} |J^P, k^\sigma\rangle &= P\sigma (-1)^J |J^P, k^\sigma\rangle, \\ R_{2\bar{y}} |J^P, k^\sigma\rangle &= \sigma (-1)^{J+k} |J^P, k^\sigma\rangle, \\ IR_{2\bar{z}} |J^P, k^\sigma\rangle &= P(-1)^k |J^P, k^\sigma\rangle. \end{aligned} \quad (7.60)$$

Comparing Eqs. (7.60) with the characters  $C_{2v}$  from Table 7.7, we obtain the following correlations for  $\bar{z}$  cluster (axis  $\bar{z}$  lies in the plane of the molecule  $XY_2$ ; it is perpendicular to the axis  $\bar{Y}$ , or to the axis  $C_2$ ).

$\bar{z} -$		cluster			
$J -$ even		$J -$ odd			
$\left( \begin{array}{l}  A_1, 0_2\rangle \\  B_1, 0_2\rangle \\  A_1, 1_2\rangle \\  B_1, 1_2\rangle \end{array} \right)$	$\longleftrightarrow$	$\left( \begin{array}{l}  J^+, k^+\rangle \\  J^-, k^-\rangle \\  J^-, k^-\rangle \\  J^+, k^+\rangle \end{array} \right)$	$\left( \begin{array}{l}  A_1, 0_2\rangle \\  B_1, 0_2\rangle \\  A_1, 1_2\rangle \\  B_1, 1_2\rangle \end{array} \right)$	$\longleftrightarrow$	$\left( \begin{array}{l}  J^+, k^-\rangle \\  J^-, k^+\rangle \\  J^-, k^+\rangle \\  J^+, k^-\rangle \end{array} \right)$

(7.61)

In Eq. (7.61) we have omitted all the correlations with symmetries  $A_2$  and  $B_2$ , as the rotation clusters can not incorporate such symmetries. Really, the action of the operator  $IR_{2\bar{x}}$  upon the rotational functions of the molecule  $XY_2$  is equivalent to a unit transformation, so that the functions (7.59), which change sign upon this operation, can not describe the rotational states of the molecule  $XY_2$  with symmetry  $C_{2v}$ .

Analogous formulas for the  $\bar{x}$ -cluster have the form:

$\bar{x}$ -	cluster
$J$ - even	$J$ - odd
$\begin{pmatrix}  A_1, 0_2\rangle \\  B_1, 0_2\rangle \\  A_1, 1_2\rangle \\  B_1, 1_2\rangle \end{pmatrix} \longleftrightarrow \begin{pmatrix}  J^+, k^+\rangle \\  J^+, k^-\rangle \\  J^-, k^+\rangle \\  J^-, k^-\rangle \end{pmatrix}$	$\begin{pmatrix}  A_1, 0_2\rangle \\  B_1, 0_2\rangle \\  A_1, 1_2\rangle \\  B_1, 1_2\rangle \end{pmatrix} \longleftrightarrow \begin{pmatrix}  J^+, k^-\rangle \\  J^+, k^+\rangle \\  J^-, k^-\rangle \\  J^-, k^+\rangle \end{pmatrix}$

(7.62)

Here the quantum number  $k$  is the projection of momentum  $\mathbf{J}$  upon the molecular axis  $\bar{x}$ . Equations (7.62) are obtained from Eqs. (7.61) with the help of two consecutive transformations: first, the substitution  $k^+ \leftrightarrow k^-$  in clusters  $(1_2)$ , and then  $J^P \leftrightarrow J^{-P}$  in clusters  $(B_1)$ . This follows from the fact, that the operators  $R_{2\bar{x}}, R_{2\bar{y}}, R_{2\bar{z}}$  act upon the state  $|J^P, k_{\bar{x}}^\sigma\rangle$  in the same way, as the operators  $R_{2\bar{y}}, R_{2\bar{z}}, R_{2\bar{x}}$  do upon the state  $|J^P, k_{\bar{x}}^\sigma\rangle$ <sup>30</sup>.

We note, that for low  $J$  not all the states with arbitrary symmetry can be constructed from the functions  $|J^P, k^\sigma\rangle$ . Thus, one can easily see that for  $J = 1$  in the clusters  $(0_{2\bar{x}})$  and  $(0_{2\bar{z}})$  there are no states with symmetry  $A_1 : |A_1 0_{2\bar{z}}\rangle; |A_1 0_{2\bar{x}}\rangle$ . The equations (7.61) and (7.62) determine the parity  $P$  and the indices of inner symmetry  $\bar{C}_{2v}$  of the rotation cluster states for given  $J$  and  $k_{\bar{x}, \bar{z}}^\sigma$ , which agree with the full symmetry  $O(3)^* \bar{C}_{2v}$ . For the molecule  $XY_2$  the dependence between indices of symmetry  $O(3)^* \bar{C}_{2v}$  and the standard indices of rotation states in the representations of group  $D_2$  can be found easily. Comparing the characters of groups  $C_{2v}$  and  $D_2$  (Table 7.7), and taking into consideration the parity of states  $P$ , we find with the help of Eqs. (7.60) – (7.62) the following correlation relations:

$C_{2v}$ group	$D_2$ group
$\bar{z}$ - cluster	
$\left\{  A_1, 0_2, (J_{e,o}^+, k^{+-})\rangle,  B_1, 0_2, (J_{e,o}^-, k^{-+})\rangle \right\}$	$(A_1, B_2)$
$\left\{  A_1, 1_2, (J_{e,o}^-, k^{+-})\rangle,  B_1, 1_2, (J_{e,o}^+, k^{-+})\rangle \right\}$	$(A_2, B_1)$
$\bar{x}$ - cluster	
$\left\{  A_1, 0_2, (J_{e,o}^+, k^{+-})\rangle,  B_1, 0_2, (J_{e,o}^+, k^{-+})\rangle \right\}$	$(A_1, B_1)$
$\left\{  A_1, 1_2, (J_{e,o}^-, k^{+-})\rangle,  B_1, 1_2, (J_{e,o}^-, k^{-+})\rangle \right\}$	$(A_2, B_2)$

(7.63)

<sup>30</sup>Eqs. (7.60) in the present case take the form:

$$\begin{aligned} IR_{2\bar{x}} |J^P, k^\sigma\rangle &= P(-1)^k |J^P, k^\sigma\rangle, \\ R_{2\bar{y}} |J^P, k^\sigma\rangle &= \sigma(-1)^J |J^P, k^\sigma\rangle, \\ IR_{2\bar{z}} |J^P, k^\sigma\rangle &= P\sigma(-1)^{J+k} |J^P, k^\sigma\rangle. \end{aligned}$$

In the derivation of Eq. (7.63) we have taken into account, that for even parity states  $P = +1$  the symmetries with respect to groups  $C_{2v}$  and  $D_2$  coincide ( $A_1 \leftrightarrow A_1$ ,  $B_1 \leftrightarrow B_1$ ), while for odd parity states  $P = -1$  the relation between the symmetries is the following:  $A_1 \leftrightarrow A_2$ ,  $B_1 \leftrightarrow B_2$ .

The obtained expansion of rotation clusters  $k_2$  for the molecule  $XY_2$  in the irreducible representations of group  $D_2$  coincide fully with the splitted rotation clusters of an asymmetric top in Fig. 7.10. More to it, the correlation formulas (7.63) enable us to determine the parity of rotational level with definite type of symmetry, group  $D_2$ . Really, the levels of rotation symmetry ( $A_1, B_1$ ) must be even, as in the opposite case (odd) they would have symmetry ( $A_2, B_2$ ) from group  $C_{2v}$ , which is impossible. On the contrary, the levels of rotational symmetry ( $A_2, B_2$ ) should be odd to obtain the symmetry ( $A_1, B_1$ ) of the group  $C_{2v}$ . It is exactly this type of correspondence between the representations of groups  $C_{2v}$  and  $D_2$  that the relations (7.63) demonstrate.

With the help of the provided consideration the parity of levels in clusters depicted in Fig. 7.10 can be found:

$$\begin{aligned} \bar{x} - \text{cluster}, J = 10 \\ (10^+ A_1, 10^+ B_1), (9^- A_2, 9^- B_2), \dots \\ \bar{z} - \text{cluster}, J = 10 \\ (10^+ A_1, 10^- B_2), (9^- A_2, 9^+ B_1), \dots \end{aligned} \quad (7.64)$$

Here the number in brackets is the quantum number ( $k_C$  or  $k_A$ ) of the classical orbit, while the indices ( $A_i, B_i$ ) enumerate the irreducible representations of group  $D_2$ .

The permutation symmetry of the full wavefunction determines the symmetry of the spin state with given symmetry of the rotational level. For the rigid molecule  $XY_2$  the operation of inversion  $IR_{2\bar{z}}$  in the plane  $\bar{x}\bar{y}$  is equivalent to the permutation of similar nuclei  $Y$  in the molecule. Thus, for Bose statistics the rotational level of  $A_1$  symmetry, group  $C_{2v}$ , will have a symmetrical spin part (ortho-function), while the level of  $B_1$  symmetry – an antisymmetric spin component (para-function). In the case of Fermi statistics the symmetry of coordinate and spin components is the opposite one: the rotational level of symmetry  $A_1$  and a spin para-function, or a rotational level of symmetry  $B_1$  with ortho-function for the spin component.

Fermi and Bose statistics in molecules  $XY_2$  can be illustrated by the examples of molecules  $H_2O$  (spin 1/2) and  $D_2O$  (spin 1). Ortho- and para-water  $H_2O$  corresponds to  $B_1$  and  $A_1$  functions with total nuclear spins  $I = 1$  and  $I = 0$  correspondingly. Para-heavy water  $D_2O$  corresponds to function  $B_1$  with nuclear spin  $I = 1$ , while the ortho-heavy water – to functions  $A_1$  with nuclear spin  $I = 0, 2$ .

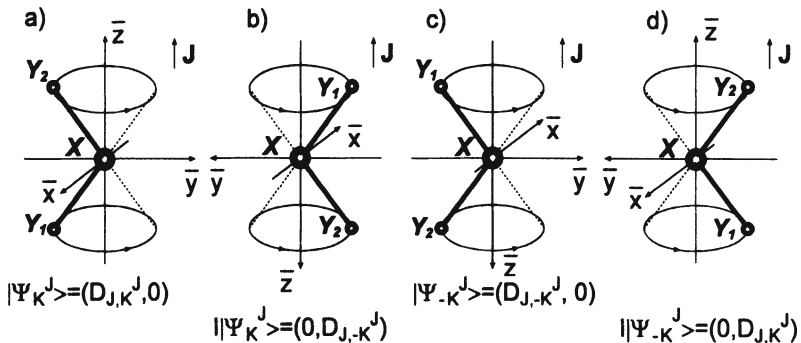


Figure 7.17: The trajectory of nuclei  $Y$  in the laboratory frame for rotational states of  $\bar{z}$  cluster. The corresponding wavefunctions are written out beneath each plot, states with  $k = \langle J \rangle = \pm J$ . The mass  $m_X$  is infinite.

From Eqs. (7.63) and (7.64) it can be seen easily, that the  $\bar{z}$ -clusters consist of levels of opposite parity, while  $\bar{x}$ -clusters – of similar parity. Because of that the rotational levels in  $\bar{z}$ -clusters do not mix with each other, even if the interaction with nuclear spins is comparable to the tunneling interaction. Thus, in  $\bar{z}$ -clusters the symmetry of levels  $A_1$  and  $B_1$  is preserved, so that the spin components of the wavefunction have some definite symmetry, which will be preserved as well. In other words, the molecule  $XY_2$  will remain in the para- or ortho- state for all the rotation levels from  $\bar{z}$ -clusters, irrespective of the magnitude of interaction between the rotation and the nuclear spins. In  $\bar{x}$ -clusters there are no exception rules with respect to parity, so that levels of different symmetry get mixed at high enough values of the perturbing interaction.

The preceding consideration of the parity of rotational levels in the cluster and of the mixing process can be instructively illustrated with the help of Figs. 7.17 - 7.18. These demonstrate, what does the rotation of a rigid molecule  $XY_2$  in the laboratory system look like. The trajectories of nuclei  $Y$  in the laboratory system, which refer to  $\bar{z}$ - and  $\bar{x}$ -clusters are shown, and the corresponding wavefunctions are written out. To be more exact, written out are the functions, the transformational properties of which coincide with those for the trajectories from the cluster. Thus, the exact wavefunctions will be formed by linear combinations of the functions, provided in Figs. 7.17 - 7.18.

Of the four basis functions, presented in Figs. 7.17 – 7.18 only two linear combinations are formed,  $|\Psi_+^J(k)\rangle$  and  $|\Psi_-^J(k)\rangle$ , which satisfy the condition:

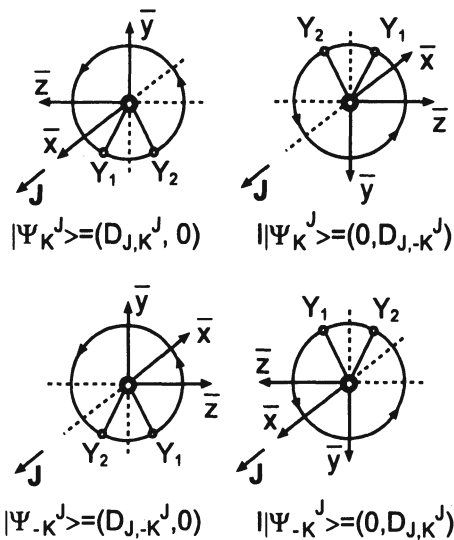


Figure 7.18: The trajectory of nuclei  $Y$  in the laboratory frame for rotational states of  $\bar{x}$  cluster. The wavefunctions with the corresponding transformation properties are written out beneath each plot. The mass  $m_x$  is infinite.

$$(P_{\bar{y}\bar{z}} = IR_{2\bar{x}}) |\Psi_{\pm}^J(k)\rangle = |\Psi_{\pm}^J(k)\rangle \text{ so that } I = R_{2\bar{x}}. \quad (7.65)$$

This is the necessary requirement for the inversion operation  $P_{\bar{y}\bar{z}}$  in the molecular plane  $XY_2$  to be equal to unit.

The functions, that satisfy Eq. (7.65) and belong to  $\bar{z}$  cluster or  $\bar{x}$  cluster respectively have the form:

$$\begin{aligned} \bar{z} - \text{cluster} \\ |\Psi_{\pm}^J(k)\rangle &= \left( \begin{array}{c} (D_k^J \pm D_{-k}^J) \\ \pm (-1)^k (D_{-k}^J \pm D_k^J) \end{array} \right); \\ \bar{x} - \text{cluster} \\ |\Psi_{\pm}^J(k)\rangle &= \left( \begin{array}{c} (D_k^J \pm D_{-k}^J) \\ (-1)^k (D_{-k}^J \pm D_k^J) \end{array} \right). \end{aligned}$$

Here the first index in the function  $D^J$  is omitted and only the second one  $k$  is left, as we are interested in the internal symmetry of the molecule. Index  $k$  of the function  $D^J$  in the  $\bar{x}$ -cluster specifies the projection of the momentum  $\mathbf{J}$  upon axis  $\bar{x}$ . The exact rotational functions have the same

properties under the transformations from the  $C_{2v}$  group as the columns from the functions  $D^J$ , written out above. Taking into account the definition of the inversion operator  $I$  in Figs. 7.17 – 7.18, one can easily find that the parity  $P$  of the provided rotational functions of the  $\bar{z}$ -cluster and  $\bar{x}$ -cluster with respect to inversion and permutation of the nuclei  $P_{12}$  are given by the formulas:

$$\begin{array}{ll} \bar{z} - \text{cluster} & \bar{x} - \text{cluster} \\ |\Psi_{\pm}^J(k)\rangle \rightarrow P_{\pm} = \pm (-1)^J; & |\Psi_{\pm}^J(k)\rangle \rightarrow P_{\pm} = (-1)^k; \\ P_{12\pm} = \pm (-1)^{J+k}. & P_{12\pm} = \pm (-1)^J. \end{array}$$

These equations and the rules of transformation of  $D^J$  functions under rotations  $R_{2\bar{x}}, R_{2\bar{y}}, R_{2\bar{z}}$  lead to the following symmetry of the groups  $C_{2v}$  and  $D_2$ , which characterize the levels of  $\bar{z}$  and  $\bar{x}$ -clusters respectively:

$$\begin{aligned} \bar{z} - \text{cluster} \\ S_{C\pm} = & \begin{cases} A_1, & \text{if } \pm (-1)^{J+k} = 1, \\ B_1, & \text{if } \pm (-1)^{J+k} = -1, \end{cases}; \\ S_{D\pm} = & \begin{cases} A_1, & \text{if } S_{C\pm} = A_1, \text{ and } (-1)^k = 1, \\ A_2, & \text{if } S_{C\pm} = A_1, \text{ and } (-1)^k = -1, \\ B_1, & \text{if } S_{C\pm} = B_1, \text{ and } (-1)^k = -1, \\ B_2, & \text{if } S_{C\pm} = B_1, \text{ and } (-1)^k = 1. \end{cases} \end{aligned}$$

$$\begin{aligned} \bar{x} - \text{cluster} \\ S_{C\pm} = & \begin{cases} A_1, & \text{if } \pm (-1)^J = 1, \\ B_1, & \text{if } \pm (-1)^J = -1, \end{cases} \\ S_{D\pm} = & \begin{cases} A_1, & \text{if } S_{C\pm} = A_1, \text{ and } (-1)^k = 1, \\ A_2, & \text{if } S_{C\pm} = A_1, \text{ and } (-1)^k = -1, \\ B_1, & \text{if } S_{C\pm} = B_1, \text{ and } (-1)^k = 1, \\ B_2, & \text{if } S_{C\pm} = B_1, \text{ and } (-1)^k = -1. \end{cases} \end{aligned}$$

Here the indices  $C$  and  $D$  specify the symmetry groups  $C_{2v}$  and  $D_2$  for the functions  $|\Psi_{\pm}^J\rangle$  in correspondence to the signs + or -. We note that even values of  $k$  have  $(0_2)$  clusters in correspondence, while odd  $k$  correspond to  $(1_2)$  - clusters. The obtained formulas for the symmetries of the rotational clusters' levels obviously fully coincide with Eqs. (7.61) - (7.63). This last representation of the symmetries, however, can be more convenient, as it provides the analytical expressions through the quantum numbers  $J, k, \sigma = \pm 1$ .

It can be seen from Fig. 7.17, that the inversion of nuclei position changes the trajectory of the nuclei: in fact, the nuclei 1 and 2 exchange trajectories with each other. In other words, the inversion operation transforms one phase curve of the system into another, different from the original one. Consequently, the corresponding wavefunction gets transformed into another

one – orthogonal to the original one, which belongs though to the same cluster  $|k| = const$ . The latter means, that the cluster will contain two levels of opposite parity  $P = \pm 1$  and opposite permutation symmetry  $P_{12}$ , as  $P_{12} = (-1)^k P$  (see Fig. 7.17).

Thus, the levels of  $A_1$  and  $B_1$  symmetries in the  $\bar{x}$ -cluster do not get mixed, so that the ortho and para spin states are preserved.

For the  $\bar{x}$ -cluster the situation is the opposite one (see Fig. 7.18). The inversion  $I$  leads to the shift of the nuclei along the trajectory, and, correspondingly, along the phase curve. Thus, the phase curve is invariant with respect to inversion, and, consequently, the wavefunction has some definite parity. As, on the other hand, the trajectories of nuclei rotation in opposite directions with respect to  $\bar{x}$ -axis get transformed into each other with the help of the rotation operator  $R_{2\bar{y}}$ , which commutes with inversion  $I$ , we arrive at the conclusion, that the rotational states in the  $\bar{x}$ -cluster have similar parity. At the same time, these states have opposite permutation symmetry, as  $P_{12} = \pm (-1)^J$  (see Fig. 7.18). Thus, in the  $\bar{x}$ -cluster the rotational levels of different permutation symmetry (with similar parity) will get mixed at a high enough strength of rotational – nuclear-spin interaction. Simultaneously, the mixing of ortho- and para- spin states will take place.

In other words, if the nuclei trajectories are invariant with respect to inversion, the states in the cluster are of the same parity, and mixing of levels takes place; in the opposite case the levels in the cluster have opposite parity and there is no mixing of states. The consideration provided refers to the molecule  $XY_2$ . As far as octahedral molecules  $XY_6$  are concerned, they will always have non-equivalent nuclei trajectories with respect to inversion, so that every cluster will contain levels of opposite parity. States of same parity will be obviously present as well (the number of states in clusters  $XY_6$  is greater than six). Thus, in the clusters of molecule  $XY_6$  the rotational levels get split into two groups with different parity, so that the levels get mixed within the group, but do not mix with levels from other groups. More details on the interrelation of rotation level symmetry in the cluster with the parity for octahedral molecules  $XY_6$  can be found in Refs. [116, 115, 117, 118].

We provide here without proof the cyclic diagram (Fig. 7.19), which enables the determination of the number and type of irreducible representations of octahedral symmetry group  $O$  in the representation  $D^J$  of the group of rotations  $O(3)$ , [110].

To determine the symmetries which compose the  $J$ -shell of rotational states, one has to find the corresponding number  $J$  on the arrows of the inner and outer cycles, and enumerate, moving from one arrow to the other (counter clockwise along the inner circle, or clockwise along the outer circle), the irreducible representations, which are contained in the ring between the arrows. For example, taking  $J = 6$ , and moving along the outer cycle, we pass the symmetries:  $E \oplus T_2 \oplus A_2 \oplus T_2 \oplus T_1 \oplus A_1 = E \oplus 2T_2 \oplus T_1 \oplus A_1 \oplus A_2$ . The dimensionality of this representation is  $2 + 6 + 3 + 1 + 1 = 13 = 2J + 1$ ,

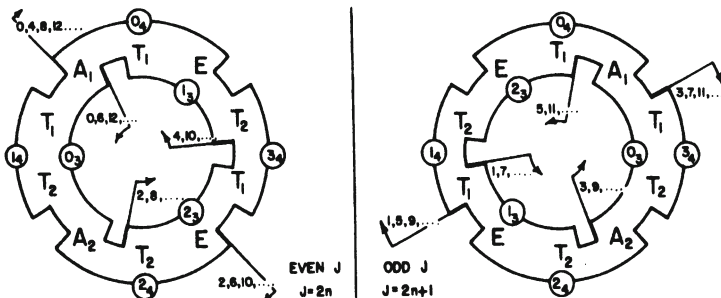


Figure 7.19: The irreducible representations of the cubic group in the spectrum of Hamiltonian  $g(J_x^4 + J_y^4 + J_z^4)$ , which enter the representation  $D^J$  of the group  $O(3)$ .

as it should be. From the same diagram we find, that in the shell there are the levels from the following clusters:  $(0_4), (1_4), (2_4), (0_3), (2_3)$ . These cyclic diagrams play the role of equations (7.61) – (7.62) in the case of cubic symmetry  $O$ .

Now let us consider the extreme forms of destruction of rotational symmetry and hyper-fine mixing, compared to those of the  $\bar{x}$ -clusters, considered above. Such extreme forms of symmetry violation happen when the equivalent nuclei move along the orbits, which differ drastically in their physical properties, or when the phase trajectories, corresponding to permutations of equivalent nuclei, are related to wavefunctions with anomalously small overlap. This can happen to semi-rigid molecules  $XY_2$ , the RE surface of which and the nuclei trajectories are shown in Fig. 7.11. The quantum state, corresponding to such a motion, is a combination of four rotational functions of the group  $D_2$  ( $A_1, B_1, A_2, B_2$ ). Really, according to Fig. 7.11 (a) each trajectory on the RE surface has in correspondence four equivalent trajectories (including itself), which are obtained with the help of the four operations of group  $D_2$  ( $1, R_{2\bar{x}}, R_{2\bar{y}}, R_{2\bar{z}}$ ). Consequently, the wavefunction of any of the trajectories is formed by a combination of all four rotational functions of group  $D_2$ .

The stationary wavefunctions of this cluster will be formed by ortho- or para- combinations of the even pair of states  $A_1$  and  $B_1$ , or of the odd pair  $A_2$  and  $B_2$ . One of the reasons for the violation of symmetry (destruction of trajectories) comes from the different surroundings of the equivalent nuclei (see Fig. 7.11 (b)). The nucleus 1 is situated closer to the  $\bar{z}$  axis, than nucleus 2, and consequently their nuclear spins will feel different magnetic fields, generated by molecule rotation.

Another origin for the violation of symmetry (destruction of trajectories)

arises from the extremely low values of tunneling between equivalent trajectories. This fact leads practically to the destruction of rotational symmetry of group  $D_2$ , as the transition time from one trajectory to the other can reach several years (see Tables 7.1 and 7.2). During the time of the experiment the molecule thus has no chance to "feel" the symmetry of its surface. One may never know, which one of the two nucleus  $Y$  rotates in state 1, and which in state 2, as there are no special labels to distinguish them. However, if nucleus  $Y$  has a nonzero spin, this can serve as a temporary distinguishing mark. In the case of spin  $S = 1/2$  it is relatively simple to learn how the mixing of para-  $A_1$  and ortho-  $B_1$  functions takes place.

Let us consider the state  $m_I = 0$  of para- and ortho- functions. The para- state has a symmetrical  $A_1$  space component  $|1, 2\rangle$  with antisymmetric spin component  $\begin{pmatrix} 1 \\ 2 \end{pmatrix}$ , the latter being singlet with zero total spin  $I = 0$ .

The ortho- state has an antisymmetric  $B_1$  space component  $\begin{pmatrix} 1 \\ 2 \end{pmatrix}$  with symmetric spin component  $|1, 2\rangle$ , the latter being triplet with total spin  $I = 1$ . These states can be related to the Slatter determinant, where spin orientations up or down serve as a label of the rotational state. One of these states is the following:

$$\begin{pmatrix} 1 \uparrow \\ 2 \downarrow \end{pmatrix} = \frac{1}{\sqrt{2}} \left( \begin{pmatrix} A_1, 1 & 2 & \uparrow \\ \downarrow \end{pmatrix} - \begin{pmatrix} B_1, 1 & 2 & \uparrow & \downarrow \end{pmatrix} \right), \quad (7.66)$$

where the nucleus in state 1 has spin orientation up, and the nucleus in state 2 – spin down. This state has the energy, differing slightly from the energy of the state with inverted spins:

$$\begin{pmatrix} 1 \downarrow \\ 2 \uparrow \end{pmatrix} = \frac{1}{\sqrt{2}} \left( \begin{pmatrix} A_1, 1 & 2 & \uparrow \\ \downarrow \end{pmatrix} + \begin{pmatrix} B_1, 1 & 2 & \uparrow & \downarrow \end{pmatrix} \right), \quad (7.67)$$

as the magnetic surroundings of nuclei in the states (7.66) and (7.67) are different, Fig. 7.11. If this difference is big as compared to the super-fine splitting of  $A_1$  and  $B_1$  functions, then mixtures  $(A_1, B_1)$  similar to Eqs. (7.66) and (7.67) will be formed – that is, hyper-fine splitting occurs.

The relation between superfine and hyperfine structures is analogous to the limits of weak and strong coupling for electrons in atoms ( $LS$  and  $jj$ -type bonds).

Thus, we arrive at the conclusion, that at high rotational excitation  $J \gg 1$  the dynamic violation of symmetry takes place, which leads to the lowering of the symmetry of trajectories on the RE surface, as compared to the total symmetry of the surface itself. The transitions between equivalent trajectories due to tunneling matrix elements have extremely low probability. The overturns of the molecule become very rare occasions, so that at

experimental times the precession axis of momentum vector  $\mathbf{J}$  in the body system will be practically frozen, and the energy spectrum of rotational levels will resemble closely the spectrum of a symmetric top, if  $J \sim k \gg 1$ .

At long time, or, equivalently, in the high-definition spectra, the symmetry group of the RE surface reveals itself in the symmetry of rotational levels, in the clusters, – if the interaction of nuclear spin with rotation can be neglected. Otherwise, the symmetry of RE surface (or the symmetry of the effective rotational Hamiltonian  $H(\mathbf{J})$ ) gets destructed due to the addition of rotational – nuclear-spin interaction with another symmetry. The latter typically reduces the initial space symmetry, as positioning spins with various projections on equivalent nuclei makes those non-equivalent, and effectively reduces the point symmetry of the molecule. The reduction of symmetry leads to the increase of the number of rotational levels in the cluster, and, as a rule, to the appearance of prohibited lines in the IR spectra.

## Chapter 8

# Interaction of vibrations and rotations; polyads and their spectra

In this Chapter we will consider with the help of a model Hamiltonian the interaction of vibrations and rotations. It will be shown, that this interaction leads to the strengthening of localization. This is due to the fact, that in this case, along with the tunneling of the vibrational excitation, the tunneling of the vector of momentum  $\mathbf{J}$  with respect to the body frame is required "flip-flop". This last process is very slow for large values of  $J$  and  $J_k$  – flip-flops for fast rotation are prohibited.

The second Section is dedicated to the phenomenological theory of changes of the vibration-rotation spectra during the passage through the bifurcation points on the energy (RE) surface  $E_v(J_x, J_y, J_z)$ , where  $v$  is the set of vibration quantum numbers. The material is presented in the spirit of the phenomenological theory of phase transitions by Landau and in the notations of quantum orbit theory by WKB. Additional help in the understanding of the material can be provided by the monograph [128]

In Section 8.3 we consider the effect of Fermi resonances upon the vibrational spectrum within the two-boson model with interaction, which preserves its number  $v_1 + v_2 = \text{const}$ . At high excitation levels ( $v \gg 1$ ) the quasiclassical approach is valid, and the study of the structure of the vibrations spectrum is reduced to the analysis of the corresponding phase space for classic motion. In the present case, this is the Hamiltonian system with a single degree of freedom, the phase space of which is a sphere. The position of stable points on the sphere and of the unstable (saddle) ones is determined, along with the separatrix lines. After that the phase trajectories are classified, and their relation to the structure of vibrational spectrum is revealed. The peculiarities of the vibration spectrum due to Fermi resonances and to the resonant (periodic) orbits in phase space are investigated.

All the necessary background information is provided in Chapter 7 of the monograph [128]. The required skills include the use of canonical transformations for the simplification of the problem, and of the corresponding unitary transformations in the quasiclassical limit, as explained in detail in Ref. [58].

## 8.1 Interaction of local vibration modes and rotation in hydrides

In the preceding Sections we found, that in the strongly nonlinear systems such as the molecules  $H_2O$ ,  $C_6H_6$ ,  $CH_4$ , and others the strong vibrational excitation of a local mode ( $XY$  bond) leads to the destruction of initial symmetry of equivalent bonds, and to the extremely strong clusterization of vibrational levels. Clusterization grows exponentially with the increase of the excitation level in contrast to the vibrational spectrum of normal modes, where the space between the levels grows proportionally to the excitation of the level  $\Delta E_v \sim v\Delta\omega_H$ . The other aspect of this phenomenon is the 'freezing' of vibration energy on a single bond, and the extreme slow-down of its transfer to other bonds, in contrast to normal vibrations, when the energy quickly (characteristic time  $\tau \sim \beta^{-1} \sim 10^{-13} \div 10^{-12}$  s) goes over from one bond to the other. In the latter case the symmetry of equivalent bonds is revealed clearly in all the relevant interactions. At the same time it has been found, that a freely rotating molecule in a non-degenerate vibrational state is described by an effective rotational Hamiltonian  $H(\mathbf{J})$ . Such a system is essentially nonlinear, and its Hamiltonian  $H(\mathbf{J})$  has the symmetry of the direct product of the molecular point group and of the inversion group,  $C_i = \{1, I\}$ . Again, as in the case of oscillators, at high excitation levels ( $J \gg 1$ ) the symmetry gets violated. It is revealed in the freezing of the precession axis of vector  $\mathbf{J}$  in the body system in some definite positions, and in the reduced probability of its tunneling into another equivalent position (of an abrupt change of vector  $\mathbf{J}$  direction in the body system). In the energy spectrum the slow-down of tunneling is revealed in the pronounced clusterization of rotation levels in full analogy with the system of nonlinear oscillators.

A question arises, how do the effects of tunneling and level clusterization change with the account of the interaction of local modes with molecular rotation? This interaction should be properly accounted for, when there exists a shell of degenerate vibration levels (several bonds  $CH, OH$ , etc.), and when the tunneling probability is comparable to the tunnel matrix elements of rotational levels:  $\varepsilon_N$  from Eqs. (5.6), (5.24) is comparable to the elements  $S, T, U$  of tunnel matrices (7.42), (7.43). In this case it is impossible to obtain a single rotation Hamiltonian  $H(\mathbf{J})$  with the help of the canonical transformations. One arrives to a matrix of rotation operators  $H_{i,k}(\mathbf{J})$

<sup>1</sup> instead, each element relating the  $i$ -th and  $k$ -th degenerate vibrational levels.

On the basis of general considerations one could expect, that the probability of a simultaneous transfer of a vibrational excitation from one bond to another, and of vector  $\mathbf{J}$  tunneling from one position in the body system into another one, is proportional to the product of the overlap of vibrational functions and rotational functions  $\sim \frac{\epsilon S}{\omega_v \Omega_{rot}} \ll \min \left\{ \frac{\epsilon}{\omega_v}, \frac{S}{\Omega_{rot}} \right\}$ . Consequently, the probability of a simultaneous tunneling is decreased many times compared to the transfer probability of each excitation, vibrational and rotational, separately, if it would be possible. At the same time, the clusterization of levels is increased further, as it will be apparent from the calculations below. We will consider this effect within the simple model suggested by K.K.Lehman [38]. This model, being simple and transparent, reveals the physical background of the effect and leads to qualitative results in good agreement with the experiment. As it has been noted above, the nonlinear interactions, which in the traditional spectroscopy are considered as small perturbations, in fact change even the topology of motion. An instructive illustration of such changes is provided in the course of the transition from normal to local modes for the vibrational overtones of most part of symmetric hydrides [51, 6].

A first systematic study of the influence of local modes upon the molecule rotation has been provided in the work by L.Halonen and A.G.Robiette for the molecules  $XY_2$ ,  $XY_3$ ,  $XY_4$  [36]. Assuming the vibrational potential to be equal to the sum of potentials for unbounded Morse oscillators, the authors of the cited paper derived several relations between the resonant terms of the operator  $H_{2,2}$ . This operator contains terms of the form  $q_i q_j J_a J_b$ , and plays a dominant role in the determination of rotational structure dependence upon the vibrations. An interesting prediction of this model is the similarity of the rotational structure of the molecule  $XH_4$  with the rotational structure of a symmetric top, including the factor 2 in the statistical weight for high overtones levels with  $k = 3n$ . This effect has been observed in fact in the overtone spectra of  $GeH_4$  [121],  $SiH_4$  [122], and  $SnH_4$  [37].

Here we would like to note also the work of K.K.Lehman on the vibrational - rotational spectrum of molecule  $CH_4$ , where the similarity of the rotational structure with the corresponding structure of a symmetric top has been observed [123]. Independently this effect has been found in [124] as well. In Ref. [125] it has been demonstrated, that the fitting of the observed vibrational-rotational spectrum of the first overtones for the molecule  $SiH_4$  with the accuracy  $0.003 \text{ cm}^{-1}$  can be achieved with the help of two fitting parameters in the effective Hamiltonian from Ref. [124].

---

<sup>1</sup>Such a structure of the rotation Hamiltonian has in correspondence a set of RE surfaces. The operators  $H_{ik}(J)$  give rise to transitions between equivalent (within the full symmetry of  $H_{ik}(J)$ ) trajectories on the  $i$ -th and  $k$ -th RE surfaces respectively.

The emerging rotational structure for the molecule  $XY_4$  in the course of excitation of overtones' vibrational band, when the excitation is localized on a single  $XY$  bond, and the similarity of the rotational structure with that of a symmetric top can be interpreted on the basis of a simple consideration. The strong vibrational excitation of a single  $XY$  bond, along with the extremely slow (due to nonlinearity of vibrations) excitation transfer to other bonds, reduce the symmetry of the tetrahedron to the symmetry group  $C_{3v}$ . A molecule with such point symmetry group, obviously, is a symmetric top. The latter is revealed in the rotational structure of the overtone band [121, 122, 37, 123]. The experimental proof of the effects of violation of tetrahedron symmetry in the spectra requires extremely high-definition measurements to resolve the intra-cluster structure of vibration-rotation levels.

The molecule  $XH_4$  with a vibrational excitation localized on one  $XH$  bond looks like a prolate top, as the excited bond on average is slightly longer than the other ones. The geometrical structure, averaged over vibrations, provides an interpretation to only some part of the dependencies of the rotation spectrum upon the vibrational strengths. However, the model, which takes into account only this dependency, predicts the symmetry of the effective rotational Hamiltonian correctly, and provides good qualitative results. For example, an interesting fact, derived below with the help of model Hamiltonians, is the confirmation of the slow-down of tunneling processes. This slow-down turns out to be considerable in fact, and leads the stabilization of the molecule for a considerable time ( $\tau \gg 10^{-10} s$ ) in a state, when all the vibrational excitation is localized entirely on some bond.

#### Molecules $XH_2$ .

Let us consider  $XH_2$  molecules in a localized state  $|n_1\rangle$  when  $n$  quanta are on the first valence bond  $XH$ . Due to symmetry the state  $|n_2\rangle$  will have the same energy  $G_0$ . These two degenerate states get transformed one into another due to tunneling, so that the corresponding Hamiltonian has the form:  $\lambda(|n_1\rangle\langle n_2| + |n_2\rangle\langle n_1|)$ .

Here  $\lambda$  is the excitation transition rate from one bond to the other. This rate decreases exponentially with the increasing number of the vibrational excitation, Eqs. (5.6), (5.24). This interaction between the modes produces the following eigenvectors:  $\psi_{s,a} = (|n_1\rangle \pm |n_2\rangle)$  with energies  $E_{s,a} = G_0 \pm \lambda$ . In each vibrational state  $|n_{1,2}\rangle$  the rotational motion is described by the Hamiltonian of an asymmetric top. Due to the increase (on average) of the length of the excited bond, the dynamical violation of molecular  $C_{2v}$  symmetry takes place. The latter leads to the rotation of the principal axes by an angle  $\theta$  with respect to the initial axes of the non-excited molecule, Fig. 8.1. The rotation of axes proceeds in such a way, that the excited (the longer one) bond reduces its smaller acute angle with the principal axis, while the non-excited bond increases it. The rotated axes ( $x_{1,2}, y_{1,2}, z_{1,2}$ ) have in correspondence the rotational constants  $A$ ,  $B$  and  $C$ . The latter do

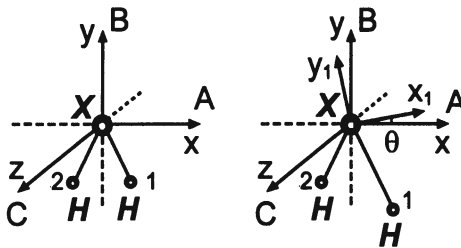


Figure 8.1: (a) Coordinate axes for the non-excited molecule  $XH_2$ ; (b) One bond excited: turning of principal axes.

not depend upon which of the bonds is excited. In the non-excited molecule the role of the  $C_{2v}$  axis is played by  $y$ , and not by  $z$ , which is perpendicular to the molecular plane, as shown in the figure. The rotation of axes is produced by the interaction term  $q_s q_a (J_x J_y + J_y J_x)$  in the Hamilton operator  $H_{2,2}$ . As the state with the excited local mode is a mixture of the symmetric  $A_2$  and antisymmetric  $B_1$  function of symmetry  $C_{2v}$ , the operator  $q_s q_a$  has a nonzero average value in vibrational functions of local modes,  $\langle v | q_s q_a | v \rangle$ . The latter changes the average value of the inertia tensor, averaged over vibrations, and rotates the principal axes. Thus, the effective Hamiltonian, which describes the dynamics of rotational tunneling states  $|n_1\rangle$  and  $|n_2\rangle$ , acquires the form:

$$\begin{aligned} H = & (G_0 + AJ_{x_1}^2 + BJ_{y_1}^2 + CJ_{z_1}^2) |n_1\rangle \langle n_1| \\ & + (G_0 + AJ_{x_2}^2 + BJ_{y_2}^2 + CJ_{z_2}^2) |n_2\rangle \langle n_2| \\ & + \lambda (|n_1\rangle \langle n_2| + |n_2\rangle \langle n_1|). \end{aligned} \quad (8.1)$$

Here the operators  $J_{x_i}$  are related to the initial ones  $J_x$  by the following equations:

$$\begin{aligned} J_{x_1} &= J_x \cos \theta + J_y \sin \theta, \\ J_{y_1} &= -J_x \sin \theta + J_y \cos \theta, \\ J_{x_2} &= J_x \cos \theta - J_y \sin \theta, \\ J_{y_2} &= J_x \sin \theta + J_y \cos \theta, \\ J_{z_1} &= J_{z_2} = J_z. \end{aligned} \quad (8.2)$$

Going over to the symmetric  $|s\rangle = 2^{-\frac{1}{2}} (|n_1\rangle + |n_2\rangle)$  and antisymmetric  $|s\rangle = 2^{-\frac{1}{2}} (|n_1\rangle - |n_2\rangle)$  vibrational states and to the operators  $J_x$ ,  $J_y$ ,  $J_z$ , we obtain the molecular Hamiltonian in the initial coordinate set:

$$\begin{aligned}
H = & \left( G_0 + \lambda + A_s J_x^2 + B_s J_y^2 + C_s J_z^2 \right) |s\rangle \langle s| \\
& + \left( G_0 - \lambda + A_a J_x^2 + B_a J_y^2 + C_a J_z^2 \right) |a\rangle \langle a| \\
& + \frac{d_{sa}}{2} \{J_x, J_y\} (|a\rangle \langle s| + |s\rangle \langle a|), \tag{8.3}
\end{aligned}$$

where

$$\begin{aligned}
\{J_x, J_y\} &= J_x J_y + J_y J_x, \\
A_s &= A_a = A \cos^2 \theta + B \sin^2 \theta, \\
B_s &= B_a = A \sin^2 \theta + B \cos^2 \theta, \\
C_s &= C_a = C, \\
d_{sa} &= (A - B) \sin 2\theta. \tag{8.4}
\end{aligned}$$

Such a Hamiltonian has been used in Refs. [36, 38] in the analysis of local modes' interaction with molecular rotation.

In the course of absorption processes from the ground state, there will be transitions into the  $x$ -polarized states  $|a\rangle$  and into  $y$ -polarized states  $|s\rangle$ , belonging to the rotational-vibrational basis set. We would like to note here, that though it seems plausible to estimate the relation of  $x$  and  $y$  matrix elements on the basis of bonds' projections upon these directions (assuming the dipole nature of transitions along the bond), such an approximation turns out to be unsatisfactory in fact.

In the Hamiltonian (8.3) some of the interactions are lacking, and that requires some additional comment. First, the Coriolis interaction between the states  $|n_1\rangle$  and  $|n_2\rangle$  is neglected. Due to symmetry, there exists the C-axis of Coriolis interaction between the  $s$  and  $a$  stretching vibrations. However, the Coriolis interaction strength is low,  $\sim \frac{m_H}{m_X} \ll 1$ , as in the absence of mixing of bending (torsion) vibrations with stretching ones only the central atom contributes to this interaction [36]. Besides, the low value of the matrix element  $\langle n| p |0\rangle \langle 0| q |n\rangle \sim n! \left(\frac{x_e}{\omega}\right)^{n-1}$  for vibrational overtones  $\frac{x_e}{\omega} \sim 0.01$  contributes to the smallness of Coriolis interaction. Halonen [126] found numerically, that the Coriolis interaction decreases rapidly, when the limit of local modes is reached.

There are also small rotational corrections to the interaction strength  $\lambda$ . However,  $\lambda$  is extremely low  $\sim \langle 2n| H |0\rangle$ , so that there is no reason to take into account these additional small corrections.

For numerical calculations the Hamiltonian in the form (8.3) is more convenient. In this representation the basis functions have the form  $D^{J(s)}(\varphi, \theta, \chi)|s\rangle$  and  $D^{J(a)}(\varphi, \theta, \chi)|a\rangle$ , and are purely symmetric or antisymmetric with respect to the permutations of the vibrational excitation. Of convenience are the common molecular axes for the rotational functions

$z$ cluster	$k_C = k_o$ - even		$k_C = k_o$ - odd	
-	$A_1$	$B_2$	$A_2$	$B_1$
$ s\rangle$	$e^{iS} + e^{-iS}$	$e^{iS} - e^{-iS}$	$e^{iS} - e^{-iS}$	$e^{iS} + e^{-iS}$
$ a\rangle$	$e^{iS} + e^{-iS}$	$e^{iS} - e^{-iS}$	$e^{iS} - e^{-iS}$	$e^{iS} + e^{-iS}$
$x$ cluster	$k_A = k_p$ - even		$k_A = k_p$ - odd	
-	$A_1$	$B_1$	$A_2$	$B_2$
$ s\rangle$	$e^{iS} + e^{-iS}$	$e^{iS} - e^{-iS}$	$e^{iS} - e^{-iS}$	$e^{iS} + e^{-iS}$
$ a\rangle$	$e^{iS} + e^{-iS}$	$e^{iS} - e^{-iS}$	$e^{iS} - e^{-iS}$	$e^{iS} + e^{-iS}$

Table 8.1: Symmetries of rotational-vibrational states with respect to the group  $D_2$  in the absence of tunneling.  $S(\gamma)$  is the classical action for the rotational part of the Hamiltonian Eq. (8.3); the non-prohibited transitions are determined by the matrix elements of the perturbation operator  $\{J_x, J_y\}_+$ , which has the symmetry of  $B_2$  type. The quantities  $k_0, k_p$  refer to the oblate and prolate symmetric rotator.

$D^J(\varphi, \theta, \chi)$ . Analogously, calculations can be performed easier in such a basis for other symmetric molecules like  $XH_3$ ,  $XH_4$ , etc. A useful parameter is provided by  $\eta$ , which characterizes the mixing of  $|s\rangle$  and  $|a\rangle$  states:

$$\eta\% = \frac{1}{2} \left[ 1 - \frac{\|D_s\|^2 - \|D_a\|^2}{\|D_s\|^2 + \|D_a\|^2} \right] \cdot 100\%, \quad (8.5)$$

where  $\|D\|^2 = \int d(\varphi, \theta, \chi) |D|^2$  – is the norm of the rotation function. From the form of Hamiltonian (8.3) some conclusions on the form of the spectrum can be derived. If the interaction can be neglected,  $d_{s,a} = 0$ , the states of the Hamiltonian can be classified according to the symmetries of group  $D_2$  in the following way (see Table 8.1).

The following estimates hold:

$$\begin{aligned} 4 \langle e^{iS} | B_2 | e^{+iS} \rangle &= \left\langle (e^{iS} + e^{-iS}) \begin{array}{c} A_1 \\ B_1 \end{array} \middle| B_2 \middle| \begin{array}{c} B_2 \\ A_2 \end{array} (e^{iS} - e^{-iS}) \right\rangle \\ &+ \left\langle (e^{iS} - e^{-iS}) \begin{array}{c} B_2 \\ A_2 \end{array} \middle| B_2 \middle| \begin{array}{c} A_1 \\ B_1 \end{array} (e^{iS} + e^{-iS}) \right\rangle \\ &+ \left\langle (e^{iS} + e^{-iS}) \begin{array}{c} A_1 \\ B_1 \end{array} \middle| B_2 \middle| \begin{array}{c} A_1 \\ B_1 \end{array} (e^{iS} + e^{-iS}) \right\rangle \\ &+ \left\langle (e^{iS} - e^{-iS}) \begin{array}{c} B_2 \\ A_2 \end{array} \middle| B_2 \middle| \begin{array}{c} B_2 \\ A_2 \end{array} (e^{iS} - e^{-iS}) \right\rangle \\ &= \left\langle (e^{iS} + e^{-iS}) \begin{array}{c} A_1 \\ B_1 \end{array} \middle| B_2 \middle| \begin{array}{c} B_2 \\ A_2 \end{array} (e^{iS} - e^{-iS}) \right\rangle \end{aligned}$$

$$\begin{aligned}
& + \left( \left\langle \left( e^{iS} + e^{-iS} \right) \begin{array}{c} A_1 \\ B_1 \end{array} \middle| B_2 \middle| \begin{array}{c} B_2 \\ A_2 \end{array} \left( e^{iS} - e^{-iS} \right) \right\rangle \right)^* \\
= & i \left( \left\langle \begin{array}{c} A_1 \\ B_1 \end{array} \cos S \middle| B_2 \middle| \begin{array}{c} B_2 \\ A_2 \end{array} \sin S \right\rangle - \left\langle \begin{array}{c} A_1 \\ B_1 \end{array} \cos S \middle| B_2 \middle| \begin{array}{c} B_2 \\ A_2 \end{array} \sin S \right\rangle \right) \\
\equiv & 0,
\end{aligned} \tag{8.6}$$

or, in other words,  $\langle e^{\pm iS} | \{J_x, J_y\}_+ | e^{\pm iS} \rangle \equiv 0$ , where

$$\begin{aligned}
& \left\langle f_1(S) \begin{pmatrix} A_1 \\ B_1 \end{pmatrix} \middle| B_2 \middle| \begin{pmatrix} B_2 \\ A_2 \end{pmatrix} f_2(S) \right\rangle \\
= & \left( \begin{array}{l} \langle f_1(S), A_1 | \{J_x, J_y\}_+ | B_2, f_2(S) \rangle \\ \langle f_1(S), B_1 | \{J_x, J_y\}_+ | A_2, f_2(S) \rangle \end{array} \right).
\end{aligned}$$

Here  $B_2$  denotes the symmetry type of the operator  $\{J_x, J_y\}_+$  with respect to the group  $D_2$ ;  $\exp(iS)$  is the quasi-classical rotation function, which corresponds to some definite trajectory on the RE surface;  $[\exp(iS) \pm \exp(-iS)]$  are the wavefunctions of the rotation cluster with symmetry  $(A_1, B_2)$  or  $(B_1, A_2)$  in  $z$ -cluster, and  $(A_1, B_1)$  or  $(B_2, A_2)$  in  $x$ -cluster, Table 8.1. In the derivation of Eq. (8.6) the characters of the group  $D_2$  (Table 7.7) have been taken into account, along with the theorem of Wigner – Eckart on the selection rules.

As the exact wavefunctions differ from the quasi-classical ones by exponentially small correction terms (in the overlap integrals, at least), from Eq. (8.6) the following estimates hold:

$$\begin{aligned}
\langle A_1 | \{J_x, J_y\}_+ | B_2 \rangle & \sim \langle A_2 | \{J_x, J_y\}_+ | B_1 \rangle \\
\sim \langle e^{-iS} | \{J_x, J_y\}_+ | e^{iS} \rangle & \sim \exp \{-const \cdot J\},
\end{aligned} \tag{8.7}$$

if  $k_C = k_o = k_z \sim J$ .

The matrix elements for any other pair of symmetries are equal to zero, including the diagonal ones.

Thus, on the basis of Eq. (8.7) we conclude, that the matrix elements of the perturbation operator  $\{J_x, J_y\}$  for any states from the  $x$ -cluster are equal to zero, while for the  $\bar{z}$  cluster they are nonzero for the states of different rotation symmetry, and in fact are exponentially small  $\sim \exp(-const \cdot J)$  for  $k_C = k_o = k_z \sim J \gg 1$ .

The intra-cluster matrix elements of the perturbation operator  $W$  determine the shift of levels in the first order in the interaction strength  $d_{sa}$ . However, according to Eq. (8.7) it is exponentially small, or equal to zero for  $x$ -clusters. Thus, the main contribution to the shift and to the splitting of levels is provided by energy corrections of the second order for large values of  $J$ :

$$\Delta E_k^A(s) = \frac{d_{sa}^2}{4} \sum_{k' \neq k} \frac{\left| \langle A, k | \{J_x, J_y\}_+ | B, k' \rangle \right|^2}{E_k^A - E_{k'}^B + 2\lambda}, \quad (8.8)$$

$$\Delta E_k^A(a) = \frac{d_{sa}^2}{4} \sum_{k' \neq k} \frac{\left| \langle A, k | \{J_x, J_y\}_+ | B, k' \rangle \right|^2}{E_k^A - E_{k'}^B - 2\lambda}, \text{ so that:}$$

$$\delta E_k^A = \Delta E_k^A(a) - \Delta E_k^A(s) = \lambda d_{sa}^2 \sum_{k' \neq k} \frac{\left| \langle A, k | \{J_x, J_y\}_+ | B, k' \rangle \right|^2}{(E_k^A - E_{k'}^B)^2 - 4\lambda^2},$$

$$\delta E_k^B = \Delta E_k^B(a) - \Delta E_k^B(s) = \lambda d_{sa}^2 \sum_{k' \neq k} \frac{\left| \langle B, k | \{J_x, J_y\}_+ | A, k' \rangle \right|^2}{(E_k^B - E_{k'}^A)^2 - 4\lambda^2}.$$

Here the condition has been used, that the constant  $\lambda$  exceeds greatly the rotational tunneling term, that is,  $|E_k^A - E_k^B| \ll \lambda$ .

The pairs  $(A, B)$  in Eq. (8.8) correspond to the pairs in Table 8.1, which are connected by symmetry operators like  $B_2$ :  $(A_1, B_2)$  and  $(A_2, B_1)$ . From Eqs. (8.8) and (8.3) we find the final result for the splitting:

$$\begin{aligned} \Delta E_k^A &= E_k^A(a) - E_k^A(s) = -\lambda \left[ 2 - d_{sa}^2 \sum_{k' \neq k} \frac{\left| \langle A, k | \{J_x, J_y\}_+ | B, k' \rangle \right|^2}{(E_k^A - E_{k'}^B)^2 - 4\lambda^2} \right], \\ \Delta E_k^B &= E_k^B(a) - E_k^B(s) = -\lambda \left[ 2 - d_{sa}^2 \sum_{k' \neq k} \frac{\left| \langle B, k | \{J_x, J_y\}_+ | A, k' \rangle \right|^2}{(E_k^B - E_{k'}^A)^2 - 4\lambda^2} \right], \end{aligned} \quad (8.9)$$

where  $(E_k^A, E_k^B)$  are the rotation energies of the cluster  $k$ .

Equations (8.8), (8.9) along with Table 8.1, which classifies all the possible states for  $d_{sa} = 0$  according to the representations of group  $D_2$ , provide a qualitative understanding of the position of levels as function of quantum numbers  $(k_C, k_A)$ . As it has been demonstrated earlier  $k_C + k_A = J$  or  $J+1$ .

Below we provide the results of a numerical calculation with parameters chosen close to those of the molecule  $SeH_2$  in a vibrationally excited state  $n = 3$  [38]:

$$\begin{aligned} A(s) &= A(a) = 7,83, \quad B(s) = B(a) = 7,39, \quad C = 3,74 \quad (cm^{-1}), \\ d_{as} &= 0,6 \quad (cm^{-1}), \quad \lambda = -0,06 \quad (cm^{-1}), \quad \vartheta_{rot} = \pm 27^\circ. \end{aligned} \quad (8.10)$$

As, according to Eq. (8.8) the energy corrections are determined by the second order of perturbation theory, to estimate the energy splitting of degenerate levels we use Eq. (8.9). Levels with large  $k_C \sim J$  correspond to an oblate top, while those with  $k_A \sim J$  correspond to a prolate top. Thus, with the increase of the difference  $k_A - k_C$  we go over from lower levels to the upper ones. For  $k_A - k_C \ll -1$  the sum in Eq. (8.9) is small  $\sim \frac{d_{sa}^2 J^2}{4(A-C)^2 k^2} \sim \frac{d_{sa}^2}{4(A-C)^2} \sim 10^{-2}$ , and so the splitting is nearly the same as in the absence of rotation:  $\Delta(E_a - E_s) \sim 0.12 \text{ cm}^{-1}$ . Thus, for  $k_C \sim J$  and  $k_A \ll J$ , when the sums in Eq. (8.9) are small, the relative splitting of levels does not change appreciable, and there are always two pairs of similar rotational  $z$ -clusters of ( $s$ ) and ( $a$ ) symmetry, shifted one from another by energy  $2\lambda = 0.12 \text{ cm}^{-1}$ :

$$\begin{aligned} \begin{pmatrix} A_1 \\ B_2 \end{pmatrix} &= (a), \quad \text{or} \quad \begin{pmatrix} A_2 \\ B_1 \end{pmatrix} = (a), \\ \begin{pmatrix} A_1 \\ B_2 \end{pmatrix} &= (s) \quad \quad \quad \begin{pmatrix} A_2 \\ B_1 \end{pmatrix} = (s). \end{aligned}$$

In this case there is practically no mixing of levels ( $s$ ) and ( $a$ ), as its value is of the same order as the sums in Eq. (8.9).

As the difference  $k_A - k_C$  increases, the classical trajectories on the RE surface, which correspond to quantum number  $k_C$ , approach the separatrix (see Fig. 7.2, implying it is rotated by  $90^\circ$  with respect to axis  $y$ ). Close to the separatrix the difference  $E_k - E_{k'}$  decreases (the frequency of motion along the orbits tends to zero), while the matrix elements  $\langle k | \{J_x, J_y\}_+ | k' \rangle$  increase, as the fast oscillations of wavefunctions' phases, decreasing the matrix elements, vanish. As a result, the sums in Eq. (8.9) increase, and, correspondingly, the splitting of levels  $\Delta E^A$  and  $\Delta E^B$  decreases. Simultaneously, the asymmetry in the splitting of  $\Delta E^A$  and  $\Delta E^B$  arises, as the motion is not quasi-classical then, so that  $|\langle k, A | \{J_x, J_y\}_+ | k', B \rangle|^2 \neq |\langle k, B | \{J_x, J_y\}_+ | k', A \rangle|^2$ , and the latter expressions in Eq. (8.9) produce different results. This is accompanied by the increased mixing of ( $a$ ) and ( $s$ ) states with the increase of the difference  $k_A - k_C$ .

With the subsequent increase of  $k_A - k_C$  the trajectories on the RE surface separate further from the separatrix line and enter the region of the  $x$ -cluster, where the quasi-classical approach applies again. Consequently,  $|\langle k, A | \{J_x, J_y\}_+ | k', B \rangle|^2 = |\langle k, B | \{J_x, J_y\}_+ | k', A \rangle|^2$ , and the splitting is  $\Delta E^A = \Delta E^B$ . The considered top in the  $x$ -cluster resembles the symmetrical prolate one. The latter brings about the decrease of the denominators  $[(E_k - E_{k'})^2 - \lambda^2]$  in the sums in Eq. (8.9). Thus, the sums in Eq. (8.9) start to grow again, while the difference  $\Delta E = E(a) - E(s)$  of levels ( $a$ )

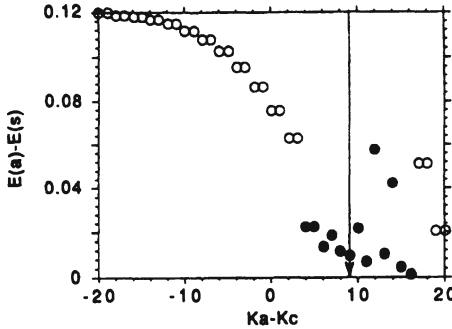


Figure 8.2: The energy splitting of levels  $|s\rangle$  and  $|a\rangle$ . The rotational functions and the energy splitting depend appreciably upon the type of symmetry only in the vicinity of the separatrix line  $k_A - k_C \sim 10$ ,  $J = 20$ .

and  $(s)$  will decrease, increasing their mixing. The described dependence of  $\Delta E^{A,B}$  upon the difference  $k_A - k_C$  is backed up entirely on a qualitative level by the exact calculation, see Table 8.2 from Ref. [38]. Fig. 8.2 reproduces the plot of this functional dependence, while Fig. 8.3 demonstrates the amount of mixing.

The curve  $\Delta E(k_A - k_C)$  in Fig. 8.2 reveals clearly the dependencies, discussed above. Really, when  $k_A - k_C$  belongs to the interval  $(-20, 2)$ , the splittings  $E^A(a) - E^A(s)$  and  $E^B(a) - E^B(s)$  are equal, and decrease simultaneously from 0.12 to 0.063 for  $k_A = 11$  and  $k_C = 9$ . Further on, for the motion, close to the separatrix line the quasi-classical approximation becomes invalid, so that  $\Delta E^A \neq \Delta E^B$ , and the functional dependence  $\Delta E^{A,B}(k_A - k_C)$  is no longer monotonous. Then, one enters the region of  $x$ -cluster, where again  $\Delta E^A = \Delta E^B$ , and  $\Delta E$  decreases monotonously with the increase of  $k_A - k_C$ . The curve  $\eta(k_A - k_C)$  correlates entirely with the dependence  $\Delta E(k_A - k_C)$ . The monotonous decrease of  $\Delta E$  corresponds to the monotonous increase in mixing, the irregularity in the dependence  $\Delta E(k_A)$  is accompanied by the irregularity in  $\eta(k_A)$ , and, finally, if  $\Delta E^A = \Delta E^B$ , then  $\eta^A = \eta^B$ .

These results can be instructively interpreted with the help of the Hamiltonian in representation (8.1) and the concept of RE surface. Below we will utilize the following conditions, in accordance with Eq. (8.10):

$$\frac{A - B}{C} \sim 0, 1 \ll 1, \quad J \cdot \vartheta_{rot} = 20 \cdot 27^\circ = 540^\circ. \quad (8.11)$$

The states with  $k_C = k_z \sim J = 20$  are of quasiclassical nature, and are of two-fold degeneracy. Thus, their wavefunctions can be represented in the form:

$k_A$	$k_C$	$\psi_{vib} \sim s$	$\psi_{vib} \sim a$	$\Delta E$	% mixing
0	20	1647.77	1647.89	0.120	0
1	20				
1	19	1797.96	1798.08	0.119	0
2	19				
2	18	1940.41	1940.52	0.118	0
3	18				
3	17	2075.09	2075.20	0.117	1
4	17				
4	16	2202.00	2202.11	0.115	2
5	16				
5	15	2321.12	2321.24	0.112	3
6	15				
6	14	2432.44	2432.55	0.108	5
7	14				
7	13	2535.92	2536.02	0.103	7
8	13				
8	12	2631.50	2631.60	0.096	10
9	12				
9	11	2719.13	2719.22	0.087	14
10	11				
10	10	2798.70	2798.77	0.076	18
11	10				
11	9	2870.00	2870.06	0.063	25
12	9				
12	8	2932.59	2932.61	0.023	42
13	8	2932.85	2932.87	0.023	38
13	7	2984.82	2984.83	0.014	44
14	7	2987.23	2987.25	0.019	42
14	6	3022.88	3022.89	0.012	45
15	6	3035.10	3035.11	0.010	46
15	5	3050.94	3050.96	0.022	40
16	5	3081.40	3081.41	0.007	47
16	4	3084.89	3084.95	0.058	26
17	4	3131.44	3131.45	0.010	47
17	3	3131.81	3131.85	0.042	32
18	3	3187.53	3187.54	0.005	48
18	2	3187.56	3187.56	0.001	49
19	2	3249.63	3249.68	0.051	28
19	1				
20	1	3317.29	3317.31	0.021	41
20	0				

Table 8.2: Rotation-tunneling energy levels in  $cm^{-1}$  for  $XH_2$   $J = 20$ .

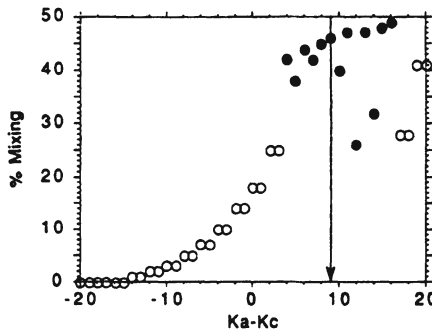


Figure 8.3: The amount of mixing  $\eta$  % of the vibrational states  $|s\rangle$  and  $|a\rangle$ .

$$(|k_C\rangle \pm |-k_C\rangle) |n_1\rangle, \quad \exp\{-2iJ_z\vartheta_{rot}\} (|k_C\rangle \pm |-k_C\rangle) |n_2\rangle. \quad (8.12)$$

The first wavefunction corresponds to the excitation of the first bond, when the principal axes are rotated by  $27^\circ$  with respect to the initial ones, while the second wavefunction corresponds to the excitation of the other bond with the axes rotated with respect to the first ones by  $-54^\circ$ . The overlap matrix elements of the wavefunctions (8.12) are:

$$\begin{aligned} \langle n_1 | H | n_2 \rangle &= \frac{\lambda}{2} (\langle k_C | \pm \langle -k_C |) \exp\{-2iJ_z\vartheta_{rot}\} (\langle k_C | \pm \langle -k_C |) \\ &= \lambda \begin{pmatrix} \cos(2k_C\vartheta_{rot}) \\ \mp i \sin(2k_C\vartheta_{rot}) \end{pmatrix} = \begin{pmatrix} \lambda \\ 0 \end{pmatrix}, \quad \text{if } k_C = J. \end{aligned} \quad (8.13)$$

Here the quasiclassical condition

$$f(J_z) |k_C\rangle = f(k_C) |k_C\rangle$$

has been utilized. For  $k_C = J$  the overlap is equal to  $\lambda$ , so that the level splitting is  $2\lambda$ , as in the absence of rotation.

With the decrease of  $k_C$  the overlap decreases as well, and the dependence  $\Delta E(k_C) = 2\langle 1 | H | 2 \rangle$  takes up a cosine form. Obviously, the plot of the functional dependence  $\Delta E(k_C)$  in its monotonous part resembles closely  $\cos(k_C\theta)$ . This fact can be proved rigorously enough in the case  $\theta_{rot} \ll 1$ ,  $2J\theta_{rot} = 2\pi$ .

From Eq. (8.13) in the present case it follows that  $\langle n_1 | H | n_2 \rangle$  as function of  $k_C$  will obey the cosine dependence in the entire quasiclassical region, at least until the value of  $\sin(2k_C\vartheta_{rot})$  becomes too large. The influence of

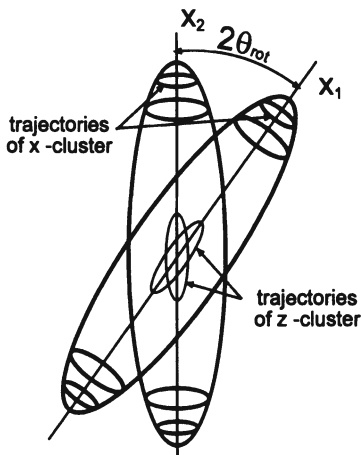


Figure 8.4: The intersecting RE surfaces of  $|n_1\rangle$  and  $|n_2\rangle$  terms. Axis  $z$  is perpendicular to the plane of the plot.

sine terms can be taken into account by the addition in cosine of an slowly varying phase  $\delta(k_C)$ :

$$\Delta E \approx 2\lambda \cos(2k_C\vartheta_{rot} + \delta(k_C)). \quad (8.14)$$

Thus, the splitting  $\Delta E(k)$  represents a cosine-type dependence with phase modulation, which in the vicinity of the separatrix line produces the irregularity in the behavior of  $\Delta E(k)$ . Upon entering the region of  $x$ -cluster, the phase  $\delta(k_C)$  acquires a slow dependence upon  $k_C$ , which produces the same cosine, shifted however by a constant phase. The latter agrees completely with the curve  $(E(a) - E(s))$ , function of  $k_C$ , in Fig. 8.2.

The above discussion can be illustrated conveniently with the help of two plotted rotated RE surfaces, which correspond to vibration terms  $|n_1\rangle$  and  $|n_2\rangle$ , see Fig. 8.4.

The trajectories of  $z$ -clusters at small rotation angle have overlaps of the order of 1, as the corresponding rotational functions differ by a small rotation with respect to axis  $Z(C)$ . With the decrease of  $k_C$  the trajectories of  $z$ -clusters will expand more and more, each on its own RE surface, and elongating along their axes  $x_1$  and  $x_2$ . At the same time, the overlap of trajectories, and, correspondingly, of the wavefunctions, will decrease. The decrease of the overlap is accompanied by the reduction in level splitting. This effect can be termed 'rotational cancellation of vibrational excitation's tunneling'. Upon entering the  $x$ -clusters, the trajectories encircle the  $x_1$  and

$x_2$  axes according to the excited mode, and the overlap is reduced further. The trajectories, which embrace the very tops of RE surface of the  $x$  axes do not overlap at all. This corresponds to the anomalously small overlap of wavefunctions, and to the corresponding low splitting of energy levels.

Symmetrical hydrides  $XH_3$  and  $XH_4$  can be considered in an analogous way, Ref. [38]. We note here, that the non-adiabatic vibrational - rotational motion in the molecule  $NH_3$  have been studied by M.Ya.Ovchinnikova in Ref. [127]. There the vibrational - rotational excitation and its tunneling have been analyzed with the account of the inversion transition from the right configuration into the left one, and vice versa. It has been shown [127], that the rotational spectrum of the molecule  $NH_3$  at high vibrational excitation resembles at small  $\lambda$  the spectrum of an asymmetric top with an  $A, C$  hybrid band.

The theoretical and experimental analysis of the rotation-vibration band in molecule  $CH_4$  with a highly-excited stretching vibration has been provided by K.Lehman, [123]. In particular, it has been shown, that the rotational structure of the molecule  $CH_4$  resembles the rotational structure of a symmetric top. The analysis of the vibration-rotation interaction in the considered molecule becomes more complex due to the strong resonance interaction between the stretching and bending modes. However, the obtained result agrees with the general law: rotation suppresses the tunneling of the vibrational excitation of the high overtone, so that the rotational structure of the molecular spectrum loses the initial molecular symmetry and acquires the new reduced symmetry. In the case of an excited molecule  $CH_4$  it is the spectrum of a symmetrical top, instead of the spectrum of a spheric top, as it would be for a non-excited molecule.

However, as it has been mentioned above, with the increase of the resolution of the spectrum, the initial total inner symmetry of the molecule (the symmetry of the system of RE surfaces, corresponding to different excitations of LMs) is manifested in the superfine structure of the vibrational-rotational cluster. For example, at average resolution the rotational structure of a symmetric top is observed, while at a higher resolution the symmetry group  $T_d$  is revealed (molecules  $^{116}S_nH_4$  in Ref. [37] and  $CH_4$  in Ref. [123]).

All the cited papers which provided the fitting of calculated spectra to experimental data demonstrate, that the highly excited vibrations reveal the character of local modes, when the entire vibrational excitation is localized on a single valance bond. The entire shell of vibrational states is composed of linear combinations of such states. Such a description of vibrational excitations requires the minimal number of fitting parameters for the vibrational-rotational spectrum ( see Refs. [37, 123, 124] and references therein). For example, in Ref. [37] with the help of 32 parameters in the effective Hamiltonian (of which 21 parameters were merely fitting ones) 1290 lines of IR spectrum were correctly specified.

## 8.2 Rotational - vibrational spectrum in the vicinity of bifurcation points

In the present Section we will consider the qualitative changes in the structure of rotational spectra, produced by changes of the parameters in the Hamiltonian or of constants of motion (such as momentum  $J$ ). These changes reveal a number of common qualitative features that do not depend upon the particular numeric values of the parameters and are of a topological nature (see, for example, [19]). Really, upon the change of parameters or of the momentum  $J$  the RE surface of the molecule gets transformed, so that for some particular values a bifurcation point on the RE surface can emerge – i.e. a point, where  $\left| \frac{\partial^2 E}{\partial x_i \partial x_k} \right| = 0$  with  $x_i, x_k$  – any two variables that determine the direction of momentum  $\mathbf{J}$  and, correspondingly, the energy  $E(\mathbf{J})$ . The behavior of the set of RE surfaces in the vicinity of the bifurcation point  $(x_{1b}, x_{2b}; t_{1b}, \dots t_{rb})$ , where  $(t_1, \dots t_r)$  are governing parameters, are studied within the theory of catastrophes [128]. It has been proved, that for  $r \leq 5$  there are only 11 distinct qualitatively different stable catastrophes, which determine the universal behavior (or topology) of the surface  $E(x_1, x_2; t_1, \dots t_5)$  in the vicinity of bifurcation point  $(x_{1b}, x_{2b}; t_{1b}, \dots t_{5b})$  (see the Thom theorem in Chapter 7, Section 7 of Ref. [128]). Any family of RE surfaces  $E(x_1, x_2; t_1, \dots t_5)$  will reveal a universal behavior in the vicinity of bifurcation manifold  $B\{x_{1b}, x_{2b}; t_{1b}, \dots t_{5b}\}$ , which is topologically equivalent to one of the eleven catastrophes, enumerated in Thoma theorem.

In the theory of catastrophes it is proved, that for a one-parametric family of surfaces  $E(x, y | J)$  some continuous transformation of variables  $(x, y) \rightarrow (u, v)$  can be performed, so that in the vicinity of the bifurcation manifold the dependence  $E(u, v)$  takes the form:

$$\begin{aligned} E(u, v; J) &= E(x(u, v), y(u, v); J) \\ &= u^3 - 3\alpha^2(J - J_c)u + v^2 + E_0. \end{aligned} \quad (8.15)$$

Here a local coordinate set has been used, where the  $E$  axis is orthogonal to the RE surface at point  $E_0$ . Such a surface models the appearance of a stable and an unstable rotation axis with the molecular momentum changing from  $J < J_c$  to  $J > J_c$ . Really, the stationary rotation axis is determined by the equation:

$$\frac{\partial E}{\partial u} = \frac{\partial E}{\partial v} = 0. \quad (8.16)$$

The latter at  $J > J_c$  has two solutions for the function (8.15), while at  $J < J_c$  in the vicinity of  $u = v = 0$  there are no solutions. Figure 8.5 demonstrates the classical trajectories on the RE surface in the vicinity of  $u = v = 0$  below and above the transition. At  $J < J_c$  the trajectory goes

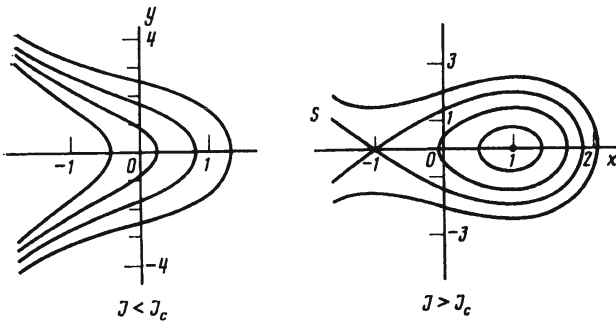


Figure 8.5: Classical trajectories on the RE surface, which correspond to stable and unstable rotation axes of  $C_1$  local symmetry.

away from the origin, which means that vector  $\mathbf{J}$  precesses with respect to some axis away from the point  $u = v = 0$ . When  $J$  exceeds  $J_c$  there appear two axes – a stable one at point  $(\alpha\sqrt{J - J_c}, 0)$ , and an unstable one at  $(-\alpha\sqrt{J - J_c}, 0)$ .

From the point of view of quantum mechanics it means, that some part of levels, which correspond to infinite trajectories does not suffer qualitative changes and remains in the same cluster, to which they belonged before the transition. However, some part of the infinite trajectories transforms into closed ones, localized close to the origin of the coordinate set. These trajectories give rise to new rotational levels with drastically different wavefunctions. Thus, in the transition point there emerges a new rotation cluster, corresponding to the appearance of a new stable rotation axis. For small values of  $|J - J_c|$  the number of such levels is low, as in the case when the rotation axis is close to the coordinate origin, the number of quantized trajectories is small. From Eqs. (8.16) and (8.15) it follows, that  $E''(J) = \mp \frac{3}{2} |\alpha|^3 |J - J_c|^{-\frac{1}{2}}$ . Such a singularity is typical for the second derivative of the thermodynamic potential over temperature in the vicinity of the Curie point of the second order phase transition within Landau theory. This is coincidence in fact, as in both cases the qualitative changes in the system are produced by the violation of symmetry (destruction of order parameter).

More varied phenomena occur, if the classical trajectories in the considered point of RE surface, where the new axis emerges, have some local symmetry. Let us assume, that it would be symmetry of the type  $C_2$ ,  $C_{2v}$ , or  $C_s$ . Besides, let the new stationary rotation axis emerge at  $J = J_c$  with energy  $E(J_c)$ . Then the family of RE surfaces in the vicinity of bifurcations takes the form:

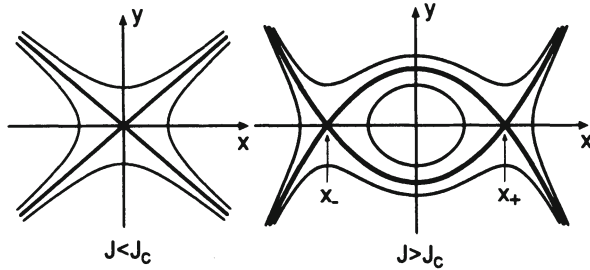


Figure 8.6: Set of classical trajectories on the RE surface in the vicinity of the bifurcation point for a non-local critical phenomenon with local symmetry group  $C_{2v}$ .

$$E(x, y; J) = E_0(J_c) - \alpha(J - J_c)x^2 + a_{20}y^2 + a_{04}x^4. \quad (8.17)$$

Here again a local coordinate set has been chosen. We note, that in the presence of a single governing parameter there always exists some continuous transformation of variables in the vicinity of a bifurcation manifold, which transforms the one-parametric family of surfaces  $F(x_1, \dots, x_n; t)$  to the form  $f(u, \tau) + \sum_{i=2}^n u_i^2$ . This theorem has been proved in the theory of catastrophes [128]. Thus, the local form, Eq. (8.17), of RE surface with  $C_{2v}$  symmetry is universal. It can be always assumed, that the dependence on the second variable is of a quadratic type. Substituting Eq. (8.17) into Eq. (8.16), we obtain the equations, which determine the position of stationary rotation axes in the vicinity of the transition  $J \sim J_c$ :

$$\begin{aligned} 2\alpha(J - J_c)x &= 4x^3a_{04}, \quad y = 0, \\ x_0 = 0, \quad x_{\pm} &= \pm\sqrt{\frac{\alpha(J - J_c)}{2a_{04}}}. \end{aligned} \quad (8.18)$$

We assume  $\alpha a_{04} > 0$ . This is no limitation in fact, as otherwise the only difference will be the change of the regions  $J > J_c$  and  $J < J_c$ . The critical phenomena belong to one of the two types, depending on the sign of  $a_{20}a_{04}$ .

First, let us consider the case  $a_{20}a_{04} < 0$ . It corresponds to a nonlocal critical phenomenon. Really, the equation (8.17) then takes the form:

$$\begin{aligned} |\alpha(J - J_c)|x^2 - |a_{20}|y^2 &= \text{const}, \quad J < J_c \quad - \text{hyperbole}; \\ |a_{04}|x^4 - |\alpha(J - J_c)|x^2 - |a_{20}|y^2 &= \text{const}, \quad J > J_c. \end{aligned} \quad (8.19)$$

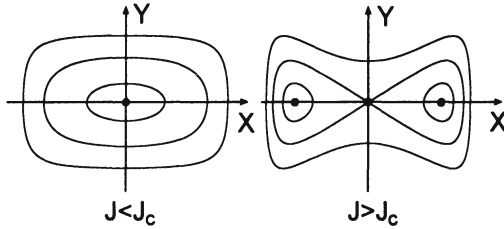


Figure 8.7: Set of trajectories on the RE surface in the vicinity of the bifurcation point for a local critical phenomenon with local symmetry group  $C_{2v}$ .

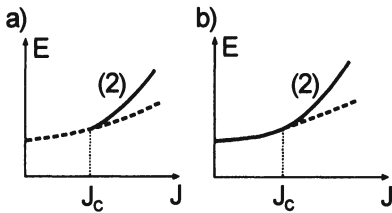


Figure 8.8: Bifurcation diagram for a non-local (a) and local (b) critical phenomenon with local symmetry  $C_{2v}$ . Dashed line corresponds to an unstable rotation axis. Number in parenthesis specifies the number of axes with violated  $C_{2v}$  symmetry.

In the derivation of Eq. (8.19) we have taken into account the inequalities  $\alpha a_{04} > 0$ ,  $a_{20}a_{04} < 0$ . Corresponding curves are plotted in Fig. 8.6.

Next we consider the case  $a_{20}a_{04} > 0$ . The critical phenomenon is of a local character. Then Eq. (8.17) describes the surface:

$$\begin{aligned} |\alpha(J - J_c)|x^2 + |a_{20}|y^2 &= \text{const}, \quad J < J_c \quad \text{- ellipsis;} \\ |a_{04}|x^4 - |\alpha(J - J_c)|x^2 + |a_{20}|y^2 &= \text{const}, \quad J > J_c. \end{aligned} \quad (8.20)$$

The curves (8.20) are plotted in Fig. 8.7.

The critical phenomenon, depicted in Fig. 8.6, corresponds to the emergence of one stable rotation axis of symmetry  $C_{2v}$  in place of an unstable axis of the same local symmetry  $C_{2v}$ . Besides, there appear two unstable rotation axes at points  $x_+$  and  $x_-$  with a violated local  $C_{2v}$  symmetry. These axes are transformed one into another by operations from the group  $C_{2v}$ . From the geometrical point of view, the appearance of a stable rotation axis signifies the emergence of a small hollow or a small hill in the saddle point of

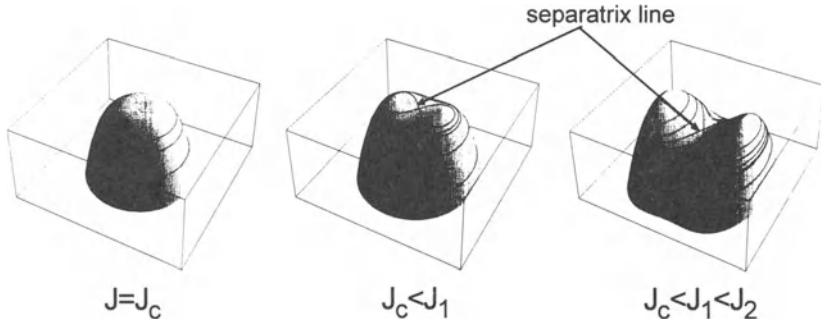


Figure 8.9: Formation of a new rotation cluster in a critical phenomenon of local type with  $C_{2v}$  symmetry.

the RE surface. As a result of the emergence of a hollow (hill) there appear closed local trajectories, which encircle the new  $C_2$  axis. These trajectories correspond to the emerging rotational levels, and the number of the latter grows with the increase of the depth of the hollow (height of the hill). This critical phenomenon and the appearance of the stable axis  $C_2$  are termed nonlocal, as most part of the trajectories go away from the point, where the new axis emerges. The local and global trajectories are separated by separatrix lines. The latter are nothing but slightly deformed former trajectories. In a qualitative way these phenomena can be represented by a bifurcation diagram, which shows the dependence of the stationary point energy upon  $J$  in variables  $(E, J)$ , Fig. 8.8 (a). Dashed lines in the diagrams correspond to unstable rotation axes. Numbers in parentheses show the number of axes with violated  $C_{2v}$  symmetry.

In the case of a local critical phenomenon, depicted in Fig. 8.7, one stable  $C_2$  axis gives rise to two equivalent stable axes with violated  $C_{2v}$  symmetry at points  $x_{\pm}$ , and to one unstable axis at point  $x = 0$ . All the trajectories in the vicinity of bifurcation are localized close to the critical point, and thus the phenomenon is termed local.

As a result of the "phase transition", pairs of equivalent trajectories appear with the corresponding pairs of degenerate rotation levels. Rotational levels with different quantum numbers stick together, creating the rotational cluster. Schematically this process on the RE surface is depicted in Fig. 8.9.

The bifurcation diagram of this phenomenon is presented in Fig. 8.8 (b). Comparing it to Fig. 8.9 we find, that the continuous curve corresponds to trajectories on the emerging small hills. The typical behavior of the rotation cluster energy  $E_n(J)$  is depicted in Fig. 8.10 from Ref. [19]. Here  $n$  is the level number, ordered with the increase of energy. The energy is measured with respect to the energy of the separatrix. Figures 8.9 and

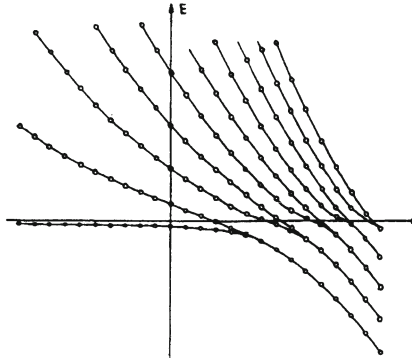


Figure 8.10: Typical behavior of a quantum system of energy levels as function of the variation of the constant of motion  $J$  in the neighborhood of the critical value for a local critical phenomenon with  $C_{2v}$  local symmetry group.

8.10 are in correspondence to each other, if  $\frac{dE}{dk_c} < 0$ , and the origin of the radius-vector of the points on RE surface, Fig. 8.9, is situated on top. Another way of establishing correspondence between Figs. 8.9 and 8.10 is the symmetry inversion of the curve Fig. 8.10 with respect to axis  $J$ . The plot of the functional dependence  $E_n(J)$  demonstrates that when the classical trajectories separate between different hills, they join the separatrix line with  $E = 0$ , and their levels now belong to the same rotational cluster. The energy splitting is determined by tunneling, which decreases with the increase of the difference  $J - J_c$ . Simultaneously the trajectories go away from the separatrix, in full agreement with Figs. 8.10 and 8.9. The universal Hamiltonian, which describes correctly the rotational spectra in the vicinity of bifurcation points for axes of various symmetry can be found in Refs. [129, 130]. In the second cited work the shape of RE surfaces in the vicinity of bifurcation, function of a single governing parameter  $J$ , which describe the emergence and disappearance of rotation axes for all symmetries of the type  $C_n$  and  $C_{2v}$  are provided. A harmonic approximation for the quantum description of vector  $\mathbf{J}$  precession is constructed as well.

Next let us consider the case of degenerate vibrational levels. The effective Hamiltonian is constructed then of rotational operators  $H_{m,n}(J_{\bar{x}_i})$ . The latter connect the subspaces of the  $m$ -th and  $n$ -th vibrational levels with  $|E_m^{(vib)} - E_n^{(vib)}| \lesssim \hbar\Omega_{rot}$ . All the levels of the vibrational multiplet, that satisfy this condition, interact effectively with the molecular rotation, the latter interaction characterized by the operator matrix  $H_{m,n}(J_{x_i})$ . If this multiplet consists of levels with two close vibrational frequencies  $\nu, \nu'$ , they call it a dyad  $\nu/\nu'$  of vibrational-rotational levels. A system of levels with

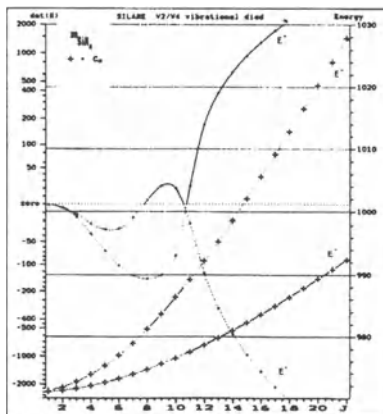


Figure 8.11: Hessian values for the stationary  $C_2$  rotation axis for the classical energy surface corresponding to the lower branch of the  $\nu_2$  state of  $^{28}\text{SiH}_4$ . By + sign the energy of stationary points with  $C_2$  local symmetry on the rotational energy surface is marked. Bold sign + is the Hessian value for  $C_2$  type stationary points. The curves, coming out from the point 'zero' represent the dependence of the Hessian on  $J$ .

three close vibrational frequencies  $\nu, \nu', \nu''$  they call a triad of vibrational-rotational levels. For example, in a tetrahedral  $AB_4$  molecule there is a dyad  $\nu_2/\nu_4$ , corresponding to the interaction of molecular rotation with the vibrations of bond angles, and another diad  $\nu_1/\nu_3$ , characterizing the vibrations of  $AB$ -bonds and rotation.

At high rotational excitation the molecular rotation is of classical type, so that the operators  $J_{\bar{x}_i}$  can be substituted by usual functions  $J_{\bar{x}_i}(J, \theta, \varphi)$ , where  $(\theta, \varphi, J)$  determine the direction and the length of vector  $\mathbf{J}$  in the body system frame. Then the Hermitian matrix  $H_{m,n}(\theta, \varphi, J)$  with eigenvalues  $E_1(\theta, \varphi, J), E_2(\theta, \varphi, J)$ , etc., determines the family of RE surfaces, which depend upon  $J$  as a parameter, each one corresponding to every eigenvalue  $E_n$ .

In the present case there are two possible reasons for the qualitative restructuring of the rotational-vibrational spectrum with the change of momentum  $J$ . The first one is the passage through a bifurcation point on a separate RE surface. The second one is the formation of crossing points of two RE surfaces, which refer to different eigenvalues:  $E_m(J_c, \theta_c, \varphi_c) = E_n(J_c, \theta_c, \varphi_c)$ .

The first case has been considered above, when there was a single nondegenerate vibrational level, and correspondingly one RE surface  $E = H(J, \theta, \varphi)$ .

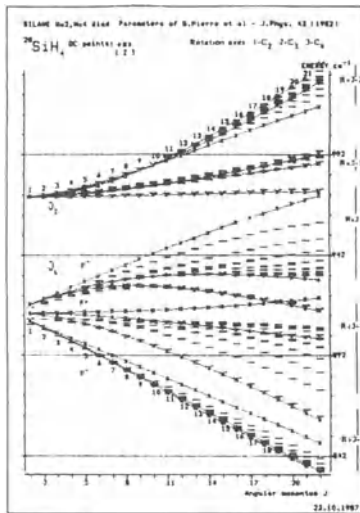


Figure 8.12: The system of energy levels and the energy of the  $C_2, C_3, C_4$  stationary points of the classical energy surfaces for the  $\nu_2/\nu_4$  dyad of  $^{28}\text{SiH}_4$ . Here  $x$  is the energy of  $C_4$  axis,  $\square$  is the energy of  $C_3$  axis,  $\circ$  - energy of  $C_2$  axis.

For a vibrational multiplet all the critical phenomena in the vicinity of bifurcation point for a single RE surface are in complete analogy to the consideration above. This fact can be seen clearly in Fig. 8.11 from Ref. [19]. The dependency of the Hessian  $\det(H^\pm)$  upon momentum  $J$  for the stationary  $C_2$  rotation axis for the RE surface corresponding to  $E^\pm$ -term of the mode  $\nu_2$  ( $v = 1$ ) of a molecule  $\text{SiH}_4$  is provided. From the plots it can be seen, that the Hessian of  $E^+(J)$ -term is a positive value at  $J \geq 11$ . It means that in the term  $E^+(J)$  at  $J > 11$  there appear 12-fold rotational clusters, which correspond to the formation of 12 equivalent stable  $C_2$  axis on the RE surface (Fig. 8.6). Transitions, incorporated into 12-fold clusters are revealed in experimental data. Tables 8.3 and 8.4 demonstrate the 12-fold clusters in the system of energy levels for  $\text{CH}_4$  and  $\text{SiH}_4$ . The rotational bands of these clusters can be seen most clearly in Fig. 8.12 from Ref. [19]. Obviously, among the levels of  $\nu_2$  mode in the region  $J = 12$  there splits apart a band which can be interpreted as the band of a 12-fold cluster, corresponding to the molecular rotation with respect to the appearing stable  $C_2$  axes, as demonstrated in Fig. 8.6.

It is worth mentioning, that the appearance of a 12-fold cluster has been forecast with the help of a simple effective Hamiltonian, which takes into

J energies in	symmetry of the	type levels clusters	and	Cluster width	Energy	separation
					from the upper level	closest lower level
			(cm <sup>-1</sup> )	(cm <sup>-1</sup> )	(cm <sup>-1</sup> )	(cm <sup>-1</sup> )
12	<i>F</i> <sub>1</sub>	13	2357.904 788			
12	<i>E</i>	9	2357.860 680			
12	<i>F</i> <sub>1</sub>	12	2357.740 393	0.55	10.5	0.5
12	<i>F</i> <sub>2</sub>	13	2357.630 423			
12	<i>A</i> <sub>2</sub>	4	2357.355 851			
13	<i>F</i> <sub>2</sub>	14	2494.569 540			
13	<i>E</i>	9	2494.467 041			
13	<i>F</i> <sub>1</sub>	14	2494.348 674	0.33	12.1	1.0
13	<i>A</i> <sub>1</sub>	5	2494.300 630			
13	<i>F</i> <sub>2</sub>	13	2494.237 198			
14	<i>A</i> <sub>2</sub>	5	2641.567 524			
14	<i>F</i> <sub>2</sub>	15	2641.484 712			
14	<i>F</i> <sub>1</sub>	15	2641.417 247	0.34	13.8	1.1
14	<i>E</i>	10	2641.247 288			
14	<i>F</i> <sub>1</sub>	14	2641.221 743			
15	<i>F</i> <sub>2</sub>	16	2798.764 098			
15	<i>A</i> <sub>1</sub>	5	2798.720 861			
15	<i>F</i> <sub>1</sub>	16	2798.684 588	0.30	15.3	1.5
15	<i>E</i>	11	2798.621 582			
15	<i>F</i> <sub>2</sub>	15	2798.458 606			
16	<i>F</i> <sub>1</sub>	17	2966.264 290			
16	<i>E</i>	11	2966.247 810			
16	<i>F</i> <sub>1</sub>	16	2966.155 522	0.32	17.0	1.7
16	<i>F</i> <sub>2</sub>	17	2966.071 832			
16	<i>A</i> <sub>2</sub>	6	2966.952 947			
17	<i>F</i> <sub>2</sub>	18	3144.000 141			
17	<i>E</i>	12	3143.911 174			
17	<i>F</i> <sub>1</sub>	18	3143.863 189	0.23	18.0	1.9
17	<i>A</i> <sub>1</sub>	6	3143.841 769			
17	<i>F</i> <sub>2</sub>	17	3143.775 683			

Table 8.3: 12-fold rotational clusters in the energy spectrum of <sup>12</sup>CH<sub>4</sub>.

J energies in	symmetry of the	type levels clusters	and	Cluster width	Energy	separation
					from the upper level	closest lower level
			(cm <sup>-1</sup> )	(cm <sup>-1</sup> )	(cm <sup>-1</sup> )	(cm <sup>-1</sup> )
14	$A_2$	5	1581.605 667			
14	$F_2$	15	1581.539 325			
14	$F_1$	15	1581.479 692	0.26	16.2	0.5
14	$E$	10	1581.387 901			
14	$F_1$	14	1581.342 038			
15	$F_2$	16	1668.100 683			
15	$E$	11	1668.013 921			
15	$F_1$	16	1667.969 200	0.22	17.9	0.7
15	$A_1$	5	1667.935 175			
15	$F_2$	15	1667.885 390			
16	$F_1$	17	1760.262 672			
16	$E$	11	1760.256 652			
16	$F_1$	16	1760.180 643	0.23	19.6	1.0
16	$F_2$	17	1760.121 334			
16	$A_2$	6	1760.033 110			
17	$F_2$	18	1858.108 758			
17	$A_1$	6	1858.066 133			
17	$F_1$	18	1858.055 310	0.16	21.0	1.0
17	$E$	12	1858.027 375			
17	$F_2$	17	1857.947 292			
18	$A_2$	6	1961.605 533			
18	$F_2$	19	1961.564 825			
18	$F_1$	19	1961.521 797	0.14	22.4	1.3
18	$E$	13	1961.470 811			
18	$F_1$	18	1961.466 926			
19	$F_2$	20	2070.662 857			
19	$E$	13	2070.611 973			
19	$F_1$	20	2070.602 380	0.11	23.8	1.3
19	$A_1$	7	2070.596 850			
19	$F_2$	19	2070.548 881			

Table 8.4: 12-fold rotational clusters in the energy spectrum of  $^{28}SiH_4$ .

account the vibrational shell of  $\nu_2$  mode solely, and which incorporated only two tensor contributions [131]:

$$H = \left[ (a_2^+ a_2)^E R^{2(2,E)} \right]^{A_1} + u \left[ (a_2^+ a_2)^{A_2} R^{3(3,A_2)} \right]^{A_1}. \quad (8.21)$$

Here  $R^{m(K,C)}$  signifies, that operator  $R$  is a polynomial of order  $m$  in operators  $J_{\bar{x}_i}$ . The latter are transformed according to the irreducible representation  $K$  of the rotation group and the irreducible representation  $C$  of the point symmetry group of molecule (in the present case it is  $T_d$ ). The birth and annihilation operators  $a_{21}^+, a_{22}^+$  and  $a_{21}, a_{22}$  for the mode  $\nu_2$  are transformed according to the representation  $E$  of the point group  $T_d$ <sup>2</sup>, each pair correspondingly. The bilinear combinations  $a_{2i}^+ a_{2j}$  incorporate the representation  $E, A_1$  and  $A_2$  of the group  $T_d$ . The operator (8.21), obviously, is invariant with respect to the group of inner symmetry  $T_d$ .

The Hamiltonian (8.21) enables one to forecast correctly the emergence of 12-fold clusters in  $CH_4$  and  $SiH_4$  under a suitable choice of numeric parameters. However, the operator (8.21) does not provide the best possible description of the vibrational-rotational spectrum of molecules  $CH_4$  and  $SiH_4$ . This fact is revealed clearly by a substantial change of the fitting parameter  $u$  in passing to the effective Hamiltonian, which takes into account the interaction with the  $\nu_4$  mode. Consequently, the model Hamiltonian (8.21) in second order provides an incorrect result.

Thus, we arrived at the situation, when a more accurate calculation of the spectrum requires the account of several RE surfaces of the quasi-degenerate vibrational multiplet. Presently that would be the RE surface of a  $\nu_2/\nu_4$  dyad. The necessity of taking into account the interaction of RE surfaces means, that we are close to the cross-section of some two RE surfaces. This is exactly the second cited case, when it is necessary to consider the entire vibrational manifold, and when the distribution of rotational-vibrational levels in the manifold is influenced substantially by the presence of cross-section points of RE surfaces.

The nature of the cross-section of the two RE surfaces, corresponding to different eigenvalues of a Hermitian matrix, is depicted in Fig. 8.13, Ref. [19]. In the vicinity of the cross-section of two RE surfaces a cone is formed. It follows from the fact, that the dimension of the parametric manifold  $(J, \theta, \varphi)$ , at which the eigenvalues of a Hermitian matrix coincide with each other  $E_m(J, \theta, \varphi) = E_n(J, \theta, \varphi)$ , is of zero measure [113]. The latter means, that the section points  $(\theta_c, \varphi_c, J_c)$  are isolated ones, so that the equation of the RE surface in their vicinity acquires the form <sup>3</sup>:

---

<sup>2</sup>It follows from the fact, that  $a_1$  and  $a_2$  should be transformed one through the other, and  $E$  is the sole two-dimensional representation of group  $T_d$ .

<sup>3</sup>From the point of view of the theory of catastrophes the cross-section points of two RE surfaces form a bifurcation manifold of zero measure, where  $\frac{\partial^2 E}{\partial u \partial v}$  is zero along with all its minors.

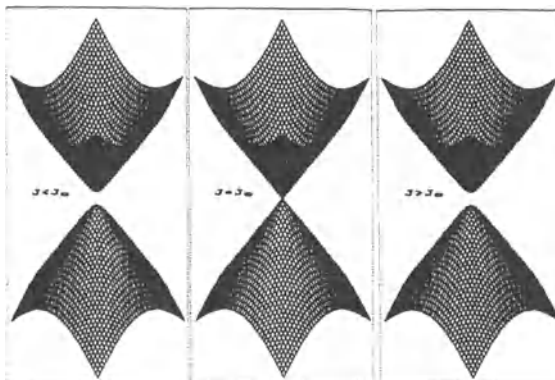


Figure 8.13: Modification of the two energy surfaces showing the formation of a conical intersection (diabolic) point at  $J = J_c$ .

$$A(\theta - \theta_c)^2 + B(\phi - \phi_c)^2 + C(J - J_c)^2 = (E - E_c)^2. \quad (8.22)$$

Corresponding surfaces are shown in Fig. 8.13. In the vicinity of these points the adiabaticity conditions of the vibrational-rotational motion are violated, and the corresponding wavefunctions suffer qualitative modifications under the change of momentum from  $J < J_c$  to  $J > J_c$  in the close neighborhood.

Thus it is obvious, that the presence of the intersection points of RE surfaces leads to the mixing of rotational-vibrational states of different vibrational bands of the manifold. Such intersections of RE surfaces are called diabolic points.

The plots, presented in Fig. 8.12 are results of experiments on IR spectra of a tetrahedral molecule  $SiH_4$ . These results can be reproduced with the help of a model Hamiltonian of the following form [19]:

$$H = \frac{\nu_2 - \nu_4}{2} \left[ \sum_{\alpha=1}^2 a_{2\alpha}^+ a_{2\alpha} - \sum_{\beta=1}^3 a_{4\beta}^+ a_{4\beta} \right] + t \left[ (V^{+(2)} V^{(2)})^{(1)} R^{(1)} \right]^{(0)}. \quad (8.23)$$

The first term characterizes the splitting of frequencies of  $\nu_2$  and  $\nu_4$  modes in the molecule  $AB_4$  (symmetry group  $T_d$ ). The second term is the Coriolis interaction between states  $\nu_2$  and  $\nu_4$ , under the condition, that the interaction is  $SO(3)$  invariant. Consequently, the five operators  $(a_{2\alpha}^+, a_{4\beta}^+)$

and  $(a_{2\alpha}, a_{4\beta})$  are transformed as spheric functions  $Y_m^{(2)}(\Omega)$  with the help of operators  $J_{\bar{x}}$  from group  $SO(3)$ :

$$J_{\bar{x}_i} = \exp \left\{ i J'_{\bar{x}_j} n_j \right\} J'_{\bar{x}_i} \exp \left\{ -i J'_{\bar{x}_j} n_j \right\} = \Lambda_{ij}^{(1)} J'_{\bar{x}_j}.$$

Thus, the bilinear combination of vibration operators  $V^{+(2)}, V^{(2)}$  in Eq. (8.23) is chosen so that it transforms according to the irreducible representation of rank  $j = 1$ . In other words, during rotation of the inner body system frame this quantity behaves like a vector. It is possible to compose its product with rotational operators, which are linear in momenta  $J_{\bar{x}_i}$ , in a  $SO(3)$  invariant form.

$SO(3)$ -invariant Hamiltonians have been used by many authors in the study of vibrational-rotational spectra of molecules of a spherical top type. Corresponding references can be found in [19] (in particular, see references 75 and 76 therein). The fact, that the operators  $(a_{2\alpha}, a_{4\beta})$  in molecules  $AB_4$  during rotation of the body system frame are transformed like  $Y_m^{(2)}(\Omega)$ , follows from such a consideration: Modes  $\nu_2$  and  $\nu_4$  describe the vibrations of the valent angle  $\angle BAB$ . The magnitude of the valent angle  $\gamma_{i,j}$  with the changes of bond length neglected, are determined by vector  $\mathbf{AB}_i \times \mathbf{AB}_j$ . All in all there are  $C_4^2 = 6$  such vectors, with only five independent ones, as the valent angles  $B_i AB_j$  have vertex  $A$  in common. Thus, the space of angular displacement is five-dimensional. Taking into account the smallness of displacements compared to the equilibrium values of the angles, it can be seen easily, that the vectors of displacements  $(\mathbf{AB}_i \times \mathbf{AB}_j) - (\mathbf{AB}_i^{(0)} \times \mathbf{AB}_j^{(0)})$  are transformed linearly one through the other during the rotation of the body system frame, and, additionally, do not have invariant subspaces. The latter means, that the vectors of angular displacements are transformed according to the irreducible five-dimensional representation, that is, as spheric functions  $Y_m^{(2)}(\Omega)$  with rank 2. Obviously, the conjugate momenta  $p = i \frac{\partial}{\partial \gamma}$  will be transformed in a similar way. Consequently, the five birth operators  $(a_{2\alpha}^+, a_{4\beta}^+)$  and, separately, five annihilation operators  $(a_{2\alpha}, a_{4\beta})$  will be transformed according to the representation  $D^{(2)}$  of group  $SO(3)$ .

It is worth mentioning, that  $SO(3)$  invariance we are talking about is nothing but a hypothesis, justified to some accuracy. Thus, for example, the first term in Eq. (8.23) is not  $SO(3)$  invariant. This is no contradiction to the isotropy of space, as in the present case  $SO(3)$  signifies the group of inner rotations or transitions from one body system frame to another. The operators of inner rotation group  $\exp \{i J_{\bar{x}_j} n_j\}$  commute with the operators of momenta projections upon the laboratory frame, axes  $J_{x_j}$ , and vice versa,  $[\exp \{i J_{\bar{x}_j} n_j\}, J_{x_k}] = 0$ . Thus, the invariance of molecular momentum  $\mathbf{J}$  does not depend on whether the Hamiltonian is  $SO(3)$  invariant or not.

We note also, that a  $SO(3)$ -invariant Hamiltonian provides a good zero order approximation for the effective Hamiltonian  $H_{mn}(J_{\bar{x}_j})$  of molecules of

spherical top type (references 75 and 76 in [19]). In the analysis of  $\nu_2$  and  $\nu_4$  diad in tetrahedral molecules  $AB_4$  such a Hamiltonian can be represented by a sum of following terms:

$$\left[ \left( V^{+(2)} V^{(2)} \right)^{(K)} R^{\Omega(K)} \right]^{(0)}. \quad (8.24)$$

Here  $K = 4, 3, 2, 1, 0$  is the rank of an irreducible representation of group  $SO(3)$ , from the direct product of vibration operators  $a_{s_1}^+ a_{s_2}$ .  $R^{\Omega(K)}$  is a polynomial in  $J_{\bar{x}_j}$  operator of order  $\Omega$  which is transformed according to the irreducible representation  $D_{mn}^{(K)}$ . In general, for each value of the quantity  $\Omega - K = 0, 2, 4, \dots$  there are five different vibration-rotation operators, invariant with respect to the transformations from group  $SO(3)$ .

However, the  $SO(3)$  - invariance is, in fact, an approximation, and more accurate is the symmetry of point group ( $T_d$  for a molecule  $AB_4$ ). Then one should add to Eq. (8.24) the terms, invariant with respect to this point group:

$$\left[ \left( V^{+(2)} V^{(2)} \right)_p^{(K)} R_p^{\Omega(K)} \right]^{(0)}, \quad p = (n, \Gamma). \quad (8.25)$$

Here  $\Gamma$  is the index of the irreducible representation of molecular point group, and  $n$  enumerates the representations of type  $\Gamma$  contained in the tensor representation of order  $K$ <sup>4</sup>,  $A_1$  is a unique representation of point group. The operator (8.25) produces the fine structure, which emerges in the spectrum of  $SO(3)$  invariant operator (8.24). All the vibration-rotation states of the  $\nu_2/\nu_4$  diad, generated by Hamiltonian (8.24) in the case of a one-quantum vibrational excitation can be represented in the form:

$$\left| \Psi^{(R)} \right\rangle = \sum_{\Lambda=-J, S=1}^{+J, 5} C_{\Lambda, S} D_{M\Lambda}^{(J)}(\alpha, \beta, \gamma) a_S^+ |0\rangle, \quad (8.26)$$

where  $(\alpha, \beta, \gamma)$  are Euler angles, specifying the orientation of the molecule  $AB_4$ ,  $a_S^+ = a_{21}^+, a_{22}^+, a_{41}^+, a_{42}^+, a_{43}^+$ ,  $D_{M\Lambda}^{(J)}$  is the Wigner function, and  $|0\rangle$  is the vibrational ground state of the molecule (vibrational vacuum). Vector  $|\Psi^{(R)}\rangle$  belongs to the space, which is a direct product  $D^{(J)} \otimes D^{(2)} = D^{(J+2)} \oplus D^{(J+1)} \oplus D^{(J)} \oplus D^{(J-1)} \oplus D^{(J-2)}$ . Due to  $SO(3)$  invariance of the Hamiltonian (8.24) this vector will belong to one of the subspaces  $D^{(R)}$  forming the direct product  $D^{(J)} \otimes D^{(2)}$ . In other words, the eigenvalues of the Hamiltonian (8.24) are characterized by two quantum numbers: momentum  $J$  and the number  $R = J \pm 2, J \pm 1, J$ . Each level is  $(2R+1)(2J+1)$  - fold degenerate. This classification is a natural generalization of the well-known

---

<sup>4</sup>The irreducible  $(K)$  representation of group  $SO(3)$  is, generally speaking, a reducible representation of point group, and index  $p = (n, \Gamma)$  enumerates the representations of this point group.

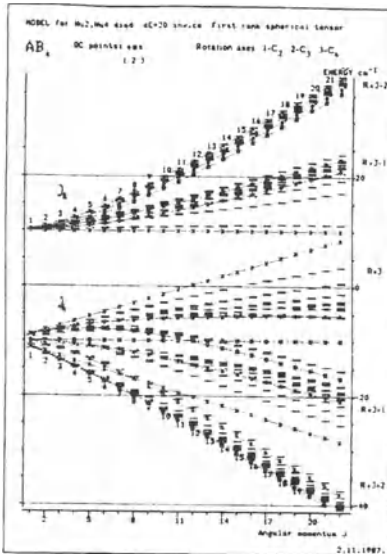


Figure 8.14: System of energy levels versus rotational monenta with respect to the stationary axes  $C_2, C_3, C_4$  for the model Hamiltonian (8.23). The notations are the same as in Fig. 8.12.

classification of rotational-vibrational states of the  $F_2$  vibrational level, split-up by Coriolis interaction into three bands  $J \pm 1, J$ . Thus, each rotational band of the  $\nu_2/\nu_4$  diad in molecule  $AB_4$  is split-up by interaction (8.24) into five rotation bands  $J \rightarrow (J+2), (J+1), J, (J-1), (J-2)$ .

It is implied here, that in the initial most crude approximation  $\nu_2 = \nu_4$  and the molecule is a spheric top. The next correction is based on the assumption, that the main additional term in the Hamiltonian is  $SO(3)$  invariant and has the shape (8.24). As a result, there emerge five rotation bands instead of one at  $J$ , which split apart from each other with increasing  $J$  (see Fig. 8.12 and 8.14). Next we take into account the fact, that the molecule  $AB_4$  has symmetry  $T_d$  and, consequently, one should add to the Hamiltonian (8.24) some small perturbing  $T_d$ - invariant operator (8.25). This operator splits every  $(R, J)$  level of the  $R$ -band into some number of levels. This number of splitted levels depends upon  $R$  and is determined by the number of irreducible representations of group  $T_d$ , contained in the  $D^{(R)}$  representation of group  $SO(3)$  (see Fig. 8.12 and 8.14). Thus, the perturbation in the form (8.25) gives rise to the fine structure in the  $R$ -band of a tetrahedral molecule  $AB_4$ , and besides produces the clusterization of levels.

With the increase of  $J$  and, correspondingly, of  $R$  the distance between the rotational clusters increases, while their width drops exponentially, as the overlap of wavefunctions belonging to the cluster decreases rapidly.

So, to obtain five bands of the rotation-vibration  $\nu_2/\nu_4$  dyad with fine structure of levels inside each band it is sufficient to adopt the Hamiltonian in the form of a sum of a  $SO(3)$  - invariant operator and a  $T_d$  - invariant operator. This is exactly the form of Hamiltonian (8.23). The  $T_d$  - invariant term in it  $\frac{1}{2}\Delta\nu(a_2^+a_2 - a_4^+a_4)$  differs from the operators (8.25) with  $\Omega \neq 0$  by the fact, that it produces the splitting of levels for the  $\nu_2/\nu_4$  dyad into two bands at small  $J$ , in correspondence with the observed spectra of molecule  $SiH_4$ , Fig. 8.12. The splitting of frequencies  $\nu_2$  and  $\nu_4$  at small  $J$  is a general rule, as it is produced by the potential and kinematics ( $m_A/m_B$ ) interaction of vibrational modes, and does not depend on the rotation of molecule. Thus, for the calculation of the  $\nu_2/\nu_4$  dyad in  $SiH_4$  it is reasonable to adopt the model Hamiltonian (8.23).

The diagram of energy levels and the results of the classical calculations with this Hamiltonian are presented in Fig. 8.14. At small  $J$  the two groups of levels can be attributed to the rotational structure of  $\nu_2$  and  $\nu_4$  vibrational states, as the term  $\sim (\nu_2 - \nu_4)$  in Eq. (8.23) is the leading one in the present case. Simultaneously, the Coriolis interaction (the second term in Eq. (8.23)) splits the  $F_2$  mode into three bands, and the  $E$  mode into two bands. At high values of  $J$  the Coriolis interaction in Eq. (8.23) becomes the leading one, and it splits the levels into five bands, as it should for  $SO(3)$  invariant operators.

Then the small perturbation is constituted by the  $T_d$  - invariant first term in Eq. (8.23) which generates the fine structure of each band. The transition from one system to another with the increase of  $J$  is due to the formation of three cone cross-section points of RE surfaces, Fig. 8.13. Qualitatively the redistribution of energy levels between the bands, produced by the model Hamiltonian (8.23) agrees with the one, observed in experiment for the molecule  $SiH_4$  (cf. Fig. 8.12 and 8.14). The analysis of changes in the redistribution of levels between the bands, introduced by terms of the form (8.25) with  $\Omega \neq 0$  leads to the conclusion, that they are of second order in magnitude. Consequently, the operator (8.23) is exact up to terms of second order, and it reproduces correctly the redistribution of energy levels between different bands in the spectrum.

Finally, to sum up the present consideration, we would like to reproduce an instructive citation from Ref. [19]:

"(1) Qualitative methods enable one to clearly visualize the complicated effective Hamiltonian and to find their generic qualitative changes.

(2) The general phenomenological classification of the generic qualitative changes is based on the number of dynamic variables and on the molecular symmetry group.

(3) The proper knowledge of the singularities (bifurcation and diabolic

points) is of primary importance for an adequate description of the dynamic systems. Accordingly, it is desirable to perform the experimental study of molecular systems close to the peculiarities of the energy spectra.

(4) The reasonable extrapolation of the experimental data for the same molecule or within some class of molecular systems might take advantage of a proper description of the qualitative changes, i.e., the singularity points.

(5) Along with the phenomenological Landau type theory of the qualitative changes discussed above the further next step is the formulation of the microscopic theory of qualitative changes.

(6) From the point of view of their possible applications to the study of qualitative features of excited states of quantum systems with small finite number of degrees of freedom, a more general comparative analysis of the qualitative methods of macroscopic physics is needed for further developments."

### 8.3 Spectral properties of systems with Fermi resonances

The inherent limitations of the conventional normal-mode theory in the interpretation of molecular vibrational spectra are most clearly revealed for systems with Fermi resonances. In this case the dependencies of the vibrational spectrum on the parameters of the molecule are some more complex functions of the energy and other quantum numbers in the considered spectral region.

It turns out, that there exists a simple and physically transparent relation between the nature of spectral lines and the corresponding structure of the family of classical phase trajectories.

This relation exists for the high values of quantum numbers, when the quasiclassical approach is relevant. The general theoretical analysis of this phenomenon, and its application to particular molecules with Fermi resonances has been studied in detail in the papers by M.E.Kellman et. al. [132, 133, 134, 135, 136, 137, 138, 139, 140]. A detailed discussion of this approach to the analysis of the vibrational-rotational spectra, and of the prospects of its development, can be found in the review [141]. Below the idea of the inter-relation between the spectrum and the structure of phase space is analyzed on the basis of a particular example of stretching vibrations in molecules of the type:  $H_2O$ ,  $CO_2$ ,  $CHD_3$  and  $(CF_3)_3CH$  [33].

The following conclusion concerning the typical characteristics of the spectrum of stretching vibrations in  $XY_2$  molecules can be reached from the previous considerations: If the anharmonicity of vibrations is negligible, than the spectrum is of an additive nature  $m\omega_1 + n\omega_2$ , where  $\omega_1$  and  $\omega_2$  are the fundamental frequencies of symmetric and antisymmetric vibrations. If the vibrations correspond to purely local highly anharmonic modes,

than in the vibrational spectrum doublet lines are necessarily formed, whose clusterization increases for higher excitation levels. Thus, in the first most rough approximation two opposite situations are revealed: 1) in the case of two normal modes the spectral lines are spread uniformly in energy of the vibrational multiplet; 2) in the case of two local modes the spectral lines group in doublets. However, pure local and pure normal vibrations are an idealization. In reality the regions of local and normal vibrations are positioned side by side in energy, or even overlap. As a consequence, spectral regions exist, where there is no neither pronounced clusterization, nor uniform distribution of levels in energy. The spectrum has a more complicated nature, which cannot be identified easily at first sight. This is especially true for systems with Fermi resonances. In such a case, due to the interaction between resonant levels their position is shifted additionally, which makes the interpretation even more complicated<sup>5</sup>.

M. E. Kellman et.al. [33] suggested the use of a more detailed characteristic of the spectrum: the dependence of the inter-level spacing on their average energy  $\Delta E(E) = E_{i+1} - E_i = f\left(\frac{E_i + E_{i+1}}{2}\right)$ . All the other quantum numbers of these levels coincide. Obviously, for normal modes this quantity is constant  $f_\omega = \omega_\nu = \text{const}$  because of the equidistant position of levels and due to their independence from other normal modes. For an anharmonic oscillator, on the contrary, the frequency is energy dependent, and consequently the level spacing is nonuniform  $\Delta E(E) \neq \text{const}$ .

It turns out, that in the two-mode system with Fermi resonance  $\omega_s : \omega_b = 2 : 1$  the curve  $\Delta E(E)$  has a V-shape cusp at the energy, corresponding to the separatrix line in the classical phase space (Fig. 8.15(d)). As it will be shown below, the existence of a separatrix is a sufficient condition for the formation of a deep gap (cusp) in the spectrum. The separatrix is formed in the case of strong enough resonant interaction only.

Let us consider the following Hamiltonian [33] as an example of the above statements:

$$H = H_0 + V_{2:1},$$

$$H_0 = \left(n_s + \frac{1}{2}\right) \omega_s^{(0)} + \left(n_b + \frac{1}{2}\right) \omega_b^{(0)} + X_{ss} \left(n_s + \frac{1}{2}\right)^2$$

---

<sup>5</sup>With the increase of energy the frequencies of anharmonic modes are reduced. Then the number of different nonlinear Fermi resonances in the corresponding region of phase space grows, and their characteristics change drastically even with minor displacements in position space. This leads to stochasticization of motion in the classical approach, and to the complete irrelevance of the traditional description of the spectrum with the help of conventional formulas of the type  $E_{\{n\}} = G(n_1, \dots, n_s)$ , where  $n_1, \dots, n_s$  are the excitation numbers for vibrational modes. Interpretation of vibrational spectra of molecules within classical dynamics for high excitations and even in the stochasticity region are discussed in [20]

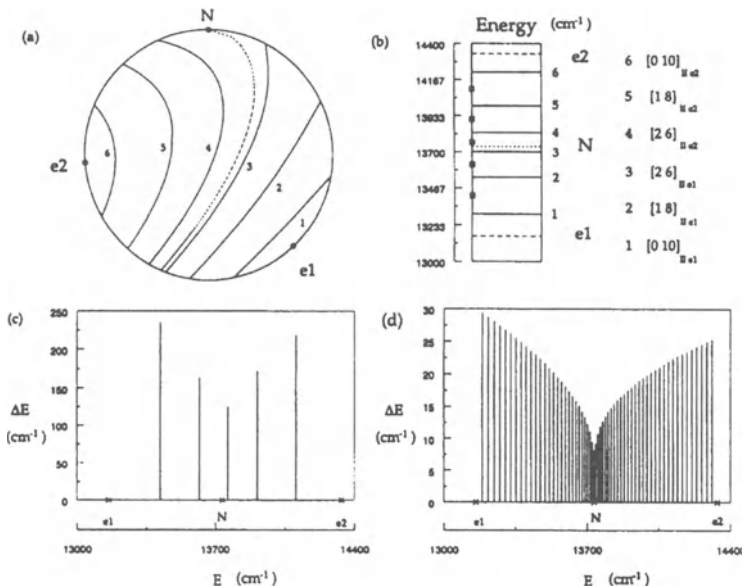


Figure 8.15: (a) Phase sphere, (b) energy levels, and (c,d) energy level spacings for the  $P = 5$  polyad of  $(CH_3)_3CH$ , a polyad in zone II of the catastrophe map, Fig. 8.17. The elliptic fixed points are labeled  $e_1, e_2$ . The separatrix, which passes through the cusp point  $N$  on the phase sphere is indicated by the dashed line on the sphere (a). The black tick marks in (b) indicate the midpoint between adjacent levels, plotted in (c) as the energy spacings between adjacent levels. (c) Indicates the energy of the fixed points  $e_1, e_2, N$  as x's on the horizontal axis. The smooth nature of the dip in (c) is seen clearly in (d) with Planck constant  $\hbar$  reduced.

$$+X_{sb} \left( n_s + \frac{1}{2} \right) \left( n_b + \frac{1}{2} \right) + X_{bb} \left( n_b + \frac{1}{2} \right)^2, \\ V_{2:1} = \frac{K_{bbb}}{\sqrt{2}} \left( a_s^+ (a_b)^2 + a_s (a_b^+)^2 \right), \quad (8.27)$$

where

$$n_s = a_s^+ a_s, \quad n_b = a_b^+ a_b. \quad (8.28)$$

Here  $a, a^+$  are usual Bose operators of annihilation and creation. With a suitable choice of parameters this Hamiltonian models correctly the symmetrical stretching mode  $a_s$  and the bond-bending mode  $a_b$  in a molecule  $XY_2$  (Fig. 8.16).

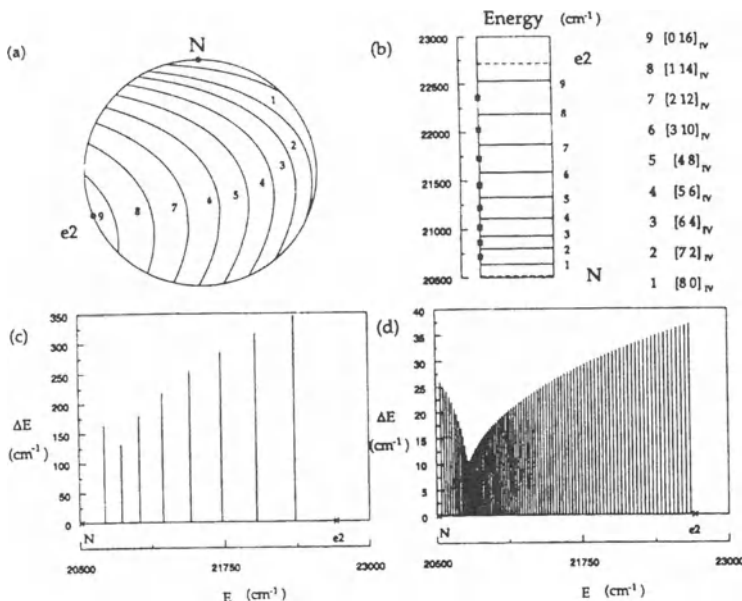


Figure 8.16: (a) Phase sphere, (b) energy levels and assignments, and (c,d) energy level spacings for the  $P = 8$  polyad of  $(CH_3)_3CH$ , a polyad in zone IV of the catastrophe map Fig. 8.17. There are two elliptic fixed points  $e_1, e_2$ . The energy spacing diagram in (c) shows a 'pseudodip' which is the residue of the zone III separatrix; the smooth nature of the pseudodip is seen in (d) with Planck constant  $\hbar$  reduced. Notations are the same, as in Fig. 8.15.

This very same Hamiltonian models well the vibrational spectrum of the molecule  $(CF_3)_3CH$  in the vicinity of Fermi resonance [137, 138]. The molecule  $(CF_3)_3CH$  can be thought of as a  $CH_4$  tetrahedron, in which the three  $H$  atoms are substituted by complexes  $CF_3$ . The stretching vibration  $a_s$  is a  $CH$  - mode, while the bending  $a_b$  mode is a symmetrical twisting of the angle between the  $CH$  and  $C - CF_3$  bonds.

The Hamiltonian (8.27) has a constant of motion:

$$P = n_s + \frac{1}{2}n_b. \quad (8.29)$$

The quantum number  $P$  enumerates the multiplets, which in vibrational spectroscopy are called polyads.

With a suitable choice of parameters in the Hamiltonian (8.27) it is pos-

Polyads fitted	P=1-6	P=1-5	P=1-4	P=1-3
$\omega_s$	3111.22	3122.48	3127.19	3105.31
$\omega_b$	1367.03	1364.62	1365.38	1367.48
$X_{ss}$	-56.53	-59.48	-61.40	-53.55
$X_{sb}$	-14.10	-15.30	-13.92	-11.88
$X_{bb}$	-0.55	0.11	-0.22	-1.21
$K_{sbb}$	-64.97	-68.78	-68.17	-56.60
RMS deviation <sup>a)</sup>	9.50	6.38	6.64	8.40
RMS deviation <sup>b)</sup>	9.50	16.36	23.00	30.00

Table 8.5: Fitting parameters for the molecule  $(CF_3)_3CH$  with the resonance Hamiltonian (8.32). <sup>a)</sup>RMS deviation of the resonance fit to the experimental levels belonging to the polyads listed at the head of the column. <sup>b)</sup>RMS deviation of the resonance fit to the full experimental spectrum (P=1-6), including the prediction of levels above those not used in the actual fitting process.

sible to model the experimental vibrational spectrum of molecules  $CO_2$  and  $(CF_3)_3CH$  with the spectrum of Eq. (8.27) in the region of Fermi resonance for each polyad. The fitting parameters for the molecule  $(CF_3)_3CH$  are provided in Table 8.5. As it can be seen, the accuracy with which the frequencies and energy levels are reproduced is higher than 1%.

The authors of Ref. [33] utilized the diagonal operator  $H_0$  with cubic terms in  $n_s$  and  $n_b$  as the fitting Hamiltonian. The corresponding results, provided in Table 8.6, show that the fitting parameters in this case change from one polyad to another in a much more pronounced way, than in the first case. The same is true for the fitting Hamiltonians of other molecular spectra as well [141]. Hence a conclusion can be drawn, that the Fermi resonances exist in reality, and are no artifact, arising from the choice of the fitting Hamiltonian.

Due to the stated reasons in the future we will consider Eq. (8.27) to be the 'true' Hamiltonian of the Fermi-resonant system. The vibrational spectrum of its polyads corresponds to the experimental spectrum. As a polyad  $P$  comprises a finite number of states, its spectrum can be found by diagonalization of the matrix, the order of which is not too high, as the vibrational quantum numbers  $v$  typically do not exceed 10.

The spectrum and the function  $\Delta E(E)$  for the polyads  $P = 5$  and  $P = 8$  of the molecule  $(CF_3)_3CH$  are depicted in Figs. 8.15 (b,c) and 8.16 (b,c) correspondingly. Here we imply  $P = n_s + \frac{1}{2}n_b$  as before. The parameters of the calculation have been taken from Table 8.5. Comparing Figs. 8.15 (c) and 8.16 (c) we note, that for the polyad  $P = 5$  the V-shaped cusp in the curve  $\Delta E(E) \simeq \omega(E)$  is deeper and more pronounced, than for  $P = 8$ . Below we will show, that this is no coincidence.

Polyads fitted	P=1-6	P=1-5	P=1-4	P=1-3
$\omega_s$	3176.03	3155.51	3093.00	3096.83
$\omega_b$	1365.40	1354.12	1372.36	1354.56
$X_{ss}$	-97.51	-91.16	-64.96	-60.13
$X_{sb}$	3.08	12.56	34.41	15.33
$X_{bb}$	-1.92	-0.21	-10.07	-0.41
$X_{sss}$	8.25	7.76	4.76	2.42
$X_{ssb}$	-3.02	-4.59	-9.08	-2.25
$X_{sbb}$	-1.89	-2.50	-3.77	-3.77
$X_{bbb}$	0.00	-0.08	0.90	0.00
RMS deviation <sup>a)</sup>	8.40	7.50	5.20	0.00 <sup>c)</sup>
RMS deviation <sup>b)</sup>	8.40	15.14	114.80	35.76

Table 8.6: Fitting parameters for a diagonal operator  $H_0$  with cubic terms in  $n_s$  and  $n_b$ , molecule  $(CF_3)_3CH$ . <sup>a)</sup>RMS deviation of the diagonal fit to the experimental levels belonging to the polyads listed at the head of the column. <sup>b)</sup>RMS deviation of the diagonal fit to the full experimental spectrum (P=1-6), including the prediction of levels above those not used in the actual fitting process. <sup>c)</sup>There are only eight experimentally observed levels in polyads P=1-3, so these levels can be fit exactly with nine adjustable parameters in the fitting Hamiltonian.

Let us now solve this very problem in the classical approach. First, we write out the classical Hamiltonian, corresponding to operator (8.27). The correspondence relations are:

$$a_s \rightarrow \sqrt{I_s} \exp(-i\Psi_s), \quad a_b \rightarrow \sqrt{I_b} \exp(-i\Psi_b), \quad (8.30)$$

where  $(I_\alpha, \Psi_\alpha)$  are the action and angular variable of the classical oscillator. In these notations  $n_b \rightarrow I_b$ ,  $n_s \rightarrow I_s$ . After such a change of variables Eq. (8.27) becomes a classic Hamiltonian function in the four dimensional phase space  $(I_s, \Psi_s; I_b, \Psi_b)$ .

It is convenient to make the following canonical transformation <sup>6</sup>:

$$\begin{aligned} \Phi &= \frac{1}{5}(2\Psi_s + \Psi_b), \quad I = \frac{1}{2}\left(I_s + \frac{1}{2}I_b\right), \\ \Psi &= \Psi_s - 2\Psi_b, \quad I_z = \frac{1}{5}(I_s - 2I_b) + \frac{3}{5}I. \end{aligned} \quad (8.31)$$

Substituting Eqs. (8.30) and (8.31) into (8.27), we obtain the following Hamiltonian [33]:

$$H(I_z, \Psi; I) = H_0(I_z, I) + H_{2:1}(I_z, \Psi; I)$$

<sup>6</sup>The transformation of the variables (8.31) is the product of the canonical transformation with a subsequent elongation of the scale for the constant of motion  $I$  and the shift of the action variable  $I_z$ .

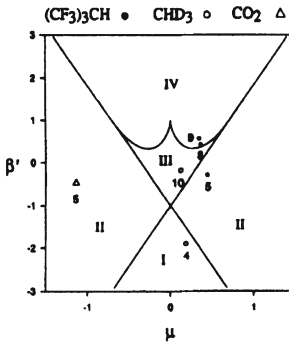


Figure 8.17: Catastrophe map for the 2:1 resonance. The closed circles represent  $(CF_3)_3CH$ , the open triangle  $CO_2$ , and the open circles  $CHD_3$ . Each symbol corresponds to an individual phase sphere for the molecule, with the polyad number shown next to the symbol.

$$= 2\gamma_2 \left[ \beta' I_z I + \frac{I_z^2}{2} + 2\mu\sqrt{I(I+I_z)}(I-I_z)\cos\Psi \right] + C(I), \quad (8.32)$$

where

$$\begin{aligned} \omega_s &= \omega_s^{(0)} + X_{ss} + \frac{1}{2}X_{sb}, \\ \omega_b &= \omega_b^{(0)} + X_{bb} + \frac{1}{2}X_{sb}, \\ \gamma_1 &= X_{ss} + 4X_{bb} + 2X_{sb}, \\ \gamma_2 &= X_{ss} + 4X_{bb} - 2X_{sb}, \\ \beta' &= \frac{\omega_s - 2\omega_b + 2(X_{ss} - 4X_{bb})I}{2\gamma_2 I}, \\ \mu &= \frac{K_{sbb}\sqrt{2}}{\gamma_2\sqrt{I}}, \\ C &= (\omega_s + 2\omega_b)I + \gamma_1 I^2. \end{aligned} \quad (8.33)$$

The parameters in Eq. (8.33) are taken from Eq. (8.27). The Hamiltonian (8.32) corresponds to a system with one degree of freedom, and it depends on  $I$  parametrically. In the quantum form the quantum number  $2I = P$  is the number of the polyad. The phase space of the system (8.32) is a sphere of radius  $I$ . The azimuth angle of the point on the sphere is  $\Psi$ , while its projection on  $z$  axis is  $I_z = I \cos\Theta$ , with  $\Theta$  — the polar angle. The phase

trajectories of the system (8.32) are on this sphere (phase sphere). The transformation of the sphere into itself under the action of the Hamilton equations keeps invariant its area, as the form  $dI \wedge d\Psi = I \sin\Theta \, d\Theta \wedge d\Psi$ , characterizing the area of a spherical element, is invariant under Hamilton transformations.

The phase curves with  $P = 5$  and  $P = 8$  are depicted in Figs. 8.15(a) and 8.16(a) correspondingly. There is a separatrix on the phase sphere for  $P = 5$ , while for  $P = 8$  there is none. On the other hand, if we construct the function  $\Delta E(E)$  with a reduced Planck's constant  $\hbar$ , we will obtain a frequency comb, shown in Figs. 8.15(d) and 8.16(d). Comparing these two combs we find a deep gap at  $\omega \rightarrow 0$  in Fig. 8.15(d) when the separatrix is present, and the absence of a gap in the absence of the separatrix, Fig. 8.16. A conclusion follows: a separatrix in phase space and a deep gap at  $\omega(E) \rightarrow 0$  in the dependence  $\Delta E(E) = \omega(E)$  either exist or do not exist simultaneously in pairs. Changing the parameter  $2I = P$  in the Hamiltonian (8.32) we pass over from one phase sphere to another, with a corresponding change of phase trajectories. For some values of the parameter  $I = I_s$  this structure changes abruptly and qualitatively. An example of it is the emergence and disappearance of the separatrix, and, correspondingly, of a deep gap in the dependence  $\Delta E(E) = \omega(E)$ . The nature of the changes in the phase space can be depicted transparently with the help of a map of catastrophes [33], Fig. 8.17.

In region 1 there is no separatrix, in 2 there is one separatrix, in region 3 there is a hyperbolic point with a self-intersecting separatrix, and in 4 no separatrix again. The method of catastrophe map provides a convenient and transparent mean of qualitative study of the phase space structure, and correspondingly of the function  $\Delta E(E)$ . It is sufficient to know to which region of the map the parameters of the Hamiltonian (8.33) correspond to. A more detail discussion of the relation between the multimode resonances and the shape of the vibrational-rotational molecular spectra can be found in Refs. [142, 35].

## Chapter 9

# Intramolecular relaxation of vibrations in the presence of local modes

In the previous Chapters it has been shown that, if the molecule possesses equivalent (degenerate) vibrational modes (such as several  $C - H$  bonds, for example), the nonlinearity of intramolecular vibrations leads to the appearance of Local Modes (LM) and to highly pronounced clusterization of vibrational levels. The same applies to the rotational evolution (motion) of the molecule, as rotations are governed by a nonlinear Hamiltonian. The rotational levels group into clusters of two or more ones, depending on the point symmetry of the effective Hamiltonian for rotations  $H(J)$ . The same is true for the rotational - vibrational states in the case of degeneracy of the vibrational level.

The analysis of the molecular rotational - vibrational spectra, introduced above, implied the absence of the continuous or quasi-continuous spectrum (density of levels) the local mode can interact with. Such an interaction increases the level widths and affects the decay of corresponding states. In this case it is necessary to estimate the decay time of local modes, to make sure LMs exist at all. Really, for oscillation frequency of order of  $\omega_l \sim 1000 \text{ cm}^{-1}$ , the level width  $\Gamma \sim 1 \div 10 \text{ cm}^{-1}$  can be regarded as satisfactory for LM existence, as long as it is smaller than the anharmonicity coefficient  $x_c \sim 50 \text{ cm}^{-1}$  and the inter-mode interaction  $\beta \sim 50 \text{ cm}^{-1}$ . If, on the contrary, the calculations gave  $\Gamma \sim 100 \text{ cm}^{-1}$ , there would be no local modes, and the stationary states would be in fact some mixtures of a large number of LMs. Then the state will be 'delocalized' considerably over the modes.

Before the calculation of the local level widths  $\Gamma$ , let us discuss briefly the nature of the continuous (quasi-continuous) spectrum, which provokes the decay of LMs. With dissociation processes left apart, the spectrum of small molecules is discrete strictly, and the previous consideration of local

modes and level clusterization is directly applicable. In this case a 'small' molecule is one of  $XY_2$  type. On the contrary, in 'big' molecules (of  $XY_3$  type already) at high vibrational excitation level one has to take into account the quasi-continuum nature of the spectrum. The density of vibrational levels can be estimated with the help of the formula:

$$\rho(E) \sim \bar{\omega}^{-1} \left( \frac{E}{\bar{\omega}} \right)^{s-1} = \bar{\omega}^{-1} N^{s-1}, \quad (9.1)$$

where  $\bar{\omega}$  is the average oscillation frequency ( $\sim 1000 \text{ cm}^{-1}$ ),  $E$  is the vibration energy, and  $s$  - the number of vibrational modes. For a molecule  $XY_2$  and excitation level  $N = 10$  we find  $\rho(10) \sim 10^{-3} 10^2 \sim 10^{-1} (\text{cm})$  which corresponds to 1 level per  $10 \text{ cm}^{-1}$ . Whereas in  $XY_3$  we obtain  $\rho(10) \sim 10^{-3} 10^5 \sim 10^2 (\text{cm})$ , i.e. 100 levels per  $1 \text{ cm}^{-1}$ . In the widely studied molecule  $SF_6$  the level density at  $N = 10$  is  $\sim 10^{11} (\text{cm})$ , which corresponds to interlevel distance of  $\Delta E \sim 10^{-11} (\text{cm}^{-1})$ . Such level density from experimental point of view is equivalent to a continuous one, as the resolution equals  $\Delta E \sim 10^{-4} \text{ cm}^{-1}$ . Implying that the 'experimental continuous' spectrum starts at  $\rho \sim 10^4 \text{ cm}$ , with the use of Eq. (9.1) we obtain the value of the minimal excitation level  $N_{st}$ , which is already in the continuum spectrum:

$$N_{st} \sim [\bar{\omega} \rho(E_{st})]^{1/(s-1)} \sim 10^{7/(s-1)}. \quad (9.2)$$

Here  $E_{st} \approx N_{st} \bar{\omega}$  denotes the energy of stochastization. The latter can be roughly identified with the energy, at which the spectrum can be considered continuous  $\rho(E_{st}) \sim 10^4 \text{ cm}$ , that is, the neighboring levels can not be resolved separately. Such a definition of  $E_{st}$  seems reasonable, as from the classical point of view, if the levels inside some energy interval  $\Delta E$  can not be identified, the phase trajectories fills uniformly some layer with thickness  $\Delta E$  in the phase space, and they do not preserve any constant of motion except for the total energy  $E$ . This fact signifies the ergodicity of the trajectories and the lack of possibility to distinguish them one from another in the experiment. This is in fact the complete mixing of modes and the destruction of any initial correlations during the observation time.

It is instructive to apply the formulas (9.1) and (9.2) to the molecule  $H_2O$  ( $D \sim \frac{\omega^2}{4x_e} = 4 \cdot 10^4 \text{ cm}^{-1}$ ), to compare the density of levels  $\rho(D)$  close to the dissociation limit to the corresponding density at the stochastization threshold  $10^4 \text{ cm}^{-1}$ . Of interest also is the comparison of the excitation levels for dissociation  $N_D \sim 40$  and for stochastization  $N_{st}$ :

$$\begin{aligned} \rho_\omega(E_D) &\sim \frac{1}{1000} \left( \frac{40000}{1000} \right)^2 \sim 1 \text{ (cm)}, \\ N_{st} &\sim 10^{7/2} \approx 1000 \gg 40 = N_D. \end{aligned} \quad (9.3)$$

Eq. (9.3) reveals the fact, that for  $E \sim E_D$  the bound states of the molecule  $H_2O$  have a clearly resolved discrete experimental spectrum, while the continuous spectrum is produced by the states, referring to the dissociated molecule. The excitation number  $N_{st}$ , which corresponds to the beginning of the quasi-continuous spectrum (stochasticization threshold)<sup>1</sup> according to Eq. (9.3) is of the order of  $\sim 3000$ . Thus the molecule  $H_2O$  would decay sooner, than the stochasticization of intra-molecular vibrations could occur.

From Eqs. (9.1), (9.2) it follows, that the density of levels with excitation level  $N$  fixed, grows exponentially with the increase of the number of modes  $s$  (or of the number of atoms in the molecule). At the same time, the excitation number  $N_{st}$ , corresponding to vibration stochasticization threshold tends to 1 for  $s \rightarrow \infty$  as  $1 + o(s^{-1})$ . We should note here, that Eqs. (9.1) and (9.2) are valid asymptotically only, when  $N \gg s \gg 1$ . Thus, more correct is the assertion on the decrease of excitation level, corresponding to stochasticization threshold with the increase of the number of atoms in the molecule. In the study of some highly excited local vibration with the energy in the stochastic region, all the resonances between this vibration and other modes should be taken into account, and the corresponding interaction strengths should be estimated. Only after such a study it becomes possible to judge whether the discussed local vibration in the molecule really exists (has a sufficiently long lifetime), or decays rapidly (and is practically non-existent). This point will be addressed below. Thus, in a polyatomic molecule (number of atoms greater than four) at high excitation levels the quasi-continuous spectrum exists, its levels interacting with the local vibrations, and causing their decay. Only in the case, when the widening of a local level is much smaller than the frequency of the local vibration ( $\Gamma_{loc} \ll \omega_{loc}$ ), can we speak of a local mode.

Another type of broadening of local levels due to their interaction with the states of the 'truly' continuous spectrum is realized in molecular crystals, like  $N_2$ ,  $NO$ , etc. Here the highly excited intra-molecular vibrations decay due to their interaction with the continuous spectrum of inter-molecular vibrations (phonons, rotons, etc.). It is in this case that the differences in the nature of intra-molecular vibrations depending on the degree of nonlinearity are revealed most transparently.

As it has been shown in 1969 by A.A.Ovchinnikov [12], in molecular crystals of the type  $N_2$ ,  $O_2$ ,  $H_2$ ,  $NO$ , etc. long-living highly excited intra-molecular vibrations should exist. The latter are, in fact, nothing but vibrational excitons with the lifetime up to several seconds, and at helium temperatures – up to  $\sim 10^5 \div 10^6$  s. Later such states have been observed in the crystals  $N_2$  [143, 14].

---

<sup>1</sup>Strictly speaking, for the stochasticization of vibrations to occur, the magnitude of the mixing interaction  $V$  should greatly exceed the average distance between the levels  $\Delta E$ . Otherwise, the levels keep their identity, despite the quasi-continuous nature of the spectrum.

The description of the general methods of calculation of local modes' lifetime and vibrational energy relaxation we will precede by the estimate of the lifetime of molecular vibrations in  $N_2$  crystals, [12]. This simple example will illustrate most transparently the physical nature of the discussed effects. The second reason is that the long-living vibrations in crystalline  $N_2$  have been observed in an impressive experiment, worth of a detailed consideration ([14], see below).

In short, this Chapter is devoted to the effects of vibrational energy localization in molecular crystals and to related phenomena. The lifetime of localized states is calculated. The mathematical model of decay of a discrete level, interacting with a continuous spectrum, is considered in detail. This model is of great use in the estimates of the lifetimes for the localized intramolecular vibrations in polyatomic molecules, as well as for the radiation broadening of levels.

For the proper understanding of the presented material the knowledge of quantum mechanics within a University course, or, for example, within the presentation of Ref. [81], is sufficient.

## 9.1 Localized long - living vibrational states in molecular crystals

The Hamiltonian of a simple molecular crystal  $X_2$  can be chosen in the following form <sup>2</sup>:

$$H = \sum_{n=1}^N H_0(x_n) + \sum_{n=1}^N \left\{ -\frac{\hbar^2}{2m} \frac{\partial^2}{\partial q_n^2} + \frac{m\omega_0^2}{8} (q_n - q_{n+1})^2 \right\} + \sum_{n=1}^N (q_n - q_{n+1}) \cdot [\alpha_1 x_n + \alpha_2 x_{n+1} + \beta_{11} x_n^2 + \beta_{22} x_{n+1}^2 + \beta_{12} x_n x_{n+1}] . \quad (9.4)$$

Here  $x_n$  is the distance between the nuclei  $X$  in the  $n$ -th molecule, and  $q_n$  are the coordinates of the center of mass of the  $n$ -th molecule. The fact, that the crystal (9.4) is one-dimensional is of no importance, as the decay of the highly-excited intra-molecular vibration of the  $n$ -th molecule is determined by the interaction with the intra-molecular vibration of the nearest (say,  $(n+1)$ -th) molecule and by the relative distance  $q = q_n - q_{n+1}$  between them. The potential energy in the Hamiltonian  $H_0(x_n)$  can be taken in Morse form, as the energy spectrum of intra-molecular vibrations is provided by the formula:

$$E_s^{(0)} = \Omega \left[ (s + 1/2) - x_e (s + 1/2)^2 \right] . \quad (9.5)$$

---

<sup>2</sup>In this Section we follow Ref. [12].

The frequency  $\omega_0$  in Eq. (9.4) is the Debai phonon frequency, which for molecular crystals is of the order of  $100 \text{ cm}^{-1}$  (for  $N_2 — \omega_\nu \sim 69 \text{ cm}^{-1}$ ). In Eq. (9.4) we have written out explicitly only the phonons, related to the oscillations of relative distance between the molecules, and neglected the interaction of intra-molecular vibrations with relative rotations. The account of the latter, however, can not change the final estimates considerably, as the quasi-rotational vibration mode has the Debai libration or torsion frequency of the same order, and its dynamic interaction with intra-molecular vibrations is, obviously, weaker. Assume some molecule in the crystal be excited to the  $s$ -th level with energy given by Eq. (9.5). Let us consider the processes, occurring in the crystal after the excitation. First, with some probability this excitations will migrate as a whole among the molecules. This is the motion of vibrational excitons in the band, corresponding to the  $s$ -th excitation level. Second, the initial vibration excitons can decay, so that the excitation level  $s$  diminishes. Let us consider these processes in more detail.

First of all, these are radiation processes. Molecules with a small dipole moment ( $CO$ ,  $NO$ , etc.) the radiation lifetime for the transition  $s \rightarrow s-1$  is of the order of 1 s, and is proportional to  $s$ . For molecules with no dipole moment (such, as  $O_2$ ,  $H_2$ ,  $N_2$ ) the dipole transition is prohibited, and only the quadrupole tradition is possible. The characteristic lifetime for the quadrupole transition  $s \rightarrow s-1$  is proportional to  $s^2$  and for the transition  $1 \rightarrow 0$  can be estimated as:  $10^6 \div 10^7$  s. The most important processes, which change  $s$ , are the radiationless transitions with the absorption of several phonons, corresponding to the translational vibrations of the molecule. Really, as  $E_s - E_{s-1} < E_1 - E_0$  (see Eq. (9.5)), the transfer of one intra-molecular quantum to the neighboring molecule is inevitably accompanied by absorption of phonons from the crystal. A radiationless transition  $s \rightarrow s-2$ , though not forbidden by energetic considerations at zero temperature, has, however, a very low probability, as it requires creation of a large number of phonons in the crystal. The number of created phonons can be estimated according to the formula:

$$N_F = \frac{\Omega}{\omega_0} \sim 10 \div 20, \quad (9.6)$$

where  $\Omega$  are the intra-molecular vibration frequencies ( $\sim 1 \div 2 \cdot 10^3 \text{ cm}^{-1}$ ), while  $\omega_0$  is the Debai phonon frequency  $\sim 10^2 \text{ cm}^{-1}$ .

Let us estimate the probability of a thermal transition with one quantum  $\hbar\Omega$  transferred to the neighboring molecule. We assume that absorbed are the most high-frequency optical phonons. In the theory of radiationless transitions [144] it is shown, that such processes are most probable. Thus, we will limit our consideration to the translational vibration of two diatomic molecules, situated in one crystal cell. Then the Hamiltonian of a molecular crystal (9.4) is reduced to the following form:

$$\begin{aligned} H &= \sum_{n=1}^2 H_0(x_n) + \left[ -\frac{\hbar^2}{2m} \frac{\partial^2}{\partial q^2} + \frac{m\omega_0^2}{8} q^2 \right] + qU(x_1, x_2), \\ U(x_1, x_2) &= [\alpha_1 x_1 + \alpha_2 x_2 + \beta_{11} x_1^2 + \beta_{22} x_2^2 + \beta_{12} x_1 x_2]. \end{aligned} \quad (9.7)$$

Here  $\alpha_i$  and  $\beta_{ij}$  are harmonic and anharmonic constants for intra-molecular and inter-molecular vibrations. Obviously, the model Hamiltonian (9.7) for the lifetime  $\tau$  of intra-molecular highly-excited vibration will provide the result of the same order of magnitude, as the more exact Hamiltonian (9.4).

The frequencies of intra-molecular vibrations are much higher than those for inter-molecular ones ( $\Omega/\omega_0 \sim 10$ ). Consequently, the motion of molecules can be considered in the adiabatic approximation. Then the wavefunctions  $\psi_s(x_1, x_2\dots)$  and the eigenvalues  $E_s(q)$  will depend on  $q$  as a parameter. In the first order in perturbation theory in  $U(x_1, x_2\dots)$  we obtain:

$$\begin{aligned} E_s &= E_s^{(0)} + qU_{ss}, \\ \psi_s(x_1, x_2; q) &= \psi_s^{(0)}(x_1, x_2) + q \sum_{s \neq s'} \frac{U_{s's}}{E_s^{(0)} - E_{s'}^{(0)}} \psi_{s'}^{(0)}(x_1, x_2). \end{aligned} \quad (9.8)$$

Here  $\psi_s^{(0)}(x_1, x_2)$  and  $E_s^{(0)}$  are wavefunctions and eigenvalues of the Hamiltonian  $\sum_{n=1}^2 H_0(x_n)$ , and

$$U_{s's} = \int \int \psi_{s'}^{(0)}(x_1, x_2) U(x_1, x_2) \psi_s^{(0)}(x_1, x_2) dx_1 dx_2. \quad (9.9)$$

In the adiabatic approximation the complete wavefunction is a product of wavefunctions for intra-molecular and inter-molecular motion:

$$\begin{aligned} \Phi_{sv}(x_1, x_2, q) &= \psi_s(x_1, x_2; q) \cdot \varphi_v^{(s)}(q), \\ \left[ -\frac{\hbar^2}{2m} \frac{\partial^2}{\partial q^2} + \frac{m\omega_0^2}{8} q^2 + (E_s^{(0)} + qU_{ss}) \right] \varphi_v^{(s)}(q) &= E_{sv} \varphi_v^{(s)}(q), \\ E_{sv} &= E_s^{(0)} - \frac{U_{ss}^2}{2m\omega_0^2} + (v + 1/2) \hbar\omega_0. \end{aligned} \quad (9.10)$$

We note, that the second term of the energy eigenvalue  $E_{sv}$  satisfies the inequality:

$$\frac{U_{ss}^2}{2m\omega_0^2} \ll \hbar\omega_0. \quad (9.11)$$

The left hand side of Eq. (9.11) characterizes the order of magnitude of second-order corrections to the inter-molecular frequencies. Obviously, the former should be much smaller than the latter in the case, when the adiabatic approximation is applicable. The quantity  $U_{ss}^2/\hbar m\omega_0^3$  for molecular crystals is smaller or of the order of  $10^{-1}$ . At high values of this parameter, the interaction of inter-molecular and intra-molecular modes becomes strong, so that they get mixed in a considerable way, and the crystal can no longer be considered a molecular one.

The non-adiabaticity operator  $M \sim 2\frac{\partial\psi}{\partial q}\frac{\partial\varphi}{\partial q}$ , which gives rise to transitions in the system, has the following matrix elements:

$$M_{vs}^{v's'} = -\frac{\hbar^2}{m} \frac{U_{s's}}{E_s^{(0)} - E_{s'}^{(0)}} \int dq \left[ \varphi_{v'}^{(s')} (q)^* \frac{\partial}{\partial q} \varphi_v^{(s)} (q) \right]. \quad (9.12)$$

According to Fermi Golden rule the transition rate of the molecule from state  $s$  into  $s'$  is given by the formula:

$$W_s^{s'} = \frac{2\pi}{\hbar} \sum_v \frac{\exp\left[-\frac{E_{sv}}{kT}\right]}{\sum_{\tilde{v}} \exp\left[-\frac{E_{s\tilde{v}}}{kT}\right]} \cdot \sum_{v'} \left| M_{vs}^{v's'} \right|^2 \\ \times \delta \left( E_s^{(0)} - \frac{U_{ss}^2}{2m\omega_0^2} - E_{s'}^{(0)} + \frac{U_{s's'}^2}{2m\omega_0^2} + \hbar\omega_0 (v - v') \right), \quad (9.13)$$

where  $T$  is the absolute temperature of the gas of optical phonons ( $T \leq 100 \text{ cm}^{-1}$ ), and  $k$  is Boltzman's constant. The sum (9.13) has been calculator in Ref. [145]. We will provide the calculation for the case  $\frac{\hbar\omega_0}{kT} \gg 1$ . In a simple molecular crystal this inequality for optical phonons is always satisfied, as  $\hbar\omega_0 \sim 100 \text{ cm}^{-1}$ ,  $kT \sim 20 \text{ cm}^{-1}$ . Substituting Eq. (9.12) into Eq. (9.13), we obtain:

$$W_s^{s'} = \frac{2\pi}{\hbar} \cdot \frac{\hbar^4}{m^2} \frac{U_{s's}^2}{\left( E_s^{(0)} - E_{s'}^{(0)} - \frac{U_{ss}^2}{2m\omega_0^2} + \frac{U_{s's'}^2}{2m\omega_0^2} \right)^2} \\ \times \sum_v \frac{\exp\left[-\frac{\hbar\omega_0 v}{kT}\right]}{\sum_{\tilde{v}} \exp\left[-\frac{\hbar\omega_0 \tilde{v}}{kT}\right]} \cdot \sum_{v'} \left| \left\langle v' s' \left| \frac{\partial}{\partial q} \right| vs \right\rangle \right|^2 \\ \times \delta \left( E_s^{(0)} - E_{s'}^{(0)} - \frac{U_{ss}^2 - U_{s's'}^2}{2m\omega_0^2} + \hbar\omega_0 (v - v') \right). \quad (9.14)$$

Here the expression  $\left\langle v' s' \left| \frac{\partial}{\partial q} \right| vs \right\rangle$  is determined by the formula:

$$\begin{aligned}
\left\langle v' s' \left| \frac{\partial}{\partial q} \right| vs \right\rangle &= \int_{-\infty}^{\infty} dq \left[ \varphi_v^{(s')} (q)^* \frac{\partial}{\partial q} \varphi_v^{(s)} (q) \right] \\
&= \sum_{\tilde{v}} \left\langle v' s' \left| \tilde{v} s \right\rangle \langle \tilde{v} s | \frac{\partial}{\partial q} | vs \right\rangle \\
&= \left\langle v' s' \left| v - 1, s \right\rangle \langle v - 1 | \frac{\partial}{\partial q} | v \rangle + \left\langle v' s' \left| v + 1, s \right\rangle \langle v + 1 | \frac{\partial}{\partial q} | v \rangle \right. \\
&= \sqrt{\frac{m\omega_0}{2\hbar}} \left\{ \left\langle v' s' \left| v - 1, s \right\rangle \sqrt{v} - \left\langle v' s' \left| v + 1, s \right\rangle \sqrt{v+1} \right\} . \quad (9.15)
\end{aligned}$$

In the derivation of Eq. (9.15) we have used the fact, that the function  $\langle q | vs \rangle = \varphi_v^{(s)} (q)$  is a solution of equation (9.10), and represents in fact a shifted Hermit function:

$$\varphi_v^{(s)} (q) = \left( \frac{m\omega_0}{\pi\hbar} \right)^{1/4} \frac{1}{\sqrt{2^v v!}} \exp \left[ -\frac{m\omega_0}{2\hbar} (q + q_s)^2 \right] H_v \left( \sqrt{\frac{m\omega_0}{\hbar}} (q + q_s) \right), \quad (9.16)$$

where

$$q_s = \frac{U_{ss}}{m\omega_0^2}, \quad (9.17)$$

and  $H_v(x)$  is Hermit polynomial.

Utilizing Eq. (9.16) we calculate the overlap matrix element  $\langle v' s' | vs \rangle$ , which enters to Eq. (9.15):

$$\begin{aligned}
\langle v' s' | vs \rangle &= \frac{\exp[-a^2]}{\sqrt{\pi 2^{v+v'} v! v'!}} \int_{-\infty}^{\infty} dq \cdot e^{-q^2} H_{v'}(q+a) H_v(q-a) \\
&= \frac{\exp[-a^2]}{\sqrt{2^{v+v'} v! v'!}} \left[ \frac{d^{v+v'}}{dt_1^v dt_2^{v'}} e^{2t_1 t_2 + 2a(t_1-t_2)} \right] \Big|_{t_1=0, t_2=0} \\
&\approx \sqrt{\frac{2^{v-v'}}{v! v'!}} a^{|v-v'|} \Bigg|_{a \rightarrow 0} \quad (9.18)
\end{aligned}$$

where

$$a = \frac{q_s' - q_s}{2\sqrt{\hbar/m\omega_0}} = \frac{U_{s's'} - U_{ss}}{2\sqrt{\hbar m\omega_0^3}} \ll 1. \quad (9.19)$$

Inequality (9.19) follows from Eq. (9.11). The integral (9.18) is calculated with the help of the generating function for Hermit polynomials:

$$f(x, t) = \exp(2xt - t^2) = \sum_n H_n(x) \frac{t^n}{n!}.$$

Substituting Eq. (9.18) into Eq. (9.15), and, subsequently, into Eq. (9.14) with the account of Eq. (9.19) we find:

$$\begin{aligned} W_s^{s'} &= \frac{\pi\hbar^2\omega_0}{m} \frac{U_{s's}^2}{(E_s^{(0)} - E_{s'}^{(0)})^2} \sum_{v=0}^{\infty} \frac{\exp[-\frac{\hbar\omega_0 v}{kT}]}{\sum_{\tilde{v}} \exp[-\frac{\hbar\omega_0 \tilde{v}}{kT}]} \\ &\times \sum_{v'=0}^{\infty} \left( \frac{2a^2}{(v-1)!v'!} \right)^{v-1-v'} v \delta \left[ (E_{s'}^{(0)} - E_s^{(0)}) + \hbar\omega_0 (v' - v) \right] \\ &= \frac{\pi\hbar}{m} \frac{U_{s's}^2}{(E_s^{(0)} - E_{s'}^{(0)})^2} (2a^2)^{\frac{E_s^{(0)} - E_{s'}^{(0)}}{\hbar\omega_0} - 1} \sum_{v=0}^{\infty} v \exp \left[ -\frac{\hbar\omega_0 v}{kT} \right] \\ &\times \frac{1}{(\nu-1)!} \int_{-\infty}^{\infty} \frac{\delta \left[ \frac{(E_{s'}^{(0)} - E_s^{(0)})}{\hbar\omega_0} - (v - v') \right]}{[v - (v - v')!]!} d(v - v') \quad (9.20) \\ &\approx \frac{\pi\hbar}{m} \frac{U_{s's}^2}{(E_s^{(0)} - E_{s'}^{(0)})^2} (2a^2)^{(p-1)} \frac{p}{(p-1)!} [n(T, \omega_0)]^p, \end{aligned}$$

where  $p = \frac{E_{s'}^{(0)} - E_s^{(0)}}{\hbar\omega_0}$  is the number of optical phonons to be absorbed from the crystal during the transition  $s \rightarrow s'$ , and  $n(T, \omega_0) = (\exp[\frac{\hbar\omega_0}{kT}] - 1)^{-1} \approx \exp[-\frac{\hbar\omega_0}{kT}]$  is the average number of optical phonons per one inter-molecular bond. This number is small due to the inequality  $\frac{\hbar\omega_0}{kT} \gg 1$ . For the same reason the sum  $\sum_{v=0}^{\infty} \exp[-\frac{\hbar\omega_0 v}{kT}]$  in Eq. (9.20) is assumed equal to 1.

The number of absorbed phonons  $p$  generally is not an integer, so to satisfy the energy conservation law, typically one acoustic phonon with low frequency is absorbed. This fact complicates the estimate considerably, but thus not change the order of magnitude of the result. Because of that, the transition rate  $W_s^{s'}$  below will be calculated according to Eq. (9.20), assuming that  $p$  can be non-integer.

In the derivation of Eq. (9.20) the sum  $\sum_{v'}$  has been substituted by an integral  $\int dv'$ . As a result, the obtained formula, from the formal point of view, is accurate up to time  $\tau \ll \omega_0^{-1}$ . According to Eq. (9.20), the decay rate is then anomalously low due to  $a^2 \ll 1$  and  $p \gg 1$ . The account of the fact that the optical phonons form a band, does not change the estimate of

the decay rate for the  $s$ -level, but make the equation (9.20) applicable at time  $\tau \lesssim (W_s^{s'})^{-1} \gg \omega_0^{-1}$ .

Next we utilize Eq. (9.20) to obtain numeric estimates of the decay rate for a highly excited vibrational level in crystal  $N_2$ .

Let us consider the case, when initially the first oscillator is at the  $n$ -th level, while the second is at zero level. In the final state the first oscillator is at the  $(n-1)$ -th level, while the second – at the first one. Then, utilizing equations (9.5), (9.7), (9.9) and (9.19) we obtain the following expressions for the parameters in Eq. (9.20):

$$\begin{aligned} p &= p_n = \frac{2x_e\Omega(n-1)}{\omega_0}, \quad 2a^2 \simeq \frac{\xi^4(\beta_{11} - \beta_{22})^2}{2\hbar m\omega_0^3}, \\ \gamma &= \left[ \frac{U_{s's}}{E_s^{(0)} - E_{s'}^{(0)}} \right]^2 = \frac{\xi^4\beta_{12}^2 n}{4\hbar m\omega_0^3 p_n^2}, \quad \xi^2 = \frac{\hbar}{m\Omega}. \end{aligned} \quad (9.21)$$

The matrix elements  $U_{ss'}$  are calculated in the harmonic approximation. The temperature dependence of the decay rate is of activation type:

$$W_s^{s'} \sim \exp \left[ -\frac{E_{s'}^{(0)} - E_s^{(0)}}{kT} \right], \quad (9.22)$$

according to Eq. (9.20) and the condition  $\hbar\omega_0 \gg kT$ . The last inequality is always satisfied for simple molecular crystals, as at higher temperatures they melt.

Next we provide numeric estimates of the decay rate  $W_n$  for  $n = 7$  and  $n = 10$ . In the crystal  $N_2$  there are two branches of inter-molecular modes: a translational one with  $\hbar\omega_0 = 69 \text{ cm}^{-1}$  and a quasi-rotational one with  $\hbar\omega_0 \simeq 49 \text{ cm}^{-1}$ . As an estimate we choose the first frequency – it provides a higher value of  $W_n$ . All the requirement parameters of the crystal  $N_2$  are known from experiment and have the following values:

$$\begin{aligned} \Omega &= 2500 \text{ cm}^{-1}, \quad \omega_0 = 69 \text{ cm}^{-1}, \quad x_e = 0,0061, \\ x_e\Omega &= 30 \text{ cm}^{-1}, \quad \beta_{ij} \frac{\hbar}{m\Omega} \sqrt{\frac{\hbar}{m\omega_0}} \approx 1 \text{ cm}^{-1}. \end{aligned} \quad (9.23)$$

With the account of Eq. (9.23) the parameters (9.21) are given by:

$$\begin{aligned} p &= p_n = 0,442 \cdot (n-1), \quad 2a^2 \approx 10^{-4}, \\ \gamma &= \gamma_n \approx \frac{a^2 n}{p_n^2}. \end{aligned} \quad (9.24)$$

Then, equation (9.20) with the account of Eqs. (9.23), (9.24) can be written down in the form:

$$\begin{aligned} W_n &\simeq \frac{\pi\omega_0 n}{2(p_n)!} \cdot \left( 2a^2 \exp \left[ -\frac{\hbar\omega_0}{kT} \right] \right)^{p_n} \\ &\simeq \frac{110n}{[0,442(n-1)]!} \left( 10^{-\left( 4+0,43\frac{\hbar\omega_0}{kT} \right)} \right)^{0,442(n-1)} \end{aligned} \quad (9.25)$$

With the help of Eq. (9.25) with  $n = 7, 10$  and  $T = 30^\circ k = 20 \text{ cm}^{-1}$  we obtain the following values of  $W_n$  and  $\tau_n = W_n^{-1}$ :

$$\begin{aligned} W_7 &\simeq 0.4 \cdot 10^{-12} \text{ cm}^{-1} \sim 0,77 \text{ s}^{-1}, \quad \tau_7 \sim 10 \text{ s}; \\ W_{10} &\simeq 0.4 \cdot 10^{-20} \text{ cm}^{-1} \sim 0,77 \cdot 10^{-8} \text{ s}^{-1}, \quad \tau_{10} \sim 10^9 \text{ s}. \end{aligned} \quad (9.26)$$

It can be seen clearly from Eq. (9.26), that the lifetime of intra-molecular vibrational excitations in crystal  $N_2$  is of a macroscopic scale, and grows exponentially  $\sim (2a^2)^{-n}$  with the increase of the excitation number  $n$ . The temperature dependence is of activation type, Eq. (9.25), so that at room temperature the estimates provide an additional factor  $\sim 10^{4p_n}$ , and the excitation energy does not decay practically until it gets emitted ( $\sim 10^5 \div 10^6 \text{ s}$ ).

The estimates provided characterize the conditions of existence of such excitations, and provide information on possible methods of their stabilization. A similar picture is realized in crystals  $O_2$ ,  $CO$ ,  $NO$ . In the last two molecules the excitations get emitted rather quickly,  $\sim 10 \text{ s}$ .

We would like to note further, that according to Eq. (9.6) and (9.20) the probability that one intra-molecular quantum gets split-up into inter-molecular quanta is very low and can be neglected due to the estimate  $p_n \sim 10 \div 20$ . Simultaneously, in Eq. (9.20) the temperature factor should be omitted. Consequently, the excited state with  $n = 1$  exists, until this quantum gets emitted, even for polar molecules like  $HCl$ . The existence of such long-lasting localized states can lead to the emergence of extremely narrow lines in the inelastic scattering of neutrons in such crystals.

Thus, the provided analysis demonstrates, that the nonlinearity of intra-molecular vibrations leads to anomalously long lifetimes  $\tau \gg 10^{-12} \text{ s}$  of local vibrational excitations in simple molecular crystals. This time in the absence of the dipole moment of the molecule is much greater than one second. In the case, one the molecule has a nonzero dipole moment (like  $CO$ ,  $NO$ ), the lifetime is determined by the radiation lifetime  $\tau_r$ , which of the order of magnitude  $\sim 10^{-6} \div 10^{-4} \text{ s}$ . Such long-living vibrational excitations have been observed in experiment in crystals  $N_2$  in 1975 by Dressper et.al., [14]. The observed lifetime was of the order of  $\sim 1 \text{ s}$ . In [146] the excitation lifetime in molecule  $CO$  has been observed to be  $\tau \sim 10^{-5} \text{ s}$ .

The consideration above suggests that in simple molecular crystals the total number of vibrational quanta  $\hbar\Omega$  is approximately conserved, at least up to times, which exceed greatly the typical time of propagation of the intramolecular vibrational energy in the crystal  $\tau \sim 10^{-12} \div 10^{-14}$  s. This fact makes possible the creation of highly-excited vibrational states in molecular crystals of the type  $N_2$ , [147], considered in detail in the next Section.

## 9.2 Population inversion of localized long - living vibrational states in a cold lattice

As it has been shown in the previous Section, the total number of intramolecular vibrational quanta (in short, vibrons)  $N$  in simple molecular crystals of type  $X_2$  at low temperature ( $T \lesssim 30$  K) is approximately preserved. It makes possible the search of a stationary distribution at given temperature of the lattice  $T_1$  and given  $N$ . Our goal is to find the distribution of molecules over the vibrational states  $n(r) = n_r$  under the condition, that the energy is given by:

$$E_r = r - x_e r^2, \quad r \ll r_0 = \frac{1}{2x}, \quad x_e = \frac{1}{4D}, \quad (9.27)$$

where  $D$  is the dissociation energy, and  $\omega_e = 1$ .

According to Eq. (9.27) the energy of two-quanta state is smaller than the sum of the two energies of one-quantum states. The same remains true for the higher energy states as well:

$$E_r + E_0 \leq E_{r-1} + E_1. \quad (9.28)$$

If the temperature of the lattice is low, the state with the lowest energy is realized. With  $N$  given, an anomalously large number of highly excited molecules with big  $r$  emerges due to the reduction of ones with low  $r = 1, 2, \dots$ . The norm is provided by  $n_r$  – the number of excited molecules per one molecule on average, so that

$$\sum_{r=0}^{r_0} n_r = 1, \quad \sum_{r=0}^{r_0} r n_r = N. \quad (9.29)$$

With such a norm introduced,  $n_r$  and  $N$  are nothing but concentrations of  $r$  – excitations and of the total number of quanta per molecule.

In the true thermodynamic equilibrium the system (in the present case the molecule  $X_2$ ) which has a single exact constant of motion – the energy – is described by the distribution function:

$$n_r = C \exp(-\beta E_r), \quad \beta = \frac{1}{kT_1}, \quad (9.30)$$

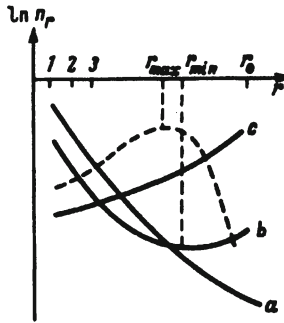


Figure 9.1: The distribution function of vibronic excitations  $n(r) = n_r$  for various temperatures and pumping regimes.

where  $T_1$  is the temperature. If we consider the molecule at times much smaller than the time of vibrational quanta' decay into phonons, there emerges an approximate constant of motion – the number of vibrons  $N$ . Then the distribution function  $n_r$  is represented by a grand canonical ensemble:

$$n_r = C \exp [\beta (\mu r - E_r)], \quad (9.31)$$

where  $\mu$  – is the chemical potential. The constants  $C$  and  $\mu$  are determined with the help of conditions (9.29). In the harmonic case we have  $E_r = r$ , and  $n_r$  is provided by a distribution:

$$n_r = (1 - \gamma) \gamma^r, \quad \gamma = \frac{N}{N + 1} = e^{\beta(\mu - 1)}. \quad (9.32)$$

The latter does not depend upon the temperature, as the exchange of vibrons takes place without the participation of the lattice.

In true equilibrium ( $\mu = 0$ ,  $N_1 = (e^\beta - 1)^{-1}$ ) the distribution  $n(r)$  decreases monotonously with the increase of  $r$  up to  $r_0$  (curve  $a$ , Fig. 9.1). If  $N$  exceeds the equilibrium value ( $N > N_1$ ) then  $n(r)$  has a minimum, determined from the condition:

$$\begin{aligned} \frac{d(E_r \beta - \mu r \beta)}{dr} &= \beta(1 - 2x_e r_{\min}) - \beta \mu = 0, \\ r_{\min} &= \frac{\beta(1 - \mu)}{2\beta x_e} \approx \frac{\ln(\gamma^{-1})}{2\beta x_e} = \frac{\ln(\frac{N+1}{N})}{2\beta x_e} \approx \frac{\ln(\frac{1}{N})}{2\beta x_e}. \end{aligned} \quad (9.33)$$

In Eq. (9.33) it has been taken into account, that in molecular crystals of type  $X_2$  the following inequalities hold:  $\beta \rightarrow \beta \omega_e \gg 1$ ,  $N \sim [e^{\beta(1-\mu)} - 1]^{-1} \ll 1$ .

In Fig. 9.1 the corresponding curve is denoted by  $b$ . Eq. (9.33) determines the position of the distribution minimum  $r_{\min}$  as function of temperature  $\beta$  and of the approximately conserved number of vibrons  $N$ . With the decrease of temperature the minimum  $r_{\min}$  is shifted to the left, and at low enough temperatures  $x_e \beta \gg 1$  it can become equal to 1 (curve  $c$ ). It is convenient to introduce the temperature  $T_2(N)$ , which corresponds to the situation, when the total number of vibrons equals the equilibrium one for the distribution (9.30) (the true distribution). The approximate expression for  $T_2$  is  $T_2 = |\ln N|^{-1}$ , and correspondingly,  $r_{\min} = r_0 T_1 T_2^{-1}$ , where  $r_0 = (2x_e)^{-1}$ .

At large values of  $r$  and  $r > r_{\min}$  the important fact is the "drift" of the molecules to the state with  $r = r_0$  quanta, as after the dissociation limit is reached the number of vibrons changes that way. The drift velocity in the stationary regime is proportional to  $n_{r_{\min}}$ , so that  $r_{\min}$  plays the role of a barrier in the process. It can be found easily, that the following estimates hold:

$$\begin{aligned} n_{r_{\min}} &\sim \exp(-\beta x_e r_{\min}^2) \\ &\sim \exp\left(-\frac{|\ln N|^2}{4\beta x_e}\right) \sim \exp\left[-\frac{DT_1}{T_2^2}\right]. \end{aligned} \quad (9.34)$$

The study of the distribution  $n(r)$  in the region  $r_{\min} < r < r_0$  is complicated. It is obvious though, that it differs there from the canonical distributions (9.30) and (9.31), and its values are low and determined by the quantity  $n_{r_{\min}}$ , Eq. (9.34).

Our goal is to calculate the stationary distribution function  $n(r)$  under the condition of constant pumping with quanta  $\hbar\omega_e = 1$  in the course of IR-absorption. It turns out that under these conditions the inversed population with respect to thermal equilibrium (9.31) is possible.

Let  $i_0$  single-quantum excitations emerge per molecule per unit time. The kinetic equation for  $n(r, t)$  should take into account the following processes: the transitions  $r \rightarrow r - 1$  with the emission of a photon  $\hbar\omega_e$  with characteristic time  $t_p \sim 10^{-6}$  s, radiationless transitions  $|r; 0\rangle \rightarrow |r - 1; 1\rangle$  with the absorption of a phonon from the lattice, and radiationless transitions  $|r - 1; 1\rangle \rightarrow |r; 0\rangle$  with the emission of a phonon. The last two processes, according to Eq. (9.20), have the following transition rates:

$$\begin{aligned} \bar{W}_r &= W_r e^{-\Delta E_r \beta} = W_r e^{-2\beta x_e(r-1)}, \\ W_r &= \tau_r^{-1} = \tau_0^{-1} \cdot e^{-pr}, \end{aligned} \quad (9.35)$$

where  $\tau_0 \sim 100/\Omega \sim 10^{-12}$  s,  $\Omega$  is the Debye frequency, and  $p \approx 1 \div 4$  for typical molecular crystals.

Implying that there are no correlations between excitations on different molecules, the kinetic equation can be presented in the form [147], analogous to the one for the growth of drops from the over-saturated vapor:

$$\begin{aligned}\frac{dn_r}{dt} &= W_r n_{r-1} n_1 - W_{r+1} n_r n_1 + \bar{W}_{r+1} n_{r+1} \\ &\quad - \bar{W}_r n_r + \frac{1}{t_{rad}} (n_{r+1} - n_r) + i_0 \delta_{r1}.\end{aligned}\quad (9.36)$$

In the stationary case we have  $\frac{dn_r}{dt} = 0$ , and from Eq. (9.36) we find:

$$\begin{aligned}W_r n_{r-1} n_1 - \bar{W}_r n_r - \frac{1}{t_{rad}} n_r &= 0, \quad \text{if } r \geq 2 \\ n_1 &= t_{rad} i_0,\end{aligned}\quad (9.37)$$

where from

$$\begin{aligned}n_r &= \frac{n_1}{\bar{W}_r/W_r + 1/(W_r t_{rad})} \cdot n_{r-1} = \frac{n_1}{e^{-\Delta E_r \beta} + \tau_r/t_{rad}} \cdot n_{r-1} \\ &= \frac{n_1^2}{(e^{-\Delta E_r \beta} + \tau_r/t_{rad})(e^{-\Delta E_{r-1} \beta} + \tau_{r-1}/t_{rad})} \cdot n_{r-2} = \dots \\ &= \frac{n_1^r e^{-\beta(E_r - E_1 r)}}{\prod_{k=2}^r [1 + (\tau_k/t_{rad}) e^{\beta \Delta E_k}]},\end{aligned}\quad (9.38)$$

with

$$\Delta E_k = (E_{k-1} + E_1 - E_k - E_0) = 2x_e(k-1), \quad \tau_k = \tau_0 e^{pk}. \quad (9.39)$$

In the derivation of equations (9.38), (9.39) we have taken into expressions (9.27) for  $E_r$  and (9.35) for the transition rates  $W_r$  and  $\bar{W}_r$ . The quantity  $\frac{\tau_0}{t_{rad}}$  can be estimated as  $\sim 10^{-6}$  according to Eq. (9.35),  $t_{rad} \sim 10^{-6}$  s. As  $\beta x_e \sim 1$ , we find, that the dependence (9.38) at  $1 \leq r \leq r_\beta = \frac{\ln(t_{rad}/\tau_0)}{p+2\beta x_e}$  has the canonical form (9.31) with  $\mu = E_1 + \beta^{-1} \ln(n_1)$ . At  $r \gtrsim r_\beta$  the quantity  $n_r$  grows, reaching its maximum at

$$r_{\max} = \frac{1}{p} \left[ \ln \left( \frac{t_{rad} i_0}{\tau_0} \right) - p \right]. \quad (9.40)$$

Equation (9.40) is valid under the condition:

$$\begin{aligned}n_1 e^{2\beta x_e r_{\max}} &\sim t_{rad} i_0 e^{2\beta x_e r_{\max}} > 1, \\ (\tau_0/t_{rad}) e^p e^{(p+2\beta x_e)r} &\ll 1, \quad \text{if } r \ll r_{\max}.\end{aligned}\quad (9.41)$$

The function  $n(r)$  for  $r > r_{max}$  is proportional to  $\exp(-pr^2/2)$  and for  $r \rightarrow r_0 \sim \infty$  it decreases rapidly. The corresponding functional dependence is presented in Fig. 9.1 as a dashed line.

Thus under stationary pumping with one-quantum excitations with intensity  $i_0$  the stationary distribution function  $n(r)$ , Eq. (9.38), reveals three distinctive regions, where the behavior of  $n(r)$  differs significantly:

$$\begin{aligned}
1 &\leqslant r \leqslant r_\beta \simeq \frac{\ln\left(\frac{t_{rad}}{\tau_0}\right)}{p + 2\beta x_e}, \\
n(r) &\sim e^{(E_1 r - E_r)\beta} \cdot n_1^r \sim \exp\left\{\left[\left(E_1 + \frac{\ln n_1}{\beta}\right)r - E_r\right]\beta\right\} \\
&\sim \exp[(\mu r - E_r)\beta], \\
&\quad -\text{curve (b), the canonical distribution;} \\
r_\beta &\leqslant r \leqslant r_{max} \simeq \frac{1}{p} \ln\left(\frac{i_{rad}^2 i_0}{\tau_0}\right) - 1, \\
&\quad -\text{the vicinity of the maximum of the dashed curve;} \\
r_{max} &\leqslant r \leqslant r_0, \quad n(r) \sim e^{-pr^2/2}, \\
&\quad -\text{the falling part of the dashed curve.}
\end{aligned} \tag{9.42}$$

In the case  $r_\beta \sim 1$  the dependence  $n(r)$  is plotted as a dashed curve in Fig. 9.1. Then the distribution  $n(r)$  differs significantly from the canonical one (9.31), so that system is in a strongly inverted state  $n(r_{max}) > n_1$ . This fact can be used for the experimental observation of vibrational quanta condensation.

It is worth noting, that the population inversion takes place for  $r > 1$ , that is, for frequencies differing from the illumination frequency  $\hbar\omega_e = 1$ . After the illumination ceases, the inversion of the transition  $r = 2 \rightarrow r = 1$  grows – the shape of the dashed curve differs considerably from the canonical distributions, curves (a) and (b).

The considered effect of the is most clearly revealed at low temperatures in simple molecular crystals of the type  $N_2, H_2, O_2, NO$ . Of interest are also the crystals like  $HCl$ , where the single-quantum levels can be excited with much ease due to a large dipole momentum of the molecule  $HCl$ .

The entire consideration above applies with some modifications to gases and liquids as well. The temperatures then, however, should be low enough.

### 9.3 Interaction of isolated levels with the continuous spectrum

One of the most important characteristics of molecular vibrational states is their lifetime  $\tau$ , or, in other words, the width of the vibrational level

$\Gamma \sim \tau^{-1}$ . The width of the vibrational level increases due to two possible reasons: the interaction with the quasi-continual spectrum of other modes<sup>3</sup> and the radiational transitions. The radiation widening vibrational levels is of the order of  $\sim 10^{-5} \text{ cm}^{-1}$ , which is much less than the vibrational-rotational transition frequencies  $\Omega \gtrsim 1 \text{ cm}^{-1}$ . Thus, the interaction with the electromagnetic field influences only the super-fine structure of the vibronic spectrum. The interaction between different modes, on the contrary, can produce a considerable widening of vibrational-rotational levels  $\Gamma \gg \Omega$ , so that there is, in fact, no more level and no corresponding stationary state. Due to this fact, below we ignore the radiation interaction and consider only the potential and kinematical interaction of modes in a polyatomic molecule.

In the analysis of physical characteristics of the considered group of vibrational-rotational levels we are supposed to find an answer to the following question: what are the widths (or lifetimes) after the inclusion of a small additional interaction between modes? One can qualify the individual properties of levels from the group, stable with respect to small variations of interaction, only if the widths satisfy the inequality  $\Gamma_i \ll \Omega$ . Otherwise the mixing (stochasticization) of these levels in between them or with the levels of other modes takes place during the time  $\tau$  which is much less than the period of motion  $T \sim \Omega^{-1}$ . Then the levels of the considered group lose their individuality, except for the energy characteristic.

The calculation of the level width  $\Gamma$  we will analyze with the help of a simple model system, which can be solved exactly, and which reveals clearly the underlying physics of the process.

Let us assume the existence of a discrete level  $|0\rangle$  and a set of states  $|x\rangle$  with continuous spectrum, having the unperturbed energies  $\varepsilon_0 = 0$  and  $\varepsilon(x)$ , respectively. The continuous variable  $x$ , the function  $\varepsilon(x)$ , and the ket-vector  $|x\rangle$  satisfy the following conditions:

$$\begin{aligned} \underline{x} &\leqslant x \leqslant \bar{x}, \quad \underline{\varepsilon} = \varepsilon(\underline{x}), \quad \bar{\varepsilon} = \varepsilon(\bar{x}), \\ \frac{d\varepsilon}{dx} &> 0; \quad \langle 0 | 0 \rangle = 1, \quad \langle 0 | x \rangle = \langle x | 0 \rangle = 0, \\ \langle x | x \rangle &= \delta(x - x'). \end{aligned} \tag{9.43}$$

An arbitrary ket-vector  $|\Psi\rangle$  has the form:

$$|\Psi\rangle = \psi_0 |0\rangle + \int_{\underline{x}}^{\bar{x}} \psi(x) |x\rangle dx,$$

---

<sup>3</sup>The density of states for small molecules reaches the values of  $\sim 10^5 \text{ cm}^{-1}$ , so that the spectrum of polyatomic molecules can be considered continuous.

$$\langle \Phi | \Psi \rangle = \varphi_0^* \psi_0 + \int_{\underline{x}}^{\bar{x}} \varphi^*(x) \psi(x) |x\rangle dx. \quad (9.44)$$

The Hamiltonian of the system we choose in the form:

$$\hat{H} = |0\rangle 0\langle 0| + \int_{\underline{x}}^{\bar{x}} |x\rangle \varepsilon(x) \langle x| dx + |0\rangle \int_{\underline{x}}^{\bar{x}} F(x) \langle x| dx + \int_{\underline{x}}^{\bar{x}} |x\rangle F^*(x) dx \langle 0|. \quad (9.45)$$

In matrix notation, this Hamiltonian has nonzero values in the first row and first column. The eigenfunction  $(\varphi_0, \psi(x)) = (1, \psi(x))$  is determined from the equation:

$$\begin{aligned} 0 \cdot 1 + \int_{\underline{x}}^{\bar{x}} F(x) \psi(x) dx &= \lambda, \\ \varepsilon(x) \psi(x) + F^*(x) &= \lambda \psi(x). \end{aligned} \quad (9.46)$$

This set has two solutions, corresponding to two discrete energy levels  $\underline{\lambda}$  and  $\bar{\lambda}$ , determined by the equations:

$$\int_{\underline{x}}^{\bar{x}} \frac{|F(x)|^2}{\underline{\lambda} - \varepsilon(x)} dx = \underline{\lambda}, \quad \int_{\underline{x}}^{\bar{x}} \frac{|F(x)|^2}{\bar{\lambda} - \varepsilon(x)} dx = \bar{\lambda}. \quad (9.47)$$

The corresponding ket-vectors are:

$$\begin{aligned} |\underline{\lambda}\rangle &= |0\rangle + \int_{\underline{x}}^{\bar{x}} |x\rangle \frac{F^*(x) dx}{\underline{\lambda} - \varepsilon(x)}, \\ |\bar{\lambda}\rangle &= |0\rangle + \int_{\underline{x}}^{\bar{x}} |x\rangle \frac{F^*(x) dx}{\bar{\lambda} - \varepsilon(x)}. \end{aligned} \quad (9.48)$$

With the account of Eq. (9.44) the norm of these states takes the form:

$$\langle \lambda_\alpha | \lambda_\alpha \rangle = 1 + \int_{\underline{x}}^{\bar{x}} \frac{|F(x)|^2}{(\lambda_\alpha - \varepsilon(x))^2} dx, \quad \lambda_\alpha = \underline{\lambda}, \bar{\lambda}. \quad (9.49)$$

It can be seen easily, that the functions from the continuum spectrum with  $\underline{\varepsilon} \leq \lambda \leq \bar{\varepsilon}$ , satisfying Eq. (9.48), are:

$$|\lambda\rangle = |0\rangle + P \int_{\underline{x}}^{\bar{x}} |x\rangle dx \times \left\{ \frac{F^*(x)}{\lambda - \varepsilon(x)} + \frac{\frac{d\varepsilon}{dx}(x)}{F(x)} \left[ \lambda - P \int_{\underline{x}}^{\bar{x}} \frac{|F(x')|^2}{\lambda - \varepsilon(x')} dx' \right] \delta(\lambda - \varepsilon(x)) \right\}, \quad (9.50)$$

where the integral  $P \int_{\underline{x}}^{\bar{x}} dx \dots$  is understood as the principal value. Ket-vectors (9.50) have the norm:

$$\begin{aligned} \langle \mu | \lambda \rangle &= \rho(\mu) \delta(\mu - \lambda), \\ \rho(\mu) &= \pi^2 \frac{|F(x(\mu))|^2}{\frac{d\varepsilon}{dx}(x(\mu))} + \frac{\frac{d\varepsilon}{dx}(x(\mu))}{|F(x(\mu))|^2} \left[ \mu - P \int_{\underline{x}}^{\bar{x}} \frac{|F(x)|^2}{\mu - \varepsilon(x)} dx \right]^2. \end{aligned} \quad (9.51)$$

The norm function  $\rho(\mu)$  emerges in the calculation of scalar product of the vectors  $|\Phi\rangle = \int \Phi(\lambda) d\lambda |\lambda\rangle$  and  $|\Psi\rangle = \int \Psi(\lambda) d\lambda |\lambda\rangle$  with the account of the well-known formula of mathematical analysis:

$$\begin{aligned} &\int G(x) dx P \int \frac{f(\lambda) d\lambda}{\lambda - x} P \int \frac{h(\mu) d\mu}{\mu - x} \\ &= \int f(\lambda) d\lambda \int h(\mu) d\mu P \int \frac{G(x) dx}{(\lambda - x)(\mu - x)} + \pi^2 \int G(x) f(x) h(x) dx. \end{aligned}$$

The norm function  $\rho(\lambda)$  has the dimension of energy, so that the scalar product  $\langle \lambda \mu \rangle$  is dimensionless, while the functions  $\Psi(\lambda)$  in  $\lambda$ -representation ( $|\Psi\rangle = \int \Psi(\lambda) d\lambda |\lambda\rangle$ ) have the dimension of inverse energy. The scalar product in  $\lambda$ -representation takes the form:

$$\langle \Psi | \Phi \rangle = \int \psi^*(\lambda) \varphi(\lambda) \rho(\lambda) d\lambda + \frac{\langle \Psi | \bar{\lambda} \rangle \langle \bar{\lambda} | \Phi \rangle}{\langle \bar{\lambda} | \bar{\lambda} \rangle} + \frac{\langle \Psi | \Delta \rangle \langle \Delta | \Phi \rangle}{\langle \Delta | \Delta \rangle}. \quad (9.52)$$

From equations (9.47)–(9.52) it follows, that the interaction  $F(x)$  transforms the states of the continuum spectrum  $|x\rangle$  into states  $|\lambda\rangle$ , Eq. (9.50), and produces two normalizable states (9.48).

The study of a discrete level decay within the considered model is reduced to the calculation of a vector  $|\Psi(t)\rangle$  under the condition  $|\Psi(0)\rangle = |0\rangle$ . Then the decay rate  $\Gamma(t)$  is determined by the probability amplitude  $\langle 0 | \Psi(t) \rangle$  with the help of the formula:

$$\Gamma(t) = -\frac{d}{dt} \ln |\langle 0 | \Psi(t) \rangle|^2. \quad (9.53)$$

From equations (9.48)–(9.52) it follows that vector  $|0\rangle$  in  $\lambda$ -representation acquires the following form:

$$|0\rangle = \frac{|\bar{\lambda}\rangle}{\langle\bar{\lambda}|\bar{\lambda}\rangle} + \frac{|\lambda\rangle}{\langle\lambda|\lambda\rangle} + \int_{\varepsilon}^{\bar{\varepsilon}} d\lambda \frac{|\lambda\rangle}{\rho(\lambda)}. \quad (9.54)$$

From Eq. (9.54) it follows that

$$|\Psi(t)\rangle = e^{-i\hat{H}t} |0\rangle = \frac{e^{-i\bar{\lambda}t} |\bar{\lambda}\rangle}{\langle\bar{\lambda}|\bar{\lambda}\rangle} + \frac{e^{-i\lambda t} |\lambda\rangle}{\langle\lambda|\lambda\rangle} + \int_{\varepsilon}^{\bar{\varepsilon}} d\lambda \frac{e^{-i\lambda t} |\lambda\rangle}{\rho(\lambda)}.$$

The amplitude  $\langle 0 | \Psi(t) \rangle$ , correspondingly, is

$$\langle 0 | \Psi(t) \rangle = \frac{e^{-i\bar{\lambda}t}}{\langle\bar{\lambda}|\bar{\lambda}\rangle} + \frac{e^{-i\lambda t}}{\langle\lambda|\lambda\rangle} + \int_{\varepsilon}^{\bar{\varepsilon}} d\lambda \frac{e^{-i\lambda t}}{\rho(\lambda)}. \quad (9.55)$$

Eq. (9.55) together with Eqs. (9.49) and (9.51) provides the exact solution of the problem of level  $\varepsilon_0 = 0$  decay in the model under consideration. Taking into account the fact, that the norms  $\langle\lambda|\lambda\rangle$  and  $\langle\bar{\lambda}|\bar{\lambda}\rangle$  satisfy the inequalities

$$\begin{aligned} 1 &\leq \langle\lambda|\lambda\rangle < \infty, \\ 1 &\leq \langle\bar{\lambda}|\bar{\lambda}\rangle < \infty, \end{aligned}$$

we find the two limiting regimes for the time-dependence of the amplitude (9.55).

In the first case, when  $|F| \gg (\bar{\varepsilon} - \varepsilon)$  and, correspondingly,  $\langle\lambda|\lambda\rangle \sim \langle\bar{\lambda}|\bar{\lambda}\rangle \sim 2$ ,  $|\lambda| \sim |\bar{\lambda}|$ , the amplitude  $\langle 0 | \Psi(t) \rangle$  is of the order of  $\sim \cos(|\lambda|t)$ . It means that the initial state  $|0\rangle$  is a superposition of two bound states  $|0\rangle = 2^{-1/2} (|\bar{\lambda}\rangle \pm |\lambda\rangle)$ , and there is no decay at all. Then the system oscillates between the states  $2^{-1/2} (|\bar{\lambda}\rangle + |\lambda\rangle)$  and  $2^{-1/2} (|\bar{\lambda}\rangle - |\lambda\rangle)$  with period  $T_{osc} \approx \pi / |\lambda|$ .

In the other limiting case we have  $|F(x)| \ll (\bar{\varepsilon} - \varepsilon)$  and  $\varepsilon < 0 < \bar{\varepsilon}$ . Then the norms satisfy  $\langle\lambda|\lambda\rangle \gg 1$ ,  $\langle\bar{\lambda}|\bar{\lambda}\rangle \gg 1$ , and, consequently, the contribution of bound states in the representation (9.55) is vanishingly small. Thus, the initial state  $|0\rangle$  is composed of states from the continuum spectrum, so that the probability amplitudes can be estimated as  $\langle 0 | \Psi(t) \rangle \sim \int_{\varepsilon}^{\bar{\varepsilon}} d\lambda \rho^{-1}(\lambda) e^{-i\lambda t} \rightarrow 0$ ,  $t \rightarrow \infty$ . This is the case of complete decay of the initial state.

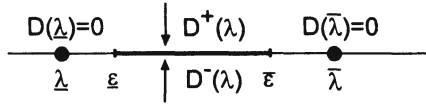


Figure 9.2: The region of analyticity for the function  $D(\lambda)$ . Physical sheet. The cut is shown by a solid line,  $(\underline{\varepsilon}, \bar{\varepsilon})$ .

The other cases, when only some part of the initial state  $|0\rangle$  decays  $(\langle 0 | \Psi(t) \rangle^2 \rightarrow p > 0 \text{ as } t \rightarrow \infty)$  are intermediate between the considered limiting cases.

Let us study the expression (9.55) of the amplitude  $\langle 0 | \Psi(t) \rangle$  in more detail. The norm function (9.51) we present in the following more convenient way:

$$\begin{aligned} \rho(\lambda) &= D^+(\lambda) \cdot D^-(\lambda) \cdot \frac{\frac{d\varepsilon}{dx}(x(\lambda))}{|F(x(\lambda))|^2}, \\ D^\pm(\lambda) &= \lambda - \int_{\underline{\varepsilon}}^{\bar{\varepsilon}} \frac{|F(x)|^2}{(\lambda \pm i\delta) - \varepsilon(x)} dx = \lambda - \int_{\underline{\varepsilon}}^{\bar{\varepsilon}} \frac{G(z)}{(\lambda \pm i\delta) - z} dz, \\ G(z) &= \frac{|F(\varepsilon^{-1}(z))|^2}{\varepsilon'(\varepsilon^{-1}(z))} > 0. \end{aligned} \quad (9.56)$$

The functions  $D^\pm(\lambda)$  are the limiting values above and below the cut  $\underline{\varepsilon} \leq \lambda \leq \bar{\varepsilon}$  of the unique analytic function  $D(\lambda)$ . The region of its analyticity, along with the cut across which it can be continued in the case of analyticity of the function  $G(z)$  is shown in Fig. 9.2.

It can be demonstrated on the basis of Eq. (9.56) that the function  $D(\lambda)$  goes to zero at points  $\underline{\lambda}$  and  $\bar{\lambda}$  only. In the rest part of the complex plane, including the cut  $(\underline{\varepsilon}, \bar{\varepsilon})$ , the function  $D(\lambda)$  is nonzero. This property originates from the fact, that the operator  $H$  is Hermitian, the discrete spectrum of which is determined by the zeros of  $D(\lambda)$ .

On the basis of the analytic properties of  $D(\lambda)$ , shown in Fig. 9.2, and of the relations

$$\begin{aligned} D(\bar{\lambda}) &= D(\underline{\lambda}) = 0, \quad D'(\bar{\lambda}) = \langle \bar{\lambda} | \bar{\lambda} \rangle, \quad D'(\underline{\lambda}) = \langle \underline{\lambda} | \underline{\lambda} \rangle, \\ \rho(\lambda) &= D^+(\lambda) \cdot D^-(\lambda) \cdot [G(\lambda)]^{-1}, \end{aligned}$$

the probability amplitude (9.55) can be represented in the form of a contour integral:

$$\begin{aligned}
A(t) &= \langle 0 | \Psi(t) \rangle = \frac{1}{2\pi i} \oint_C \frac{e^{-i\lambda t}}{D(\lambda)} d\lambda \\
&= \frac{1}{2\pi i} \oint_C \frac{e^{-i\lambda t}}{\lambda - \int_{\bar{\varepsilon}}^{\bar{\varepsilon}} \frac{G(z)}{\lambda - z} dz} d\lambda, \quad \text{if } t > 0. \tag{9.57}
\end{aligned}$$

Contour  $C$  surrounds counterclockwise the segment  $[\underline{\lambda}, \bar{\lambda}]$  of the real axis  $\operatorname{Re} \lambda$ , Fig. 9.2. The cut  $[\underline{\varepsilon}, \bar{\varepsilon}]$  on the physical sheet of the plane  $\lambda$  finds itself inside the contour  $C$  as well.

At  $t = 0$  the integral (9.57) along the contour  $C$  can be transformed into an integral  $\frac{1}{2\pi i} \oint_{|\lambda|=R} \frac{d\lambda}{\lambda} = 1$  along the circle of radius  $R \rightarrow \infty$ .<sup>4</sup> In other words  $A(0) = \langle 0 | 0 \rangle = 1$ , as it should be. At  $t > 0$  the integral (9.57) is transformed into an integral (9.55). The dependence  $A(t)$  can be analyzed, if the integral (9.57) is transformed into an integral along contour  $\underline{C}$ , some part of which is situated on the unphysical sheet – as the zeros of the function  $D(\lambda)$ , which correspond to quasi-stationary states, are situated there. To perform the analytic continuation of the function  $D(\lambda) = D^+(\lambda)$  down through the cut, we use the well-known equation from the theory of analytic functions utilized for the analytic continuation of Cauchi integrals through the integration contour:

$$\begin{aligned}
D(\lambda + i\delta) &= D^+(\lambda) = D^-(\lambda) + 2\pi i G(\lambda) = D(\lambda - i\delta) + 2\pi i G(\lambda), \\
\underline{\varepsilon} &< \lambda \leq \bar{\varepsilon}. \tag{9.58}
\end{aligned}$$

With the use of Eq. (9.58) we transform the integral (9.57) to the following form:

$$\begin{aligned}
A(t) &= \frac{1}{2\pi i} \oint_{\bar{C}} \frac{e^{-i\lambda t}}{D(\lambda + i\delta)} d\lambda \\
&= \frac{e^{-i\bar{\lambda}t}}{D'(\bar{\lambda})} + \frac{e^{-i\bar{\lambda}t}}{D'(\bar{\lambda})} + \frac{1}{2\pi i} \oint_{C_l} \frac{e^{-i\lambda t}}{D(\lambda)} d\lambda \\
&\quad + \frac{1}{2\pi i} \oint_{C_r} \frac{e^{-i\lambda t}}{D(\lambda)} d\lambda + \frac{1}{2\pi i} \sum_k \oint_{\gamma_k} \frac{e^{-i\lambda t}}{D(\lambda)} d\lambda. \tag{9.59}
\end{aligned}$$

Here the contour  $C_l$  surrounds the point  $\underline{\varepsilon}$  going counterclockwise: coming from the unphysical sheet at  $\operatorname{Im} \lambda = -\infty$  and going then to the physical

---

<sup>4</sup>Here it is taken into account that  $D(\lambda) = \lambda^{-1} + O(\lambda^{-1})$  according to Eq.(9.56).

sheet to  $\text{Im } \lambda = -\infty$ . The contour  $C_r$  surrounds the point  $\bar{\varepsilon}$  counterclockwise as well: coming from the physical sheet at  $\text{Im } \lambda = -\infty$  and going then to the unphysical sheet to  $\text{Im } \lambda = -\infty$ .

The contours  $C_l$  and  $C_r$  have one branch on the physical sheet where  $D(\lambda)$  is determined by Eq. (9.56), and another branch on the unphysical sheet, where  $D(\lambda)$  is the analytic continuation through the cut in accordance with Eq. (9.58). We note, that  $D^-(\lambda) = D^+(\lambda) = D(\lambda)$  for all points  $\lambda$  on the physical sheet, which do not belong to the cut. The last sum in Eq. (9.59) is the sum of residues in the zeros of the function  $D(\lambda)$ , corresponding to quasi-stationary levels (resonances). The representation (9.59) of the probability amplitude makes possible the analysis of all the forms of  $A(t)$ , including the limiting cases, mentioned above:  $|F| \gg |\bar{\varepsilon} - \varepsilon|$  and  $|F| \ll |\bar{\varepsilon} - \varepsilon|$ <sup>5</sup>. First we consider the case of strong interaction:

$$F^2 = \int_{\underline{x}}^{\bar{x}} |F(x)|^2 dx \gg (\varepsilon^2 + \bar{\varepsilon}^2). \quad (9.60)$$

Here the discrete levels, determined from Eq. (9.47) are:

$$\bar{\lambda}, \lambda = \pm \sqrt{\int_{\underline{x}}^{\bar{x}} |F(x)|^2 dx}. \quad (9.61)$$

The norms, determined by Eq. (9.49) are given by:

$$D'(\lambda) = D'(\bar{\lambda}) = \langle \lambda | \lambda \rangle = \langle \bar{\lambda} | \bar{\lambda} \rangle \approx 2. \quad (9.62)$$

Consequently, the first two terms in Eq. (9.59) give  $A(t) \sim \cos \lambda t$ . The other terms in Eq. (9.59) go to zero as  $t \rightarrow \infty$ . Really, the integrals over the contours  $C_r$  and  $C_l$  tend to zero as  $t \rightarrow \infty$  due to the condition  $\text{Im } \lambda < 0$  on these contours. The sum of residues in the points  $\gamma_k$  of the lower semi-plane is given by exponentially decaying terms, which go to zero for  $t \rightarrow \infty$  as well. Thus, at large  $t$  in the representation (9.59) of the probability amplitude  $A(t)$  only the first two terms survive, giving

$$A(t) \simeq \cos \left[ \sqrt{\int_{\underline{x}}^{\bar{x}} |F(x)|^2 dx t} \right], \quad (9.63)$$

with no decay. Such a probability amplitude  $\langle 0 | \Phi(t) \rangle$  is provided by a state, which at  $t = 0$  is represented by the vector:

---

<sup>5</sup>The sufficient condition for the representation (9.59) is provided by the analyticity of the function  $G(z)$  in the stripe  $\text{Im } \lambda \leq 0$ , and  $\varepsilon \leq \text{Re } \lambda \leq \bar{\varepsilon}$ , and by the convergence of integrals along the contours  $C_r$  and  $C_l$ , or by the condition that  $\left| \frac{\exp(-|\text{Im } \lambda|t)}{D(\lambda)} \right|$  tends to zero rapidly enough.

$$|\Phi(0)\rangle = (|\lambda\rangle + |\bar{\lambda}\rangle)/\sqrt{2}.$$

The ket vector  $|\Phi(t)\rangle$  rotates with a constant angular velocity  $|\dot{\lambda}| = |\bar{\lambda}|$  in the plane, generated by vectors

$$(|\lambda\rangle + |\bar{\lambda}\rangle)/\sqrt{2} = |0\rangle, \quad (|\lambda\rangle - |\bar{\lambda}\rangle)/\sqrt{2} = \int_{\underline{x}}^{\bar{x}} a(x)|x\rangle dx.$$

The last equations follow from Eqs. (9.47) and (9.48) with the account of Eqs. (9.60) and (9.61). It is obvious, that in the limit of strong interaction the system goes over from state  $|0\rangle$  into the state  $a(x)$ , composed of vectors  $|x\rangle$  from the continuum spectrum, and then back from  $a(x)$  to  $|0\rangle$ , etc. The period of such oscillations is given by  $T = 2\pi/\bar{\lambda}$ . Thus, we arrived to the same result, which has been formulated briefly above.

In the terms of stationary states the interaction  $F(x)$ , which satisfies the condition (9.60), binds the unperturbed bounded state  $|0\rangle$  with the wavepacket  $\int a(x)|x\rangle dx$ , producing two new bounded states:  $|0\rangle \pm \int a(x)|x\rangle dx = |\bar{\lambda}\rangle$ . In the considered limiting case, according to Eq. (9.48) we have  $a(x) = F^*(x)(\lambda)^{-1}$ . This resembles in fact the case of Fermi resonance, where the wavepacket  $\int a(x)|x\rangle dx$  plays the role of one of the resonant levels.

The other limiting case corresponds to weak interaction

$$F^2 = \int_{\underline{x}}^{\bar{x}} |F(x)|^2 dx \ll (\varepsilon - \bar{\varepsilon})^2. \quad (9.64)$$

Then three different physical situations are possible, characterized by the following conditions <sup>6</sup>:

- a)  $\varepsilon_0 - \varepsilon \gg |F|^2(\bar{\varepsilon} - \underline{\varepsilon})^{-1}$ , and  $\bar{\varepsilon} - \varepsilon_0 \gg |F|^2(\bar{\varepsilon} - \underline{\varepsilon})^{-1}$ ;
- b)  $|\varepsilon_0 - \varepsilon| \sim |F|^2(\bar{\varepsilon} - \underline{\varepsilon})^{-1}$ , or  $|\bar{\varepsilon} - \varepsilon_0| \sim |F|^2(\bar{\varepsilon} - \underline{\varepsilon})^{-1}$ ;
- c)  $\underline{\varepsilon} - \varepsilon_0 \gg |F|^2(\bar{\varepsilon} - \underline{\varepsilon})^{-1}$ , or  $\varepsilon_0 - \bar{\varepsilon} \gg |F|^2(\bar{\varepsilon} - \underline{\varepsilon})^{-1}$ .

The three regimes, corresponding to Eq. (9.65) are shown schematically in Fig. 9.3. The physical consequences of it are commented in the caption. Below we apply the representation (9.59) to the analysis of conditions a), b), and c).

In the case a), when the energy of level  $\varepsilon_0 = 0$  is approximately in the middle of the band  $(\underline{\varepsilon}, \bar{\varepsilon})$ , both levels  $\lambda$  and  $\bar{\lambda}$  lie close to the boundary of

---

<sup>6</sup>The energy of the unperturbed discrete level  $\varepsilon_0$  has been chosen to be zero.

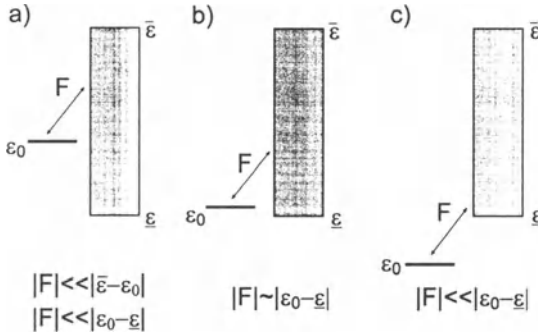


Figure 9.3: Different situations in the interaction of a discrete level with the continuous spectrum: a) complete decay; b) partial decay; c) absence of decay, applicability of the perturbation theory.

the continuum spectrum  $\lambda \sim \underline{\varepsilon}$  and  $\bar{\lambda} \sim \bar{\varepsilon}$ . Then according to Eq. (9.49) the following estimates hold:  $\langle \bar{\lambda} | \bar{\lambda} \rangle = D'(\bar{\lambda}) \gg 1$ ,  $\langle \lambda | \lambda \rangle = D'(\lambda) \gg 1$ , and, consequently, the first two terms in Eq. (9.59) are small and can be neglected. Due to the same reason the integrals along the contours  $C_l$  and  $C_r$  in Eq. (9.59) can be neglected as well (the contours start at points  $\underline{\varepsilon}$  and  $\bar{\varepsilon}$ , where  $D(\varepsilon) = \infty$ ).

Thus there are left only the residues in the zeros of the function  $D(\lambda)$  on the unphysical sheet in the lower semi-plane (points  $\gamma_k$  in Eq. (9.59)). The main contribution comes from  $\gamma_0$  with the smallest imaginary part  $\text{Im } \gamma_0$ . The root  $\gamma_0$  is determined from the equation:

$$D(\gamma_0) = 0, \quad D^-(\gamma_0) + 2\pi i G(\gamma_0) = 0. \quad (9.66)$$

Here the formula (9.58) for the analytic continuation to the unphysical sheet has been used. Substituting Eq. (9.56) into Eq. (9.66) and assuming  $|\text{Im } \gamma_0| \ll \bar{\varepsilon} - \underline{\varepsilon}$  (this assumption will be confirmed by the final result) we transform Eq. (9.66) to the following form:

$$\begin{aligned} \lambda_0 &= P \int_{\underline{\varepsilon}}^{\bar{\varepsilon}} \frac{G(z)}{\lambda_0 - z} dz = P \int_{\underline{\varepsilon}}^{\bar{\varepsilon}} \frac{|F(x)|^2 dx}{\lambda_0 - \varepsilon(x)} \approx P \int_{\underline{\varepsilon}}^{\bar{\varepsilon}} \frac{|F(x)|^2 dx}{0 - \varepsilon(x)}, \\ 0 &= -i \frac{\Gamma}{2} - \pi i G(\lambda_0) + 2\pi i G(\lambda_0), \text{ so that} \\ \Gamma &= 2\pi G(\lambda_0) = 2\pi |F(\lambda_0)|^2 \frac{dx}{d\varepsilon}(\lambda_0), \end{aligned} \quad (9.67)$$

where the root is given by  $\gamma_0 = \lambda_0 - i \frac{\Gamma}{2}$ . In the derivation the relation

$G(\lambda_0 - i\frac{\Gamma}{2}) \simeq G(\lambda_0)$  has been used, which follows from the conditions

$$G'(\lambda_0) \sim \frac{F^2}{\varepsilon^2} \ll 1, \quad \Gamma \sim G(\lambda_0) \sim \frac{F^2}{\varepsilon}, \quad G'(\lambda_0)\Gamma \sim \frac{F^4}{\varepsilon^3} \ll \frac{F^2}{\varepsilon} \sim G(\lambda_0).$$

The first equation in (9.67) determines the shift  $\lambda_0$  of the initial discrete level  $\varepsilon_0$ , while the second specifies the damping constant  $\Gamma$  in full accordance with the golden rule from the perturbation theory. For a weak interaction the shift of the level  $\lambda_0$  and its width  $\Gamma$  are much smaller, then the typical energy in the unperturbed Hamiltonian  $\varepsilon = \bar{\varepsilon} - \underline{\varepsilon}$ :

$$\begin{aligned} \lambda_0 &= P \int_{\underline{x}}^{\bar{x}} \frac{|F(x)|^2 dx}{\lambda_0 - \varepsilon(x)} \sim P \int_{\underline{x}}^{\bar{x}} \frac{|F(x)|^2}{\varepsilon(x)} dx \sim \frac{F^2}{\varepsilon} \ll \varepsilon, \\ \Gamma &\sim \frac{F^2}{\varepsilon} \ll \varepsilon. \end{aligned} \quad (9.68)$$

The residue at point  $\gamma_0$  is determined by the derivative  $D'(\gamma_0)$ , the magnitude of which can be estimated as:

$$\begin{aligned} D'(\gamma_0) &= D^-(\gamma_0)' + 2\pi i G'(\gamma_0) \approx D^-(\gamma_0)' \\ &\approx \frac{d}{d\lambda} \left[ \lambda - P \int_{\underline{x}}^{\bar{x}} \frac{|F(x)|^2 dx}{\lambda - \varepsilon(x)} \right] \sim 1, \quad \text{if } \lambda = \lambda_0. \end{aligned} \quad (9.69)$$

Thus the magnitude of the residue is  $A(t) \simeq \exp(-i\gamma_0 t)$ , and consequently the contributions of other terms in Eq. (9.59) are of the order of  $F^2/\varepsilon^2 \ll 1$ . Thus the main contribution to the probability amplitude  $A(t)$  comes from the last term in Eq. (9.59). The residue should be calculated at point  $\gamma_0$ , which is closest to the real axis:

$$A(t) = \exp \left[ -i\lambda_0 t - \frac{\Gamma}{2}t \right] \left\{ 1 + O\left(\frac{F^2}{\varepsilon^2}\right) \right\}. \quad (9.70)$$

The shift of the energy  $\lambda_0$  and the width of the level  $\Gamma$  are determined by the formulas (9.67), which coincide exactly with the results of perturbation theory for the correction terms to the energy  $\Delta\varepsilon_0$  and the decay rate  $\Gamma$  (relaxation decrement).

The case c) is a simple one (see Fig. 9.3). Here the perturbation theory is valid, which shifts slightly the energy level  $\varepsilon_0$  ( $\Delta\varepsilon_0 \sim \frac{F^2}{\varepsilon}$ ) and admixes somehow the states of the continuum spectrum  $\int \nu(x) |x\rangle dx$  to the unperturbed state  $|0\rangle$ , where  $\int \nu^2(x) dx \sim \frac{F^2}{\varepsilon^2} \ll 1$ .

Case b), when the discrete level  $\varepsilon_0 = 0$  is in resonance with the edge of the continuum spectrum  $\underline{\varepsilon} \sim \varepsilon_0$  is more complicated. To simplify the

analysis and to demonstrate transparently the transition from case *a*) to *c*) we consider the following example:

$$F(x) = F, \quad \varepsilon(x) = \underline{\varepsilon} + \varepsilon x, \quad \bar{\varepsilon} = \varepsilon(1) = \underline{\varepsilon} + \varepsilon, \quad 0 \leq x \leq 1.$$

Then from Eq. (9.47) we find the following expression for the shift of the energy level  $\underline{\lambda}$  from the edge of the continuous spectrum  $\underline{\varepsilon}$ :

$$\underline{\varepsilon} - \underline{\lambda} = \begin{cases} \varepsilon \exp [-(\varepsilon_0 - \underline{\varepsilon}) \varepsilon F^{-2}], & \text{case (a),} \\ 2|F|^2 \varepsilon^{-1} \ln |\varepsilon F^{-1}|, & \text{case (b),} \\ |F|^2 \varepsilon^{-1} \ln [(\bar{\varepsilon} - \varepsilon_0)(\underline{\varepsilon} - \varepsilon_0)^{-1}], & \text{case (c).} \end{cases} \quad (9.71)$$

We note that in all the previous cases (a) – (c) the following inequality holds:  $|F| \ll \varepsilon$ . Then, according to Eq. (9.71), one of the two relations is satisfied:  $\underline{\lambda} \sim \underline{\varepsilon}$  or  $\underline{\lambda} \sim \varepsilon_0$ . The factor, preceding the exponent  $\exp(-i\underline{\lambda}t)$  in Eq. (9.59) can be found with the help of Eq. (9.49) in the following form:

$$D'(\underline{\lambda}) = \langle \underline{\lambda} | \underline{\lambda} \rangle = 1 + \begin{cases} F^2 \varepsilon^{-2} \exp [(\varepsilon_0 - \underline{\varepsilon}) \varepsilon F^{-2}], & \text{case (a),} \\ 2 \ln^{-1} |\varepsilon F^{-1}|, & \text{case (b),} \\ |F|^2 (\underline{\varepsilon} - \varepsilon_0)^{-1} (\bar{\varepsilon} - \varepsilon_0)^{-1}, & \text{case (c).} \end{cases} \quad (9.72)$$

According to Eq. (9.55) the quantity  $|\langle \underline{\lambda} | \underline{\lambda} \rangle|^{-2}$  determines the contribution of the discrete state  $|\underline{\lambda}\rangle$  to the wavevector  $|\Psi(t)\rangle$ . Correspondingly, it characterizes the component of the initial state, which does not decay despite of the interaction with the continuum spectrum. From Eq. (9.72) with the account of Eq. (9.55) it follows, that passing from case (a) to cases (b) and (c) we go over from complete decay to the the situation, when the admixture of continuum states is small  $F^2 \varepsilon^{-2} \ll 1$ , so that there is practically no decay. All the consideration above is valid for the case of small interaction  $|F\varepsilon^{-1}| \ll 1$ .

Obviously, the transition from case (a) to (c) occurs in a continuous fashion. It follows from Eqs. (9.71) and (9.72) with the change of the parameter  $\varepsilon_0 - \underline{\varepsilon}$  from the values  $\varepsilon_0 - \underline{\varepsilon} \gg |F|$  through  $|\varepsilon_0 - \underline{\varepsilon}| \sim |F|$  and down to the values  $\underline{\varepsilon} - \varepsilon_0 \gg |F|$ . The eigenvalue  $\underline{\lambda}$  changes simultaneously from  $\underline{\lambda} \sim \underline{\varepsilon}$  to  $\underline{\lambda} \sim \varepsilon_0$ . The same consideration holds true for the eigenvalue  $\bar{\lambda}$  as well, when  $\varepsilon_0$  shifts into the region  $\varepsilon_0 \gg \bar{\varepsilon}$ .

In the graphical form the solution of equation (9.47) for the root  $\underline{\lambda}$  in all the cases (a), (b), (c) is presented in Fig. 9.4. The corresponding dependence  $\underline{\lambda}(\varepsilon)$  with  $\varepsilon$  fixed and  $\varepsilon_0 = 0$  is shown in Fig. 9.5.

Thus, there is a smooth transition from the situation of total decay to the pure bound stationary state  $|\underline{\lambda}\rangle$ , when the region of continuum spectrum  $(\underline{\varepsilon}, \bar{\varepsilon})$  shifts to the right in passing from case (a) to case (c), Fig. 9.6. The

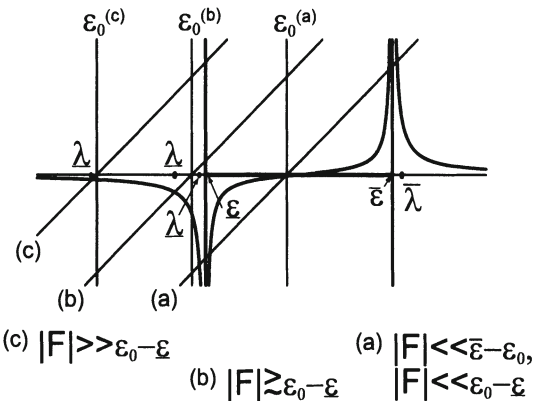


Figure 9.4: The graphical determination of the root  $\lambda$  of Eq. (9.47): a) total decay; b) partial decay; c) absence of decay, small correction to the energy of the unperturbed root  $\varepsilon_0$ .

same takes place during the transition to the left with the only difference that the decay state  $|0\rangle$  transforms into the stationary state  $|\bar{\lambda}\rangle$ .

To find the time dependence of the decay in case (b), when some part of the initial state  $|0\rangle$  suffers decay ( $A(t) < 1$  for  $t \rightarrow \infty$ ) one has to calculate the integrals along contours  $C_l$  and  $C_r$  and the residue in the zeros of  $D(\lambda)$  on the unphysical sheet. These calculations depend upon the particular form of the functions  $F(x)$  and  $\varepsilon(x)$ , which determine  $D(\lambda)$  according to the formulas (9.56) and (9.58).

The consideration above makes it possible to examine whether some particular states in a polyatomic molecule exist or not. Let us assume, that within some approximation some particular vibrational-rotational state with

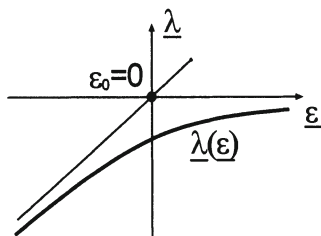


Figure 9.5: The dependence of the position of the lowest level  $\lambda$  upon the lower edge of the continuum spectrum  $\lambda(\varepsilon)$ .

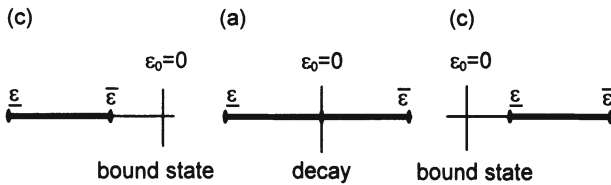


Figure 9.6: The nature of the interaction of the discrete level  $\varepsilon_0$  with the continuum spectrum as function of their relative position.

energy  $\varepsilon_0$  exists. Let then some additional weak interaction be switched on. The question arises whether the initial state will survive the introduction of the small additional interaction or not? If the state decays, how fast the process will be? If the decay (stochasticization) is fast enough, there is no reason to speak of the existence of the level in question.

The model consideration above provides answers to such questions at least in principle. To obtain qualitative answers it is sufficient to find the energy of the state  $\varepsilon_0$ , the region of continuum spectrum  $(\varepsilon, \bar{\varepsilon})$  with which the considered state is interacting, the strength of the interaction (like oscillator strengths), and to use it in the obtained formulas to estimate the widening of the level and the portion of the initial state that has decayed  $\lim [1 - A(t)]^2$  along with the shift of the level  $\Delta\varepsilon_0 \simeq \int |F(x)|^2 \varepsilon^{-1}(x) dx$ .

The theory of intramolecular relaxation and its relation to the radiation widening of levels is considered in detail in the review of T.Uzera [148]. Besides, there is an Appendix, written by W.H.Miller, where the relation between the width of radiation widening, intramolecular redistribution of vibrational energy, and the molecular decay rate is analyzed. Extensive bibliography on the matter can be found there as well. The methods of analysis of intramolecular vibrational energy relaxation, considered in this review will be analyzed in the next Chapter. The model of a discrete level decay, studied above in the present chapter provides the mathematical basis for such a study.

# Chapter 10

## IR spectra and intramolecular relaxation

In this Chapter we consider the effect of multi-mode intra-molecular resonances on the process of energy redistribution among the vibration modes. Studies of these resonances' effect upon the lineshape in IR absorption spectra are presented on a quantitative level. The properties of IR spectra due to the anharmonicity of vibrations are investigated.

For the proper understanding of this Chapter the knowledge of quantum mechanics within the University course or, for example, Ref. [81] is required, along with the technique of Green's functions in the amount, necessary for manipulations with formulas of Kubo type.

### 10.1 Redistribution of intramolecular energy: influence of multimode resonance

We will study the processes of energy relaxation of a high-frequency mode ( $\omega \sim 3000 \text{ cm}^{-1}$ ) in a polyatomic molecule. A good approximation is provided by a model, consisting of a relatively small number of high-frequency anharmonic oscillators interacting with a much larger number of other oscillators, which can be assumed harmonic. The Hamiltonian of the system has the form:

$$H = H_0 + H_B + W, \quad (10.1)$$

where  $H_0$  is the Hamiltonian of high-frequency modes,  $H_B$  is the Hamiltonian of harmonic oscillators, called usually "thermal bath", and  $W$  is the interaction of high-frequency modes with the bath. Obviously, the vibrational temperature of the molecule  $T_{vib}$  is determined by the total energy  $E_{vib} = \bar{E}$  of the set of harmonic oscillators. In thermal equilibrium the population of excited high-frequency modes is distributed according to Gibbs

law:  $\rho \sim \exp(-H_0/T_{vib})$ . As usually the inequality  $T_{vib} \ll \omega_0$  holds the high-frequency modes practically are not excited. However, if we excite them, for example with the help of a laser, the inequilibrium population is produced, and relaxation of high-frequency mode energy into the thermal bath starts. Due to the low magnitude of  $T_{vib}$  as compared to  $\omega_0$ , practically all the excitation energy goes over to the low-frequency oscillators. What is the rate of such transition (decay rate), the question arises.

In the calculations of decay rate  $\Gamma$  typically the inequality  $\Gamma \ll \Gamma_b$  is assumed, where  $\Gamma_b$  is the relaxation rate for correlations (fluctuations) in the thermal bath. In such a case the only good quantum number (constant of motion) for the bath is solely the energy  $E_b$ . The microscopic state of the bath will be characterized by energy  $E_b$  and by the number of states  $N(E_b)$  in the energy layer  $E_b - \frac{\Gamma_b}{2} < E < E_b + \frac{\Gamma_b}{2}$ <sup>1</sup>. The vibrational states of the entire molecule can be described by pairs of numbers  $(K, k), (J, j)$ , etc., where  $K, J$  are quantum numbers, which enumerate the eigenstates of the Hamiltonian  $H_0$ , while  $k$  refer to eigenstates of Hamiltonian  $H_B$  in the energy layer  $(E - E_0(K) - \frac{\Gamma_b}{2}, E - E_0(K) + \frac{\Gamma_b}{2})$ , and analogously for  $j$ . The indices  $k, j$  take values 1 through  $N(K)$  and 1 through  $N(J)$  respectively. Any vibrational state of the molecule will be characterized by the following quantities: total energy  $E$ , quantum numbers of the high-frequency mode  $K$  with energy  $E_0(K)$ , energy of the thermal bath  $E_b = E - E_0(K)$ , and the number of states for the bath  $N(K)$ . Our goal is to provide a description for the relaxation process of such macroscopic states, which is in fact observed in experiments.

Let  $b_{kK}(t)$  be the probability amplitude to find the molecule in a state with quantum numbers  $K$  and  $k$ ,  $1 \leq k \leq N(K)$  at time  $t$ . The amplitudes  $b_{kK}(t)$  and  $b_{jJ}(t)$  are related through the equations:

$$\begin{aligned} b_{kK}(t) &= \sum_{j,J} \langle k, K | e^{-iH(t-t_0)} | j, J \rangle b_{jJ}(t_0) \\ &= \sum_{j,J} U_{kK,jJ} b_{jJ}(t_0). \end{aligned} \quad (10.2)$$

The probability of a microscopic state  $K$  at time  $t$  is defined by the equation:

$$P_K(t) = \sum_{k=1}^{N_K} |b_{kK}(t)|^2. \quad (10.3)$$

Substituting Eq. (10.2) into Eq. (10.3) we obtain:

---

<sup>1</sup>Obviously,  $\Gamma_b \ll E_b$ , so that such a description of microscopic states is reasonable.

$$\begin{aligned}
P_K(t) &= \sum_{k=1}^{N_K} \left| \sum_{j,J} U_{kK,jJ}(t-t_0) b_{jJ}(t_0) \right|^2 \\
&= \sum_{k=1}^{N_K} \sum_{j=1}^{N_j} |U_{kK,jJ}(t-t_0)|^2 |b_{jJ}(t_0)|^2 \\
&\quad + \sum_{k=1}^{N_K} \sum_J \sum_{j'=1}^{N_j} \sum_{j=1}^{N_{j'}} \sum_{j'=1}^{N_{j'}} U_{kK,jJ}(t-t_0) U_{kK,j'j'}(t-t_0)^* \\
&\quad \times b_{jJ}(t_0) b_{j'j'}(t_0)^*. \tag{10.4}
\end{aligned}$$

The second term in Eq. (10.4) vanishes, as the dephasing process in it occurs during the time  $\tau_b \sim \Gamma_b^{-1}$ , whereas  $(t-t_0) \gg \Gamma_b^{-1}$ , and at the same time  $(t-t_0) \ll \hbar |E_b(j+1) - E_b(j)|^{-1}$  – thus the second term can be estimated as  $\exp[-(t-t_0)\tau_b^{-1}] \ll 1$ . Consequently, for  $P_K(t)$  we find:

$$P_K(t) = \sum_{k=1}^{N_K} \sum_{j=1}^{N_j} |U_{kK,jJ}(t-t_0)|^2 |b_{jJ}(t_0)|^2. \tag{10.5}$$

Equation (10.5) can be simplified, if one takes into account, that the sums

$$\sum_{k=1}^{N_K} |U_{kK,jJ}(t-t_0)|^2 \quad \text{and} \quad \sum_{j=1}^{N_j} |U_{kK,jJ}(t-t_0)|^2$$

do not depend upon  $j$  and  $k$  respectively. This statement follows from the fact, that the sum over  $j$ , for example, provides the probability of state  $k$  from the layer  $K$ , when the initial state is the macroscopic state  $J$  ( $P_{jJ} = 1$ ). But the macroscopic state  $J$  during the time  $(t-t_0) \gg \tau_b$  transforms into another macroscopic state only, which means, that  $P_{kK}$  does not depend upon  $k$ . The same is true for the sum over  $k$  due to the reversibility in time of the quantity

$$U_{kK,jJ}(t-t_0)^* = (U^{-1}(t-t_0))_{jJ,kK} = (U(t_0-t))_{jJ,kK},$$

which means, that any macroscopic state  $P_{kK} = P_{k'K}$  at time  $t$  is obtained from a macroscopic state  $P_{j'J} = P_{jJ}$  at time  $t_0$  with overwhelming probability. Thus, Eq. (10.5) can be transformed to the following form:

$$P_K(t) = \sum_J \left( \sum_{k=1}^{N_K} |U_{kK,jJ}(t-t_0)|^2 \right) \underbrace{\sum_{j=1}^{N_j} |b_{jJ}(t_0)|^2}_{P_J}$$

$$\begin{aligned}
&= \sum_J \left\{ \frac{1}{N_j} \sum_{j=1}^{N_j} \left( \sum_{k=1}^{N_K} |U_{kK,jJ}(t - t_0)|^2 \right) \right\} P_J, \\
P_K(t) &= \sum_J Y_{K,J}(t - t_0) P_J(t_0), \\
Y_{K,J}(t - t_0) &= \frac{1}{N_J} \sum_{j=1}^{N_J} \left( \sum_{k=1}^{N_K} |U_{kK,jJ}(t - t_0)|^2 \right). \quad (10.6)
\end{aligned}$$

Matrix  $Y_{K,J}(t - t_0)$  describes a Markovian process. Really,

$$\begin{aligned}
&\sum_L Y_{K,L}(t_1) Y_{L,J}(t_2) \\
&= \sum_L \left( \sum_{k=1}^{N_K} |U_{kK,lL}(t_1)|^2 \right) \frac{N_L}{N_J} \left( \sum_{j=1}^{N_J} |U_{lL,Jj}(t_2)|^2 \right) \\
&= \sum_{k=1}^{N_K} \sum_{j=1}^{N_J} \frac{1}{N_J} \sum_{l=1, L}^{N_L} |U_{kK,lL}(t_1)|^2 |U_{lL,Jj}(t_2)|^2 \\
&= \frac{1}{N_J} \sum_{k=1, j=1}^{N_K, N_J} \sum_{l=1, L}^{N_L} U_{kK,lL}(t_1) U_{lL,Jj}(t_2) (U_{kK,lL}(t_1) U_{lL,Jj}(t_2))^* \\
&= \frac{1}{N_J} \sum_{k=1, j=1}^{N_K, N_J} \sum_{l=1, L}^{N_L} U_{kK,lL}(t_1) U_{lL,Jj}(t_2) \left( \sum_{l'=1, L'}^{N_L} U_{kK,l'L'}(t_1) U_{l'L', Jj}(t_2) \right)^* \\
&= \frac{1}{N_J} \sum_{k=1, j=1}^{N_K, N_J} U_{kK,jJ}(t_1 + t_2) U_{kK,jJ}^*(t_1 + t_2) = Y_{K,J}(t_1 + t_2),
\end{aligned}$$

which means, that the Markovian condition is fulfilled. In the preceding derivation the following condition has been used:

$$\sum_{k=1}^{N_K} U_{kK,lL}(t) U_{kK,l'L'}^*(t) = 0, \quad \text{if } (l, L) \neq (l', L').$$

The latter follows from the absence of phase correlations (or dephasing) of the products of matrix elements  $U_{kK,lL}(t) U_{k'K', l'L'}^*(t)$ . The Markov process, describing the evolution of macroscopic states  $\sum_{k=1} a_{kK} |kK\rangle$  is homogeneous, as

$$Y(t_1 + t_2) = Y(t_1) \cdot Y(t_2), \quad Y(0) = I. \quad (10.7)$$

Consequently, the matrix  $Y(t)$  can be represented in the form:

$$Y(t) = e^{K \cdot t}. \quad (10.8)$$

Taking into account Eqs. (10.6) and (10.8) we find the following differential equation for the probabilities  $P_J(t)$ :

$$\dot{P}_J(t) = \sum_L K_{JL} \cdot P_L(t). \quad (10.9)$$

With the use of the unitary property of the matrix  $U_{kK,lL}$  we obtain from Eqs. (10.6) and (10.8) the following conditions for the transfer probabilities  $Y_{JL}$  and transfer rates  $K_{JL}$ :

$$\left\{ \begin{array}{l} \sum_J Y_{JL} = 1, \quad Y_{JL} \geq 0 \\ K_{JJ} \leq 0, \quad K_{JL} \geq 0, \end{array} \right\} \Rightarrow \sum_J K_{JL} = 0, \quad (10.10)$$

as it should have been in accordance with the physical meaning of the quantities  $Y_{JL}$  and  $K_{JL}$ .

From Eq. (10.10) the following limitations upon the eigenvalues of the rate matrix  $K$  follow:

$$\lambda_0 = 0, \quad \operatorname{Re} \lambda_n \leq 0, \quad \text{if } n \neq 0. \quad (10.11)$$

The existence of zero eigenvalue  $\lambda_0$  is a consequence of the fact, that the determinant of the matrix  $\|K_{JL}\|$  is zero. The fact, that  $\operatorname{Re} \lambda_n$  is not positive follows from the bounded values of the probabilities  $0 \leq P_J \leq 1$  which is a formal consequence of Eq. (10.4). The master equations (10.9) are a consequence of the fast enough dephasing process (decay of correlations) in the states  $\sum_{j \in J} a_j \exp(\varepsilon_j t) |jJ\rangle$  from the energy layer  $E(J)$  of the macroscopic state of the thermal bath: the dephasing rate is determined by the energy width  $\varepsilon_J$  of the manifold of states from the energy layer  $E(J)$ . Really, the fast decay of correlations is equivalent to:

$$K_{JL} \leq \varepsilon_J. \quad (10.12)$$

The inequality (10.12) coincides with Eq. (9.68) from the preceding paragraph, where the model problem of a discrete level' decay has been considered. It has been shown, that Eq. (9.68) determines the range of validity for the calculation of level's decay with the help of the "golden rule". Thus the inequality (10.12) determines the range of validity for equation (10.9) as well, and guarantees simultaneously the applicability of the golden rule to the calculation of transition rate  $K_{JL}$ <sup>2</sup>:

---

<sup>2</sup>The matrix element  $W_{jJ,lL}$  is of the order of  $N^{-1/2}$ , as the eigenfunctions in the layer are represented by a superposition of purely oscillatory functions with coefficients of the

$$K_{JL} = \frac{2\pi}{\hbar} \cdot \frac{1}{N_J} \sum_j |W_{lL,jJ}|^2 \cdot \frac{1}{(\Delta\varepsilon_J)} \simeq \frac{2\pi}{\hbar} |W_{L,J}|^2 \varepsilon_J^{-1}. \quad (10.13)$$

Thus, relaxation can be studied by the calculation of transition rates  $K_{JL}$  according to Fermi's golden rule and by the subsequent verification of the condition (10.12). If the latter is satisfied, the process is Markovian, and the level populations  $P_J(t)$  are governed by the master equation (10.9) with the matrix  $K_{JL}$ , calculated according to the golden rule. In the opposite case a purely quantum mechanical consideration is required, which takes into account the interference between the probability amplitudes  $\langle jJ|\Phi(t)\rangle$  and  $\langle j'J|\Phi(t)\rangle$ . In the model of discrete level decay that corresponds to the case of no decay, when the condition (9.60) is satisfied, and the energy flows periodically from one mode into the other.

The form of the master equation together with the conditions (10.10) and (10.11) for the matrix  $K_{JL}$  enables one to derive some general conclusions on the time evolution of the population  $P_J(t)$ . In the absence of special reasons the matrix  $K_{JL}$  has all different eigenvalues, so that the general solution of equation (10.9) takes the form of superposition of exponents:

$$P_J(t) = P_J^{(0)} + \sum_n \left[ B_J^{(n)} e^{-i\Omega_n t} + \left( B_J^{(n)} \right)^* e^{i\Omega_n t} \right] \cdot e^{-\gamma_n t} C_n, \quad (10.14)$$

where  $P_J^{(0)}$  is a stationary distribution corresponding to  $\lambda_0 = 0$ , and  $B_J^{(n)} e^{-i\Omega_n t - \gamma_n t}$  is the solution of the equation, which corresponds to the eigenvalue  $\lambda_n = -\gamma_n - i\Omega_n$ . The function  $P_J(t)$  describes the decay of  $J$ -th macroscopic state population, or of the  $J$ -th level of a small subsystem of high-frequency modes in a big polyatomic molecule to its equilibrium value  $P_J^{(0)} \sim \exp(-E_J/T_b)$ . If radiation transitions from the  $J$ -th state are possible, and, besides  $\gamma_n \gg \gamma_{rad}$ , then  $P_J(t)$  characterizes the time dependence of the integral intensity of radiation. From Eq. (10.14) it can be seen, that the intensity can be oscillatory in time. These oscillations, called quantum beats, have been observed experimentally by many researchers, see, for example, [149]. A theoretical interpretation of quantum beats, the discussion of the possibility of their observation in experiments and of the necessary conditions have been provided in Ref. [150].

From Eqs. (10.9) – (10.14) an important conclusion can be derived: for  $T_b \rightarrow 0$  the absorption spectrum into the  $J$  – state is of Lorentz type. Really,

---

order of  $N_J^{-1/2} \ll 1$ , as  $N_J \gg 1$ . Thus, the sum in Eq. (10.13) has a finite value  $|W_{LJ}|^2$ . Its independence of  $l$  has been explained above. The quantity  $\varepsilon_J = N_J \Delta\varepsilon_J$  plays the role of the continuum spectrum' energy width  $\varepsilon = \bar{\varepsilon} - \varepsilon$  in the problem of discrete level' decay, see Fig. 3.3 and Eqs. (9.43). Equation Eq. (10.13) coincides exactly with Eq. (9.67) in the case, when the discrete level decays completely.

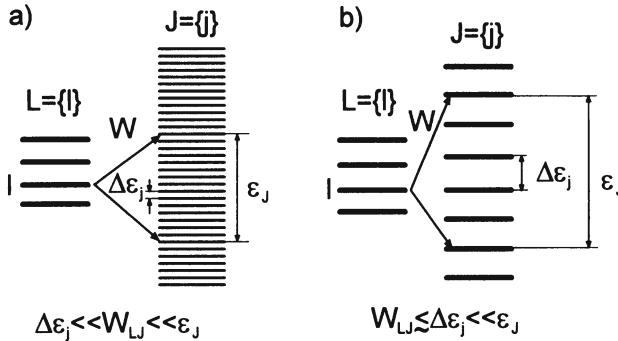


Figure 10.1: Different cases of the interaction of the high - frequency mode  $L$  with the thermal bath  $\{\varepsilon_j\}$ .

at  $T_b = 0$  the transitions from the  $J$ -th level of the local mode are possible to the levels  $(J-1), (J-2), \dots, 0$  only as there are no vibrational quanta in other modes. It means, that the transition rates  $K_{JL}$  are equal to zero for  $L < J$ . Thus, from Eq. (10.9) for the population of the  $J$ -th level of the local mode we find:  $P_J = -K_{JJ}P_J$ ,  $P_J = e^{-K_{JJ}t} = e^{-\gamma_J t}$ . Then for the probability amplitude of any  $|J\rangle$  - state from the  $J$ -th layer we obtain:

$$A_{JJ}(t) = \sqrt{P_J(t)} = e^{-\gamma_J t/2 - i\omega_J t}.$$

Consequently the absorption lineshape  $I(\omega) \sim \text{Im} \int_0^\infty \exp(i\omega t) A_{JJ}(t) dt$  in  $|J\rangle$  - state will be of Lorentz type:

$$I(\omega) = \frac{1}{\pi} \cdot \frac{\gamma_J/2}{(\omega - \omega_{JJ})^2 + (\gamma_J/2)^2}.$$

In the case of nonzero temperature  $T_b \neq 0$  the population  $P_J(t)$  is presented by a sum of decaying exponentials, and, correspondingly, the amplitude and the shape of the spectrum  $A_{JJ}(t) = \sqrt{P_J(t)} \sim \sqrt{\sum_n \exp(-\gamma_n t)} A_n$  will be complicated, though at low temperatures  $T_b \ll \bar{\omega}_b$  it will still be close to Lorentz shape.

The consideration above is illustrated with the help of Fig. 10.1. When the effective matrix element  $W_{J,L}$ , which connects the groups of levels like  $\{l\} = L$  and  $\{j\} = J$  exceeds greatly the distance between the levels  $\Delta\varepsilon_{jj+1} = \Delta\varepsilon_J$  and the others from the group, where the transition is performed  $L \rightarrow J$ , and at the same time it is much smaller, than the dephasing  $\varepsilon_J$  in the layer  $J$  (i.e.  $K_{JL} = |W_{JL}|^2 \varepsilon_J^{-1} \ll \varepsilon_J$ ), the population relaxation  $P_J$  is governed by master equations (10.9). The case  $|W_{JL}| \ll \Delta\varepsilon_J \ll \varepsilon_J$

corresponds to a small molecule, when the inter-mode interaction slightly shifts the vibration levels. Only the close levels experience significant shifts  $\Delta\epsilon_{jl} \lesssim W_{jJ;ll}$  (Fermi resonance).

If the matrix element  $W_{JL}$  is equal to zero or is sufficiently small, then one has to find in the layers  $J$  and  $L$  such states, which are connected via the perturbation of the second or third order in  $W$ :

$$\begin{aligned} R_{jJ,LL}^{(2)} &= \sum_{k,K} \langle jJ | W | kK \rangle \frac{1}{E_{jJ} - E_{kK}} \langle kK | W | lL \rangle, \\ R_{jJ,LL}^{(3)} &= \sum_{k,K} \sum_{q,Q} \langle jJ | W | kK \rangle \frac{1}{E_{jJ} - E_{kK}} \langle kK | W | qQ \rangle \\ &\quad \frac{1}{E_{jJ} - E_{qQ}} \langle qQ | W | lL \rangle, \end{aligned} \quad (10.15)$$

etc. In the general case one has to find all the possible paths of the transition, and to construct subsequently the matrix element  $R_{jJ,LL}$  according to the formula:

$$R_{jJ,LL} = \sum_m R_{jJ,LL}^{(m)},$$

along with the effective matrix element  $W_{JL}$ :

$$|W_{JL}|^2 = \sum_{j=1}^{N_J} |R_{jJ,LL}|^2, \quad W_{JL} = \sqrt{|W_{JL}|^2}. \quad (10.16)$$

The latter should be substituted into Eq. (10.13) for the calculation of transition rates according to the golden rule. However, the use of Eq. (10.13) is not quite convenient, as it comprises the decay rate of correlations  $\epsilon_J$ , which is hard to be determined, instead of the well-defined density of levels  $\Delta\epsilon_J$ . To avoid the inconvenience, let us determine  $w_{JL}$  according to the formula:

$$|w_{JL}|^2 = \frac{1}{N_J} \sum_{j=1}^{N_J} |R_{jJ,LL}|^2, \quad w_{JL} = \sqrt{|w_{JL}|^2}. \quad (10.17)$$

Then Eq. (10.13) reduces to the standard form:

$$K_{JL} = \frac{2\pi}{\hbar} |w_{JL}|^2 \frac{1}{\Delta\epsilon_J} = \frac{2\pi}{\hbar} |w_{JL}|^2 \rho(\epsilon_J), \quad (10.18)$$

where  $\rho(\epsilon_J)$  characterizes the density of levels at  $E = E_J$ . Comparing equations (10.18) and (10.13) one can note, that the latter comprises more transparent physical parameters. Really, the quantity  $\tau_J = \hbar\epsilon_J^{-1}$  is the time of decay of the fluctuation in mode  $J$ , which has been formed for

the acceptance of the corresponding energy from mode  $L$ . The portion of this energy is related to the admixture of wavefunction  $\Psi_J$ , mode  $J$  to the unperturbed wavefunction  $\Psi_L$ , mode  $L$ . The weight of this admixture according to perturbation theory can be estimated as <sup>3</sup>  $\sim \sum_j \left| \frac{W_{jL}}{\epsilon_j} \right|^2 = \left| \frac{W_{JL}}{\epsilon_J} \right|^2$ . It will disperse over the mode  $J$  during the time  $\hbar\epsilon_J^{-1}$ . Consequently, the transition rate will be  $\sim \frac{|W_{JL}|^2}{\hbar\epsilon_J}$ , which coincides with Eq. (10.13).

Equation (10.18) does not allow such a simple physical interpretation, as here the inequality always holds  $\left| \frac{w_{JL}}{\Delta\epsilon_J} \right| \gg 1$ . This formula is of quantum origin, and it does not incorporate the vaguely defined decay time of correlations  $\hbar\epsilon_J^{-1}$ . On the contrary, all the quantities entering it are well defined:  $|w_{JL}|^2 = N_J \sum_j |W_{jJ;JL}|^2$  is a self-averaging quantity, and  $\Delta\epsilon_J \sim \epsilon_{jJ} - \epsilon_{j'J}$  is the distance between adjacent levels, which is also self-averaging. Below we define  $w_{JL}$  through the quantities  $R_{jJ;JL}$  according to Eq. (10.17), and, correspondingly, we calculate the relaxation rates  $K_{JL}$  according to the golden rule in its traditional form (10.18).

Equation (10.15) and (10.16) reveal the role of resonances in the processes of vibrational relaxation of the excited high-frequency mode. Let us assume, that the interaction  $W$  leads to the exchange, excitation and absorption processes with only to vibrational quanta of two different modes involved. In other words, let  $W(q)$  have the shape:

$$W(q_1, q_2 \dots) = \sum_{i \neq j} \beta_{ij} q_i q_j, \quad (10.19)$$

where  $q_i$  are coordinates of vibrational modes, and  $\beta_{ij}$  are interaction strengths between the modes.

It can be seen from Eqs. (10.19) and (10.15), that the more vibrational quanta take part in the process of transformation of the initial state  $\Psi_{N_0 N_1 \dots N_\nu}$  into the resonant state  $\Psi_{N'_0 N'_1 \dots N'_\nu}$ <sup>4</sup>, the higher is the order of the matrix element  $R_{jJ;JL}$  in the interaction  $W$ , and, consequently, the higher is the order of  $R_{jJ;JL}$  in the small parameter  $\overline{\beta\omega}^{-1}$ . (Each successive order of the operator  $W$  in the small parameter  $\overline{\beta\omega}^{-1}$  introduces two vibrational quanta into the transformation of the interacting modes, and, consequently, into the redistribution of energy.)

On the other hand, the higher is the order of resonance  $m$ , the more dense is their distribution, as there are more possibilities for the approximate redistribution of energy in the vibrational system. This leads to the increase in the number of matrix elements of the type  $R_{jJ;JL}^{(m)}$ , which bind the more

<sup>3</sup>We would like to note, that Eq. (10.13) is correct under the condition  $|W_{JL}|^2 \epsilon_J^{-2} \ll 1$ , as it should be for the correction term to the probability.

<sup>4</sup>We note, that the total number of vibrational quanta, taking part in the transformation of molecular state, is called the order of resonance  $m$ , see Chapter 2, Section 1.

densely positioned levels in the modes  $L$  and  $J$ . In other words, the density of interacting levels in modes  $L$  and  $J$  increases with the growing order of resonance  $m$ .

Thus, with the increase of  $m$  the magnitude of the matrix element  $W_{jJ;IL}$  decreases, but the number of nonzero matrix elements grows sharply. There are two possibilities: 1) the decrease of matrix elements  $W_{jJ;IL}^{(m)}$  with increasing  $m$  and the growth of the density of levels  $\rho_m$  (connected with the initial level by resonances of order  $m$ ) satisfy the inequality:

$$|W_{jJ;IL}(m)| \ll \rho_m^{-1}, \quad \text{for any } m, \quad (10.20)$$

and 2) the decrease of  $W_{jJ;IL}^{(m)}$  and increase of  $\rho_m$  change the sign of the inequality (10.20) for some values of  $m$ .

In the first case the level remains a discrete one and suffers a shift only with no relaxation introduced. In the terms of classical mechanics the shift of resonance exceeds the perturbing interaction, so that the nature of the unperturbed motion is preserved. This situation is typical to small molecules with low vibrational excitation.

In the second case the initial level decays, and the vibrational energy of the high-frequency mode dissociates into the subsystem of other vibrational modes – the thermal bath. In classical terms this signifies the dramatic change of the region of phase space, which is filled up with the trajectory of the system.

A priori it is hard to forecast the contribution of some particular resonances into the decay of the initial state, as there is a competing influence of the decreasing matrix elements  $W_{jJ;IL}^{(m)}$  and the increasing density of levels  $\rho_m$ . In principle, both the monotonous decrease of the contribution to the decay rate (with increasing  $m$ ) due to  $m$ -th resonance or the existence of some optimal resonance value  $m^*$ , which provides the maximal contribution to the decay rate  $\gamma$  are possible.

Fig. 10.2 from Ref. [151] shows the dependence of the contribution  $\gamma_m$  upon the number  $m$  of the resonance to the decay rate  $\gamma$ , calculated for the molecule  $CF_3I$ . The potential of the interaction between the high-frequency mode  $Q$  and the thermal bath of harmonic oscillators has been chosen in the form:

$$W = Q \sum_{m=2}^{\infty} \frac{1}{m!} \sum_{\alpha_1 \dots \alpha_m}^s \lambda^{m+1} q_{\alpha_1} \dots q_{\alpha_m}. \quad (10.21)$$

The high-frequency mode has been assumed to be harmonic with a frequency  $\omega_1(T)$ , which is function of the temperature of the bath. The decay rate  $\gamma_1$  has been calculated according to the formulas, obtained by the authors of the cited work:

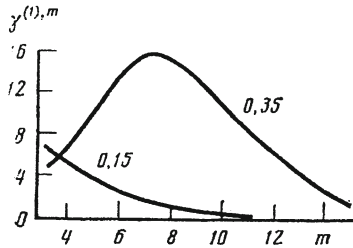


Figure 10.2: The dependence of the contribution of the  $m$ -th resonance to the decay rate  $\gamma_m$  as function of  $m$ : a) rigid molecule; b) soft molecule.

$$\gamma_1 = \pi \sum_{m=2}^r \lambda^{2(m+1)} \frac{\bar{n}^m}{2^{m+1}} \sum_{l=0}^m \left(1 + \frac{1}{\bar{n}}\right)^l \rho_m(\omega_1, l), \quad (10.22)$$

where  $\bar{n}$  is the population of the oscillators from the thermal bath, and  $\rho_m(\omega, l)$  is the density of resonant combinations:  $\omega_1 = \omega_{\alpha_1} + \omega_{\alpha_2} + \dots + \omega_{\alpha_l} - \omega_{\alpha_{l+1}} - \omega_{\alpha_{l+2}} - \dots - \omega_{\alpha_m}$ . For  $\rho_m(\omega, l)$  the following approximation has been used:

$$\rho_m(\omega, l) = \frac{(s-1)^m}{l!(m-l)!} \cdot \frac{\exp\left\{-\frac{[\bar{\omega}(2l-m)-\omega]^2}{2\sigma^2 m}\right\}}{\sqrt{2\pi m\sigma}}, \quad (10.23)$$

where  $s$  is the number of modes in the molecule,  $\bar{\omega}$  is some average frequency of the modes in the bath,  $\sigma$  is their dispersion. The results of the corresponding calculations with the use of these formulas with  $s = 9$  and  $\lambda \ll 1$  (rigid molecule) and  $\lambda \sim 1$  (soft molecule) are presented in Fig. 10.2. Obviously, in a rigid molecule the contribution of resonances decreases gradually with their number, while in a soft molecule there exists a maximal contribution from resonance  $m^*$ .

In small molecules only sufficiently high resonance can govern the decay, as at low values of  $m$  and small interaction the condition (10.20) holds always. Thus, the decay rate  $\gamma$  for small molecules is much smaller, then the inter-mode interaction  $\beta$ . Consequently, one should speak then of the not too highly excited vibrational states of the high-frequency local modes. If the mode is strongly anharmonic, then with the change of its excitation level the optimal type of resonance, providing the principal contribution to the decay rate, changes as well, as the frequency depends strongly upon the excitation number  $v$ . This leads to a strongly irregular dependence of the decay rate  $\gamma$  upon the number of the level  $v$ . The corresponding calculations for the  $CH$  mode vibrations in the crystal  $CH_4$  have been performed in [152],

$v$	1	2	3	4	5	6	7	8	9	10
$\gamma_v, \text{cm}^{-1}$	10	10	10	10	10	$10^{-6}$	$10^{-1}$	$10^{-1}$	$10^{-2}$	$10^{-2}$

Table 10.1: The widths  $\gamma$  of the vibrational levels for the valent  $CH$  bonds' vibrations in the molecule  $CH_4$  as functions of the excitation number  $v$ .

and strong irregularity of the dependence of level width upon the number  $\gamma(v)$  has been observed. Among all the levels with  $1 \leq v \leq 10$  the width of the level with  $v = 7$  was much smaller, then that of the rest, Table 10.2 <sup>5</sup>.

The preceding consideration of vibrational energy relaxation in polyatomic molecules revealed the fact, that the approximation of a Markovian process in the description of relaxation is in fact reduced to the model of decay of a discrete level, interacting with a continuum spectrum.

## 10.2 Relation between the absorption linewidths, intramolecular vibrations evolution, and unimolecular decay rates

In the preceding Section it has been mentioned already, that the widening of levels due to vibrational relaxation determines the level width and molecular absorption in the IR spectra, and the exponential decay of the vibrational excitation in time produces the Lorentz shape of the absorption line. On the other hand, the high-definition spectra should produce a comb of narrow radiation lines, whose envelope has Lorentz shape with the width of the corresponding vibrational level. Thus, if the definition is not too high ( $\sim 1 \text{ cm}^{-1}$ ), the Lorentz shape of the absorption line should be observed. Examples are provided by the radiation excitation of overtones of  $CH$  vibrations in polyatomic molecules, [153, 154, 155]. The width of the absorption line ( $\sim 10 \div 100 \text{ cm}^{-1}$ ) is typically interpreted as the decay rate in the process of vibrational relaxation of the local mode, initially excited by radiation (like, for example, the  $CH$  mode). If the resolution of the spectra would have been of the order of  $\sim 10^{-5} \div 10^{-6} \text{ cm}^{-1}$ , then in the cited experiments the absorption spectra would have had the form of a comb with a Lorentz envelope. The theoretical background for such an assertion lies in the strict discreteness of the molecular energy spectrum in the region of vibrational overtones, and the big enough distance (exceeding  $10^{-6} \text{ cm}^{-1}$ ) between the optically-active levels.

An entirely different situation occurs in the experiments of photodissociation, when the molecule is excited in the region of continuum spectrum, and the width of the excited quasistationary state  $|n\rangle$  satisfies  $\Gamma_n \gg \Gamma_r$  and is comparable to the vibrational relaxation decay rates  $\sim 10 \div 100 \text{ cm}^{-1}$ .

---

<sup>5</sup>  $\gamma_1$  is the delocalization velocity of a single-quantum excitation in the crystal.

The absorption spectra in the process of ethylene dimers dissociation have the widths of the order of  $\sim 10 \text{ cm}^{-1}$  (see [156, 157, 158]), so it is quite unclear to what it corresponds: either to the decay rate of the LM vibrational excitation, or to the dissociation rate of the dimer, or to something in between? The lines, observed in these experiments are of Lorentz type according to the most stringent standards, and, contrary to the excitation of overtones of the *CH* mode, preserve apparently the form of a single smooth Lorentz line even with the indefinite increase of the resolution.

The answer to the question on how the absorption spectrum in the cited experiments of photodissociation is obtained, and how its form is related to the parameters of the molecule, is provided below on the basis of a simple model system as an example. The consideration in this Section follows closely the analysis by W.H.Miller in the Appendix of Ref. [148].

The model employed is a standard one in the theory of radiationless transitions [159]: in zero order the state  $|a\rangle$  are bound to the states  $|n\rangle$  of the thermal bath. The state  $|a\rangle$  incorporates all the oscillator strengths from the ground state  $|g\rangle$ , that is the dipole matrix elements  $\langle g | d | n \rangle \equiv 0$ , while  $\langle g | d | a \rangle \neq 0$ . The state  $|n\rangle$  is characterized by complex energies  $E_n - i\frac{\Gamma_n}{2}$ , where  $\Gamma_n$  is the rate of the unimolecular decay or the width of the state  $|n\rangle$ . It is assumed that there is no dissociation of the molecule from the optically active state  $|a\rangle$ , that is the dissociation from  $|a\rangle$  proceeds through the state  $|n\rangle$ .

Such a molecular system is described by the following Hamiltonian [160]:

$$H = \begin{pmatrix} E_a & H_{a1} & \dots & H_{an} & \dots \\ H_{1a} & E_1 - i\Gamma_1/2 & 0 & 0 & 0 \\ \dots & 0 & \dots & 0 & 0 \\ H_{na} & 0 & 0 & E_n - i\Gamma_n/2 & 0 \\ \dots & 0 & 0 & 0 & \dots \end{pmatrix}, \quad (10.24)$$

where  $H_{an}$  is the binding matrix element between state  $|a\rangle$  and state  $|n\rangle$  of the thermal bath. The complex energies of this matrix define the energy and lifetime of the metastable states of the isolated molecule.

The spectrum of absorption from the ground state  $|g\rangle \rightarrow |a\rangle$  is determined by the formulas<sup>6</sup>:

$$I(E) = -\frac{1}{\pi} \operatorname{Im} \langle g | dGd | g \rangle, \quad (10.25)$$

$$G(E) = \lim_{\epsilon \rightarrow 0} \left( \frac{1}{E + i\epsilon - H} \right), \quad E = \hbar\omega + E_g. \quad (10.26)$$

---

<sup>6</sup>The formula below is valid for the dipole interaction of photons with the molecules:  $W_p = (b_p^+ + b_p) d$ , if one takes into account the relation  $I(E) \sim \sigma(E)$ , where  $\sigma(E)$  is the total cross-section for the absorption of a photon with energy  $E$ .

As  $\langle g | d | n \rangle = 0$ , from Eq. (10.25) we find:

$$I(E) = |\langle g | d | a \rangle|^2 \left( -\frac{1}{\pi} \right) \text{Im} \langle a | G(E) | a \rangle. \quad (10.27)$$

Of interest also is the probability of the survival of the initial state  $|a\rangle$ :

$$P_{a \rightarrow a}(t) = \left| \left\langle a \left| e^{-iHt/\hbar} \right| a \right\rangle \right|^2, \quad (10.28)$$

and the probability  $P(t)$  that the molecule survives:

$$P(t) = P_{a \rightarrow a}(t) + \sum_n P_{a \rightarrow n \rightarrow a}(t), \quad (10.29)$$

$$P_{a \rightarrow n \rightarrow a}(t) = \left| \left\langle n \left| e^{-iHt/\hbar} \right| a \right\rangle \right|^2. \quad (10.30)$$

The quantity  $P_{a \rightarrow a}(t)$  is the probability of the event, that during time  $t$  the system is still in its initially excited state  $|a\rangle$ , while  $P(t)$  is the probability that during time  $t$  the molecule does not dissociate. If  $\Gamma_n = 0$  then the matrix  $\exp(-iHt/\hbar)$  is unitary, and the total probability  $P(t)$  is preserved, that is  $P(t) \equiv 1$ . Such a situation typically occurs for radiationless transitions, when the molecule is excited below the dissociation threshold  $D$ . For example, it happens under radiational excitation of overtones for the  $CH$ -mode:  $P(t) = 1$ , but  $P_{a \rightarrow a}(t) < 1$ , as the redistribution of  $CH$ -mode energy over other modes takes place.

The matrix elements (10.28) – (10.30) can be obtained easily by Fourier transforming the Green's function:

$$e^{-iHt/\hbar} = -\frac{1}{2\pi i} \int_{-\infty}^{+\infty} dE e^{-iEt/\hbar} G(E), \quad (10.31)$$

so that:

$$\begin{aligned} P_{a \rightarrow a}(t) &= \left| -\frac{1}{2\pi i} \int_{-\infty}^{+\infty} dE e^{-iEt/\hbar} \langle a | G(E) | a \rangle \right|^2, \\ P_{a \rightarrow n \rightarrow a}(t) &= \left| -\frac{1}{2\pi i} \int_{-\infty}^{+\infty} dE e^{-iEt/\hbar} \langle n | G(E) | a \rangle \right|^2. \end{aligned} \quad (10.32)$$

The equations for the matrix elements of the Green's functions  $\langle \Phi | G(E) | \Phi \rangle$  of the model with Hamiltonian (10.24) can be solved exactly <sup>7</sup>:

---

<sup>7</sup> Obviously, the model considered is a discrete analogue of the model from Section 3, Chapter 9.

$$\begin{aligned}\langle a | G(E) | a \rangle &= \left( E - E_a - \sum_n \frac{|H_{na}|^2}{E - E_n + i\Gamma_n/2} \right)^{-1}, \\ \langle n | G(E) | a \rangle &= \frac{H_{na}}{E - E_n + i\Gamma_n/2} \langle a | G(E) | a \rangle.\end{aligned}\quad (10.33)$$

To proceed further one has to know the values of the energies  $E_a$ ,  $E_n$  and of the lifetime  $\Gamma_n$ , along with the matrix elements  $H_{an}$ . In principle, these quantities can be found from *ab initio* quantum-chemical calculations. Let us consider the simplified version of the model, first introduced by Bixon and Jortner [161], when

$$E_n = n\varepsilon, \quad n = 0, \pm 1, \pm 2, \dots; \quad \Gamma_n = \Gamma_D; \quad H_{na} = V. \quad (10.34)$$

Substituting Eq. (10.34) into Eq. (10.33), we obtain numerical sums, which can be calculated exactly. As a result, for the matrix elements of the Green's functions we find the following expressions:

$$\begin{aligned}\langle a | G(E) | a \rangle &= \left[ E - E_a - \frac{1}{2}\Gamma_1 \cot \left( \frac{\pi E}{\varepsilon} + i\pi \frac{\Gamma_D}{2\varepsilon} \right) \right]^{-1}, \\ \langle n | G(E) | a \rangle &= \left( \frac{\varepsilon \Gamma_1}{2\pi} \right)^{\frac{1}{2}} \frac{1}{E - n\varepsilon + i\Gamma_D/2} \langle a | G(E) | a \rangle,\end{aligned}\quad (10.35)$$

$$\Gamma_1 = \frac{2\pi V^2}{\varepsilon}. \quad (10.36)$$

Thus, the model is specified by the dissociation rate  $\Gamma_D$  and by the rates of vibrational relaxation  $\Gamma_1$ , according to the golden rule for the state  $|a\rangle$ . Below we assume  $\varepsilon = 1$  and  $E_a = 0$ <sup>8</sup>. With the help of Eq. (10.35) the expression (10.27) is reduced to the form:

$$\begin{aligned}I(E) &= \frac{\Gamma}{2\pi} |\langle a | d | g \rangle|^2 \left( (E - \Delta)^2 + (\Gamma/2)^2 \right)^{-1}, \\ \Gamma &= \Gamma_1 \frac{T(1+t^2)}{T^2+t^2}, \quad \Delta = \frac{\Gamma_1}{2} \cdot \frac{t(1-T^2)}{T^2+t^2},\end{aligned}\quad (10.37)$$

where  $t = \tan(\pi E)$ ,  $T = \tanh(\frac{1}{2}\pi\Gamma_D)$ . From Eq. (10.37) the important case  $\Gamma_D \gg 1$  can be derived easily. In that case we have  $\Delta = 0$  and  $\Gamma = \Gamma_1$ , so that the lineshape  $I(E)$  takes the simple Lorentz form, centered at the

---

<sup>8</sup>The choice  $E_a \neq 0$  introduces insignificant corrections to the shape of the line  $I(E)$ , basically shifting it as a whole.

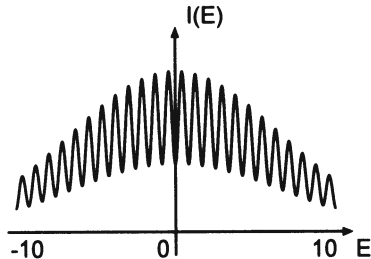


Figure 10.3: The absorption spectrum (arbitrary units) from Eq. (10.37) with  $\Gamma_D = 0.5$ ,  $\Gamma_1 = 10$ . The bath inter-level spacing is  $\varepsilon = 1$ .

energy of the optically active level  $E = 0$ , which has the width  $\Gamma_1$ , equal to the vibrational relaxation rate of the state  $|a\rangle$ . This result is in fact obvious: for  $\Gamma_D \gg \Gamma_1$  the dissociation rate from the state  $|a\rangle$  is limited by the relaxation rate of the excitation  $\Gamma_1$ , which determines the absorption linewidth in the state  $|a\rangle$ . This conclusion is backed up by the functional form of the dependencies  $P_{a \leftarrow a}(t)$  and  $P(t)$  for  $\Gamma_D \gg 1$ , derived from Eqs. (10.32) – (10.36):

$$P_{a \leftarrow a}(t) = e^{-\Gamma_1 t / \hbar}, \quad P(t) = \frac{\Gamma_1 e^{-\Gamma_D t / \hbar} - \Gamma_D e^{-\Gamma_1 t / \hbar}}{\Gamma_1 - \Gamma_D}. \quad (10.38)$$

Figures 10.3 - 10.5 show the absorption lineshape  $I(E)$ , calculated according to Eq. (10.37) for three cases:  $\Gamma_D = 0.5 < 1$ ,  $\Gamma_D = 1$ , and  $\Gamma_D = 2 > 1$  with  $\Gamma_1 = 10$ . We note here, that the increase of  $\Gamma_D$  from 2 to  $\Gamma_D \gg 2$  changes the spectrum in Fig. 10.5 insignificantly.

Figure 10.3 reveals clearly the fact, that if the dissociation rate is smaller, than the distance between the vibrational levels of the bath,  $\Gamma_D \ll 1$ , into

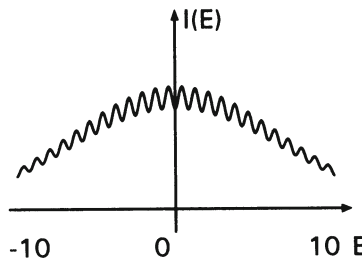


Figure 10.4: The absorption spectrum (arbitrary units) from Eq. (10.37) with  $\Gamma_D = 1$ ,  $\Gamma_1 = 10$ . The bath inter-level spacing is  $\varepsilon = 1$ .

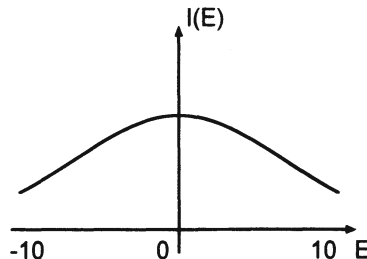


Figure 10.5: The absorption spectrum (arbitrary units) from Eq. (10.37) with  $\Gamma_D = 2$ ,  $\Gamma_1 = 10$ . The bath inter-level spacing is  $\epsilon = 1$ .

which the optically excited vibration transfers its energy, then the absorption spectrum reveals clearly its fine structure. The width of narrow peaks  $\sim \Gamma_D$ , or, in other words, the information on the dissociation rate, is contained in the fine structure of the spectrum. The envelope of these peaks has the width  $\Gamma_1$  — it is determined by the relaxation rate of the excited state.

For  $\Gamma_D = 1$  the fine structure in the spectra  $I(E)$ , Fig. 10.4, is detectable, though not quite well seen. The determination of  $\Gamma_D$  from the shape of the function  $I(E)$  in that case is not accurate.

In the case  $\Gamma_D = 2 > 1$  the fine structure in the spectrum  $I(E)$ , Fig. 10.5, is lost and the latter provides no information on the dissociation rate  $\Gamma_D$ . The function  $I(E)$  in that case has the width  $\Gamma_1$ .

The equations (10.36) – (10.38) and the corresponding figures 10.3 – 10.5 lead us to the following conclusions:

1) If  $\Gamma_D$  is smaller than the distance between the levels in the molecule, than the width of individual lines in the absorption spectrum (narrow peaks) characterizes the rate of unimolecular decay  $\Gamma_D/\hbar$ ;

2) If  $\Gamma_D$  exceeded the distance between the levels there is no way to determine the dissociation rate from the analysis of absorption spectra;

3) In all the cases, both for  $\Gamma_D < 1$  and  $\Gamma_D > 1$ , figures 10.3 – 10.5, the width of the band (with a resolved fine structure, or not) can be interpreted as the vibrational relaxation rate  $\Gamma_1$ , which is the decay rate for the initially excited optically active state  $|a\rangle$ .

Thus, a question arises on what information can be derived from the observed Lorentz-like absorption lineshape, which is realized in the experiments on photodissociation of ethylene dimers [156, 157, 158]? The widening of the lines in these experiments obviously greatly exceeds the inter-level distance, which can be estimated in the statistical approximation. The observed linewidth can be securely identified with the vibrational relaxation rate  $\Gamma_1$ , which characterizes the decay rate of the initially excited level  $E_a$ . The only information on the dissociation rate  $\Gamma_D$ , which can be derived, is

contained in the inequality  $\varepsilon < \Gamma_D < \Gamma_1$  ( $\varepsilon$  is the inter-level distance). In this case the dissociation rate  $\Gamma_D$  can not be derived from the absorption spectra even at an indefinitely high resolution<sup>9</sup>.

### 10.3 Effect of anharmonicity on IR spectra of polyatomic molecules

In this section we will demonstrate the relation between the form of the anharmonic potential and the shape of the IR absorption spectrum on the basis of a quasi-harmonic model [162]. In this model the molecule is represented by two subsystems: one is the high-frequency harmonic oscillator with frequency  $\omega(E)$  – function of the total energy of the molecule, and the second is the large subsystem of harmonic oscillators (the thermal bath), which interacts with the high-frequency oscillator. This interaction  $V_A$  we choose to be anharmonic. Our goal is to find out, how the form of this interaction is related to the absorption lineshape. That would enable one to extract information on the type of interaction from the analysis of IR absorption spectra.

The vibration Hamiltonian we choose in the form:

$$\begin{aligned} H &= \omega_p(E) a^+ a + \sum_{q=1}^s \Omega_q b_q^+ b_q + V_A, \\ V_A &= \sum_k (a^+ a)^k B_k(q_1, \dots, q_s). \end{aligned} \quad (10.39)$$

Here  $\omega_p(E)$  is the frequency of the high-frequency mode, which is function of the energy  $E$  of the molecule, and  $T$  is the vibrational temperature of the molecule. The interaction  $V_A$  is assumed to be small, so that in the main approximation its effect is reduced to the introduction of energy correction terms  $\delta E_{n\nu} = \langle n\nu | V_A | n\nu \rangle$ , where  $\nu$  is the set of vibrational excitations  $\nu_1 \dots \nu_s$  of the oscillators from the thermal bath, and  $n$  is the excitation number of the high-frequency oscillator of the considered mode. The eigenfunctions of the operator (10.39) in the consideration below are taken in zero approximation, that is in the form of harmonic functions.

As it has been noted already, the absorption spectrum lineshape is proportional to the difference of the cross-sections for photon absorption and stimulated emission. In the case of dipole interaction of the considered mode with the electromagnetic field this leads to the well-known formula:

---

<sup>9</sup>In principle, other mechanisms of excitation, different from the dipole one, can exist, which would allow the determination of dissociation rate  $\Gamma_D$  in this case. This is possible for the excitation of eigenstates of the molecular Hamiltonian.

$$I(\omega) = \frac{1}{\pi} \operatorname{Re} \int_0^\infty dt e^{i\omega t} \langle [d(t), d(0)] \rangle, \quad (10.40)$$

where  $d(t)$  is the Heisenberg operator of the dipole momentum in the linear approximation, and the brackets  $\langle \rangle$  denote the statistical averaging with the equilibrium density matrix  $\bar{f} = Sp\{f\rho_T\}$ , where  $T$  is the temperature<sup>10</sup>. For a non-interacting harmonic oscillator from Eq. (10.40) we obtain the resonance line of infinite intensity:

$$\begin{aligned} I_H(\omega) &= \frac{1}{\pi} \operatorname{Re} \left\{ \int_0^\infty dt e^{i\omega t} \langle [[a, a^+], e^{-i\omega_0 t}, [a^+, a]] | e^{i\omega_0 t} \rangle \right\} \\ &= \frac{1}{\pi} \operatorname{Re} \int_0^\infty dt \left( e^{i(\omega-\omega_0)t-\delta t} + e^{i(\omega+\omega_0)t-\delta t} \right) \\ &= \frac{1}{\pi} \lim_{\delta \rightarrow 0} \left( \frac{1}{\delta - i(\omega - \omega_0)} + \frac{1}{\delta - i(\omega + \omega_0)} \right) \\ &= \delta(\omega - \omega_0) + \delta(\omega + \omega_0), \Rightarrow I_H(\omega) = \delta(\omega - \omega_0). \end{aligned}$$

In the general case the interaction widens the resonance peak, and the absorption spectrum can take a very complicated form (see below). For the quasi-harmonic model the equations (10.40) lead to the expression:

$$\begin{aligned} I(\omega) &= \frac{1}{\pi} \sum_{n,\nu} 1 \operatorname{Re} \int_0^\infty dt e^{i\omega t} \sum_{n,\nu} \langle n, \nu | [e^{iHt} d(0) e^{-iHt}, d(0)] | n, \nu \rangle \\ &= \frac{\operatorname{Re} \int_0^\infty dt e^{i\omega t} \sum_{n\nu; m\mu} |\langle n, \nu | d(0) | m, \mu \rangle|^2 \{ e^{i(E_{n\nu} - E_{m\mu})t} - e^{-i(E_{n\nu} - E_{m\mu})t} \}}{\pi \left( \sum_{n,\nu} 1 \right)} \\ &= \frac{1}{\pi} \sum_{n', \nu'} 1 \operatorname{Re} \int_0^\infty e^{i\omega t} dt \sum_{n,\nu} \left\{ |\langle n | d(0) | n+1 \rangle|^2 e^{i(E_{n\nu} - E_{n+1,\nu})t} \right. \\ &\quad \left. - |\langle n-1 | d(0) | n \rangle|^2 e^{i(E_{n-1,\nu} - E_{n,\nu})t} \right\}, \quad (10.41) \\ \text{or } I(\omega) &= \frac{\operatorname{Re} \int_0^\infty e^{i\omega t} dt}{\pi \sum_{n', \nu'} 1} \sum_n \left( \sum_{\lambda, n=const} 1 \right) \sum_{\nu, n=const} \end{aligned}$$

<sup>10</sup>For an isolated molecule the micro-canonical distribution for the vibrational subsystem is adopted. Then the  $\omega(E)$ -mode obeys the Gibbs distribution  $\sim \exp\left(-\frac{n\omega(E)}{T}\right)$ .

$$\begin{aligned}
& \times \frac{|\langle n | d(0) | n+1 \rangle|^2 e^{i(E_{n\nu} - E_{n+1,\nu})t} - |\langle n-1 | d(0) | n \rangle|^2 e^{i(E_{n-1,\nu} - E_{n\nu})t}}{\sum_{\lambda, n=const} 1} \\
& = \frac{1}{\pi} Re \int_0^\infty e^{i\omega t} dt \cdot \rho_{nn}(T) \left( |d_{n,n+1}|^2 \frac{\rho_{n+1,n}(t)}{\rho_{n+1,n}(0)} - |d_{n-1,n}|^2 \frac{\rho_{n,n-1}(t)}{\rho_{n,n-1}(0)} \right) \\
& = \frac{1}{\pi} Re \int_0^\infty e^{i\omega t} dt \cdot \sum_{n=0}^\infty |d_{n,n+1}|^2 \frac{\rho_{n+1,n}(t)}{\rho_{n+1,n}(0)} \cdot [\rho_{nn}(T) - \rho_{n+1,n+1}(T)].
\end{aligned}$$

Here  $\rho_{mn}(t)$  are the elements of the time-dependent density matrix,  $\rho_{nn}(T) = \sum_{n\nu=const} 1 / \sum_{n\nu} 1$  – is the diagonal element of the equilibrium density matrix  $\sim \exp\left(-\frac{n\omega_p(E)}{T}\right)$ , corresponding to the pumping mode. In the derivation of Eq. (10.41) it has been taken into account, that the matrix elements of the dipole moment are diagonal in the vibrational quantum numbers of the thermal bath, that is  $\langle m\mu | d | n\nu \rangle = d_{mn}\delta_{\mu\nu}$ .

One can verify easily, that  $I(\omega) = \delta(\omega - \omega_0)$ , if the density matrices  $\rho_{mn}(t)$  and  $\rho_{mn}(T)$  correspond to an isolated harmonic oscillator:

$$\begin{aligned}
\rho_{mn}(t) &= \rho_{mn}(0) \exp[-i(m-n)\omega t] \quad \text{and} \\
\rho_{mn}(T) &= [1 - \exp(-\omega/T)]^{-1} \exp(-m\omega/T).
\end{aligned}$$

In Eq. (10.41) we neglect the nonlinear dependence of the energy of the considered mode (due to interaction  $V_A$ ) upon the excitation number  $n$  ( $n$  is an exact quantum number), so that

$$\rho_{nn}(T) = [1 - \exp(-\omega_p/T)] \exp(-n\omega_p/T),$$

Besides, we take into account the fact, that in the linear approximation the matrix elements of the dipole moment  $d = a^+ + a$  are given by:

$$d_{n,n+1} = \sqrt{n+1}.$$

Then the formula (10.41) for the spectral dependence  $I(\omega)$  can be represented in the form:

$$\begin{aligned}
I(\omega) &= \pi^{-1} \left(1 - e^{-\omega_p/T}\right) \sum_{n=0}^\infty (n+1) e^{-\frac{n\omega_p}{T}} \\
&\times Re \int_0^\infty e^{i\omega t} dt \cdot \frac{\rho_{n+1,n}(t)}{\rho_{n+1,n}(0)}. \tag{10.42}
\end{aligned}$$

Thus, to obtain the spectral function  $I(\omega)$  one has to find the time dependence of the element  $\rho_{n+1,n}(t)$  of the density matrix. The equations

for the density matrix  $\rho$  with the account of relaxation can be written as [162]<sup>11</sup>:

$$\frac{\partial \rho}{\partial t} = -i [H_p, \rho] + I_R(\rho), \quad (10.43)$$

where  $H_p = \omega_p(E) a^\dagger a$ , while  $I_R(\rho)$  is the relaxation operator, linear in the density matrix. The explicit form of this operator in Markov approximation for the quasi-harmonic model can be found in Refs. [163, 164]:

$$\begin{aligned} I_R(\rho) &= -\sum_{k,k'} \text{Im} G_{kk'} (\omega \rightarrow 0) \cdot \left[ (a^\dagger a)^k (a^\dagger a)^{k'}, \rho \right], \\ G_{kk'} (\omega) &= i \int_0^\infty \left[ \langle B_k(\tau) \cdot B_{k'}(0) \rangle - \langle B_k \rangle \cdot \langle B_{k'} \rangle \right] e^{i\omega\tau} d\tau. \end{aligned} \quad (10.44)$$

In the simplest case  $k = 1$ ,  $V_A = a^\dagger a B_1(q)$  the equation (10.43) in the interaction representation  $\rho = \exp(-iH_p t) \sigma \exp(iH_p t)$  takes the form:

$$\frac{d\sigma_{mn}}{dt} = -\gamma_1 (m-n)^2 \sigma_{mn}, \quad \text{where } \gamma_1 = G_{11}(\omega \rightarrow 0), \quad (10.45)$$

and, consequently,

$$\rho_{mn}(t) = e^{-i\omega_p t(m-n)-\gamma_1 t(m-n)^2} \rho_{mn}(0). \quad (10.46)$$

Substituting Eq. (10.46) into Eq. (10.42) we find the expression for  $I(\omega)$ :

$$I(\omega) = \frac{\gamma_1}{\pi \left[ (\omega - \omega_p)^2 + \gamma_1^2 \right]}. \quad (10.47)$$

This is a well-known result, giving the Lorentz spectrum for the oscillator with a quickly fluctuating frequency.

In the more complicated case  $k = 2$ ,  $V_A = (a^\dagger a)^2 B_2(q)$  the equation (10.43) for the density matrix is:

$$\frac{d\sigma_{mn}}{dt} = -\gamma_2 (m^2 - n^2)^2 \sigma_{mn}, \quad \text{where } \sigma_{mn} = e^{i\omega_p t(m-n)} \rho_{mn}(t), \quad (10.48)$$

and, correspondingly,

$$\rho_{mn}(t) = \rho_{mn}(0) \cdot e^{-i\omega_p t(m-n)-\gamma_2 (m^2-n^2)^2 t}, \quad (10.49)$$

---

<sup>11</sup>In the subsequent consideration we follow Ref. [162].

where  $\gamma_2 = G_{22}(\omega \rightarrow 0)$ . Substituting Eq. (10.49) into Eq. (10.42), we find:

$$\begin{aligned} I(\omega) &= \frac{1}{\pi} \left(1 - e^{-\frac{\omega_p}{T}}\right)^2 \sum_{n=0}^{\infty} (n+1) e^{-\frac{n\omega_p}{T}} \\ &\times \operatorname{Re} \left[ \frac{1}{(2n+1)^2 \gamma_2 - i(\omega - \omega_p)} \right]. \end{aligned} \quad (10.50)$$

We would like to note, that the vibrational temperature  $T$  is defined through the total energy of the molecule  $E$  in such a way, that the distribution of the population of the pumped mode  $n$  is of Gibbs type<sup>12</sup>. From Eq. (10.50) it can be found, that the spectrum in the present case is represented by a superposition of different Lorentz lines with increasing widths.

Let us consider the spectrum in more detailed. In the case  $\frac{\hbar\omega_p}{kT} \gg 1$  only the term with  $n = 0$  is left in the sum (10.50), and the spectrum is of Lorentz type with the width  $\gamma_2$ .

In the more interesting case of the highly excited molecule  $\frac{\hbar\omega_p}{kT} \ll 1$  in Eq. (10.50) all the terms should be kept. Treating  $n$  like a continuous variable, we transform Eq. (10.50) to the form:

$$I(\omega) = \frac{(\omega_p/T)^2 \gamma_2}{\pi} \int_0^{\infty} \frac{(2x+1)^2 (x+1)}{(2x+1)^4 \gamma_2^2 + (\omega - \omega_p)^2} e^{-(\omega_p/T)x} dx. \quad (10.51)$$

It is hard to analyze this integral in the general case. However, with the help of the condition  $\frac{\hbar\omega_p}{kT} \ll 1$  it can be presented in the form of the following analytic expressions in the three different areas of its arguments  $\varepsilon = \frac{\omega - \omega_p}{\gamma_2}$ ,  $\alpha = \frac{\hbar\omega_p}{kT}$ :

(1) in the area of maximal absorption  $\varepsilon \ll 1$ ,  $\alpha \ll 1$ :

$$I(\varepsilon) = \frac{\alpha^2}{4\pi\gamma_2} (1 - C + \ln(2/\alpha) - 0,45\varepsilon^2); \quad (10.52)$$

(2) in the intermediate region  $1 \ll \varepsilon \ll \alpha^{-2}$ ,  $\alpha \ll 1$ :

$$I(\varepsilon) = \frac{\alpha^2}{4\pi\gamma_2} (\ln(2/\alpha) - C - \ln \varepsilon^{1/2}); \quad (10.53)$$

(3) in the sidebands of the absorption  $\alpha^{-2} \ll \varepsilon$ ,  $\alpha \ll 1$ :

$$I(\varepsilon) = \frac{24}{\pi\alpha^2\varepsilon^2\gamma_2}, \text{ if } \alpha^{-2} \ll \varepsilon, \quad \alpha \ll 1, \quad (10.54)$$

---

<sup>12</sup>The entire vibrational system of the molecule obeys the micro-canonical distribution, so that its small subsystem, the pumped-up mode, is governed by Gibbs distribution on the basis of general principles. This gives the dependence  $\omega_p(E, T)$ .

where  $C = 0.5772\dots$  is the Euler's constant.

The dependence of the shape of the absorption  $I(\omega)$  upon the temperature in the limit of high  $T$  can be analyzed on the basis of these formulas. The maximal value of the absorption we find from Eq. (10.52):

$$\begin{aligned} I_{res} &= I(0) = I(\omega \simeq \omega_p) = \frac{\alpha^2}{4\pi\gamma_2} (1 - C + \ln(2/\alpha)) \\ &\simeq \frac{\alpha^2}{4\pi\gamma_2} \ln(2/\alpha) \sim \frac{\ln T}{T^2}. \end{aligned} \quad (10.55)$$

The half-width, defined by the condition  $I\left(\delta\omega_{\frac{1}{2}}\right) = \frac{1}{2}I_{res}$ , we find from the comparison of equations (10.52) and (10.53):

$$\delta\omega_{1/2} = \gamma_2 \cdot \frac{2}{\alpha} \cdot e^{-(1+C)} \sim \gamma_2 \cdot \frac{T}{\omega_p}. \quad (10.56)$$

This quantity determines the width of the resonance peak. It belongs to the intermediate region of  $\varepsilon$ , as  $1 \ll \varepsilon_{\frac{1}{2}} \sim \frac{\delta\omega_{\frac{1}{2}}}{\gamma_2} \sim \frac{kT}{\hbar\omega_p} \sim \alpha^{-1} \ll \alpha^{-2}$ . Besides, one can calculate the half-width of the effective Lorentzian, the wings of which coincide asymptotically with the curve of Eq. (10.54). This quantity,  $\delta\omega_w$ , characterizing the width of the wings of the real spectrum:

$$\delta\omega_w = 24\alpha^{-2}\gamma_2 \sim \gamma_2 \cdot \left(\frac{T}{\omega_p}\right)^2. \quad (10.57)$$

Comparing equations (10.56) and (10.57) we find, that the width of the resonance peak  $\delta\omega_{\frac{1}{2}}$  grows with temperature much slower, then the width of the spectrum wings  $\delta\omega_w$ . Besides, the product  $I_{res}\delta\omega_{\frac{1}{2}}$  tends to zero as  $T \rightarrow \infty$ , as

$$I_{res}\delta\omega_{1/2} = \alpha \ln\left(\frac{2}{\alpha}\right) = \frac{\omega_p}{T} \ln\left(\frac{2T}{\omega_p}\right) \rightarrow 0. \quad (10.58)$$

From the last two facts one can derive the conclusion, that at high excitation levels  $\frac{kT}{\hbar\omega_p} \gg 1$  the transition strength redistributes quickly from the center of the resonance peak into the wings of the contour (the entire integral  $\int I(\omega) d\omega = 1$  does not depend upon the excitation level). The results of the calculation of  $I(\omega)$  according to Eq. (10.50) at various excitation levels, plotted in Fig. 10.6 from Ref. [162], back up nicely the consideration above.

The product  $I_{res}\delta\omega_{\frac{1}{2}}$  typically is used to estimate the total transition strength for the experimental spectrum under the assumption, that its form is of Lorentz type. Then this product is independent upon the vibrational energy of the molecule.

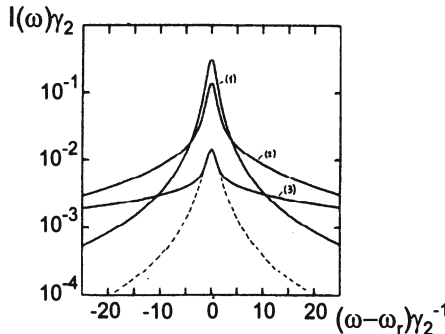


Figure 10.6: The shape of the IR absorption spectrum  $I(\omega - \omega_p)$  for various excitation levels  $n$ . The dashed line corresponds to a simple Lorentz approximation of the real spectrum close to the maximum of absorption.

From the consideration above it follows, that with  $V_A = (a^+a)^2 B_2(q)$  the absorption spectrum is non-Lorentzian, and the quantity  $I_{res}\delta\omega_{\frac{1}{2}}$  decreases with the growing vibrational excitation energy of the molecule. It means, that as  $T \rightarrow \infty$  the contribution of the resonance part of the spectrum into the total intensity of absorption tends to zero, and the basic contribution is provided by the wings of the absorption spectrum. Such dependencies of the absorption spectra has even observed in the experiment in molecules  $C_6F_{12}$  at excitation level  $E \approx 60000 \text{ cm}^{-1}$  [165]. Thus, the anharmonicity of high order in the coordinate of the pumped-up mode plays an important role in the intra-molecular relaxation and in the IR absorption spectra of polyatomic molecules at high excitation of vibrational levels. It is reasonable to suppose, that the observed decrease of the contribution of the resonant part of the spectrum into the integral intensity, as compared to the wings of the spectral contour, signify the strong effect of anharmonic terms of inter-mode interaction upon the rate and the character of vibrational relaxation in the molecule.

## 10.4 Correlation between structure and IR spectra in polyatomic molecules

To conclude the book, we end with the Section, devoted to the use in experimental studies of some semi-empirical dependencies, which relate the anharmonic parameters of polyatomic molecules to the characteristics of their IR spectra. It is demonstrated, how the use of this relation helps to determine from the IR spectrum the lengths of valence bonds and angles in polyatomic molecules with valent bonds of similar type. Results of the cor-

responding quantum-chemical calculations, supporting these relations, are provided.

In the present Section we consider a simple and accurate (up to  $\sim 10^{-3}$   $\text{\AA}$ ) method of measurement of bond lengths in polyatomic molecules through the spectroscopic characteristics of the overtone spectra[166, 15].

In the last two decades a great number of theoretical and experimental works on IR spectroscopy of vibrational overtones in polyatomic molecules has been performed. It has been proved, that the IR spectra of stretching vibrations of  $XH$  bonds are successfully reproduced and interpreted within the model of weakly bound anharmonic Morse oscillators. More to it, in passing to higher overtones this model works even better and better. Here we would like to reproduce a citation from the paper by B.R.Henry and M.G.Sowat [39]:

"One of the main thrusts of our research over the last ten years has been to use the local mode model and overtone spectra to investigate changes in molecular structure and conformation between similar molecules. We proposed the local mode model in order to understand  $XH$ -stretching vibrational overtone spectra, where  $X$  is some heavier atom like  $C$ ,  $N$ , or  $O$ . This model is now routinely used to analyze these high energy overtone spectra. The model predicts that the dominant transitions in these spectra involve vibrationally excited states whose components have all of the vibrational energy localized in one of a set of equivalent  $XH$  oscillators. For example, even in molecules like the methyl halides where the three hydrogens are joined to a common carbon, the spectrally active  $CH$ -stretching overtone states for  $\Delta\nu_{CH} \geq 3$  correspond primarily to linear combinations of components  $|v, 0, 0\rangle$ ,  $|0, v, 0\rangle$  and  $|0, 0, v\rangle$ . These individual components can be thought of as products of one-dimensional wavefunctions localized on each of the three  $CH$  bonds, i.e.  $|v, 0, 0\rangle = |v\rangle|0\rangle|0\rangle$ . These localized wavefunctions are unharmonic but only weakly coupled. The effective coupling decreases with increasing vibrational energy, and the splitting between the various linear combinations ( $|v, 0, 0\rangle \pm |0, v, 0\rangle \pm |0, 0, v\rangle$ ) also decreases. Thus for the higher overtones, these various linear combinations are effectively degenerate. These local mode characteristics are even more pronounced in a molecule like benzene because the hydrogens are bonded to different carbons. Indeed, most of the higher energy gas phase overtone transitions in benzene appear as simple Lorentzian peaks".

Thus, at  $v \gg 1$  the overwhelming contribution to the intensity of IR spectra is provided by the localized states of the type  $|v, 0\dots 0\rangle$ . Consequently, the characteristics of these spectra are very sensitive to the properties of  $XH$  bonds. Really, it has been found in the experiment, that the shifts of transition frequencies  $\Delta\bar{\nu}$  are proportional to the lengths of  $XH$  bonds [167]:

$$r_{CH}^{LM}(A^0) = 1,084 - \left( \frac{\Delta\bar{\nu}}{11\Delta\nu_{CH}} \right) \cdot 0,001. \quad (10.59)$$

Here  $r_{CH}^{LM}$  is the length of the  $CH$  bond, the vibration spectrum of which is determined from the IR spectrum. The length of  $CH$  bond in the molecule of benzene,  $1.084 \text{ \AA}$ , is adopted as the length unit, and all the changes of the  $CH$  bond length are measured with respect to it.

For the potential of the vibrationally excited oscillator ( $C - H$  bond) B.R.Henry and M.G.Sowat suggested the following truncated Morse function:

$$\begin{aligned} V(r \leq r_a) &= \infty, \\ V(r \geq r_a) &= V_a(r) = D_e \left[ \left( 1 - e^{-\alpha_e(r-r_e)^2} \right)^2 - 1 \right], \end{aligned} \quad (10.60)$$

where  $D_e$  is the dissociation energy,  $r_a$  is the minimal distance, at which the atoms can approach one another (the radius of the hard core of atom  $X$ ). It is assumed, that the parameters  $r_a$  and  $V_a$  are constant for the elements from the same row of the Mendeleev table. For example, the atoms  $C$ ,  $N$ , and  $O$  have  $V_a = 37.5 \text{ ev}$ , and  $r_a = 33.5 \cdot 10^{-12} \text{ m}$ . If the atom  $X$  becomes excited, then  $V_a$  is substituted by  $V_a + T_e$ , where  $T_e$  is the electronic excitation energy.

From Eq. (10.60) we find:

$$\alpha_e = \frac{\ln \left[ 1 + (V_a/D_e + 1)^{1/2} \right]}{r_e - r_a}. \quad (10.61)$$

The parameters  $\alpha_e$  and  $D_e$  of the Morse potential are related to the vibrational frequency  $\omega_e$  and the anharmonicity parameter  $x_e$  by the following formula:

$$\begin{aligned} D_e &= \frac{\omega_e^2}{4x_e}, \\ \alpha_e &= \frac{1}{2\hbar} \left( \frac{2\mu}{D_e} \right)^{1/2} \omega_e = \frac{(2\mu x_e)^{1/2}}{\hbar}, \end{aligned} \quad (10.62)$$

where  $\omega_e$  and  $x_e$  are measured in energy units. From Eqs. (10.61) and (10.62) we obtain the following dependence of  $(r_e - r_a)$  upon  $\omega_e$  and  $x_e$ :

$$(r_e - r_a) = \frac{\hbar}{(2\mu x_e)^{1/2}} \ln \left[ 1 + \left( 1 + \frac{4V_a x_e}{\omega_e^2} \right)^{1/2} \right]. \quad (10.63)$$

Then the changes in the bond lengths  $\delta r_e$  are determined by the differential  $dr_e = \delta r_e$  under the condition  $dr_a = \delta r_a \equiv 0$ :

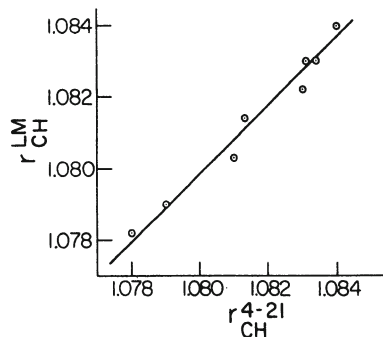


Figure 10.7: Correlation between  $CH$  bondlengths in fluorinated benzenes, which are obtained from frequency shifts in the overtone spectra, and  $CH$  bondlengths from ab initio molecular orbital calculations at the 4-21G level, from Ref. [167]

$$\begin{aligned}\delta r_e = & \frac{\left(\hbar/(2\mu x_e)^{1/2}\right)(-4V_a x_e)}{\omega_e^3 (1 + 4V_a x_e/\omega_e^2)^{1/2} \left[1 + (1 + 4V_a x_e/\omega_e^2)^{1/2}\right]} \delta \omega_e \\ & + \frac{\left(\hbar/(2\mu x_e)^{1/2}\right)(4V_a \omega_e^{-2})}{(1 + 4V_a x_e \omega_e^{-2})^{1/2} \left[1 + (1 + 4V_a x_e \omega_e^{-2})^{1/2}\right]} \delta x_e \\ & - \frac{\hbar}{2(2\mu x_e^3)^{1/2}} \ln \left[1 + \left(1 + \frac{4V_a x_e}{\omega_e^2}\right)^{1/2}\right] \delta x_e.\end{aligned}\quad (10.64)$$

Equation (10.64) enables one to find the correction to the bond length  $\delta r_e$  based on the information on the frequency shifts  $\delta \omega_e$  and the changes of the anharmonicity parameter  $\delta x_e$ , if the length of  $XH$  bond is known for any one molecule from the considered row. For example, that could be the  $CH$  bond in benzene. Then, given the IR spectra of benzene and of the  $CH$  bond of the studied molecule, one finds  $\delta \omega_e$  and  $\delta x_e$ , and, subsequently,  $\delta r_e$  and  $r_e = (r_e)_{benzene}$  with the help of Eq. (10.64).

The accuracy of this method of determination of bond lengths is of the order of  $10^{-3} \text{ \AA}$ , and in fact it is at least comparable to the accuracy of quantum-chemical calculations [39]. Fig. 10.7 shows the correlation between the calculated lengths of  $CH$  bonds in the molecules of fluorinated benzenes and the bond lengths, found with the help of Eq. (10.64) from the spectroscopic characteristics of vibrational IR spectrum. The agreement in

Molecule	$\omega,$ $cm^{-1}$	$x,$ $cm^{-1}$	$D,$ $eV$	$r_{ex},$ $pm$	$\Delta r_e,$ $pm$	$\Delta r_H,$ $pm$	$\Delta r_B,$ $pm$
FB $H_2$	3199	58,6	5,411	108,1	-0,1	-4,8	-5,4
FB $H_3, H_4$	3187	60,3	5,222	108,3	-0,7	-5,0	-5,4
1,2-FB $H_3$	3192	57,3	5,513	108,1	0,4	-4,6	-5,3
1,2-FB $H_4$	3188	58,7	5,366	108,2	-0,1	-4,8	-5,3
1,3-FB $H_2$	3218	57,5	5,581	107,9	0,2	-4,7	-5,4
1,3-FB $H_4$	3209	58,8	5,428	108,0	-0,2	-4,8	-5,4
1,3-FB $H_5$	3193	59,9	5,275	108,2	-0,6	-4,9	-5,4
1,4-FB	3201	57,9	5,485	108,1	0,1	-4,7	-5,4
1,3,5-FB	3221	56,6	5,680	107,8	0,6	-4,5	-5,4
1,2,5-FB	3214	58,9	5,436	108,0	-0,2	-4,8	-5,5
1,2,3,5-FB	3231	59,1	5,475	107,8	-0,4	-4,9	-5,6
1,2,4,5-FB	3217	57,6	5,568	107,9	0,2	-4,7	-5,4
$CH_2Cl_2$	3207	63,2	5,043	108,5	-2,0	-5,6	-5,9
$C_6H_6$	3157	57,1	5,411	108,4	0,6	-4,5	-5,1

Table 10.2: Calculated values of the bond length  $r_e$  for a series of  $CH$  oscillators from observed values of  $\omega_e$  and  $x_e$ . These values are compared with experimental values, and with those calculated by Huggins' method,  $r_H$ , and by Badger's rule,  $r_B$ .  $\Delta$  denotes the deviation of the calculated parameter from the experimental value, for example,  $\Delta r_e = r_e - r_{ex}$ . FB - Fluorinated benzene with atoms  $F$  in the specified positions.

fact is amazing. At present this method of determination of bond lengths is the most accurate.

In conclusion we provide the table with the calculated  $CH$  bond lengths according to Eq. (10.64) in a number of molecules, along with the corresponding results obtained by different methods [166]. The experimental values of  $r_{CH}$  in Table 10.2 were obtained by a fitting procedure to the empirical dependencies which relate structural and spectroscopic characteristics.

# Chapter 11

## Conclusion

In this book we have discussed the effects of nonlinearity in the vibrational-rotational motion in polyatomic molecules and in simple molecular crystals like  $N_2$ ,  $CO$ , etc. This nonlinearity is revealed most transparently at high excitation levels of the vibrational/rotational mode in the presence of a point symmetry of the initial Hamiltonian. Then the strong excitation leads to the dynamical violation of the initial symmetry. The IR spectra under insufficient resolution demonstrate lowered symmetry in the rotational spectra. For example, in place of the octahedral symmetry in the molecule  $XY_4$  the symmetry  $C_{3v}$  of a symmetric top will be observed. Thus the determination of the real symmetry of the intramolecular Hamiltonian, and the reconstruction of the potential energy surface of the intramolecular interaction requires the great enhancement in the resolution of the IR spectral lines ( $\sim 10^6 \div 10^{-8} \text{ cm}^{-1}$ ). This will enable the determination of the interaction with nuclear spins and the correct interpretation of the lines in IR spectra as well.

There is another basic conclusion from the analysis of the motion of finite (molecules) and infinite (crystals) nonlinear systems — a kind of complementarity (asymmetry). In molecules the conditionally-periodic motions with different frequencies  $\omega_1 \neq \omega_2$  due to high excitation of one degree of freedom lead to the appearance of LMs, whereas the NM appears from the resonance  $\omega_1 = \omega_2$  and corresponds to the equal excitation of equivalent bonds ( $XY_2$  molecules). In the latter case the energy is dispersed over valent bonds. In nonlinear lattices the breathers (localized excitations), on the contrary, are formed from resonant orbits, whereas the tori of conditionally-periodic motion  $\omega_1 \neq \omega_2$  are destroyed necessarily due to the inevitable resonance with the frequencies of the phonon spectrum because of the nonlinearity. Thus, one can expect, that the intramolecular local modes in crystals can be at most long-living with anomalously long decay times, while the NM of resonant orbits are transformed into breathers with infinite lifetime. The reasonable assumption then is that the breather states in the quantum case correspond to a narrow band of discrete localized states, analogous to the

states of the impurity band in semiconductors. The linewidth in the IR spectra of such states will be governed purely by the radiation-like mechanism.

# Bibliography

- [1] M.Toda, Theory of Nonlinear Lattices, Berlin, 1981.
- [2] R.K.Dodd, J.C.Eilbeck, J.D.Gibbon, H.C.Morris, Solitons and Non-linear Waves, Academic Press, New York, 1982.
- [3] G.Eilenberger, Solitons. Mathematical Methods for Physicists. Springer, Berlin, 1981.
- [4] M.Toda, Phys.Rep. 18 (1975) 1.
- [5] G.Herzberg, Molecular Spectra and Molecular Structure, vol.2, Infrared and Raman Spectra of Polyatomic Molecules, van Nostrand, New York, 1945 (2nd edn., 1950).
- [6] M.S.Child, L.Halonen, Advances in Chemical Physics, 57 (1984) 1.
- [7] V.I.Arnold, Mathematical Methods of Classical Mechanics, Springer, New-York, 1978.
- [8] A.N.Kolmogorov, Doklady Academii Nauk (USSR), 98 (1954) 527.
- [9] V.I.Arnold, Uspekhi Matem. Nauk (USSR), 18 (1963) 13.
- [10] V.I.Arnold, Uspekhi Matem. Nauk (USSR), 18 (1963) 81.
- [11] E.B.Wilson, J.C.Decius, P.C.Cross, Molecular Vibrations, McGraw-Hill, 1955.
- [12] A.A.Ovchinnikov, Zh.Eksp.Teor.Phys. (USSR), 57 (1969) 263, (Eng. transl.: Sov. Phys. JETP 30 (1970) 147).
- [13] A.A.Ovchinnikov, Teor.Mat.Phys. (USSR), 11 (1972) 366.
- [14] K. Dressler, O.Oehler, D.A.Smith, Phys.Rev.Lett., 34 (1975) 364.
- [15] B.R.Henry, Accounts of Chemical Research, 20 (1987) 429.
- [16] E.L.Sibert, W.P.Reinhardt, J.T.Hynes, J.Chem.Phys., 77 (1982) 3583.
- [17] S.C.Althorpe, D.C.Clary, J.Chem.Phys., 102 (1995) 4390.

- [18] W.J.Harter, G.W.Patterson, *J.Chem.Phys.*, 80 (1984) 4241.
- [19] D.A.Sadovskii, B.I.Zhilinskii, J.P.Chamption, G.Pierre, *J.Chem.Phys.*, 92 (1990) 1523.
- [20] J.M.Gomes Llorente and E.Pollak, *Ann.Rev.Phys.Chem.*, 43 (1992) 91.
- [21] O.Brass, J.Tennyson, E.Pollak, *J.Chem.Phys.*, 92 (1990) 3005, *ibid*, 3377.
- [22] B.R.Johnson, J.L.Kinsey, *Phys.Rev.Lett.*, 62 (1989) 1607.
- [23] A.Carrington, I.R.McNab, *Acc.Chem.Res.*, 22 (1989) 218.
- [24] A.Carrington, R.A.Kennedy, *J.Chem.Phys.*, 81 (1984) 91.
- [25] R.V.Jensen, Proceedings of the US-Mexico Workshop on Atomic and Molecular Physics, 1991.
- [26] B.Eckhardt, J.M.Gomes Llorente, E.Pollak, *Chem.Phys.Lett.*, 174 (1990) 325.
- [27] E.J.Heller, in: *Proceedings 1989 Les Houches Summer School on Chaos and Quantum Physics*, ed. by A.Varos, M.J.Griannoni, J.Justin, Elsevier, Amsterdam, 1990.
- [28] H.G.Kjaergaard, Hengutai Yu, B.J.Schattka, B.R.Henry, A.W.Tarr, *J.Chem.Phys.*, 93 (1990) 6239.
- [29] H.G.Kjaergaard, B.R.Henry, *J.Phys.Chem.*, 99 (1995) 899.
- [30] H.G.Kjaergaard, B.R.Henry, *Mol.Phys.*, 83 (1994) 1099.
- [31] M.M.Law, J.L.Duncan, *Mol.Phys.* 83 (1994) 757.
- [32] A.C.Albrecht, in: *Advances in Laser Chemistry*, ed. by A.H.Zeweil, Springer, Berlin, 1978, p.235 (*Springer Series in Chemical Physics*, v.3).
- [33] J.Svitak, Z.Li, J.Rose, M.E.Kellman, *J.Chem.Phys.*, 102 (1995) 4340.
- [34] J.P.Rose, M.E.Kellman, *J.Chem.Phys.*, 103 (1995) 7255.
- [35] M.E.Kellman, *Ann.Rev.Phys.Chem.*, 46 (1995) 395.
- [36] L.Halonen, A.G.Robiette, *J.Chem.Phys.*, 84 (1986) 6861.
- [37] M.Halonen, L.Halonen, H.Burger, S.Sommer, *J.Chem.Phys.*, 93 (1990) 1607.

- [38] K.K.Lehman, J.Chem.Phys., 95 (1991) 2361.
- [39] B.R.Henry, M.G.Sowa, Prog.Analyt.Spectrosc. 12 (1989) 349.
- [40] C.L.Siegel, J.K.Moser, Lectures on Celestial Mechanics, Springer, 1971.
- [41] S.Sternberg, Celestial Mechanics 1, 2, N.Y., Benjamin, 1969.
- [42] L.D.Landau, E.M.Lifshitz, Mechanik, Lehrbuch der Theoretischen Physik I, Akademie-Verlag, Berlin, 1991.
- [43] P.M.Morse, H.Feshbach, Methods of Theoretical Physics, New York, 1953.
- [44] V.I.Arnold, Doklady Academii Nauk (USSR), 156 (1964) 9.
- [45] G.M.Zaslavskii, B.V.Chirikov, Uspehi Fiz. Nauk (USSR), 105 (1971) 3.
- [46] S.M.Ulam, A Collection of Mathematical Problems, Los Alamos Scientific Laboratories, New Mexico.
- [47] J.Ford, J.Waters, J.Math. Phys., 4 (1963) 1293.
- [48] F.M.Izrailev, A.I.Hisamutdinov, B.V.Chirikov, Preprint, Institute of Nuclear Physics, Siberian branch of the Academy of Sciences of USSR.
- [49] V.M.Burlakov, S.A.Kiselev, V.I.Rupesov, Pis'ma ZHETF (USSR), 51 (1990) 481, (Eng. transl.: JETP Letters 51 (1990) 544).
- [50] J.K.Moser, Math.Ann., 169 (1967) 136.
- [51] A.A.Ovchinnikov, N.S.Erikhman, Uspekhi Fiz. Nauk (USSR), 138 (1982) 289, (Eng. transl.: Sov.Phys.Usp., 25 (1982) 737).
- [52] C.Jaffe, P.Brumer, J.Chem.Phys., 73 (1980) 5647.
- [53] R.Wallace, Chem.Phys., 11 (1975) 189.
- [54] G.A.Korn, J.M.Korn, Mathematical Handbook for Scientists and Engineers, Mc. Graw - Hill Book Company, 1968.
- [55] R.T.Lawton, M.S.Child, Mol.Phys., 37 (1979) 1799.
- [56] B.Henry, I.Hung, Chem.Phys., 29 (1978) 465.
- [57] D.A.Kirzhnic, Field Methods of Many-Particle Theory, Gosatomisdat (USSR), Moscow, 1963.
- [58] P.A.M.Dirac, The Principles of Quantum Mechanics, Oxford, 1958.

- [59] N.N.Nehoroshev, Functionalnii Analiz I Ego Prilozheniya (USSR), 5, (1971) 82.
- [60] A.P.Prudnikov, Yu.A.Brichkov, O.I.Marichev, Integrals and Series, Nauka, Moscow, 1981 (in Russian),  
I.S.Gradshteyn, I.M.Rizhik, Tables of Integrals, Series, and Products, Nauka, Moscow, 1971.
- [61] A.J.Sievers, S.Takeno, Phys.Rev.Lett., 61 (1988) 970.
- [62] S.Takeno, A.J.Sievers, Sol.St.Comm., 67 (1988) 1023.
- [63] S.Takeno, et.al., Progr.Theor.Phys., 94 (1988) 242.
- [64] S.Flach, C.R.Willis, Phys.Rep., 295 (1998) 184.
- [65] H.Segur, M.D.Kruscal, Phys.Rev.Lett., 58 (1987) 747.
- [66] J.Giecke, Phys.Rev.E, 49 (1994) 3539.
- [67] S.Elytin, A.Maimistov, E. Manukin, Phys.Lett.A, 142 (1989) 493.
- [68] R.Trautman-Michalska, J.Opt.Spect.America, 6 (1989) 36.
- [69] S.Flach, Phys.Rev.E, 50 (1994) 3134.
- [70] S.Flach, Phys.Rev.E, 51 (1995) 1503.
- [71] S.Flach, Phys.Rev.E, 51 (1995) 3579.
- [72] S.Flach, Existence and properties of discrete breathers, in: E.Alfinito, M.Boiti, L.Martina, F.Pempinelli, editors, Nonlinear Physics. Theory and Experiment, World Scientific, Singapore, 1996, p.390.
- [73] D.Cai, A.R.Bishop, N.Gronbech-Jensen, Phys.Rev.E, 52 (1995) 5784.
- [74] R.S.Mac-Kay, S.Aubry, Nonlinearity, 7 (1994) 1623.
- [75] W.H.Press, B.P.Flannery, S.A.Teukolsky, W.T.Vetterling, Numerical Recipes: The Art of Scientific Computing, Cambridge University Press, Cambridge, 1986.
- [76] S.Flach, C.R.Willis, E.Olbrich, Phys.Rev.E, 49 (1994) 836.
- [77] A.A.Ovchinnikov, S.Flach, Phys.Rev.Lett., 83 (1999) 248.
- [78] A.J.Sievers, S.Takeno, Phys.Rev.Lett., 61 (1988) 970.
- [79] J.B.Page, Phys.Rev.B, 41 (1990) 7835.

- [80] A.J.Sievers, J.B.Page, Unusual anharmonic local mode systems, in: G.K.Horton and A.A.Maradudin, editors, *Dynamical Properties of Solids VII (Phonon Physics: The Cutting Edge)*, Elsevier, Amsterdam, 1995, p.137.
- [81] L.D.Landau, E.M.Lifshitz, Quantenmechanik, Lehrbuch der Theoretischen Physik III, Akademie-Verlag, Berlin, 1991.
- [82] A.A.Ovchinnikov, N.S.Erikman, Optika i Spektroscopia. (USSR), 34 (1973) 690, (Eng. transl.: Opt. Spectrosc. 34 (1973) 398).
- [83] M.S.Child, R.T.Lawton, Faraday Discuss. Chem. Soc., 71 (1981) 273.
- [84] H.S.Heeps, G.Herzberg, Z.Physik, 133 (1952) 48.
- [85] L.V.Gurvich et. al., *Thermodynamic Properties of Individual Substances*, 4-th Ed. (Hemisphere, NewYork, 1991).
- [86] I.A.Watson, B.R.Henry, I.G.Ross, Spectrochim. Acta, 37A (1981) 857.
- [87] M.S.Child, R.T.Lawton, Chem.Phys.Lett., 87 (1982) 217.
- [88] P.R.Stannard, M.L.Elert, W.M.Gelbart, J.Chem.Phys., 74 (1981) 6050.
- [89] H.S.Moller, O.S.Mortensen, Chem.Phys.Lett., 66 (1979) 539.
- [90] L.D.Landau, E.M.Lifshitz, Feldtheorie, Lehrbuch der Theoretischen Physik II, Akademie-Verlag, Berlin, 1991.
- [91] P.R.Bunker, R.E.Moss, Mol.Phys., 33 (1977) 417.
- [92] P.R.Bunker, C.J McLarnon, R.E.Moss, Mol.Phys., 33 (1977) 425.
- [93] P.R.Bunker, R.E.Moss, J.Mol.Spectrosc., 80 (1980) 217.
- [94] H.Essen, Am.J.Phys., 46 (1978) 983.
- [95] H.Grum, H.G.Kjaergaard, O.S.Mortensen, Am.J.Phys., 58 (1990) 344.
- [96] D.Papousek, M.Aliev, Molecular Vibrational / Rotational spectra, Academia, Prague, 1982, 323 p.
- [97] J.K.G.Watson, Mol.Phys., 15 (1968) 479.
- [98] M.R.Aliev, J.K.G.Watson, in: *Molecular Spectroscopy: Modern Research*, v.3, p.1, ed. by K.N.Rao, Academic Press, 1985, pp.2-67.
- [99] C.Camy-Peyret, J.M.Flaud, in: *Molecular Spectroscopy: Modern Research*, v.3, p.69, ed. by K.N.Rao, Academic Press, 1985, pp.69-110.

- [100] H.A.Jahn, E.Teller, Proc.Roy.Soc.A, 161 (1937) 220.
- [101] M.S.Krishnan, T.Carrington, J.Chem.Phys., 95 (1991) 1884.
- [102] M.S.Krishnan, T.Carrington, J.Chem.Phys., 94 (1991) 461.
- [103] M.Dubs, D.Harradine, E.Schweitzer, J.I.Steinfield, C.W.Patterson, J.Chem.Phys., 77 (1982) 3824.
- [104] M.Takami, H.Kuze, J.Chem.Phys., 78 (1983) 2204.
- [105] G.A.Laguna, K.C.Kim, C.W.Patterson, M.I.Reisfeld, D.M.Seitz, Chem.Phys.Lett., 75 (1980) 357.
- [106] K.Fox, H.W.Galbreith, B.I.Krohn, J.D.Louck, Phys.Rev.A, 15 (1977) 1363.
- [107] A.J.Dorney, J.K.G.Watson, J.Mol.Spectrosc., 42 (1972) 135.
- [108] J.Heading, An Introduction to Phase-Integral Methods, London: Methuen, New York: John Wiley, 1962, 160 p.
- [109] B.J.Krohn, Los Alamos Report LA-6554-MS, 1976.
- [110] W.G.Harter, C.W.Patterson, J.Chem.Phys., 66 (1977) 4872.
- [111] W.G.Harter, C.W.Patterson, J.Chem.Phys., 66 (1977) 4886.
- [112] W.G.Harter, C.W.Patterson, F.J. da Paihao Rev.Mod.Phys., 50 (1978) 37.
- [113] E.P.Wigner, Group Theory and Its Application to the Quantum Mechanics of Atomic Spectra, New York and London, 1959.
- [114] R.S.McDowell, C.W.Patteron, W.G.Harter, Los Alamos, Sci 3, (1982) 38.
- [115] W.G.Harter, C.W.Patterson, Phys.Rev.A, 10, (1979) 2277.
- [116] J.Borde et.al., Phys.Rev.Lett., 45 (1980) 14.
- [117] W.G.Harter, Phys.Rev.A, 24 (1981) 192.
- [118] J.Borde, Ch.J.Borde, Chem.Phys. 71 (1982) 417.
- [119] J.D.Louck, H.W.Galbraith, Rev.Mod.Phys., 48 (1976) 69.
- [120] G.S.Ezra, Symmetry Properties of Molecules: Lecture Notes in Chemistry, vol.28, Springer, New York, 1982, p.41.
- [121] Q.Zhu, B.A.Thrush, Chem.Phys.Lett., 150 (1988) 181.

- [122] Q.Zhu, B.Zhang, Y. Ma, H. Qian, Chem.Phys.Lett., 164 (1989) 596.
- [123] K.Lehmann, J.Chem.Phys., 96 (1992) 7402.
- [124] F.Michelot, J.Moret-Bailly, A.De-Martino, Chem.Phys.Lett., 148 (1988) 52.
- [125] M.Chevalier, A.De-Martino, F.Michelot, J.Mol.Spectrosc., 131 (1988) 382.
- [126] L.Halonen, J.Chem.Phys., 86 (1987) 588.
- [127] M.Ya.Ovchinnikova, Chem.Phys., 120 (1989) 249.
- [128] T.Poston, I.Stewart, Catastrophe Theory and Its Applications, Pitman, London, San Fransisco, Melbourne, 1978.
- [129] I.M.Pavlichenkov, B.I.Zhilinskii, Chem.Phys., 100 (1985) 339.
- [130] B.I.Zhilinskii, I.M.Pavlichenkov, Optica i Spectroscopia (USSR), 92 (1987) 387.
- [131] D.A.Sadovskii, B.I.Zhilinskii, Mol.Phys., 65 (1988) 109.
- [132] M.E.Kellman, L.Xiao, Chem.Phys.Lett., 162 (1989) 486.
- [133] M.E.Kellman, L.Xiao, J.Chem.Phys. 93 (1990) 5821.
- [134] Z.Li, L.Xiao, M.E.Kellman, J.Chem.Phys. 92 (1990) 2251.
- [135] Z.Li, L.Xiao, M.E.Kellman, J.Chem.Phys. 93 (1990) 5805.
- [136] M.E.Kellman, J.Chem.Phys. 83 (1985) 3843.
- [137] M.E.Kellman, E.D.Lynch, J.Chem.Phys. 85 (1986) 7216.
- [138] L.Xiao, M.E.Kellman, J.Chem.Phys. 90 (1989) 6086.
- [139] M.E.Kellman, J.Chem.Phys. 93 (1990) 6630.
- [140] M.E.Kellman, G.Chen, J.Chem.Phys. 95 (1991) 8671.
- [141] M.E.Kellman, in Molecular Dynamics and Spectroscopy by Stimulated Emission Pumping, edited by H.L.Dai and R.W.Field, World Scientific Singapore.
- [142] J.Rose and M.E.Kellman, J.Chem.Phys. 103 (1995) 17.
- [143] D.S.Tinitit, G.W.Robinson, J.Chem.Phys., 49 (1968) 3229.
- [144] R.Kubo, Y.Toyozawa, Progr.Theor.Phys., 13 (1955) 160.

- [145] H.Kun, A. Rhys, Proc.Roy.Soc. A, 204 (1950) 406.
- [146] K.Takahashi, M.Yokota, Mol.Phys., 20 (1971) 663.
- [147] Ya.B.Zel'dovich, A.A.Ovchinnikov, Pis'ma Zh.Eksp.Teor.Fiz, 13 (1971) 636, (Eng. transl.: JETP Lett., 13 (1971) 452).
- [148] T.Uzer, Phys.Rep., 199 (1991) 1.
- [149] J.M.Y.Ha, H.J.Maris, W.M.Risen Jr., J.Tauc, C.Thomson Z.Vardeny, Phys.Rev.Lett., 57 (1986) 3302; see also references in [148].
- [150] V.Plotnikov, G.Konoplev, Sov.Phys. JETP, 38 (1974) 476.
- [151] A.Stuchebrukhov, S.Ionov, V.Letokhov, J.Phys.Chem., 93 (1989) 5357.
- [152] A.A.Ovchinnikov, N.S.Erikhman, Sov.Phys.Solid State, 14 (1973) 2453.
- [153] B.R.Henry, Acc.Chem.Res., 10 (1977) 207.
- [154] R.G.Bray, M.J.Berry, J.Chem.Phys., 71 (1979) 4909.
- [155] K.F.Reddy, D.F.Heller, M.J.Berry, J.Chem.Phys., 76 (1982) 2814.
- [156] M.P.Cassassa, D.S.Bomse, K.C.Janda, J.Chem.Phys., 74 (1981) 5044.
- [157] M.A.Hoffbauer, K.Liu, C.F.Giese, W.R.Gentry, J.Chem.Phys., 78 (1983) 5567.
- [158] G.Fischer, R.E.Miller, R.O.Watts, Chem.Phys., 80 (1983) 147.
- [159] P.Avouris et al., Chem.Rev., 77 (1977) 793.
- [160] D.F.Heller, M.L.Elert, W.M.Gelbart, J.Chem.Phys., 69 (1978) 4061.
- [161] M.Bixon, J.Jortner, J.Chem.Phys., 50 (1969) 3284; ibid, 4061.
- [162] A.A.Stuchebrukhov, I.E.Khromov, Chem.Phys.Lett., 134 (1987) 251.
- [163] M.V.Kuzmin, V.S.Letokhov, A.A.Stuchebrukhov, ZHETP (USSR), 90 (1986) 458, (Eng. transl.: Sov.Phys. JETP, 63 (1986) 264).
- [164] A.A.Stuchebrukhov, Sov.Phys. – JETP, 64, (1986) 1195.
- [165] V.N.Bagratashvili, V.N.Burimov, S.I.Ionov, A.P.Sviridov, A.A.Stuchebrukhov, L.M.Turovets, Spectrochim.Acta, Proceedings of the International Conference on Chemistry by IR Lasers, 1986.

- [166] D.J.Swanton, B.R.Henry, *J.Chem.Phys.*, 86 (1987) 4801.
- [167] K.M.Gough, B.R.Henry, *J.Am.Chem.Soc.*, 106 (1984) 2781;  
*J.Phys.Chem.*, 88 (1984) 1298.

# Index

- Absorption
  - lineshape, 329
  - linewidth, 334
  - spectrum, 338, 346
- Anharmonicity, 13, 26, 71
  - of stretching vibrations, 178
  - parameter, 14, 185
- Arnold diffusion, 32
- Asymmetric top, 199, 216, 220
- Averaged Hamiltonian, 39
- Beat effect, 14, 34
- Bifurcation
  - diagram, 271, 272
  - manifold, 270
  - point, 253, 268, 270, 274
- Body frame, 157, 163, 165, 178, 180, 193, 212, 252, 253
- Bond length, 184, 347, 349
- Breather, 107, 351
  - discrete, 107, 110
  - multi-frequency, 114
- Canonical transformation, 29, 74, 89, 99, 192, 289
- Catastrophe map, 290
- Cluster
  - of rotation levels, 207, 243, 245, 246, 248, 249
  - of vibrational-rotational levels, 260
- Clusterization
  - of rotational levels, 177, 187, 188, 252, 254
  - of vibrational levels, 129, 140, 145, 154, 254
- of vibrational-rotational levels, 25, 178
- Combined symmetry, 241
- Completely integrable system, 31, 32
- Condensation of vibrational excitations, 308
- Conditionally-periodic motion, 31, 32, 120
- Contact transformation, 153, 170
- Coriolis interaction, 169, 184
- Correlation
  - structure-spectrum, 346
  - table, 219, 220, 225, 231, 237, 242
- Critical phenomenon, 270–272, 275
- Cusp (gap) in the spectrum, 285
- Decay rate (level width), 311, 318, 324, 334
- Diabolic point, 279
- Differential form, 42
- Eckart conditions, 156
- Effective Hamiltonian, 25, 171, 173, 188, 190, 191, 252, 254
- Euler angles, 191
- Fermi resonance, 253, 284
- Freezing effect, 239
- Generating function, 28
- Hamiltonian
  - equations, 30, 111, 198
  - in tensor form, 278, 279
  - lattice, 107, 110, 125

- Hyperfine splitting, 129, 207, 241, 251
- Initial vector, 218
- Integrals in involution, 30
- Internal symmetry, 187, 216, 242
- Intramolecular relaxation, 323
- Invariant torus, 62
- KAM theory, 17, 69, 87, 116
- Kolmogorov theorem, 20, 27, 31, 35, 108
- Laplace operator in covariant form, 153, 157
- Lissajou curve, 15, 21
- Local Mode (LM), 17, 21, 32, 42, 65, 68, 70, 78, 96, 107, 146, 150, 254, 347
- lifetime, 87, 296, 303
  - split-off, 81, 82
- Local symmetry, 217, 219, 270
- Master equation, 329
- Method of averaging, 37, 40, 74
- Metric tensor, 158
- Mixing of states
- of different symmetry, 259, 265
  - of different vibrational bands, 279
- Morse oscillator, 27, 35, 40, 70, 131, 347
- Multimode resonance, 291, 323, 333
- Nonresonant torus, 31, 32, 35, 42, 69, 87
- Normal Mode (NM), 12, 13, 42, 65, 68, 70, 78, 146, 150, 157
- Order of resonance, 30, 331
- Overlap of states, 209, 226, 260
- Overtone spectrum, 130
- Permutation symmetry, 239
- Phase
- portrait, 50, 54
- sphere, 286, 287, 291
- trajectory, 16, 19, 31, 34, 41, 195, 207
- vibrations, 62
- Poincare section, 56, 62, 120
- Point group invariance, 281, 283
- Poisson brackets, 88
- Polyad, 253, 286, 287, 290
- R-band of dyad, 282
- RE surface, 187, 198, 206, 214, 217, 220, 255, 266, 268, 278
- of rigid molecule (top), 199
  - of semirigid molecule, 200
- Redistribution of levels between the bands of a dyad, 283
- Relaxation operator, 343
- Resonance width, 65, 78
- Resonant (periodic) orbit, 19, 76, 111, 253
- Resonant torus, 19, 32, 69
- Rigid molecule, 12, 165, 167, 187, 201, 246
- Rotation Hamiltonian, 175, 177, 186, 187
- in operator matrix form, 273, 274
  - of rigid molecule, 190, 201
  - of semirigid molecule, 190, 211, 212
- Rotational deformation, 190, 216
- Rotational spectrum, 188, 215, 268
- Semirigid molecule, 156, 187, 201, 239
- Separatrix, 49, 79, 206, 220, 253, 262, 263, 272, 285, 287, 291
- $SO(3)$ -invariant Hamiltonian, 280, 283
- Spherical top, 190, 200, 215, 242
- Splitting of dyad levels, 283
- Stochastization of vibrations, 62

- Stretching vibration, 14, 71, 85, 129, 143, 157, 238, 347
- Super-hyperfine splitting, 239, 240
- Superfine splitting, 207, 237, 239, 240, 251
- Symmetric top, 199
- Symmetry
  - of RE surface, 242, 252
  - of split-up levels, 215
- Symmetry analysis
  - of rotation clusters, 214, 226, 242
- Theory of catastrophes, 270
- Thoma theorem, 268
- Tunneling integral, 209, 228
- Tunneling matrix, 187, 226, 227, 234, 238, 251, 254
- Unitary transformation, 89, 154, 170
- Valence coordinates, 179, 180, 184
- Variables action-angle, 27, 35, 41
- Vibration
  - Hamiltonian, 173, 176, 177
  - overtone, 185
- Vibrational excitation, 254
- Vibrational multiplet, 278
- Vibrational relaxation, 26, 293
- Vibrational spectrum, 23, 154, 253
- Vibrational-rotational dyad, 273, 275, 278
- Vibrational-rotational excitation, 267
- Vibrational-rotational Hamiltonian, 153, 170, 178
- Vibrational-rotational spectrum, 25, 155, 157, 167, 179, 185, 255, 291
- Violation of symmetry, 189, 240, 250, 254, 269, 271